SYNTHESIS, CHARACTERIZATION AND APPLICATION OF N-SUBSTITUTED AND C-SUBSTITUTED NICKEL CYCLAM CATAYLSTS IN HYDRODEHALOGENATION REACTIONS.

by

JAMES ALAN TOWNSEND

MChem., The Nottingham Trent University, 2003

AN ABSTRACT OF A DISSERTATION

submitted in partial fulfillment of the requirements for the degree

DOCTOR OF PHILOSOPHY

Department of Chemistry
College of Arts and Science

KANSAS STATE UNIVERSITY
Manhattan, Kansas

2009

Abstract

Highly toxic aromatic halogenated compounds such as PCB's, PCDF's and PCDD's act as persistent organic pollutants and can bio-accumulate. These compounds are highly stable to oxidation, reduction and thermal degradation. Current remediation technologies are expensive and can cause the formation of even more toxic byproducts. It is clear that an environmentally friendly and inexpensive remediation technology is required.

Our goal was the synthesis of dehalogenation catalysts incorporating aromatic side arms for the pre-concentration of the substrates to the catalysts. We envisioned that aromatic side arms would allow the aggregation of catalyst and substrate to form a pre-complex that would enhance rates of dehalogenation. Rapid and stereochemically predictable synthesis of N and C functionalized nickel cyclam complexes were a priority for this project.

Synthesis of N-functionalized cyclam molecules and subsequent metal incorporation proceeds smoothly to form *trans*(III) nickel cyclam complexes. However longer reaction times, initiation periods and short catalyst lifetimes made these complexes unsuitable for long-term study.

Cyclization of dipeptides and tetrapeptides using a metal template in basic conditions led to the formation of cyclopeptide nickel complexes with stereochemistry retained from the peptide precursors. Free cyclopeptides could be isolated from the nickel complexes by treatment with HCl.

Cyclopeptides are reduced to the cyclam molecules via a LAH reduction in low to moderate yields. Nickel incorporation into the cyclam molecules produced C-functionalized nickel catalysts with stereochemical integrity maintained throughout the synthesis. Intermolecular CH-π interactions can be seen in the solid state for the nickel cyclam complexes with aromatic side arms.

Reduction data show that the C-functionalized catalysts do not show improved rates of reduction for several aromatic substrates but small rate enhancements are observed for the reduction of chloronaphthalene over the unfunctionalized catalyst.

SYNTHESIS, CHARACTERIZATION AND APPLICATION OF N-SUBSTITUTED AND
C-SUBSTITUTED NICKEL CYCLAM CATAYLSTS IN HYDRODEHALOGENATION
REACTIONS.

by

JAMES TOWNSEND

MChem., The Nottingham Trent University, 2003

A DISSERTATION

submitted in partial fulfillment of the requirements for the degree

DOCTOR OF PHILSOPHY

Department of Chemistry
College of Arts and Science

KANSAS STATE UNIVERSITY
Manhattan, Kansas

2009

Approved by:

Major Professor
Dr S. Kraft

Copyright

JAMES TOWNSEND

2009

Abstract

Highly toxic aromatic halogenated compounds such as PCB's, PCDF's and PCDD's act as persistent organic pollutants and can bio-accumulate. These compounds are highly stable to oxidation, reduction and thermal degradation. Current remediation technologies are expensive and can cause the formation of even more toxic byproducts. It is clear that an environmentally friendly and inexpensive remediation technology is required.

Our goal was the synthesis of dehalogenation catalysts incorporating aromatic side arms for the pre-concentration of the substrates to the catalysts. We envisioned that aromatic side arms would allow the aggregation of catalyst and substrate to form a pre-complex that would enhance rates of dehalogenation. Rapid and stereochemically predictable synthesis of N and C functionalized nickel cyclam complexes were a priority for this project.

Synthesis of N-functionalized cyclam molecules and subsequent metal incorporation proceeds smoothly to form *trans*(III) nickel cyclam complexes. However longer reaction times, initiation periods and short catalyst lifetimes made these complexes unsuitable for long-term study.

Cyclization of dipeptides and tetrapeptides using a metal template in basic conditions led to the formation of cyclopeptide nickel complexes with stereochemistry retained from the peptide precursors. Free cyclopeptides could be isolated from the nickel complexes by treatment with HCl.

Cyclopeptides are reduced to the cyclam molecules via a LAH reduction in low to moderate yields. Nickel incorporation into the cyclam molecules produced C-functionalized nickel catalysts with stereochemical integrity maintained throughout the synthesis. Intermolecular CH-π interactions can be seen in the solid state for the nickel cyclam complexes with aromatic side arms.

Reduction data show that the C-functionalized catalysts do not show improved rates of reduction for several aromatic substrates but small rate enhancements are observed for the reduction of chloronaphthalene over the unfunctionalized catalyst.

Table of Contents

List of Figures

List of Tables

Acknowledgements

I would like to thank Kansas State University and the Terry. C. Johnson center for basic cancer research for funding.

I would like to thank Dr's Kraft, Culbertson, Hua, and Levy for their excellent teaching. The courses that I have had the privilege to take at Kansas State University have made me a more rounded chemist with a deeper understanding of inorganic, organic separation and spectroscopic chemistry and I thank you all for your dedication to learning, and for putting up with me.

I would like to thank my committee members, Dr's Kraft, Culbertson, Tomich, Smith and Pfromm for their guidance during both my proposition oral and my thesis. The support of such great people will never be forgotten.

I would like to make a special mention of Dr's Aakeroy, Bossmann and Tomich with whom I enjoyed countless hours of discussion, chemistry related and otherwise. Gentlemen your insight into my work has proven to be invaluable and I thank you all from the bottom of my heart.

I would like to thank Dr Tomich, Dr Hiromasa, and Dr Iwamoto for the generous donation of their time and use of the mass spectrum machines, Alvaro and Leila for all of their help with the NMR machines and John Desper for providing me with X-ray crystal structures.

A special thank you to all the ladies in the chemistry department office for all of their hard work behind the scenes. All of your efforts have not gone unnoticed and I thank you all for your help and understanding when it has been needed.

I would like to thank my friends at Kansas State University Michelle Smith, Dipesh Prima and Kris Mijares for their support; fun times were had by all. I look forward to a long lasting friendship with each of you over the coming years.

I would like to thank Nick Lloyd (AKA rich uncle Nicky/Terrance) for his friendship, care packages and continued support throughout my five and a half years away from England. Thank you for every beer and kebab you bought this poor student on his visits home and for letting me stay with you during my visits to Nottingham. I have been blessed with having such a

great best friend and have been thankful for the 12 years that we have known each other. Long may our friendship continue buddy!!

I would like to make special mention of Ben Scott and Abhijeet Sinha. No one could ever ask for a better pair of roommates. Thank you for putting up with me in the hard times and the good.

I would like to thank the families Eakes and Fasulo for their love and support over the past few years. To my lady Markie, thank you for your patience and understanding over the past few months. I know it must have been hard to deal with me under these conditions and I thank you from the bottom of my heart for your love and support; you are the best babe!

Dedication

This thesis is dedicated to my parents Peter and Jackie Townsend, my brothers David and Lee, and to my great auntie Anne and uncle Douglas Cameron for their unwavering love and support throughout both my undergraduate and graduate career. Without their help none of this would have been possible. Thank you with all my heart.

CHAPTER 1 - Non-functionalized and N-functionalized Nickel Cyclam Complexes and Hydrodehalogenation.

1.1   Introduction

There are many halogenated aromatic hydrocarbons that have been produced either intentionally as useful chemicals[1] or as side products of reactions/remediation of compounds over the years. These range from simple halogenated benzenes (used as intermediates in synthesizing pesticides[2]) to more complex polyhalogenated and polyaromatic systems such as polychlorinated biphenyls (PCB's) which were intentionally synthesized during most of the 20th century[3], polychlorinated dibenzo-p-dioxins (PCDD's), and polychlorinated dibenzofurans (PCDF's) both are unintentionally produced as by-products of the incineration of organic compounds[4] (Figure 1.1). These compounds are costly to remove with clean up of PCB's from the Hudson River exceeding 460 million dollars[5]. There are two main processes by which halogenated organic pollutants are removed from the environment, plasma burning and sodium columns[6]. Homogeneous catalysis in aqueous solutions may one day provide an efficient and cost effective means of remediation of these pollutants.
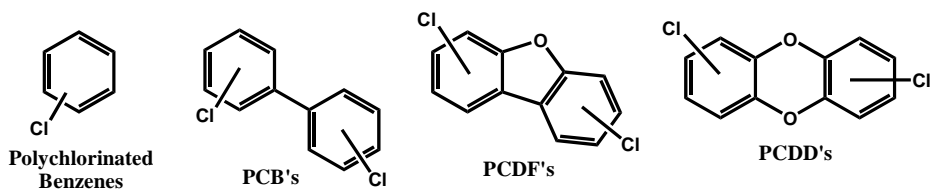
Figure 1.1: -Pollutants of concern.

1.1.1   Previous Methods of Hydrodehalogenation.

There are many methods available for the dehalogenation of aromatic compounds[7]. Alkaline earth metals for single electron transfer reductions (SET)[8]. Metal hydrides such as silanes[9] act as good hydrogen donors in SET reactions with aryl halides.

Pd/C, Pd/TiO$_2$ or Pd/Al$_2$O$_3$ catalysts can reduce aryl halides though hydrogenation reactions in polar media such as propanol/methanol mixtures at 30°C[10] or ethanol:water mixtures[11]. Pd(OAc)$_2$ has also been utilized as a dehalogenation catalyst. It is very effective under basic conditions in alcoholic solvents for the dehalogenation of a wide range of halogenated materials[12].

Electrochemical dechlorination of polychlorinated benzenes occurs readily in acetonitrile in the presence of naphthalene and occurs via SET mechanism[13]. Hydroxide ions can be utilized as an electron source for photo-dehalogenation reactions in high yields[14].

Homogenous ruthenium catalysts with phosphine ligands have been utilized in the reduction of sp^2 hybridised C-halogen bonds via insertion elimination mechanisms[15].

Active homogenous FeCl$_2$ catalysts in the presence of Li powder and an electron carrier such as 4,4'-di-*tert*-butylbiphenyl (DTBB) can reduce many aryl halides in THF[16].

Sodium borohydride acts as a dehalogenation promoter at high temperatures and have been shown to work better in glyme solvents[17].

Raney nickel catalysts have been utilized in the removal of halogens from polychlorinated benzene to some effect under high temperatures in the presence of base and protic solvents[18]. Na-H nanoparticles in the presence of Ni(OAc)$_2$ and I-PrONa show a strong ability to dehalogenate polychlorinated biphenyls in >99% yields[19]. NiCl$_2$ in the presence of Li and DTBB at –20°C work in over 85% yields to remove chlorines from aryl halides and again occur though electron transfer mechanisms[20].

Biological C-Cl bond breaking may well occur utilizing vitamin B12 (Co) and its derivatives[21], factor F$_{430}$ (Ni)[22] or hematin (Fe)[21a]. F$_{430}$ is a nickel-hydrocorphinoid prosthetic group of the enzyme methyl coenzyme M reductase[22] (MCR) (Figure 1.2). However F$_{430}$ not a very efficient catalyst for the reduction and remediation of halogenated aromatic compounds[23].
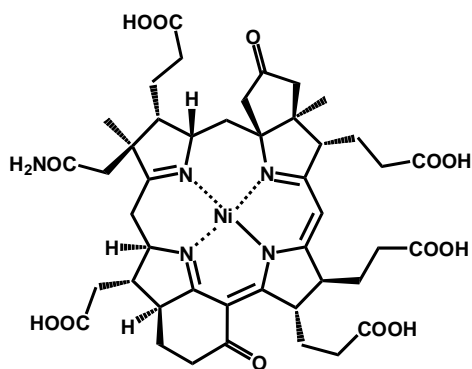
Figure 1.2: - Structure of F$_{430}$.

Several examples of nickel complexes based on F$_{430}$ have been developed to study the dehalogenation reaction with Ni(I)/Ni-H species[24/22] and some are shown below (Figure 1.3).
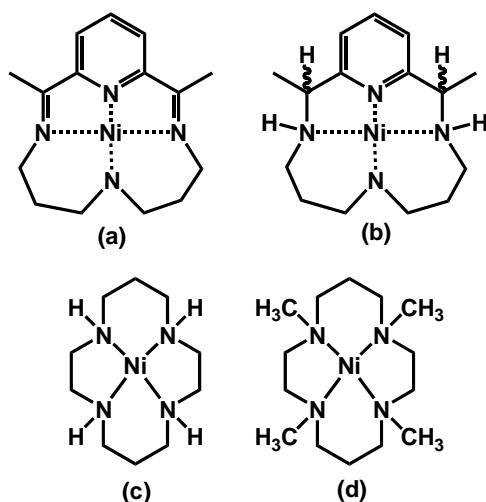
Figure 1.3: - Several catalysts developed to study hydrodehalogenation reactions.

There is much confusion over the apparent mechanism of dehalogenation mediated by F$_{430}$ and its analogues with SET[24], hydride delivery[25] and insertion/elimination[26] pathways all being proposed.

Stiles utilized a limited series of tetraazamacrocyclic compounds (a and b Figure 1.3) and performed reactions incorporating deuterium or protons into the dehalogenated product (naphthalene) and noticed that the vast majority of the protons/deuterons came from the borohydride (84%) (borohydride has the ability to donate hydrogen atoms[24]) with some hydrogen atoms coming from the solvent (16%) (Ethanol, water, AcCN were

used as solvents) (Figure 1.23) Cumene was also seen to retard the reaction indicating radical pathways[24].

EPR experiments led to the discovery of a possible nickel hydride formation in $F_{430.}$ Possible insertion and β-hydride elimination mechanisms for non-aromatic substrates have been deduced using this system[22].

Dunach's cyclization of aromatic halides suggests Ni-Aryl intermediates based on a 2e$^-$ reaction. Ni(I) inserts into a C-Br bond to give a Ni(III) species that rearranges to form a cyclized intermediate and is then reduced to Ni(II) whereby the C deprotonates a solvent molecule and the catalyst is regenerated. Evidence for this process can be seen in the CV data obtained for the reaction and the generation of coupled products[26/24b] (Figure1.22).

1.1.2 Artificial Enzymes

Much work has been performed in the field of artificial enzymes in recent years with many examples available in the literature[27]. These enzymes have been designed to mimic natural enzymes by utilizing hydrogen bonding and hydrophobic effects to pre-organize substrates for reaction and to stabilize transition states[27].

One of the most well known example of artificial enzymes are functionalized cyclodextrins that catalyze the hydrolysis of cyclic phosphates with an apparent 120fold rate acceleration over the uncatalyzed process[28]. Neighboring imidazoles cooperate, show stronger binding to the starting material and can control the outcome of the reaction (Figure 1.4). 4-*tert*-butylcatechol cyclic phosphate binds though complementary size and hydrophobic effects to the interior of the cyclodextrins with binding being entropically favorable[28].

Cooperative binding and pre-alignment of starting materials to a catalyst is often cited as the cause of rate increases during the course of a reaction[27]. It has also been shown that hydrophobic interactions can contribute to the binding of substrates to active sites of enzymes and appear to be the dominant effect for the induced fit model of drugs into binding sites[29].

(a)

(b)
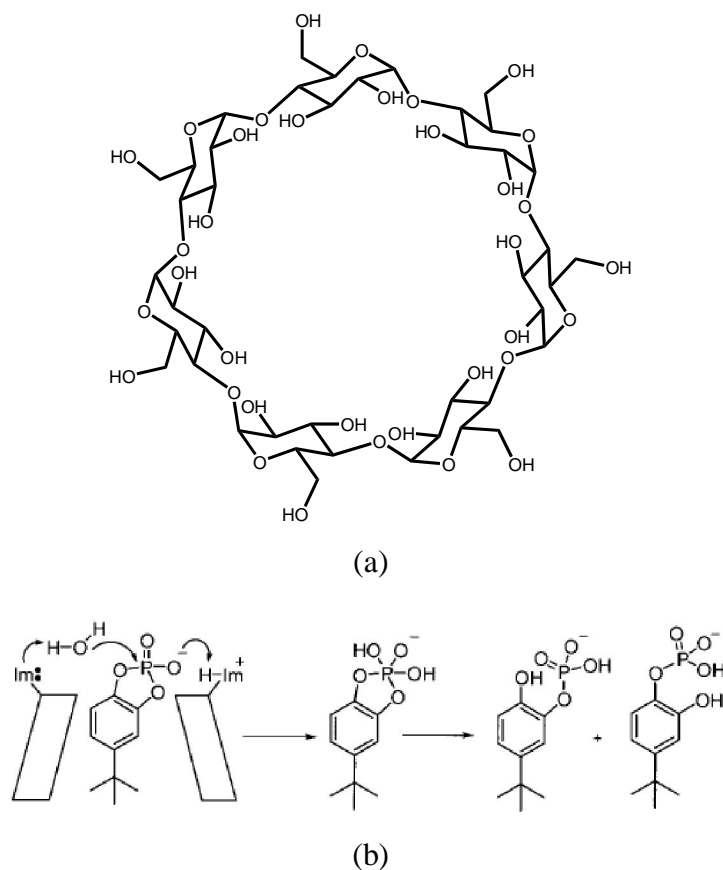
Figure 1.4: - (a) β-Cyclodextrin; (b) Proposed cooperation of imidazoles in hydrolysis of the phosphate[27a].

1.1.3 π-π stacking effects in catalysis

Several papers have recently shown that π-π interactions can play a role in the outcome of chemical reactions. The development of alternating styrene-pentaflurostyrene co-polymers has been noted due to the favorable interaction of one π-surface to the other has been demonstrated for a radical polymerisation reaction[30].

Interestingly π-π interactions have also been shown to aid in the increase of *ee* of a reaction based upon the orientation of π-π compatible catalysts and substrates (Figure 1.5)[31]. The alignment of the π-π interaction (as well as the hydrogen bonding interactions) helps to dictate the orientation of the 1,4 unsaturated aldehydes. This π-π interaction

effectively blocks one side of the starting material forcing cyclopentene to approach the alkene from only one direction, leading to an increase in the *ee*.

(a)

(b)
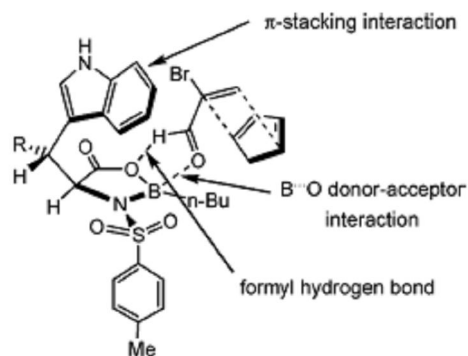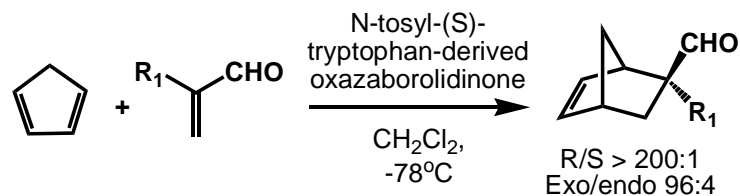
Figure 1.5: - (a) Diels Alder reaction of functionalized aldehydes with cyclopentadiene in the presence of a N-tosyl-(S)-tryptophan-derived oxazaborolidinone catalyst; (b) Proposed intermediate leading to high ee for the Diels Alder reaction[31].

Perhaps one of the most interesting and impressive aspects of π-π interactions in catalysis maybe the increase in rates of reaction observed for certain examples. Sharpless *et al* performed a comprehensive study on osmium-catalyzed asymmetric dihydroxylation reactions and found that aromatic ligands combined with aromatic alkene substrates gave *drastically* higher k values than that of aliphatic substrates or ligands[32] (Figure1.6). It is believed that mutually attractive π-π interactions bring the reactants into close proximity to one another, allowing a *pre-concentration* and *alignment* of the reactant and catalyst to occur. This effect is enhanced in more polar solvent (such as t-butanol) and with a larger degree of π surface in the ligand[30] (Figure 1.6).
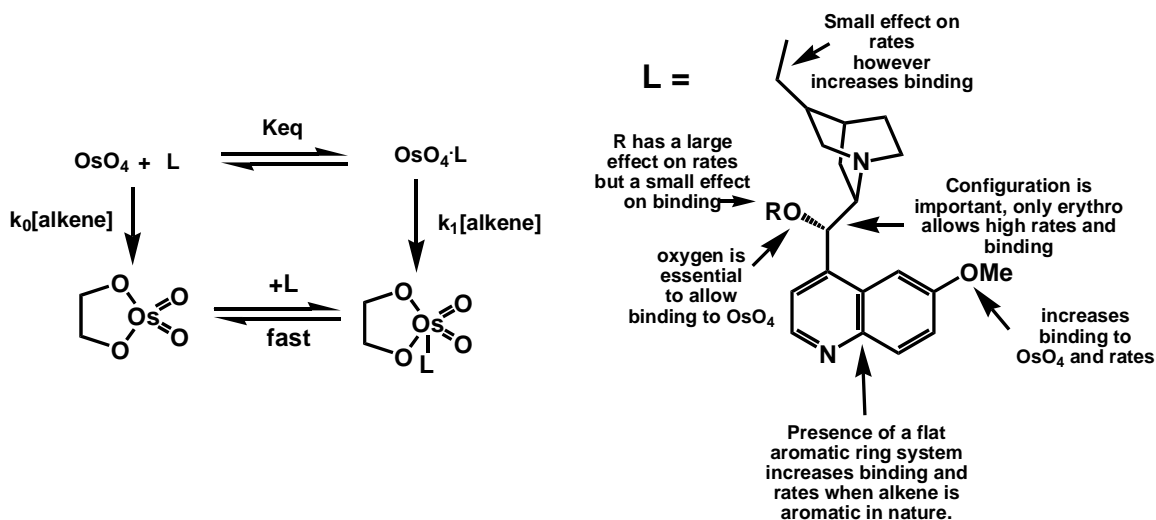
Figure 1.6: - Sharpless ligand system, showing increased rates of alkene oxidation due to aromatic π-π interactions.

1.2   Aims

The goal of our research was the generation of nickel tetraazamacrocyclic compounds with aromatic side arms capable of interacting with the planar aromatic halogenated molecules via π-π or π-CH interactions in a similar fashion to that shown by Sharpless system (Figures 1.6). These interactions were hoped to artificially increase concentrations and orientate the substrate toward the reactive center of the Ni catalyst.

Whilst π-π and T-stacking interactions are electrostatic in nature, their effect is relatively weak, with the energy of the interactions known to be around 2-5.5 KJmol^{-1} [33]. PCB's and other halogenated polyaromatic pollutants have extremely low water solubility[34] and as such they self assemble due to hydrophobic effects. This coming together of hydrophobic molecules has shown large rate increases for various reactions in polar solvents such as water[35].

We wished to utilize π-π/π-CH interactions between catalysts and reactants to pre-bind the substrate to the catalyst. The pre-binding of the substrate followed by its reduction should lead to an increase in observed rates when compared to catalysts without this pre-concentration. Mutual aggregation is the bringing together of compounds of a similar nature. In this case the hydrophobic effects in polar solvents should aggregate the non-polar catalyst side arms and substrates, artificially enhancing their concentrations

and aligning the substrate with the reactive center of our complex, allowing reduction to occur at a quicker rate.

The ligand systems that we have chosen to investigate are based around the cyclam molecules utilized by Stolzenberg[20] (Figure 1.7). The ligand periphery shall be functionalized with aromatic side arms of varying sizes either on one of the nitrogen atoms or on one or two of the carbons atoms indicated below in figure 1.8.
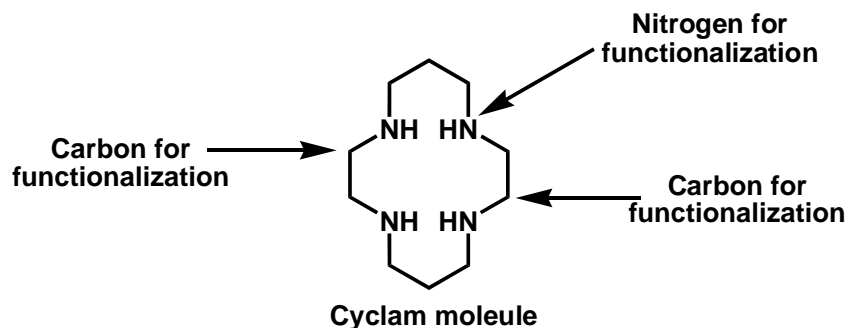
Figure 1.7: - Diagram of the basic cyclam ligand system showing where functionalization will occur.

It was our intent study the hydrodehalogenation of aromatic hydrocarbons in the presence of nickel-based catalysts. To this end compounds such as bromonaphthalene, chloronaphthalene, P and M-bromobiphenyl and 2-bromofluroene were chosen, having flat aromatic surfaces with which to bind to the aromatically functionalized catalysts (Figure 1.1). These compounds contain varying degrees of planarity, stacking ability and have a range of reduction potentials[36] that was hoped would allow us to investigate the dehalogenation reactions.

Singularly halogenated aromatic compounds are more difficult to reduce than multiply functionalized ones due to the aromatic rings being more electron rich, leading to higher reduction potentials. It is often the final dehalogenation step that takes the longest and as such these rates become interesting in comparative studies. The dehalogenation of singularly halogenated aromatic compounds also allows us to identify just one product in the reaction mixture.

We wished to utilize π-π/π-CH interactions between catalysts and reactants in the reduction of halogenated aromatic compounds to increase rates of reaction through mutual aggregation.

N-functionalised cyclam molecules with aromatic side arms ranging from the small phenyl ring up to the larger 4-fused ring system pyrene were to be synthesized as a means of testing this theory. We hoped that π-π/π-CH interactions between the side arm on the catalyst and the aromatic halogenated substrates, such as bromonaphthalene, in polar solvents such as DMSO, DMSO:EtOH mixtures would lead to a rate increase due to close contact aggregation of the substrate and the catalyst through mutual attraction[37] (Figure 1.8).
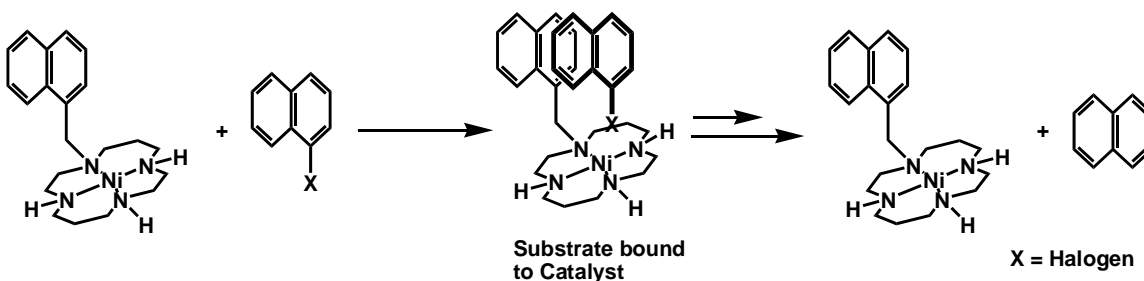
Figure 1.8: - Halogenated substrate bound to catalyst showing pre-concentration.

Second generation catalysts were to focus on C-functionalized cyclam molecules however mono-N-functionalized cyclam molecules were seen as a rapidly generated series of catalysts with the correct properties to ascertain the viability of the π-stacking idea. We wished to utilize mono-functionalized cyclams because the Bis-functionalized cyclams have several drawbacks.

The first drawback of Bis-functionalized cyclams is the controllable functionalization of the cyclam molecule with respect to the attachment of the second alkyl group. One can form either the cis or the trans cyclam with the Cis having a 2:1 statistical advantage over the Trans. Isolation and characterization of these molecules would take a lot of time. Cis Bis-alkylated cyclam synthesis has been accomplished selectively utilizing protecting groups to block off two amines yielding only the 1, 4-dialkylated products[38].

Another drawback of Bis-functionalized cyclams is the distance between the aryl units. In both the Cis and Trans Bis-functionalized cyclams the distance between the aryl units is less than 6Å, less than twice the distance of a π-π interaction[39] and thus would not enhance binding through cooperative binding (the formation of a tweezer like pincer that could bind the aromatic substrate, Figure 1.9b), but may through the catalysts having a higher degree of π surfaces with which to bind.
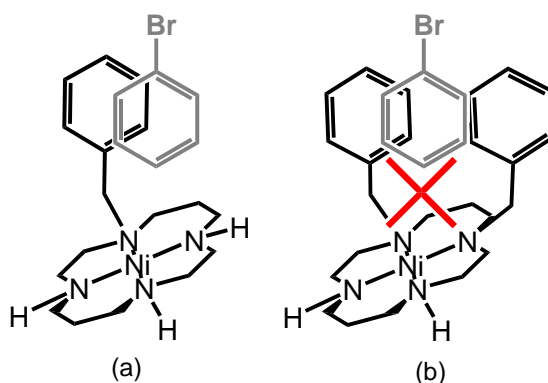
Figure 1.9: - (a) Binding of aromatic substrate to the catalyst. (b) Tweezer like complex utilizing cooperative binding not formed.

The final and most prominent drawback of utilizing multiple N-functionalized cyclam catalysts is that cyclam-metal complexes are known to have several isomers pertaining to the relative positions of the N-H or N-R groups that do not make up the macrocycle scaffold[40] (Figure 1.10).
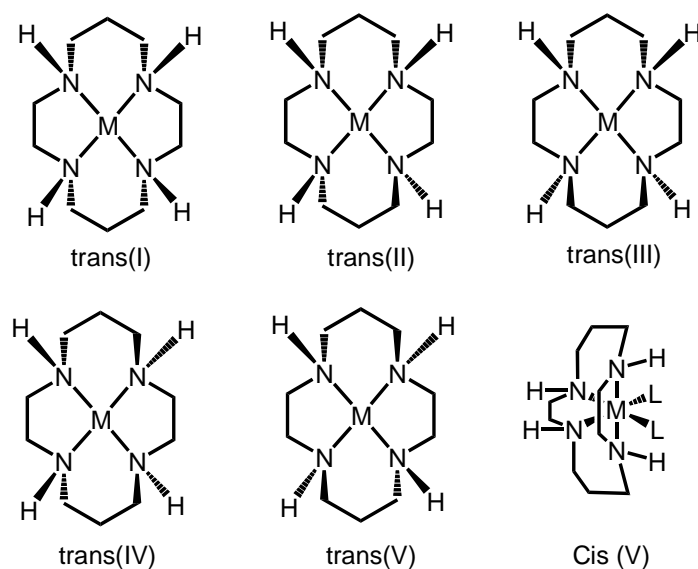
Figure 1.10: - The five configurations of metal cyclam complexes[2]

Determining the exact geometry of each complex and isolating the desired one is very difficult as the complex has the ability to form any of the configurations discussed in figure 1.3. For example (IR,2R,4S,7S,8R,9R,11S,14S)-1,2,4,7,8,9,11,14-Oetamethyl-1,4,8,11-tetraazacyclotetradecanenickel(II)perchlorate adopts the *trans*(I) configuration[41], although the *trans*(III) isomer tends to be preferred in the solid state as it is the most thermodynamically stable[42]. Hence selective and controllable stereochemistry derived from multiple N-alkylation reactions is impractical.

1.3   Mono N-Functionalized Cyclams: - Synthesis

There have been several examples of papers showing the synthesis of N-functionalized cyclam molecules from the basic 1,4,8,11-tetraazacyclotetradecane starting material, each with a unique way to avoid over-alkylation[43,44]. These methods can include cyclam protection[6] and alkylation or the use of stoichiometry to overcome the over-alkylation problem.

Perhaps one of the simplest ways to avoid over-alkylation is to use the 1,4,8,11-tetraazacyclotetradecane in large excess and in high dilution[45]. Statistically one is more likely to find a mono-alkylated cyclam molecule than the Bis, tris or tetra-alkylated cyclams (Figure 1.11).
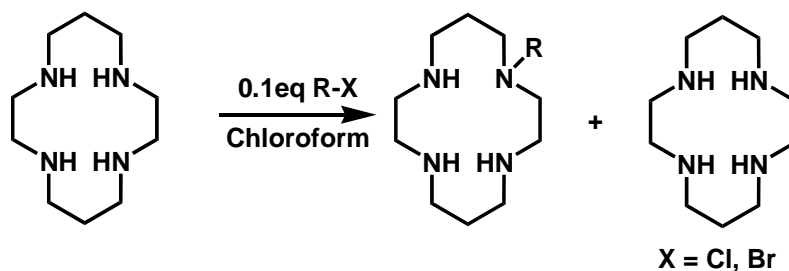
Figure 1.11: - Mono-alkylation via high dilution and excess of cyclam.

The main drawback to this method is the large excesses of cyclam needed[11]. This problem is however overcome by the fact that recovery of the starting material does not tend to be problematic[11]. Either a column or even simple filtration of the product from the starting material using differences in solubility can be utilized for starting material recovery in high yields[11].

Utilizing the high dilution low equivalence technique several cyclam ligands were synthesized in high yield (Figure 1.12) Purification of these ligands was very simple. All products were soluble in cold acetone whilst the starting material, 1,4,8,11-tetraazacyclotetradecane was not. Simple filtration purified the reactions and the starting material was recovered and reused.

R = Phenyl (1.2a), 9-anthracenyl (1.2b), 1-pyrenyl (1.2c)
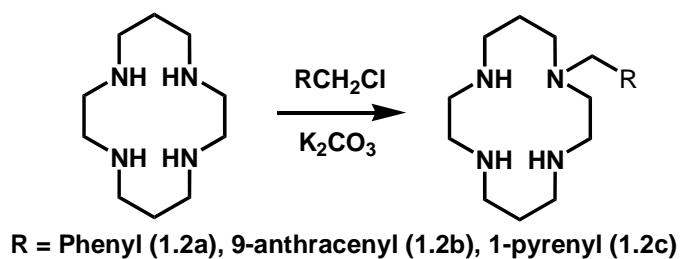
Figure 1.12: - Synthesis of N-functionalized cyclam ligands.

Table 1.1: - Yield of synthesized mono N-functionalized cyclams.

Compound Number	R	Yield%
1.2a	Phenyl	85
1.2b	9-Anthracenyl	85
1.2c	1-Pyrenyl	100

1.4 Synthesis of N-Functionalized Nickel Cyclam Complexes

With the ligands synthesized, incorporation of the metal centre proved to be fairly straightforward. Simply refluxing each ligand with NiX_2 in methanol leads to complex formation[46] (Figure 1.13).

R = H, CH$_2$-Phenyl, CH$_2$-9-anthracenyl, CH$_2$-1-pyrenyl

X = Cl, ClO$_4$, BPh$_4$
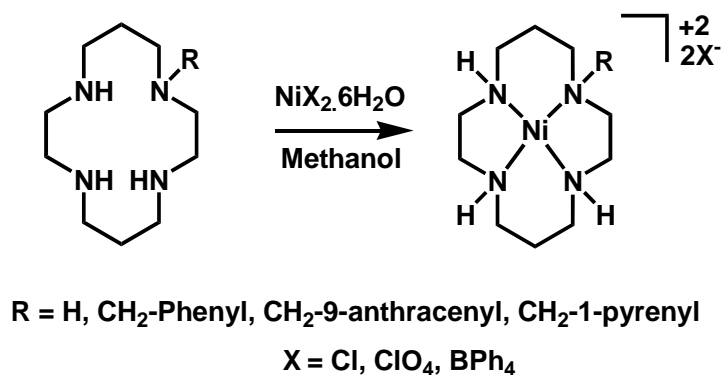
Figure 1.13: - Synthesis of nickel cyclam complexes.

Table 1.2: - Yields of the nickel complexes formed in solution.

Compound Number	X	R	Yield%
1.3	ClO$_4$	CH$_2$Phenyl[47]	30
1.4	ClO$_4$	CH$_2$(9-Anthracenyl)[48]	36.8
1.5	ClO$_4$	CH$_2$(1-Pyrenyl)	30
1.6a	Cl	H[49]	95
1.6b	BPh$_4$	H[50]	76
1.6c	ClO$_4$	H[51]	95
1.6d	BH$_4$	H	81.4
1.6e	BD$_4$	H	75.7

Ni(II) species can exist in an octahedral environment, which is paramagnetic[52], or a square planar environment, which is diamagnetic[53]. Much of the coordination geometry of the complexes depends on the anion and the solvent it is dissolved in. Solvents that have lone pairs to donate such as acetonitrile, water, pyridine and acetic acid can form the octahedral complexes that are paramagnetic. ^{1}HNMR data was checked over a range of –100 to 100ppm as the paramagnetic nature of the complexes causes such large changes in ppm values.

Several of these nickel cyclam complexes were purified by recrystallization/precipitation and X-ray quality crystals were grown for compounds **1.3**, **1.4**, **1.6a**, **1.6b**, and **1.6c** with X-ray crystal data being obtained for compounds **1.4, 1.6b** and **1.6d**, whilst the other compounds (**1.3, 1.6a** and **1.6c**) have crystal structure data previously reported in the literature[14,15,16].

Complex **1.3** sits in the thermodynamically favored *trans*(III) configuration, with no π-π interactions visible in the packing (for the copper complex)[12]. The ^{1}HNMR data for **1.3** proved to be complicated with conformational isomers present in small amounts, even from a very crystalline purified solid, indicating some isomerization in solution[54].

Excellent ^{1}HNMR data was gathered for complex **1.4** (Figures 1.14). The ligand ring structure gives a somewhat complex set of proton signals between –1.24ppm and

3.3ppm that can be attributed to the formation of several stereocenters on the nitrogens of the ligand. In this case one configuration seems to be preferred although exact details are difficult to decipher due to the complexity of the ^{1}HNMR spectrum. This complexity did not allow the assignment of one particular configuration from the data available. There are some large splittings for several NH and CH protons, most like due to the proximity of these protons to the metal center. Having a ^{1}HNMR that shows low broadening and a small ppm range also indicate that the complex is square planar and has no axial ligands (either the counter anion or solvent). The reaction of **1.2b** with nickel perchlorate (an non-coordinating counter anion) in methanol generated the **1.4** without axial ligands. In this case it appears the solvent was not a strong enough coordinator to interact with the nickel. This suggests that the nickel is diamagnetic, having a square planar geometry around the metal and not paramagnetic, having an octahedral geometry around the metal center. For complex **1.6a** axial ligands (chloride) induce paramagnetism leading to broad and wide ranging ^{1}HNMR spectra (Figure 1.15).
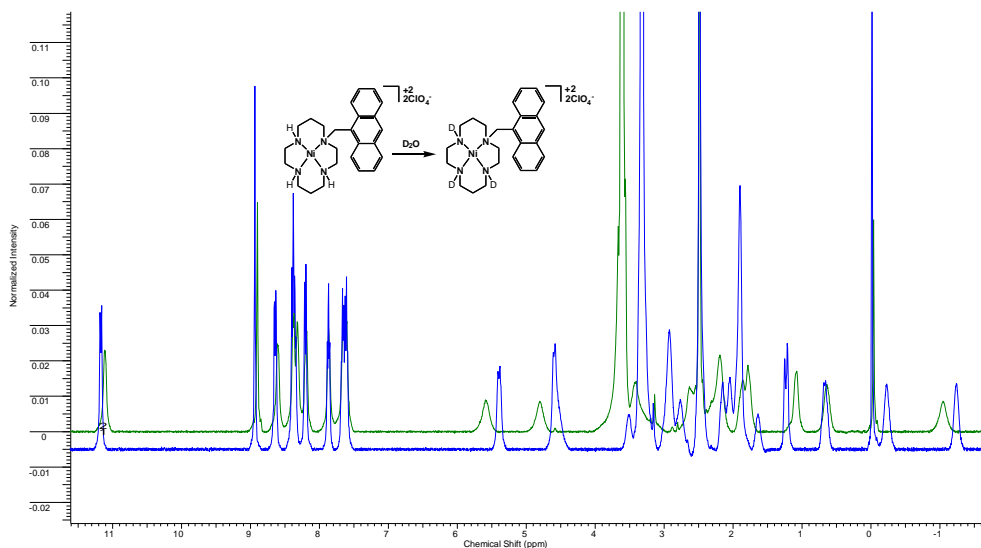
Figure 1.14: - (1, Blue line) NMR of 1.4 with NH bonds, (2, green line) NMR of 1.4 with ND bonds after treatment with D$_2$O.

Complex **1.5**, isolated as a sandy solid, has a ^{1}HNMR showing the characteristic wide-ranging spectra observed for paramagnetic octahedral nickel complexes. The nickel centre had generated peaks that can be seen as high as 32ppm and as low as –24ppm.

Although a reasonably good spectrum was obtained, not all of the protons have been accounted for. Broad peaks in the baseline and peaks overlapping solvent peaks make characterization of the ligand periphery difficult. Full characterization of the pyrene protons was accomplished because of the increased distance from the metal centre.

It is possible that dissolving the complexes allows for equilibrium to form between different configurations. Sadler *et al* showed that the uptake of Zn by cyclam ligands form an equilibrium of *trans*(III), *cis*(V) and *trans*(I) configurations in solution after 100 minutes[55] . The reaction mixture for the complexes **1.3** and **1.5** could not be purified to give one configuration in solution. It is probable that the side arm in complex **1.4** forces the complex to adopt the *trans*(III) configuration, even in solution, due to the 1,3 syn axial steric repulsion experienced between the functionalized and unfunctionalized nitrogens, which is much less of a problem when non of the nitrogens are functionalized.

^{1}HNMR data for the 1,4,8,11-tetraazacyclotetradecane nickel complex **1.6a** shows broadening indicating a paramagnetic complex (Figure 1.15). In this case there is Cl^{-} in the axial positions of the complex as shown by the crystal structure previously obtained[56].
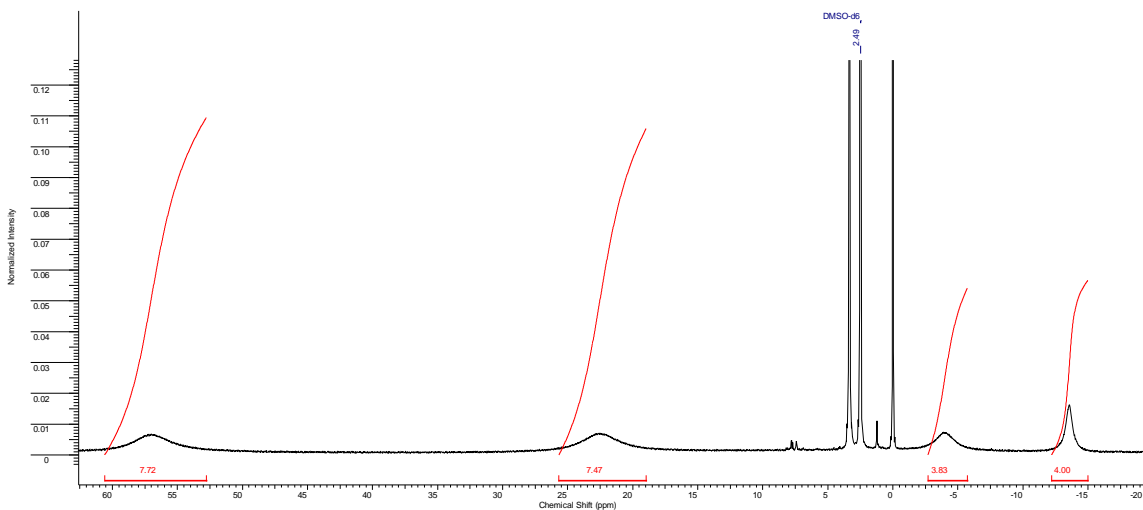
Figure 1.15: - NMR of the (1,4,8,11-tetraazacyclotetradecane)Nickel(II) Bis chloride complex 1.6a in DMSO (δ –20-75)

The ^{1}HNMR of complex **1.6b** also suggested that it was paramagnetic, typical of octahedral complexes. BPh_4^- is a none-coordinating anion and as such would not take up

the coordination sites in the axial position. However in **1.6b** two acetonitrile molecules, delivered during crystallization from acetonitrile, occupy the axial positions leading to an overall octahedral and thus paramagnetic complex.

The presence of more than one configuration in solution is somewhat of a concern when it comes to comparative rate studies. It is possible to have 6 different configurations of the complex in the solution, which may lead to 6 different rate constants in one reaction mixture (Figure 1.10). Any rate increase/decrease observed for each complex may not be related to its overall structure but to the configurations that the complex can achieve in solution.

1.4.1 X-ray Crystal Structures of Nickel Cyclam Complexes.

Crystals of the 1-(9-Anthraceneyl)-1,4,8,11-tetraazacyclotetradecane nickel Bis(perchlorate) complex (**1.4**) (Figure 1.16). and 1,4,8,11-tetraazacyclotetradecane nickel Bis(chloride) complex (**1.6b**) (Figure 1.17) and - X-ray crystal structure of the (1,4,8,11-tetraazacyclotetradecane)nickel(II) Bis-borohydride complex **1.6d** were isolated and X-ray crystal structures were obtained (Figure 1.18). The other complexes generated (**1.3**, **1.5**, **1.6a**, **1.6c**) have all had crystal structures previously reported in the literature.
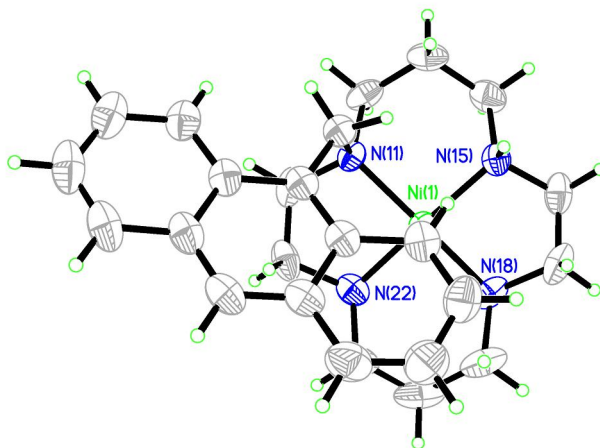
Figure 1.16: - X-ray of (1-(9-Anthraceneyl)-1,4,8,11-Tetraazacycotetradecane) Nickel(II) Bis(perchlorate) complex 1.4 (perchlorate removed for clarity).
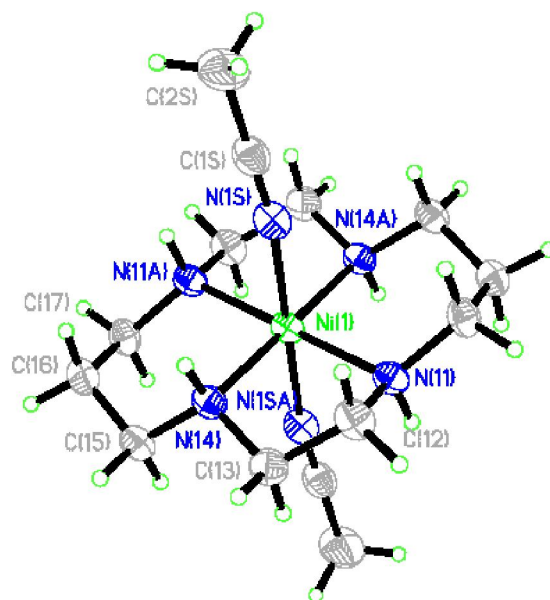
Figure 1.17: - X-ray of (1,4,8,11-Tetraazacycotetradecane)nickel(II) Bis(tetraphenylborate) complex 1.6b (BPh$_4^-$ Removed for Clarity) .
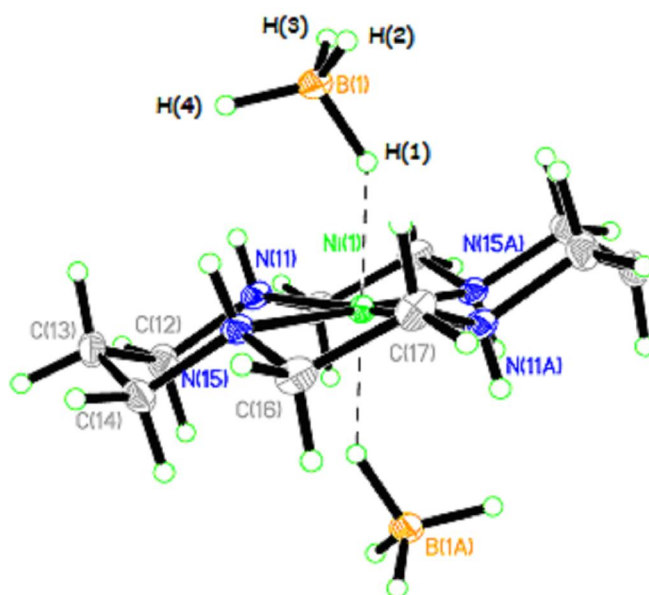
Figure 1.18: - X-ray crystal structure of the (1,4,8,11-tetraazacyclotetradecane)nickel(II) Bis-borohydride complex 1.6d.

Table 1.3: - Selected X-ray crystal structure information for complexes 1.4, 1.6b and 1.6d.

Complex	Configuration	Selected Bond Lengths	Selected Bond Angles
1.4	*Trans*(III)	N(11)-Ni (1.971Å), N(15)-Ni (1.961Å), N(18)-Ni (1.950Å), N(22)-Ni (1.940Å).	N(11)-Ni-N(15) (93.96°), N(15)-Ni-N(18) (86.51°), N(18)-Ni-N(22) (91.13°), N(22)-Ni-N(11) (88.47°), N(11)-Ni-N(18) (179.19°), N(22)-Ni-N(15) (173.93°).
1.6b	*Trans*(III)	N(11/11A)-Ni (2.066Å), N(14/14A)-Ni (2.059Å), N(1S/1SA)-Ni (2.143Å).	N(11)-Ni-N(14A) (85.92°), N(14A)-Ni-N(11) (94.09°), N(11)-Ni-N(14) (85.92°), N(14)-Ni-N(11) (94.08°), N(1S)-Ni-N(11) (87.88°), N(1S)-Ni-N(11) (92.12°), N(1S)-Ni-N(14) (88.43°), N(1S)-Ni-N(14A) (91.57°), N(11)-Ni-N(11A) (180°), N(14)-Ni-N(14A) (180°).
1.6d	*Trans*(III)	N(11/11A)-Ni (2.061Å), N(15/15A)-Ni (2.065Å), H(1)-Ni (1.819Å), H(1)-B (1.166Å), H(2)-B (1.039Å), H(3)-B (1.053Å), H(4)-B (1.098Å).	N(11)-Ni-N(15A) (85.13°), N(15A)-Ni-N(11A) (94.87°), N(11A)-Ni-N(15) (85.13°), N(15)-Ni-N(11) (94.87°), H(1)-Ni-N(11) (93.00°), H(1)-Ni-N(15A) (88.93°), H(1)-Ni-N(11A) (87.00°), H(1)-Ni-N(15) (91.07°), N(11)-Ni-N(11A) (180°), N(15)-Ni-N(15A) (180°).

As was speculated from the ^{1}HNMR data obtained for **1.4** the crystal structure shows no axial ligands on the metal center and thus can be diamagnetic[57]. The N-Ni bond lengths in **1.4** are shorter than that seen for **1.6b** or **1.6d**. A possible explanation is that the extra electron density pushed onto the nickel by the axial ligands in **1.6b** or **1.6d** means that less electron density is needed from the equatorial ligands. The crystal structure of **1.4** shows no intermolecular or intramolecular π-π or π-CH interactions.

The X-ray data for **1.6b** shows acetonitrile acting as axial ligands forming an octahedral paramagnetic nickel complex. Bond lengths increase between the equatorial nitrogens and the nickel, when compared to complex **1.4**, due to the increased electron density pushed onto the metal from the axial acetonitrile. Complex **1.6c** was synthesized and crystallized in methanol to overcome the axial ligand problem encountered from acetonitrile crystallizations. Other solvents for the crystallization of complex **1.6b** could be used however these options were never attempted due to the formation of complex **1.6c** and the choice of complex **1.6a** as the reference complex for halide reductions monitored by HPLC (chapter 4).

From the reaction of **1.6c** with sodium borohydride in acetonitrile a green crystalline solid was isolated. IR and X-ray spectroscopy on this complex revealed that it to be the complex **1.6d** (Figure 1.18). Multiple attempts at repeating this reaction in acetonitrile did not yield the desired complex as a crystalline solid. However repeating the reaction in THF yielded the complex as a powder (identified by IR, figure 1.19). Repeating this reaction with NaBD$_4$ led to the formation of the deuteride analogue **1.6e** as characterized by the large shifts in wave numbers (cm^{-1}) for the borohydride/deuteride peaks (2320cm^{-1}→1744cm^{-1}, 2197cm^{-1}→1605cm^{-1}, 2116cm^{-1}→1548cm^{-1}) (Figure 1.19).
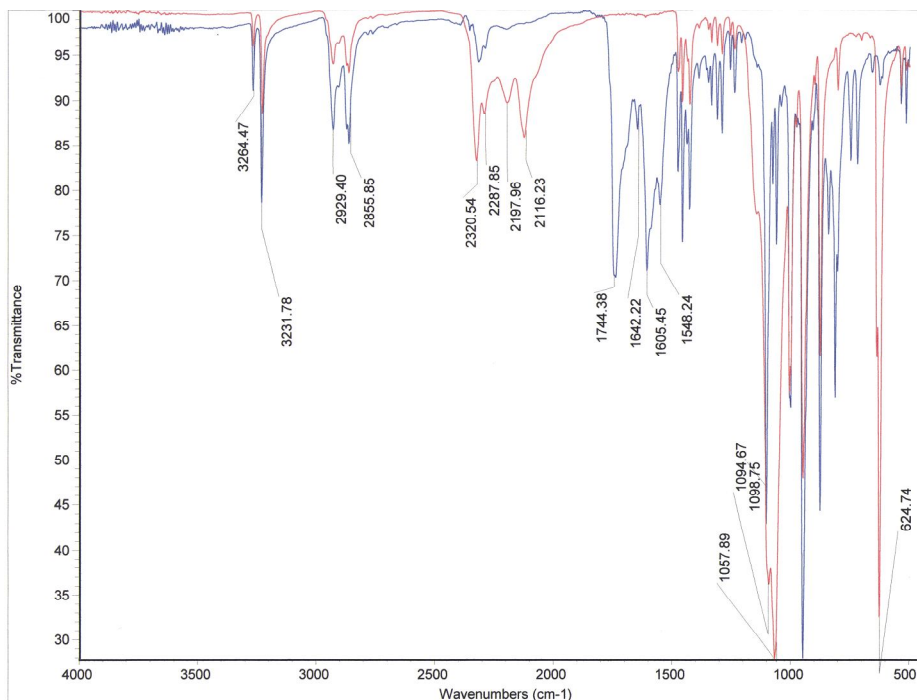
Figure 1.19: - IR of 1.6d (red line). IR of 1.6e (blue line).

The bond lengths between the terminal hydrogens and the boron in complex **1.6d** are shorter than the bridging hydrogen coordinated to the nickel centre. The Ni-H bond length in **1.6d** is close to that reported in the literature for other bridging borohydrides (1.84Å and 1.93Å[58], 1.71Å[59]). Ni-H-Ni (μ2) bonds have been reported in the order of 1.58Å[60], whilst cyanoborohydride complexes have shown slightly longer Ni-H bonds of 2.145Å[61]

1.5   Mechanistic studies

Whilst several papers have undertaken mechanistic studies involving hydrodehalogenations coupled with nickel catalysts much conjecture still remains as to the actual mechanism/mechanisms[62].

Mechanisms including single electron transfer[63] (Figure 1.20), hydride reductions[64] (Figure 1.21) and nickel insertion/elimination reaction have all been proposed[27b] (Figure 1.22) and each is viable for the reaction conditions used. We have attempted to elucidate the mechanism under our reaction conditions.

21
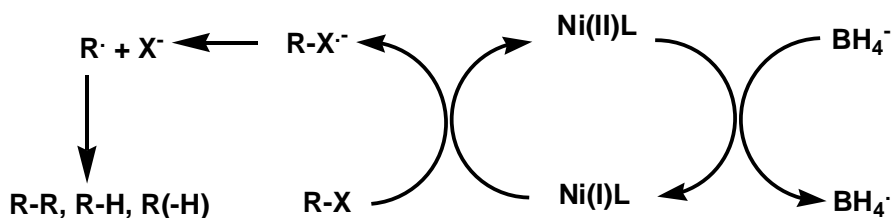
Figure 1.20: - Proposed single electron transfer (SET) mechanism of hydrodehalogenation (L = tetraazamacrocyclic ligand)
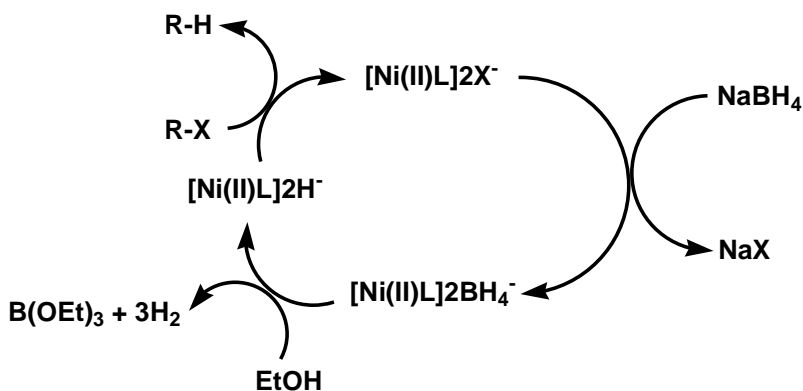
Figure 1.21: - Proposed hydride reduction mechanism of hydrodehalogenation (L = tetraazamacrocyclic ligand, X = halogen)
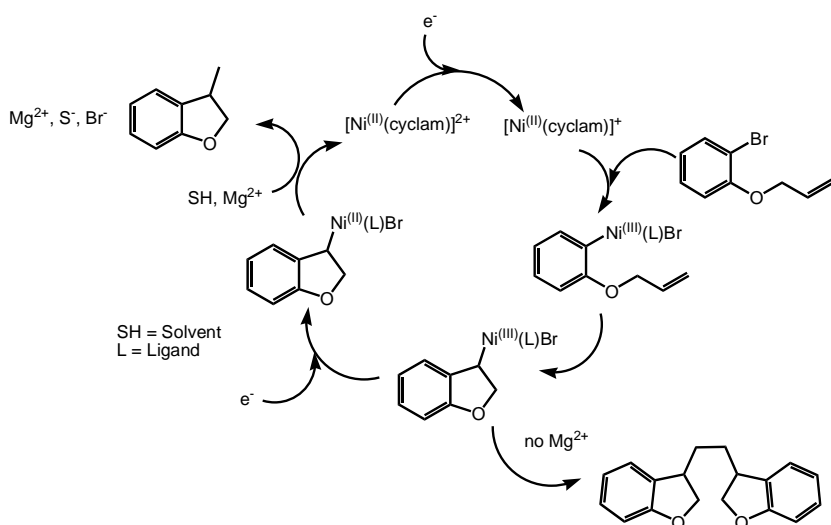
Figure 1.22 Nickel insertion mechanism proposed by Dunach ((L = tetraazamacrocyclic ligand).

1.5.1 Deuterium Incorporation Experiments

Deuterium labeling experiments utilizing $NaBH_4$ in deuterated $DMSO:CD_3OD$ and a separate experiment was performed utilizing $NaBD_4$ in protio DMSO:Ethanol to ascertain where the proton(deuterium)/hydride(deuteride) originates during the reduction of the bromonaphthalene under our conditions (Figure 1.23).
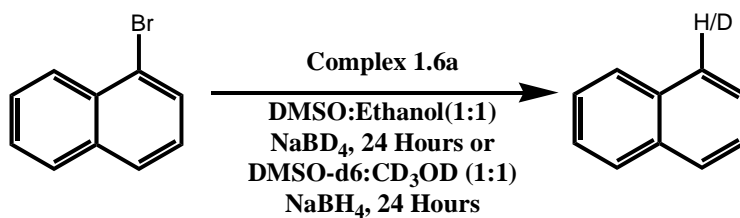
Figure 1.23: - Labeling study using $NaBD_4$ in protio DMSO:EtOH (1:1) or $NaBH_4$ in DMSO-d6:CD_3OD (1:1).

For the experiment utilizing $NaBD_4$ in none deuterated solvents 84% deuterium incorporation into naphthalene is observed by integration in ^{1}HNMR. The protons on carbons 4, 6 and 9 give an integration of 3.16 (84% D incorporation) at 7.86ppm when compared to the 4.00 (100% protons) for the protons on carbons 2, 3, 7 and 8 shown at 7.48ppm in the ^{1}HNMR. This result would suggest that the vast majority of the hydride/deuteride comes from the $NaBD_4$ with solvent having only a 16% incorporation of protons into the naphthalene product (Figure 1.24).

The second experiment utilizing $NaBH_4$ in deuterated solvents DMSO-d6:CD_3OD showed no deuterium incorporation by ^{1}HNMR. Again this reinforces the concept that the borohydride is the major source of the proton/deuteron attached at the 1 position of the naphthalene (Figure 1.25). These results are in concurrence with labeling experiments performed by Stiles (84% deuteride incorporation with $NaBD_4$ in $D_2O:CH_3CN$, 0% incorporation with $NaBH_4$ in $D_2O:CH_3CN$ for tetrachlorobenzene)[28d]. Our results also show that naphthyl anions are not a major contributor to the mechanism, as deprotonation of the methanol would occur from the OH if this were the case.
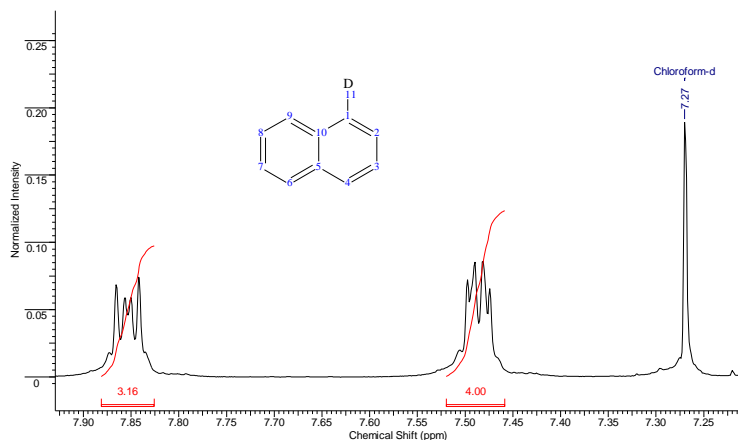
Figure 1.24: - ¹HNMR of naphthalene product (reaction conditions: - NaBD₄ and DMSO:EtOH (1:1)) with integration values compared against each other.
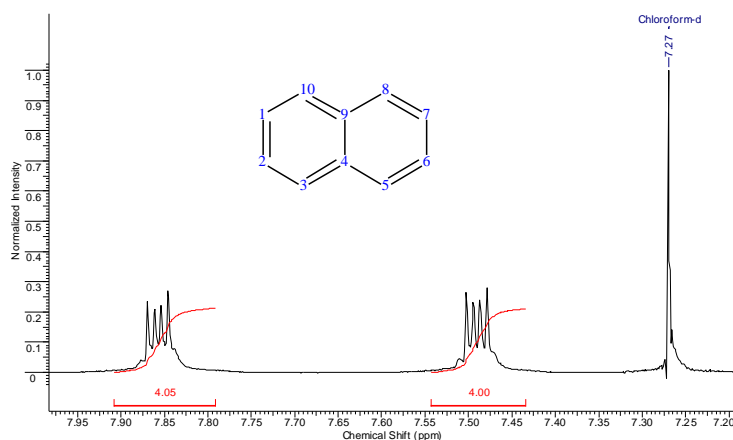
Figure 1.25: - ¹HNMR of naphthalene product (reaction conditions: - NaBH₄ in DMSO-d6:CD₃OD (1:1)) with integration values compared against each other.

There are several conceivable mechanisms for the incorporation of the hydride from the sodium borohydride.

Figure 1.20 show the formation of a Ni(I) species from the reduction of the Ni(II)cyclam complex by the sodium borohydride. This Ni(I)cyclam can then perform a single electron transfer, probably through an outer-sphere electron transfer into the π^* orbital of the aromatic ring, although the oxidation potential for the Ni(I) complex is significantly lower than that of the reduction potential of the halogenated substrate. The radical anion then breaks down to give a radical and an anion. The radical can then further react with the borohydride to extract a hydrogen atom[28d].

24

Another possibility is the formation of a nickel hydride species capable of delivering the hydride directly to the substrate or to form hydride radicals that can react with the substrate (Figure 1.21).

A ^{1}HNMR study of **1.6d** in acetonitrile shows that no change occurs in the spectra upon the addition of bromonaphthalene over 12hours. However when a drop of D_2O was added to the mixture bubbling was observed (the formation of hydrogen) and some naphthalene was generated (Figure 1.26) the dehalogenation observed after 10 minutes did not change over a period of 3 days.
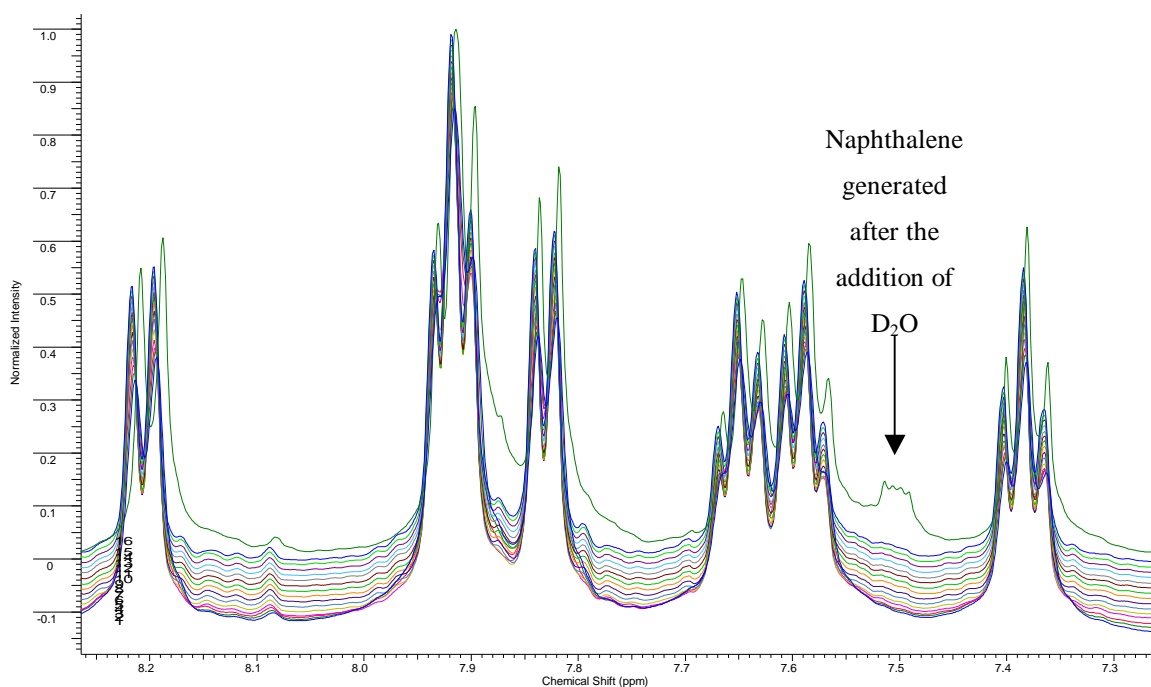
Figure 1.26: - A stack plot of the aromatic region of the reaction of bromonaphthalene (6eq) with the 1.6d in acetonitrile at 10 minute intervals over 3 hours. The final spectrum was taken after the addition of D_2O (10 minutes) after 12 hours of having the bromonaphthalene mixed with the complex showing no sign disappearance of starting material.

The reduction of bromonaphthalene utilizing complex **1.6d** (10%) generates 17.3% of the naphthalene product in DMSO:EtOH (1:1), indicating that only 2 of the hydrides in complex **1.6d** are utilized in the reaction (Figure 1.27).

25
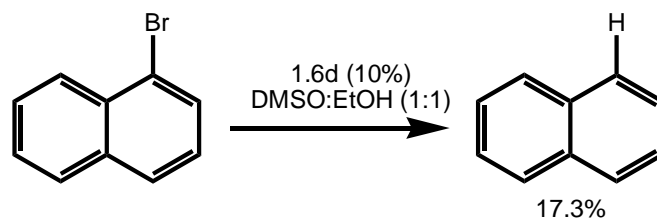
Figure 1.27: - Reduction of bromonaphthalene utilizing complex 1.6d (10%) in DMSO:EtOH (1:1)

Looking at the results observed in figures 1.26 and 1.27 it is reasonable to assume that the formation of borates increases leaving ability of the hydride and facilitates the formation of the nickel hydride species through increased electron donation to the boron and increased back strain from the alkoxy units (Figure 1.28).
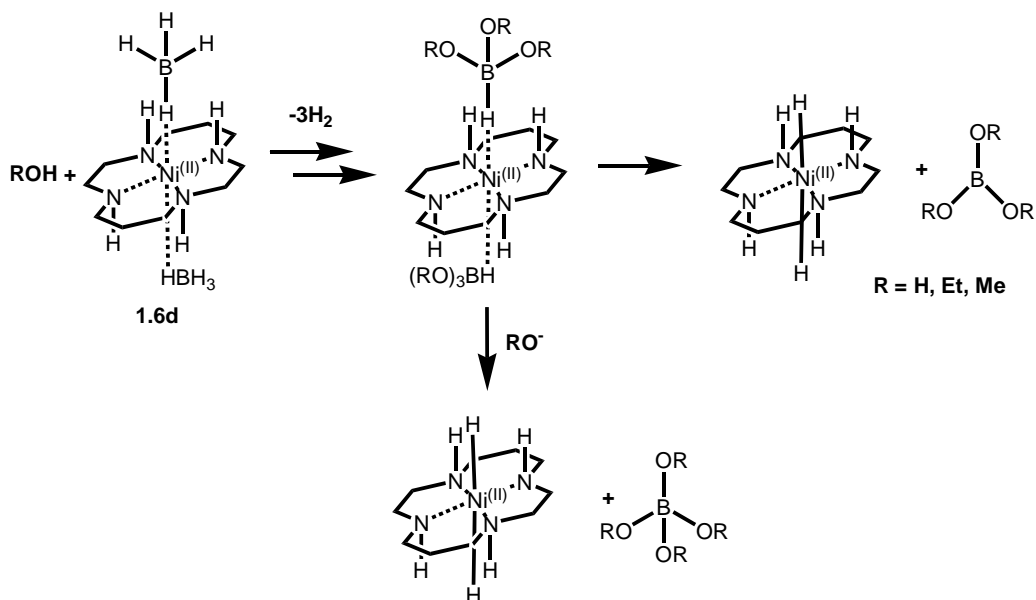
Figure 1.28: - Possible reaction of 1.6d with alcohols/water to produce a nickel hydride complex and borates.

Further evidence to support the reaction of hydrides with the bromonaphthalene came from a reaction run utilizing complex **1.6a** in DMSO:EtOH (1:1) with excess $NaBH_4$ performed in the presence of air.

In the presence of oxygen the formation of Ni(I) should be perturbed and if the reaction involves Ni(I) species the reduction should not occur, or occur at a much slower rate. After 2.5 hours at 25°C nearly all of the bromonaphthalene had been completely converted to naphthalene (>94%) and the purple colour of the solution remained strong perhaps indicating that Ni(II)-H/BH$_4$ play an important role in the reduction of aryl halides not Ni(I) under these reaction conditions.

A reduction run without the catalyst produced a small quantity of the naphthalene product (3.5%) after 2.5 hours at 25°C, significantly slower than without the catalyst.

1.5.2 Ni(I) and Na/Hg Amalgam Reductions of Bromonaphthalene

Reduction of a **1.6c** in acetonitrile utilizing Hg/Na amalgam generated a Ni(I) complex **1.**7 that was isolated by filtration (Figure 1.29). Complex **1.7** shows a characteristic purple color in the UV-Vis spectra at 559nm indicative of Ni(I) complexes[65] (Figure 1.30).
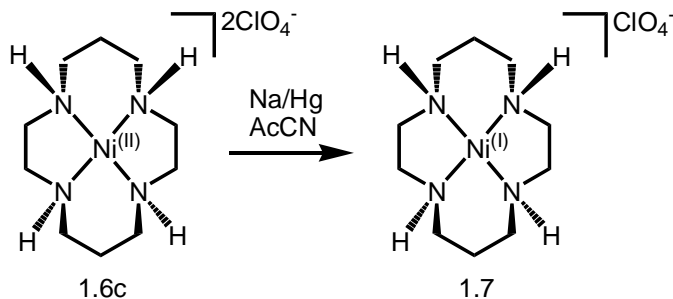
Figure 1.29: - Generation of a Ni(I) 1.7 from the Ni(II) complex 1.6c

#	Name	Peaks (nm)	Abs (AU)	#	Name	Peaks (nm)	Abs (AU)
1		341.0	0.47519	1		***	***
1		559.0	0.20120	1		***	***
1		477.0	0.19461				
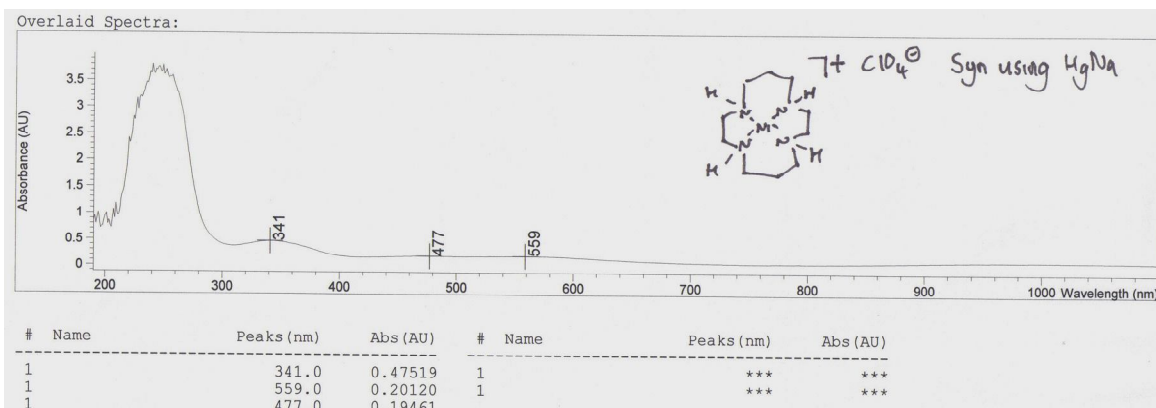
Figure 1.30: - UV-Vis spectra of 1.7.

1.7, in acetonitrile, was treated with bromonaphthalene for 12 hours at 50^oC under inert conditions (a change in color from purple to brown was observed after 5-6 hours). At the end of the reaction, when the Ni(I) had be oxidized to Ni(II) as observed by a loss of the peak at 559nm, a sample was taken for ^{1}HNMR analysis. No conversion of the bromonaphthalene was observed. Previous experience with complex **1.7** suggests that the lifetime of this complex is over several hours.

A UV/Vis experiment was also performed where monitoring of the 559nm wavelength (d-d transition for Ni(I)) in **1.**7 over several hours showed no signs of the disappearance of this peak after the addition of bromonaphthalene. Overall every peak on the spectra decreased over time at the same extent, a consequence of a baseline error. No reduction of the bromonaphthalene was observed (by HPLC analysis). It was observed that Ni(I) generated from Na/Hg amalgam is air sensitive. The purple color of the solution in acetonitrile rapidly converts to an orange colored solution upon exposure to air confirming the presence of the Ni(I) species.

The fact that independently synthesized Ni(I) complexes were unable to convert bromonaphthalene to naphthalene excludes that Ni(I) species play an important role under catalytic hydro-dehalogenation reactions.

Previous experiments have however shown that Ni(I), generated via a variety of methods, can act as a reductant following the formation of alkyl-nickel intermediates[27b], that break down to radical intermediates. However most of these reactions were carried out on alkyl-halides not aryl-halides and similar reductions were not observed under these conditions in our experiments.

A run whereby Na/Hg was allowed to react with the bromonaphthalene in DMSO without the presence of the nickel cyclam complex shows that the single electron reduction from this reductant can indeed reduce the bromonaphthalene to naphthalene[66]. Na is a much stronger electron donor than Ni(I) and has previously been used as a large scale method of dehalogenation[67] and although Na/Hg is a weaker electron donor than Na it is strong enough to perform the reaction as well.

1.6 Cyclam and N-functionalized Cyclam Nickel Complexes As Hydrodehalogenation Catalysts.

^{1}HNMR testing was performed to identify the reactivity of the nickel cyclam complexes hydrodehalogenation reactions. Bromonaphthalene was chosen as the test compound due to its flat aromatic surface, which was hoped, may interact with the side arms built into the complexes (Figure 1.31).
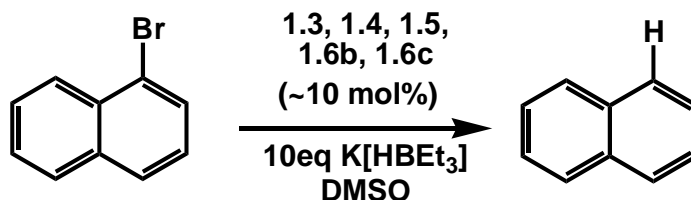
Figure 1.31: - Reduction of bromonaphthalene utilizing nickel cyclam complexes under ^{1}HNMR conditions with superhydride.

Each of the catalysts was weighed into an NMR tube and the co-reductant, in this case super hydride (potassium triethylborohydride) was added. This was shaken for a few minutes to allow the generation of the active reductive species. To this mixture was added the bromonaphthalene and ^{1}HNMR's were taken at regular intervals. By measuring the relative peak heights for the bromonaphthalene and the naphthalene product one could monitor conversion over time (Figure 1.32).
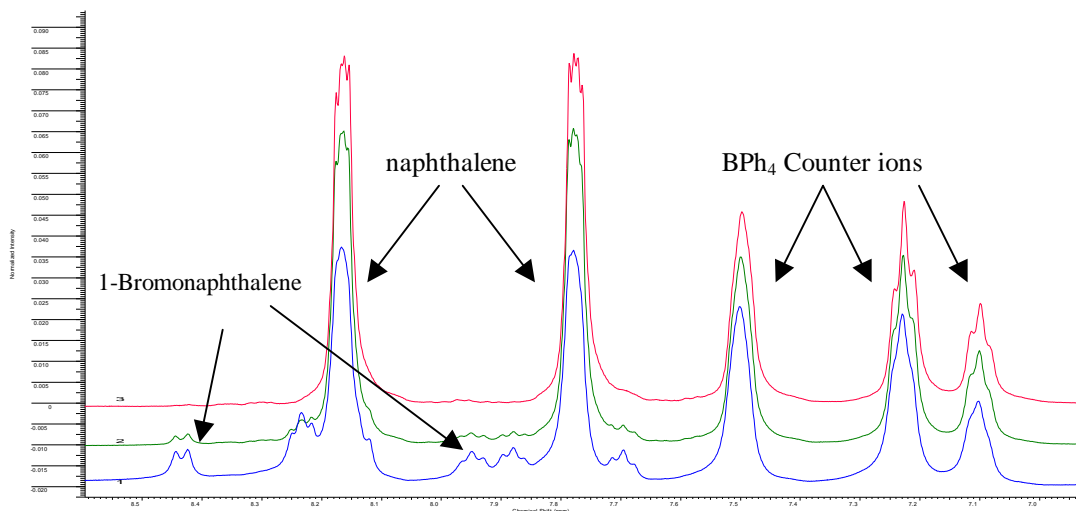
Figure 1.32: - Stack plot ^{1}HNMR of bromonaphthalene reduction using 13.1 Mol% 1.6b and Superhydride, in DMSO over time (1=19min, 2=25min, 3=29min).

By using the BPh$_4$ peaks as an internal standard it was possible to accurately integrate the bromonaphthalene peaks in order to obtain a rate constant for the reduction (Figure 1.33).
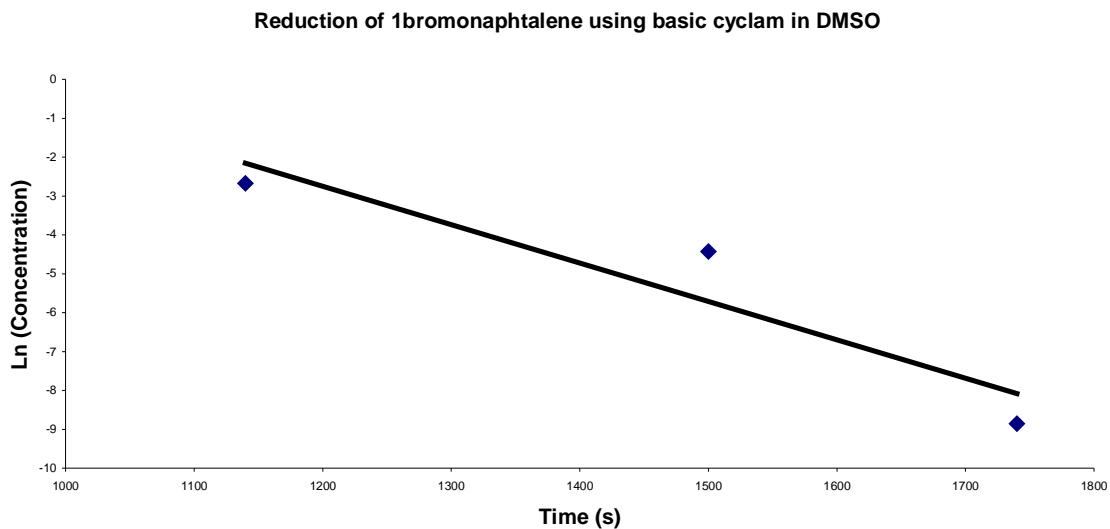
Figure 1.33: - Plot of Ln(Concentration) vs. Time(s) for bromonaphthalene reduction using 13.1 Mol% 1.6b and Superhydride in DMSO.

The graph gives us a k^{obs} value from the slope which, when divided by the concentration of the catalyst, yields the k value (rate constant) for the reaction. In this

case when you divide the slope ($-0.0063 Ms^{-1}$) by the concentration of the catalyst (0.0187M) you arrive at the number $-0.337 s^{-1}$ at $25^{o}C$.

1.6.1 ^{1}HNMR Monitored Reduction Tests on Bromonaphthalene Utilizing Benzyl and Anthracenyl Functionalized Nickel Cyclam Complexes with Superhydride as the Co-reductant/hydride source.

When attempts were made at performing the ^{1}HNMR reduction test as performed on complex **1.6b** utilizing the benzyl and anthracenyl nickel cyclam complexes (**1.3** and **1.4**) measurement of rates became impossible. Under these conditions the reaction occurs so fast that during the shimming procedure on the NMR machine the reaction had gone to completion, between 4-5 minutes (the time taken to shim the machine) even with extra dilution and lowering catalyst concentrations. This means that N-functionalized compounds react significantly faster than the unfunctionalized ones (at least 7.5 times faster) under these reaction conditions. There are several explanations for this.

N-alkylation produces a tertiary amine; in this case the benzyl/anthracenyl arm pulls electron density away from the amine and ultimately from the nickel center. This makes the Ni(II) more electrophilic[68] and thus a rate increase may be observed by having forming the hydride/borohydride nickel complex more quickly. This theory would mean that the formation of the Ni(II)-H intermediate would have to be part of the rate law and as such the rate of hydride formation may be on a longer or on a similar scale to the actual reduction. In this case the rate-determining step (RDS) could be the hydride formation. This theory my be reinforced by previous work undertaken by Stolzenberg[22] showing that a tetramethylated Ni-cyclam complex is actually ten times less active in the reduction of bromocyclohexane than the unfunctionalized cyclam nickel complex (Figure 1.34). The extra electron density pushed onto the nickel center by the methyl groups, inductively, may decrease the rate at which the hydride is formed, reducing its activity. This theory would only be correct if the rate-determining step (RDS) in this reaction is the Ni(II) hydride formation not the actual hydride delivery/halide loss.

The tetramethylated complex also has a large amount of steric hindrance and thus the formation of a possible hydride/borohydride complex may be more difficult and interactions with substrates may also become less favorable (Figure 1.34).
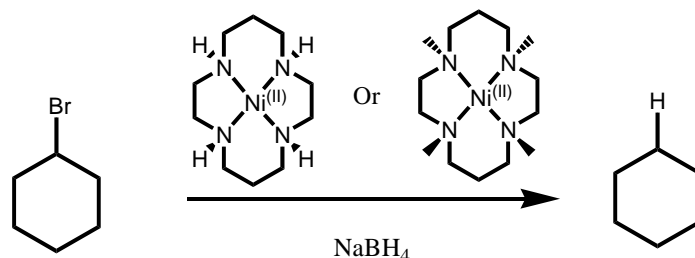
Figure 1.34: - Reduction of bromocyclohexane utilizing nickel cyclam catalysts[34].

π stacking attraction may bring the substrate into close proximity and the reaction proceeds as was initially hoped, although such large reduction rates for the phenyl complex was not expected due to the small π surface in this complex. Reduction rates on similar to that of complex **1.6b** might be expected for such a small π surface if only electrostatic interactions, not electronic effects were to play a role in the reduction rates.

A final explanation for this rather large reduction rate would be the formation of other active nickel species such as Ni(0) during the course of the reaction that maybe more reactive than hydride species (small amounts of black metallic material was observed after then reaction in the NMR machine). In order to better understand the reaction, reduction runs were performed under milder conditions with HPLC monitoring.

1.6.1.1 *HPLC Monitored Reduction Tests on Bromonaphthalene Using Non-functionalized and N-functionalized Nickel Cyclam Catalysts Utilizing Sodium Borohydride as the Co-reductant/hydride source.*

To test the reaction under different conditions runs were performed with **1.3**, **1.4**, and **1.6c** in a DMSO:EtOH mixture using sodium borohydride as the reductant and 1,3-dimethoxybenzene (DMB) as the internal standard (Figure1.35).
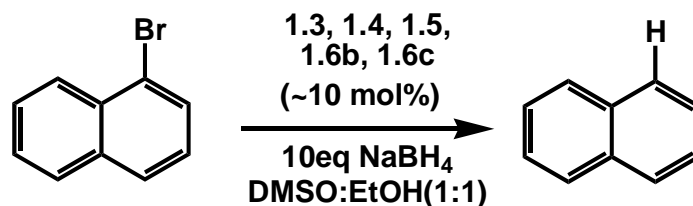
Figure 1.35: - HPLC reaction conditions for bromonaphthalene reductions.

The reduction of bromonaphthalene under our reaction conditions was *presumed* to follow the rate equation 1 below, where the active catalyst is generated and reformed more quickly than the actual reduction occurs. In this case the reduction of bromonaphthalene to naphthalene is assumed to be the rate determining step (RDS) for the reaction. This therefore means that the rate can be perceived as pseudo first order with respect to bromonaphthalene (equation 2). In this case plots of Ln[bromonaphthalene t = x]/][Bromonaphthalene t=0] vs. time (s) should lead to a straight line with the slope of that line being k^{obs}. k can be obtained by dividing k^{obs} by the concentration of the catalyst (equation 3). This proved to be the case for complexes **1.6c**, **1.3** and **1.5**, leading us to believe that the RDS is in fact the reduction of the substrate not the formation of the active species.

1. Rate = k[Active catalyst][Bromonaphthalene]
2. Rate = k[Bromonaphthalene]
3. k = k^{obs}/[catalyst]

For reaction monitoring we took small aliquots out of the reaction mixture and quench them in saturated ammonium chloride at given time intervals (to kill the active complex). The sample is extracted using ethyl acetate and run on the HPLC system to give integrations for each component. It is known that different solvent conditions show differences in product distribution and rates[24] so only the same solvent mixtures can be compared against each other. An observation made during the hydrodehalogenation experiments is that the complexes **1.3-1.5** have life times of several hours (2-4 hours) in DMSO:EtOH (1:1) with an excess of borohydride whereas **1.6a-1.6c** have lifetimes on the order of 48 hours under the same condition by color change (the active species

appears to be violet/purple in solution whereas the inactive species becomes orange in solution and Ni metal drops out of the mixture).

Table 1.4: - Selected reduction data from bromonaphthalene reductions in DMSO:EtOH as monitored by HPLC with dimethoxybenzene as the internal standard (DMB) at 22°C.

Catalyst (mol%)	Time (s)	Con^c of BrNap (M)	Starting Con^c of BrNap (M)	k^{obs}(Ms^{-1})	k(s^{-1})	k^{rel}	R^2
1.6c **(10)**	0	0.05	0.05	-3.936X10^{-5}	-0.0068	1	92.0
	240	0.0488					
	360	0.0486					
	960	0.0477					
	1200	0.0474					
1.3 **(5.7)**	300	0.0493	0.05	-2.95X10^{-6}	-0.001	-6.8	99.5
	600	0.0492					
	900	0.0491					
	1800	0.0490					
	3600	0.0488					
1.5 **(8.4)**	300	0.0405	0.05	-3.1X10^{-3}	-0.525	77.2	97.4
	600	0.0145					
	900	0.00349					
	1200	0.00164					
	1800	0.000416					

The reduction of bromonaphthalene using complex **1.6c** in DMSO:EtOH (1:1) gave a reduction rate constant of -0.0068s^{-1}, 49 times slower than the superhydride system with complex **1.6b** in DMSO. Complex **1.3** gave a rate constant 6.8 times *slower* than that of the unfunctionalized complex **1.6c** (Table 1.4). Complex **1.5** gave a reduction rate 77 times faster than complex **1.6c** after an apparent initiation period (to be discussed

in more detail shortly). These reductions showed the formation of only naphthalene, as identified via HPLC (Figure 1.36).
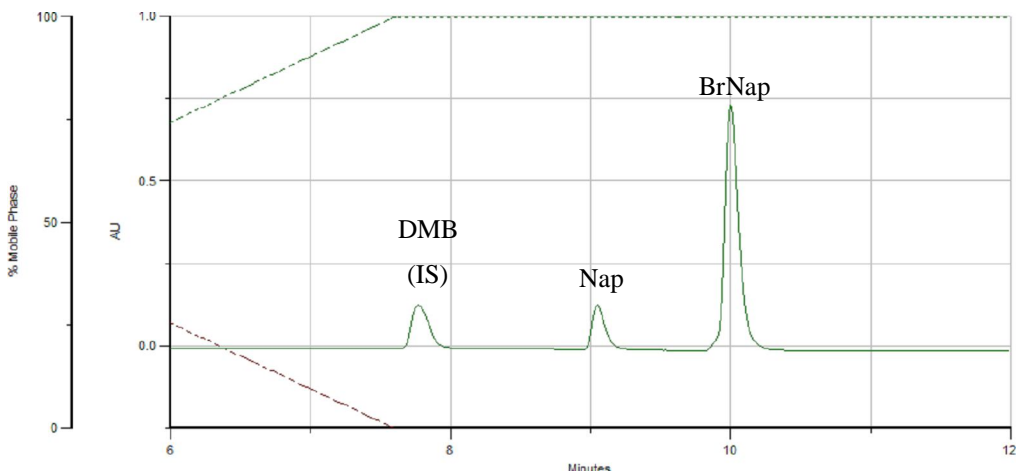
Figure 1.36: - HPLC trace of a 1-bromonaphthalene reduction using 1.6a, DMSO:EtOH (1:1) with sodium borohydride co-reductant and 1,3-dimethoxybenzene internal standard (IS) at 254nm (after 20minutes).

Complications arose when reacting complex **1.4** under these conditions. During the reaction the formation of a dark particulate suspension was observed. After 40 minutes the dark suspension had disappeared to be replaced by the original purple solution. The HPLC spectrum of this reaction shows the build up of several new, and unknown, peaks in the trace (Figure 1.37).
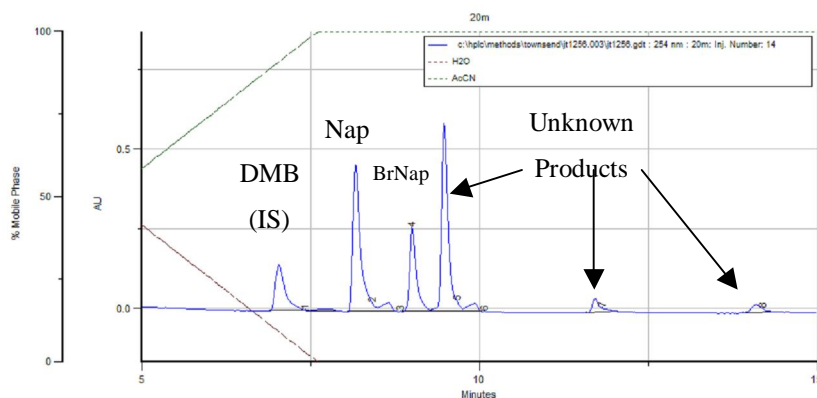
Figure 1.37: - HPLC trace of a 1-bromonaphthalene reduction using N-9-anthracenyl-cyclam nickel perchlorate, DMSO:EtOH (1:1) with sodium borohydride co-reductant (after 20minutes).

35

When studies were performed with complex **1.5** the reaction appears to have an initiation period, somewhat surprising, as the other catalysts in this series do not show this. Under the ^{1}HNMR experimental conditions no reduction was observed over a period of 8 minutes. As the ^{1}HNMR reaction was deemed to be inactive it was halted and the NMR tube removed from the machine. Shortly after the removal of the NMR tube from the instrument a sharp change in color from violet to orange was observed. A ^{1}HNMR was immediately run to check the reaction. No starting material was seen after 27 minutes (Figure 1.38).
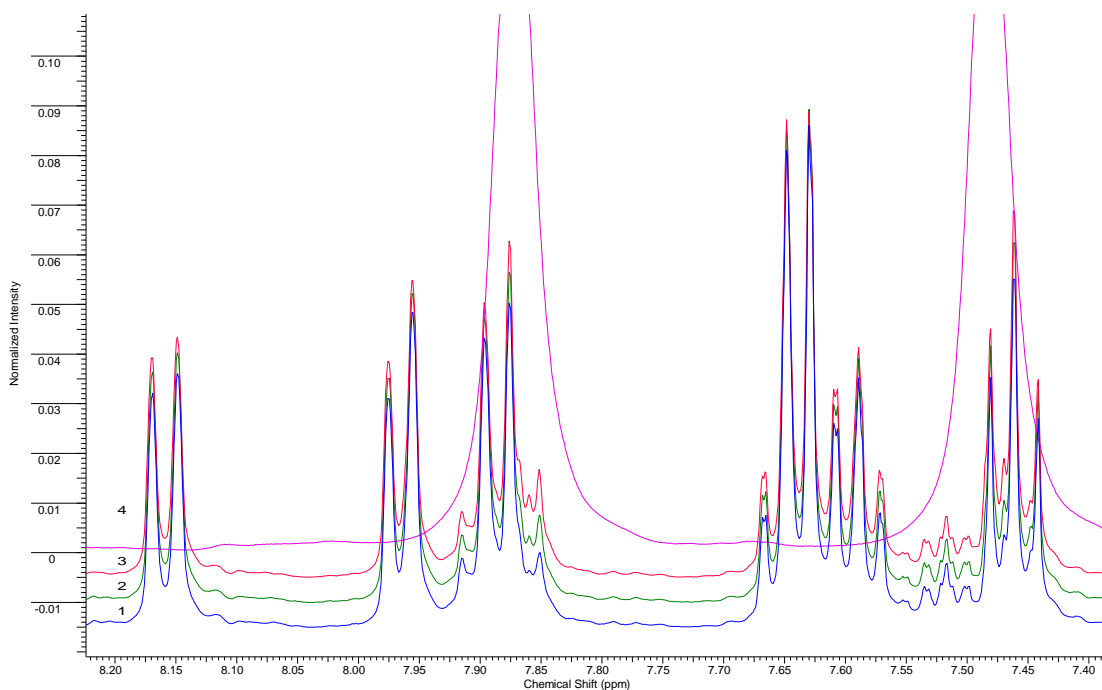
Figure 1.38: - NMR data showing the reduction of bromonaphthalene by 2.2c after (1) T=0min, (2) T=3min, (3) T=7Min 30s (4) 28min.

A reduction run for this complex was performed using sodium borohydride in a DMSO:EtOH mixture and HPLC monitoring of the reaction was employed to overcome the time issues involved with ^{1}HNMR monitoring. Samples were taken at 5, 10, 20, 30, 40, 74 minutes.

It was observed that a small amount of reduction had occurred over the 5 minute time period that did not change up to the 40-minute sample. When a sample was taken

after 74 minutes an orange color was observed in the solution and almost all of the bromonaphthalene had been converted to naphthalene product (Figure 1.39).

A graph showing Ln(%BrNap) vs Time
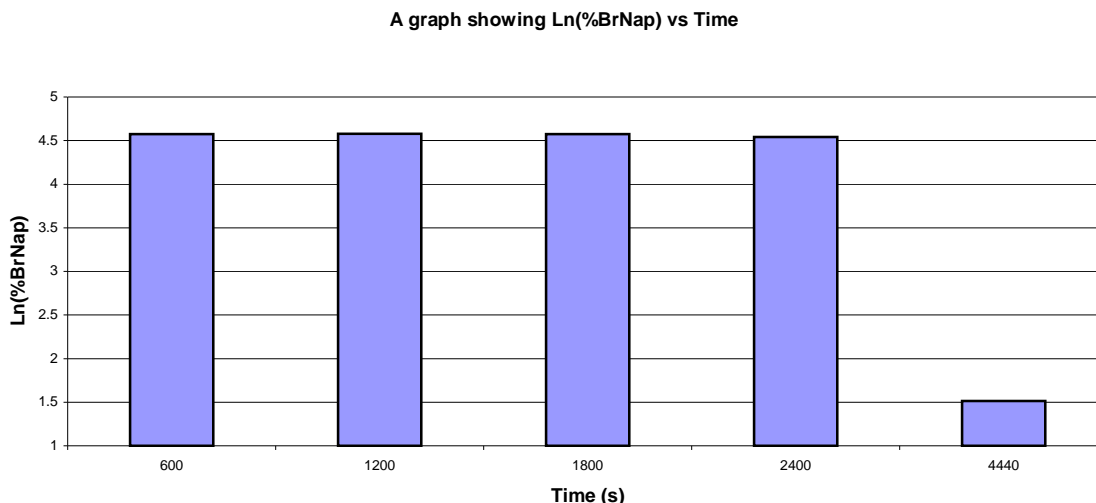
Figure 1.39: - Bar chart showing conversion of bromonaphthalene to naphthalene in DMSO:EtOH (1:1) using complex 1.5 and sodium borohydride as a co-reductant.

A blank run where no bromonaphthalene was added to the reaction mixture produced no change in color over a 2-hour period, perhaps indicating that something in the mixture is reacting over this time before hydrodehalogenation is affected. The catalyst lifetime appear to be between 4-5 hours as the purple color disappears and small traces of nickel metal can be seen after this time.

A second run was performed whereby **1.5** was allowed to react with $NaBH_4$ for 2-hours before the bromonaphthalene was added. This reaction showed that the purple Ni species of the complex **1.5** could be maintained over this period. This species might be the borohydride/hydride complex of **1.5** (Figure 1.40) Addition of the bromonaphthalene caused a large amount of bubbling (hydrogen production) in the initial stages. Samples were taken every 5 minutes for 30 minutes until the solution turned orange and the bubbling ceased (Figure 1.41). In this case no products bar naphthalene were observed in the HPLC trace and reduction proceeded smoothly over the given time period.

37
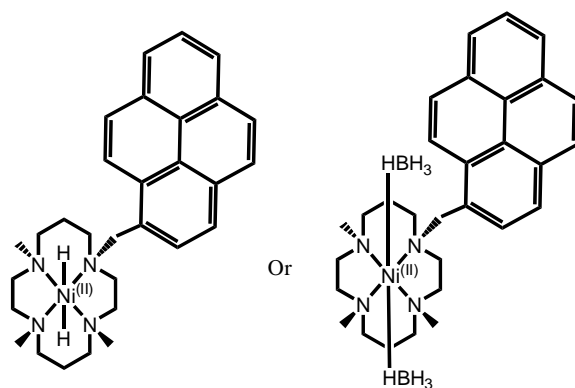
Figure 1.40: - Proposed intermediates in the reduction of bromonaphthalene utilizing complex 1.5.

Ln(concBrNap/ConcBrNap(t=0)) Vs time

$y = -0.0029x + 0.2596$
$R^2 = 0.9748$
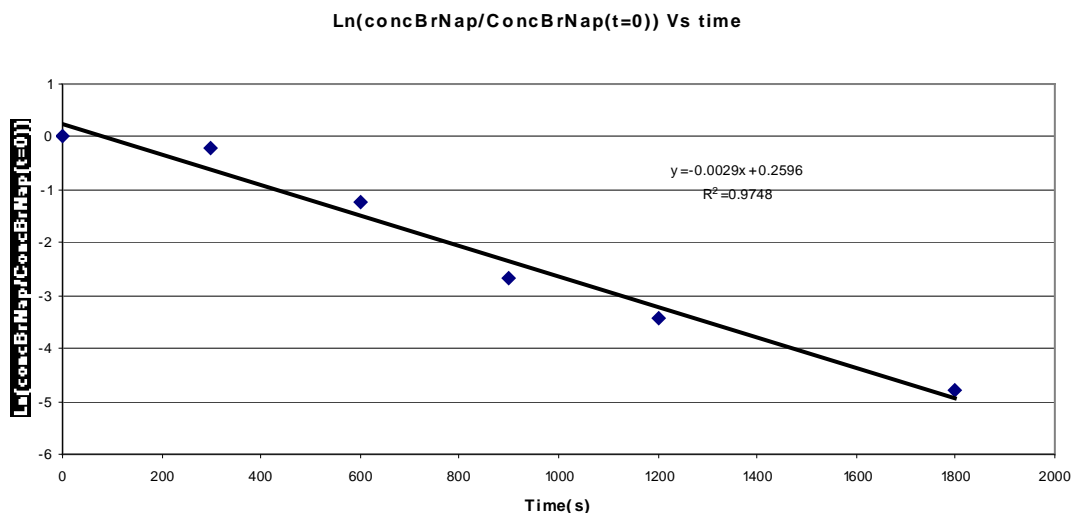
Figure 1.41: - Reduction graph of bromonaphthalene to naphthalene in DMSO:EtOH (1:1) using complex 1.5 and sodium borohydride as a co-reductant (2 hour delay before the addition of bromonaphthalene).

It is likely that there may be an unidentified intermediate built up before the reaction takes place to allow the dehalogenation to occur. The build up of a purple solution with **1.5** and borohydride/superhydride occurs rapidly as it does for all other complexes (**1.3-1.6c**) in either DMSO or DMSO:EtOH (1:1) solutions.

The large size of the pyrene ring maybe sterically inhibiting the formation of the reactive species and thus the initiation period for this reaction might be longer than for other similar complexes.

38

Another explanation for this delay time is that there is an impurity in the pyrene complex that is being consumed before the reaction with bromonaphthalene is initiated. ^{1}HNMR data for this complex is unclear due its paramagnetic nature although the aromatic region is sharp and clean for one product (Figure 1.42).
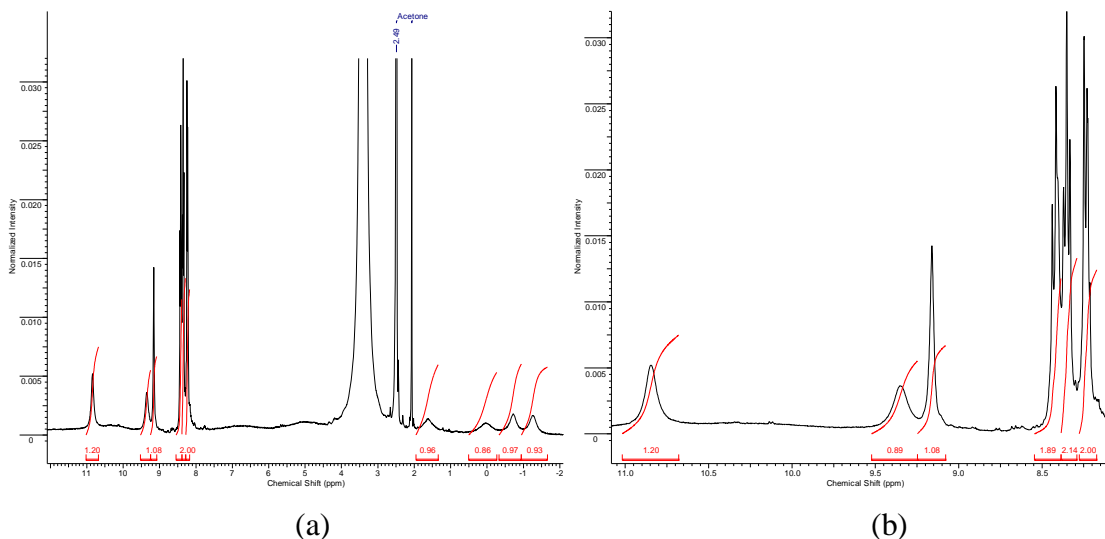
Figure 1.42: - (a) ^{1}HNMR of complex 1.5. (b) expanded ^{1}HNMR of the aromatic region for complex 1.5.

The rate constant for the reduction of bromonaphthalene using complex **1.6c** gave a reduction rate constant of -0.0068s^{-1} in the DMSO:EtOH (1:1) solvent. This is just under 77 times slower than the complex **1.5** meaning that the side arm does provide a large rate increase over **1.6c** (Table 1.4).

1.7 Conclusions

Synthesis of the N-functionalized cyclam ligands proved to be straightforward with high yielding reactions and simple isolation. Nickel complex formation was straightforward. However paramagnetic complexes **1.6b**, **1.6d** and **1.6e** were difficult to identify by ^{1}HNMR. In these cases IR, MS and X-ray crystallography were utilized to identify the compounds.

Mechanistic studies suggest that the reaction occurs through the formation of active borohydride/hydride intermediate as isolated in complexes **1.6d**, and **1.6e** as no

reactive was observed utilizing **1.7**. The complex **1.6d** reacted with roughly two equivalents of bromonaphthalene in solution. This result suggests that only two of the hydrides in **1.6d** are active in this reaction. **1.6d** does not react (over 12 hours) with bromonaphthalene in AcCN or DMSO. When D_2O (in AcCN) or CD_3OD (in DMSO) was added to the reduction of bromonaphthalene was observed. This result might suggest that a reactive intermediate is generated from **1.6d**. As we have concluded that Ni(I) does not play a major role in this reduction it is envisioned that Ni-H intermediates are the reactive species[69].

k^{obs} values were not obtained for the complexes **1.3**, **1.4**, and **1.5** in the ^{1}HNMR experiments with superhydride. However these rates were clearly much greater than those obtained for **1.6c**. The slower analogous reactions in DMSO:EtOH mixtures utilizing sodium borohydride as the hydride source gave interesting results. **1.3** shows a *slower* rate of reduction under these conditions than the unfunctionalized complex **1.6c** whilst complex **1.4** reacted unpredictably with the formation of side products. Complex **1.5** is very much a quandary. An apparent initiation period, followed by rapid reduction rates was observed under both reaction conditions. No solid explanation for this process is available. It may be possible that reaction of complexes **1.3**, **1.4**, and **1.5** with superhydride progress by an alternate reaction pathway to the analogous reaction with sodium borohydride as no reduction was seen utilizing sodium borohydride in DMSO of catalyst **1.6d**. The possibility of Ni(0) (black metal was observed after the reaction) or single electron transfer reductions cannot be ruled out.

The N-functionalized nickel cyclam complexes have shown to be very unpredictable in their reaction with bromonaphthalene with the generation of side products (possibly binaphthalene using complex **1.4**, initiation periods for complex **1.5**, and slower rates than the unfunctionalized cyclams noted for complex **1.3** in DMSO:EtOH(1:1) with $NaBH_4$.

Overall it became obvious that N-functionalized nickel cyclam complexes had far too many complications to be a viable candidate for the long-term study of the pre-concentration hypotheses and an alternative solution was needed. Under that notion the synthesis of the second generation, C-functionalized nickel cyclam complexes, became a target. C-functionalized nickel cyclam complexes will allow for the formation of tweezer

like cavities to trap the halogenated aromatic substrates and keeping the nitrogens in the cyclam complex free of substitution will minimize 1,3-synaxial interactions and electronic effects through the R-N-Ni bonds. Efforts toward the synthesis, characterization and application of C-functionalized nickel cyclam complexes shall be discussed in the following chapters.

1.8   Experimental.

All chemicals were purchased from Aldrich, Acros Organics and Fischer and used without further purification.

1.8.1   N-Functionalized Cyclam Ligand Synthesis.

1-(Chloromethyl)pyrene (1.1)
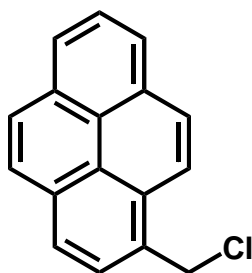
1-methylhydroxypyrene (500mg, 2.15mmol) was suspended in toluene (20mL) and thionyl chloride (0.32mL, 4.5mmol) added dropwise. The mixture was then heated to reflux for 2.5 hours. The solvent was removed *in vacuo* to yield the product. Yield 539mg, 100%. ^{1}H NMR (400 MHz, CDCl$_3$) δ 5.31 (s, 2 H) 7.97 - 8.08 (m, 4 H) 8.10 (t, *J*=8.00 Hz, 1 H) 8.14 - 8.23 (m, 3 H) 8.36 (d, *J*=9.37 Hz, 1 H). ^{13}C NMR (101 MHz, CDCl$_3$). δ 44.75, 122.71, 124.71, 125.62, 126.16, 127.26, 127.64, 127.99, 128.21, 128.35, 129.01, 129.12, 130.27, 130.67, 131.14, 131.95.

General Synthesis of Mono N-Functionalized Cyclams

To 1,4,8,11-tetraazacyclotetradecane (500mg, 2.50mmol) in chloroform (20mL) was added the aryl chloride (0.25mmol) and potassium carbonate (500mg, 3.62mmol). This was stirred at RT for 12 hours and filtered to remove any solid potassium carbonate. The solvent was removed *in vacuo* and the product extracted from the solid 5 times with acetone.

1-Benzyl-1,4,8,11-tetraazacyclotetradecane (1.2a)
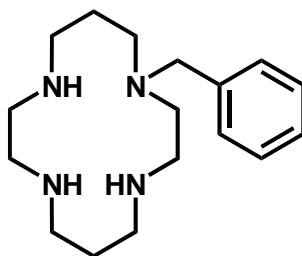
Yield 71.1mg, 80%. ^{1}H NMR (400 MHz, CHLOROFORM-D) δ 1.73 (dt, *J*=10.54, 5.27 Hz, 2 H) 1.81 - 1.90 (m, *J*=10.79, 5.66, 5.44, 5.44 Hz, 2 H) 2.51 - 2.59 (m, 4 H) 2.60 - 2.66 (m, 4 H) 2.69 - 2.76 (m, 4 H) 2.78 - 2.83 (m, 2 H) 2.83 - 2.87 (m, 2 H) 3.48 (m, 3 H) 3.57 (s, 2 H) 7.24 - 7.36 (m, 5 H). ^{13}C NMR (101 MHz, CDCl$_3$) δ 26.05, 27.99, 47.31, 47.80, 49.04, 49.22, 49.50, 50.67, 53.71, 54.28, 58.12, 127.18, 128.34, 129.43, 138.86.

1-(Anthracen-9-ylmethyl)-1,4,8,11-tetraazacyclotetradecane (1.2b)
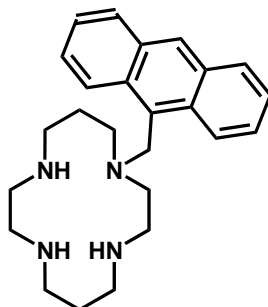
Yield 122mg, 85%. ^{1}H NMR (400 MHz, CDCl$_3$) δ 1.53 (ddd, J=10.74, 5.27, 5.08 Hz, 2 H) 1.78 (ddd, J=11.13, 5.86, 5.66 Hz, 2 H) 2.14 - 2.26 (m, 3 H) 2.40 - 2.48 (m, 4 H) 2.52 - 2.61 (m, 6 H) 2.65 - 2.74 (m, 6 H) 4.47 (s, 2 H) 7.39 - 7.50 (m, 4 H) 7.95 (d, J=7.81 Hz, 2 H) 8.37 (s, 1 H) 8.51 (d, J=8.59 Hz, 2 H). ^{13}C NMR (101 MHz, CDCl$_3$) δ 26.82, 27.72, 47.94, 48.05, 48.76, 49.12, 50.22, 50.83, 52.51, 54.43, 55.14, 124.90, 125.01, 125.17, 125.85, 127.93, 129.36, 131.48, 131.60.

1-(1-pyrenylmethyl)-1,4,8,11-tetraazacyclotetradecane (1.2c)
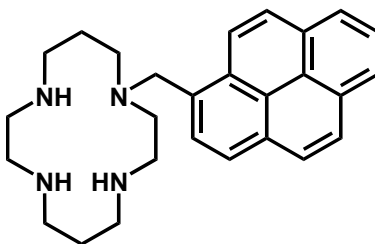
Yield 250mg, 100%. ^{1}H NMR (400 MHz, CDCl$_3$) δ 1.62 (dt, J=10.54, 5.27 Hz, 2 H) 1.88 (dt, J=10.93, 5.47 Hz, 2 H) 2.45 - 2.51 (m, 2 H) 2.51 - 2.56 (m, 2 H) 2.59 - 2.65 (m, 2 H) 2.66 - 2.71 (m, 4 H) 2.73 (s, 1 H) 2.75 - 2.80 (m, 3 H) 2.81 - 2.88 (m, 2 H) 3.22 - 3.34 (m, 3 H) 4.20 (s, 2 H) 7.95 - 8.00 (m, 1 H) 8.02 (s, 2 H) 8.06 - 8.08 (m, 1 H) 8.10 (d, J=3.90 Hz, 2 H) 8.12 - 8.18 (m, 2 H) 8.48 (d, J=9.37 Hz, 1 H). ^{13}C NMR (101 MHz, CDCl$_3$) δ 26.58, 27.93, 47.61, 47.70, 48.43, 48.84, 49.05, 50.44, 54.34, 54.86, 57.21,

123.73, 124.75, 124.96, 125.02, 125.07, 125.23, 125.98, 127.22, 127.32, 127.58, 128.31, 129.80, 130.76, 130.87, 131.45, 132.97.

1.8.2 N-Functionalized Nickel Cyclam Ligand Synthesis.

(1-Benzyl-1,4,8,11-tetraazacyclotetradecane)Nickel(II) Bis(perchlorate) (1.3)
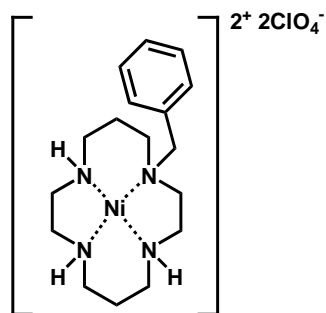
1-Benzyl-1,4,8,11-tetraazacyclotetradecane (71.1mg, 0.23mmol) and $Ni(ClO_4)_2$ (80mg, 0.23mmol) were dissolved in methanol (5mL) and mixed together. The initial orange color of the cyclam became darker upon the addition of the nickel. The solvent was removed in vacuo and the sample taken up in a little methanol. Crystals formed quickly. The mixture was placed in the fridge for a few minutes then removed and left at RT overnight. The orange solid was filtered off and washed with a little methanol. The crystals were then dried in vacuo. Yield 37mg, 30%. MS: *m/z* calculated for $C_{17}H_{30}N_4Ni$ = 348.1824, actual *m/z* (M-H) = 347.133. IR: υ 3201, 2958, 2887, 1659, 1548, 1453, 1429, 1067, 733, 710, 618cm^{-1}.

(1-(Anthracen-9-ylmethyl)-1,4,8,11-tetraazacyclotetradecane)Nickel(II) Bis(perchlorate) (1.4)
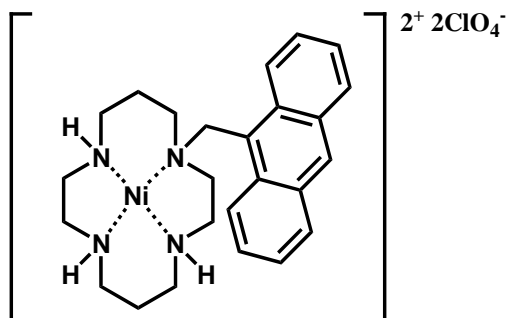
To 1-(Anthracen-9-ylmethyl)-1,4,8,11-tetraazacyclotetradecane (122mg, 0.31mmol) in methanol (5mL) was added the $Ni(ClO_4)_2$ (113mg, 0.31mmol) in methanol (2mL). The product was crystallized from methanol. Yield 74mg, 36.8%. ^{1}H NMR (200 MHz, DMSO-D6) δ ppm -1.24 (s, 1 H) -0.21 (s, 1 H) 0.56 - 0.80 (m, 1 H) 1.22 (d, J=15.38 Hz, 1 H) 1.64 (s, 2 H) 1.92 (s, 7 H) 2.59 - 2.81 (m, 3 H) 2.82 - 3.04 (m, 4 H) 3.04 - 3.19 (m, 2 H) 4.56 (d, J=13.92 Hz, 2 H) 5.36 (d, J=12.82 Hz, 1 H) 7.55 - 7.75 (m, 2 H) 7.88 (t, J=8.06, 7.33 Hz, 1 H) 8.22 (d, J=7.69 Hz, 1 H) 8.38 (m, 2 H) 8.66 (d, J=8.06 Hz, 1 H) 8.95 (s, 1 H) 11.19 (d, J=8.42 Hz, 1 H). ^{13}C NMR (101 MHz, DMSO-D6) δ 23.61, 25.20, 46.77, 47.26, 49.07, 49.82, 53.58, 58.53, 62.89, 124.42, 125.77, 126.03, 127.46, 128.37, 129.45, 130.07, 130.36, 130.41, 131.03, 131.22, 131.35, 132.10. MS: *m/z* calculated for $C_{25}H_{34}N_4Ni$ = 448.2137, actual *m/z* (M-H) = 447.941. See X-ray crystal structure for structural configuration.

(1-(1-pyrenylmethyl)-1,4,8,11-tetraazacyclotetradecane)Nickel(II) Bis(perchlorate) (1.5)
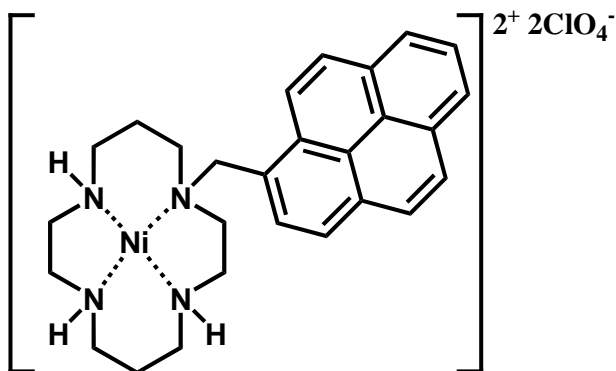
To 1-(1-pyrenylmethyl)-1,4,8,11-tetraazacyclotetradecane (101mg, 0.244mmol) in methanol (5mL) was added the $Ni(ClO_4)_2$ (89.2mg, 0.244mmol) in methanol (2mL). The product was crystallized from methanol. Yield 44.7mg, 29.1%. (Not all protons are accounted for) 1H NMR (400 MHz, DMSO-D6) δ ppm -20.37 (bs, 2 H) -16.37 (bs, 5 H) -0.47 (s, 2 H) -0.07 - 0.57 (m, 2 H) 1.33 - 1.96 (m, 1 H) 3.62 - 4.58 (m, 1 H) 5.64 (s, 2 H) 8.23 (s, 2 H) 8.29 - 8.53 (m, 4 H) 9.07 (s, 1 H) 9.22 - 9.43 (m, 1 H) 10.72 (s, 1 H) 13.76 - 16.95 (m, 1 H). MS: *m/z* calculated for $C_{27}H_{34}N_4Ni$ = 472.2137, actual *m/z* (M-H) = 471.144. IR: υ 3252, 3193, 2962, 2939, 2875, 1627, 1592, 1457, 1429, 1059, 1019, 849, 714, 630cm^{-1}.

(1,4,8,11-Tetraazacyclotetradecane)nickel(II) Bis(chloride) (1.6a)
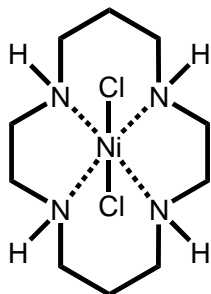
The cyclam (162mg, 0.681mmol) was dissolved in ethanol (20mL) and the $NiCl_2$ (137mg, 0.681mmol) was added. The reaction mixture was heated for ten minutes and allowed to cool. A purple crystalline solid fell out of solution and was collected by filtration and washed with cold methanol. Yield 71.2%. MS: *m/z* calculated for $C_{10}H_{24}N_4Ni$ = 258.1354, actual *m/z* (M-H) = 256.918. ^{1}H NMR (400 MHz, DMSO-D6) δ -14.83 - -12.26 (m, 4 H) -6.32 - -2.46 (m, 4 H) 18.42 - 26.06 (m, 8 H) 52.96 - 60.40 (m, 8 H) IR (KBr pellet): υ 3264, 3211, 2932, 2859, 1633, 1447, 1096, 1003, 983, 943, 870cm^{-1}.

(1,4,8,11-Tetraazacyclotetradecane)nickel(II) Bis(Tetraphenylborate) (1.6b)
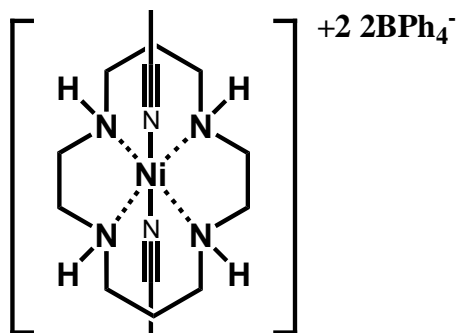
The 1,4,8,11-tetraazacyclotetradecane (500mg, 2.5mmol) and $NiCl_2$ (320mg, 2.5mmol) were dissolved in methanol and water (2:5, 20mL) and refluxed for 10 minutes until a change of colour to orange was observed. To this mixture was added the sodium

tetraphenylborate (171mg, 5mmol). The solvent was then removed and the crude taken up into acetonitrile and filtered to remove any excess salt. The compound was then left to recrystallize from acetonitrile. Yield 1.84g, 76% IR: υ 3154, 3129, 3117, 3060, 2978, 2953, 1580, 1474, 1462, 1417, 1298, 1270, 1241, 1127, 1094, 1070, 882, 833, 804, 747, 702, 612cm^{-1}. Structure confirmed by X-ray crystal analysis.

(1,4,8,11-Tetraazacyclotetradecane)nickel(II) Bis(perchlorate) (1.6c)
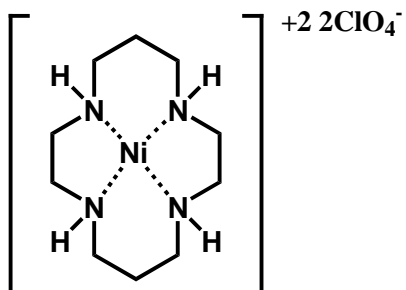
To a solution of 1,4,8,11-tetraazacyclotetradecane (294, 1.47mmol) in Methanol (10mL) was added the nickel perchlorate (511mg, 1.47mmol). The crystalline product dropped out of solution and collected by filtration. Yield 595mg, 88.4%. IR: υ 3358, 3309, 3207, 3141, 2966, 2880, 1666, 1621, 193, 1462, 1446, 1384, 1225, 1074, 1066, 1049, 1008, 767, 726, 616cm^{-1}.

(1,4,8,11-Tetraazacyclotetradecane)nickel(II) Bis(Borohydride) (1.6d)
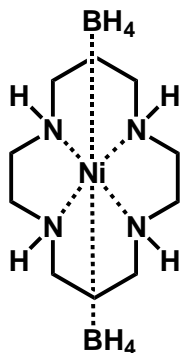
To a suspension of (1,4,8,11-Tetraazacyclotetradecane)nickel(II) Bis(perchlorate) (173mg, 0.378mmol) in THF (10mL) was added potassium borohydride (40.8mg, 0.756mmol). This mixture was allowed to stir for 12 hours. The generated light green powder was then collected by filtration. Yield 86.6mg, 79.4%. IR: υ 3260, 3235, 2933, 2864, 2328, 2279, 2197, 2124, 1470, 1454, 1425, 1098, 1012, 951, 874, 620cm^{-1}. Structure confirmed by X-ray crystal analysis.

(1,4,8,11-Tetraazacyclotetradecane)nickel(II) Bis(Borodeuteride) (1.6d)
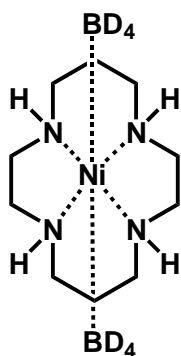
To a suspension of (1,4,8,11-Tetraazacyclotetradecane)nickel(II) Bis(perchlorate) (47.2mg, 0.103mmol) in THF (10mL) was added sodium borodueteride (8.62mg, 0.206mmol). This mixture was allowed to stir for 12 hours. The generated light green powder was then collected by filtration. Yield 23.1mg, 75.7%. IR: υ 3268, 3235, 2945, 2859, 1736, 1642, 1605, 1556, 1458, 1421, 1339, 1307, 1286, 1102, 1061, 1012, 947, 878, 800, 747, 710cm^{-1}.

References: - Chapter 1

[1] (a) B. SanMartin, R. Churruca, F. Dominguez, E. Urtiaga, M. Karmele, A. M. Isabel, *Organometallics.*, 2008, **27**, 2833-2839; (b) B. Basudeb D. Sajal, K. Sekhar; M. Bablee, *Synlett.,* 2008, **2**, 255-259.

[2] http://www.epa.gov/wastemin/factshts/tetchlben.pdf

[3] M. D. Erickson, *Analytical chemistry of PCB's*, Ann Arbor science, Butterworth publishing, 1997.

[4] http://www.epa.gov/fishadvisories/files/dioxin.pdf

[5] http://www.washingtonpost.com/ac2/wp-dyn?pagename=article&contentId=A46648-2001Dec31

[6] (a) http://www.powertechlabs.com/cfm/index.cfm?It=902&Id=4

(b) http://www.jesconet.co.jp/eg/pcb/pcb.html#cat05; (c) Y. Noma, Y. Mitsuhara, K. Matsuyama, S-I. Sakai, *Chemosphere.*, 2007, **68**, 871-879;

(d) http://www.oceta.on.ca/profiles/oht/pcb/low-temp.html.

[7] F. Alonso, I. P. Beletskaya and M. Yus, *Chem. Rev.*, 2002, **102**, 4009-4091

[8] (a) A. Guijarro, D. J. Ramo´n, M. Yus, *Tetrahedron,* 1993, **49**, 469; (b) E. Austin, R. A. Alonso, R. A. Rossi, *J. Chem. Res., Synop.* 1990, 190. (c) E. Austin, C. G. Ferrayoli, R. A. Alonso, R. A. Rossi, *Tetrahedron,* 1993, **49**, 4495.

[9] (a) C. Chatgilialoglu, A.Guerrini, G. Seconi, *Synlett,* 1990, 219; (b) C. Chatgilialoglu, M. Guerra, A. Guerrini, G. Seconi, *J. Org. Chem.,* 1992, **57**, 2427. (c) M. Ballestri, C. Chatgilialoglu, K. B. Clark, D. Griller, B. Giese, B. Kopping, *J. Org. Chem,.* 1991, **56**, 678. (d) M. Ballestri, C. Chatgilialoglu, N. Cardi, A. Sommazzi, *Tetrahedron Lett.,* 1992, **33**, 1787. (e) C. Chatgilialoglu, A. Guerrini, M. Lucarini, *J. Org. Chem,.* 1992, **57**, 3405. (f) J. Yang, M. Brookhart, *Adv. Synth. Catal.,* 2009, **351**,175-187. (g) J. Yang, M. Brookhart, *J. Am. Chem. Soc.,* 2007, **129**, 12656-1267; (h) D. Karshtedt, A. T. Bell, T. T. Don, *Organometallics*, 2006, **25**, 4471-4482.

[10] Y. Ukisu, *Applied Catalysis A*, 2008, 229-232.

[11] H-Y. Wee, J. A. Cunningham, *J. Haz. Mat.,* 2008, **155**, 1-9

[12] J. Chen, Y. Zhang, L. Yang, X. Zhang, J. Liu, L. Li, H. Zhang*, Tetrahedron*, 2007, **63**, 4266-4270.

[13] A. A. Jalil, N. Fatimah, A. Panjang, S. Akhbar, M. Sundang, N. Tajuddin, S. Triwahyono, *J. Haz. Mat.,* 2007, **148**, 1-5.

[14] Y. Yoshimi, A. Ishise, H. Oda, Y. Moriguchi, H. Kanezaki, Y. Nakaya, K. Katsuno, T. Itou, S. Inagaki, T. Morito, M. Hatanaka, *Tetrahedron Lett.,* 2008, **49**, 3400-3404.

[15] A. A. Peterson, K. McNeill, *Organometallics*, 2006, **25**, 4938-4940.

[16] Y. Moglie, F. Alsonso, C. Vitale, M. Yus, G. Radivory, *Applied Catalysis A: General,* 2006, **313**, 94-100.

[17] (a) C. Yang, C. U. Pittman, *Tetrahedron Lett.* 1997, **38**, 6561;(b) C. Yang, C. U. Pittmann, *Synth. Commun.* 1998, **28**,517; (c) C. Yang, *Diss. Abstr. Int., B,* 1998, **58**, 6589;(d) C. Yang, C. U. Pittman, *J. Hazard.Mater.* 2001, **B82**, 299.

[18] S. Zinovyev, A. Shelepchikov and P. Tundo, *Applid Catalysis B: Environmental,* 2007, 289-298.

[19] W. Wu, J. Xu, H. Zhao, Q. Zhang, S. Liao, *Chemosphere*, 2005, **60**, 944-950.

[20] F. Alonso, G. Ravivoy, M. Yus, *Russ. Chem.Bull. Int. Ed.,* 2003, **52**, 2563-2576.

[21] S. Kliegman, K. McNeill, *Dalton Trans.,* 2008, 4191-4201; (b) J. M. Fritsch, K. McNeill, *Inog. Chem.,* 2005, **44**, 4852-4861.

[22] A. M. Stolzenberg and Z. Zhang, *Inorg. Chem.,* 1997, **36**, 593-600.

[23] C. J. Gantzer, L. P. Wackett, *Environ. Sci. Technol.,* 1991, **25**, 715-722.

[24] M. Stiles, *J. Org. Chem.,* 1994, **59**, 5381-5385; (b) A. Bakac and J. H. Espenson, *J. Am. Chem. Soc.,* 1986, **108**, 713-719.

[25] (a) see reference 20 (b) J. Harmer, C. Finazzo, R. Piskorshi, S. Ebner, E. C. Duin, M. Goenrich, R. K. Thauer, M. Reiher, A. Schweiger, D. Hinderberger and B. Jaun, *J. Am. Chem. Soc.,* 2008, **130**, 10907-10920. (c) G. K. Lahiri, A. M. Stolzenberg, *Inorg. Chem.,* 1993, **32**, 4409-4413.

[26] S. Olivero, J-P. Rolland and E. Dunach, *Organometallics.*, 1998, **17**, 3747-3753.

[27] (a) W. B. Motherwell, M. J. Bingham, Y. Six, *Tetrahedron*, 2001, **57**, 4663, 4686; (b) R. Breslow, *Artificial Enzymes,* Wiley VCH, 2005; (c) T. R. Ward, *Angew. Chem. Int. Ed.,* 2008, **47.** 7802-7803; (d) T. Darbre, J-L Reymond, *Acc. Chem. Res.*, 2006, **39**, 925-934; (e) J. Suh, *Acc. Chem. Res.*, 2003, **36**, 562-570; (f) I. Tabushi, *Tetrahedron,* 1984, **40**, 269-292.(g) A. Kuzuya, M. Komiyana, *Cur. Org. Chem.,* 2007, **11**, 150-1459;

[28] (a) R. Breslow, C. J. Schmuck, *J. Am. Chem. Soc.* 1996, **118**, 6601-6605; (b) R. Breslow, E. Anslyn, *J. Am. Chem. Soc.,* 1989, **111**, 8931-8932.

[29] S. J. Teague, A. M. Davis, *Angew. Chem. Int. Ed.,* 1999, **38**, 736-749.

[30] C. Pugh, C. N. Tang, M. Paz-Pazos, O. Samtani, A. H. Dao, *Macromolecules*, 2007, **40**, 8178-8188.

[31] (a) E. J. Corey, T.-P. Loh, *J. Am. Chem. Soc.* 1991, **113**, 8966; (b) E. J. Corey, T.-P. Loh, T. D. Roper, M. D. Azimioara, *J. Am. Chem. Soc.,* 1992, **114**, 8290; (c) M. W. Wong, *J. Org. Chem.*, 2005, **70**, 5487-5493.

[32] H. C. Kolb, P. G. Andersson, K. B. Sharpless, *J. Am. Chem. Soc.*, 1994, **116**, 1278-1291.

[33] M. M. Ito, J. Kato, S. Takagi, E. Nakashiro, T. Sato, Y. Yamada, H. Saito, T. Namiki, I. Takamura, K. Wakatsuki, T. Suzuki and T. Endo, *J. Am. Chem. Soc.,* 1988, **110**, 5147; (b) H. Adams, F. J. Carver, C. A Hunter, J. C. Morales, E. M. Seward, *Angew. Chem. Int. Ed. Engl.,* 1996, **35**, 1542-1544; (c) S. L Cockroft, C. A. Hunter, K. R. Lawson, J. Perkins, C. J. Urch, *J. Am. Chem. Soc.,* 2005, **127**, 8594-8595; (d) G. Chessari, C. A. Hunter, C. M. R. Low, M. J. Packer, J. G. Vinter, C. Zonta, *Chem. Eur. J.,* 2002, **8**, 2860-2867.

[34] (a) G-N. Lu, Z. Dang, X-Q. Tao. C. Yang and X-Y Yi., *QSAR Comb. Sci.*, 2008, **27** 618 – 626; (b) J. Reza, A. Trejo, and L. E. Vera-Avila, *Chemosphere*, 2002, **47**, 933-945.

[35] R. Breslow, *J. Phys. Org. Chem.,* 2006, **19**, 813-822.

[36] J. W. Sease, F. G. Burton and S. L. Nickol, *J. Am. Soc.*, 1967, **90**, 2595-2598 (b) A Matsunaga, A. Yasuhara., *Environmental science & technology.* 2003, **37**, 3435-3441; (c) C. Costentin, M. Robert and J-M. Saveant, *J. Am. Chem. Soc.,* 2004, **126**, 16051-16057.

[37] (a) Silverman. R.B.; Rev. ed. San Diego, Calif. "Organic chemistry of enzyme-catalyzed reactions" London : Academic Press, 2002. (b) A. Warshel, *J. Biol. Chem.,* 1998, **273**, 27035-27038; (c) M. H. M. Olsson, W. W. Parson, A. Warshel, *Chem. Rev.* 2006, **106**, 1737-1756; (d) A. Warshel, *Computer Modeling of Chemical Reactions in Enzymes and Solutions*; John Wiley & Sons: New York, 1997. (e) A. Warshel, *Proc. Natl. Acad. Sci. U.S.A.,* 1978, **75**, 5250. (f) S. Kraft, *NSF proposal*, 2007.

[38] F. Bellouard, F. Chuburu, N. Kervarec, L. Toupet, S. Triki, Y. Le Mest and H. Handel, *J. Chem. Soc.*, *Perkin Trans 1.*, 1999, 3499–3505

[39] D. Ranganathan, V. Haridas, R. Gilardi, I. L. Karle, *J. Am. Chem. Soc.,* 1988, **120**, 10793-10800

[40] X. Liang, J. A. Parkinson, S. Parsons, M. Weisha, and P. J. Sadler, *Inorg. Chem.,* 2002, **41**, 4539-4537.

[41] T. Ito, H. Ito, K. Toriumi., *Acta Cryst.* 1981, **B37**, 1415-1416

[42] B. Bosnich, C. K. Poon, T. Tobe, *Inorg. Chem.,* 1965, **4**, 1102–1108.

[43] (a) C. Schickaneder, F. W. Heinemann, R. Alsfasser, *Eur. J. Inorg. Chem.,* 2006, **12**, 2357-2363; (b) T. Kitagawa, A. Dey, P. Lugo-Mas, J. B. Benedict, W. Kaminsky, E. Solomon, J. A. Kovacs, *J. Am. Chem. Soc.,* 2006, **128**, 14448-14449; (c) G. Byk, M. Frederic, D. Scherman, *Tettrahedron Lett.*, 1997, **38**, 3219-3222; (d) B. Boitrel, B. Andrioletti, M. Lachkar, R. Guilard., *Tettrahedron. Lett.*, 1995, **36**, 4995-8.

[44] A. E. Goeta, J. A. K. Howard, D. Maffeo, H. Puschmann, J. A. G.Williams and D. S. Yufit, *J. Chem. Soc., Dalton Trans.,* 2000, 1873; (b) M. Le Baccon, F. O. Chuburu, L. Toupet, H. Handel, M.Soibinet, I. De-champs-Olivier, JP. Barbier*c* and M. Aplincourtc, *New Journal of Chemistry,* 2001, **25**, 1168-1174.

[45] I. M. Helps, D. Parker, J. R. Morphy and J. Chapman, *Tetrahedron,* 1989, **45**, 219-226.

[46] (a) A. V. Powell, R. J. E. Lees, A. M. Chippindale, *Inorg. Chem.*, 2006, **45**, 4261-4267; (b) T. V. Mitkina, D. Y. Naumov, O. A. Gerasko, F. M. Dolgushin, C. V. R. Llusar, M. N. Sokolov, V. P. Fedin., *Rus. Chem. Bull.*, 2004, **53**, 2519-2524; (c) Y. Dong, G. A. Lawrance, L. F. Lindoy, P. Turner, *Dalton Trans.*, 2003, **8**, 1567-1576.

[47] (a) Y. Dong, L. F. Lindoy, P. Turner, G. Wei, *Dalton Trans.*, 2004, **8**, 1264-1270; (b) See reference 9c; (c) E. K. Barefield, F. Wagner, K. D. Hodges, *Inorg. Chem.,* 1976, **15**, 1370-1377

[48] (a) P. Rowinski, R. Bilewicz, *Sci. Eng. Commun.,* 2001, **C18**, 177-183; (b) G. De Santis, L. Fabbrizzi, M. Licchelli, S. N. Maurizo, A. H. Velders, *Chem. Eur. J.*, 1996, **2**, 1243-1250.

[49] (a) S. Matsuoka, K. Yamamoto, C. Pac, Y. Chyongjin, S. Yanagida, *Chem. Lett.,* 1991, **12**, 12099-2100; (b) H. Bock, T. Dieck, *Angewandte Chemie,* 1966, **5**, 520-522; (c) P. O. Whimp, N. F. Curtis, *J. Chem. Soc.,* 1966, **7**, 867-871.

[50] (a) J. D. Koola, J. K. Kochi, *Inorg. Chem.,* 1987, **26**, 908-16; (b) E. Iwawmoto, K. Imai, Y. Yamamoto, *Inorg. Chem.,* 1984, **23**, 986-988.

[51] K. Q. Ferreira, F. G. Doro, E. Tfouni, *Inorg. Chimi. Acta.,* 2003, **355**, 205-212

[52] R. Prakash, S. Kandoi and R. C. Srivastava, *Transition Metal Chemistry*, 2002, **27**, 598–603.

[53] T. M. Hunter, I. W. McNae, D. P. Simpson , A. M. Smith , S. Moggach, F. White, M. D. Walkinshaw, S. Parsons, P.J. Sadler, *Chemistry – A European Journal.,* 2006, **13**, 40-50.s

[54] X. Liang, J. A. Parkinson, M. Weishaupl, R. O. Gould, S. J. Paisey, H. Park, T. M. Hunter, C. A. Blindauer, S. Parsons and P. Sadler, *J. Am. Chem. Soc.*, 2002, **124**, 9105-9112

[55] S. J. Paisey, P. J. Sadler, *Chem. Commun,.* 2004, 306-307

[56] T. Ito, M. Kato, H. Ito, *Bull. Chem. Soc. Jpn.,* 1984, **57**, 2641

[57] (a) S. Surgden, *J. Chem. Soc.*, 1932, 246–250: (b) H. Cavell, S. Surgden, *J. Chem. Soc.*, 1935, 621–624.

[58] Y. Journaux, V. Lozan, J. Kinele, B. Kersting, *Chem. Commun.,* 2006, 83-84

[59] N. Carr, D. F. Mullica, E. L. Sappenfield, F. G. A. Stone, *Inorg. Chem.,* 1994, **33**, 1666-1673.

[60] I. Bach, R. Goddard, C. Kopiske, K. Seevogel, K-R. Porschke, *Organometallics*, 1999, **18**, 10-20

[61] B. G. Segal, S. J. Lippard, *Inorg. Chem.,* 1977, **16**, 1623-1629.

[62] (a) see reference 24b; (b) S. Olivero, J-P. Rolland and E. Dunach, *Organometallics*, 1998, **17**, 3747-3753; (e) see reference 24a; (f) J. Harmer, C. Finazzo, R. Piskorshi, S. Ebner, E. C. Duin, M. Goenrich, R. K. Thauer, M. Reiher, A. Schweiger, D. Hinderberger and B. Jaun, *J. Am. Chem. Soc.,* 2008, **130**, 10907-10920.

[63] (a) J. T. Groves, K. W. Ma, *J. Am. Chem. Soc.,* 1974, **96**, 6527; (b) J. A. Barltrop, D. Bradbury, *J. Am. Chem. Soc.,* 1973, **95**, 5085. (c) J. F. Bunnett, *Acc. Chem. Res.*, 1992, **25**, 2-9; (d) see reference 24

[64] (a) See reference 27. (b) J. Harmer, C. Finazzo, R. Piskorshi, S. Ebner, E. C. Duin, M. Goenrich, R. K. Thauer, M. Reiher, A. Schweiger, D. Hinderberger and B. Jaun, *J. Am. Chem. Soc.,* 2008, **130**, 10907-10920.

[65] M. P. Suh, H. K. Kim, M. J. Kim, K. Y. Oh, *Inorg. Chem.,* 1992, **31**, 3620-3625.

[66] Y. Mirua, H. Oka, E. Yamano, M. Mortia., *J. Org. Chem.,* 1997, **62**, 1188-1190.

[67] (a) http://www.powertechlabs.com/cfm/index.cfm?It=902&Id=4

(b) http://www.jesconet.co.jp/eg/pcb/pcb.html#cat05; (c) Y. Noma, Y. Mitsuhara, K. Matsuyama, S-I. Sakai, *Chemosphere*, 2007, **68**, 871-879;

(d) http://www.oceta.on.ca/profiles/oht/pcb/low-temp.html.

[68] Y. Dong, G. A. Lawance, L. F. Lindoy and P. Turner, *Dalton Trans.,* 2003, 1567-1576

[69] D. W. Lamson, P. Ulrich, R. O. Hutchins, *J. Org. Chem.,* 1973, **38**, 2928-2930.

CHAPTER 2 - C-Functionalized Cyclam Synthesis: - Linear Dipeptide and Tetrapeptide Precursors For Cyclopeptide Synthesis.

2.1   Introduction

Our previous N-functionalized nickel cyclam catalysts with **1.3** and **1.5** showed increased rates of hydrodehalogenation when compared to the unfunctionalized versions **1.6a-1.6c**, depending on conditions used (Table 1.4). However several problems with these molecules quickly became evident. The first is that the catalyst lifetimes are much lower than that of the unfunctionalized version. The second is that the exact nature of the change in rates is not immediately evident. The rate increases could be due to the electron withdrawing nature of the side arms pulling electron density out of the coordinating ligand, this in turn makes the nickel more willing to accept the hydride from the borohydride and ultimately the reactive intermediate. Possible Ni(0) formation also became an issue in DMSO:EtOH:NaBH$_4$ and DMSO:KHBEt$_3$ mixtures.

Synthesis of C-functionalized cyclam molecules with well-defined and controlled stereochemistry became a goal for this project. With well-defined stereochemistries in catalysts rate changes can be attributed to differences in the catalyst side arms or stereochemistry. However if the stereochemistry of the catalysts are not controlled and multiple stereochemistries are present in the reaction mixture difficulties are encountered in defining any rate increases/losses as these could be attributed to one or two minor complexes in the mixture.

It was theorized that incorporation of aromatic side arms on cyclam nickel complexes would allow the formation of π-π interactions with aromatic halogenated hydrocarbons[1], while a 3-bond distance between the sidearm and the coordinating amine in the cyclam should mean the reduction potentials of the complex are left unaffected. The π-π interactions were expected to pre-bind the substrate to the catalyst and any

increase in rates of dehalogenation or enhance selectivity for halogenated aromatics[2] would then only be due to the pre-binding. Any reduction in rate could in turn be attributed to increased steric hindrance on the catalyst. It was also hoped that the absence of side arms on the nitrogens would allow a longer catalytic lifetime, more comparable to the un-functionalized nickel cyclam catalysts. Whilst the factors governing lifetimes for these catalysts is not fully understood experimental visualization suggests that catalysts that are not functionalized on the nitrogens (**1.6a-1.6c**) have longer lifetimes than those that are (**1.3-1.5**)

We envisioned four types of C-substituted Ni-cyclam complexes that can theoretically cause pre-binding of aromatic substrates. The first kind is known as a molecular tweezer, conformation **2.1**, and according to molecular modeling would have a distance between aromatic side arms of 6.5-7Å, roughly twice that of the average π-π interaction[3]. This was modeled to occur when the C-functionalization occurs on the 1-6 carbons (Figures 2.1, 3.2). The second kind of cyclam would be conformation **2.2**, an L-shaped complex with one wall and one floor as π surfaces (Figures 2.1, 3.2). This catalyst has one sidearm in the plane of the cyclam and the other sits orthogonally to it and is capable of causing not only π-π interaction but also T-stacking (herringbone stacking) of aromatic substrates to the catalyst. The third kind of complex, conformation **2.3**, is the paddle wheel (Figure 2.1). This cyclam has one aromatic unit that is used for binding on either side of the ligand equator in both the T-stacking and face to face stacking π-π motifs. The final complex, conformation **2.4** is the single walled catalyst, similar in nature to the N-functionalized compounds that have only one sidearm that can be used as either a π-π stacker, or a T-stacker (Figure 2.1)

2.1   2.2   2.3   2.4
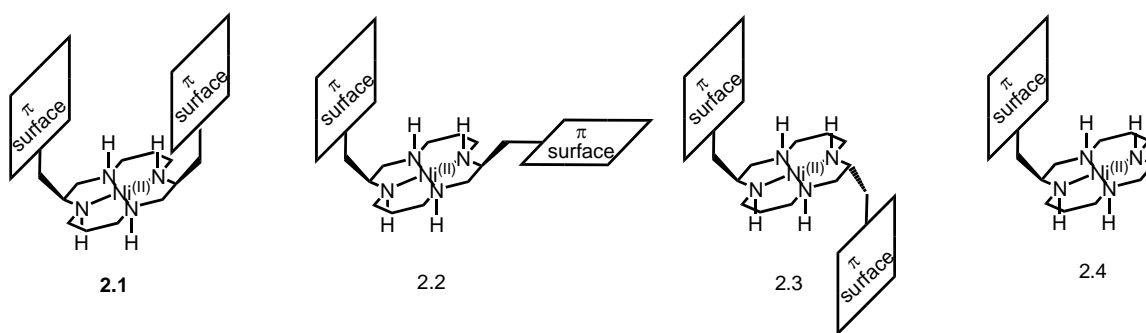
Figure 2.1:- Diagram showing (2.1) Tweezer shaped nickel cyclam (2.2) L shaped nickel cyclam (2.3) paddle wheel shaped nickel cyclam (2.4) Single walled nickel cyclam

(**2.1**)   (**2.2**)
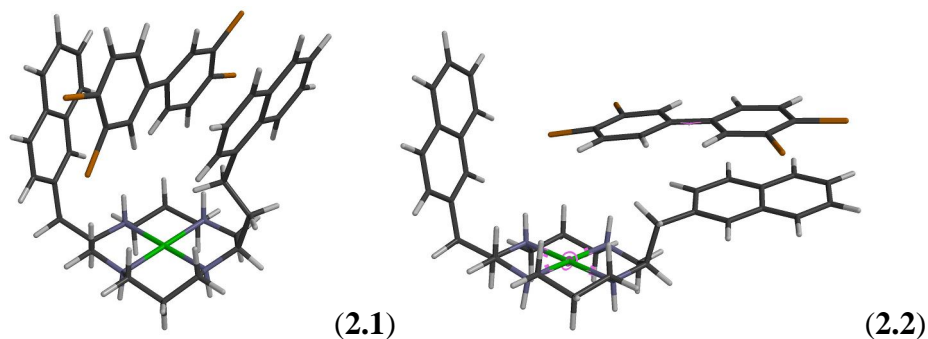
Figure 2.2: - Molecular modeling of 2.1 (naphthyl side arms) Tweezer shaped nickel cyclam complex binding a PCB, a representative aromatic substrate. 2.2 is a model of the L-shaped nickel cyclam complex binding a PCB.

2.1.1 Introduction to General Cyclam Synthesis

Previous efforts of macrocycle formation (leading to cyclam synthesis) have mostly focused around the formation of a macrocyclic amide through the ring closure of linear amines. There are many reported methods of doing this and include, but are not limited to, the reaction of polyamines (with primary amine termini) **2.5** with diethyl malonate [4], diacid chlorides or diazide[5] (**2.6**) (Figure 2.3), methyl acrylates[6] (**2.9**) (Figure 2.4) or diacids (**2.13**) and DCC[7] (Figure 2.5). Metal templated imine formation from **2.15** leads to **2.16**, which can be reduced to form the cyclen **2.17**, a close relative to cyclams[8] (Figure 2.6).

2.5   2.6   2.7   2.8

X = OEt, N₃, Cl
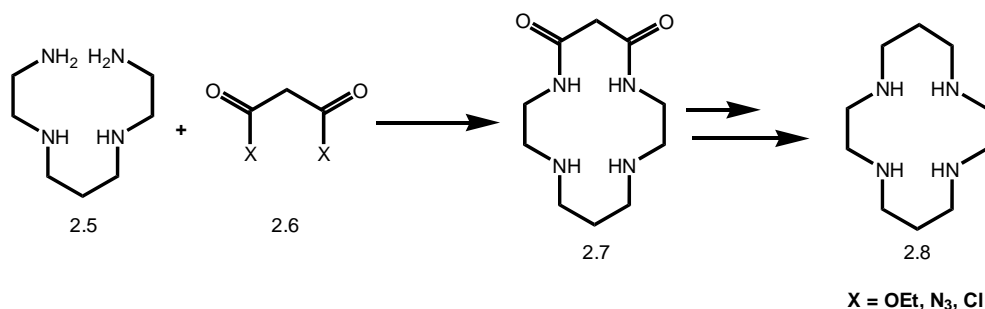
Figure 2.3: - Ring closure using malonates, diacids chlorides or diazides.
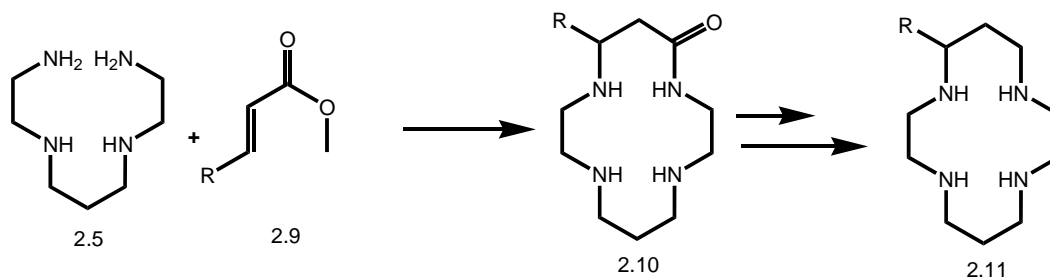
Figure 2.4: - Ring closure using methyl acrylates.
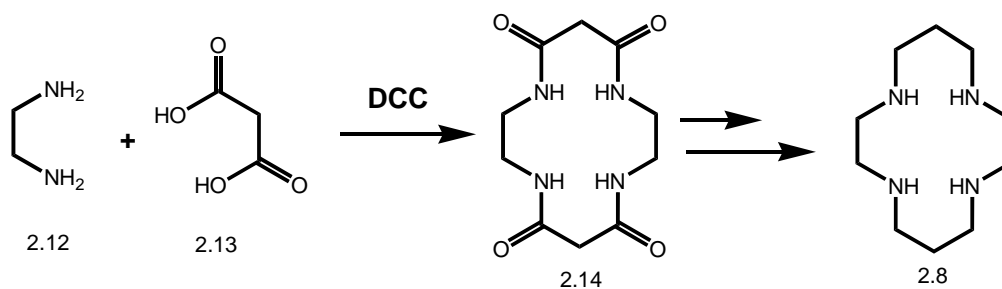
Figure 2.5: - Ring formation using amide bond formations.
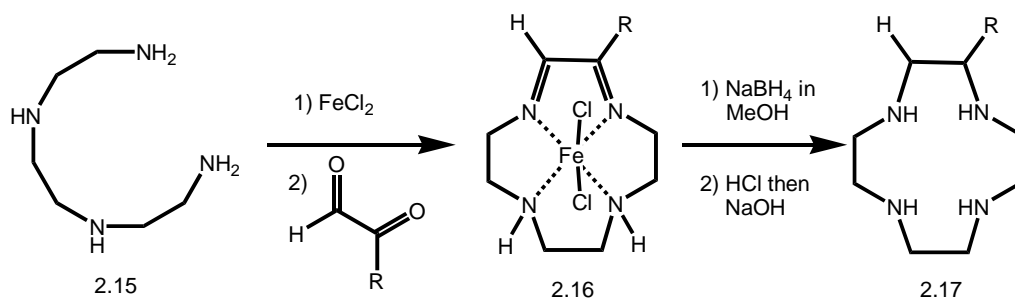
Figure 2.6: - Ring formation using metal templated imine formation followed by reduction.

There are many methods to form marcocycles and most (as in the given examples) utilize amines to form amides, which can later be reduced to form the cyclam molecules.

In the above examples carbon functionalization can be seen in the case of methyl acrylate ring closure and metal templated imine formation, however stereochemical control of the cyclam/cyclen was not achieved.

2.1.2 Stereoselective Carbon-Functionalized Cyclam Synthesis

In order to achieve the goal of stereoselectively synthesizing C-functionalized cyclams a synthesis was required that would allow the incorporation of various side arms in a controllable and selective manner. Of the examples of macrocycle formation selected (Figures **2.3-2.6**) one can clearly see that the formation of amides usually occurs during the ring synthesis. These amides can then simply be reduced using the appropriate reductant (BH_3, LAH) to form the cyclams.

In order to control the orientation of the aromatic group on the cyclam ligand we must have the ability to control R and S configurations during the synthesis. To increase the efficiency of the cyclam synthesis it was concluded that starting materials should be purchasable with defined stereochemistry, should be relatively inexpensive and should lend itself to rapid automated synthesis. Amino acids fit all of these parameters. They are purchased enantiomerically pure, they are inexpensive and peptide synthesis lends itself readily to automation both in solution phase[9] and solid phase chemistries.[10]

2.1.2.1 Stereospecific Synthesis of 1-5 C-Functionalized Cyclam Precursors.

Literature searches on the formation of stereospecifically synthesized carbon functionalized 14-membered amide containing macrocycles/cyclam/cyclen molecules produced very few hits (as will discussed shortly) and all seemed to use amino acids as the method of introducing the predefined stereocenters, as we envisioned.

C. J. Burrows developed a synthesis that incorporated two stereo-specifically defined carbon centres into a cyclam precursor[11] this was based on Tabushi's method (Figure 2.3)[4]. The synthesis, outlined in figure 2.6, shows the formation of a macrocyclic cyclam precursor **2.**20 with side arm configurations predefined from the amino acid starting material **2.18** (Figure 2.7).
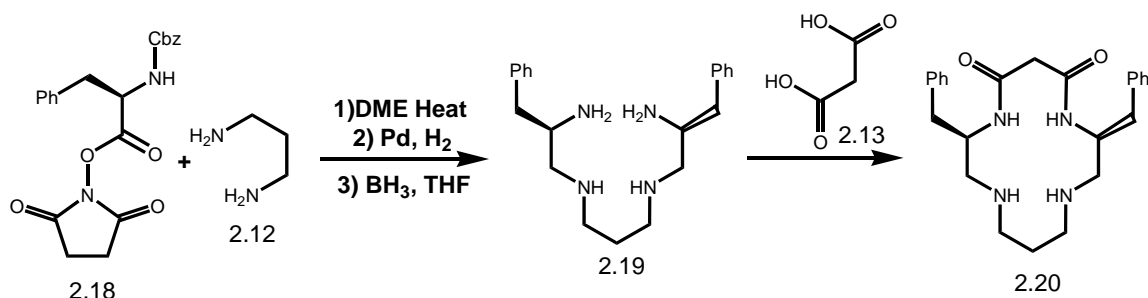
Figure 2.7: - Stereo-controlled synthesis of a macrocyclic cyclam precursor (Yield 7 12%).

There are two problems with this synthesis that make it an unfavourable route for our cyclam formation. The first is that the carbons that have been functionalized (1 and 5) are not the carbons that we wish to functionalize (1 and 6) and the second is that modifications to this route to allow SR stereocenters to be involved would require a mono-protected amine and the use of S and R amino acids in order to achieve the cis configuration of the side arms. The yield of the macrocycle formation is also very bad 7-12%.

2.1.2.2 Synthesis of 1-6 C-functionalized Cyclam Precursors and Cyclams

J. Jurczak *et al* used linearly synthesized tetraaza compounds to generate C_2 symmetric C-functionalized cyclams with 1-6 carbon functionalization[12]. In this case a diamine-ester was synthesized from an N-protected, O-activated ethanolamine followed by a divergent-convergent synthesis leading to a linear tetraaza compound. This compound was then cyclized in solution to yield a cyclopeptide precursor that was then reduced to yield the C-functionalized cyclams (Figure 2.8)
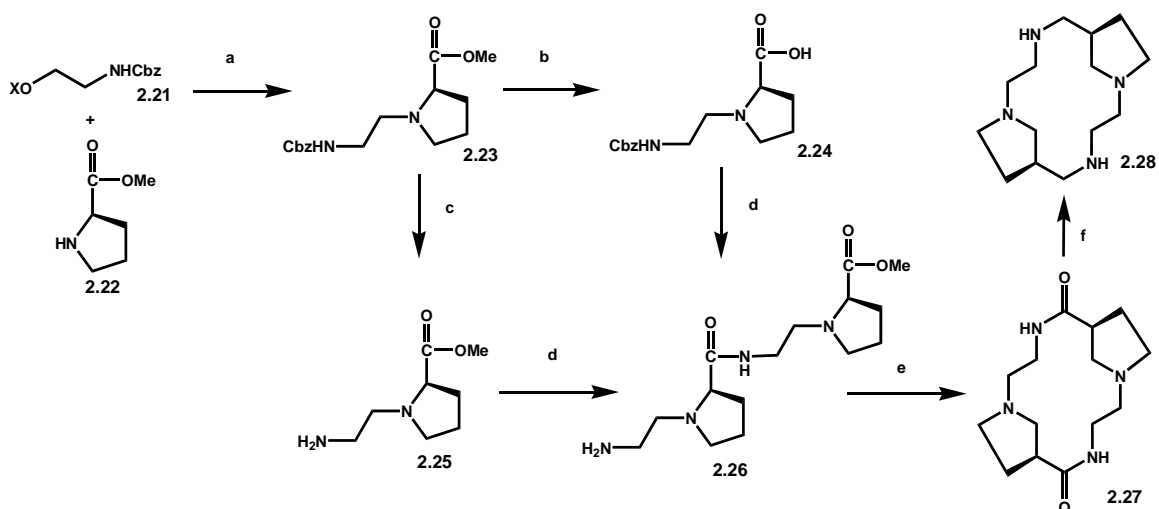
Figure 2.8: - 1-6 C-functionalized cyclams from amino acid starting materials. (a) TEA, MeCN heat. (b) H2O Heat. (c) H2 Pd/C, HCl MeOH (d) ^tButOCOCl, TEA, DCM -20oC-0oC, H2 Pd/C (e) NaOMe or NaOH in MeOH (f) BMS, THF, reflux, 20h.

Whilst an intriguing synthesis, there are several setbacks to this technique. One major setback to this synthesis is the length of time it takes to cyclize the material in solution, 28 days. Another problem is the synthesis can yield a 2:1 mixture of the SS and SR product, therefore increasing the workload via excessive purifications. In the authors opinion racemization occurs at the saponification stage of the synthesis and not during the cyclization, however this was not proven. The authors also note the formation of **2.28** as a side product of the cyclization, (Figure 2.9), indicating an intramolecular 6-exo-trig cyclization (favored by the Baldwin rules[13]) to form a 6-membered macrocycle.

2.28
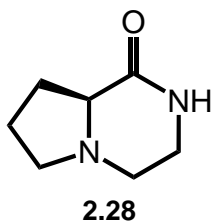
Figure 2.9: - (8a*S*)-hexahydropyrrolo[1,2-*a*]pyrazin-1(2*H*)-one (2.28), a side product of cyclization in the Jurczak's cyclization.

2.1.2.3 Cyclization of linear tetraamine ligands.

Another method of forming C-functionalized cyclam complexes is derived from the metal templated cyclization of linear amines[14] in a similar fashion to figure 2.6 (nickel template is used in this case). Here a tetraamine is coordinated to a nickel metal center and a condensation reaction with glycol proceeds to form an imine intermediate. This intermediate is then reduced with $NaBH_4$ to yield the metal complex. This methodology has several lacks stereochemical control of final products and as such was not pursued. However it must be noted that many crystal structures of C-functionalized cyclam complexes have been analyzed in literate[15].

2.1.2.4 Metal Templated Dipeptide and Tetrapeptide Cyclizations.

Several papers by Beck *et al*[16] have shown the formation of both the 1-6 C-functionalized cyclopeptides and crucially the formation of the 1-6 C-functionalized cyclams from those cyclopeptides. In these cases dipeptides (**2.29**) were synthesized and cyclized around a metal template (Pd, Ni, Cu) in good yield 70-80%. The metal template ensures that no unwanted intramolecular cyclizations occur. The cyclization leads to the formation of a metal containing tetrapeptide species and does not require high dilution or long reaction times. Freeing the cyclopeptide ligand from the metal involves treating the complex with HCl to yield **2.30** and reduction of **2.30** leads to the *cis* C_2 cyclam molecule **2.31** (Figure 2.10).
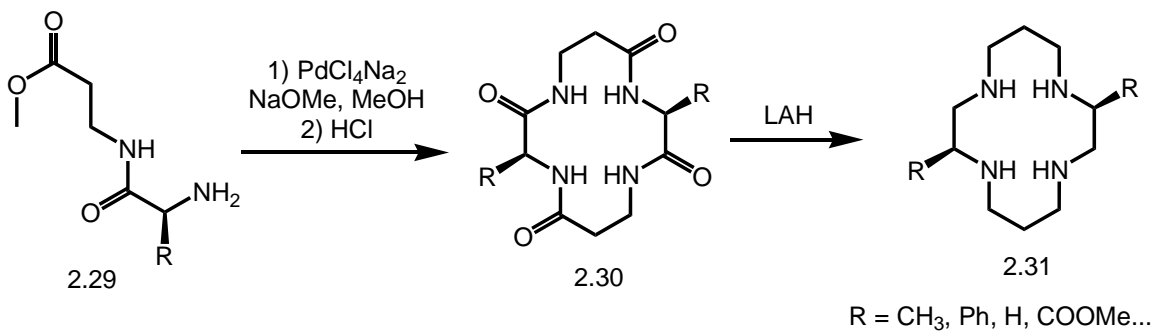
Figure 2.10: - Beck's route to cyclams utilizing amino acid cyclization.

This route was chosen as our means to synthesize the cyclams and modifications to the peptides used were envisioned to allow us to incorporate aromatic side arms including (L)-phenylalanine (previously accomplished by Beck[14a]) and 2-naphthylalanine (both L and D), a commercially available unnatural amino acid.

Modifications to Beck's approach can be utilized to form any C_2, C_i or C_1 14-membered cyclopeptide/cyclams from tetrapeptides. It must be noted that a 13-membered cyclopeptide has previously been synthesized by Beck from the tetrapeptide **3.32**, MeO-βala-ala-gly-gly-NH$_2$[14c] (Figure 2.11).
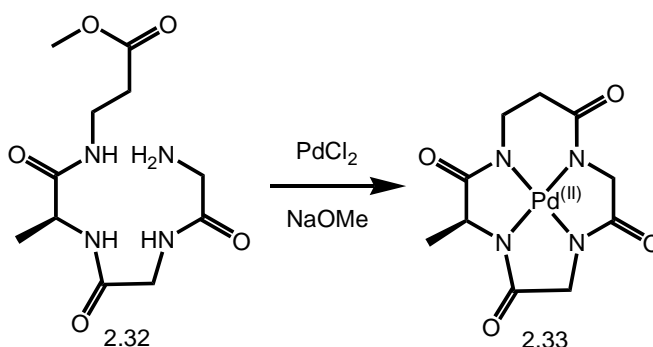
Figure 2.11: - Synthesis of a 13-membered cyclopeptide palladium complex from a tetrapeptide precursor.

Tetrapeptides can be generated by solution or solid phase chemistries, by either sequential or segment condensations. These linear peptides can then be cyclized around a nickel template to form a cyclopeptide nickel complex in a similar fashion to that shown in figure 2.11. The cyclopeptide can then be isolated by nickel removal, and the cyclopeptide can be subsequently reduced to form the desired cyclam **2.31** (Figure 2.10) Beck's synthesis will be discussed in more detail in chapter 4 but is the basis for the generation of our cyclam ligands.

For the synthesis of a 14-membered cyclam macrocycle the tetrapeptide used to form the cyclopeptide must contain two β-amino acids and two α-amino acids. Molecular modelling indicates that the aromatic arms would be more likely to form a cooperative interaction with the aromatic substrate (Figure 2.2) in the five membered rings of the nickel cyclam complex than those placed in the six membered rings of the nickel complex. This can be achieved by staring with functionalized α-amino acids in the

peptide starting materials. β-alanine is used to generate the six membered ring in the nickel cyclam complex (Figure 2.12). This is fortunate as stereospecific functionalized β-amino acids are less common and more expensive than α-amino acids.
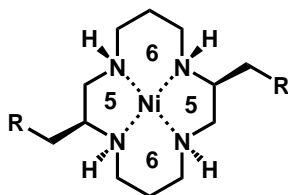
R = H, Alkyl, Aryl

Figure 2.12: - A diagram of a nickel cyclam complex, showing the five and six membered ring systems.

2.2   Solution Phase Synthesis of Dipeptides

In order to form cyclopeptides and cyclams the linear dipeptide (**2.29**) and tetrapeptide precursors (**2.34**) must be synthesized (Figure 2.13).

2.29   2.34
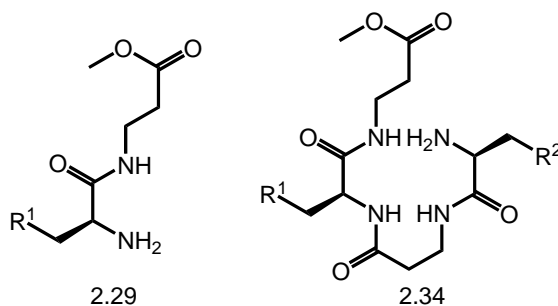
R^1, R^2 = H, Ph, 2-Nap, (4Me)Phe.

Figure 2.13: - (a) Dipeptide precursor to 14-membered cyclopeptides (b) Tetrapeptide precursor to 14-membered cyclopeptides.

The following describes the procedures and protocols developed to allow the synthesis of a large amount of dipeptide (**2.29**) and tetrapeptide (**2.34**) starting materials. Standard methods of peptide synthesis involve the use of HOBt and DCC in dry peptide grade DMF[17]. However low yields plagued this methodology in my hands. Alternative

reaction conditions were sought that would negate the DCC urea side product and allow the use of a less expensive and more easily removed solvent than DMF.

A reagent known as EDCI, a DCC mimic, was seen to have desirable properties such as increased water solubility of the urea side product due to its charge[18]. Performing the peptide coupling reaction in DCM generates products in >95% yields after 3 hours (Figure 2.14). Work up involves simply washing the DCM with water and brine to remove excess HOBt and EDCI urea with no column chromatography required to further purify the compounds generated (Figure 2.14).
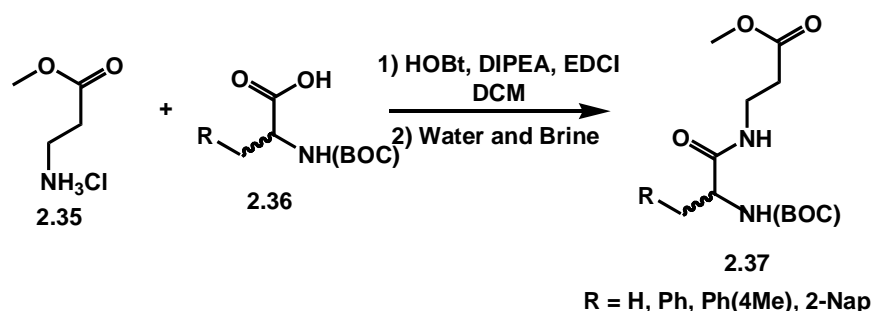
Figure 2.14: - Dipeptide synthesis utilizing EDCI, HOBt and DIPEA in DCM.

The dipeptides synthesized were a good starting point for the synthesis of the tetrapeptides and several were synthesized in good yield (Table 2.1).

Table 2.1: - Dipeptides synthesized.

Compound Name/number	Yield %	Compound Name/number	Yield %
Boc-Phe(L)-βala-OMe (2.37a)	95	Boc-Nap(D)-βala-OMe (2.37d)	94
Boc-Phe(D)-βala-OMe (2.37b)	95	Boc-Para methyl-Phe(L)-βala-OMe (2.37e)	93
Boc-Nap(L)-βala-OMe (2.37c)	93	Boc-Ala(L)-βala-OMe (2.37f)	90

2.2.1   *Crystal structure of Boc-Phe(L)-βala-OMe 2.37a*

Crystals of compound **2.37a** were grown from DCM and analysed by X-ray crystallography (Figure 2.15). The structure shown has only one configuration and is presumed to be S as was dialled into the molecule.

(a)   (b)
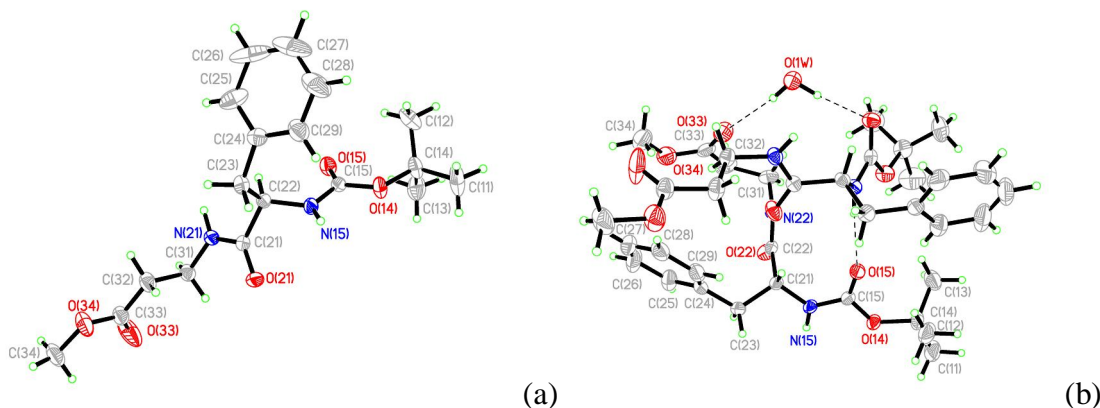
Figure 2.15: - (a) X-ray crystal structure of dipeptide 2.37a. (b) Unit cell of the dipeptide 2.37a showing hydrogen bond N-H···O interactions between two peptides and a water molecule bridging the dipeptides with O···H-O hydrogen bond interactions in 2.37a.

2.3   Synthesis: - Tetrapeptide Synthesis Through Selective Dipeptide De-protection and Coupling Reactions

2.3.1   Boc Protecting Group Removal

The BOC deprotection was accomplished via standard protocols using trifluoroacetic acid (TFA)[19] or HCl[20]. In most cases HCl was preferred as the reaction afforded a solid salt instead of oils when TFA was used (Figure 2.16).
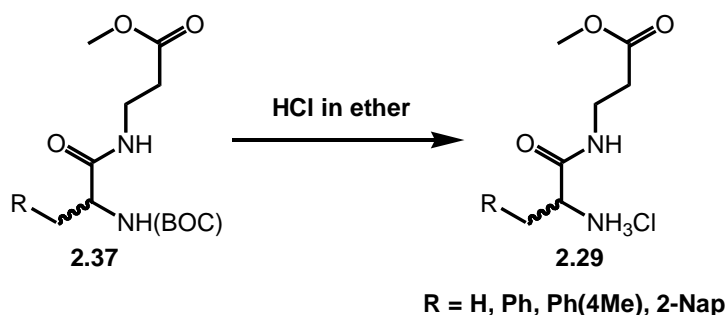
Figure 2.16: - BOC deprotection with HCl.

It is important that the reaction is monitored carefully by TLC and stopped as soon as possible. Too much acid combined with a long reaction time and heat may lead to racemization of the peptides[21]. A two-fold excess of acid was used at room temperature and the reaction was usually quenched after an hour (or when starting material was consumed by TLC). Some of the ammonium salts synthesized are shown in table 2.2. It should be noted that stereochemical integrity of the dipeptides in table 2.3 were not established at this stage of our synthesis.

Table 2.2: - Ammonium salts formed by Boc removal.

Compound Name/Number	Yield %	Compound Name/Number	Yield %
ClNH$_3$-Phe(L)- βala-OMe (2.29a)	95	ClNH$_3$-Para methyl-Phe(L)- βala-OMe (2.29d)	99
ClNH$_3$-Nap(L)- βala-OMe (2.29b)	99	ClNH$_3$-Ala-(L)- βala-OMe (2.29e)	99
ClNH$_3$-Nap(D)- βala-OMe (2.29c)	98		

2.3.3 Tetrapeptide Synthesis From Dipeptide Segment Condensations.

Retrosynthetic analysis of the desired tetrapeptides (Figure 2.17) showed that they could be synthesized from selectively deprotected dipeptides via a segment condensation.
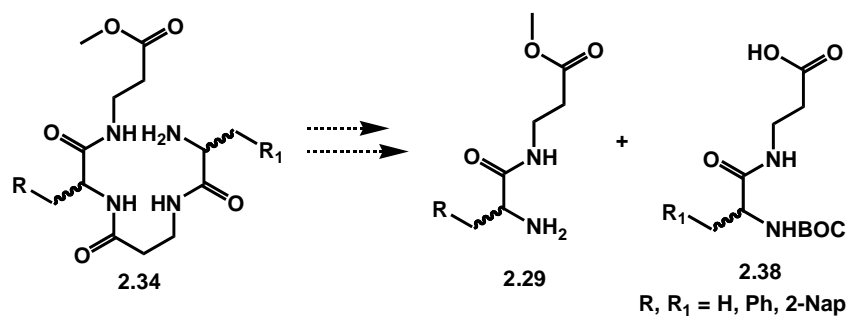
Figure 2.17: - Retrosynthetic analysis of tetrapeptide formation.

Both the ammonium salt (compounds **2.29a-e**) and the carboxylic acid dipeptide derivatives (compounds **2.38a-e**) can be synthesized directly form the dipeptide by removing the appropriate protecting group. Ester functionalities are base sensitive[22] while BOC groups are acid sensitive[10-11]. This orthogonal protecting group combination allows for the selective removal of one protecting group over the other.

2.3.4 Saponification of the Dipeptide Ester.

Ester groups can be removed easily using hydroxides in water mixtures. Some reports indicate that amino acid stereo-integrity can be compromised by prolonged exposure to strongly basic conditions[23]. Therefore during the synthesis it is important to use only a minimum amount of hydroxide (2 equivalents), monitor the conversion by TLC and work up the reaction as soon as the starting material is consumed. In this case stereochemical integrity is maintained more easily than in other cases as it is usually the carbon alpha to the ester/carboxylic acid that is affected most by basic conditions. Fortunately the dipeptide ester moiety is located on the β-alanine and this has no alpha stereocenter. Alpha protons in peptides are known to racemize under prolonged exposure to bases at elevated temperatures[21], so the reaction was closely monitored by TLC and worked up when the starting material was consumed.

Work up of the saponification reaction involves protonating the carboxylate salt and extracting the product into organic solvent. At this stage it is important to use a weak acid to protonate the salt as the acid sensitive BOC protecting group must be left in tact.

Our experiments found that 25% phosphoric acid works well for the protonation of the carboxylate salt without affecting the BOC group (Figure 2.18)
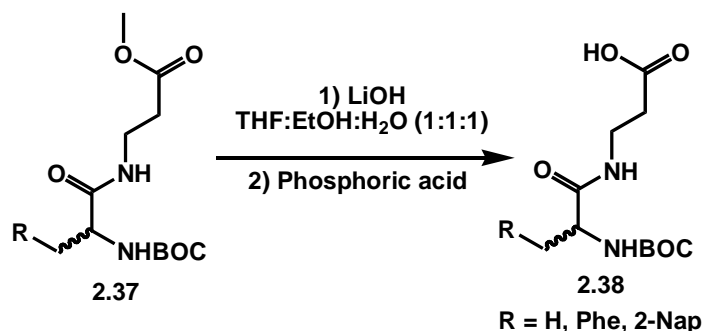
Figure 2.18: - Saponification of the dipeptide ester.

Several carboxylic acid dipeptides were synthesized to create a stock for tetrapeptide formations (Table 2.3).

Table 2.3: - Carboxylic acid dipeptides isolated.

Compound Name/Number	Yield %	Compound Name/Number	Yield %
Boc-Phe(L)-βala-OH (2.38a)	90.0	Boc-Nap(D)-βala-OH (2.38d)	84.0
Boc-Phe(D)-βala -OH (2.38b)	84.6	Boc-Ala(L)-βala -OH (2.38e)	81.0
Boc-Nap(L)-βala -OH (2.38c)	90.0		

2.3.5   Coupling of the Dipeptide Ammonium Salt and Dipeptide Carboxylic Acid: - A Segment Condensation.

The coupling of two larger peptide components (where the number of amino acids is two or more for both sides) is known as a segment condensation. This type of reaction has one major drawback. The C-terminus of the segment to be coupled often experiences

racemization when coupled and usually requires special conditions to overcome this failing[24]. However when the C-terminus does not contain any stereocenters such as in glycine and β-alanine these special conditions are no longer required and a simple EDCI/HOBt coupling can be employed with no racemization incurred. It is therefore fortunate that the C-terminus of our dipeptide acid is β-alanine or stepwise additions would need to be employed.

The coupling of a dipeptide ammonium salt (**2.29**) and a dipeptide carboxylic acid (**2.38**) precedes smoothly using similar conditions to that used to synthesize the dipeptides **3.37** (Figure 2.19). The coupling reaction takes a longer time (12-24 hours) most likely due to the increased steric bulk of the α-amino acids as the amine component[25].
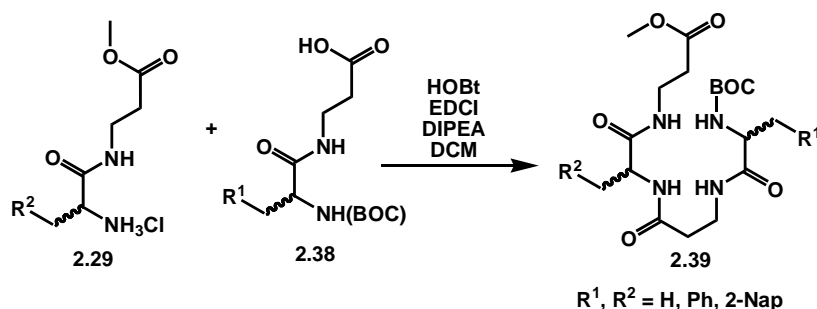
Figure 2.19: - Tetrapeptide synthesis from dipeptide ammonium salts and carboxylic acids.

Many of the tetrapeptides synthesized simply fell out of solution after synthesis. Once the product has fallen out of solution it is simply filtered and washed with water to remove any HOBt or EDCI. The tetrapeptides that did not fall out of solution (**2.39e**, **2.39f**, **2.39h** and **2.39i**) were worked up in the same manner as the dipeptides (Table 2.4).

Table 2.4: - Yields of tetrapeptides synthesized.

Compound Name/Number	Yield %	Compound Name/Number	Yield %
Boc-Phe(L)- ßala - Phe(L)- ßala -OMe (2.39a)	70-80	Boc-Nap(L)- ßala -Nap(D)- ßala -OMe (2.39f)	73.3
Boc-Phe(D)- ßala - Phe(L)- ßala -OMe (2.39b)	30.5	Boc-Phe(L)- ßala -Nap(D)- ßala -OMe (2.39g)	67.7
Boc-Ala(L)- ßala - Phe(L)- ßala -OMe (2.39c)	81.9	Boc-Ala(L)- ßala -Nap(L)- ßala -OMe (2.39h)	89.1
Boc-Ala(L)- ßala - Ala(L)- ßala -OMe (2.39d)	28	Boc-Phe (D)-ßala-Nap(D)- ßala-OMe (2.39i)	94.2
Boc-Nap(L)- ßala - Nap(L)- ßala -OMe (2.39e)	82.7		

2.3.6 BOC Removal From Tetrapeptides.

The BOC removal from the tetrapeptides (**2.39a-i**) occurs in a similar fashion to the removal of the BOC from the dipeptides (**2.29a-e**). In this case TFA is often preferred as the reagent to remove the BOC as the salts generated are solid and can be easily purified by simple washing with ether and drying (Figure 2.20, Table 2.5). However HCl is still utilized for some of the compounds.
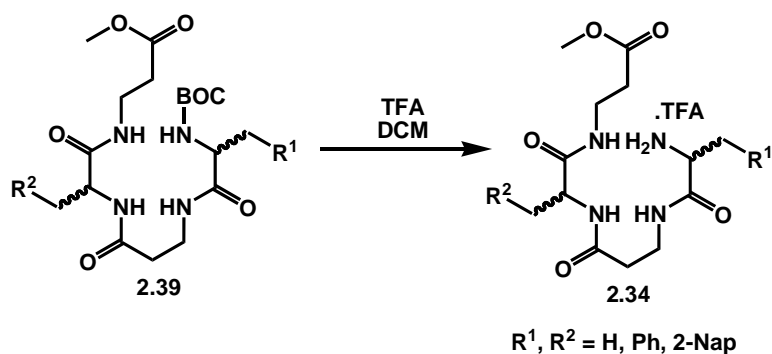
Figure 2.20: - BOC removal from tetrapeptides.

Table 2.5: - Yields of BOC removal from tetrapeptides.

Compound Name/Number	Yield %	Compound Name/Number	Yield %
H-Phe(L)- βala-Phe(L)- ßala-OMe (2.34a)	70.0	H-Ala(L)- βala-Phe(L)- ßala-OMe (2.34d)	95.0
H-Phe(L)- βala-Phe(D)- ßala-OMe (2.34b)	80.5	H-Phe(L)- βala-Nap(L)- ßala-OMe (2.34e)	95.0
H-Nap(L)- βala-Nap(L)- ßala-OMe (2.34c)	94.0	H-Nap(D)- βala-Nap(L)- ßala-OMe (2.34f)	95.0

2.4 Tetrapeptide Synthesis on Solid Support.

As well as performing solution phase tetrapeptide synthesis several tetrapeptides were synthesized on solid support using standard reaction conditions[26] including N-hydroxybenzotriazole (HOBt), diisopropylamine (DIPEA), dicyclohexyldicarbamide (DCC) and O-Benzotriazole-N,N,N',N'-tetramethyl-uronium-hexafluoro-phosphate (HBTU) (Figure 2.21, Table 2.6).

R = H, CH$_2$S(Trt), CH$_3$, (CH$_2$)$_3$NH(Trt), O(^{t}But), His(Trt), COO^{t}But, CONH$_2$.
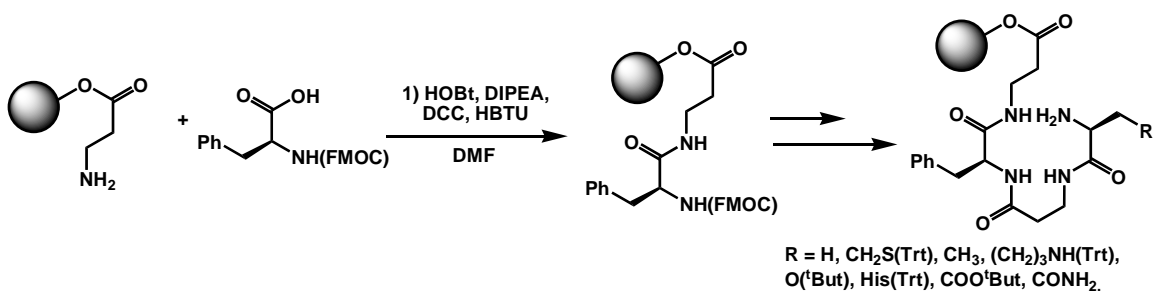
Figure 2.21: - Solid phase synthesis of tetrapeptides.

Unfortunately yields could not be determined due to variations in masses of the resins from starting materials to products. Mass spectrum analysis confirmed the presence of the products.

The stock of the trimer was synthesized in the Tomich lab with the assistance of Dr Iwamoto in high yield as shown via the ninhydrin test. Final coupling of the last amino acid was performed on a Trident Synthesizer$^®$.

Table 2.6: - Tetrapeptides synthesized on solid support.

Compound Name/Number	Mass Peak(s) *m/z*	Compound Name/Number	Mass Peak(s) *m/z*
H-Ala(L)- βala-Phe(L)- ßala-OH (2.40a)	Calculated $C_{18}H_{26}N_4O_5$ = 378.191. Actual = 379.075 (M+H)	FmocHN - His(L)(Trt)- βala-Phe(L)- ßala-OH (2.40e)	Calculated $C_{55}H_{52}N_6O_7$ = 909.038. Actual m/z 667.611 (M-Trt, +2H)
FmocHN-Ala-βala-Phe(D)-ßala-OH (2.40b)	Calculated $C_{33}H_{34}N_4O_7$ = 600.258. Actual = 601.561 (M+H)	FmocHN – Asp(L)(^{t}But)-βala-Phe(L)- βala-OH (2.40f)	Calculated $C_{37}H_{42}N_4O_9$ = 686.295. Actual = 644.610 (M-^{t}But, +H)
FmocHN – Lys(L)(Boc)-βala-Phe(L)-ßala-OH (2.40c)	Calculated $C_{41}H_{51}N_5O_9$ = 757.872 Actual m/z 658.683 (M-Boc, +H)	FmocHN – Asn(L)(Trt)- βala-Phe(L)- βala-OH (2.40g)	Calculated $C_{38}H_{44}N_4O_9$ = 700.778. Actual = 644.626(M-Trt, +H)
FmocHN – Ser(L)(^{t}But)-βala-Phe(L)-βala-OH (2.40d)	Calculated $C_{37}H_{44}N_4O_8$ = 672.767. Actual m/z 617.581(M-^{t}But+2H)	FmocHN –Ala-βala-Phe(L)- βala-OH (2.40h)	Calculated $C_{33}H_{36}N_4O_7$ = 600.662. Actual m/z 601.561(M+H)

2.5 Conclusions.

Various N-protected tetrapeptide esters of the generic formula (BOC)-NH-X-CON-βala-CON-X-CON-βala-OH were generated in high yields from dipeptides **2.29** and **2.38** using variations on standard coupling conditions. Complimentary solid support synthesis using FMOC-protected amino building blocks cleanly produced tetrapeptides as well. Yields were not determined but the small quantities obtained did not seem compatible with a multi gram demand for the further course of the project. We therefore abandoned the solid support approach.

2.6 Experimental.

All chemicals were purchased from Aldrich, Peptech Corp, Aroz Technologies, Acros Organics or Fisher Scientific and used without further purification.

2.6.1 Dipeptide synthesis.

Methyl 3-aminopropanoate hydrochloride (2.35)
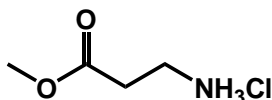
To β alanine (10.0g, 112mmol) in MeOH (100mL) at 0 °C was added thionyl chloride (19.0g, 160mmol). This was then left to stir for 10 minutes and warmed to RT. After stirring overnight the solvent was removed *in vacuo*. The residue was taken up into chloroform and the solid filtered off and dried. The solid was analyzed by NMR and showed pure product. Yield 12.8g, 82% ^{1}H NMR (400 MHz, CDCl$_3$) δ 2.95 (t, *J*=6.59 Hz, 2 H), 3.38 (t, *J*=6.78 Hz, 2 H), 3.73 - 3.76 (s, 3 H). ^{13}C NMR (101 MHz, CD$_3$OD) δ 32.07, 36.44, 52.60, 172.54.

General synthesis for dipeptides.

To the amino acid (**2.36**) (1.0 mmol), methyl 3-aminopropanoate hydrochloride (**2.35**), (152.94mg, 1.1mmol), HOBt (148.63mg, 1.1 mmol) and DIPEA (0.182mL, 1.1mmol) in DCM (20mL) at RT was slowly added EDCI (239.63mg, 1.25mmol) in small portions. This was left to stir for 4 hours. The DCM was then washed twice with water (20mL) and once with brine (20mL). The DCM was dried over magnesium sulfate and the solvent removed *in vacuo* to yield the product.

Boc-Phe(L)- βala-OMe (2.37a)
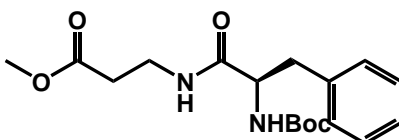
Yield 3.66g, 100%. MS: *m/z* calculated for $C_{18}H_{26}N_2O_5$ = 350.1842, actual *m/z* (M+Na) = 372.931. ^{1}H NMR (200 MHz, CDCl$_3$) δ 1.35 - 1.43 (s, 9 H) 2.26 - 2.47 (m, 2 H) 2.89 - 3.08 (m, 2 H) 3.28 - 3.52 (m, 2 H) 3.61 (s, 3 H) 4.26 (q, *J*=6.59 Hz, 1 H) 5.13 (d, *J*=8.06 Hz, 1 H) 6.37 (t, *J*=5.49 Hz, 1 H) 7.12 - 7.29 (m, 5 H). ^{13}C NMR (50 MHz, CDCl$_3$) δ 28.18, 33.49, 34.60, 38.74, 51.65, 55.91, 80.05, 126.79, 128.41, 128.52, 129.06, 129.17, 136.57, 155.19, 171.15, 172.45. IR (KBr cm^{-1}) v = 3339, 3308, 1736, 1680, 1649, 1173cm^{-1}

Boc-Phe(D)- βala-OMe (2.37b)
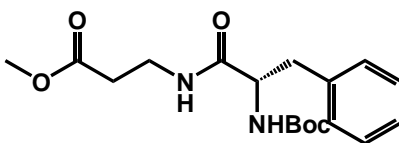
Yield 3.4g, 97%. MS: MS: *m/z* calculated for $C_{18}H_{26}N_2O_5$ = 350.1842, actual *m/z* (M+Na) = 372.931. ^{1}H NMR (400 MHz, CDCl$_3$) δ 1.41 (s, 9 H) 2.33 - 2.44 (m, 2 H) 2.97

- 3.08 (m, 2 H) 3.38 (ddd, *J*=12.40, 6.64, 6.34 Hz, 1 H) 3.48 (dt, *J*=11.81, 6.78 Hz, 1 H) 3.64 (s, 3 H) 4.28 (d, *J*=5.86 Hz, 1 H) 5.08 (s, *J*=3.51 Hz, 1 H) 6.23 - 6.34 (m, 1 H) 7.17 - 7.25 (m, 3 H) 7.26 - 7.30 (m, 2 H). ^{13}C NMR (101 MHz, CDCl$_3$) δ 28.37, 33.69, 34.82, 38.93, 51.83, 56.02, 80.13, 126.93, 128.66, 129.38, 136.84, 155.46, 171.45, 172.68.

Boc-Nap(L)-ßala-OMe (2.37c)
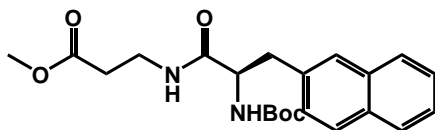
Yield 2.33g, 91.5%. MS: MS: *m/z* calculated for C$_{22}$H$_{28}$N$_2$O$_5$ = 400.1998, actual *m/z* (M+Na) = 422.975. ^{1}H NMR (400 MHz, CDCl$_3$) δ ppm 1.39 (s, 9 H) 2.27 (s, 1 H) 2.33 - 2.44 (m, 1 H) 3.14 (m, 1 H) 3.24 (m, 1H) 3.32 (m, 1 H) 3.45 (s, 3 H) 3.49 (s, 1 H) 4.35 (d, J=6.04 Hz, 1 H) 5.03 - 5.14 (m, 1 H) 6.19 - 6.30 (m, 1 H) 7.32 (d, J=8.24 Hz, 1 H) 7.39 - 7.50 (m, 2 H) 7.62 (s, 1 H) 7.73 - 7.82 (m, J=9.34 Hz, 3 H). ^{13}C NMR (50 MHz, CDCl$_3$) δ ppm 28.22, 33.46, 34.60, 38.96, 51.62, 56.02, 80.25, 125.71, 126.20, 127.29, 127.54, 127.60, 127.93, 128.36, 132.38, 133.42, 134.10, 155.24, 171.08, 172.44.

Boc-Nap(D)-ßala-OMe (2.37d)
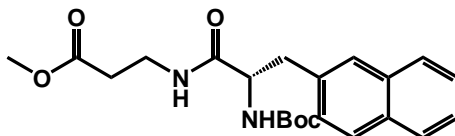
Yield 1.2g, 94.6%. ^{1}H NMR (400 MHz, CDCl$_3$) δ 1.30 - 1.46 (s, 9 H) 2.19 - 2.48 (m, 2 H) 3.09 - 3.27 (m, 2 H) 3.28 - 3.38 (m, 1 H) 3.42 - 3.47 (m, 3 H) 4.30 - 4.41 (m, 1 H) 5.12 (m, 1 H) 6.31 (s, 1 H) 7.31 (dd, *J*=8.42, 1.47 Hz, 1 H) 7.40 - 7.49 (m, 2 H) 7.61 (s, 1 H) 7.73 - 7.81 (m, 3 H). ^{13}C NMR (101 MHz, CDCl$_3$) δ 28.40, 33.67, 34.82, 39.15, 51.76, 56.14, 80.26, 125.84, 126.33, 127.52, 127.70, 127.76, 128.10, 128.47, 132.55, 133.59, 134.37, 155.44, 171.33, 172.57.

Boc-Para methyl-Phe(L)- ßala-OMe (2.37e)
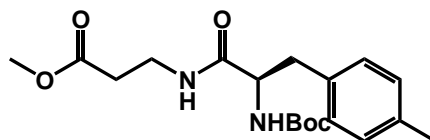
Yield 1.24g, 95%. MS: MS: *m/z* calculated for $C_{19}H_{28}N_2O_5$ = 364.1998, actual *m/z* (M+Na) = 386.992. ^{1}H NMR (200 MHz, CDCl₃) δ 1.42 (s, 9 H) 2.32 (s, 3 H) 2.34 - 2.54 (m, 2 H) 2.86 - 3.13 (m, 2 H) 3.29 - 3.59 (m, 2 H) 3.65 (s, 3 H) 4.24 (q, *J*=6.84 Hz, 1 H) 4.93 - 5.10 (m, 1 H) 6.14 - 6.30 (m, 1 H) 7.02 - 7.14 (m, 4 H). ^{13}C NMR (101 MHz, CD₃OD) δ 21.18, 28.42, 33.76, 34.84, 38.49, 51.86, 56.14, 80.18, 129.30, 129.43, 133.64, 136.57, 155.46, 171.50, 172.72.

Boc-Ala(L)-Bala-OMe (2.37f)
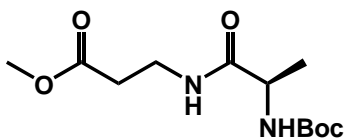
Yield 3.26g, 91.5%. MS: MS: *m/z* calculated for $C_{12}H_{22}N_2O_5$ = 274.1529, actual *m/z* (M+Na) = 296.914. ^{1}H NMR (400 MHz, CDCl₃) δ 1.28 (d, *J*=7.03 Hz, 3 H) 1.38 (s, 9 H) 2.49 (t, *J*=6.05 Hz, 2 H) 3.41 - 3.52 (m, 2 H) 3.63 (s, 3 H) 4.08 (s, 1 H) 5.20 (d, *J*=7.03 Hz, 1 H) 6.81 (s, 1 H). ^{13}C NMR (101 MHz, CDCl₃) δ 18.45, 28.20, 33.66, 34.81, 50.01, 51.65, 79.83, 155.31, 172.61, 172.79.

2.6.2 Dipeptide Ammonium Salt Synthesis.

General synthesis of dipeptide ammonium salts

The dipeptide (1mmol) was dissolved in methanol (1 mL) and HCl in methanol (1mL, 2mmol) was added. This was stirred for between 20 and 60 minutes until all starting material was consumed, as shown by TLC and the solvent was removed *in vacuo*.

ClNH$_3$-Phe-(L)-Bala-OMe (2.29a)
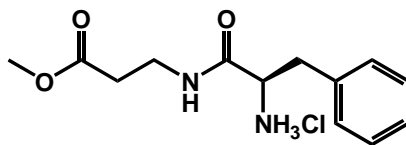
Yield 1.64g, 97.7%. MS: *m/z* calculated for C$_{13}$H$_{18}$N$_2$O$_3$ = 250.1317, actual *m/z* (M+Na) = 273.869. ^{1}H NMR (200 MHz, D$_2$O) δ 2.00 - 2.21 (m, 2 H) 2.80 - 2.99 (m, 3 H) 3.06 - 3.23 (m, 1 H) 3.31 (s, 3 H) 3.79 (dd, *J*=8.61, 6.78 Hz, 1 H) 6.85 - 6.98 (m, 2 H) 6.98 - 7.09 (m, 3 H). ^{13}C NMR (50 MHz, CDCl$_3$) δ 32.93, 35.19, 37.51, 52.01, 55.19, 128.16, 129.19, 129.25, 133.31, 168.33, 172.69.

ClNH$_3$-Nap(L)-Bala-OMe (2.29b)
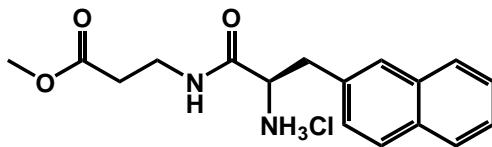
Yield 840mg, 99.6%. ^{1}H NMR (200 MHz, D$_2$O) δ ppm 1.95 - 2.12 (m, 1 H) 2.16 - 2.32 (m, 1 H) 2.91 - 3.20 (m, 2 H) 3.25 (s, 3 H) 3.28 - 3.51 (m, 2 H) 3.53 - 3.82 (m, 1 H) 4.19 (dd, *J*=9.71, 6.04 Hz, 1 H) 7.34 (d, *J*=8.42 Hz, 1 H) 7.52 (dd, *J*=5.68, 2.75 Hz, 2

H) 7.68 (s, 1 H) 7.87 (d, J=8.42 Hz, 3 H). ^{13}C NMR (50 MHz, D$_2$O) δ ppm 32.55, 34.17, 36.71, 51.71, 53.92, 126.09, 126.38, 126.60, 127.21, 127.35, 127.84, 128.35, 131.10, 132.02, 132.71, 168.28, 173.48.

ClNH$_3$-Nap(D)-Bala-OMe (2.29c)
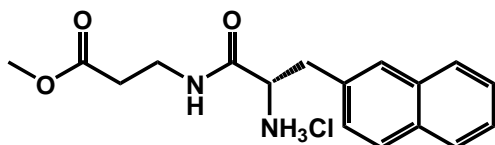
Yield 168mg, 78.9%. ^{1}H NMR (400 MHz, CD$_3$OD) δ 2.27 - 2.39 (m, 2 H) 3.21 - 3.32 (m, 4 H) 3.36 - 3.45 (m, 1 H) 3.45 - 3.51 (m, 3 H) 4.18 (t, J=7.42 Hz, 1 H) 7.35 - 7.45 (m, 3 H) 7.73 (s, 1 H) 7.76 - 7.83 (m, 3 H). ^{13}C NMR (101 MHz, CD$_3$OD) δ 34.21, 36.22, 38.70, 52.18, 55.58, 127.11, 127.36, 128.16, 128.67, 128.73, 129.56, 129.72, 133.05, 134.15, 134.88, 169.52, 173.34.

ClNH$_3$-Phe(4-Me)-(L)-Bala-OMe (2.29d)
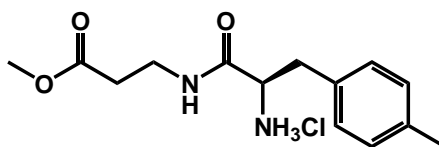
Yield 97.7%. ^{1}H NMR (400 MHz, METHANOL-D4) δ 2.16 - 2.23 (m, 3 H) 2.29 - 2.41 (m, 2 H) 2.93 - 3.04 (m, 2 H) 3.19 - 3.30 (m, 2 H) 3.32 - 3.41 (m, 1 H) 3.53 - 3.57 (m, 3 H) 3.96 (t, J=7.22 Hz, 1 H) 5.18 (none, 1 H) 7.07 (s, 4 H). ^{13}C NMR (101 MHz, CD$_3$OD) δ 19.99, 33.12, 35.07, 37.02. 51.12, 54.56, 129.26, 129.42, 131.31, 137.35, 168.41, 172.27.

TFA.NH₃-Ala(L)-Bala-OMe (2.29e)
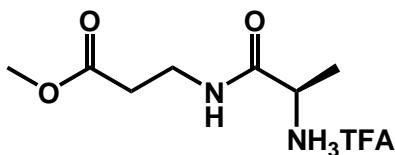
Yield 651mg, 100%. ^{1}H NMR (400 MHz, DMSO-D6) δ 1.29 (d, *J*=7.03 Hz, 3 H) 2.49 (m, 2 H) 3.27 - 3.38 (m, 2 H) 3.55 - 3.61 (m, 3 H) 3.76 (ddd, *J*=11.52, 6.05, 5.86 Hz, 1 H) 8.03 - 8.13 (m, 3 H) 8.49 (t, *J*=5.47 Hz, 1 H) ^{13}C NMR (101 MHz, DMSO-D6) δ 17.16, 33.33, 34.87, 48.16, 51.46, 169.51, 171.57.

2.6.3 Carboxylic Acid Dipeptide Synthesis.

General synthesis of dipeptide acids

The Bis-protected dipeptide (1mmol) was dissolved in Water:THF:Ethanol (1:1:1, 2mL) and the KOH (2mmol) was added. This was stirred at RT for 30 minutes until all starting material was consumed as shown by TLC. To the mixture was added diluted phosphoric acid (25%) until the solution was acidified. The product was extracted with ethyl acetate, washed with water and brine and dried over magnesium sulfate. The organic solvent was removed *in vacuo*.

Boc-Phe(L)-Bala-OH (2.38a)
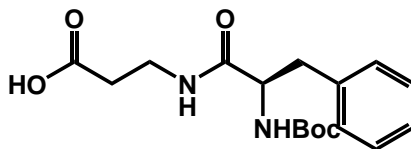
Yield 1.09g, 92.3%. ^{1}H NMR (200 MHz, CDCl$_3$) δ 1.38 (s, 9 H) 2.23 - 2.68 (m, 2 H) 2.99 (d, J=6.59 Hz, 2 H) 3.25 - 3.66 (m, 2 H) 4.58 (m, 1 H) 5.48 (d, J=6.59 Hz, 1 H) 6.85 - 7.09 (m, 1 H) 7.12 - 7.37 (m, 5 H) 10.22 - 10.82 (m, 1 H). ^{13}C NMR (101 MHz, CDCl$_3$) δ 28.43, 33.70, 34.66, 39.34, 55.75, 80.80, 127.09, 128.70, 129.46, 136.74, 156.05, 171.93, 175.64.

Boc-Phe(D)-Bala-OH (2.38b)
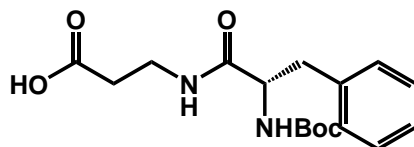
Yield 865mg, 90.2%. MS: *m/z* calculated for C$_{17}$H$_{24}$N$_2$O$_5$ = 336.1685, actual *m/z* (M+Na) = 358.946. ^{1}H NMR (200 MHz, CDCl$_3$) δ 1.23 - 1.53 (s, 9 H) 2.13 - 2.69 (m, 2 H) 2.98 (d, J=6.96 Hz, 2 H) 3.24 - 3.74 (m, 2 H) 4.23 - 4.70 (m, 1 H) 5.61 (d, J=8.79 Hz, 1 H) 6.85 - 7.39 (m, 6 H) 9.88 (bs, 1 H). ^{13}C NMR (50 MHz, CDCl$_3$) δ 28.43, 33.70, 34.67, 39.33, 55.74, 80.79, 127.09, 128.69, 129.45, 136.73, 156.05, 171.94, 175.63.

Boc-Nap(L)-Bala-OH (2.38c)
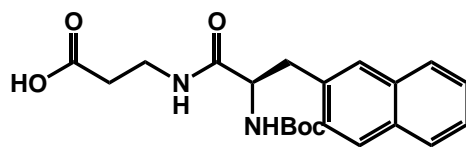
Yield 84.4mg, 98.4%. MS: *m/z* calculated for C$_{21}$H$_{26}$N$_2$O$_5$ = 386.1842, actual *m/z* (M+Na) = 409.003. ^{1}H NMR (200 MHz, CDCl$_3$) δ 1.34 (s, 9 H) 2.35 (d, J=12.45 Hz, 2 H) 3.14 (d, J=7.33 Hz, 2 H) 3.35 (m, 2 H) 4.60 (m, 1 H) 5.35 (m, 1 H) 6.86 (m, 1 H) 7.36 - 7.50 (m, 2 H) 7.61 (s, 1 H) 7.70 - 7.84 (m, 4 H). ^{13}C NMR (50 MHz, CDCl$_3$) δ 27.95, 33.30, 34.65, 38.81, 55.47, 80.16, 125.37, 125.84, 127.16, 127.31, 127.38, 127.81, 127.92, 132.16, 133.20, 133.94, 155.75, 172.12, 175.16.

Boc-Nap(D)-Bala-OH (2.38d)
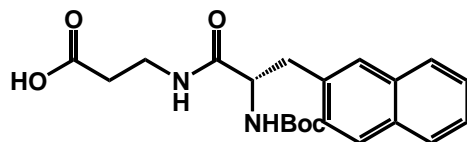
Yield 1.06g, 100%. ^{1}H NMR (400 MHz, CDCl$_3$) δ 1.31 (s, 9 H) 2.23 (m, 1 H) 2.35 (m, 1 H) 3.05 - 3.16 (m, 2 H) 3.26 (m, 1 H) 3.30 - 3.41 (m, 1 H) 4.62 (q, *J*=7.03 Hz, 1 H) 5.57 (d, *J*=7.42 Hz, 1 H) 7.02 (s, 1 H) 7.21 - 7.30 (m, 1 H) 7.33 - 7.44 (m, 2 H) 7.58 (s, 1 H) 7.67 - 7.77 (m, 3 H) 10.79 (s, 1 H). ^{13}C NMR (101 MHz, CDCl$_3$) δ 28.37, 33.62, 34.68, 39.37, 55.67, 80.85, 125.80, 126.28, 127.51, 127.66, 127.80, 128.17, 128.36, 132.57, 133.59, 134.22, 156.07, 172.03, 175.67.

Boc-Ala(L)-Bala-OH (2.38e)
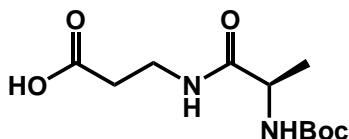
Yield 519mg, 99.5%. ^{1}H NMR (200 MHz, CDCl$_3$) δ 1.34 (d, J=6.59 Hz, 3 H) 1.43 (s, 9 H) 2.59 (d, J=5.13 Hz, 2 H) 3.54 (d, J=5.13 Hz, 2 H) 4.31 (s, 1 H) 5.44 - 5.77 (m, 1 H) 7.19 - 7.41 (m, 1 H) 9.84 (s, 1 H). ^{13}C NMR (50 MHz, CDCl$_3$) δ 18.53, 28.20, 33.66, 34.79, 49.90, 80.45, 155.83, 173.49, 175.46.

2.6.4 Tetrapeptide Synthesis.

General synthesis of tetrapeptides

To dipeptide carboxylic acid **2.38** (1mmol), the dipeptide ammonium salt **2.29** (0.9mmol), HOBt (1.1mmol) and DIPEA (1.1mmol) in DCM (20mL) was added the EDCI (1.25mmol) slowly in small portions. This was left to stir at room temperature overnight. A solid precipitate formed and was filtered, washed with DCM, water and ether. For compounds that did not drop out of solution (**2.39e-i**) the DCM was simply washed with water, brine and dried with magnesium sulfate. The solvent was then removed to yield the product.

Boc-Phe(L)-Bala-Phe(L)-Bala-OMe (2.39a)
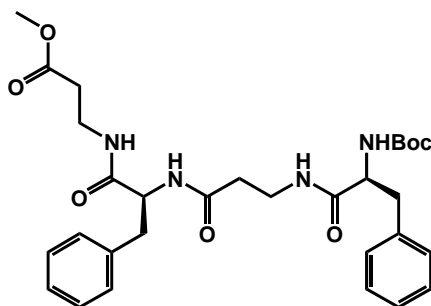
Yield 1.51g, 80.6%. MS: *m/z* calculated for $C_{30}H_{40}N_4O_7$ = 568.2897, actual *m/z* (M+Na) = 591.196. ^{1}H NMR (200 MHz, CDCl$_3$) δ 1.37 (s, 9 H) 2.09 - 2.27 (m, 1 H) 2.28 - 2.48 (m, 3 H) 2.90 - 3.08 (m, 3 H) 3.08 - 3.22 (m, 1 H) 3.23 - 3.41 (m, 2 H) 3.45 - 3.60 (m, 2 H) 3.63 (s, 3 H) 4.35 (q, *J*=6.96 Hz, 1 H) 4.50 (q, *J*=7.45 Hz, 1 H) 5.23 (d, *J*=7.69 Hz, 1 H) 6.34 (s, 1 H) 6.54 (d, *J*=7.33 Hz, 1 H) 7.00 (s, 1 H) 7.16 - 7.35 (m, 10 H). ^{13}C NMR (50 MHz, CDCl$_3$) δ 28.24, 33.40, 34.80, 36.04, 36.30, 38.09, 38.34, 51.85, 53.42, 55.32, 56.17, 80.04, 126.85, 127.06, 128.54, 128.72, 129.04, 129.30, 136.47, 136.73, 136.80, 155.68, 171.15, 171.99, 172.83.

Boc-Phe(L)-Bala-Phe(D)-Bala-OMe (2.39b)
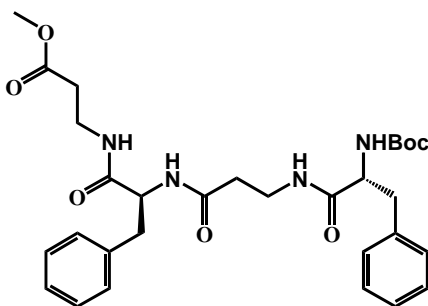
Yield 0.9g, 57.3%. MS: *m/z* calculated for $C_{30}H_{40}N_4O_7$ = 568.2897, actual *m/z* (M+Na) = 591.196. ^{1}H NMR (400 MHz, CDCl$_3$) δ 1.39 (s, 9 H) 2.13 - 2.25 (m, 1 H) 2.28 - 2.40 (m, 2 H) 2.40 - 2.50 (m, 1 H) 2.95 - 3.05 (m, 4 H) 3.31 - 3.43 (m, 3 H) 3.44 - 3.54 (m, 1 H) 3.60 - 3.69 (m, 3 H) 4.22 (q, *J*=7.29 Hz, 1 H) 4.55 (q, *J*=7.16 Hz, 1 H) 5.14 (d, *J*=7.03 Hz, 1 H) 6.27 - 6.39 (m, 2 H) 6.46 (s, 1 H) 7.11 - 7.21 (m, 5 H) 7.21 - 7.31 (m, 5 H). ^{13}C NMR (101 MHz, CDCl$_3$) δ 28.51, 33.71, 34.99, 35.65, 35.98, 38.35, 38.51, 39.17, 52.06, 54.78, 80.25, 127.07, 127.25, 128.77, 128.89, 129.35, 129.57, 136.98, 170.75, 171.38, 171.58, 172.91, 183.83.

Boc-Phe(L)-Bala-Ala(L)-Bala-OMe (2.39c)
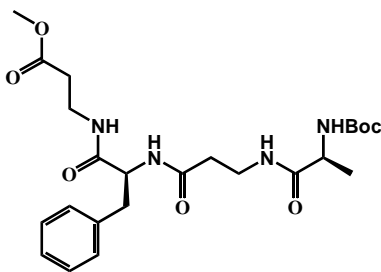
Yield 81%. ^{1}H NMR (400 MHz, CDCl$_3$) δ ppm 1.30 - 1.39 (m, 3 H) 1.39 - 1.44 (m, 9 H) 2.22 - 2.34 (m, 1 H) 2.36 - 2.46 (m, 3 H) 3.03 (d, *J*=7.42 Hz, 2 H) 3.22 (s, 1 H) 3.29 - 3.40 (m, 1 H) 3.46 - 3.56 (m, 1 H) 3.63 - 3.69 (m, 3 H) 3.78 (s, 1 H) 4.07 - 4.18 (m, 1 H) 4.51 (q, *J*=7.42 Hz, 1 H) 5.20 (d, *J*=7.03 Hz, 1 H) 6.33 (s, 1 H) 6.77 (s, 1 H) 7.19 -

7.31 (m, 6 H) ^{13}C NMR (101 MHz, CDCl$_3$) δ ppm 18.77, 28.31, 33.53, 34.83, 35.68, 38.30, 50.14, 51.78, 54.48, 79.90, 126.91, 128.56, 129.15, 136.70, 155.41, 170.79, 171.34, 172.56, 173.09,.

<u>Boc-Ala(L)-Bala-Ala(L)-Bala-OMe (2.39d)</u>
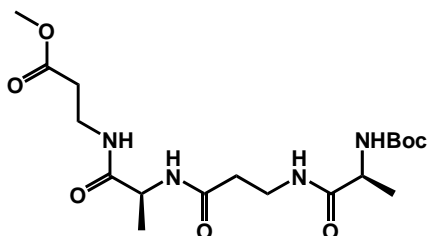
Yield 179mg, 38.8%. ^{1}H NMR (200 MHz, DMSO-D6) δ 1.11 (d, *J*=2.93 Hz, 3 H) 1.15 (d, *J*=2.93 Hz, 3 H) 1.36 (s, 9 H) 2.25 (t, *J*=6.78 Hz, 2 H) 2.39 - 2.46 (m, 1 H) 2.59 (s, 1 H) 3.14 - 3.33 (m, 4 H) 3.58 (s, 3 H) 3.76 - 3.96 (m, 1 H) 4.09 - 4.26 (m, 1 H) 6.84 (d, *J*=6.96 Hz, 1 H) 7.73 (t, *J*=5.13 Hz, 1 H) 7.92 (t, *J*=5.49 Hz, 1 H) 8.01 (d, *J*=7.33 Hz, 1 H). ^{13}C NMR (101 MHz, DMSO-D6) δ 18.16, 18.25, 28.15, 33.54, 34.68, 35.05, 35.16, 48.08, 49.71, 31, 77.95, 158.65, 170.15, 171.54, 172.38, 172.53.

<u>Boc-Nap(L)-Bala-Nap(L)-Bala-OMe (2.39e)</u>
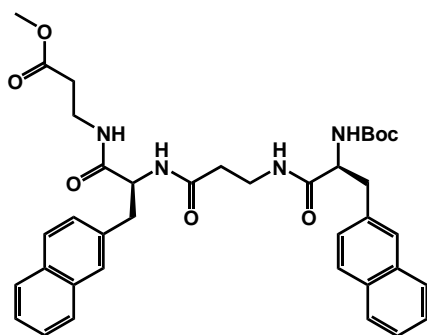
Yield 82.7%. ^{1}H NMR (200 MHz, CDCl$_3$) δ 1.27 - 1.38 (s, 9 H) 2.05 - 2.22 (m, 1 H) 2.22 - 2.43 (m, 3 H) 3.06 (d, J=6.59 Hz, 2 H) 3.10 - 3.32 (m, 4 H) 3.39 - 3.46 (m, 3 H) 3.47 - 3.70 (m, 2 H) 4.39 - 4.60 (m, 2 H) 5.31 (d, J=6.59 Hz, 1 H) 6.34 (s, 1 H) 6.48 (d, J=6.59 Hz, 1 H) 7.05 (t, J=5.49 Hz, 1 H) 7.33 (d, J=8.79 Hz, 1 H) 7.37 - 7.49 (m, 5 H)

7.58 (s, 1 H) 7.66 (s, 1 H) 7.70 - 7.75 (m, 3 H) 7.76 - 7.82 (m, 3 H). ^{13}C NMR (101 MHz, CDCl$_3$) δ 28.39, 33.57, 35.05, 36.23, 36.39, 38.41, 38.77, 51.88, 55.47, 56.27, 80.18, 125.83, 125.95, 126.29, 126.44, 127.32, 127.70, 127.82, 127.94, 128.23, 128.31, 128.53, 132.55, 133.58, 133.62, 134.40, 134.60, 155.94, 171.52, 172.16, 172.36, 172.81.

Boc-Nap(L)-Bala-Nap(D)-Bala-OMe (2.39f)
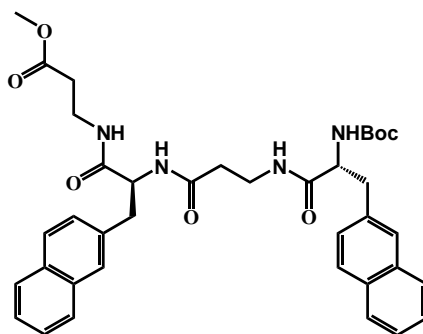
Yield 2.5g, 73.3%. ^{1}H NMR (400 MHz, DMSO-D6) δ 1.22 (s, 9 H) 2.15 - 2.21 (m, 1 H) 2.23 - 2.29 (m, 1 H) 2.33 - 2.42 (m, 2 H) 2.87 - 2.96 (m, 2 H) 3.06 - 3.17 (m, 4 H) 3.54 (s, 3 H) 4.18 (td, J=9.22, 4.10 Hz, 1 H) 4.54 (td, J=8.49, 5.56 Hz, 1 H) 6.89 (d, J=8.49 Hz, 1 H) 7.37 - 7.48 (m, 7 H) 7.69 (s, 2 H) 7.78 (s, 2 H) 7.79 (d, J=5.56 Hz, 3 H) 7.84 (d, J=8.49 Hz, 2 H) 7.92 (t, J=5.42 Hz, 1 H) 8.10 (t, J=5.42 Hz, 1 H) 8.20 (d, J=8.20 Hz, 1 H). ^{13}C NMR (101 MHz, DMSO-D6) δ 28.07, 33.47, 34.74, 35.08, 35.29, 37.84, 38.04, 51.36, 53.99, 55.72, 78.00, 125.35, 125.93, 127.31, 127.37, 127.46, 127.81, 131.80, 132.94, 135.63, 135.98, 155.18, 170.24, 171.16, 171.47, 171.66.

Boc-Phe(L)-Bala-Nap(L)-Bala-OMe (2.39g)
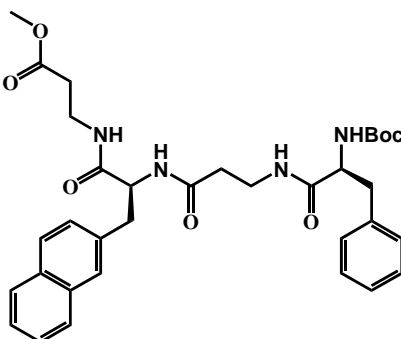
Yield 700mg, 67.7%. MS: *m/z* calculated for $C_{34}H_{42}N_4O_7$ = 618.3053, actual *m/z* (M+Na) = 641.277. ^{1}H NMR (200 MHz, CDCl$_3$) δ 1.36 (s, 9 H) 2.13 - 2.28 (m, 1 H) 2.28 - 2.45 (m, *J*=4.03 Hz, 3 H) 2.96 (s, 1 H) 3.06 - 3.29 (m, 5 H) 3.43 - 3.50 (m, 3 H) 3.51 - 3.73 (m, 2 H) 4.28 - 4.46 (m, 1 H) 4.62 (q, *J*=7.20 Hz, 1 H) 5.25 (d, *J*=7.69 Hz, 1 H) 6.42 (s, 1 H) 6.67 (d, *J*=6.96 Hz, 1 H) 7.08 (s, 1 H) 7.16 - 7.39 (m, 5 H) 7.40 - 7.53 (m, 3 H) 7.64 (s, 1 H) 7.79 (d, *J*=6.96 Hz, 3 H). ^{13}C NMR (101 MHz, CDCl$_3$) δ 28.46, 33.57, 35.05, 36.26, 36.50, 38.57, 51.93, 55.51, 56.35, 80.22, 126.02, 126.52, 127.03, 127.30, 127.73, 127.86, 127.97, 128.65, 128.73, 129.52, 132.61, 133.62, 134.36, 137.05, 155.96, 171.45, 172.20, 172.26, 172.89.

Boc-Ala(L)-Bala-Nap(L)-Bala-OMe (2.39h)
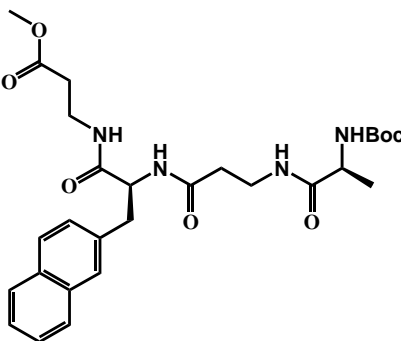
Yield 720mg, 89.1%. ^{1}H NMR (400 MHz, CDCl$_3$) δ 1.32 (d, *J*=7.42 Hz, 3 H) 1.37 - 1.45 (m, 9 H) 2.20 - 2.47 (m, 4 H) 3.15 - 3.27 (m, 4 H) 3.43 - 3.48 (m, 3 H) 3.48 - 3.57 (m, 1 H) 3.63 - 3.73 (m, 1 H) 4.11 - 4.21 (m, 1 H) 4.70 (q, *J*=7.42 Hz, 1 H) 5.50 (d,

J=7.03 Hz, 1 H) 6.90 (t, *J*=5.47 Hz, 1 H) 7.20 (d, *J*=7.42 Hz, 1 H) 7.32 (d, *J*=8.20 Hz, 1 H) 7.38 - 7.47 (m, 3 H) 7.61 (s, 1 H) 7.72 (t, *J*=4.49 Hz, 2 H) 7.73 - 7.78 (m, 1 H). ^{13}C NMR (101 MHz, CDCl₃) δ 18.46, 28.48, 33.62, 35.03, 36.35, 36.46, 38.51, 50.64, 51.82, 55.59, 79.97, 125.87, 126.37, 127.38, 127.65, 127.76, 127.91, 128.41, 132.51, 133.54, 134.48, 155.92, 171.81, 172.40, 172.68, 173.79.

Boc-Phe(D)-Bala-Nap(L)-Bala-OMe (2.39i)
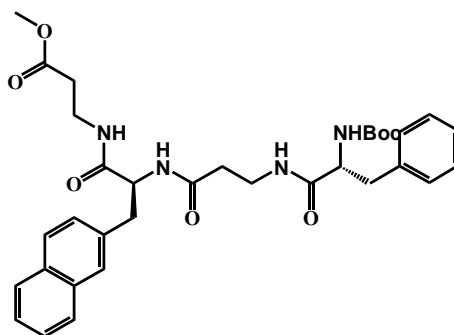
Yield 1.62g, 94.2%. ^{1}H NMR (400 MHz, CDCl₃) δ 1.31 (s, 9 H) 2.26 (m, 2 H) 2.33 - 2.41 (m, 2 H) 2.89 - 3.01 (m, 2 H) 3.14 (d, *J*=7.42 Hz, 2 H) 3.19 - 3.31 (m, 2 H) 3.37 (s, 2 H) 3.42 - 3.53 (m, 4 H) 4.40 (d, *J*=6.25 Hz, 1 H) 4.76 (q, *J*=7.29 Hz, 1 H) 5.57 (d, *J*=7.03 Hz, 1 H) 6.89 (s, 1 H) 6.97 (s, 1 H) 7.11 - 7.17 (m, 3 H) 7.19 - 7.27 (m, 3 H) 7.36 - 7.48 (m, 2 H) 7.56 (s, 1 H) 7.66 - 7.77 (m, 3 H). ^{13}C NMR (101 MHz, CDCl₃) δ 28.41, 33.65, 35.05, 35.66, 35.72, 39.13, 39.50, 51.82, 54.78, 55.90, 79.91, 125.84, 126.33, 126.82, 127.52, 127.70, 127.75, 128.01, 128.32, 128.53, 129.53, 132.50, 133.54, 134.33, 137.08, 155.53, 171.05, 171.27, 171.83, 172.48.

2.6.5 *Tetrapeptide Ammonium Salt Synthesis.*

The tetrapeptide (1mmol) was dissolved in methanol (1 mL) and HCl in Methanol (1mL, 2mmol) or TFA (1ml, 20% in DCM) was added. This was stirred for 20-60 minutes until all starting material was consumed as shown by TLC and the solvent removed *in vacuo*.

H-Phe(L)-Bala-Phe(L)-Bala-OMe (2.34a)
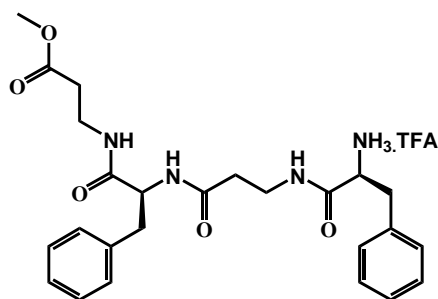
Yield 70%. MS: *m/z* calculated for $C_{25}H_{32}N_4O_5$ = 468.2373, actual *m/z* (M+Na) = 491.105. ^{1}H NMR (200 MHz, CD$_3$OD) δ 2.14 - 2.32 (m, 1 H) 2.33 - 2.53 (m, 3 H) 2.78 - 3.20 (m, 5 H) 3.33 - 3.44 (m, 3 H) 3.64 (s, 3 H) 3.97 (t, *J*=7.33 Hz, 1 H) 4.50 (dd, *J*=8.42, 6.59 Hz, 1 H) 7.10 - 7.44 (m, 10 H). ^{13}C NMR (50 MHz, CD$_3$OD) δ 34.40, 35.85, 36.19, 36.92, 38.62, 39.06, 52.22, 55.87, 56.24, 127.85, 128.86, 129.48, 130.10, 130.25, 130.46, 135.67, 138.31, 169.62, 173.22, 173.71, 173.78,

H-Phe(L)-Bala-Phe(D)-Bala-OMe (2.34b)
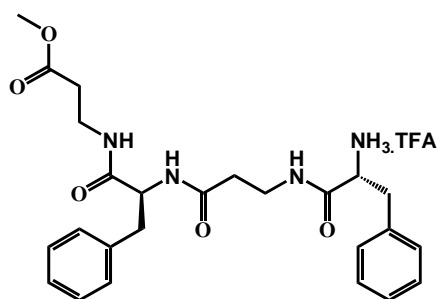
Yield 262mg, 80.5% ^{1}H NMR (400 MHz, D$_2$O) δ 2.27 - 2.35 (m, 3 H) 2.37 - 2.41 (m, 1 H) 2.91 - 3.01 (m, 2 H) 3.09 (d, *J*=7.42 Hz, 2 H) 3.17 - 3.29 (m, 2 H) 3.29 - 3.41 (m, 2 H) 3.56 - 3.67 (m, 3 H) 4.08 (t, *J*=7.42 Hz, 1 H) 4.45 (t, *J*=7.61 Hz, 1 H) 7.22 (t, *J*=7.22 Hz, 4 H) 7.27 - 7.38 (m, 6 H). ^{13}C NMR (101 MHz, CD$_3$OD) δ 34.40, 36.06, 36.19, 36.95, 38.60, 39.02, 52.18, 55.83, 56.25, 127.79, 128.78, 129.44, 130.03, 130.24, 130.48, 135.70, 138.28, 169.53, 173.17, 173.61, 173.71.

H-Nap(L)-Bala-Nap(L)-Bala-OMe (2.34c)
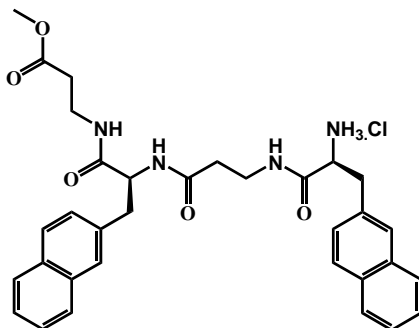
Yield 424mg, 93.6% MS: *m/z* calculated for $C_{33}H_{36}N_4O_5$ = 568.2686, actual *m/z* (M+Na) = 591.248. ^{1}H NMR (200 MHz, CD$_3$OD) δ 2.12 - 2.30 (m, 1 H) 2.30 - 2.50 (m, 3 H) 3.04 (dd, *J*=13.92, 8.79 Hz, 1 H) 3.13 - 3.26 (m, 4 H) 3.33 - 3.46 (m, 3 H) 3.48 - 3.55 (m, 3 H) 4.12 (m, 1 H) 4.61 (dd, *J*=8.61, 6.41 Hz, 1 H) 7.31 - 7.50 (m, 6 H) 7.68 (s, 1 H) 7.71 - 7.88 (m, 7 H) ^{13}C NMR (50 MHz, CD$_3$OD) δ 34.34, 35.96, 36.17, 36.92, 38.62, 39.09, 52.19, 55.71, 56.20, 126.58, 127.03, 127.09, 127.36, 128.11, 128.35, 128.53, 128.65, 128.70, 128.85, 128.99, 129.56, 129.72, 133.01, 133.72, 134.11, 134.74, 134.83, 135.78, 138.66, 169.53, 173.16, 173.55, 173.60.

H-Ala(L)-Bala-Phe(L)-Bala-OMe (2.34d)
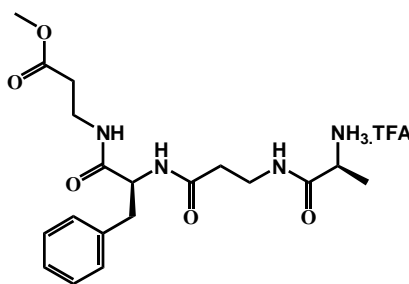
Yield 805mg, 95%. MS: *m/z* calculated for $C_{19}H28N_4O_5$ = 392.206, actual *m/z* (M+Na) = 415.033. ^{1}H NMR (200 MHz, CD$_3$OD) δ 1.24 (d, *J*=6.96 Hz, 3 H) 2.09 - 2.30 (m, 4 H) 2.66 (dd, *J*=12.45, 8.79 Hz, 1 H) 2.85 (dd, *J*=13.74, 6.78 Hz, 1 H) 3.07 - 3.27 (m, 4 H) 3.42 (s, 3 H) 3.67 (q, *J*=6.96 Hz, 1 H) 4.31 (m, 1 H) 6.93 - 7.10 (m, 5 H). [13]C

NMR (50 MHz, CD$_3$OD) δ 17.56, 34.40, 36.20, 37.03, 38.99, 50.25, 52.22, 56.25, 127.79, 129.43, 130.24, 138.31, 170.99, 173.28, 173.62, 173.74.

H-Phe(D)-Bala-Nap(L)-Bala-OMe (2.35e)
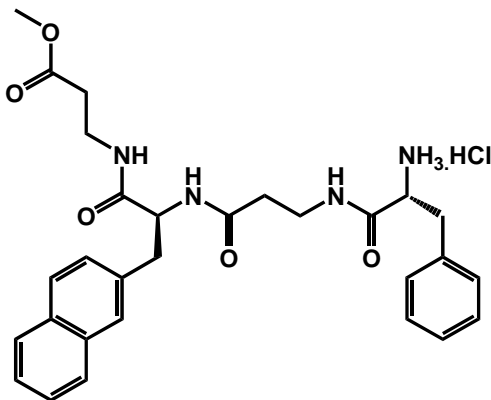
Yield 1.5g, 95% ^{1}H NMR (400 MHz, CD$_3$OD) δ 2.27 - 2.38 (m, 4 H) 3.00 (dd, J=14.06, 8.20 Hz, 1 H) 3.04 (dd, J=13.67, 8.59 Hz, 1 H) 3.16 (dd, J=14.06, 7.03 Hz, 2 H) 3.24 (dd, J=14.06, 7.42 Hz, 2 H) 3.32 - 3.43 (m, 4 H) 3.53 - 3.56 (m, 3 H) 4.00 (t, J=7.42 Hz, 1 H) 4.62 (dd, J=8.59, 6.64 Hz, 1 H) 7.24 - 7.34 (m, 5 H) 7.34 - 7.40 (m, 2 H) 7.41 - 7.44 (m, 3 H) 7.69 (s, 1 H) 7.73 - 7.81 (m, 4 H). ^{13}C NMR (101 MHz, CD$_3$OD) δ 34.36, 35.90, 36.20, 36.89, 38.53, 39.20, 52.13, 55.83, 56.21, 126.67, 127.12, 128.35, 128.57, 128.74, 128.87, 128.91, 129.07, 129.99, 130.45, 133.85, 134.86, 135.61, 135.82, 169.61, 173.26, 173.69, 173.74.

H-Nap(D)-Bala-Nap(L)-Bala-OMe (2.35f)
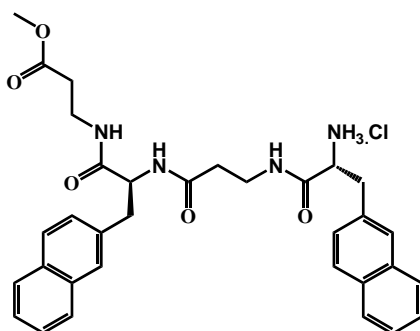
Yield 481mg, 100% MS: *m/z* calculated for $C_{33}H_{36}N_4O_5$ = 568.2686, actual *m/z* (M+Na) = 591.248. ^{1}H NMR (200 MHz, CD_3OD) δ 2.12 - 2.30 (m, 1 H) 2.30 - 2.50 (m, 3 H) 2.95 - 3.12 (m, 1 H) 3.13 - 3.26 (m, 4 H) 3.33 - 3.46 (m, 3 H) 3.48 - 3.55 (m, 3 H) 4.06 - 4.19 (m, 1 H) 4.61 (dd, *J*=8.61, 6.41 Hz, 1 H) 7.31 - 7.50 (m, 7 H) 7.68 (s, 1 H) 7.71 - 7.88 (m, 6 H). ^{13}C NMR (50 MHz, CD_3OD) δ 34.34, 35.96, 36.17, 36.92, 38.62, 39.09, 52.19, 55.71, 56.20, 126.58, 127.03, 127.09, 127.36, 128.11, 128.35, 128.53, 128.65, 128.70, 128.85, 128.99, 129.56, 129.72, 133.01, 133.72, 134.11, 134.74, 134.83, 135.78, 138.66, 169.53, 173.16, 173.55, 173.60.

,

References: - Chapter 2

[1] (a) K. Miyamura, A. Mihara, T. Fujii, Y. Gohshi, Y. Ishii. *J. Am. Chem. Soc.,* 1995, **117**, 2377-2378; (b) C. J. Janiak, *Dalton Trans.,* 2000, **21**, 3885; (c) A. S. Ionkin, W. J. Marshall, and Y. Wang, *Organometallics,* 2005**, 24***, 619-627.

[2] (a) P. Dotta, A. Magistrato, U. Rothlisberger, and P. S. Pregosin, *Organometallics,* 2002**, 21***, 3033-3041; (b) S. Negi and H. Schneider, *Tetrahedron Lett.,* 2002**, 43***, 411-414; (c) M. Q. Slagt, J. T. B. H. Jastrzebski, R. J. M. Klein Gebbink, H. J. van Ramesdonk, J. W. Verhoeven, D. D. Ellis, A. L. Spek, and G. van Koten, *Eur. J. Org. Chem.,* 2003, 1692-1703; (d) L. Ma, P. Jiao, Q. Zhang and J. Xu., *Tetrahedron: Asymmetry,* 2005, **16**, 3718–3734.

[3] A. S. Ionkin, W. J. Marshall, and Y. Wang, *Organometallics.,* 2005**, 24***,* 619-627.

[4] I. Tabushi, Y. Taniguchi, H. Kato., *Tetrahedron Lett.,* 1977, **12**, 1049-1052.

[5] E. Kimura, Y. Kurogi, S. Wada, M. Shionoya, *J. Chem. Soc. Chem. Commun.*, 1989, **12**, 781-783.

[6] (a) E. Kimura, C. A. Dalimunte, A. Yamashita, R. Machida, *J. Chem. Soc. Chem. Commun.*, 1985, **15**, 1041-1043; (b) T. Kumamaru, Y. Nitta, H. Matsuo, E. Kimura., *Bull. Chem. Soc. Jap.,* 1987, **60**, 1930-1932.

[7] R. V. Singh, A. Chaudhary, *J. Inorg. Biochem.,* 2004, **98**, 1712-1721.

[8] C. M. Reid, C. Ebikeme, M. P. Barrett, E-M. Patzewitz, S. Muller, D. J. Robins and A. Sutherland, *Bioor. & Med. Chem. Lett.,* 2008, **18**, 2455-2458.

[9] (a) N. Kuroda, T. Hattori, Y. Fujioka, D. G. Cork, C. Kitada, T. Sugawara, *Chem Pharm Bull (Tokyo).*, 2001, **49**, 1147-54; (b) P. Watts, C. Wiles, S. J. Haswell and E. Pombo-Villar., *Tetrahedron,* 2002, **58**, 5427-5439; (c) I.F. Eggen, F. T. Bakelaar, A. Petersen, and P. B. W. Ten Kortenaar, *Organic Process Research & Development.,* 2005, **9**, 98-101; (d) T. Sugawara,K. Kobayashi, T Tanaka, S. Fukushi, C. Kitada, M. Fujino, *Peptide Chemistry.*, 1996, **33**, 57-60.

[10] (a) R. M. Broyer, G. M. Quaker, and H. D. Maynard, *J. Am. Chem. Soc.,* 2008**, 130***,* 1041-1047; (b) S. Rajagopalan, T. J. Heck, T. Iwamoto, J. M. Tomich, *International Journal of Peptide & Protein Research*, 1995, **45**, 173-179; (c) I. Coin, M. Beyermann amd M. Bienert., *Nature Protocols.*, 2007, **2**, 3247-3256; (d) A. Bagno, S. Bicciato, M. Dettin, C. Di Bello., *Recent Research Developments in Peptides*, 2002, **1**, 65-77; (e) J. Alsina, F. Albericio, *Biopolymers.,* 2003, **71**, 454-77.

[11] T. R. Wagler, Y. Fang, and C.J. Burrows, *J. Org. Chem.,* 1989, **54**, 1584-1589.

[12] M. Achmatowicz and J. Jurczak, *Tetrahedron Assym.,* 2001, **12**, 111-119.

[13] J. E. Baldwin, R. C. Thomas, L. I. Kruse, L. Silberman., *J. Org. Chem.,* 1977, **42**, 3846-3852.

[14] E. K. Barefield, F. Wagner, K. D. Hodges, *Inorg. Chem.,* 1976, **15**, 1370-1377.

[15] K. R. Adams, M. Antolovich, L. G. Brigden, L. F. Lindoy, *J. Am. Soc.,* 1991, **113,** 3346-3351 (and references therein).

[16](a) K. Haas, E. Ehrenstorfer-Schäfers, K. Polborn, and W Beck, *Eur. J. Inorg. Chem.,* 1999, 465-469; (b) M. A. Lang and W. Beck, *Naturforsch.*, 2003, **58b,** 447 – 450; (c) K. Haas, W. Ponikwar, H. Nöth, and W. Beck., *Angew. Chem. Int. Ed.,* 1998, **37**, 1086-1089.

[17]T. S. Haque, J. C. Little, and S. H. Gellman, *J. Am. Chem. Soc.,* 1996**, 118***,* 6975-6985.

[18]S. Krautha, L. A. Christianson, D. R. Powell, and S. H. Gellman, *J. Am. Chem. Soc,.* 1997**, 119***,* 11719-11702 (b) http://www.actim.com/content/view/25/40/lang,en/

[19](a)N. I. Martin, J. J. Woodward, M. B. Winter, W. T Beeson, M. A. Marletta, *J. Am. Chem. Soc.,* 2007, **129***,* 12563-12570; (b) see 13c; (C) M. Wathier, P. J. Jung, M. A. Carnahan, T. Kim, M. W. Grinstaff., *J. Am. Chem. Soc., (Communication),* 2004, **126**, 12744-12745; (d) D. Orain, J. Ellard, M. Bradley, *J. Comb. Chem. (Review),* 2002, **4**, 1-16; (e) T. Haino, Y. Matsumoto, Y. Fukazawa, *J. Am. Chem. Soc. (Communication),* 2005, **127**, 8936-8937.

[20] (a) K. Gademann, Y.Bethuel, H. H. Locher, and C. Hubschwerlen, *J. Org. Chem.,* 2007, **72** (22), 8361 –8370; (b) D. Srinivas, R. Gonnade, S. Ravindranathan, and G. J. Sanjayan, *J. Org. Chem.,* 2007, 72(18), 7022–7025; (c) A. Kudaj˙ and A. Olma, *Tetrahedron Lett.,* 2007, **48** (38), 6794-6797; (d) M. Tullberg, M. Grøtli, and K. Luthman**,** *J. Org. Chem.,* 2007, **72** (1), 195 –199.

[21] (a) J. L. Bada, *J. Am. Chem. Soc.,* 1972, **94**, 1371-1373. (b) P. Lloyd-Williams, *Chemical approaches to the synthesis of peptides and proteins.*, Boca Raton: CRC Press, 1997.

[22] (a) I. M. Kovach, J. P. Elrod, and R. L. Schowen, *J. Am. Chem. Soc.,* 1980, **102**, 7530-7534; (b) H. S. Levenson, H. A. Smith*, J. Am. Chem. Soc.*, 1940, **62**, 1556-1558; (c) T. Kawasaki, H. Enoki., K. Matsumura, M. Ohyama, M. Inagawa, M. Sakamoto, *Org. Let.,* 2000, **2,** 3027-3029; (d) J. Deng, Y. Hamada, T. Shioiri, *J. Am. Chem. Soc.,* 1995, **117,** 7824-7825.

[23] (a) H. D. Darkin., *J. Bio. Chem.* 1912, 357-364 (b) H. D. Darkin., *J. Bio. Chem.* 1913, 263-269 (c) P. M. Masters and M. Friedman *J. Agric. Food Chem.,* 1979*,* **27**, 507-511 (d) P. M. Masters and M. Friedman *J. Food. Sci., 1982,* **47**, 760-764 (e) R. Liardon and S. Ledermann., *J. Agric. Food Chem.,* 1986*,* **34**, 557-565. (f) D. E. Schwass and J.

W. Finley., *J. Agric. Food Chem.,* 1984, **32**, 1377-1382 (g) S. Casal, E. Mendes, M. B. P. P. Olivereira, M. A. Ferreira., *Food. Chem.* 2005, **89**, 333-340. (h) M. Friedman, *J. Agric. Food Chem.,* 1999, **47**, 1268-1319

[24] T. Yoshiya, Y. Sohma, T. Kimura, Y Hayashi[a]and Y. Kiso, *Tetrahedron Lett.,* 2006, **47**, 7905–7909.

[25](a) M. Ni, E. Esposito, B. Kaptein, Q. B. Broxterman, and A Dal Pozzo, *Tetrahedron Lett.,* 2005, **46**, 6369–6371; (b) W. T. Wahl, F. Nefzi, A. Rohwedder, B. Sato, T. Sun, X. Mutter, *J. Am. Chem. Soc*., 1996, **118**, 9218–9227. (c) For a review, see: S. R. *J. Pept. Sci*., 2003, **9**, 545–552.

[26](a)http://web.whittier.edu/people/webpages/personalwebpages/Hashemzadeh/Solid%20 Phase%20Peptide%20Synthesis.pdf (b) C. G. Fields, D. H. Lloyd, R. L. Macdonald, K. M. Otteson, R. L. Noble, *Pept. Res.,* 1991, **4**, 95–101; (c) P. Rzepecki, H. Gallmeier, N. Geib, Katarina Cernovska, B. König, and T. Schrader *J. Org. Chem.,* 2004, **69**, 5168 –5178. (d) J. Tulla-Puche and G. Barany, *J. Org. Chem.,* 2004, **69** (12), 4101 –4107; (e) N. R. Wurtz, J. M. Turner, E. E. Baird, and P. B. Dervan, *Org. Lett.,* 2001, **3**, 1201 -1203.

CHAPTER 3 - Cyclization of Linear Peptides: - Isolation, Electrochemical Properties and Binding Studies of the Generated Nickel Cyclopeptide Complexes.

3.1   Introduction.

After the synthesis of linear peptides **2.29a-e** and **2.35a-f** we wished to utilize Beck's cyclization protocol[1] to generate several cyclopeptide metal complexes (Figure 3.1), analyse them for stereochemical integrity and perform binding tests on them with aromatic substrates to see if they would undergo π-π or CH-π interactions.
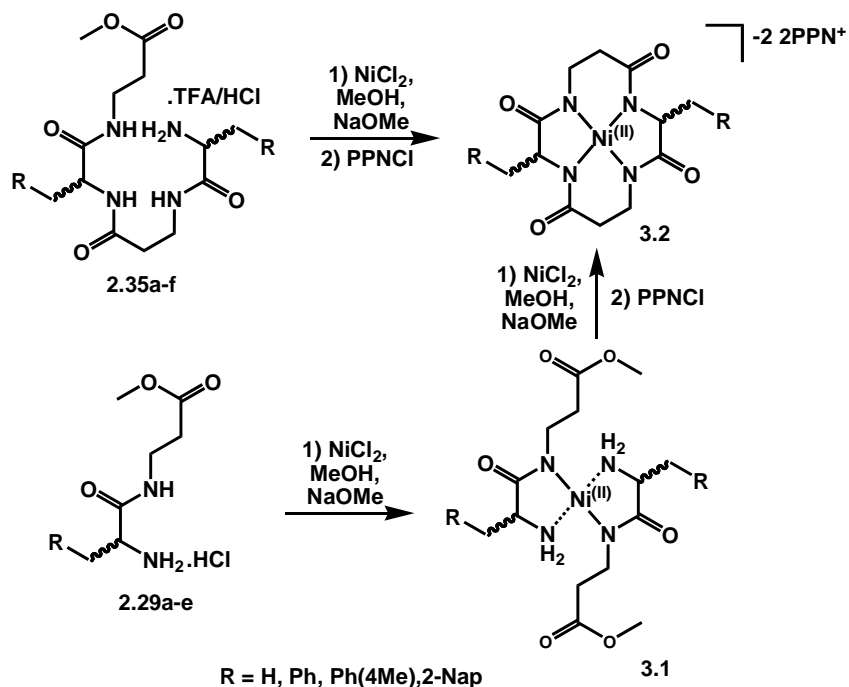
Figure 3.1: - Cyclization of a dipeptides (2.29) and tetrapeptides (2.35) utilizing Beck's metal templated technique.

Very little work has been performed on the metal assisted cyclization of peptides. Most notably several papers from Beck *et al*[1] describe the synthesis of 14 membered ring structures from linear dipeptides utilizing Pd, Ni, and Cu metal templates. The 14 membered rings that we were trying to synthesize are attainable using all three of the metals in good yield (Figure 3.1). In general metal templated cyclizations have been shown to be an effective method for the generation of cyclic systems[2], open ligand systems[3] and even for the generation of small cyclic rings[4]. These cyclizations generally occur though some kind of condensation reaction such as imine formation and are favored over the linear condensation (polymerization) due to the proximity of the reactive centers to one another. Complexes incorporating amido-metal bonds have been developed by Burrows *et al* for use as oxidation catalysts, and disulphide cross linkers[5].

Smaller ring sizes such as 12-14 membered rings were synthesized utilizing the nickel template as the smaller ionic radius of nickel(II) (63pm) allows the head to tail cyclization to occur (**3.4** and **3.5b**). Larger ring sizes such as 16-18 membered rings are accommodated only by the Pd(II) ion, ionic radius 78pm (**3.6**-**3.7**) (Figure 3.2).
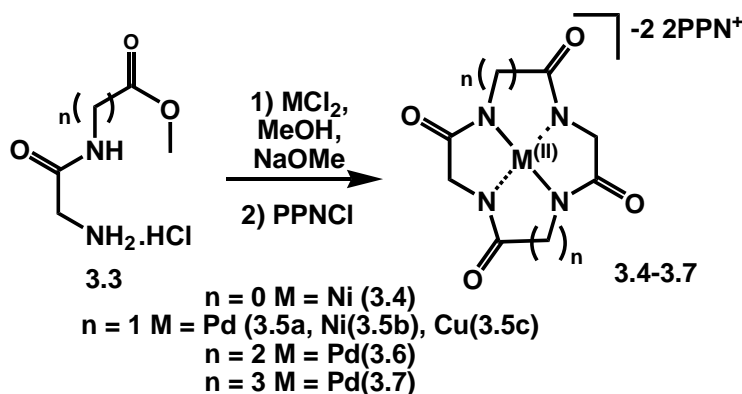
Figure 3.2: - Metal templated cyclizations: - ring sizes vs. metal template used.

In all cases high dilution of the reaction is not necessary as each peptide wraps around a metal ion, thus inducing a close proximity of head to tail (Figure 3.3). The formation of intramolecular 6-exo-trig cyclization products as seen by J. Jurczak *et al*[6] is negated by the formation of a stable complex with the metal. This prevents the amide carbonyl from being attacked by locking the linear peptide in a planar conformation.
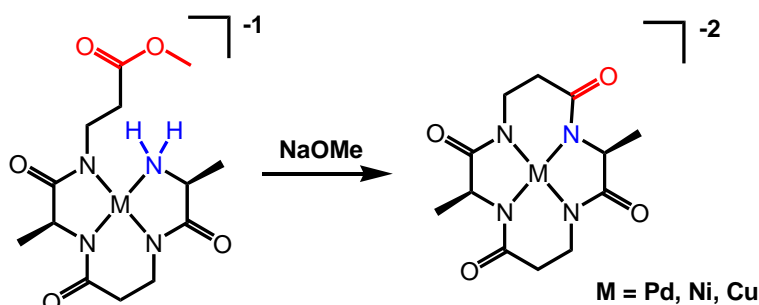
Figure 3.3: - Cyclization of open chain nickel peptide complex by "head to tail" amide bond formation.

C_2, C_1 and C_i symmetric nickel cyclopeptide complexes can be synthesized using tetrapeptide-starting materials[1c] (**2.39a-e**). Each tetrapeptide has stereochemical information "dialed in" during its synthesis (depending on the R or S starting amino acid (**2.36**) used). Thus enabling a wide range of side arms and stereochemistry's to be incorporated into the nickel cyclopeptide complex and ultimately the cyclam molecules. The position of the side arms in **3.1**-3.**4** (Figure 3.1) can be controlled by the cyclopeptides generated during the linear peptide cyclization. The formed cyclopeptide can be reduced to form the desired cyclams (Figure 2.10).

3.1.1 Dipeptide Cyclizations.

Perhaps even more useful than tetrapeptide cyclization is the fact that dipeptide esters can be cyclized to form the 14-membered cyclopeptides[1] (Figure 4.8). In this case 2 equivalents of the dipeptide form a complex with the metal ion. Here two head to tail amide bond formations occur to yield the cyclopeptide complex.

(a)   (b)

(c)
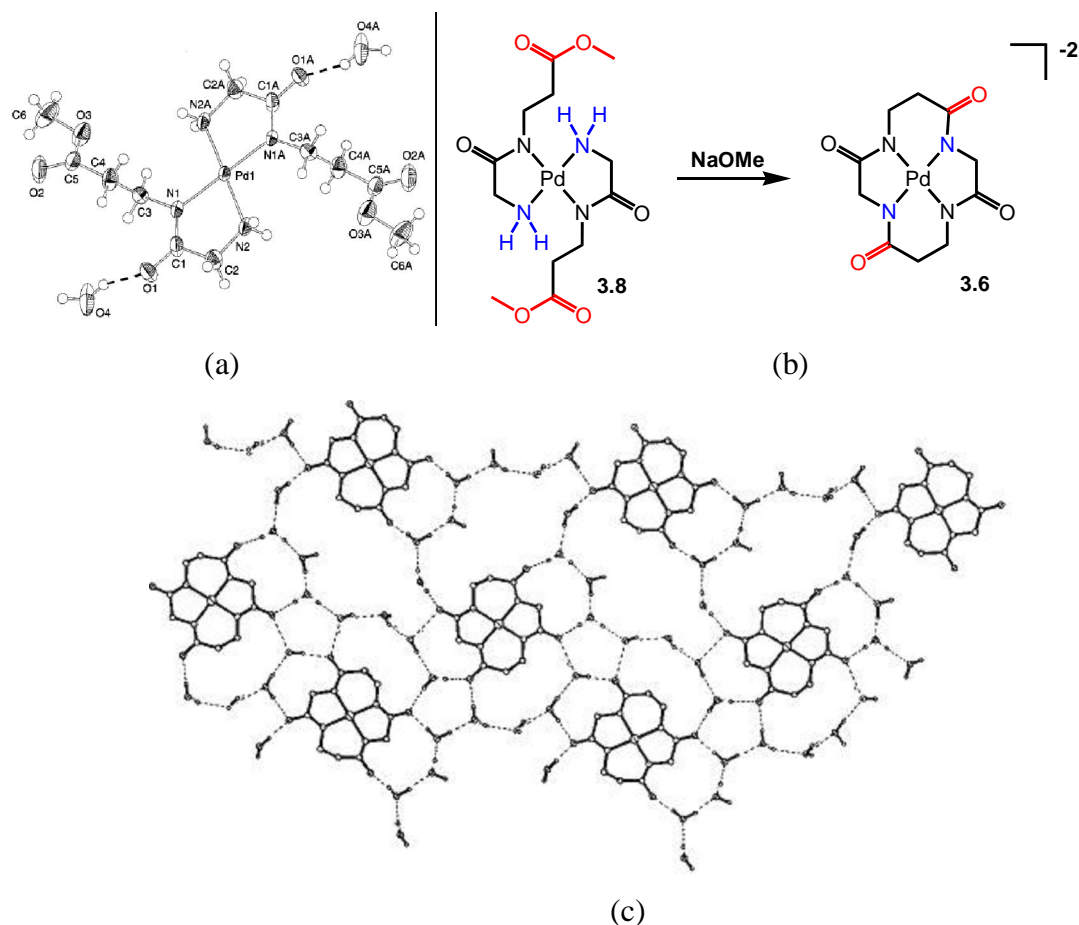
Figure 3.4: - (a) Crystal structure of Pd-(Bis-dipeptide) complex (3.8)[1c] (b) Dipeptide metal complex cyclization of 3.8 to yield 3.6 (c) Crystal structure of Pd-cyclopeptide complex. A sheet structure held together by hydrogen bonding to water molecules (PPN cations removed for clarity) as characterized by Beck[1c] .

The cyclization of dipeptide complexes leads to the formation of C_2 symmetric complexes only[1c]. The dipeptide has only one R group arranged in one stereochemistry (determined by the starting amino acid **2.36**). Cyclization of this peptide leads to the formation of the C_2 symmetric complex with a rotation axis though the metal.

Most of the previous 14-membered ring cyclopeptides synthesized utilizing the metal templated techniques are simple C_2 symmetric complexes derived from β-alanine and natural amino acids such as alanine, phenylalanine and leucine[1]. Yields after purification via recrystallization with PPN range from 17-96%.

3.2   Dipeptide Complex Formation.

Initial trials into cyclopeptide metal complex formation focused on cyclization utilizing Na_2PdCl_4 and the MeO-βala-Phe-NH_2.HCl dipeptide ammonium salt as described by Beck[1]. Under inert conditions using dry methanol Pd black would form after thirty minutes in the presence of NaOMe. Isolation and characterization of the dipeptide Pd complex or the cyclopeptide Pd complex proved impossible (Figure 4.9). Impure Pd salts or NaOMe used may be factors in explaining why this procedure was irreproducible in my hands.
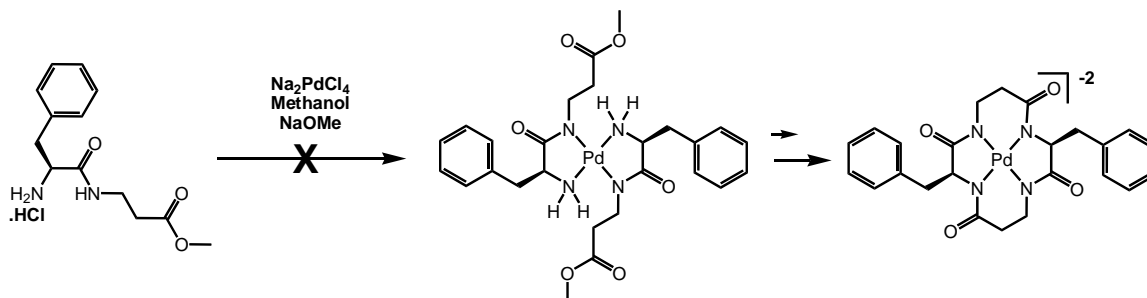
Figure 3.5: - Failed attempts at dipeptide and cyclopeptide complex formation with Pd salts following Beck's method[1].

Due to the failure with $PdCl_2$, $Ni^{(II)}$ dipeptide complexes were synthesized. The product drops out of solution after ten minutes at room temperature and can be crystallized from methanol to give X-ray quality crystals (Figure 3.7). Unfortunately these compounds tend to be highly insoluble at room temperature in MeOH, EtOH, ether, water, DCM, chloroform, acetonitrile, toluene and DMF. Some small solubility was noted in DMSO.
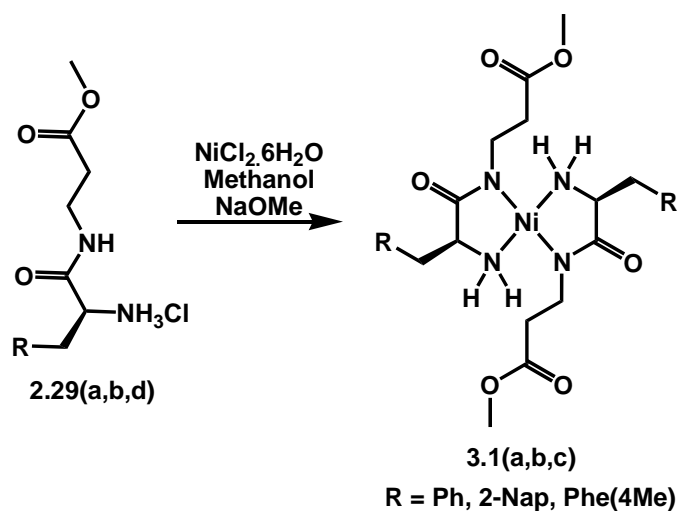
Figure 3.6: - Synthesis of dipeptide nickel complexes.

Table 3.1: - Yields of dipeptide nickel complexes.

R	Compound Number	Yield%
Ph	**3.1a**	58
4Me-Ph	**3.1b**	18
2-Nap	**3.1c**	28.5

3.2.1 X-ray Structures of Dipeptide Nickel Complexes.

Several crystal structures indicate that the stereocenters on the dipeptides withstood the coupling reaction; Boc removal and the base promoted nickel complex formation (Figure 3.7).

(a)   b)
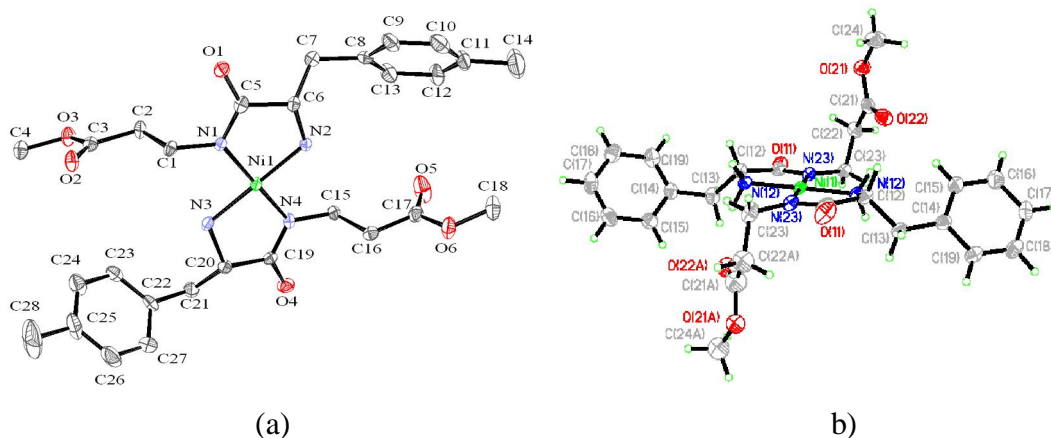
Figure 3.7: - (a) X-ray crystal structure of *trans*-Bis(4-methyl-phenyl-dipeptide ester)Ni[II] complex (3.1b). (b) X-ray crystal structure of *trans*-Bis(phenyl-dipeptide ester)Ni[II] complex (3.1a).

Table 3.2: - Table of selected bond lengths and angles for complexes 3.1a and 3.1b

Selected Bond Lengths complex 3.1a	Selected Bond Lengths complex 3.1b
Ni(1)-N(23) (1.882Å), Ni(1)-N(12) (1.909Å), C(11)-O(11) (1.250Å), C(11)-N(23) (1.329Å), C(11)-C(12) (1.520Å), C121-N121, (1.479Å).	N(1)-Ni(1) (1.892Å), N(2)-Ni(1) (1.895Å), N(3)-Ni(1) (1.896Å), N(4)-Ni(1) (1.894Å), C(19)-N(4) (1.334Å), C(5)-N(1) (1.330Å), C(5)-C(6) (1.508Å), C(5)-O(1) (1.252Å), C(19)-C(20) (1.516Å), C(19)-O(4) (1.250Å), C(17)-O(5) (1.199Å)
Selected Bond Angles 3.1a	**Selected Bond Angles 3.1b**
N23-Ni(1)-N23 (179.26°), N(23)-Ni(1)-N(12-1) (95.53°), N(23-1)-Ni(1)-N(12-1) (85.14°), N(23-2)-Ni(1)-N(12-2) (84.87°), N(23-1)-Ni(1)-N(12-2) (94.47°), N(12-1)-Ni(1)-N(12-2) (178.85°).	N(1)-Ni(1)-N(4) (177.30°), N(1)-Ni(1)-N(2) (85.14°), N(4)-Ni(1)-N(2) (95.13°), N(1)-Ni(1)-N(3) (95.98°), N(4)-Ni(1)-N(3) (83.70°), N(2)-Ni(1)-N(3) (178.37°)

104

Selected Torsion Angles 3.1a	Selected Torsion Angles 3.1b
Ni(1)-N(12)-C(12)-C(11) (19.26°), N(12)-C(12)-C(11)-N(23) (12.33°), Ni(1)-N(23)-C(11)-C(12) (-0.44°), Ni(1)-N(23)-C(11)-O(11) (176.68°),	Ni(1)-N(1)-C(5)-C(6) (-32.61°), N(1)-C(5)-C(6)-N(2) (20.02°), Ni(1)-N(2)-C(6)-C(5) (-28.52°), Ni(1)-N(1)-C(5)-O(1) (-179.72°), N(3)-C(20)-C(19)-N(4) (13.81°),

Interestingly the packing of the Ni complex **3.1a** show an N-H--O hydrogen bond (2.014Å) to other complex molecules through the carbonyl in the five membered ring and the NH_2 in the five membered ring (Figure 3.8). This differs from Beck's findings as the complexes in which case hydrogen bonding is seen through bridging water molecules and the ester as in the Pd dipeptide complexes[1a] (Figure 3.9).
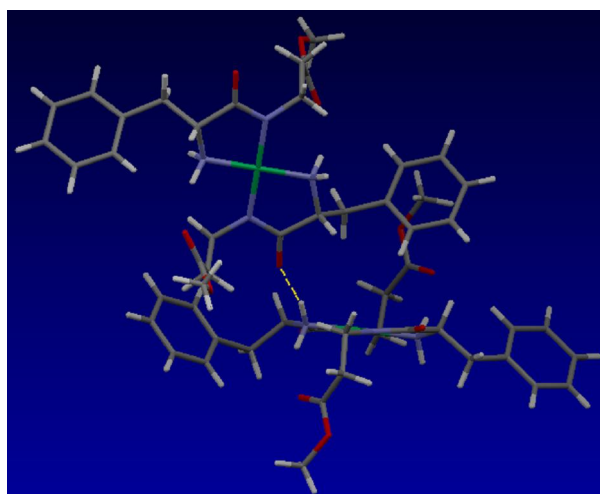
Figure 3.8: - Bridging N-H---O hydrogen bonding between two molecules of 3.1a as seen in the crystal structure.
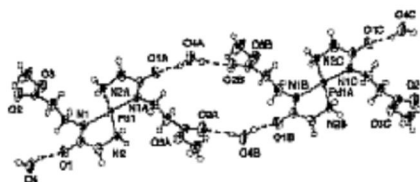
Figure 3.9: - Part of the extended chain formed by Pd(Bis-dipeptide) complexes.

The crystal structures obtained show that stereochemical integrity is maintained in the presence of the base and nickel, although this chemistry is performed at room temperature and full cyclization occurs at higher temperatures. The dipeptide complex previously obtained by Beck (Figure 3.9) has no stereocenters that could possibly undergo racemization during the reaction thus this data is useful as stereochemical integrity is a priority in the synthesis of the cyclopeptides.

3.2.2   Electrochemical Data For A Dipeptide Complex.

Electrochemical data for the dipeptide complex **3.1a** suggests that the complex dissociates upon oxidation from Ni(II) to Ni(III) (+0.773V) with no reverse wave seen (Figure 4.13). The uncyclized complexes are entropically less stable than that of a fully cyclized complex[7]. Further isolation of these intermediates was not pursued.
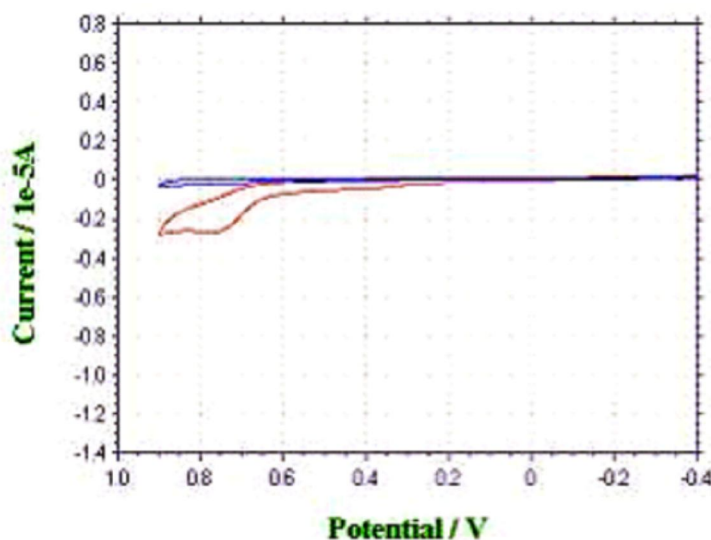
Figure 3.10: - [Ni^{II}L'$_2$] (3.1a) < 2.3 mM (not dissolved completely in DMSO)- E (Ni^{II}L'$_2$ to Ni^{III}L'$_2$) = +0.773 V vs. Ag/AgCl (irreversible, and thus cannot determine E^0.).

3.3   Isolated Nickel Cyclopeptide Complexes Derived From Linear Tetrapeptides.

Cyclization of dipeptides, in solution, using the metal template procedure (Figure 3.2) gives 75-80% pure crude nickel complexes after the reaction (impurities may include uncyclized starting materials and saponified dipeptides). In these cases pure Bis(triphenylphosphine)iminium (PPN) or Ca salts of these compounds were never isolated. The amount of impurities in the product was simply too great to allow crystallization to occur. Other purification techniques including column chromatography, HPLC (C18 and cyano), and ion exchange chromatography proved as fruitless as the crystallization in the isolation of the complexes.

To give an improved chance of isolating pure complexes the cyclization of tetrapeptides were performed (Figures 3.11). Tetrapeptides need only to undergo one amide bond-forming step, which is more efficient than the formation of two new amide bonds as in the dipeptide cyclization. This would lead to fewer side products (including saponification of the ester).

Tetrapeptide cyclization reactions worked fairly well after several modifications to Beck's original procedure, and it became obvious that this methodology was significantly cleaner than that of the dipeptide cyclization for C_2 symmetric complexes (crude ^{1}HNMR showing purities between 70-90%).

Cyclizations required between 1.2 and 2eq of base per NH to minimize the amount of unreacted starting material and complete the cyclization, whereas Beck used 1eq of base per NH. Beck's isolated yields range between 17-94% whilst yields obtained under the modified conditions ranges from 8-47.5% for isolated complexes.

Adjustments were also made to the crystallization procedure. Beck's papers suggest that simply mixing the crude Na salt with $CaCl_2$ or PPN-Cl then adding water would give pure crystalline product through simply crashing it out of solution. This procedure failed to give any pure product in my hands with lots of impurities trapped in the precipitate isolated from these procedures.

In order to achieve purification the crude Na salt was mixed with Bis(triphenylphosphine)iminium chloride (PPN-Cl) in a mixture of acetone:methanol (1:1, roughly 10mL per 0.1mmol) and water was slowly added until the mixture started to become turbid. The flask was then placed in the fridge overnight where crystallization occurred giving a 8-47% yield of very pure PPN salts generated from these slow

crystallization conditions (Figure 3.11, Table 3.2). Beck's procedure involved adding the PPN-Cl to his reaction crude reaction mixture in methanol then diluting with water to obtain his crystals. This procedure gave impure sandy solids in my hands and sometimes just the PPN-Cl was recovered, even when attempted under inert conditions.
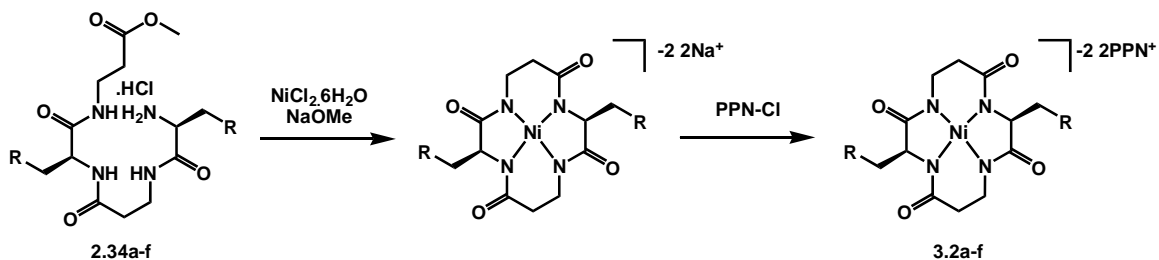
Figure 3.11: - Cyclization of tetrapeptides 2.34a-f using a nickel template.

Table 3.3: - Complexes synthesized and isolated from tetrapeptides.

Compound Name/Number	Yield %	Compound Name/Number	Yield %
[-(Phe(L)-ßala-Phe(L)-ßala)-Ni$^{(II)}$]$^{-2}$ (3.2a)	47.5	[-(2-Nap(L)-ßala-2-Nap(L)-ßala)-Ni$^{(II)}$]$^{-2}$ (3.2d)	8
[-(Ala(L)-ßala-Ala(L)-ßala)-Ni$^{(II)}$]$^{-2}$ (3.2b)	38	[-(2-Nap(L)- ßala-2-Nap(D)-ßala)-Ni$^{(II)}$]$^{-2}$ (3.2e)	30
[-(Phe(L)-ßala-Ala(L)-ßala)-Ni$^{(II)}$]$^{-2}$ (3.2c)	26.8	[-(Phe(L)-ßala-Phe(D)-ßala)-Ni$^{(II)}$]$^{-2}$ (3.2f)	28.5

3.3.1 NMR Data Showing Cyclopeptide Nickel Complex Formation from Solution Phase Reactions.

The solution phase cyclization reaction was followed by ^{1}HNMR and takes between 5-24 hours to complete using 2eq of NaOMe per NH bond. Larger naphthyl side

groups take longer to cyclize than the simple natural amino acids and are harder to crystallize.

The crystallization of the products **3.2a-f** occurs over a period of 24 hours at 5°C using a mixture of acetone:MeOH and water and leads to crystals which are ^{1}HNMR pure (Figure 4.15) and suitable for X-ray crystallography.
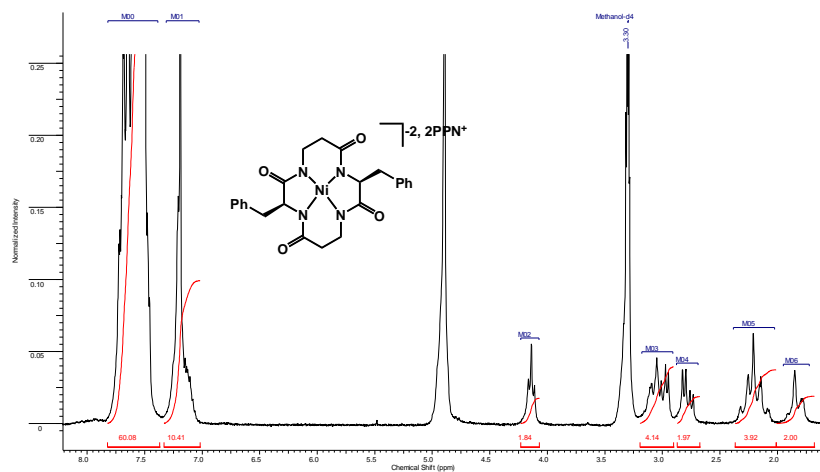
(a)
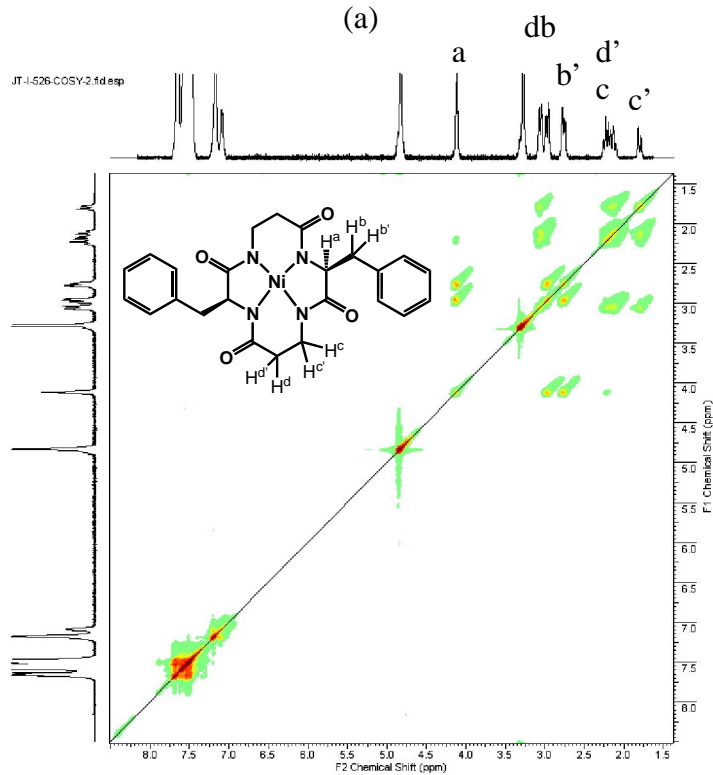
(b)

Figure 3.12: - (a) NMR of complex 3.2a (b) COSY of complex 3.2a.

The NMR and COSY of complex **3.2a** allow us to identify each of the signals within the spectra. The multiplet at 4.14ppm, corresponds to the alpha C-H next to the phenyl arm and interacts with the protons at 2.79ppm (dd) and the protons at 2.99ppm (dd), both the benzyl C-H's. Interactions between the C-H groups at 3.09ppm and the multiplets in the 2.1-2.3ppm regions and the multiplet at the 2.82ppm show these to be the C-H groups in the β-alanine part of the ring. Symmetry is maintained in the molecule that doubles the integration for each peak.

3.3.2 Solid Phase Cyclization Reactions.

Although cyclizations of compounds on solid support have previously been demonstrated utilizing cyclization release mechanisms[8] and external stimuli such as enzymes[9] or electrocycliztion[10], little work has been performed on metal mediated cyclizations on solid support. We wished to cyclize the peptides synthesized on resin to generate cyclopeptide complexes.

When the tetrapeptides on resins are treated with a solution of $Ni^{(II)}X_2$ (X = ClO_4^-, Cl^-) or $Ni^{(II)}(NH_3)_6$ in the presence of a base (NaOMe, TEA) the resin changes color to a light yellow. It would appear that the peptide on the resin is coordinating to the metal center in a similar way to the metals in the solution phase reactions. Further treatment of these metalated resins, after extensive washing, with NaOMe at $60^{\circ}C$ for 12 hours, leads to the formation of an orange solution and a lightening of the hydroxymethyl resin (Figure 3.13).

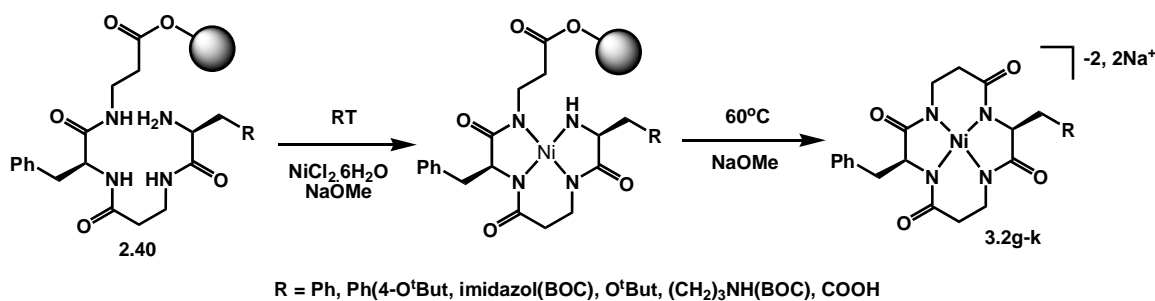R = Ph, Ph(4-O^{t}But, imidazol(BOC), O^{t}But, (CH$_2$)$_3$NH(BOC), COOH

Figure 3.13: - On resin tetrapeptide cyclization.

Purification methods including HPLC's utilizing C18 (reverse phase) columns proved ineffective at purifying the materials as they eluted with the solvent front. Ion exchange columns, amine terminated column, normal phase silica column chromatography and recrystallization from various solvents also proved ineffective in the purification of the compounds. Crystallization induced by PPN addition analogous to the solution studies in figure 3.11 was not attempted.

Although these compounds were not purified their presence was confirmed by MALDI mass spectroscopy and the major peaks correspond to either the main mass of the complex or a fragment (minus acid sensitive protecting groups) (Table 4.3).

Mechanistic studies for the cyclization/release of the nickel complexes were not performed however could proceed through one of two routes, cyclization-release or transesterification-cyclization (Figure 3.14)
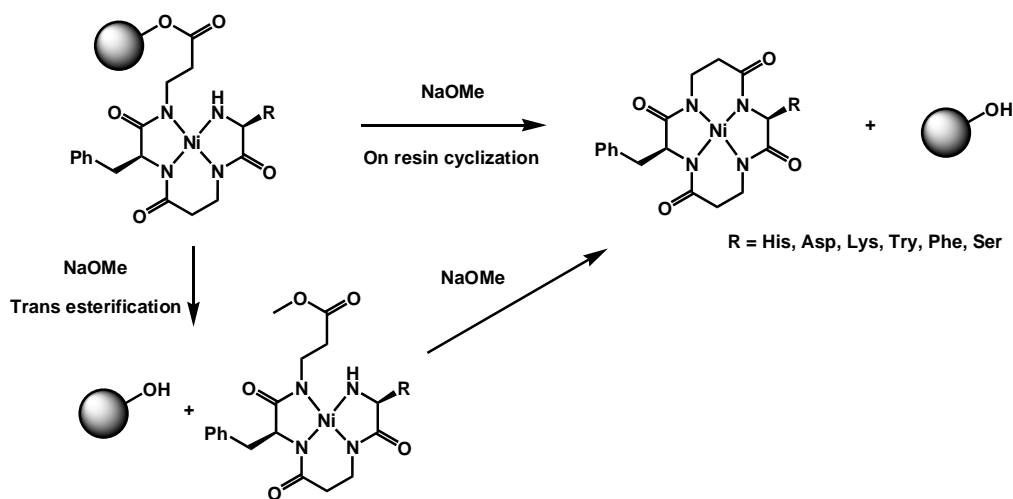

Figure 3.14: - The two possible mechanisms for cyclization products obtained from the cyclization of tetrapeptides on resins.

Table 3.4: - Mass spectrum results for on resin cyclizations.

Compound Name/Number	Mass Peak(s) *m/z*	Compound Name/Number	Mass Peak(s)
[-(His(L)(Trt)-ßala-Phe(L)-ßala)-Ni$^{(II)}$]$^{-2}$ (3.2g)	Calculated for C$_{40}$H$_{36}$N$_6$NiO$_4$ = 722.215 Actual = 725.564 (M+3H$^+$) 483.279 (M-Trt +3H$^+$)	[-(Tyr(L)(^{t}But)-ßala-Phe(L)-ßala)-Ni$^{(II)}$]$^{-2}$ (3.2j)	Calculated for C$_{28}$H$_{32}$N$_4$NiO$_5$ = 562.173 Actual = 565.145 (M-+3H$^+$) 509.042 (M-^{t}But + 3H$^+$)
[-(Asp(L)(^{t}But)-ßala-Phe(L)-ßala)-Ni$^{(II)}$]$^{-2}$ (3.2h)	Calculated for C$_{23}$H$_{28}$N$_4$NiO$_6$ = 514.136 Actual = 461.254 (M- ^{t}But +3H$^+$) 401.153 (M-Asp +2H$^+$)	[-(Phe(L)- ßala-Phe(L)- ßala)-Ni$^{(II)}$]$^{-2}$ (3.2a)	Calculated for C$_{24}$H24N$_4$NiO$_4$ = 490.115 Actual = 493.066 (M + 3H$^+$)
[-(Lys(L)(Boc)-ßala-Phe(L)-ßala)-Ni$^{(II)}$]$^{-2}$ (3.2i)	Calculated for C$_{26}$H$_{55}$N$_5$NiO$_6$ = 571.194 Actual = 574.465 (M+3H$^+$) 474.322 (M-Boc +3H$^+$)	[-(Ser(L)(^{t}But)-ßala-Phe(L)-ßala)-Ni$^{(II)}$]$^{-2}$ (3.2k)	Calculated for C$_{22}$H$_{28}$N$_4$NiO$_5$ = 486.141 Actual = 489.366(M+3H$^+$) 433.254 (M – ^{t}But +3H$^+$)

Several other metals (Fe, Zn, Pd) were utilized in the cyclization reaction but failed to produce any sign of the cyclopeptide complex under inert conditions in a trident synthesizer. The Pd templated cyclization did not occur as in Beck's solution phase synthesis for dipeptides[1]. This result is somewhat perplexing but may have been a result of impure PdCl$_2$. Iron and zinc cyclizations attempted in solution phase did not produce

cyclic complexes. This may be due to an incompatibility with the ionic radius of these metals and the 14 membered rings formed. The failed cyclizations also failed to show any sign of the tetrapeptide starting material by MS. These cases may show that complexation of the nickel is required for the cyclization or release of the tetrapeptide to occur. Simple transesterification/saponification was not observed under these basic conditions or in the presence of these Lewis acids (Fe, Pd, Zn).

This work was interesting as it shows that rapid generation of the cyclopeptide complexes can be achieved utilizing solid phase bound tetrapeptides. Our work on tetrapeptides generated in the solution phase showed that the cyclopeptides could be isolated by treatment of the *impure* nickel cyclopeptide complex with HCl. This methodology could be applied to the impure peptide complexes isolated from on resin cyclizations.

3.3.3 Stereochemical Integrity: - Racemization of Peptides/Peptide Complexes and X-ray Crystal Structure analysis of Cyclopeptide Nickel Complexes.

Beck's previously synthesized cyclopeptide complexes were never fully characterized in terms of their stereochemistry. Only ^{1}HNMR, ^{13}CNMR, IR and MS were performed on Beck's isolated products, non of which allow for the determination of the absolute stereochemistry in the case of the C_2 symmetric complexes he hoped to generate. If racemization occurred C_i symmetric complexes would be generated and would have ^{1}HNMR data very similar to the C_2 symmetric complexes. When dealing with strong bases at elevated temperatures it is possible to racemize α-protons on amino acid and peptides[11].

Our own studies at racemization of tetrapeptides show that the aromatic phenyl side chain can stabilize the formation of an anion at the alpha position in the side chain. H/D exchange reactions in CD$_3$OD over 28 hours under basic conditions for tetrapeptide H-Ala(L)-ßala-Phe(L)-ßala-OMe **(2.34d)**. The alpha proton on the phenyl side chain (4.5ppm) exchanges whilst the alpha CH from the alanine shows no racemization (this can be seen in the retention of the doublet at 1.2ppm) (Figure 3.15). This racemization is

due to the electron withdrawing nature of the phenyl group. The phenyl increases the acidity (decreases the pKa) of the alpha proton and also provides some inductive stabilizing effect for the anion formed after deprotonation. The methyl group on alanine is an electron donor, inductively, and causes a pKa increase in the alpha proton when compared to the phenyl side group, making it more difficult to deprotonate. The alpha protons on the β alanine also undergo racemization under these conditions (2.3-2.5ppm), however due to the lack of a stereocenter this is of little concern in the stereochemical integrity of the final product.

This racemization of phenylalanine was very worrisome for the maintenance of stereochemical integrity in our aromatically functionalized systems. If racemization can occur at the alpha position of phenylalanine then it is likely that the effect will be increased as the electron withdrawing nature of the side arm is increased, meaning that 2-naphthylalanine would racemize more quickly than phenyl alanine under basic conditions combined with heat. In this case stereochemical control would be lost and racemic mixtures would be isolated as our product.
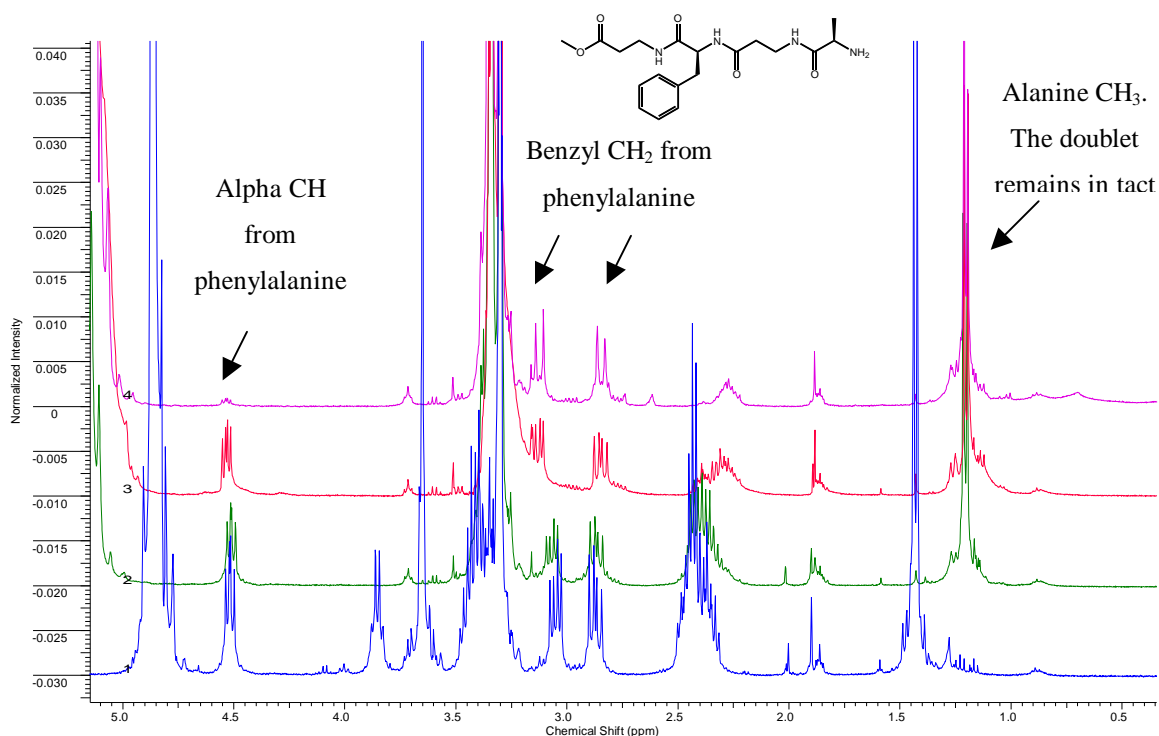

Figure 3.15: - (1) HCl salt of MeO-Bala-Phe-Bala-ala-NH₂ (blue), (2) NaOMe added to the MeO-Bala-Phe-Bala-ala-NH₂ salt t=0 (green), (3) NaOMe plus MeO-Bala-

Phe-Bala-ala-NH$_2$ t= 4 hours (red), (4) NaOMe plus MeO-Bala-Phe-Bala-ala-NH$_2$ t= 28 hours (purple).

A racemization experiment was carried out on the complex formed from the tetrapeptide **3.2c** after cyclization. This experiment showed that cyclization of the complexes leads to a stereochemically stable complex even after 80 hours under basic conditions with heat (Figure 3.16).
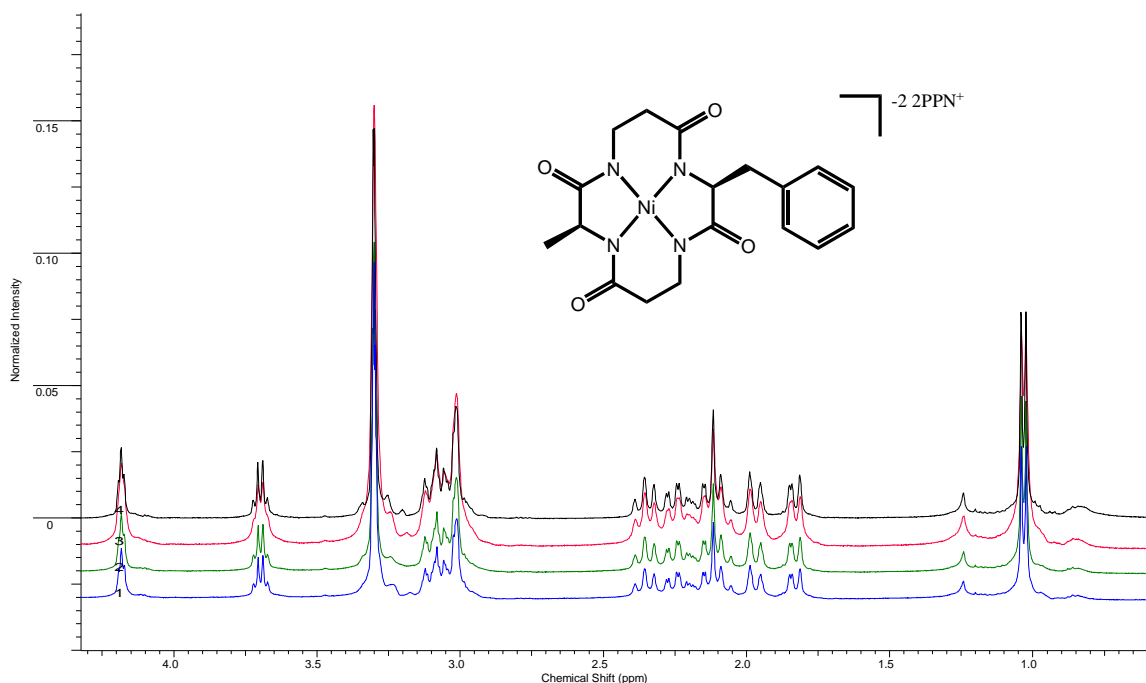

Figure 3.16: - NaOMe plus the cyclopeptide nickel complex 3.2c. (1) T=0 (blue), (2) T=1h 45m (green), (3) t=24h (red), (4) t=80h (black).

Dipeptide complex formation occurs in ten minutes under basic conditions with no loss of stereochemistry at RT, and a similarly rapid tetrapeptide complex formation is expected, followed by cyclization.

Whilst the cyclopeptide nickel complex **3.2c** does not undergo proton exchange the intermediates before cyclization may still do so. The only way to fully characterize the stereochemical information on nickel cyclopeptide complexes is to grow crystals and analyse them by X-ray crystallography.

115

3.3.3.1 [–(βala-Phe(L)-βala-Phe(L))-]Ni 2PPN (3.2a) Crystal Structure.

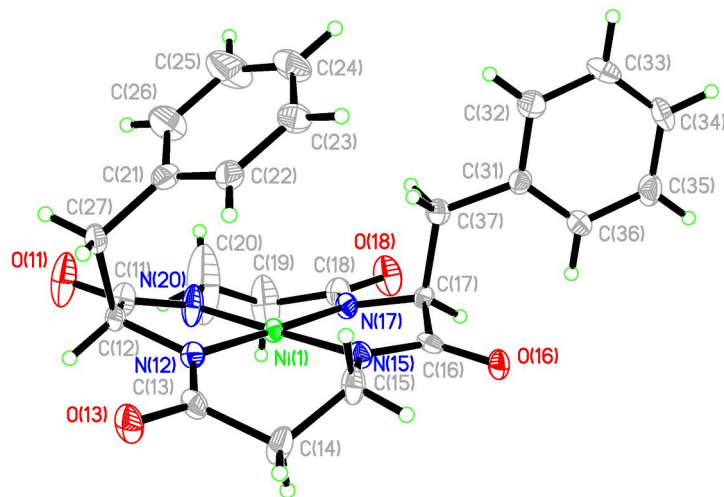X-ray data for **3.2a** was generated from isolated crystals and is shown in figure 3.17.

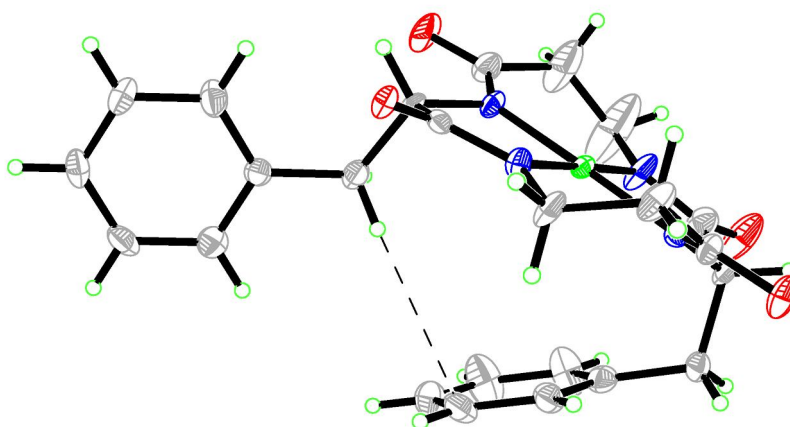**Figure 3.17: - Crystal structure of the 3.2a (PPN and solvent molecules removed for clarity).**

Figure 3.18: - Crystal structure of 3.2a showing the intramolecular π-CH bond (PPN and solvent molecules remove for clarity).
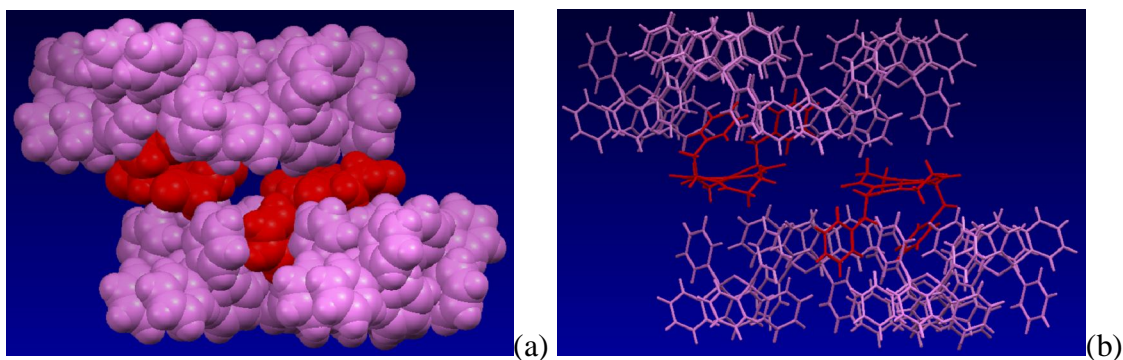
(a)

(b)

Figure 3.19:- (a) A space filling diagram showing the interaction of [–(βala-Phe(L)-βala-Phe(L))-]Ni^{-2} (red) with the PPN groups (violet) (b) A cap and stick diagram showing the interaction of [–(βala-Phe(L)-βala-Phe(L))-]Ni^{-2} (red) with the PPN groups (violet).

Table 3.5: - Selected bond lengths, bond angles, torsion angles and ring alignment for complex 3.2a.

Selected Bond Lengths	Selected Torsion Angles
Ni(1)-N(15) (1.858Å), Ni(1)-N(17) (1.863Å), Ni(1)-N(20) (1.857Å), Ni(1)-N(12) (1.888Å), N(15)-C(16) (1.317Å), N(15)-C(15) (1.460Å), N(17)-C(17) (1.476Å), N(17)-C(18) (1.297Å), N(20)-C(20) (1.461Å), N(20)-C(11) (1.338Å), N(12)-C(13) (1.306Å), N(12)-C(12) (1.455Å), C(16)-O(16) (1.281Å), C(18)-O(18) (1.283Å), C(11)-O(11) (1.262Å), C(13)-O(13) (1.249Å).	C(16)-N(15)-Ni(1)-N(17) (-10.33^{o}), C(15)-N(15)-Ni(1)-N(17) (-175.86^{o}), C(14)-C(15)-N(15)-Ni(1) (32.17^{o}), C(17)-C(16)-N(15)-Ni(1) (11.82^{o}), N(12)-C(13)-C(14)-C(15) (48.58^{o}), Ni(1)-N(12)-C(13)-C(14) (-0.66^{o}), O(16)-C(16)-C(17)-C(37) (-75.50^{o}), O(16)-C(16)-C(17)-H on C(17) (-48.81^{o}), N(17)-C(17)-C(16)-N(15) (-13.48^{o}), N(12)-C(12)-C(11)-N(20) (-6.15^{o}). C(20)-N(20)-C(11)-O(11) (2.22^{o}), C(15)-N(15)-C(16)-O(16) (3.71^{o}), C(17)-N(17)-C(18)-O(18) (0.20^{o}), C(12)-N(12)-C(13)-O(13) (0.65^{o}),

Selected Bond Angles	Six Membered Ring Alignment
N(15)-Ni(1)-N(17) (84.88°), N(17)-Ni(1)-N(20) (95.39°), N(20)-Ni(1)-N(12) (83.84°), N(12)-Ni(1)-N(15) (95.79°), N(15)-Ni(1)-N(20) (176.38°), N(12)-Ni(1)-N(17) (178.17°).	*Cis*

The bond angles show a slightly distorted square planar geometry with bond angles in between N-Ni-N ranging from 83.84-95.79° (Table 3.5). **3.2a**'s X-ray crystal structure confirms the ^{1}HNMR data in revealing that the cyclopeptide ligand system is in a square planner arrangement around the metal center.

The stereochemistry in the crystal structure is shown to be S on C(17) and S on C(12). This SS arrangement is as was "dialled in" utilizing BOC protected (S) phenylalanine in the synthesis of the tetrapeptide **2.34a**.

In **3.2a** the arrangement of the side arms appears to be that of a tweezer shaped cavity with both arms in an axial position, although the space between the two groups is under 4Å, far too short for intercalation with an aromatic guest.

To avoid steric interactions **3.2a** one might expect the side arms to be in an equatorial position. However the phenyl rings in **3.2a** occupy the axial position. A possible reason the rings are orientated like this is a π-CH interaction located intramolecularly between a phenyl ring and the methylene linker of the opposite phenyl group. This interaction (on the order of 2.5-5.5KJ/mol for intermolecular π-CH interactions[12]) may provide enough energy to overcome the steric repulsion in the solid state (Figure 3.18).

There are several π-CH intermolecular interactions in this crystal structure between the cyclopeptide complex and the PPN counter cation (6 per cyclopeptide nickel complex). These distances are between 3Å and 3.1Å and showed interactions are possible between the cyclopeptide complex and another π surface, a desired property for *cyclam* complexes to be generated from these intermediates (Figure 3.19).

3.3.3.2 [–(βala-Phe(L)-βala-Phe(D))-]Ni 2PPN (3.2f) Crystal Structure.

X-ray data for **3.2f** was generated from isolated crystals and is shown in figure 3.20 (bond length and angle data in table 3.6).
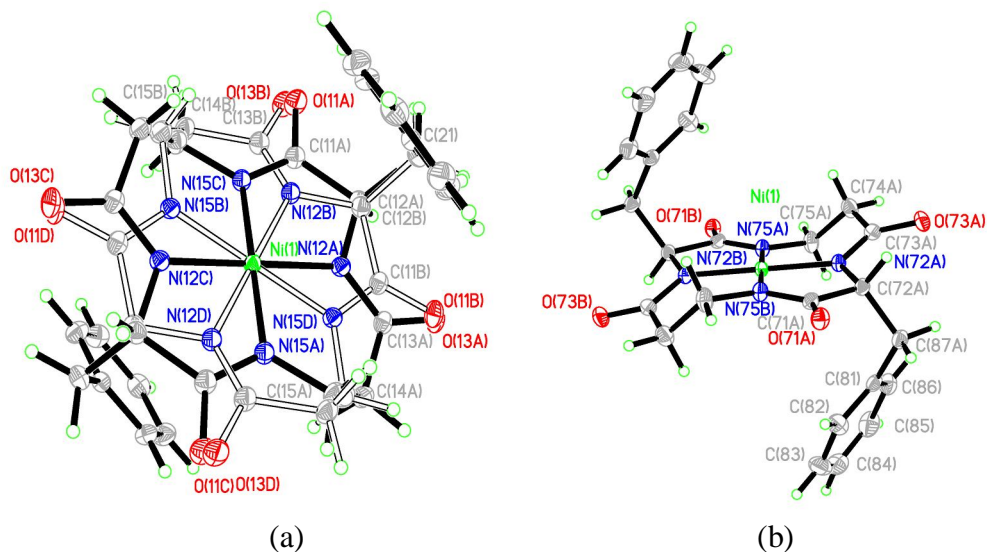

(a)   (b)

Figure 3.20: - X-ray crystal structure of 3.2f (PPN and solvents removed for clarity). (a) The two structures of the nickel complex in the solid state differing only by the direction of the peptide chain. (b) One molecule of 3.2f alone.

(a)   (b)
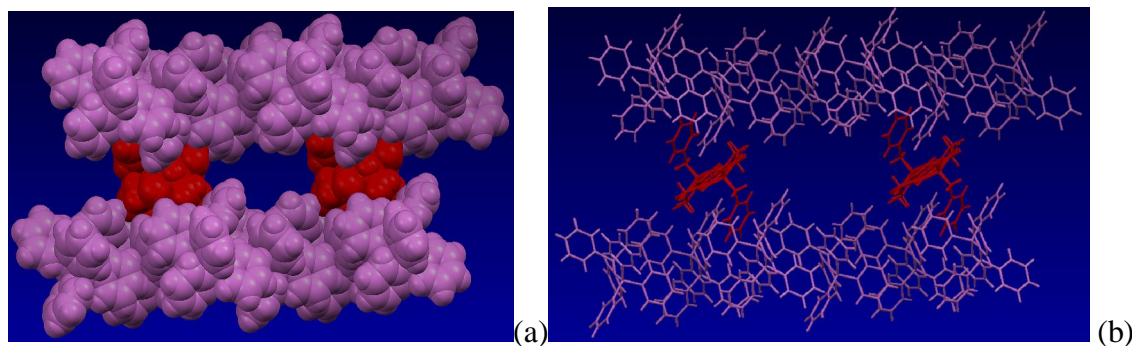
Figure 3.21: - (a) A space filling diagram showing the interaction of [–(βala-Phe(L)-βala-Phe(D))-]Ni^{-2} (red) (3.2f) with the PPN groups (violet) (a) A cap and stick diagram showing the interaction of [–(βala-Phe(L)-βala-Phe(D))-]Ni^{-2} (red) (3.2f) with the PPN groups (violet). (Solvents removed for clarity).

Table 3.6: - Selected bond lengths, bond angles, torsion angles and ring alignment for complex 3.2f.

Selected Bond Lengths	Selected Bond Angles
Ni(1)-N(15A1#1) (1.8656Å), Ni(1)-N(15A1) (1.8656Å), Ni(1)-N(15B1#1) (1.872Å), Ni(1)-N(15B1) (1.872Å), Ni(1)-N(12B1) (1.883Å), Ni(1)-N(12B1#1) (1.883Å), Ni(1)-N(12A1#1) (1.8837Å), Ni11-N(12A1) (1.8837Å), C(11A1)-(N15A1#1) (1.306Å), C(12A1)-(N12A1) (1.464Å), N(12A1)-(C(13A1) (1.331Å), C(11B1)-(O11B1) (1.290Å), C(13B1)-(O13B1) (1.290Å), C(11A2)-(O11A2) (1.297Å), C(13A2)-(O13A2) (1.266Å).	N(75A)-Ni(1)-N(72A) (84.55°), N(72A)-Ni(1)-N(75B) (95.39°), N(20)-Ni(1)-N(12) (83.84°), N(12)-Ni(1)-N(15) (95.79°), N(15)-Ni(1)-N(20) (176.38°), N(12)-Ni(1)-N(17) (178.17°).
	Six Membered Ring Alignment
	Trans

Crystals grown of **3.2f** show a marked difference in the orientation of the phenyl rings in the solid state. As predicted the arms on the ligand periphery are in a pseudo equatorial position (Figure 3.20). An interesting structural development is the fact that the rotation of the ligand periphery (which way the amide bonds flow around the ring) is not static in the crystal structure. The two rotations can be seen in the solid state in an 83:17 ratio. The structures of these compounds are identical (a flip and rotation leads to the same molecule) and the alignment of many of the atoms is very close including the phenyl rings, Ni center and carbonyl oxygens.

The stereochemistry in the crystal structure is shown to be R on C(72A) and S on C(1A). This SR arrangement is as was dialled in utilizing BOC protected (S) phenylalanine and BOC protected (R) phenylalanine in the synthesis of the tetrapeptide **2.34b**.

3.2f has C_i symmetry with an inversion center through the Ni. A marked difference between this compound, the **3.2a** and the Pd complexes shown by Beck *et al* is

the orientation of the 6 membered rings incorporating the Ni. In **3.2f** the 6 membered rings are *trans* to each other but the rings on the other complexes are *cis* giving the molecule a saddle shape with a C_2 axis passing through the nickel.

3.2f the complexes interact with both layers of the PPN counter ions in the solid state, not just one as in the complex **3.2a** did (Figure 3.21). As a consequence of both side arms of the cyclopeptide nickel complex **3.2f** interacting with different layers of the PPN counter ion each phenyl ring now has 6 π-CH interactions (3.163-2.656Å), doubling that of **3.2a**.

3.3.3.3 [–(βala-Nap(L)-βala-Nap(D))-]Ni 2PPN (3.2e) Crystal Structure.

X-ray data for **3.2e** was generated from isolated crystals and is shown in figure 3.22 (bond length and angle data in table 3.7).
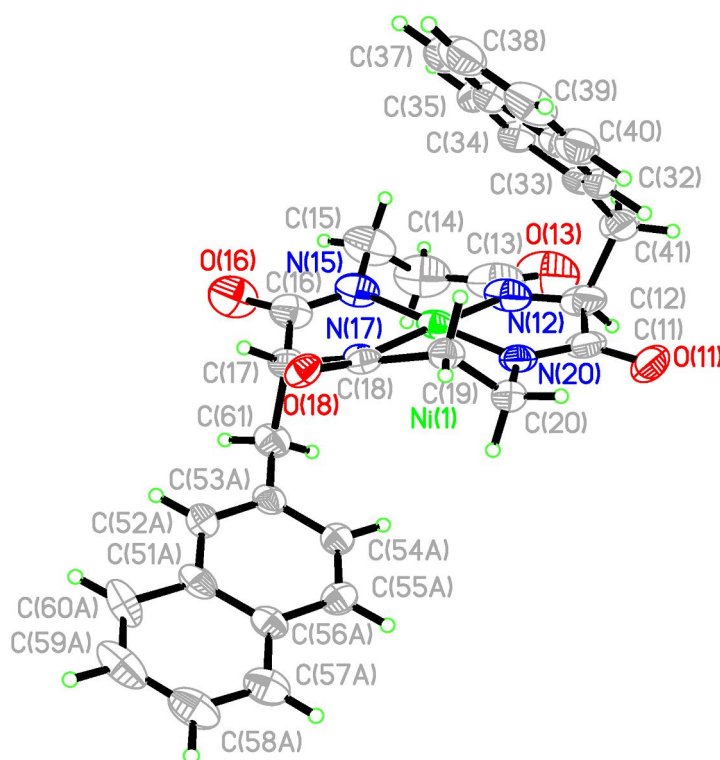
Figure 3.22: - X-ray Crystal Structure of –(βala-2-Nap(L)-βala-2-Nap(D))-Ni PPN complex (3.2e) (PPN Removed for Clarity).
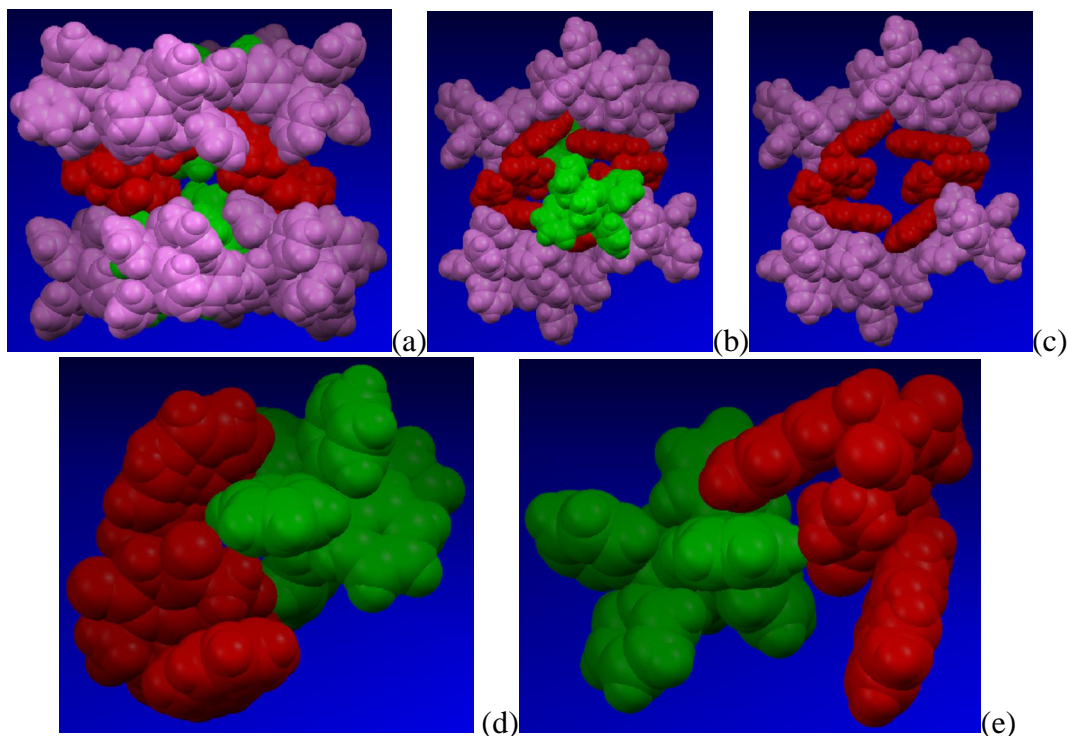
Figure 3.23: - (a) A space filled diagram showing all PPN molecules interacting with the Nap(L)Nap(D) dimer (Green PPN interacts in the gap between dimers, violet PPN interact with the dimer on the outside edge, solvents removed for clarity) (b) A space filled diagram showing the PPN interacting with the pocket (several outer PPN molecules removed for clarity) (c) A space filled diagram showing the complex dimer formed in the crystal (several outer PPN molecules and the interchelating π-π stacking PPN molecules removed for clarity) (d) A space filled diagram showing the CH-π interaction of a PPN to the Nap(L)Nap(D) complex within the cavity (all other PPN molecules removed for clarity) (e) A space filled diagram showing the π-π stacking of the PPN inside the cavity to the Nap(L)Nap(D) complex (all other PPN molecules removed for clarity).

Table 3.7: - Selected bond lengths, bond angles, torsion angles and ring alignment for complex 3.2e

Selected Bond Lengths	Selected Bond Angles
Ni(1)-N(20) (1.855Å), Ni(1)-N(12) (1.888Å), Ni(1)-N(15) (1.861Å), Ni(1)-N(17) (1.869Å), N(20)-C(11) (1.311Å), N(12)-C(13) (1.322Å), N(15)-C(16) (1.292Å), N(17)-C(18) (1.318Å), N(20)-C(20) (1.458Å), N(12)-C(12) (1.455Å), N(15)-C(15) (1.455Å), N(17)-C(17) (1.468Å), C(11)-O(11) (1.281Å), C(13)-O(13) (1.295Å), C(16)-O(16) (1.276Å), C(18)-O(18) (1.271Å).	N(20)-Ni(1)-N(12) (85.46°), N(12)-Ni(1)-N(15) (95.13°), N(15)-Ni(1)-N(17) (84.34°), N(17)-Ni(1)-N(20) (95.10°), N(20)-Ni(1)-N(15) (178.82°), N(17)-Ni(1)-N(12) (177.79°).
	Selected Torsion Angles
	O(11)-C(11)-C(12)-N(12) (174.22°), N(20)-C(11)-C(12)-N(12) (-10.05°), C(12)-N(12)-C(13)-O(13) (1.19°), C(20)-N(20)-C(11)-O(11) (3.25°), C(17)-N(17)-C(18)-O(18) (1.00°), C(15)-N(15)-C(16)-O(16) (-0.35°), O(11)-C(11)-C(12)-C (41) (-63.61°), O(16)-C(16)-C(17)-C (61) (72.15°),
	Six Membered Ring Alignment
	Trans

Another C_i symmetric compound synthesized was **3.2e**. **3.2e** shows the *trans* orientation of the 6 membered rings in the cyclopeptide nickel complexes as shown in **3.2f**.

The larger π surface in **3.2f** might be expected to form π-π interactions between the naphthyl rings within the crystal, however this does not occur. Both side arms in this case are in the pseudo axial position, more so than in complex **3.2e** and very closely rated to **3.2a**, with its *cis* orientated side arms. The large size of the side arms, and the fact that

123

they are both on opposite sides to each other may mean that the steric interactions with the carbonyls on the ligand structure are minimized by the position they take up (Figure 3.22).

Perhaps an even more important consideration in the solid-state conformation can be seen when one looks at the overall interaction of the cyclopeptide complex in the crystal (Figure 3.23). Here we can see that two of the nickel complexes T-stack to each other in the solid state forming a distinctive dimer (Figure 3.23c) very similar to a dimer observed in a molecular tweezer synthesized by Klarner *et al*[13] (Figure 3.24).
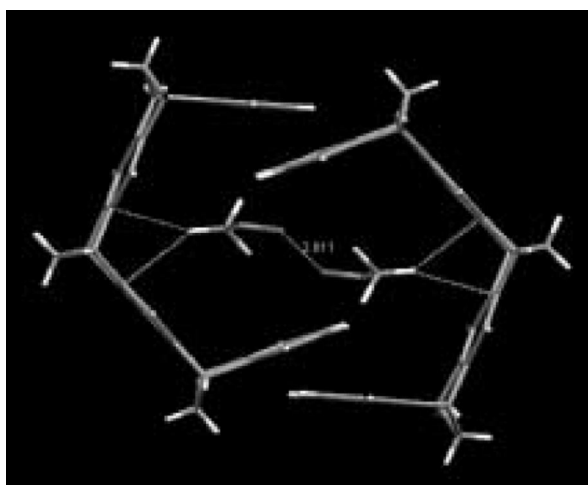
Figure 3.24: - Klarners tweezer dimer.

3.2f also interacts with the PPN counter ion to form multiple T-stacking interactions. All bond distances are around 3Å, well within the range for a π-CH interaction, this is visible in the space filled diagrams (Figures 3.23b and c). **3.2f** shows the presence of π-π interactions between 2PPN molecules and the complex with C-C distances of 3.521Å and 3.561Å (Figure 3.23e).

The crystal structures for **3.2a,e** and **f** show that complex formation under basic conditions allows the formed complex to maintain the stereochemical integrity of the tetrapeptide used in their synthesis. Whilst free peptides undergo racemization (to different extents depending on side arms), complexed peptides do not and thus stereochemical information is maintained. This discovery also lends credence to Beck's

interpretation of the stereochemical outcome of the dipeptide cyclizations performed in his lab.

3.3.4 *Electrochemical Data For Cyclopeptide Nickel Complexes.*

After the isolation of various nickel complexes electrochemical analysis was performed to determine the stability and usefulness of these complexes as single electron donors in respect to oxidation reactions with polyaromatic hydrocarbons (PAH's)[14]. Amido donors from ligand systems are capable of stabilizing high oxidation states in metal centres[15]. It was therefore considered that these ligand systems maybe capable of performing the same task by oxidizing Ni(II) to Ni(III). Beck has previously noted a side chain oxidation with nickel cyclopeptide complexes in acetonitrile and air at elevated temperatures[16].

The CV tests showed that the ligands were indeed capable of being oxidized from Ni(II) to Ni(III) with a range of 0.321-0.478eV being noted for the complexes **3.2a-f** (table 4.4) and each had a reverse wave indicating ligand and complex stability to electrochemistry (Figure 3.25).

A graph to show CV data for cyclopeptide Ni PPN complexes
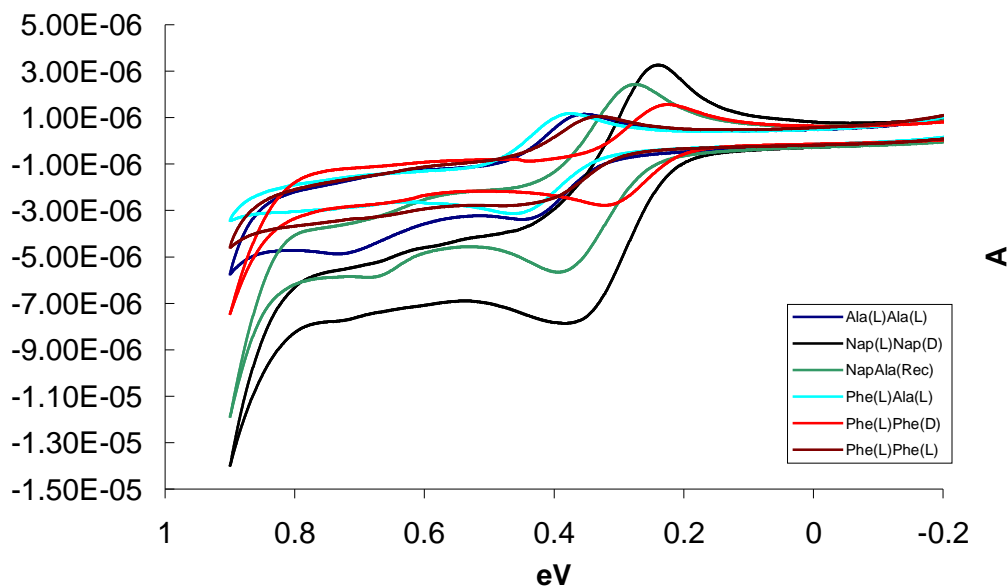
Figure 3.25: - **Electrochemical data for complexes 3.2a, b, c, e and f -[NiᴵᴵL] = 0.6 mM-** E^0(NiᴵᴵᴵL/NiᴵᴵL)**, vs. Ag/AgCl (in 3M KCl) solutions in DMSO:H$_2$O with KCl (20:1, 0.1M).**

Table 3.8: - **Cyclic voltammetry (CV) electrochemical data for complexes 3.2a, b, c, e and f.**

Complex	Ni(II)/Ni(III) wave (eV)	Ni(III)/Ni(II) wave (eV)	Half wave (eV)
Phe(S)Phe(S) (3.2a)	0.478	0.333	0.406
Ala(S)Ala(S) (3.2b)	0.447	0.348	0.398
Phe(S)Ala(S) (3.2c)	0.468	0.371	0.420
Phe(S)Phe(R) (3.2f)	0.321	0.218	0.270
Nap(S)Nap(R) (3.2e)	0.384	0.232	0.308

126

Table 3.9: - A table showing differences in Ni(II)-Ni(III) potentials (δeV) and the relative energies of stabilization between the different complexes 3.2a, b, c, e and f.

Complex	(3.2a) (SS)	(3.2b) (SS)	(3.2c) (SS)	(3.2f) (SR)	(3.2e) (SR)
(3.2a) (SS)	-	0.031eV	0.001eV	0.157eV	0.094eV
(3.2b) (SS)	2.99 KJ/Mol	-	0.021eV	0.126eV	0.063eV
(3.2c) (SS)	0.096 KJ/Mol	2.026 KJ/Mol	-	0.147eV	0.084eV
(3.2f) (SR)	15.148 KJ/Mol	12.157 KJ/Mol	14.183 KJ/Mol	-	0.063eV
(3.2e) (SR)	9.069 KJ/Mol	6.078 KJ/Mol	8.104 KJ/Mol	6.078 KJ/Mol	-
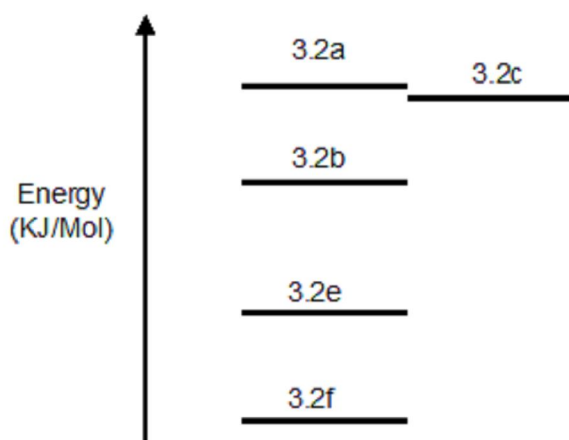
Figure 3.26: - Energy diagram showing relative stabilities of the Ni(III) complexes as deduced from CV data.

The oxidation values of complexes with *cis* orientated side arms (**3.2a, b and c**) are higher than those with trans orientated side arms (**3.2e and f**) (Table 3.8, Figure 3.26).

This may be a result of the stability of the formed product. Ni(III) (56pm)[17] has a smaller ionic radius than Ni(II) (69pm)[13], this decrease in size may in turn shorten the N-Ni bond lengths brining the side arms in closer proximity and extra strain in the ring systems may lead to more sterics between the sidearm and the carbonyls in the five and six membered rings. For the *cis* functionalized complexes this would increase the steric repulsion felt by each side arm to a greater extent than the *trans* and thus the energy to perform the reduction of Ni(II) to Ni(III) for the *cis* would be greater than that of the *trans* functionalized complexes (energy difference between **3.2a**-Ni^{III} and **3.2f**-Ni^{III} = 15.14 KJ/Mol in favor of **3.2f**). There may also be some extra ring strain involved with having both side arms in the *cis* configuration forcing the 5 membered rings to be more out of planarity than the corresponding *trans* substituted rings (Figures 3.17 and 3.20).

Table 3.10: - A table showing differences in Ni(III)-Ni(II) potentials (δeV) and the relative energies of stabilization between the different complexes 3.2a, b, c, e and f.

Complex	(3.2a) (SS)	(3.2b) (SS)	(3.2c) (SS)	(3.2f) (SR)	(3.2e) (SR)
(3.2a) (SS)	-	0.015eV	0.038eV	0.115eV	0.101eV
(3.2b) (SS)	1.447 KJ/Mol	-	0.023eV	0.13eV	0.116eV
(3.2c) (SS)	3.666 KJ/Mol	2.219 KJ/Mol	-	0.153eV	0.139eV
(3.2f) (SR)	11.096 KJ/Mol	12.543 KJ/Mol	14.762 KJ/Mol	-	0.014eV
(3.2e) (SR)	9.745 KJ/Mol	11.192 KJ/Mol	13.410 KJ/Mol	1.351 KJ/Mol	-
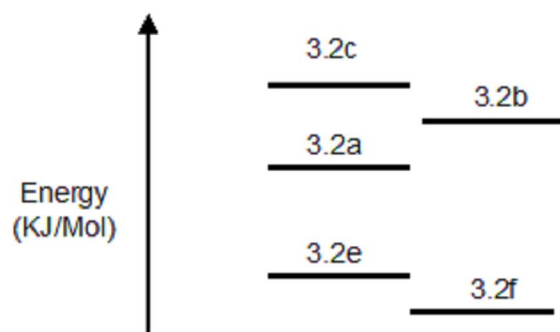
Figure 3.27: - Energy diagram showing relative stabilities of the Ni(II) complexes as deduced from CV data.

The reduction values of the Ni(III) complexes with *cis* orientated side arms (**3.2a, b and c**) are higher than those with trans orientated side arms (**3.2e and f**) (Table 3.9, Figure 3.27). This is a result of the stability of the formed product. The Ni(II) complexes experience steric hindrance to a lesser degree that the Ni(III) complexes however this effect is still present. For the *cis* functionalized complexes there is an increase the steric repulsion felt by each side arm to a greater extent than the *trans* and thus the energy to perform the reduction of Ni(III) back to Ni(II) for the *cis* would be greater than that of the *trans* functionalized complexes. In this case however there is a slight shift in the order of highest energy to lowest energy when compared to the oxidation values of the complexes. It appears that complex **3.2a** is in fact more stable than complexes **3.2b-c**. This is likely due to the presence of the internal CH-π interaction in **3.2a** that is not present in **3.2b** and less likely in **3.2c**. The internal CH-π interaction in **3.2a** stabilizes the complex by 3.66KJ/mol when compared to **3.2c**, this is close in value to the energy of a CH-π interaction, between 2KJ/Mol and 5.5KJ/Mol[18]. There may also be some extra ring strain involved with having both side arms in the *cis* configuration forcing the 5 membered rings to be more out of planarity than the corresponding *trans* substituted rings (Figures 3.17 and 3.20).

Cyclic voltammetry data can be utilized to ascertain the *cis* or *trans* relationship of side arms in the nickel complexes and thus gives us another tool in the identification of stereochemical configuration. Complexes with oxidation values (Ni(II)-Ni(III)) under 0.4eV have a *trans* configuration (as analyzed by X-ray crystallography and dialed in

configurations) whilst complexes with oxidation values above 0.4eV have the *cis* configuration (as analyzed by X-ray crystallography and dialed in configurations). Th

3.4   Binding Studies With Cyclopeptide Nickel Complexes.

After the isolation of several nickel cyclopeptide complexes it was decided that several binding studies should be performed to see if these systems were capable of pre-binding aromatic substrates. Although these systems were never intended to be used for hydrodehalogenations, similar systems (cyclic tetraamido iron complexes) had been previously used as oxidants[19] and with the electrochemical data already gained we knew that these systems could be used as single electron donors.

Several tests utilizing naphthalene and 1-hydroxy-naphthalene showed no binding induced chemical shift changes by ^{1}HNMR titration experiments (Figure 3.28).
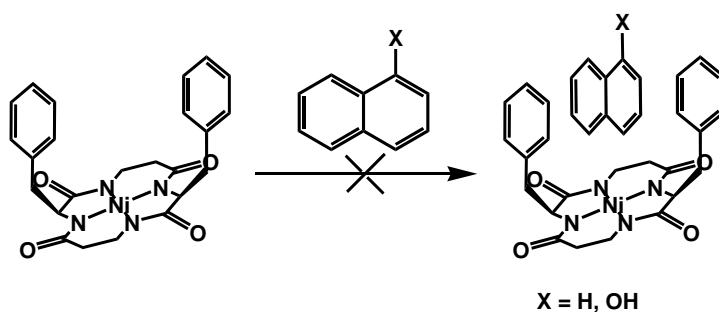
Figure 3.28: - Failed attempts at aromatic substrate binding.

3.4.1 Binding Studies With 1,10-Phenanthroline, Pyrazino[1,2,3,4 lmn][1,10]phenanthrolinediium 5,6-dihydro-dibromide, and 4,4'-Bipyridinium 1,1'-dimethyl-diiodide (dimethyl viologen).

After the binding studies with naphthalene and naphthol failed to produce π-π stacking it was decided that a larger, more electron poor aromatic substrate should be used to increase the probability of binding through having a larger surface to interact with and the electron poor nature of these compounds lowers the energy of the HUMO allowing stacking to occur more readily.

When phenanthroline was tested for binding to the complex **3.2a** no chemical shift changes were observed, as was the case for the naphthalene and naphthol. We then turned our attention to pyrazino[1,2,3,4 lmn][1,10]phenanthrolinediium, 5,6-dihydro-, dibromide (**3.12)** (Figure 3.29).

3.12
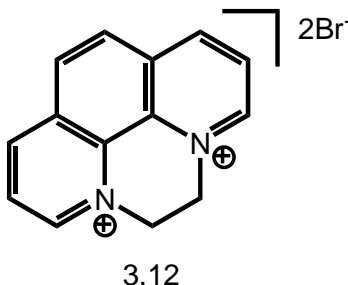
Figure 3.29: - Structure of pyrazino[1,2,3,4 lmn][1,10]phenanthrolinediium, 5,6-dihydro-, dibromide 3.12

3.12 was chosen due to its extremely electron poor nature which is better for π-π interactions with the relatively electron rich aromatic rings in the cyclopeptide complexes[20]. It was hoped that the π surface and the charge attraction in this salt would show some binding in solution. Drastic changes were observable in the ^{1}HNMR spectrum of **3.12** when complex **3.2a** was titrated into the solution (Figure 3.30).
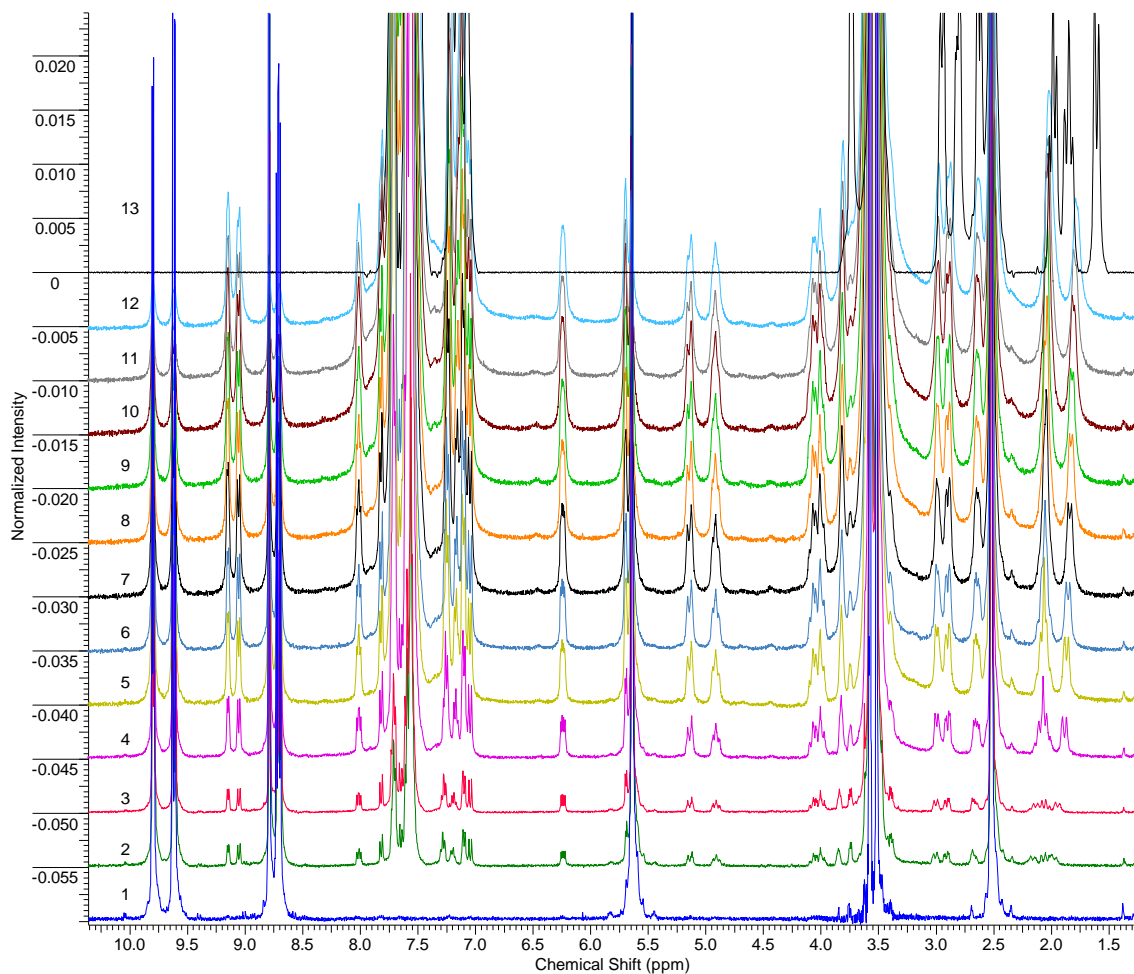
Figure 3.30: - Stack plot NMR of the complex 3.2a titrated into a solution of 3.12 in a DMSO-d6:D₂O mixture (20:1). 1= Guest, 2= 0.1eq Host in Guest, 3 = 0.2eq Host in Guest, 4 = 0.3eq Host in Guest, 5 = 0.4eq Host in Guest, 6 = 0.5eq Host in Guest, 7 = 0.6eq Host in Guest, 8 = 0.7eq Host in Guest, 9 = 0.8eq Host in Guest, 10 = 0.9eq Host in Guest, 11 = 1eq Host in Guest, 12 = 1.1eq Host in Guest, 13 = Host.
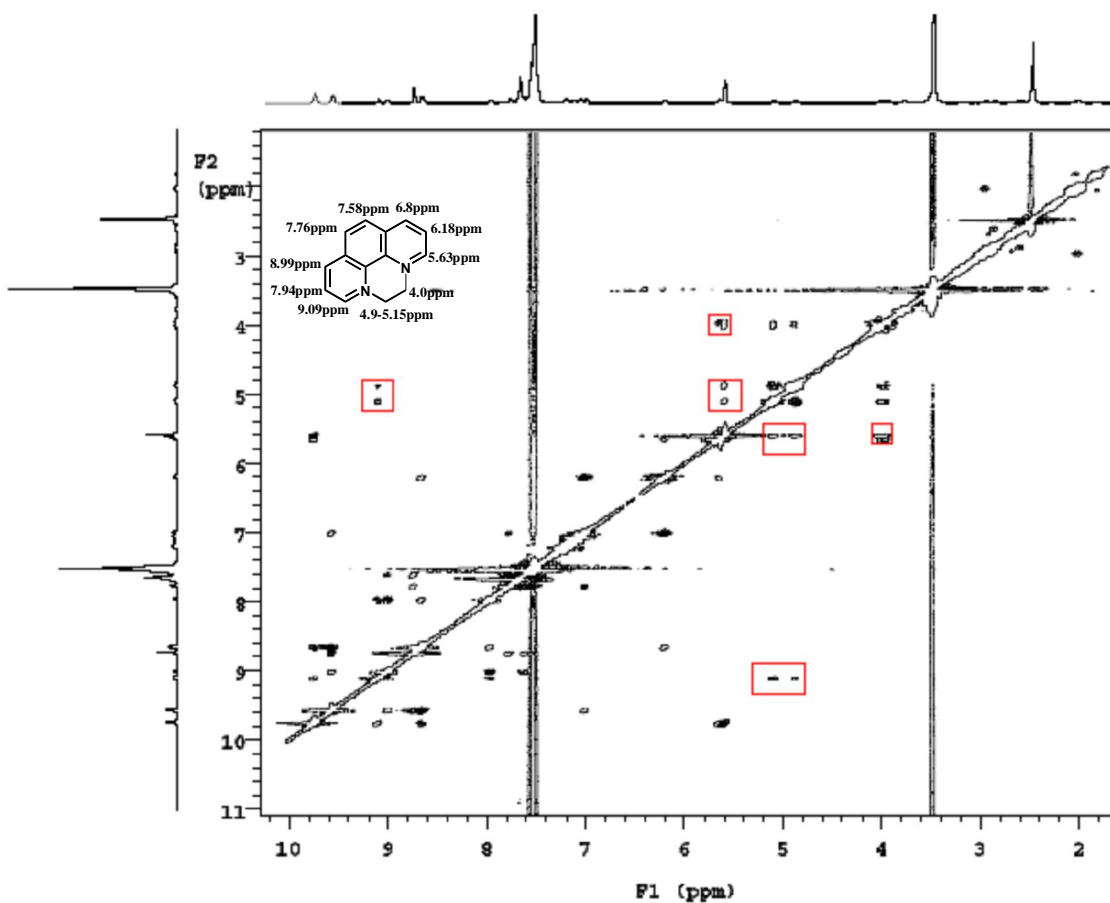
Figure 3.31: - ROSEY NMR of 3.12 combined with 3.2a in DMSO-D6:D$_2$O (20:1)

ROSEY NMR (Figure 3.31) confirms the closed nature of the bound **3.12** via cross peaks at 5.63ppm to 4.0ppm and 9.09ppm to 4.9-5.1ppm. No cross peaks between the bound **3.12** and **3.2a** were observed in the spectra leading to the belief that no chemical bond forming/breaking process is involved in the generation of the new species and a strong ion pair interaction is occurring (although no interaction between **3.12** and **3.2a** is observed). Reaction of a mixture of **3.2a** and **3.12** with phosphoric acid leads to the complete destruction of the newly formed salt interaction via protonation of the **3.2a** dianion. **3.2a** was seen to react readily with MeI to form metabolites however this reaction is retarded in the presence of **3.12** indicating that the tight ion pair reduces the nucleophilicity of the anion.
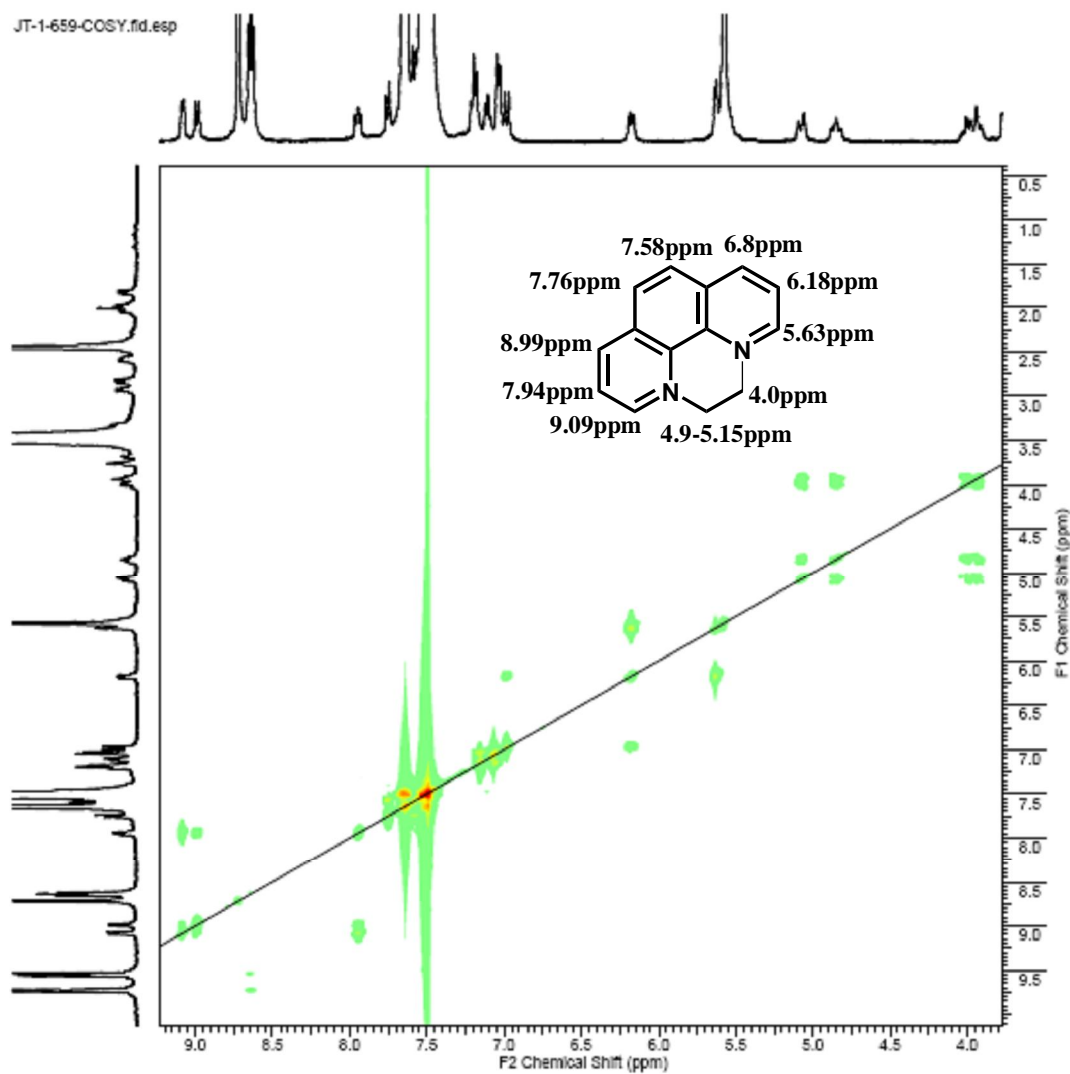
Figure 3.32: - COSY NMR of 3.12 mixed with 3.2a (DMSO-d6:D₂O 20:1)

Table 3.11: - Chemical Shift data for 3.12 and 3.12x (3.12 interacting with host)

Compound	Chemical shift in DMSO-d₂:D₂O (20:1) δ
3.12 free	5.64 (s, 4 H) 8.71 (dd, *J*=8.39, 5.66 Hz, 2 H) 8.79 (s, 2 H) 9.62 (dd, *J*=8.39, 1.37 Hz, 2 H) 9.80 (dd, *J*=5.66, 0.98 Hz, 2 H)
3.12 bound	3.87 - 3.97 (m, 1 H) 3.97 - 4.05 (m, 1 H) 4.85 (m, 1 H) 5.08 (dt, *J*=14.25, 3.9 Hz, 1 H) 5.63 (d, *J*=4.69 Hz, 1 H) 6.18 (dd, *J*=9.76, 4.69 Hz, 1 H) 6.98 (d, *J*=9.76 Hz, 1 H) 7.58 (d, *J*=8.59 Hz, 2 H) 7.75 (d, *J*=8.59 Hz, 1 H) 7.95 (dd, *J*=8.20, 5.86 Hz, 1 H) 8.99 (d, *J*=8.20 Hz, 1 H) 9.08 (d, *J*=5.08 Hz, 1 H)

Table 3.12: - Binding constants of 3.12 with complexes 3.10a-d.

Complex	Binding/equilibrium constant (k^{obs}) (M^{-1}) of 3.12	$\Delta G^o = -RT\ln(k)$ KJ/Mol
3.2a	267.97	-13.85
3.2b	217.79	-13.33
3.2c	594.15	-15.82
3.2d	280.00	-13.96

The binding study experiment was repeated for complexes **3.2b-d** with **3.12** and the binding constants were obtained (Table 3.12). The energy of this interaction was between -13.33 and –15.82KJ/Mol, far too much for the average π-π or π-CH (Figure 3.33) but not for a tight ion pair interaction[21] (Figure 3.31). Complexes **3.2b-d** all show binding of **3.12**, most unusual if π-π or π-CH host guest interactions are occurring due to the lack of aromatic side arms on complex **3.2b**. Therefore binding of the nature shown in figure 3.33 was rejected in favor of the binding of the type shown in figure 3.34.
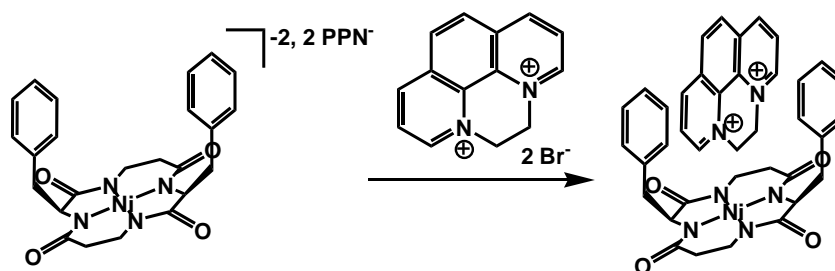
Figure 3.33: - Binding of the phenanthroline salt to the tweezer shaped cavity of the cyclopeptide nickel complex.
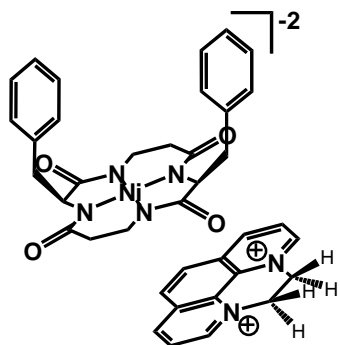
Figure 3.34: - The guest molecule in close proximity to the host molecule.

After the binding study with **3.12** it was decided that performing a test on a similar di-cation would be useful. Methyl viologen (**3.15**) was chosen as a suitable aromatic di-cation for the binding studies. It has a π surface (the twist out of the plain for the pyridine rings is representative of PCB molecules) and the same charge as the **3.12**. A mixture of **3.2a** and **3.15** failed to produce any discernable interactions in solution with no changes in ^{1}HNMR (Figure 3.35). It was therefore considered that the ion pair interaction may occur with **3.12** due to a preferred alignment of charges. **3.12** has a flat surface and charges that are approximately 2.84Å apart. **3.15** has a slightly bent surface and a charge separation of approximately 6.98Å. The distance between the nitrogens (N-Ni-N) in complex **3.2a** is around 3.715Å whilst the carbonyl oxygens have an approximate separation of 7.58Å. With this information it may be logical to assume that the charge-charge interactions occur closer to the nitrogens in both **3.12** and **3.2a** rather than between the carbonyl oxygens and the nitrogens in **3.15** and **3.2a**. Thus cationic charge separation plays an important role in the tight ion pair formation in this series of complexes.
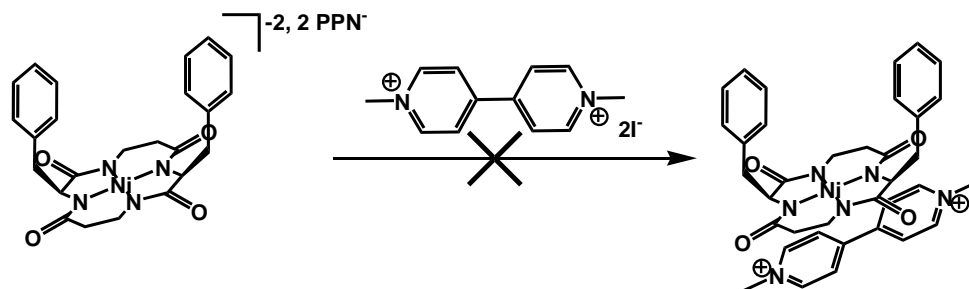
Figure 3.35: - Possible binding of methyl viologen to a nickel cyclopeptide complex through ion pair formation.

Although binding of **3.15** to **3.2a** was not observed via ^{1}HNMR preparation of a mixture of **3.2a** and **3.15** in DMSO led to the generation of a blue colored solution (in air). When shaken in air the blue color quickly disappeared and an orange color was observed.

The blue color that was observed in the ^{1}HNMR tube before mixing with air became of some interest, as this color is usually associated with viologen radicals. When the experiment was repeated under inert conditions the deep blue color remained stable for at least 24 hours (later UV studies showed the blue color to be stable for over a month). The ^{1}HNMR of **3.2a** and **3.15** under inert conditions showed no sign of the methyl viologen indicating the formation of radicals in solution.

The Ni(II) complex **3.2a** loses an electron to form a stabilized Ni(III) complex **3.16** and forms the viologen radical **3.17** which is ^{1}HNMR inactive (Figure 3.36).
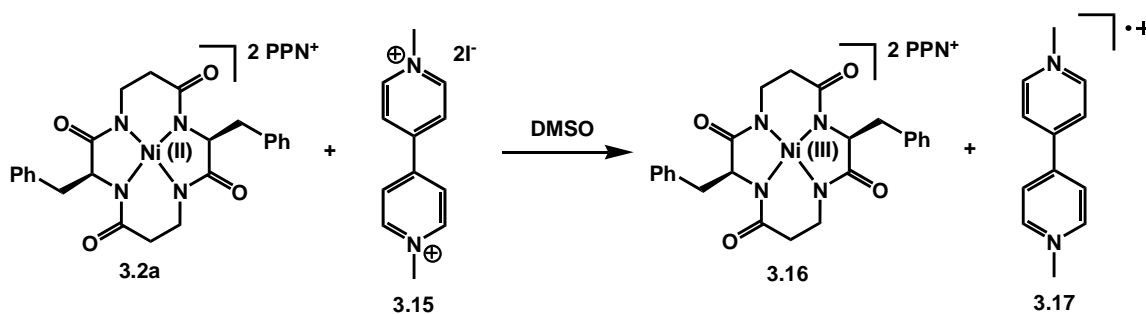
Figure 3.36: - Reduction of viologen utilizing a nickel cyclopeptide complex (3.2a).

UV spectra of a mixture of **3.2a** and **3.15** shows peaks at 268, 389, 400, 485 and 610nm. The peak at 610nm represents the methyl viologen radical (Figure 3.37).
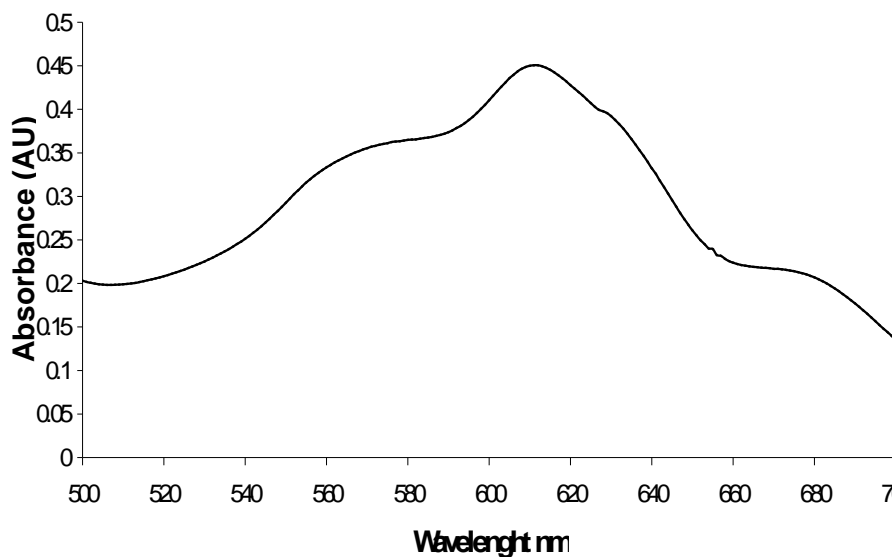
Figure 3.37: - UV trace of complex 4.4 with viologen in DMSO under inert conditions.

The addition of triethanolamine (TEOA) to the reaction mixture of complex **3.2a** and **3.15** gives a marked increase in the UV absorption at 610nm. In this case the TEOA acts as a sacrificial donor[22] to regenerate the Ni(II) complex from the Ni(III). Once this is done the electron can then be used to reduce another viologen molecule and the cycle can continue (Figure 3.38). It must be noted that once the radical of TEOA is formed from the initial reduction of **3.16** the radical cation can be utilized to reduce **3.15** as well.
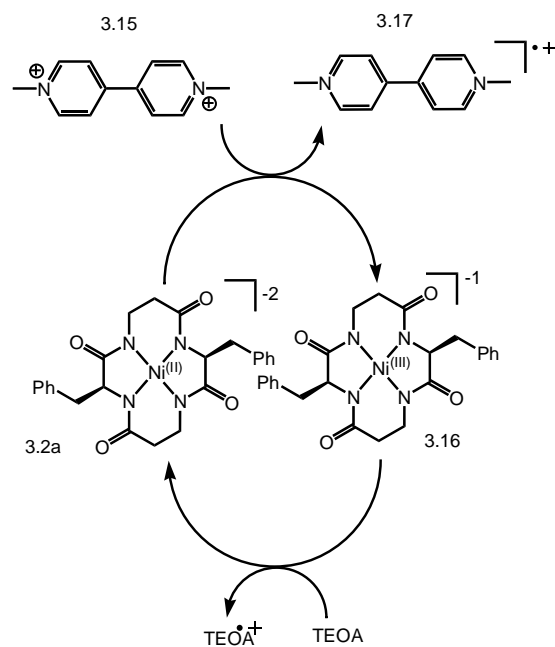
Figure 3.38: - Possible catalytic cycle observed using TEOA.

3.5 Conclusions.

In this chapter we can see that dipeptide nickel complexes can be isolated in low to moderate yield and show that the configuration of the dipeptides/tetrapeptides utilized in the synthesis is imparted to the generated complexes in the presence of a strong base at room temperature. Metal templated cyclization of dipeptides did not yield pure products in our hands. Tetrapeptide metal templated cyclizations on the other hand proved extremely effective. Not only are the cyclizations cleaner and faster using tetrapeptides, crystallizations utilizing PPN allowed the isolation of very pure X-ray quality products.

Cyclizations on solid support have been shown to be effective, although yields were not determined. Purification of these complexes was not achieved, however mass spectrum data clearly shows product formation.

X-ray quality crystals allowed for the determination of stereochemistry in the products. It was seen that all the products analyzed by X-ray crystallography showed retention of configuration imparted to them through the tetrapeptides synthesized in chapter 2. C_2, C_i and C_1 symmetric complexes were all synthesized using these

conditions. Although racemization of free peptides was shown, cyclized peptide complexes do not undergo racemization reactions under the reaction conditions.

Looking at the crystal structures we can see that the aromatic side arms of the cyclopeptide complexes interact with the aromatic rings in the PPN. This allows for the formation of interacting layers in complexes **3.2a** and **3.2f** with no interactions occurring between individual cyclopeptide complexes.

The complex **3.2e**, having larger aromatic sidearms, show a significantly increased amount of CH-π interactions when compared to complexes **3.2a** and **3.2f**. This complex also shows *π-π interactions* with the PPN and interestingly CH-π interactions with another cyclopeptide complex to form discreet dimers in the crystal. This complex loses the ordered layer structure shown by the other two complexes with counter ion interactions occurring all throughout the crystal.

The CH-π and π-π interactions shown by these molecules in the crystal structure gave us great hope that similar interactions would be possible with other aromatic substrates. However I was unable to identify π-π stacking in solution with 2-3 suitable guest molecules.

Electrochemical data was utilized to determine the relative stabilities of complexes **3.2a, b, c, e** and **f**. The data shows that *cis* functionalized cyclopeptide complexes are more difficult to oxidize than *trans* functionalized cyclopeptide complexes, probably due to the extra steric hindrance observed when the metal center contracts from Ni(II) to Ni(III), although differences in ring strain energies may also play a part in the energy differences.

Tight ion pair interactions shown between complexes **3.2a-d** and **3.12** have been identified and charge separation has been theorized as to the reason why **3.15** does not undergo the same type of ion pair formation.

A novel use for the cyclopeptide nickel complexes was found when they were seen to act as good single electron donors to viologen in DMSO, with a possible catalytic cycle being established in the presence of TEOA.

All together the isolation and characterization of the cyclopeptide metal complexes allowed us to fulfill one part of the overall goal of this project, the control of stereochemical integrity for cyclam precursors from affordable starting materials.

3.6   Experimental.

All chemicals were purchased from Aldrich, Acros Organics or Fisher Scientific and used without further purification.

3.6.1   General Synthesis of Dipeptide Nickel Complexes.

To a mixture of the dipeptide HCl salt (1.0 mmol) and $NiCl_2.(H_2O)_6$ (118.85mg, 0.5mmol) in methanol (10mL) is slowly added NaOMe (216mg, 4.0mmol) in methanol (3.0mL). Between 10 minutes and an hour of stirring at RT an orange solid drops out of solution. The solid is collected by centrifugation/filtration and recrystallized form hot methanol.

(MeO-Bala-Phe-NH2)$_2$Ni (3.1a)
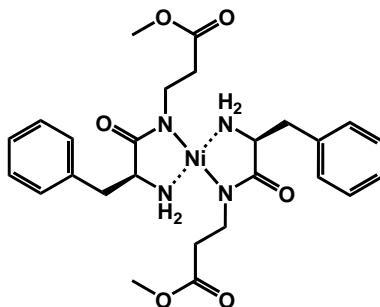
Yield 110mg, 59.3%. 1H NMR (200 MHz, DMSO-D6) δ 2.03 - 2.46 (m, 9 H) 2.54 - 2.75 (m, 2 H) 2.83 - 2.99 (m, 3 H) 3.02 (d, *J*=3.30 Hz, 1 H) 3.15 (d, *J*=4.40 Hz, 1 H) 3.55 (s, 6 H) 3.65 - 3.86 (m, 2 H) 7.16 - 7.35 (m, 10 H). ^{13}C NMR (101 MHz, DMSO-D6) δ 30.67, 33.98, 37.68, 51.20, 56.70, 126.35, 128.30, 129.27, 137.91, 173.20, 179.95. See X-ray crystal structure for stereochemical analysis.

(MeO-Bala-4methylPhe-NH₂)₂Ni (3.1b)
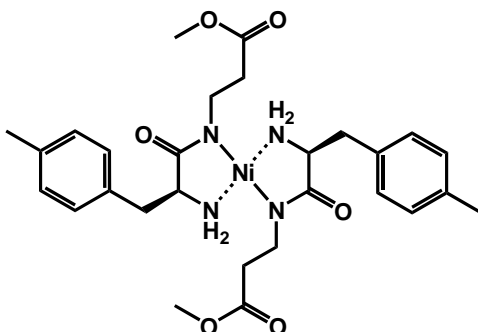
Yield 70mg, 18%. ^{1}H NMR (400 MHz, DMSO-D6) δ 2.08 - 2.20 (m, 4 H) 2.26 (s, 6 H) 2.29 - 2.40 (m, 4 H) 2.63 (dd, *J*=8.2, 14.68 Hz, 2 H) 2.86 (broad s, 2 H) 2.96 (dd, *J*=3.71, 13.86 Hz, 2 H) 3.57 (s, 6 H) 3.77 (m, 2 H) 7.12 (d, *J*=8.20 Hz, 4 H) 7.16 (d, *J*=8.20 Hz, 4 H). ^{13}C NMR (101 MHz, DMSO-D6) δ 20.66, 33.98, 37.68, 38.22, 51.17, 56.81, 128.92, 129.18, 134.65, 135.33, 173.12, 179.98. MS: *m/z* calculated for $C_{28}H_{38}N_4O_6$ = 584.2145, actual *m/z* (M+H) = 585.139. See X-ray crystal structure for stereochemical analysis.

(MeO-Bala-Nap-NH2)₂Ni (3.1c)
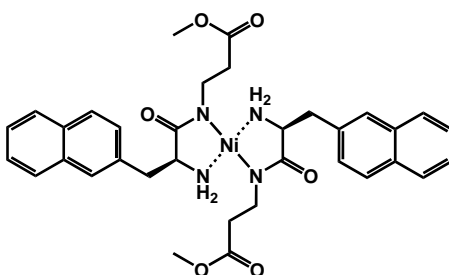
Yield 50mg, 28.5%. MS: *m/z* calculated for $C_{34}H_{38}N_4O_6$ = 656.2145, actual *m/z* (M+H) = 657.150. ^{1}H NMR (400 MHz, DMSO-D6) δ 2.03 - 2.14 (m, 4 H) 2.24 - 2.35 (m, 4 H) 2.35 - 2.44 (m, 2 H) 2.69 (dd, *J*=13.86, 8.39 Hz, 2 H) 2.97 (s, 2 H) 3.08 (dd, *J*=13.86, 2.93 Hz, 2 H) 3.36 - 3.44 (m, 6 H) 3.80 - 3.91 (m, 2 H) 7.35 (d, *J*=8.59 Hz, 2 H) 7.40 - 7.46 (m, 2 H) 7.49 (t, *J*=7.42 Hz, 2 H) 7.62 (s, 2 H) 7.79 (d, *J*=8.20 Hz, 2 H) 7.86

(t, *J*=7.81 Hz, 4 H). ^{13}C NMR (101 MHz, DMSO-D6) δ 33.96, 37.74, 38.65, 51.01, 56.63, 125.41, 125.96, 127.38, 127.45, 127.60, 127.75, 127.87, 131.90, 133.02, 135.39, 172.98, 179.86.

3.6.2   Synthesis of Cyclopeptide Complexes.

<u>[(-Bala-Phe(L)-Bala-Phe(L)-)Ni[II]][-2]2PPN[+] (3.2a)</u>
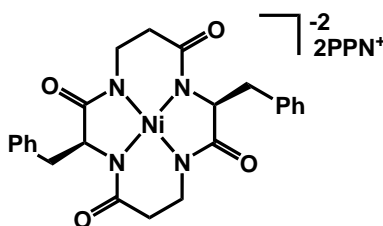
The H-Phe(L)-Bala-Phe(L)-Bala-OMe (2.34a) (845mg, 1.45mmol) and NiCl$_2$(H$_2$O)$_6$ (345mg, 1.45mmol) were dissolved in methanol (20mL) and NaOMe (470mg, 8.7mmol) was added all at once. The mixture was then stirred and heated to 65°C for between 24 hours. The solution was cooled and the precipitate that had formed was filtered off. To the orange solution was added the PPN-Cl (1.66g, 2.9mmol). The solvent was then removed and the solid taken up into acetone (~30mL). To this solution was added water until it was seen that a cloudy precipitate was about to drop out of solution. The mixture was then placed in the fridge at +5°C for 24 hours. The crystals that had formed were then filtered off to give pure product. The filtrate was again placed in the fridge and the process of crystallization repeated two more times. Total yield 1.09g, 47.9%. ^{1}H NMR (400 MHz, CD$_3$OD) δ 1.82 (d, *J*=15.28 Hz, 2 H) 2.09 - 2.19 (m, 2 H) 2.17 - 2.32 (m, 2 H) 2.79 (dd, *J*=13.05, 5.41 Hz, 2 H) 2.99 (dd, *J*=12.89, 5.25 Hz, 2 H) 3.08 (d, *J*=12.41 Hz, 2 H) 4.09 - 4.20 (m, 2 H) 7.07 - 7.15 (m, 2 H) 7.16 - 7.26 (m, 8 H) 7.42 - 7.76 (m, 60 H). ^{13}C NMR (101 MHz, CD$_3$OD) δ 39.41, 40.14, 40.93, 65.43, 126.72, 128.09, 128.10, 128.39, 129.16, 129.18, 130.55, 130.61, 130.68, 131.57, 133.41, 133.47, 133.53, 134.88, 140.64, 174.38, 180.93. See X-ray crystal structure for stereochemical analysis.

[(-Bala-Nap(L)-Bala-Nap(L)-)Ni^{II}]$^{-2}$2PPN$^+$ (3.2b)
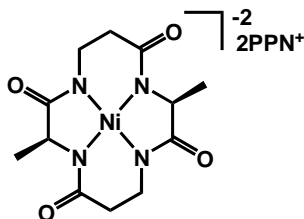
The H-Ala(L)-Bala-Ala(L)-Bala-OMe (2.39g) (113mg, 0.263mmol) and the NiCl$_2$ salt (62.5mg, 0.263mmol) with the NaOMe (freshly prepared 216mg, 4mmol) were vigorously dried under vacuum and dissolved in methanol (15ml). The reaction was then heated to 60 °C for between 12 hours. The PPN-Cl was added and any ppt was removed via centrifugation. The solvent was removed and the complex taken up in acetone/methanol and water added until just before the cloudy ppt appeared. The mixture was placed in the fridge. White crystals ppt out of solution these were removed via filtration. The solvent was removed until there was just a little water remaining and the solid was allowed to crystallize from the solution. The orange solid was then filtered off and washed with water, then dried *in vacuo*. Yield 142mg, 38%. ^{1}H NMR (400 MHz, CD$_3$OD) δ1.21 - 1.32 (d, *J*=6.64 Hz 6 H) 1.95 (m, 2 H) 2.14 (m, 2 H) 2.17 - 2.27 (m, 2 H) 2.32 (m, 2 H) 3.21 (m, 2 H) 3.95 (q, *J*=6.25 Hz, 2 H) 7.53 (m, 24 H) 7.59 (m, 24 H) 7.69 (t, *J*=7.03 Hz, 12 H). ^{13}C NMR (101 MHz, CD$_3$OD) δ 20.55, 39.50, 40.43, 60.65, 28.11, 129.20, 130.55, 130.62, 130.69, 133.43, 133.49, 133.54, 134.89, 175.14, 183.16.

[(-Bala-Phe(L)-Bala-Ala(L)-)Ni^{II}]^{-2}2PPN^{+} (3.2c)
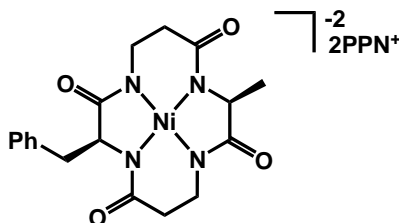
The H-Ala(L)-Bala-Phe(L)-Bala-OMe (2.34d) (52.6mg, 0.1mmol) and NiCl$_2$(H$_2$O)$_6$ (23.8mg, 0.1mmol) were dissolved in methanol (5mL) and NaOMe (43mg, 0.8mmol) was added all at once. The mixture was then stirred and heated to 65°C for 12-24 hours. The solution was cooled and the precipitate that had formed was filtered off. To the orange solution was added the PPN-Cl (115mg, 2mmol). The solvent was then removed and the solid taken up into acetone (~10mL). To this solution was added water until it was seen that a cloudy precipitate was about to drop out of solution. The mixture was then placed in the fridge at -5°C for 24 hours. The crystals that had formed were then filtered off to give pure product. Yield 40mg, 26.8%.[23] ^{1}H NMR (400 MHz, CD$_3$OD) δ 1.15 (d, *J*=6.64 Hz, 3 H) 1.60 - 1.70 (m, 2 H) 1.92 - 2.00 (dt, *J*=1.4 Hz, *J*=12 Hz, 1 H) 2.01 - 2.09 (m, 2 H) 2.29 (t, *J*=12.69 Hz, 1 H) 2.93 (dd, *J*=12.88, 3.12 Hz, 1 H) 3.03 (dd, *J*=12.88, 4.69 Hz, 1 H) 3.15 (dt, *J*=12.79, 3.37 Hz, 1 H) 3.72 (q, *J*=6.51 Hz, 1 H) 4.16 - 4.26 (t, 4 Hz, 1 H) 7.12 - 7.20 (m, 1 H) 7.20 - 7.30 (m, 4 H) 7.47 (m, 9 H) 7.48 - 7.51 (m, 17 H) 7.52 - 7.60 (m, 23 H) 7.66 (t, *J*=6.83 Hz, 12 H) ^{13}C NMR (101 MHz, CD$_3$OD) δ 20.63, 38.66, 39.00, 39.53, 39.78, 39.92, 60.74, 65.47, 127.03, 128.11, 128.37, 129.18, 130.68, 131.87, 133.52, 134.90, 139.94, 174.67, 175.03, 179.55, 182.61.

[(-Bala-Nap(L)-Bala-Nap(L)-)Ni[II]][-2]2PPN[+] (3.2d)
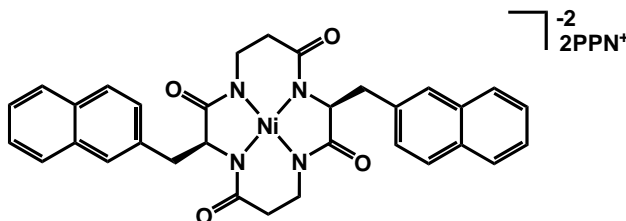
The Cl.H$_3$N-Nap(L)-Bala-Nap(L)-Bala-OMe (2.34c) (134mg, 0.22mmol) and NiCl$_2$(H$_2$O)$_6$ (52.5mg, 0.22mmol) were dissolved in methanol (15mL) and NaOMe (96.2mg, 1.78mmol) was added all at once. The mixture was then stirred and heated to 65°C for 24 hours. The solution was cooled and the precipitate that had formed was filtered off. To the orange solution was added the PPN-Cl (254mg, 442mmol). The solvent was then removed and the solid taken up into acetone (~20mL). To this solution was added water until it was seen that a cloudy precipitate appeared. The mixture was then placed in the fridge at +5°C for 24 hours. The crystals that had formed were then filtered off to give pure product. Yield 33mg, 8.9%. ^{1}H NMR (400 MHz, CD$_3$OD) δ 2.12 (td, *J*=14.54, 4.10 Hz, 2 H) 2.28 (t, *J*=12.88 Hz, 2 H) 2.54 (dd, *J*=12.69, 6.05 Hz, 2 H) 2.92 (dd, *J*=12.88, 4.69 Hz, 2 H) 3.08 (dt, *J*=12.79, 2.78 Hz, 2 H) 4.16 (t, *J*=5.27 Hz, 2 H) 7.18 (t, *J*=7.03 Hz, 2 H) 7.24 - 7.34 (m, 4 H) 7.36 (s, 2 H) 7.50 (td, *J*=7.61, 3.51 Hz, 27 H) 7.53 - 7.61 (m, 23 H) 7.61 - 7.69 (m, 16 H) 7.74 (d, *J*=8.20 Hz, 2 H). ^{13}C NMR (101 MHz, CD$_3$OD) δ 39.34, 40.19, 41.24, 65.39, 125.58, 126.21, 127.47, 128.08, 128.56, 128.71, 129.16, 129.67, 130.54, 130.61, 130.67, 133.40, 133.46, 133.52, 133.76, 134.88, 138.36, 174.24, 180.94.

[(-Bala-Nap(L)-Bala-Nap(D)-)Ni^{II}]$^{-2}$2PPN^{+} (3.2e)
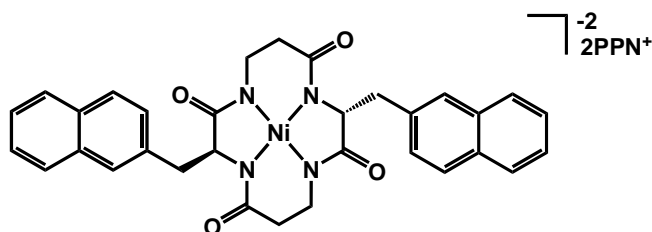
The Cl.H$_3$N-Nap(L)-Bala-Nap(D)-Bala-OMe (185mg, 0.305mmol) and NiCl$_2$(H$_2$O)$_6$ (72.5mg, 0.305mmol) were dissolved in methanol (15mL) and NaOMe (96.2mg, 1.78mmol) was added all at once. The mixture was then stirred and heated to 70°C in a schlenk flask for 24 hours. To the orange solution was added the PPN-Cl (254mg, 442mmol). The solvent was then removed and the solid taken up into acetone (~20mL). To this solution was added water until it was seen that a cloudy precipitate was observed. The mixture was then placed in the fridge at +5°C for 24 hours. The crystals that had formed were then filtered off to give pure product. Yield 150mg, 30%. ^{1}H NMR (400 MHz, CD$_3$OD) δ 1.37 - 1.48 (m, 2 H) 1.67 (m 2 H) 2.14 (m, 2 H) 2.97 - 3.09 (m, 4 H) 3.15 (m 2 H) 4.00 (m, 2 H) 7.28 (m 4 H) 7.40 (d, J=8.59 Hz, 2 H) 7.48 (d, J=1.95 Hz, 15 H) 7.49 (m, 9 H) 7.56 (m, 23 H) 7.61 - 7.68 (m, 15 H) 7.68 - 7.74 (m, 6 H)) ^{13}C NMR (50 MHz, CD$_3$OD) δ 38.71, 38.96, 39.58, 65.23, 125.67, 126.28, 127.45, 128.54, 129.60, 129.64, 129.78, 130.39, 130.46, 130.58, 130.72, 130.77, 130.90, 133.24, 133.30, 133.41, 133.53, 133.60, 133.77, 134.85, 137.73, 174.45, 179.17. See X-ray crystal structure for stereochemical analysis.

[(-Bala-Phe(L)-Bala-Phe(D)-)Ni^{II}]$^{-2}$2PPN$^+$ (3.2f)
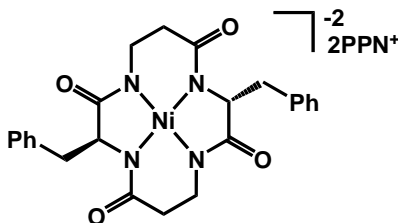
The H-Phe(L)-Bala-Phe(D)-Bala-OMe (100mg, 0.172mmol) and NiCl$_2$(H$_2$O)$_6$ (40.9mg, 0.172mmol) were dissolved in methanol (15mL) and NaOMe (81mg, 1.5mmol) was added all at once. The mixture was then stirred and heated to 70°C for 24 hours. The solution was cooled and the precipitate that had formed was filtered off. To the orange solution was added the PPN-Cl (197mg, 0.344mmol). The solvent was then removed and the solid taken up into acetone (~30mL). To this solution was added water until it was seen that a cloudy precipitate was about to drop out of solution. The mixture was then placed in the fridge at -5°C for 24 hours. The crystals that had formed were then filtered off to give pure product. Total yield 76.8mg, 28.5%. ^{1}H NMR (400 MHz, CD$_3$OD) δ 1.66 (dd, J=13.08, 4.10 Hz, 2 H) 1.70 - 1.77 (m, 2 H) 2.13 (t, J=12.49 Hz, 2 H) 2.87 (dd, J=12.88, 3.51 Hz, 2 H) 2.92 (dd, J=13.27, 5.08 Hz, 2 H) 3.14 (dt, J=12.49, 3.51 Hz, 2 H) 4.00 - 4.09 (m, J=3.51, 3.51 Hz, 2 H) 7.13 - 7.24 (m, 10 H) 7.50 (td, J=7.71, 3.32 Hz, 24 H) 7.55 - 7.61 (m, 24 H) 7.68 (td, J=7.32, 1.76 Hz, 12 H). ^{13}C NMR (101 MHz, CD$_3$OD) δ 38.67, 39.13, 39.59, 65.21, 126.91, 128.08, 128.27, 129.17, 130.54, 130.61, 130.67, 131.80, 133.41, 133.46, 133.52, 134.88, 139.95, 174.57, 179.14. See X-ray crystal structure for stereochemical analysis.

3.6.3 General Synthesis of Cyclopeptide Nickel Complexes From Resins

To the amine terminated tetrapeptide (general formula PS-CO-β-ala-X-β-ala-X-NH$_2$) on the hydroxymethyl resin (0.1mmol) was added a solution of NiCl$_2$·6H$_2$O (47.4mg, 0.2mmol) in H$_2$0:NH$_4$OH:AcCN (1:1:1) (5ml). The solution was shaken for 1

hour at RT and the resin was drained and washed 4 times with DMF (20mL) and 4 times with DCM (20mL). To the resin was added methanol (1mL) and NaOMe (10.8mg, 0.2mmol)). This was then heated at 60°C for 24 hours. The resin was filtered off and the orange solution analyzed by MS directly.

References: - Chapter 3

[1] a) K. Haas, E. Ehrenstorfer-Schäfers, K. Polborn, and W Beck, *Eur. J. Inorg. Chem.,* 1999, 465-469; (b) M. A. Lang and W. Beck, *Z. Naturforsch.*, 2003, **58b,** 447 – 450; (c) K. Haas, W. Ponikwar, H. Nöth, and W. Beck, *Angew. Chem. Int. Ed.,* 1998, **37**, 1086-1089; (d) J. Schapp, K. Haas, K. Sünkel, and W. Beck, *Eur. J. Inorg. Chem.,* 2002, **20**, 3745-3751.

[2] S. Chirachanchai, S. Phongtamrug, T. Rungsimanon, *Tet. Lett.,* 2008, **49**, 3181-3184; (b) J. E. Klee, K. Haegele, M. Przybylski, *J. Poly. Sci.,* 2003, **41**, 2047-2052; (c) A. Bertram, G. Pattenden, *Heterocycles*, 2002, **58**, 521-561; (d) A. J. Blake, J. S. Hannam, K. A. Jolloffe, G. Pattenden, *Synlett,* 2000, **10** 1515-1518; (e) A. El-Mottaleb, M. Ramadan, *Transition Met. Chem.,* 1998, **23**, 491-495; (f) Y. Kuroki, K. Ishihara, N. Hanaki, S. Ohara, H. Yananoto, *Bull. Chem. Soc. Jpn.,* 1998, **71**, 1221-1230.

[3] O. Kaufhold, A. Stasch, T. Pape, A. Hepp, P.g. Edwards, P. D. Newman, F. Ekkehardt Hahn, *J. Am. Chem. Soc.,* 2009, **131**, 306-317; (b) S. Samanta, S. Goswami, *J. Am. Chem. Soc.,* 2009, **131**, 924-925; (c) D. V. Shevchenko, S. R. Petrusenko, V. N. Kokozay, M. V. Zhigalko, R. I. Zubatyuk, O. V. Shishkin, B. W. Skelto, P. R. Raithby, *Inorganic, Chimica, Acta,* 2005, **358**, 3889-3904.

[4] O. Kaufhold, A. Flores-Figueroa, T. Pape, F. E. Hahn, *Organometallics,* 2009, **28**, 896-901.

[5] (a) C. A. Salata, M. Therese, Youinou, C. J. Burrows, *Inorg. Chem.,* 1991, **30**, 3454-3461; (b) S. A. Ross, C. J. Burrows, *Inorg. Chem,* 1998, **37**, 5358-5363.

[6] M. Achmatowicz and J. Jurczak, *Tetrahedron,* 2001, **12**, 111-119.

[7] R. T. Meyers, *Inorg. Chem.,* 1978, **17**, 952-958

[8] A. Cook, P. Hodge, B. Manzini, C. L. Ruddick, *Tetrahedron Lett.,* 2007, **48**, 6496-6499; (b) P. Virta, H. Loennberg, *J. Org. Chem.,* 2003, **68**, 8534-8538; (c) L. S. Richter, J. Y. K. Tom, J. P. Burnier, *Tetrahedron Lett.,* 1994, **35**, 5547-5550.

[9] W. Seufert, Z. Q. Beck, D. H. Sherman, *Angewandte Chemie Int. Ed.,* 2007, **46**, 9298-9300.

[10] J. I. Gavrilyuk, G. Evindat, J. Y. Chen, R. A. Batey, *J. Combi. Chem.,* 2007, **9**, 644-651

[11] (a) H. D. Darkin, *J. Bio. Chem.,* 1912, 357-364; (b) H. D. Darkin, *J. Bio. Chem.,* 1913, 263-269; (c) P. M. Masters and M. Friedman, *J. Agric. Food Chem.,* 1979, **27**, 507-511; (d) P. M. Masters and M. Friedman, *J. Food. Sci., 1982,* **47**, 760-764; (e) R. Liardon and S. Ledermann, *J. Agric. Food Chem.,* 1986, **34**, 557-565; (f) D. E. Schwass and J. W. Finley, *J. Agric. Food Chem.,* 1984, **32**, 1377-1382; (g) S. Casal, E. Mendes, M. B. P. P. Olivereira, M. A. Ferreira, *Food. Chem.,* 2005, **89**, 333-340; (h) M. Friedman, *J. Agric. Food Chem.,* 1999, **47**, 1268-1319

[12] M. M. Ito, J. Kato, S. Takagi, E. Nakashiro, T. Sato, Y. Yamada, H. Saito, T. Namiki, I. Takamura, K. Watatsuki, T. Suzuki and T. Endo., *J. Am. Chem. Soc.* 1998, **110**, 1988

[13] F-G. Klarner, M. Lobert, U. Naatz, H. Bandmann and R. Boese., *Chem. Eur. J.* 2003, **9**, 5036-5047

[14] T. Collins, N. Chahbane, D. Lenoir, A. Kettrup, K. W. Schramm, *Chemie Ingenieur Technik,* 2004, **76**, 1284.

[15] T. J. Collins, *Acc. Chem. Res.,* 1994, **27**, 279-285

[16] K. Haas, H. Dialer, H. Piotrowski, J. Schapp and W. Beck, *Angew. Chem. Int. Ed.,* 2002, **41**, 1879-1881.

[17] R. D. Shannon, *Acta Crystallographica,* 1976, **A32**, 751-767.

[18] M. M. Ito, J. Kato, S. Takagi, E. Nakashiro, T. Sato, Y. Yamada, H. Saito, T. Namiki, I. Takamura, K. Wakatsuki, T. Suzuki and T. Endo, *J. Am. Chem. Soc.,* 1988, **110**, 5147

[19] T. J. Collins, *Acc. Chem. Res.,* 2002, **35**, 782-790

[20] J. West, S. Mecozzi, D. A. Dougherty, *J. Phys. Org. Chem.,* 1997, **10**, 347-350.

[21] H. J. Schneider, T. Schiestel, and P. Zimmermann, *J. Am. Chem. Soc.*, 1992, **114**, 7698-7703.

[22] K. Kasuga, K. Nishie, M. Handa, T. Sugimori, *Inorgnica Chimica Acta*, 2000, **307**, 164-166

[23] (NB: - A trail run shows that 66% cyclization occurs after 3 hours with 2eq NaOMe/NH (1:0.5 for the integration of the CH_3 side arm) and is left unaltered after 24hours. Addition of 2eq more base per proton only marginally changed the ratio of CH_3 side arms in the NMR (1:0.41))

CHAPTER 4 - Isolation of Cyclopeptides, Their Reduction to Form Cyclams and Nickel Insertion to Form Novel C-Functionalized Cyclam Nickel(II) Complexes.

4.1   Introduction

The synthesis of 1,6 Bis-substituted cyclams from dipeptide esters has previously been reported by Beck (Figure 4.1)[1]. However stereochemical analysis of the functionalized carbons was never performed.
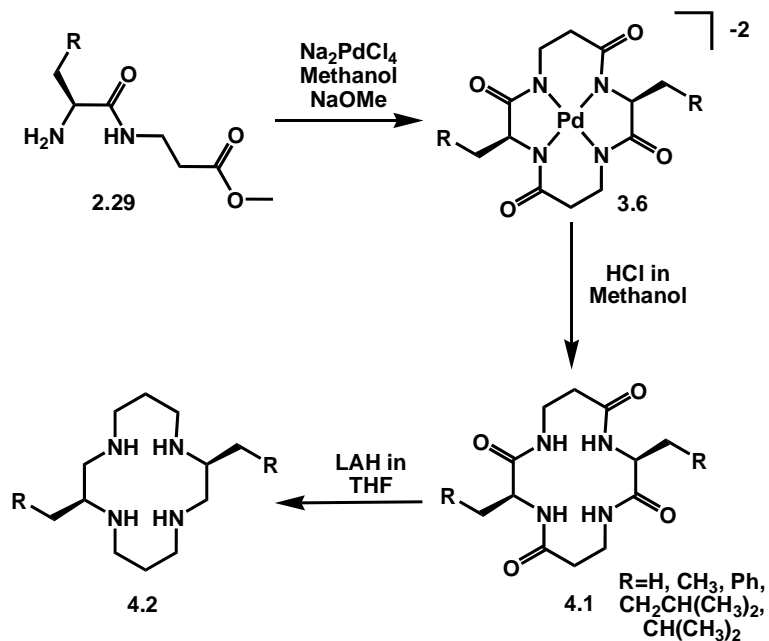
Figure 4.1: - Beck's route to C-substituted cyclams[1].

The liberated cyclopeptides (**4.1**) fall out of the methanol solution and can be isolated by simple filtration followed by minimal washing. These peptides were characterized by ^{1}HNMR using TFA:MeOH (80:20) mixtures[1]. Beck then reduced the cyclopeptide to the cyclams utilizing LAH[1].

4.2 Isolation of Cyclopeptides From Nickel Cyclopeptide Complex Precursors.

Metal free cyclopeptides were generated from Ni-cyclopeptide complexes (**3.2a, b** and **e**) via protonation with HCl. Taking advantage of the low solubility of the cyclopeptides[2] even impure samples of the Ni-cyclopeptide complexes (70-80% purity) were successfully converted to pure cyclopeptides (Figure 4.2, Table 4.1).
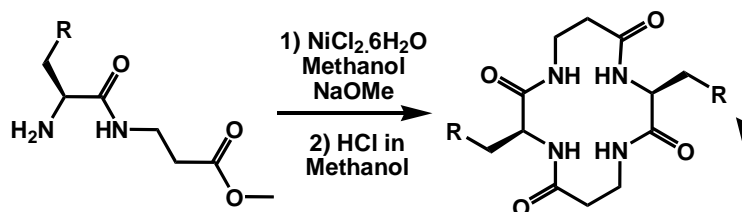
Figure 4.2: - Cyclization of dipeptides followed by liberation of cyclopeptides.

Table 4.1: - Isolated cyclopeptides from dipeptide cyclizations.

R	Compound Number	Yield%
Ph	**4.1a**	45.7
2-Nap	**4.1b**	83.5
H	**4.1c**	87.8

Unsymmetrical cyclopeptides can be synthesized in a similar manner to C_2 symmetric ones utilizing tetrapeptide starting materials (Figure 4.3, Table 4.2).
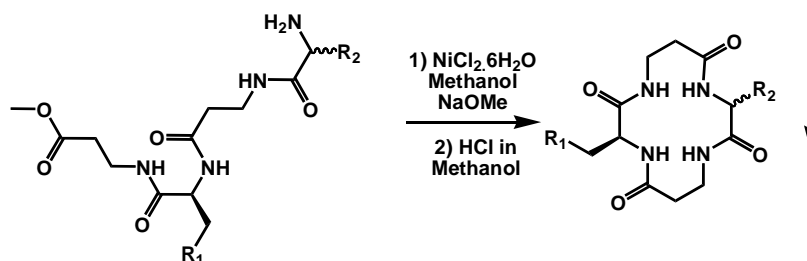
Figure 4.3: - Liberation of cyclopeptides from tetrapeptide cyclizations.

Table 4.2: - Isolated cyclopeptides from tetrapeptide cyclizations.

R_1	R_2	Compound Number	Yield%
Ph	(D)-CH$_2$Ph	**4.1d**	77.8
2-Nap	(D)-CH$_2$-2-Nap	**4.1e**	85.3
2-Nap	(L)-CH$_2$Ph	**4.1f**	64.4
2-Nap	(L)- CH$_3$	**4.1g**[b]	54.5
2-Nap	H	**4.1h**[b]	54.5

[b] **NMR insoluble characterization by IR and MS only.**

4.2.1 Insertion of Other Metals into the Cyclopeptide.

Insertion of other metals such as iron into the cyclopeptide allows the formation of Collins[3] TAML® type complexes. Reaction of the cyclopeptides is very difficult due to their innate insolubility in almost all organic solvents (THF, MeOH, DMSO, DMF, ether, DCM). Previous efforts at metal insertion into TAML ligands include the use of BuLi in THF at $-108^{o}C$[4] and the use of NaOH in water[5]. These methods are inconsistent with the solubility of our cyclopeptides and with the production of Fe complexes due to the formation of iron oxides. However when the cyclopeptide is suspended in DMSO and reacted with KH a soluble salt is formed. Reacting this salt with MCl$_2$ (M = Fe, Co) then allows the formation of a metal complex (Figure 4.4). The excess Fe is removed by treating the solution with water and filtering off the formed iron oxides (Figure 4.5). Crystal structure analysis prove the structure of the complex and shows stereochemical retention. Quick reaction times at RT prevent the isomerization of the stereocenters even in the presence of the very strong KH base. Some examples of larger peptide metal complexes are available in the literature[6]. However these systems show little practical use in catalysis or as reagents.
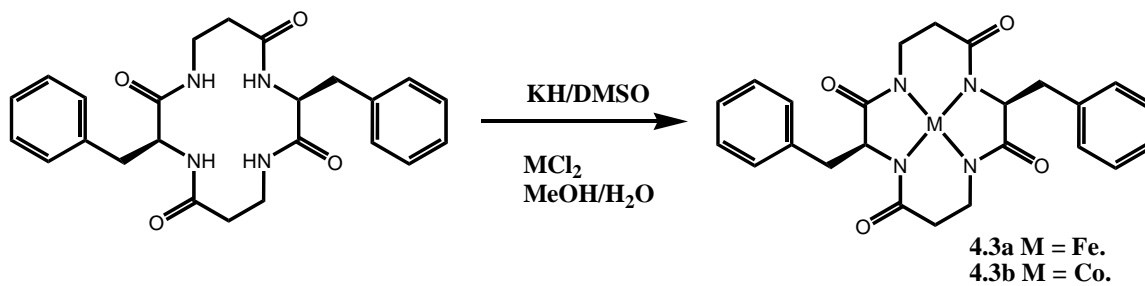
Figure 4.4:- Reaction of cyclopeptide 4.1a with KH and MCl₂ in DMSO.
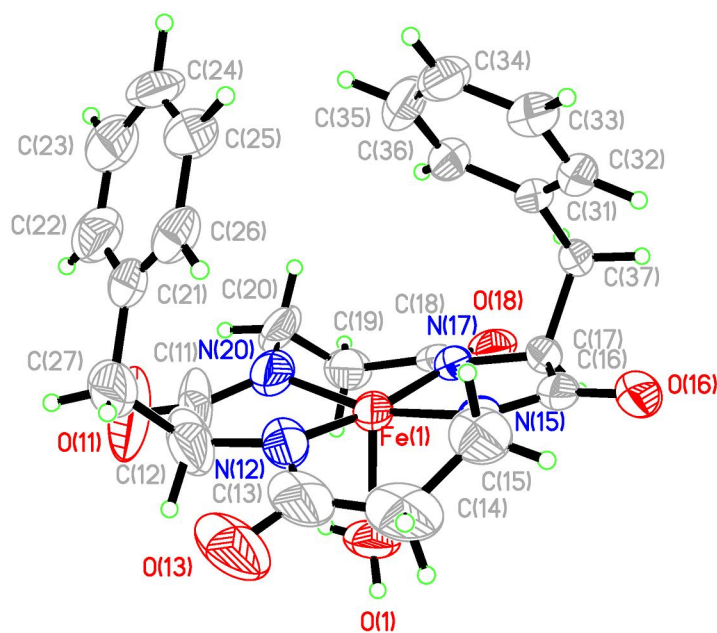
Figure 4.5: - X-ray crystal structure of 4.3a (PPN removed for clarity)

Table 4.3: - Selected crystal structure data for complex 4.3a

Selected Bond Lengths	Selected Torsion Angles
Fe(1)-N(15) (1.886Å), Fe(1)-N(17) (1.912Å), Fe(1)-N(20) (1.875Å), Fe(1)-N(12) (1.918Å), Fe(1)-O(1) (2.116Å), C(11)-O(11) (1.245Å), C(11)-N(20) (1.321Å) N(12)-C(13) (1.330Å), C(13)-O(13) (1.264Å),C(13)-C(14) (1.475Å), C(15)-N(15) (1.459Å), N(15)-C(16) (1.341Å), C(16)-O(16) (1.238Å), C(17)-N(17) (1.440Å), N(17)-C(18) (1.328Å), C(18)-O(18) (1.284Å).	Fe(1)-N(17)-C(17)-C(16) (-6.16°), Fe(1)-N(17)-C(18)-C(19) (19.84°) N(17)-C(17)-C(16)-N(15) (-10.11°), N(15)-C(15)-C(14)-C(13) (-67.36°), Fe(1)-N(12)-C(13)-C(14) (-14.38°), Fe(1)-N(12)-C(13)-O(13) (-163.56°), O(13)-C(13)-C(14)-C(15) (-144.82°).
Selected Bond Angles	**Six Membered Ring Alignment**
N(20)-Fe(1)-N(15) (163.0°), N(20)-Fe(1)-N(17) (95.2°), N(15)-Fe(1)-N(17) (83.2°), N(20)-Fe(1)-N(12) (83.6°), N(15)-Fe(1)-N(12) (95.2°), N(17)-Fe(1)-N(12) (170.5°), N(20)-Fe(1)-O(1) (94.1°), N(15)-Fe(1)-O(1) (102.9°), N(17)-Fe(1)-O(1) (94.82°), N(12)-Fe(1)-O(1) (94.6°).	*Cis*

Insertion of cobalt into the cyclopeptide and treatment of the crude solution with PPN also lead to the formation of crystals suitable for X-ray analysis (Figure 4.6).
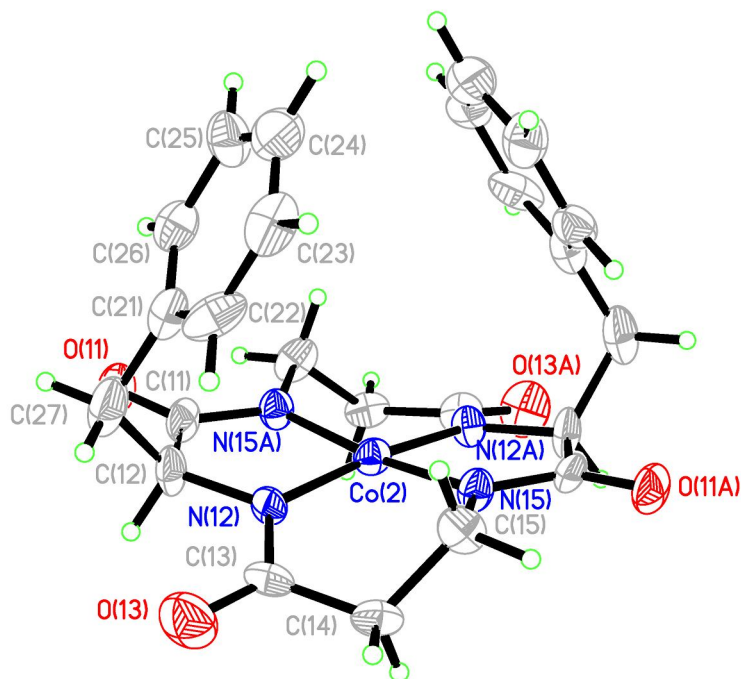
Figure 4.6: - X-ray crystal structure of 4.3b (PPN removed for clarity)

Table 4.4: - Selected crystal structure data for complex 4.3b

Selected Bond Lengths	Selected Torsion Angles
Co(2)-N(15/15A) (1.867Å), Co(2)-N(12/12A) (1.852Å), C(13)-O(13) (1.241Å), C(13A)-O(13A) (1.241Å), C(13)-N(12) (1.393Å), C(13A)-N(12A) (1.393Å), N(12)-C(12) (1.503Å), N(12A)-C(12A) (1.503Å), O(11)-C(11) (1.242Å), O(11A)-C(11A) (1.242Å), N(15)-C(11) (1.331Å), N(15A)-C(11A) (1.331Å).	Co(2)-N(12)-C(12)-C(11) (5.87°), Co(2)-N(12)-C(13)-C(14) (8.45°), Co(2)-N(15)-C(15)-C(14) (-44.10°), N(12)-C(12)-C(11)-N(15A) (-9.59°), N(112A)-C(13A)-C(14A)-C(14A) (-53.42°), Co(2)-N(12A)-C(13A)-O(13A) (-172.99°), Co(2)-N(15)-C(11A)-O(11A) (-175.26°).
Selected Bond Angles	**Six Membered Ring Alignment**
N(15)-Co(2)-N(15A) (173.12°), N(12)-Co(2)-N(12A) (164.41°), N(15A)-Co(2)-N(12A) (95.75°), N(12A)-Co(1)-N(15) (85.19°), Co(2)-N(12A)-C(12) (115.93°), Co(2)-N(15)-C(11) (116.41°), N(15)-C(11)-C(12) (115.93°), N(12)-C(13)-C(14) (115.71°).	*Cis*

With the insertion of other metals into cyclopeptides novel complexes with controllable stereochemistry can be obtained. These complexes have possible uses in oxidation chemistry, similar to that performed with the nickel complexes. Possible polyaromatic hydrocarbon degradation utilizing the iron complex could be achieved following Collins methodology[2] and substrate pre-binding with aromatic sidearms.

4.3   Reduction of the Cyclopetides to Cyclams.

Various attempts to reduce cyclopeptides with lithium aluminum hydride (LAH) (4 equivalents, work up with Na_2SO_4 solution) according to Beck's original report[1] as well as equivalent reductions using BH_3[7], produced complex mixtures. Successful generation of cyclams (in moderate yields) was eventually accomplished using a large excess of LAH (16eq) followed by a workup with $NaOH/H_2O$[8] (Figure 4.7, Table 4.4).
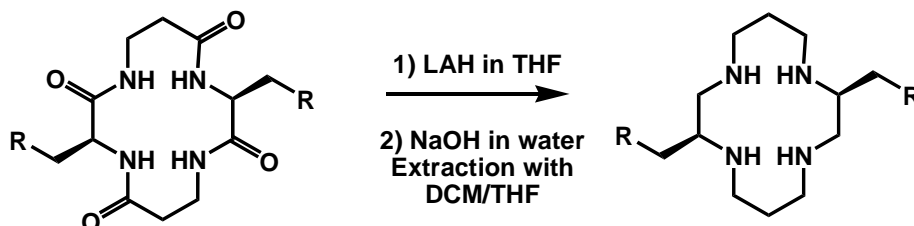
Figure 4.7: - Reduction of cyclopeptides, using LAH in THF with a NaOH workup.

Table 4.5: - Yields of cyclopeptide reductions with LAH.

R	Compound Number	Yield%
Ph	**4.2a**	38.3
2-Nap	**4.2b**	79.1
H	**4.2c**	26

4.4   Nickel Insertion into Cyclam ligands.

Ni cyclam complexes were successfully generated from cyclams **4.2a-b** and NiCl$_2$ in boiling methanol, along with complex **4.4c** that was generated through the crystallization of an impure sample of the cyclam after reaction with NiCl$_2$ (Figure 4.8). In one case **4.4d,** a perchlorate complex was successfully synthesized in that manner as well (Figure 4.8). However I was unable to produce pure Ni perchlorate complexes or BPh$_4$$^-$ complexes from cyclams **4.2a-b** and Ni(ClO$_4$)$_2$ or Ni(ClO$_4$)$_2$/NaBPh$_4$ mixtures.

Several nickel tetraazamacrocyclic complexes (similar in nature to the complexes generated here) have previously been isolated by Burrows *et al* and utilized in the epoxidation of alkenes[9], for the oxidative cleavage of DNA molecules[10] and for associative binding to guanine in DNA[11]. Other nickel cyclam complexes generated by the stereoselective reduction of planar imine complexes over Raney Ni show stereoselectively but no aromaticity[12].

4.4a R = Ph, R^1 = (S)CH$_2$Ph
4.4b R = 2-Nap, R^1 = (S) CH$_2$-(2)Nap
4.4c R = 2-Nap, R^1 = (R) CH$_2$-(2)Nap
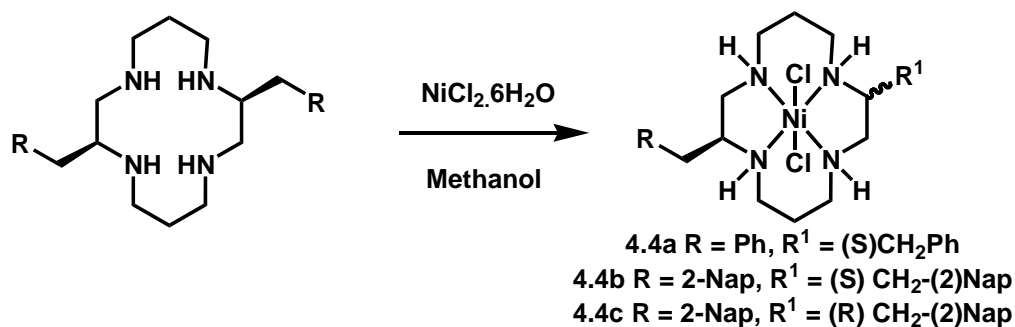
Figure 4.8: - Isolation of nickel cyclam Bis-chloride complexes.
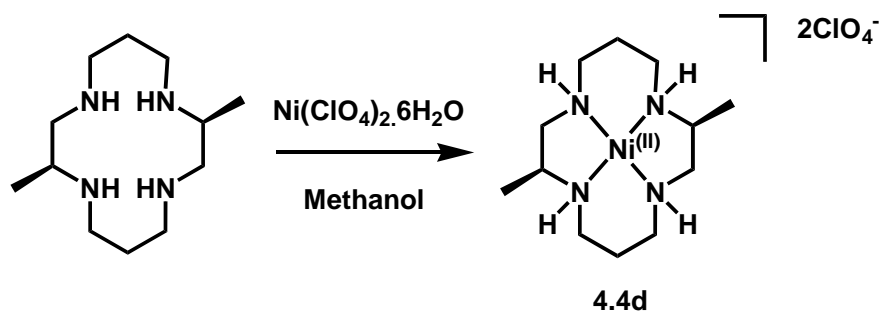
Figure 4.9: - Nickel incorporation into the cyclam 5.12 utilizing nickel perchlorate.

Table 4.6: - Yield of C-functionalized nickel chloride cyclam complexes.

R	Compound Number	Yield%
Ph (SS)	**4.4a**	38.3
2-Nap (SS)	**4.4b**	35.8
2-Nap (SR)	**4.4c**	-
H (SS)	**4.4d**	9.4

4.4.1 Structural Characterization of C-Functionalized Nickel Cyclam Complexes.

Despite previous report on Ni-cyclam napthoates that are devoid of intermolecular π-π stacking interactions[13] in the solid state (Figure 4.9) π-π stacking was observed when isonicotinic acid was used as an axial ligand in a trans(III) cyclam complex[14] (Figure 4.10). Encouraged by this finding we anticipated that the side arms in the complexes **4.4a-c** would be suitably positioned for π-π or CH-π interactions within the crystal lattice as observed with the cyclopeptide nickel complexes **3.2a**, **3.2f** and **3.2e**, leading to the possible formation of these interactions with aromatic substrates in solution.
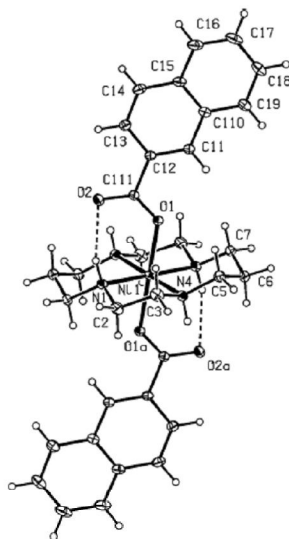
Figure 4.10: - X-ray crystal structure of a Ni-cyclam with 2 axial naphthoic acid groups that show no π-π interactions in the solid state[5].
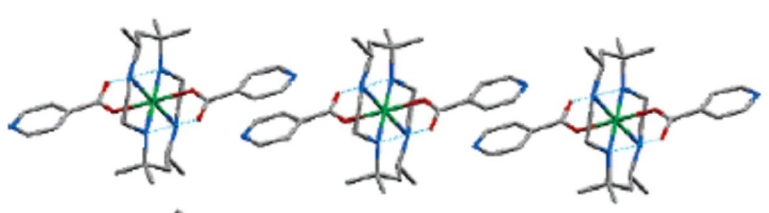
Figure 4.11: - X-ray crystal structure of a Ni-cyclam with 2 axial nicotinic acid groups that show π-π interactions in the solid state[6].

Generation of Ni-cyclam complexes with C-functionalized cyclam molecules allowed the structural determination of a variety of interactions such as π-π and CH-π and shall be discussed as follows.

4.4.1.1 X-ray Crystal Structure Analysis of Cyclam Nickel Complex 4.4a.
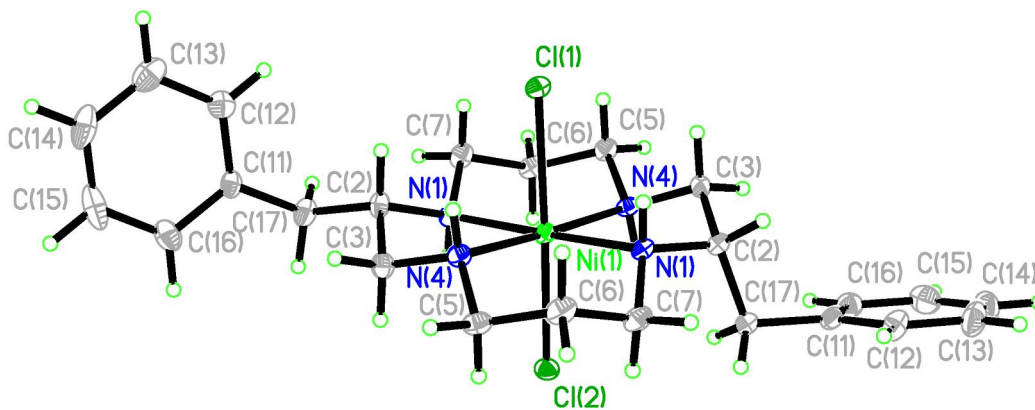
Figure 4.12: - X-ray Crystal Structure of the complex 4.4a (solvents removed for clarity).
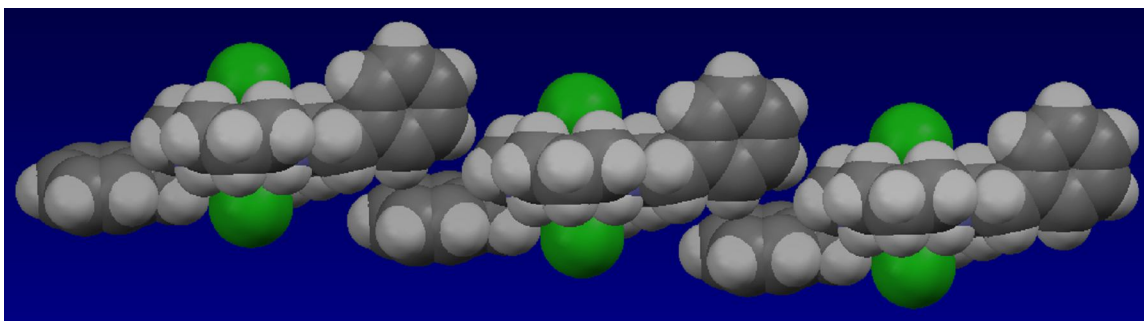
Figure 4.13: - Space filled model showing CH-π interactions in one dimension within the crystal lattice for complex 4.4a (solvents removed for clarity).
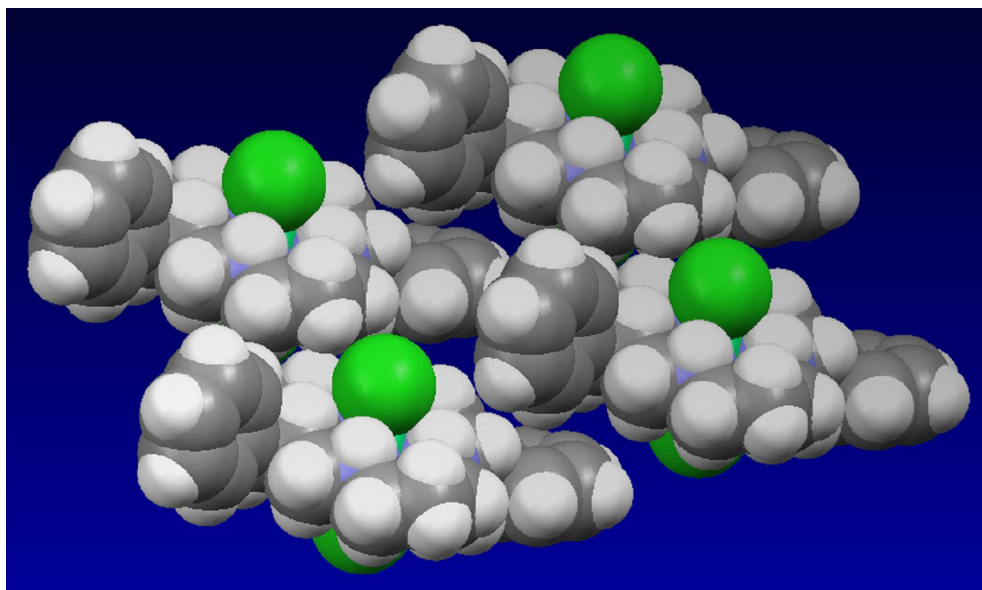
Figure 4.14: - Space filling X-ray crystal structure shows the CH-π interactions between four complexes in a two-dimensional sheet in the lattice for complex 4.4a (solvents removed for clarity).

Table 4.7: - Selected X-ray crystal data for complex 4.4a.

Selected Bond Lengths	Selected Torsion Angles
Ni(1)-N(1) (2.0633Å), Ni(1)-N(4) (2.0636Å),Ni(1)-N42 (2.0689Å), Ni(1)-N12 (2.0732Å), Ni(1)-Cl(2) (2.4940Å), Ni(1)-Cl(1) (2.5826Å), N(1)-H(1) (0.90Å), N(4)-H(4) (0.82Å), N12-H12 (0.82Å), N42-H42 (0.87Å).	N(4)-Ni(1)-N(1)-C72 (-142.85°), N42-Ni(1)-N(1)-C72 (40.75°), N12-Ni(1)-N(1)-(C72 95.6°), Cl(2)-Ni(1)-N(1)-C72 –(54.53°), Cl(1)-Ni(1)-N(1)-C72 (124.80°), N(4)-Ni(1)-N(1)-C(2) (-8.04°), N42-Ni(1)-N(1)-C(2) (175.56°), N12-Ni(1)-N(1)-C(2) (-129.6°), Cl(2)-Ni(1)-N(1)-C(2) (80.28°), Cl(1)-Ni(1)-N(1)-C(2) (-100.39°), C72-N(1)-C(2)-C(17) (42.8°), Ni(1)-N(1)-C(2)-C(17) (-91.75°), N(1)-Ni(1)-N(4)-C(5) –(145.20°), N42-Ni(1)-N(4)-C(5) (-89.3°), N12-Ni(1)-N(4)-C(5) (32.80°), Cl(2)-Ni(1)-N(4)-C(5) (120.18°), Cl(1)-Ni(1)-N(4)-C(5) (-58.25°), N(1)-Ni(1)-N(4)-C(3) (-19.09°), N42-Ni(1)-N(4)-C(3) (36.8°), N12-Ni(1)-N(4)-C(3) (158.90°), Cl(2)-Ni(1)-N(4)-C(3) (-113.72°), Cl(1)-Ni(1)-N(4)-C(3) (67.86°)

Selected Bond Angles	Configuration: - Trans(III)
N(1)-Ni(1)-N(4) (83.75°), N(1)-Ni(1)-N42 (93.80°), N(4)-Ni(1)-N42 (175.66°), N(1)-Ni(1)-N12 (177.67°), N(4)-Ni(1)-N12 (97.47°), N42-Ni(1)-N12 (84.86°), N(1)-Ni(1)-Cl(2) (94.47°), N(4)-Ni(1)-Cl(2) (88.82°), N42-Ni(1)-Cl(2) (94.95°), N12-Ni(1)-Cl(2) (87.56°), N(1)-Ni(1)-Cl(1) (87.19°), N(4)-Ni(1)-Cl(1) (92.03°), N42-Ni(1)-Cl(1) (84.26°), N12-Ni(1)-Cl(1) (90.77°), Cl(2)-Ni(1)-Cl(1) (178.209°)	**π-π interactions**: - No **CH-π interactions**: - Yes (2D), 2.829Å and 2.819Å
	Side Arm Positioning: - 1 axial, 1 equatorial.

4.4.1.2 X-ray Crystal Structure Analysis of Cyclam Nickel Complex 4.4b.
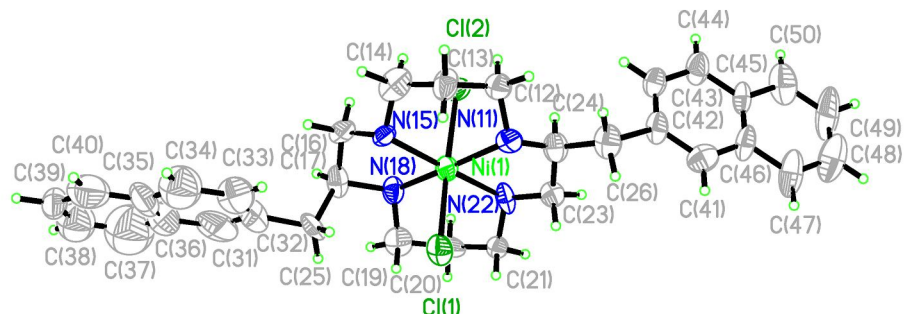
Figure 4.15: - X-ray Crystal Structure of 4.4b (solvents removed for clarity).
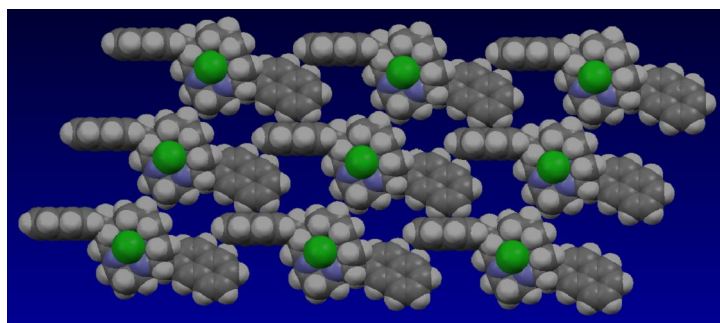
Figure 4.16: - Crystal packing of complex 4.4b in two dimensions (solvents removed for clarity).
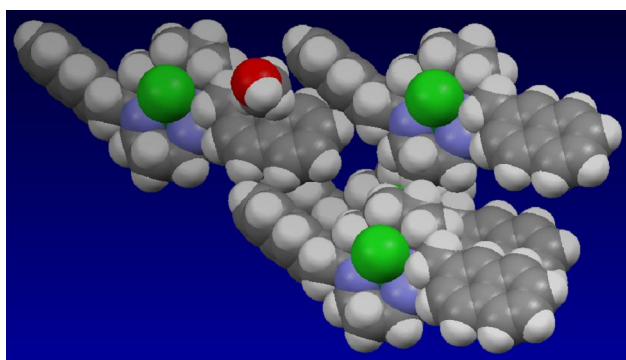
Figure 4.17: - Space filled X-ray structure showing the crystal packing of complex 4.4b in three dimensions (one solvent included to show the blocked position above the central naphthyl ring, the complex on the bottom right T-stacks to the complex on the top left).

Table 4.8: - Selected X-ray crystal data for complex 4.4b.

Selected Bond Lengths	Selected Torsion Angles
Ni(1)-N(18) (1.991Å), Ni(1)-N(15) (2.035Å), Ni(1)-N(22) (2.110Å), Ni(1)-N(11) (2.137Å), Ni(1)-Cl(1) (2.503Å), Ni(1)-Cl(2) (2.587Å).	Ni(1)-N(18)-C(16)-C(17) (44.42°), Ni(1)-N(11)-C(24)-C(23) (-39.02°), N(11)-C(24)-C(23)-N(2) (-50.46°), N(11)-C(24)-C(23)-N(2) (55.24°), N(22)-C(23)-C(24)-C(26) (159.21°), N(15)-C(16)-C(17)-C(25) (73.94°),
Selected Bond Angles	**Configuration**: - Trans(III)
N(18)-Ni(1)-N(15) (84.0°), N(18)-Ni(1)-N(22) (92.5°), N(15)-Ni(1)-N(22) (175.1°), N(18)-Ni(1)-N(11) (176.7°), N(15)-Ni(1)-N(11) (97.5°), N(22)-Ni(1)-N(11) (85.8°), N(18)-Ni(1)-Cl(1) (95.6°), N(15)-Ni(1)-Cl(1) (88.88°), N(22)-Ni(1)-Cl(1) (94.91°), N(11)-Ni(1)-Cl(1) (87.38°), N(18)-Ni(1)-Cl(2) (85.9°), N(15)-Ni(1)-Cl(2) (92.57°), N(22)-Ni(1)-Cl(2) (83.72°), Cl(1)-Ni(1)-Cl(2) (178.00°),	**π-π interactions**: - No **CH-π interactions**: - Yes (3D), 2.916Å, 2.996Å, 2.739Å and 3.071Å
	Side Arm Positioning: - 1 axial, 1 equatorial.

4.4.1.3 X-ray Crystal Structure Analysis of Cyclam Nickel Complex 4.4c.
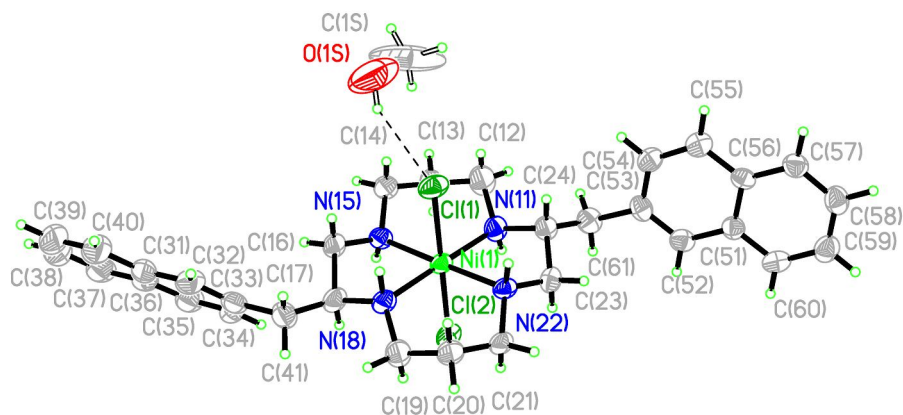
Figure 4.18: - X-ray crystal structure of complex 4.4c.
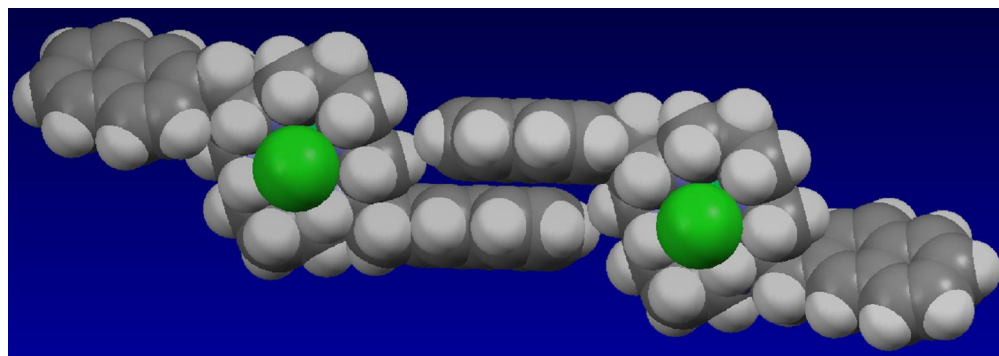
(a)
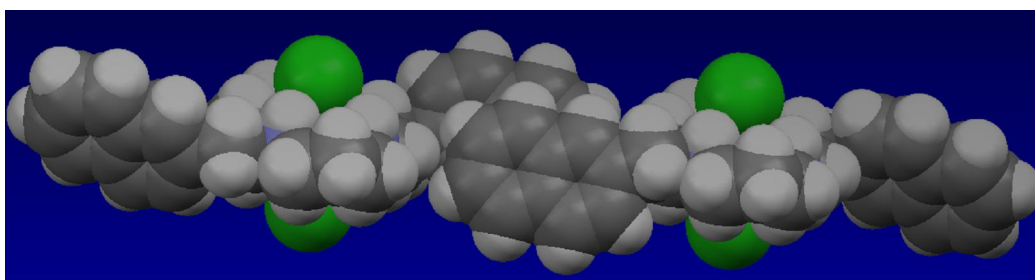
(b)

Figure 4.19: - (a) Diagram showing the π-π interactions in the complex 4.4c from a side on view (solvents removed for clarity) (b) Diagram showing the π-π interactions in the complex 4.4c from an end on view (solvents removed for clarity).

Table 4.9: - Selected X-ray crystal data for complex 4.4c.

Selected Bond Lengths	Selected Torsion Angles
Ni(1)-N(15) (2.052Å), Ni(1)-N(22) (2.056Å), Ni(1)-N(11) (2.073Å), Ni(1)-N(18) (2.078Å), Ni(1)-Cl(2) (2.4893Å), Ni(1)-Cl(1) (2.5016Å).	Ni(1)-N(1)-C(24)-C(23) (38.62^{o}), Ni(1)-N(15)-C(16)-C(17) (-45.47^{o}), N(11)-C(24)-C(23)-N(22) (-54.83^{o}), N(15)-C(16)-C(17)-N(18) (57.96^{o}), N(22)-C(23)-C(24)-C(61) (-177.75^{o}), N(15)-C(16)-C(17)-C(41) (156.90^{o}),
Selected Bond Angles	**Configuration**: - Trans(III)
N(15)-Ni(1)-N(22) (178.50^{o}), N(15)-Ni(1)-N(11) (95.28^{o}), N(22)-Ni(1)-N(11) (84.65^{o}), N(15)-Ni(1)-N(18) (84.30^{o}), N(22)-Ni(1)-N(18) (95.81^{o}), N(11)-Ni(1)-N(18) (178.42^{o}), N(15)-Ni(1)-Cl(2) (88.79^{o}), N(22)-Ni(1)-Cl(2) (92.70^{o}), N(11)-Ni(1)-Cl(2) (86.42^{o}), N(18)-Ni(1)-Cl(2) (92.05^{o}), N(15)-Ni(1)-Cl(1) (91.40^{o}), N(22)-Ni(1)-Cl(1) (87.11^{o}), N(11)-Ni(1)-Cl(1) (94.04^{o}), N(18)-Ni(1)-Cl(1) (87.50^{o}), Cl(2)-Ni(1)-Cl(1) (179.49^{o})	**π-π interactions**: - Yes, 3.519Å **CH-π interactions**: - No
	Side Arm Positioning: - 2 equatorial.
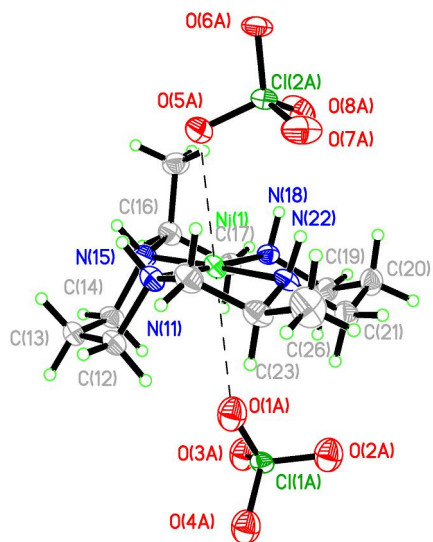
Figure 4.20:- X-ray crystal structure of complex 4.4d.
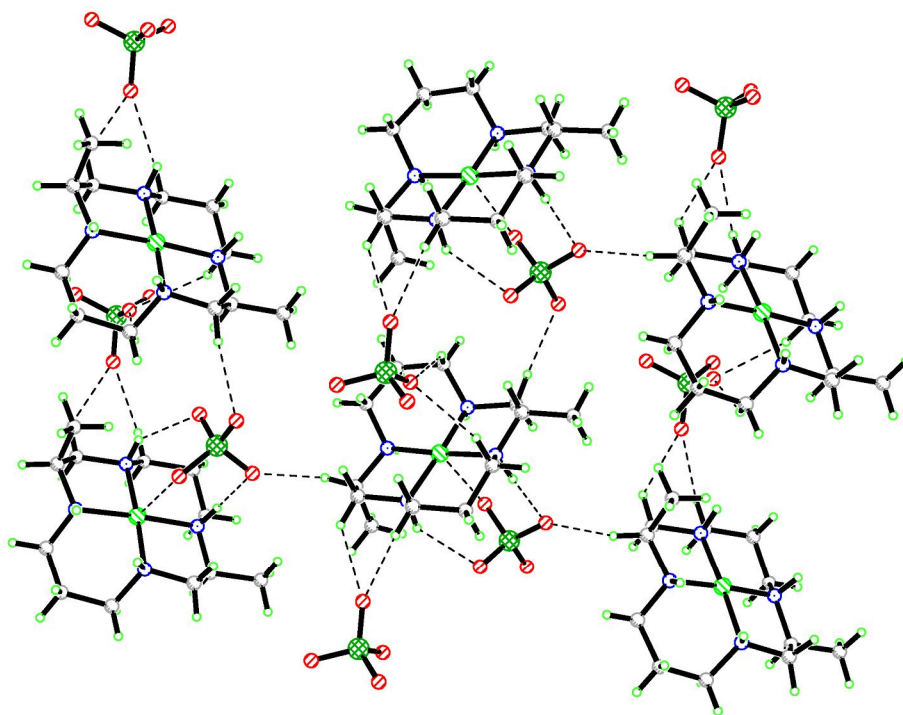
Figure 4.21: - X-ray crystal structure of complex 4.4d, showing the N-H···O interaction, Ni···O interactions and C-H···O interactions forming a network within the crystal.

Table 4.10: - Selected X-ray crystal data for complex 4.4d

Selected Bond Lengths	Selected Torsion Angles
Ni(1)-N(11) (1.922Å), Ni(1)-N(18) (1.923Å), Ni(1)-N(22) (1.937Å), Ni(1)-N(15) (1.938Å), N(11)-H(11) (0.9300Å), N(15)-H(15) (0.9300Å), N(18)-H(18) (0.9300Å), N(22)-H(22) (0.9300Å), Ni(1)-O(5A) (2.909Å), Ni(1)-O(1A) (3.108Å), H(22)-O(7A) (2.141Å), H(18)-O(8A) (2.318Å).	Ni(1)-N(15)-C(16)-C(17) (35.82°), Ni(1)-N(18)-C(19)-C(20) (-40.03°), N(15)-C(16)-C(17)-N(18) (-50.80°), N(11)-C(22)-C(23)-N(22) (49.76°), Ni(1)-N(15)-C(16)-C(24) (-84.80°), Ni(1)-N(22)-C(23)-C(26) (-161.39°),
Selected Bond Angles	**Configuration**: - Trans(I)
N(11)-Ni(1)-N(18) (175.97°), N(15)-Ni(1)-N(22) (175.97°), N(11)-Ni(1)-N(22) (88.22°), N(18)-Ni(1)-N(22) (95.80°), N(11)-Ni(1)-N(15) (88.48°), N(18)-Ni(1)-N(15) (87.50°).	**π-π interactions**: - No **CH-π interactions**: - No
	Side Arm Positioning: - 1 axial, 1 equatorial.

Complexes **4.4a-b** show intermolecular CH-π building a 2D network in the case of **4.4a** (Figures 4.12 and 4.13) and a 3D network in the case of **4.4b** (Figures 4.15 and 4.16). These complexes both have axial and equatorial sidearms with an octahedral geometry around the nickel center. Complex **4.4c** shows differences from complexes **4.4a-b.** By having two equatorial sidearms, no CH-π interactions are evident, however a new π-π interaction has been detected within the crystal structure. These CH-π and π-π interactions are exactly what we had hoped would be accomplished by incorporating the aromatic sidearms onto the ligand framework. All complexes **4.4a-c** show the *trans*(III) geometry of the nitrogens around the metal center. The complex **4.4d** having no aromatic sidearms shows no CH-π or π-π interactions. The different counter ion (perchlorate) also allows the formation of a *trans*(I) conformation with a slight shortening of the N-Ni bonds and the formation of O--H hydrogen bonding throughout the crystal structure (both N-H···O and C-H···O interactions are observed). The RS version of complex **4.4d** shows

both side arms to be in the equatorial position and the configuration of the complex is *trans*(III) as the perchlorate salt[15].

4.5   Reduction Tests Using C-functionalized Nickel Cyclams.

Reduction runs using different halogenated aromatic substrates were performed utilizing both C-functionalized and non-functionalized nickel complexes in DMSO:EtOH (1:1) mixtures with the $NaBH_4$ co-reductant and 1,3-dimethoxybenzene (DMB) was utilized as the internal standard. Monitoring of the reactions was performed over time by the removal of a small aliquot of the reaction mixture, quenching with ammonium chloride and extraction with ethyl acetate. The extracted sample was subjected to HPLC analysis and the conversion of the starting material to product was determined relative to the internal standard. These reactions were *not reproducible* and gave large variations in rate constants under the same conditions.
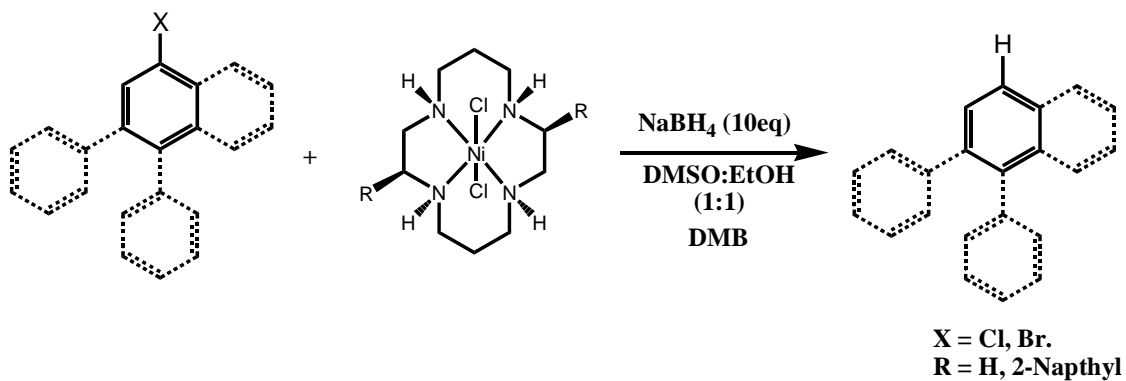
Figure 4.22: - Reduction of aromatic substrates utilizing complexes 1.6a and 4.3b.

The follow arguments are based solely on experimental data obtained in our lab and may not actually reflect the true nature of the mechanism or catalytic pathway as a more in depth analysis of the reaction is necessary: -

Rates of reduction were calculated based on the assumption that k_3 is the rate determining step (RDS) in the reduction (Figure 4.23). The first step in the reduction k_1 is shown to be the formation of complex **1.6d** from **1.6a**. This step appears to be fast via the

generation of a purple solution in the DMSO:EtOH (1:1) mixture within minutes from the original suspension of **1.6a**. The rate of generation of the *proposed* intermediate **1.6x** is unknown but seems likely to be slower than the formation of **1.6d**. The rates of k_2 and k_3 maybe close, however attack of the complex **1.6x** on aromatic substrates is believed to be slower than its formation. This hypothesis is supported by the differences in rates between all the aromatic substrates for the same catalysts **1.6a** or **4.4b** (Table 4.11).
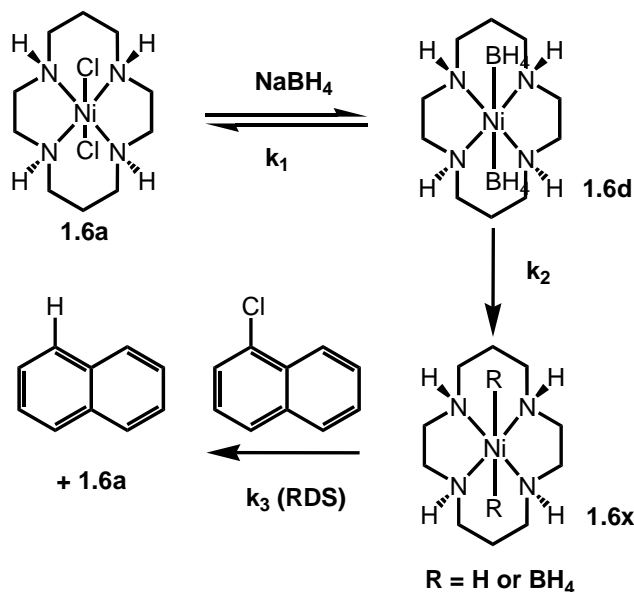
Figure 4.23: - Possible reduction pathway for the dehalogenation of bromonaphthalene.

From the reaction data gathered (Table 4.11) it is *assumed* that the rate law would be as shown in equation 1. Since the formation of **1.6x** is not *thought* to be the RDS and its concentration is assumed to not alter during the course of the reaction (in the presence of an excess of the borohydride) we have *assumed* this reaction to be pseudo first order (equation 2). This assumption bears fruit in the generation of graphs plotting Ln([Aryl-halide t = X]/[Aryl-halide t=0]) against time (s) leading to straight lines (Figure 4.24) and the slope of which gives us k^{obs}. k^{obs} is converted to k by dividing by the amount of catalyst concentration (equation 3) although this is not necessarily the case and must not be taken as a fully defined rate law.

1   Rate = k[**1.6x**][Aryl-halide]

172

2   Rate = k[Aryl-halide]

3        $k = k^{obs}/[cat]$

A graph to show Ln([ClNap]/[ClNAp t = 0]) vs time (s) for JT-I-1288

$y = -4.65565E\text{-}05x - 0.020893025$
$R^2 = 0.992325665$
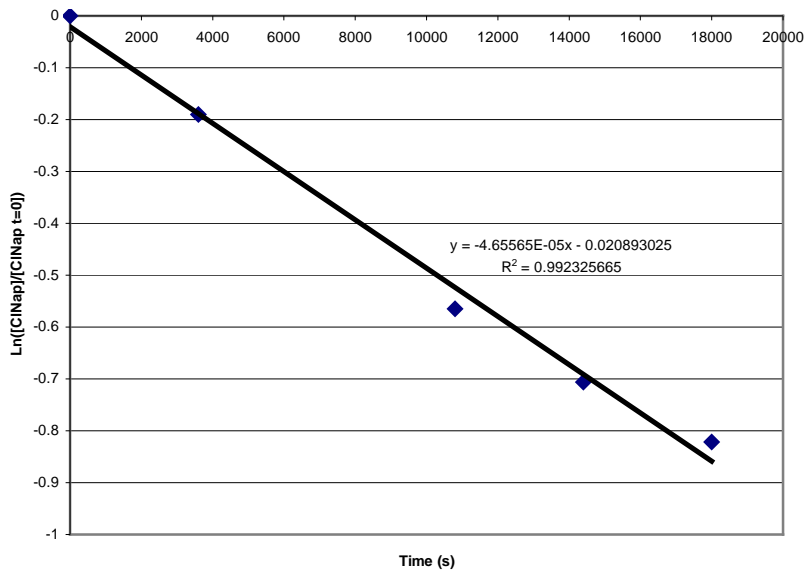
Figure 4.24: - A graph showing Ln([Clnap t = X]/[ClNap t = 0]) vs time (s)

Table 4.11: - Reduction data for complexes 1.6b and 4.3a with various halogenated compounds using DMB as an internal standard at 23°C.

Compound	Complex	K^{obs}	$k(s^{-1})$	R^2	k^{rel}
1-Bromonaphthalene	**1.6a**	3.569×10^{-4}	0.0327	90.9	1
1-Bromonaphthalene	**4.4b**	1.283×10^{-4}	0.024	96.6	-1.36
1-Chloronaphthalene	**1.6a**	4.656×10^{-5}	0.00637	99.2	1
1-Chloronaphthalene	**4.4b**	1.469×10^{-4}	0.0108	97.7	1.69
M-Bromobiphenyl	**1.6a**	7.602×10^{-5}	0.00644	97.1	1
M-Bromobiphenyl	**4.4b**	1.473×10^{-5}	0.00295	98.8	-2.25
P-Bromobiphenyl	**1.6a**	4.426×10^{-5}	0.00226	92.0	1
P-Bromobiphenyl	**4.4b**	8.274×10^{-6}	0.00146	96.4	-1.54
2-Bromofluroene	**1.6a**	4.252×10^{-5}	0.00914	99.2	1
2-Bromofluroene	**4.4b**	9.909×10^{-6}	0.00194	99.47	-4.71
Bromobenzene	**1.6a**	2.3759×10^{-5}	0.00102	96.6	-

The fact that chloronaphthalene reacts more slowly than bromonaphthalene *may* indicate that $S_{NR}1$, or SET mechanisms. If S_NAr were the mechanism one might expect that chloronaphthalene would react more quickly as it is more electronegative than bromine (bearing in mind the RDS is the attack of the hydride), however it is slower.

Although we do not see any aryl coupling products from the reaction this maybe due to the fact that the rather than being a radical chain mechanism the reaction may involve the combination of the generated radical intermediate species more rapidly than separation can occur[16]. It is also noteworthy that Ni(I) species isolated in acetonitrile do not react with bromonaphthalene to induce hydrodehalogenation indicating that the H-ion plays an important role as the reductant whether as the electron source or as a stabilizing factor in the Ni(I) complex.

It appears that the presence of aromatic sidearms reduces the rates of reduction for almost all substrates tested, except for chloronaphthalene where **4.4b** shows an increased rate of 1.69 over **1.6a** (Table 4.11). In this case the more electron poor chloronaphthalene

ring maybe able to undergo pre-concentration with the active complex though mutual π-π or CH-π interactions. Again it must be noted that the reduction tests performed are irreproducible and the rates of reduction shown are not reliable.

The reduction in rates in all other complexes could simply be due to steric hindrance blocking one side of the active complex making hydride/SET attack more difficult, effectively halving the concentration of active complex **1.6x** as only one side of the active intermediate would be available for attack.

After the failure to observe rate increases in DMSO:EtOH mixtures reactions in water were attempted. However substrate and catalyst insolubility led to this reaction being impossible to perform. The synthesis of a water-soluble glyme ester of bromonaphthalene was achieved however no reduction was observed utilizing complex **1.6a**.

4.6   Conclusions.

Cyclization of linear dipeptides and tetrapeptides followed by nickel removal from *impure* nickel cyclopeptide complexes leads to the formation of a highly insoluble cyclopeptide product than can be isolated by filtration. These cyclopeptides have proven difficult to fully characterize by ^{13}CNMR due to the extreme solvent conditions needed to dissolve them (100% TFA) leading to some breakdown of the compounds over time. ^{1}HNMR, mass spectra and IR data have been obtained for the majority of the compounds.

Reduction of the cyclopeptides to the cyclam molecules gave pure products for the C_2 symmetric compounds after the reaction without chromatography whilst the impure *Ci* Bis naphthyl compound was not purified but carried though to the next step.

Nickel insertion into the cyclam molecules proceeded smoothly. *Trans*(III) isomers were isolated for the chloride salts whilst the perchlorate salt yielded the *trans*(I) isomer, all in the desired SS or SR configuration dialed in during the peptide synthesis.

Increased CH-π interactions were observed in the solid state when the π surfaces of the side arms were increased from complex. Complex **4.4a** shows a two dimensional layered structure held together by CH-π interactions between the phenyl side arms whilst the larger naphthyl side arms in complex **4.4b** allows the formation of a three

dimensional structure, utilizing CH-π interactions. In both cases π-π interactions in the solid state were not observed as was originally envisioned. Complex **4.4c** showed π-π interactions in the solid state whilst complex **4.4d** formed no intermolecular interactions however hydrogen bonding was seen through the perchlorate counter ion.

Data for the aromatic substrates chosen shows reduction in rates for the complex **4.4b** over **4.4a**. Unfortunately meaning that the pre-concentration idea was not viable (at least in DMSO:EtOH mixtures) for the majority of substrates.

The chloronaphthalene substrate whilst being more difficult to reduce due to strong C-Cl bonds, has a more electron poor ring system and thus should interact more favorably with an electron rich π system such as the naphthalene rings in complex **4.4b** than the more electron rich bromonaphthalene substrate. Longer residence times in the presence of the catalyst should allow for the reduction to occur at a greater rate, which is shown by the results gained for chloronaphthalene reduction utilizing **4.4b** over **1.6a**.

Overall the stereo controlled synthesis of aromatic C-functionalized nickel cyclam complexes has been accomplished. Reduction rates in the DMSO:EtOH solvent mixture show that the C-functionalized Ni complex **4.4b** have a slower rate of reduction over the unfunctionalized complex **1.6a** for all substrates tested except chloronaphthalene although these reactions need to be repeated in order to fully assess the nature of the dehalogenation pathway.

4.7   Experimental.

All chemicals were purchased from Aldrich, Peptech Corp, Aroz technologies, Acros Organics or Fischer and used without further purification.

4.7.1   *General Synthesis of Cyclopeptides From Dipeptides.*

All following work was performed under nitrogen: - The dipeptide (1mmol) and nickel chloride (0.5mmol) were mixed in methanol 25mL. To this solution was slowly added a solution of fresh NaOMe (12mmol) in 50mL methanol and then the reaction was slowly heated to 70 °C. The reaction was stopped after 5hours, concentrated and filtered over celite to remove any NaCl formed. To the solution was added HCl in ether

(20mmol) and stirred for between 20 minutes and 24 hours until a white solid dropped out of solution. The solid was filtered and washed with cold methanol, water and ether then dried *in vacuo*.

cyclo-[βala-L-Phe-βala-L-Phe] (4.1a)
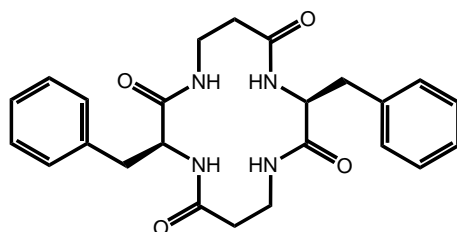
Yield 359mg, 45%. ^{1}H NMR (400 MHz, tfa) δ ppm 2.68 (s, 2 H) 2.95 (s, 2 H) 3.05 - 3.17 (m, 2 H) 3.17 - 3.28 (m, 2 H) 3.51 (s, 2 H) 3.85 (s, 2 H) 4.83 (s, 2 H) 7.14 - 7.24 (m, 4 H) 7.30 - 7.40 (m, 6 H). ^{13}C NMR (101 MHz, tfa) δ ppm 35.99, 38.06, 38.39, 58.55, 129.94, 130.96, 131.16, 136.79, 206.61. MS: *m/z* calculated for $C_{24}H_{28}N_4O_4$ = 436.2111, actual *m/z* (M+Na) = 459.172. IR (KBr pellet): υ 3457, 3303, 3047, 2934, 1644, 1541, 1439, 1357, 1111, 697cm^{-1}.

cyclo-[βala-L-(2)Nap-βala-L-(2)Nap] (4.1b)
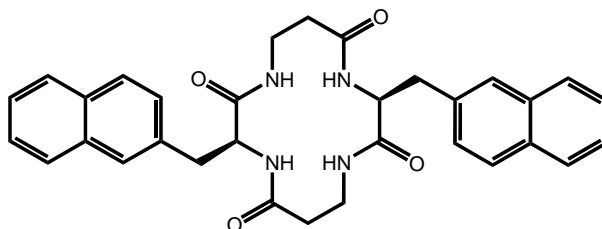
Yield 2.15g, 83.5%. ^{1}H NMR (400 MHz, CD₃OD) δ ppm 1.86 (dt, *J*=16.01, 4.49 Hz, 2 H) 2.20 (dd, *J*=15.23, 7.03 Hz, 2 H) 2.56 (dd, *J*=14.25, 8.78 Hz, 2 H) 2.71 (dd, *J*=14.06, 6.64 Hz, 2 H) 2.87 (s, 4 H) 2.89 - 2.95 (m, 4 H) 4.10 - 4.21 (m, *J*=7.61, 7.61 Hz, 2 H) 6.68 (dd, *J*=8.20, 1.56 Hz, 2 H) 6.74 - 6.84 (m, 4 H) 7.02 (s, 2 H) 7.07 - 7.18 (m, 6

H). MS: *m/z* calculated for $C_{32}H_{32}N_4O_4$ = 536.2424, actual *m/z* (M+H) = 537.085. IR (KBr pellet): υ 3441, 3308, 3062, 2914, 1644, 1541, 1439, 1357cm^{-1}.

cyclo-[βala-L-ala -βala-L-ala] (4.1c)
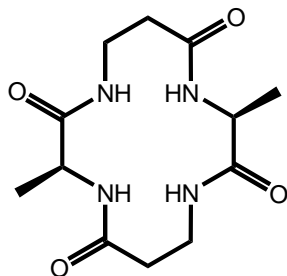
Yield 1.11g, 86.5%. ^{1}H NMR (400 MHz, CDCl$_3$) δ ppm 1.29 (d, *J*=7.03 Hz, 6 H) 2.43 (ddd, *J*=15.81, 3.90, 3.71 Hz, 2 H) 2.77 (ddd, *J*=15.71, 11.03, 4.49 Hz, 2 H) 3.41 - 3.48 (m, 2 H) 3.49 - 3.55 (m, 2 H) 4.44 (q, *J*=7.03 Hz, 2 H). MS: *m/z* calculated for $C_{12}H_{20}N_4O_4$ = 284.1485, actual *m/z* (M+H) = 285.066. IR (KBr pellet): υ 3297, 3098, 2965, 2906, 1666, 1639, 1553, 1440, 1387, 1348, 1255, 1003, 691, 665cm^{-1}.

4.7.2   General Synthesis of Cyclopeptides From Tetrapeptides.

All following work was performed under nitrogen: - The tetrapeptide (1mmol) and nickel chloride (1mmol) were mixed in methanol 25mL. To this solution was slowly added a solution of fresh NaOMe (12mmol) in 50mL methanol and then the reaction was slowly heated to 70 °C. The reaction was stopped between 3 and 24 hours (usually around 12 hours), concentrated and filtered over celite to remove any NaCl formed. To the solution was added HCl in ether (10mL, 2M, 20mmol) and stirred for between 20 minutes and 24 hours until a white solid dropped out of solution. The solid was filtered and washed with cold methanol, water and ether then dried *in vacuo*.

cyclo-[βala-L-Phe-βala-D-Phe] (4.1d)
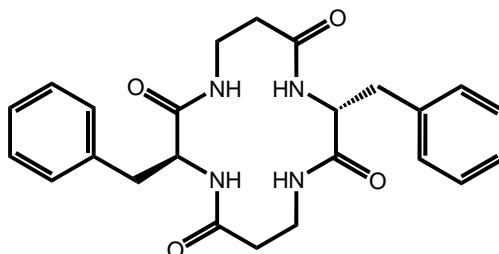
Yield 110mg, 77.8%. ^{1}H NMR (400 MHz, tfa) δ 2.35 - 2.74 (m, 3 H) 2.90 - 3.13 (m, 2 H) 3.12 - 3.32 (m, 3 H) 3.33 - 3.66 (m, 4 H) 4.36 - 4.56 (m, 1 H) 4.64 - 4.79 (m, 1 H) 7.02 - 7.38 (m, 10 H) 7.40 - 7.58 (m, 2 H) 7.73 - 7.92 (m, 2 H). MS: *m/z* calculated for $C_{24}H_{28}N_4O_4$ = 436.2111, actual *m/z* (M+H) = 437.22. IR (KBr pellet): υ 3482, 3290, 3078, 2919, 1653, 1546, 1454, 1367, 1261, 1222, 1062, 751, 711cm^{-1}.

cyclo-[βala-L-(2)Nap-βala-D-(2)Nap] (4.1e)
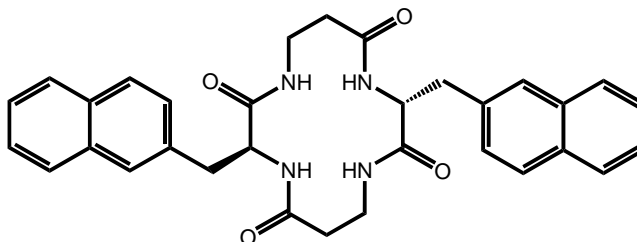
Yield 364mg, 85.3%. ^{1}H NMR (400 MHz, tfa) δ ppm 2.43 (s, 4 H) 3.03 (dd, *J*=14.18, 7.75 Hz, 2 H) 3.10 - 3.21 (m, 2 H) 3.49 (s, 4 H) 4.72 (d, *J*=6.81 Hz, 2 H) 7.09 (d, *J*=8.70 Hz, 2 H) 7.25 - 7.37 (m, 5 H) 7.38 - 7.50 (m, 6 H) 7.52 - 7.64 (m, 5 H). MS: *m/z* calculated for $C_{32}H_{32}N_4O_4$ = 536.2424, actual *m/z* (M+H) = 537.217. IR (KBr pellet): υ 3482, 3297, 3051, 2919, 1639, 1540, 1454, 1261, 1235, 1202, 744cm^{-1}

cyclo-[βala-L-(2)Nap-βala-L-Phe] (4.1f)
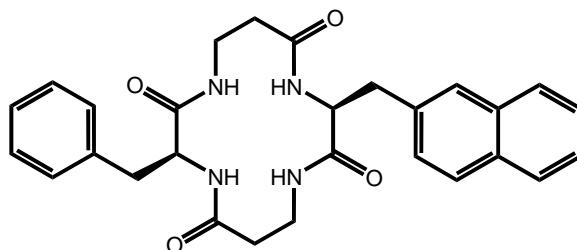
Yield 237mg, 64.4%. ^{1}H NMR (400 MHz, tfa) δ ppm 2.61 (s, 2 H) 2.94 (s, 2 H) 3.06 (s, 1 H) 3.20 (s, 2 H) 3.35 (s, 1 H) 3.45 - 3.56 (m, 2 H) 3.74 (s, 2 H) 4.77 (s, 1 H) 4.89 (s, 1 H) 7.15 (s, 2 H) 7.26 (d, J=7.03 Hz, 4 H) 7.43 (s, 2 H) 7.62 (s, 1 H) 7.75 (s, 3 H)

cyclo-[βala-L-(2)Nap-βala-gly] (4.1g)
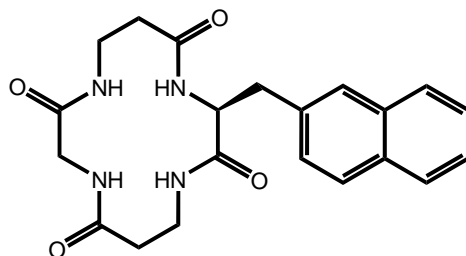
Yield 100mg, 15.3%. IR (KBr pellet): υ 3436, 3317, 2939, 1686, 1653, 1553, 1540, 1427, 1049cm^{-1}. MS: m/z calculated for $C_{21}H_{24}N_4O_4$ = 396.1798, actual m/z (M+Na) = 419.166.

cyclo-[βala-L-(2)Nap-βala-L-Ala] (4.1h)
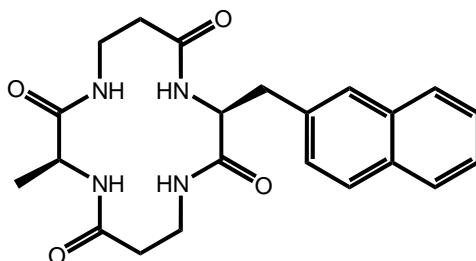
Yield 246mg, 54.5%. IR (KBr pellet): υ 3409, 3270, 2952, 1739, 1639, 1560, 1440, 1381, 1275, 1096, 1023, 804cm^{-1}. MS: *m/z* calculated for $C_{22}H_{26}N_4O_4$ = 410.1954, actual *m/z* (M+Na) = 433.170.

4.7.3 Synthesis of Metal Complexes from Liberated Cyclopeptides.

cyclo-[βala-L-Phe-βala-L-Phe]Fe$^{(III)}$ (4.3a)
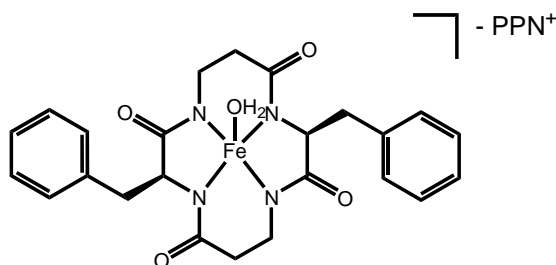
The following was performed in the glove box under a nitrogen atmosphere: - The *cyclo*-[βala-L-Phe-βala-L-Phe] (150mg, 0.344mmol) was suspended in DMSO and KH (66.2mg, 1.65mmol) added. The mixture was left to react for 10 minutes by which time all of the cyclopeptide had dissolved. To this mixture was added the FeCl$_2$ (43.6mg, 0.344mmol) and shaken for ten minutes. The color went to a dark orange. The vial was removed from the glove box and methanol and water were added. The flask was allowed to sit for 1 hour then the rust that had formed was filtered off. The DMSO was removed

in vacuo and the remaining solid was taken up in methanol and re-filtered. PPN-Cl (197mg, 0.344mmol) was then added to the methanol and slow evaporation lead to the formation of crystals. Yield 205mg, 58.1%. IR: υ 3056, 3019, 2912, 2839, 1568, 1442, 1376, 1254, 1102, 1000, 772, 686, 538cm^{-1}. Structure confirmed by X-ray crystal analysis.

cyclo-[βala-L-Phe-βala-L-Phe]Co$^{(III)}$ (4.3a)
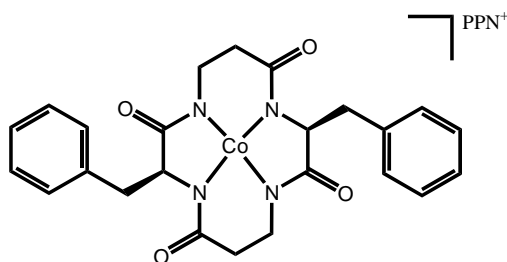
The following was performed in the glove box under a nitrogen atmosphere: - To *cyclo*-[βala-L-Phe-βala-L-Phe] (50mg, 0.115mmol) in DMSO (5mL) was added KH (20.1mg, 0.5mmol) and stirred for 5 minutes. To this mixture was added the CoCl$_2$ (14.9mg, 0.115mmol) in DMSO (2mL) the mixture then went green and was stirred for a further ten minutes. The mixture was removed from the glove box and sonicated for two minutes. To this solution was then added methanol (1ml) and the solution then went red. To the solution was added PPN-Cl (132mg, 0.23mmol) and the mixture was crystallized from water:methanol:ethanol (1:1:1) mixture. Yield 90mg, 76%. IR: υ 3060, 3019, 2937, 1715, 1609, 1585, 1564, 1474, 1446, 1372, 1270, 1213, 1102, 1000, 747, 726, 696, 534cm^{-1}. Structure confirmed by X-ray crystal analysis.

4.7.4 General Synthesis of Cyclams From Cyclopetides.

The cyclopeptide (1mmol) is placed in a Schlenk flask and THF (30mL) is added via vacuum transfer. To this was added LAH (12mmol) at –78°C and the reaction mixture is stirred for 1 hour at until the flask reaches RT and the initial bubbling stops. The flask

is then heated to 60 °C for 24-48 hours. The reaction is allowed to cool to RT and NaOH (15% w/w, 5-10mL) was added slowly and the mixture stirred for 1 hour. The mixture was diluted with wet THF (20ml) and filtered through celite to remove the solid waste. The celite is then washed with DCM and the organics dried over magnesium sulfate. The solvent is removed *in vacuo* and taken up in DCM and filtered to remove any solid particles. The solvent is removed *in vacuo* to yield product.

2S,9S-Dibenzyl-1,4,8,11-tetraazacyclotetradecane (4.2a)
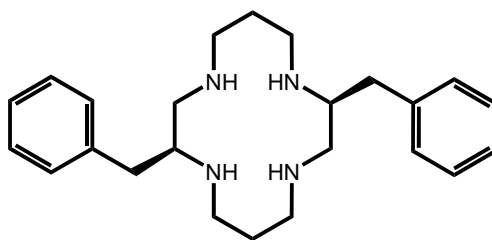
Yield 141mg, 38.3% ^{1}H NMR (400 MHz, CDCl$_3$) δ ppm 1.60 - 1.72 (m, 4 H) 2.08 (s, 4 H) 2.39 - 2.47 (m, 2 H) 2.47 - 2.53 (m, 2 H) 2.56 - 2.67 (m, 8 H) 2.80 - 2.87 (m, 2 H) 2.87 - 2.96 (m, 4 H) 7.12 - 7.19 (m, 6 H) 7.22 - 7.28 (m, 4 H). 13C NMR (101 MHz, CDCL3-D) δ ppm 29.54, 39.38, 47.32, 50.09, 52.85, 58.86, 126.17, 128.52, 129.35, 139.83.

2S,9S-Di(2-naphthyl)-1,4,8,11-tetraazacyclotetradecane (4.2b)
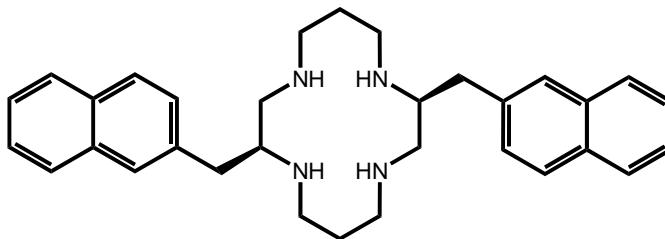
Yield 117mg, 65.1%. ^{1}H NMR (400 MHz, CDCl$_3$) δ 1.75 (s, 4 H) 2.58 (dd, *J*=11.91, 8.78 Hz, 4 H) 2.62 - 2.74 (m, 12 H) 2.94 - 3.10 (m, 4 H) 3.14 (dd, *J*=13.47, 5.27 Hz, 2 H) 7.33 (d, *J*=8.20 Hz, 2 H) 7.40 - 7.51 (m, 4 H) 7.62 (s, 2 H) 7.74 - 7.84 (m, 6 H).

^{13}C NMR (101 MHz, CDCl$_3$) δ 29.03, 39.36, 47.46, 50.15, 52.80, 58.63, 125.54, 126.22, 127.67, 127.70, 127.83, 127.89, 128.22, 132.31, 133.75, 137.08.

2S,9S-Dimethyl 1,4,8,11-tetraazacyclotetradecane (4.2c)
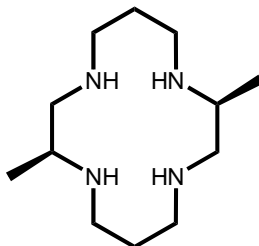
Yield 118mg, 26%. ^{1}H NMR (400 MHz, CDCl$_3$) δ 1.00 (s, 6 H) 1.76 (s, 4 H) 2.55 (s, 6 H) 2.75 (s, 6 H) 2.98 (s, 2 H). ^{13}C NMR (101 MHz, CDCl$_3$) δ 17.79, 28.86, 48.56, 50.77, 52.38, 55.62.

4.7.5 *General Synthesis of Nickel Cyclams Complexes.*

The cyclam (1mmol) is dissolved in methanol (20ml) and the nickel salt (1mmol) is added in methanol (10ml). The reaction mixture is heated to reflux for ten minutes and allowed to cool. A purple crystalline solid falls out of solution and is collected by filtration. (For the perchlorate salt recrystallization occurs in water after the removal of methanol)

2S,9S-Dibenzyl-1,4,8,11-tetraazacyclotetradecane nickel Bis-chloride (4.4a)
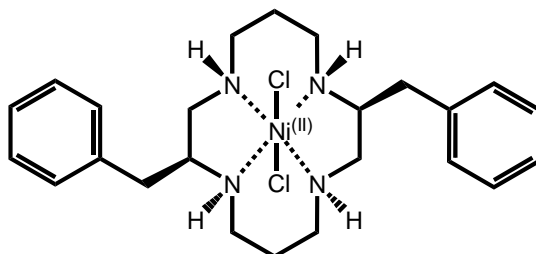
Yield 35mg, 37.3%. MS: *m/z* calculated for $C_{24}H_{36}N_4$ = 438.2293 actual *m/z* (M-H) = 437.151. IR: υ 3252, 3219, 2921, 2855, 1446, 1086, 1000, 943, 869, 755, 739, 714, 690, 637, 510cm^{-1}. Structure confirmed by X-ray analysis.

2S,9S-Di(2-naphthyl)-1,4,8,11-tetraazacyclotetradecane nickel Bis-chloride (4.4b)
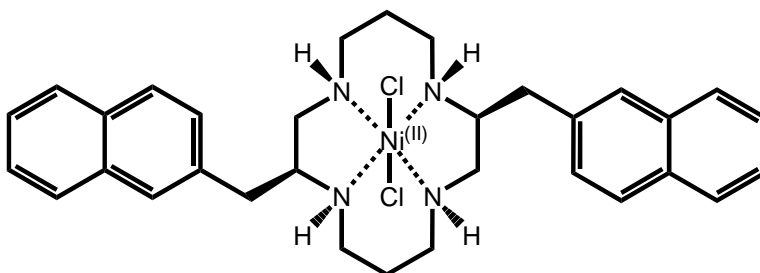
Yield 70mg, 68%. MS: *m/z* calculated for $C_{32}H_{40}N_4$ = 538.2606, actual *m/z* (M-H) = 537.178. IR: υ 3207, 3178, 2913, 2843, 1458, 1421, 1115, 1094, 1041, 939, 874, 812, 747, 735, 637, 592cm^{-1}. Structure confirmed by X-ray analysis.

2S,9R-Di(2-naphthyl)-1,4,8,11-tetraazacyclotetradecane nickel Bis-chloride (4.4c)
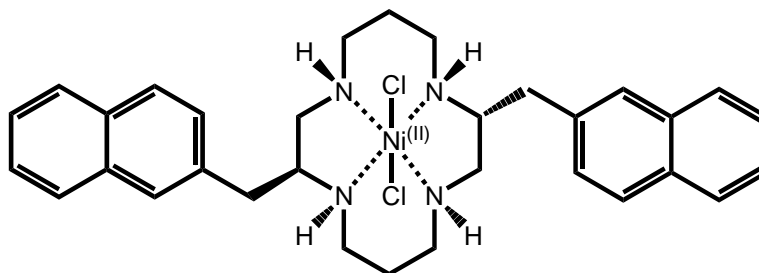
Yield 5mg, 3% over two steps.. Structure confirmed by X-ray analysis.

2S,9S-Dimethyl-1,4,8,11-tetraazacyclotetradecane nickel Bis-perchlorate (4.4d)
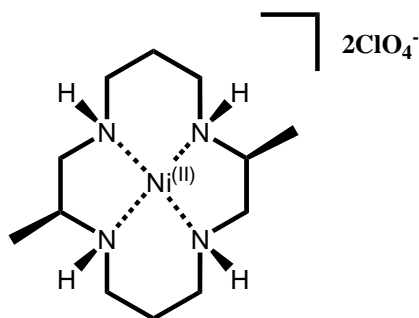
Yield 2mg, 9.41% Structure confirmed by X-ray analysis.

References: - Chapter 4.

[1] J. Schapp, K. Haas, K. Sünkel, and W. Beck., *Eur. J. Inorg. Chem.,* 2002, **20**, 3745-3751.

[2] M. Amorin, R. J. Brea, L. Castedo, and J. R. Granja. *Org. Lett.,* 2005, **7(21)**, 4681-4684 (and references therein) (b) D. Ranganathan, C. Lakshmi, V. Haridas and M. Gopikumar, *Pure. Appl. Chem.,* 200, **72(3)**, 365-372

3 T. J. Collins, *Acc. Chem. Res.,* 1994, **27**, 279-285; (b) T. J. Collins, *Acc. Chem. Res.,* 2002, **35**, 782-790; (c) S. S. Gupta, M. Stadler, C. A. Noser, A. Ghosh, B. Steinhoff, D. Lenoir, C. P. Horwitz, K-W. Schramm, T. J. Collins, *Reports*., 2002, **296**, 326-328; (d) A. Ghosh, F. T. Oliveria, T. Yano, T. Nishioka, E. S. Beach, I. Kinoshita, E. Munck, A. D. Ryabov, C. P. Hortwitz and T. J. Collins, *J. Am. Chem. Soc.,* 2004, **127**, 2505-2513. (e) A. Ghosh, D. A. Mitchell, A. Chanda, A. D. Ryabov, D. L. Popescu, E. C. Upham, G. J. Collins, T. J. Collins, *J. Am. Chem. Soc.,* 2008, **130**, 15116-15126.

4 T. J. Collins, R. D. Powell, C. Slebodnick and E. S. Uffelman, *J. Am. Chem. Soc.,* 1991, **113**, 8419-8425.

5 (a) D. W. Margerum, J. S. Rybka, *Inorg. Chem.* 1980, **19**, 2784-2790. (b) J. S. Rybka, D. W. Margerum, *Inorg. Chem.* 1981, **20***,* 1453-1458.

6 (a) A. L. Nivorozhkin, B. M. Segal, K. B. Musgrave, S. A. Kates, B. Hedman, K. O. Hodgson, R. H. Holm, *Inorg. Chem.,* 2000, **39**, 2306-2313; (b) D. J. Freeman, G. Pattenden, A. F. Drake, G. Siligardi, *J. Chem. Soc., Perkin Trans 2,* 1998, 129-135. (c) J. C. Lagarias, R. A. Houghten, H. Rapoport, *J. Am. Soc.* 1978, **100**, 8202-8209.

7 (a) M. C. Alcaro, M. Orfei, M. Chelli, M. Ginanneschi and A. M. Papini, *Tetrahedron Lett.,* 2003, **44**, 5217-5219. (b) M. Achmatowicz and J. Jurczak, *Tetrahedron: Asymmetry,* 2001, **12**, 111-119 (c) A. Kouvarakis, H. E. Katerinopoulos, *Syn. Commun.,* 1995, **25**, 3035-44 (d) L. F. Tietze, H. Braun, P. L. Steck, S. A. A. El Bialy, N. Toelle, A. Duefert, *Tetrahedron.*, 2007, **63**, 6437-6445.

8 N. Franceschini, P. Sonnet and D. Guillaume, *Org. Biomol. Chem.,* 2005, **3**, 787-793

9 (a) H. Yoon, T. R. Wagler, K. J. O'Connor, C. J. Burrows, *J. Am. Chem. Soc.,* 1990, **112**, 4568-4570; (b) J. F. Kinneray, T. R. Wagler, C. J. Burrows, *Tetrahedron Lett.,* 1988, **29**, 877-880.

10 (a) N. Ting, J. G. Muller, C. J. Burrows, S. E. Rokita, *Biochemistry*, 1999, **38**, 16648-16654; (b) J. G. Muller, X. Chen, A. C. Dadiz, S. E. Rokita, C. J. Burrows, *Pure & Appl. Chem.,* 1993, **65**, 545-550.

11 H-C. Shih, H. Kassahun, C. J. Burrows, S. E. Rokita, *Biochemistry*, 1999, **38**, 15034-15042.

12 B. Konig, M. Pelka, H. Zieg, P. G. Jones, I. Dix, *Chem. Commun.,* 1996, 471-472

[13] C. M. Zakaria, G. Ferguson, A. J. Lough, C. Glidewell, *Acta Cryst.,* 2002. **B58**, 78-93

[14] L. Jiang, X-L. Feng, T-B. Lu, C*rystal Growth and Design.,* 2005, **5**, 1469-1475

[15] Z. Urbanczyk-Lipkowska, J. W. Krajewski, P. Gluzinski, L. Parkanyi, *Pol. J. Chem.,* 1983, **57**, 85

[16] F. A. Carey, R. J. Sundberg, *Advanced Organic Chemistry 4th Ed. Part A: Structure and Mechanisms,* Kluwer Academic/Plenum Publishers: New York, 2000, 732.

Appendix A - ¹HNMR and ¹³CNMR Data.

Figure A.1: - (a) ¹HNMR (b) ¹³CNMR of 1.1
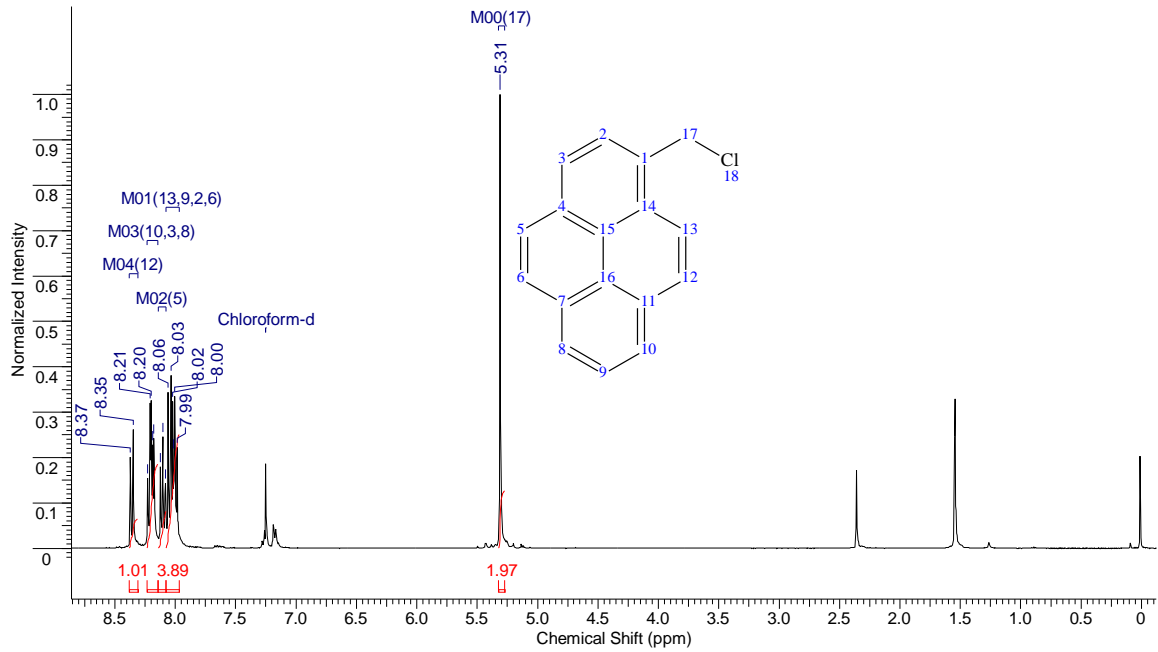
(a)
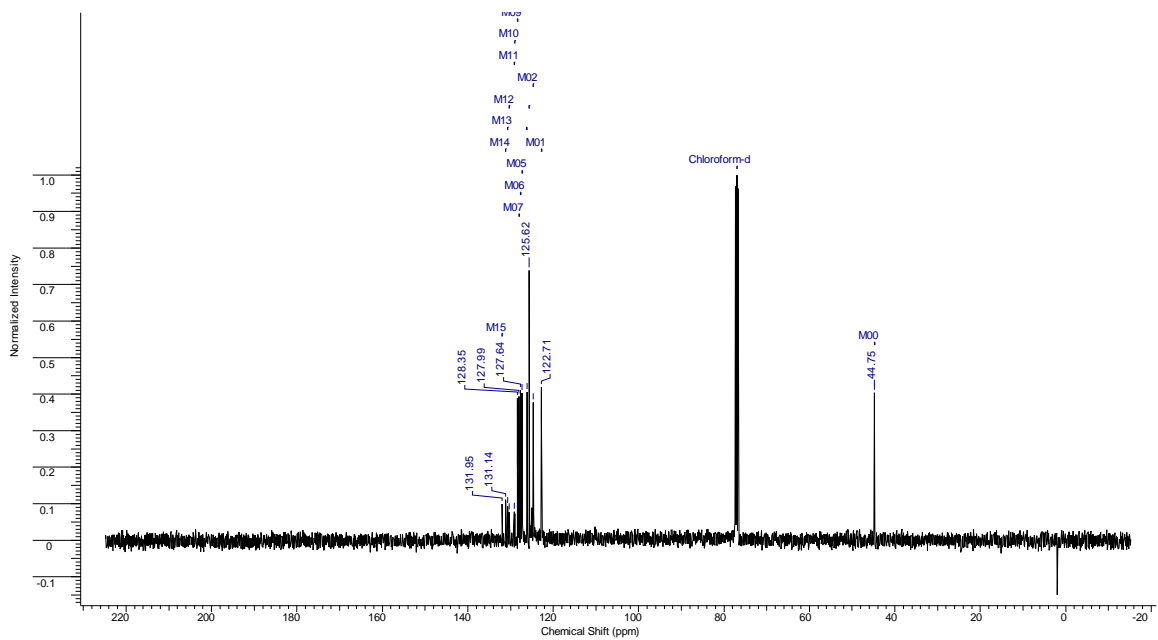
(b)

Figure A.2: - (a) ¹HNMR (b) ¹³CNMR of 1.2a
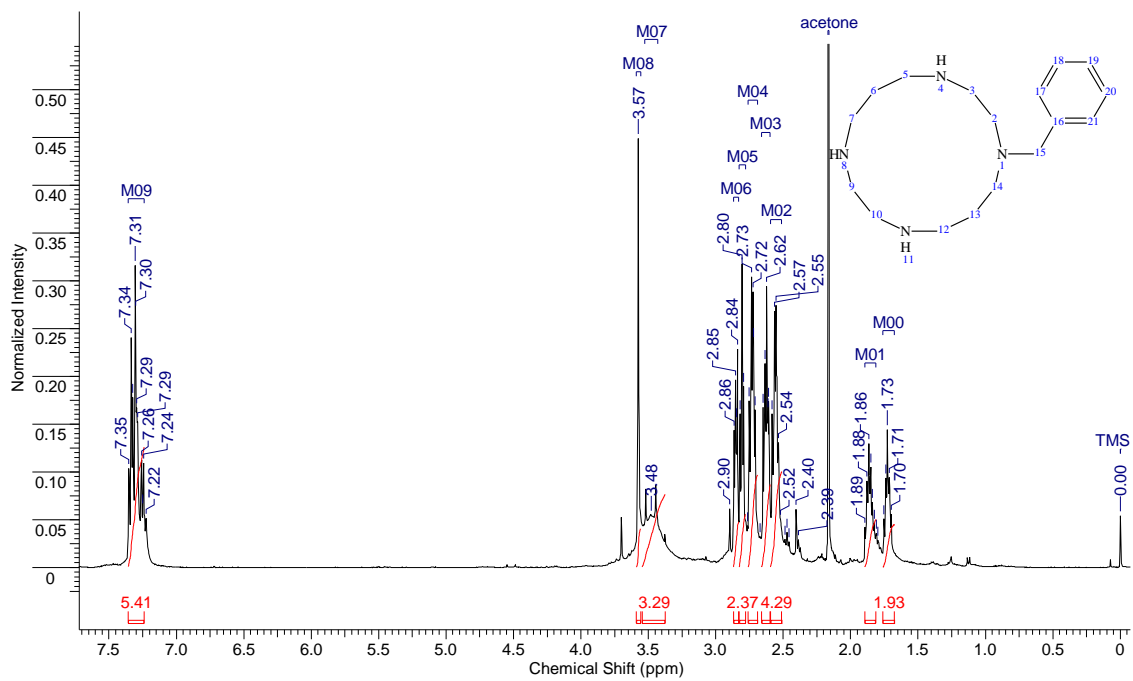
(a)
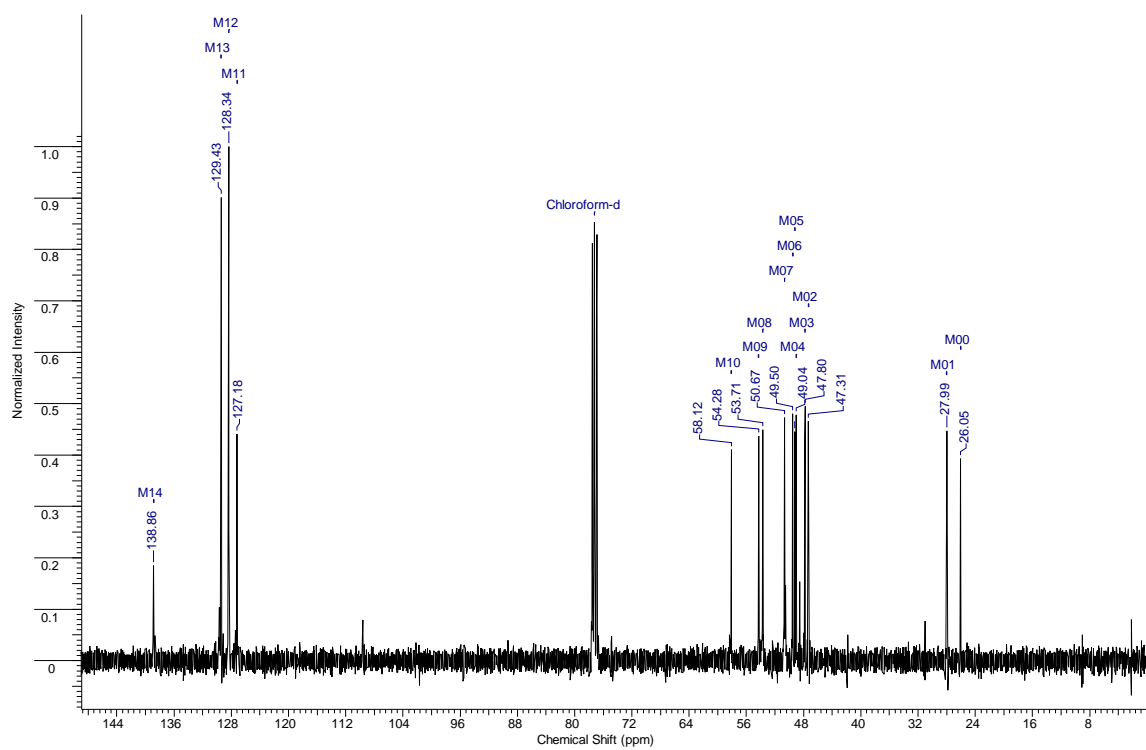
(b)
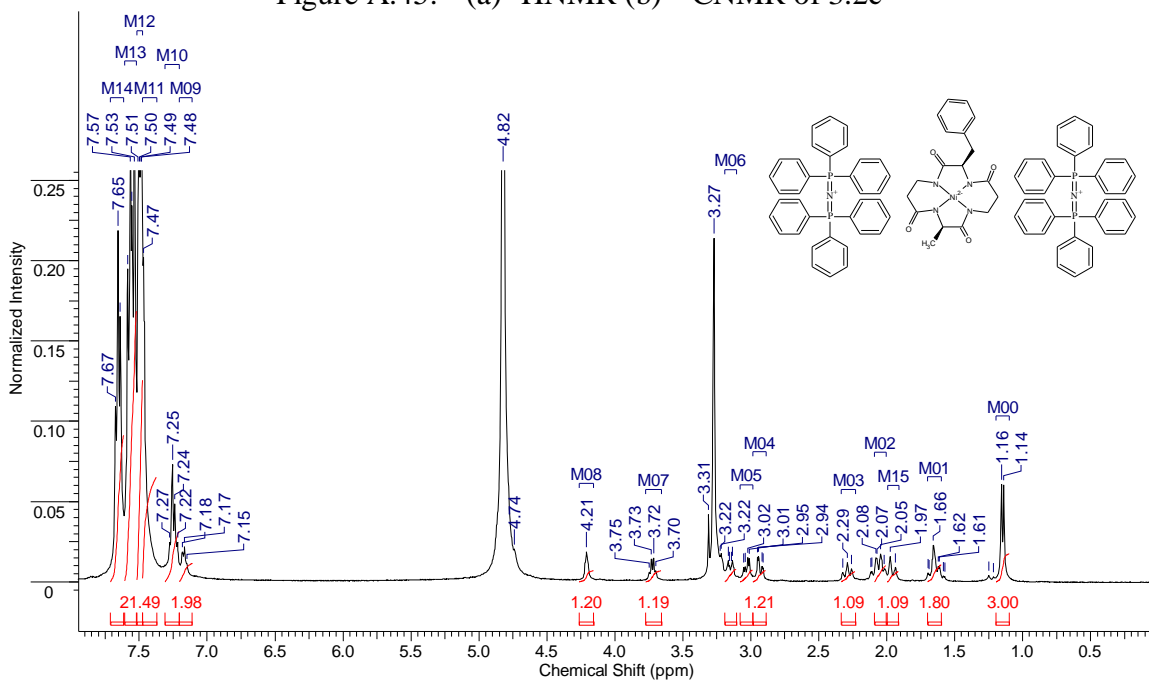
Figure A.3: - (a) ¹HNMR (b) ¹³CNMR of 1.2b
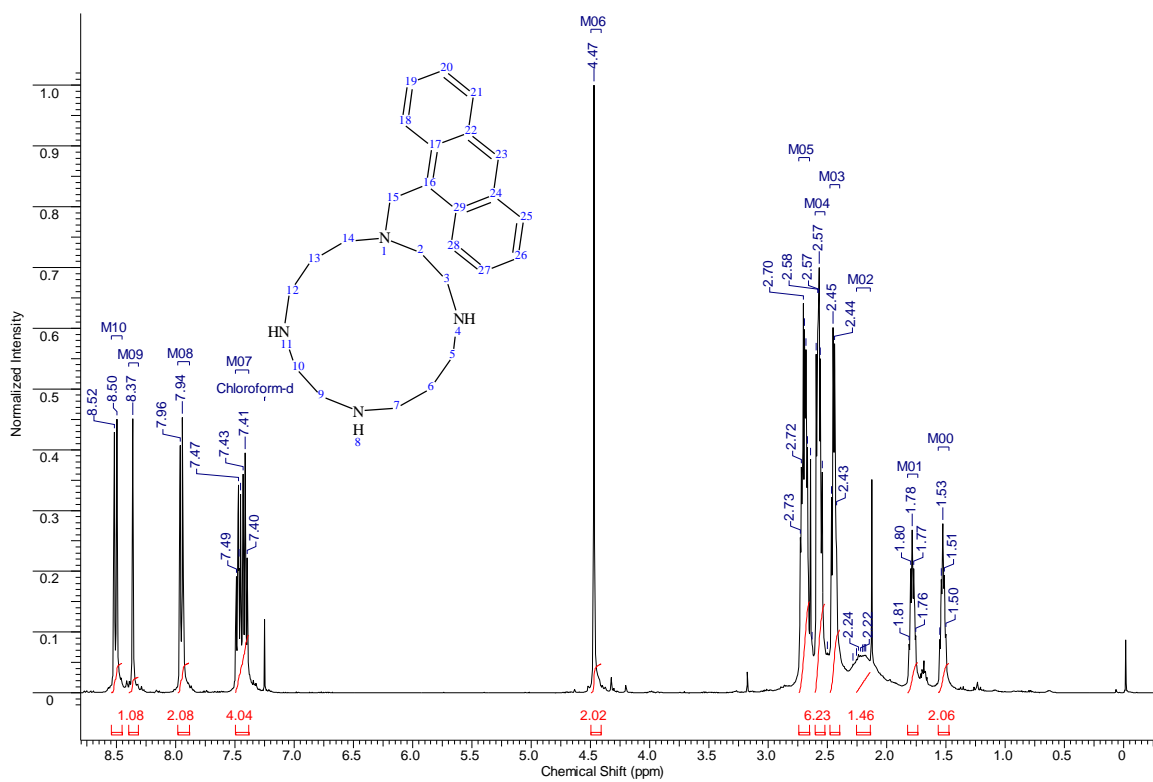
(a)
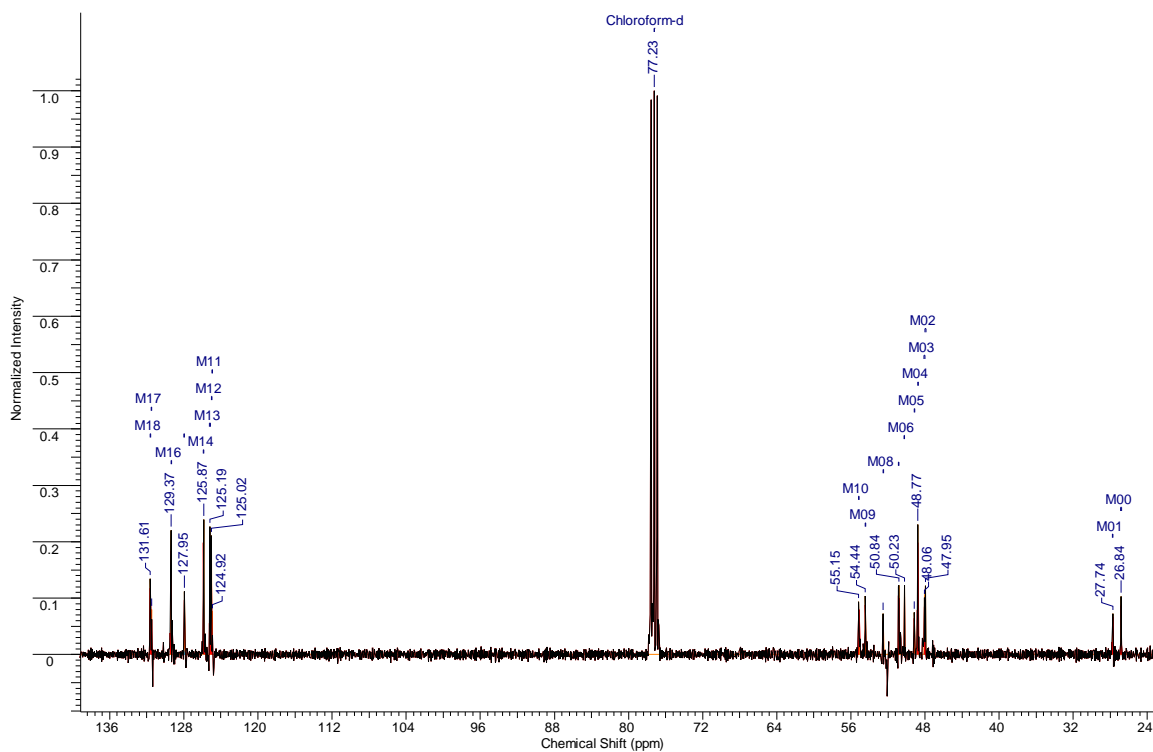
(b)
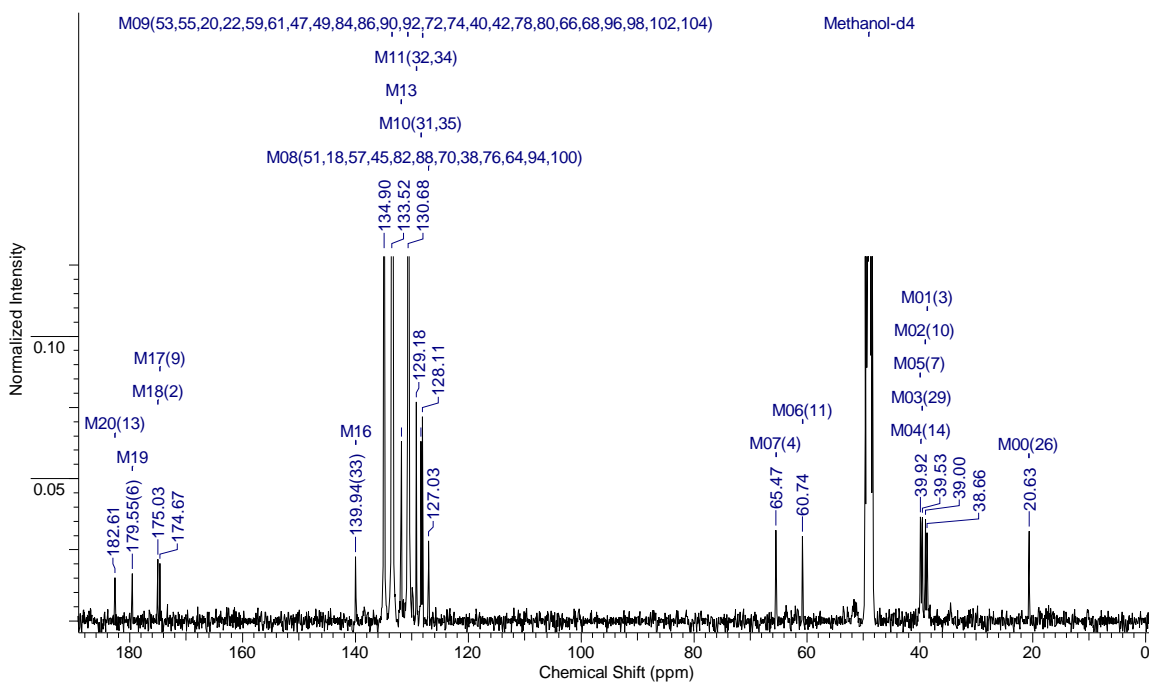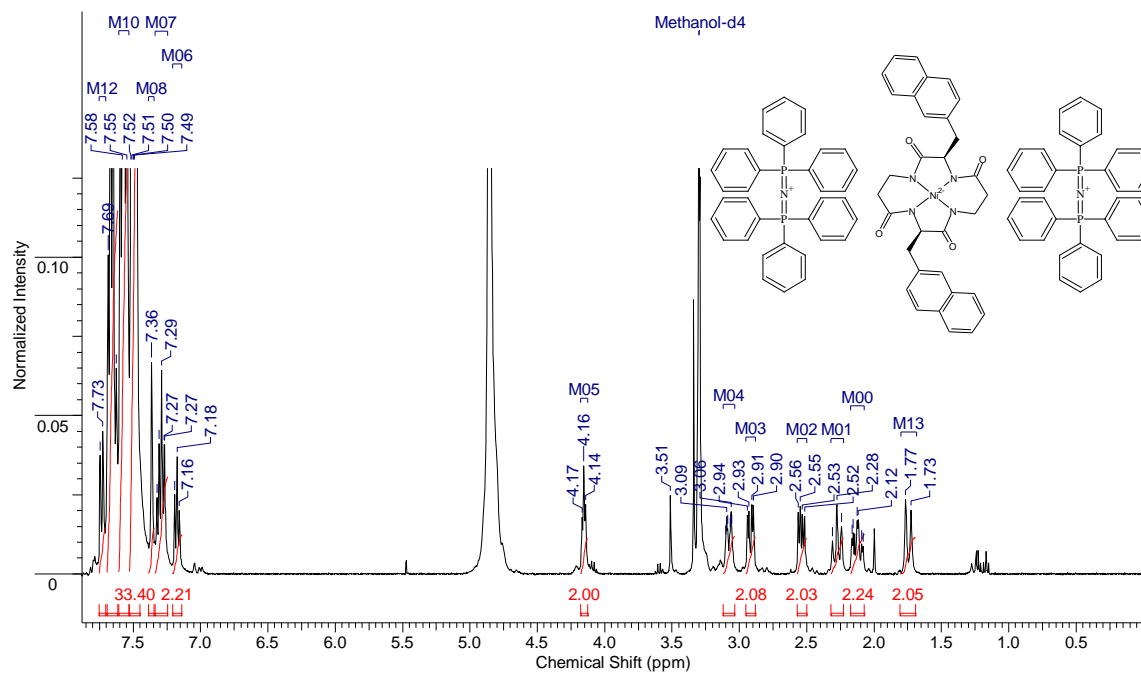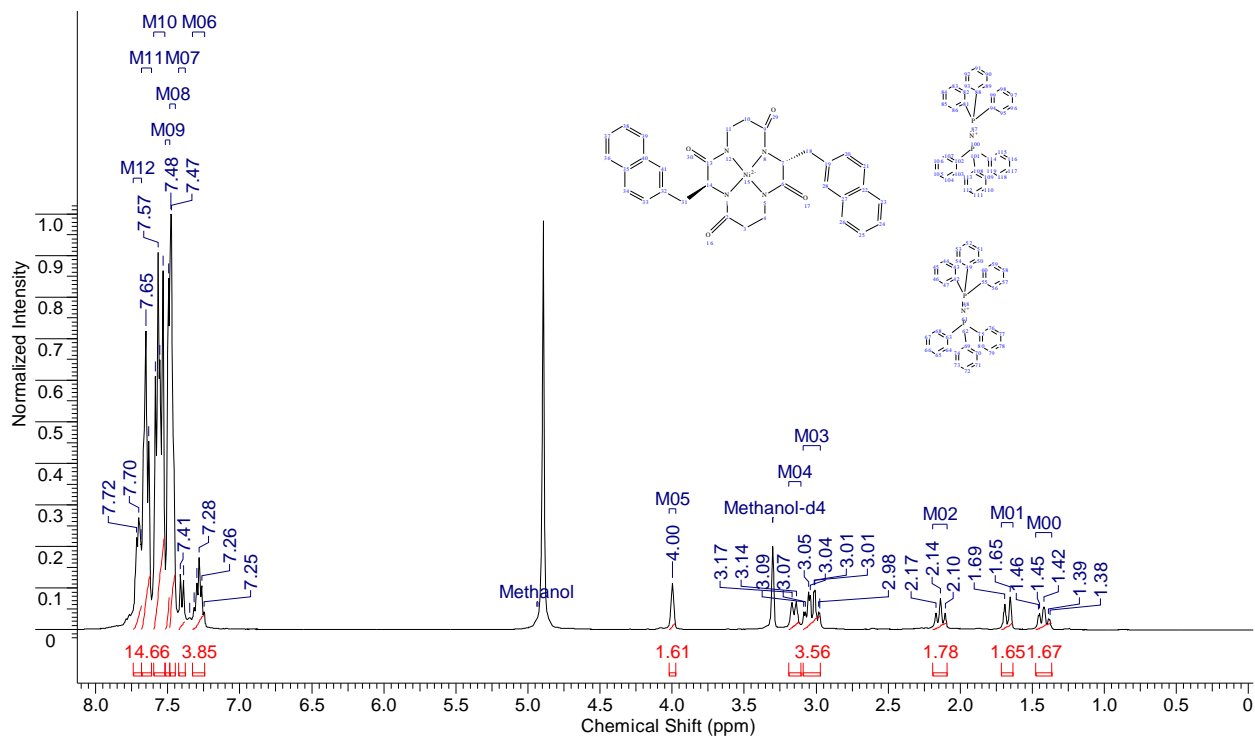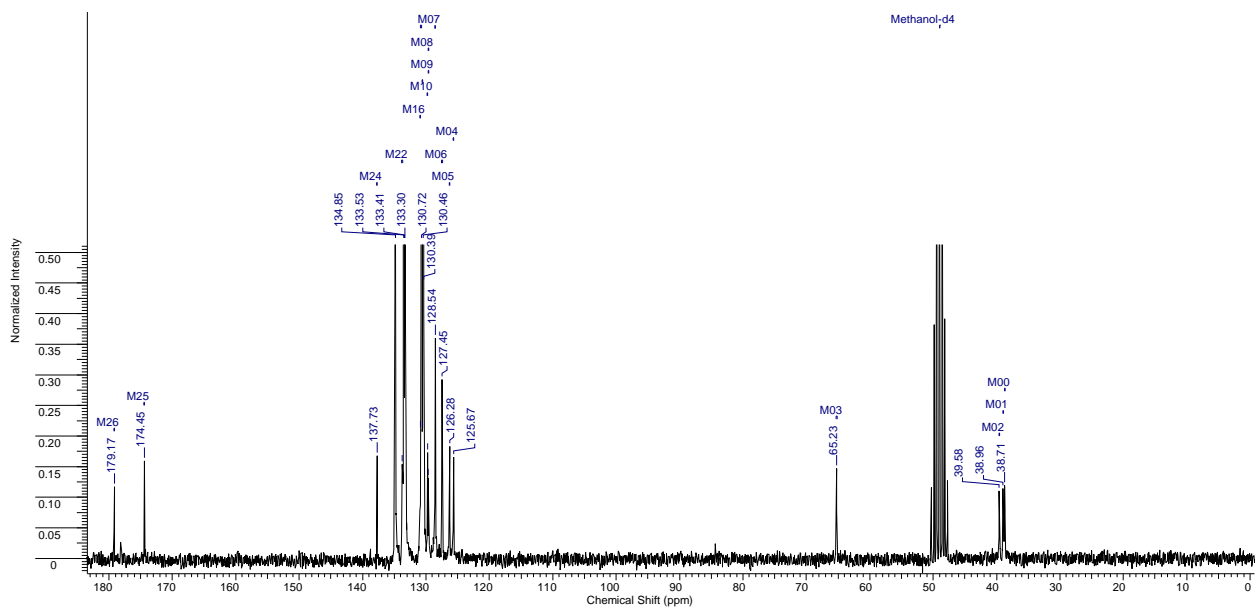
Figure A.4: - (a) ^{1}HNMR (b) ^{13}CNMR of 1.2c
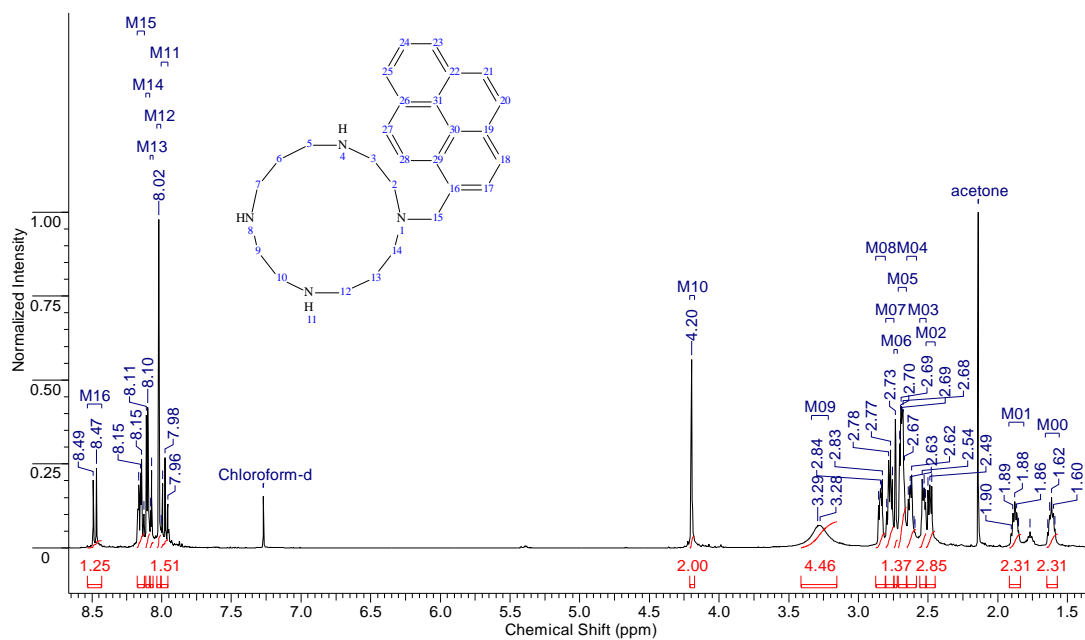
(a)
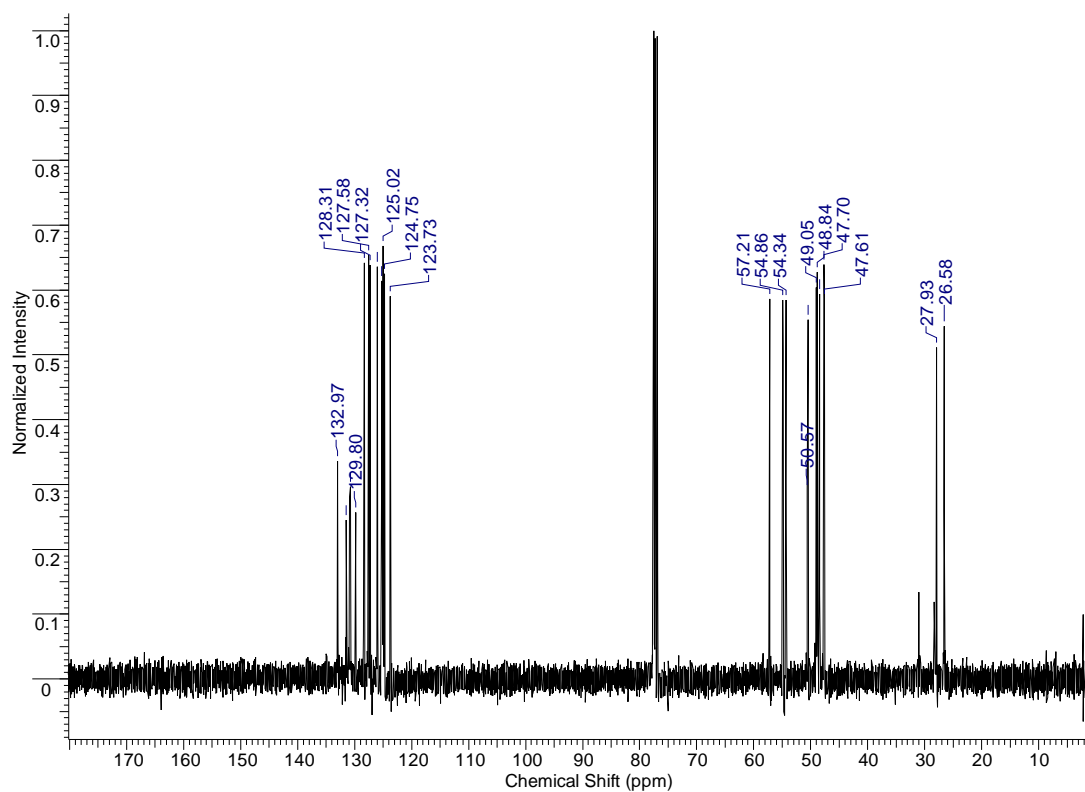
(b)

Figure A.5: - (a) ¹HNMR 1.4
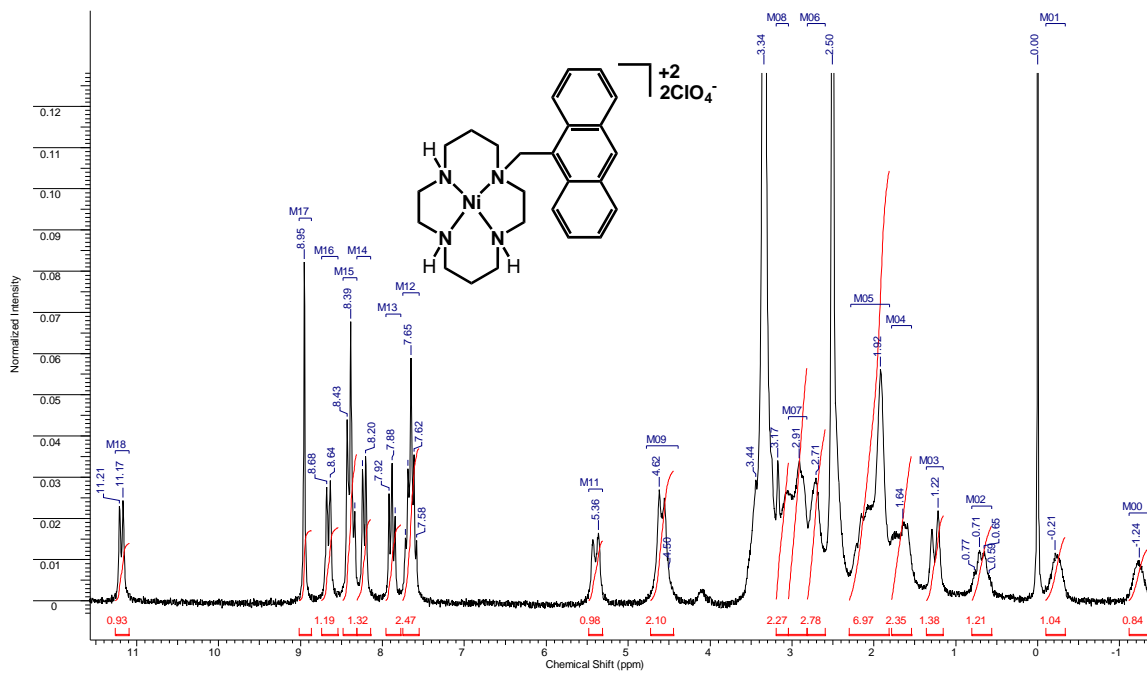
(a)

Figure A.6: - (a) ¹HNMR of 1.5
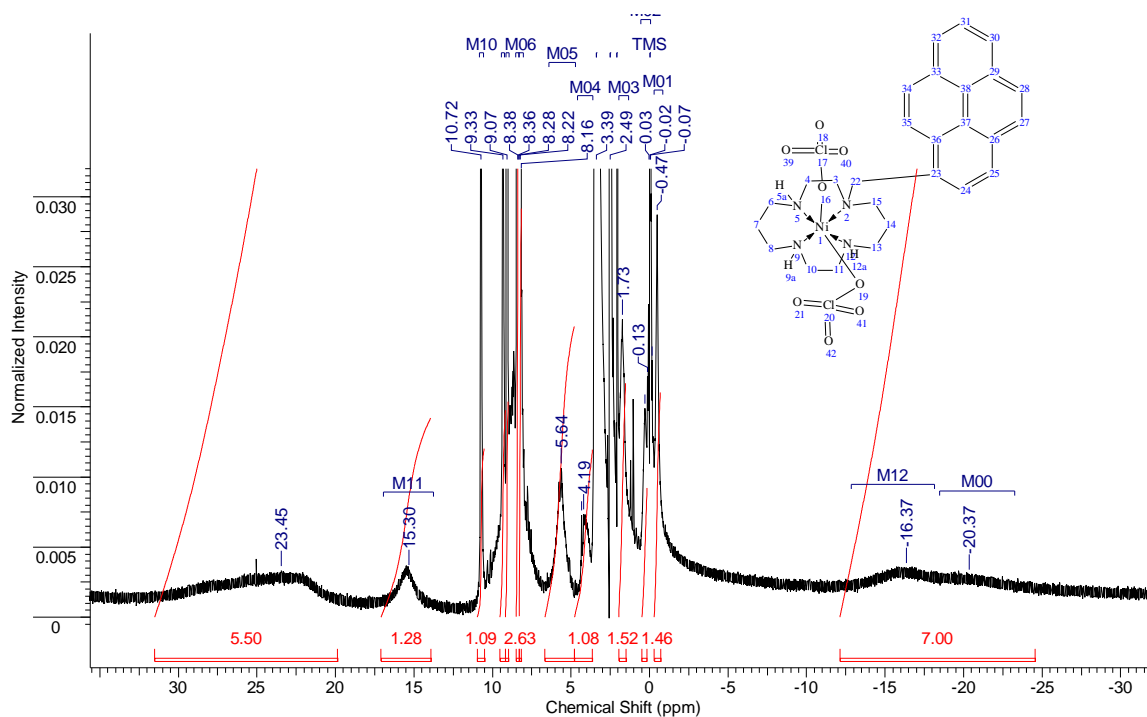
(a)

Figure A.7: - (a) ^{1}HNMR of 1.6a
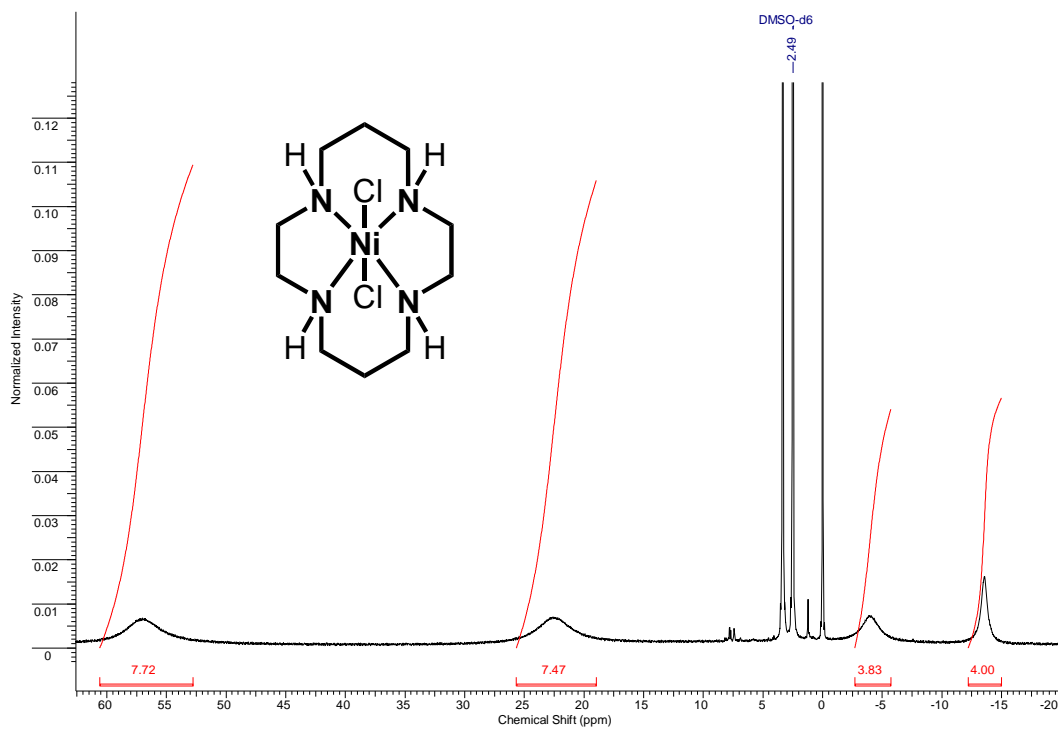
(a)

Figure A.8: - (a) ^{1}HNMR (b) ^{13}CNMR of 2.35
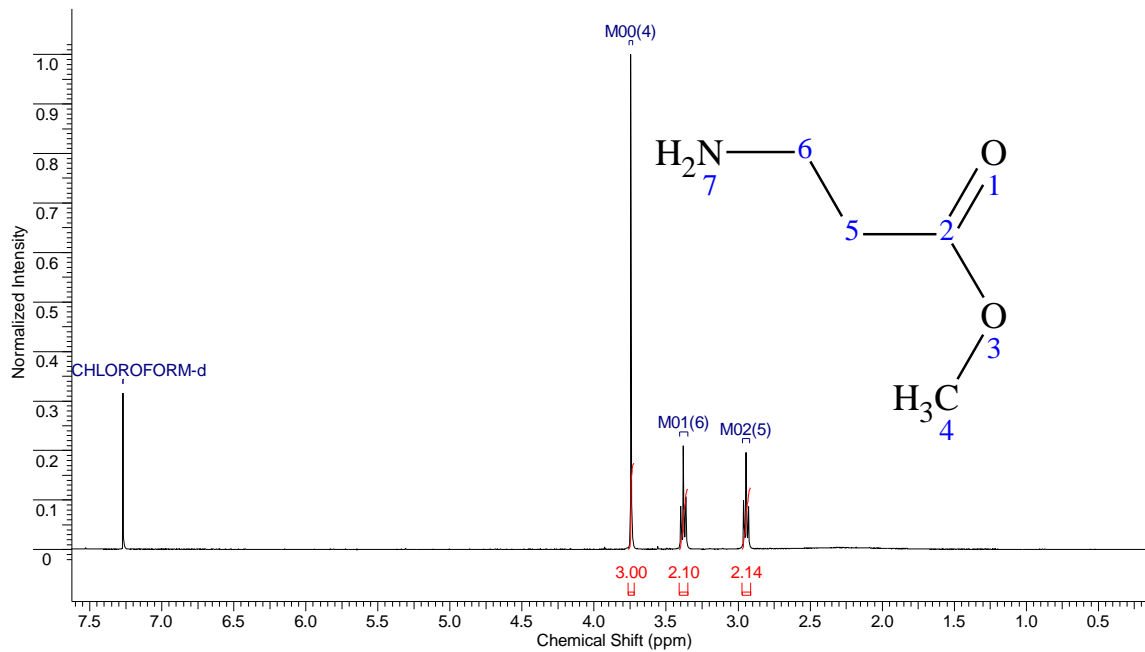
(a)
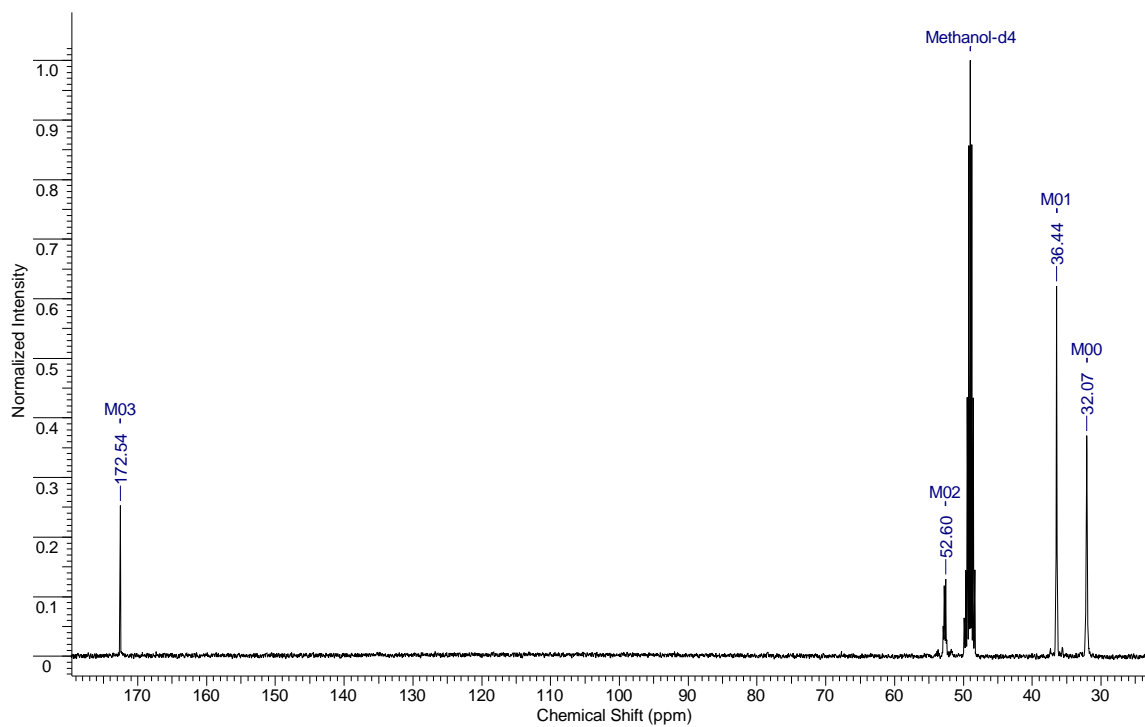
(b)

Figure A.9: - (a) ¹HNMR (b) ¹³CNMR of 2.37a
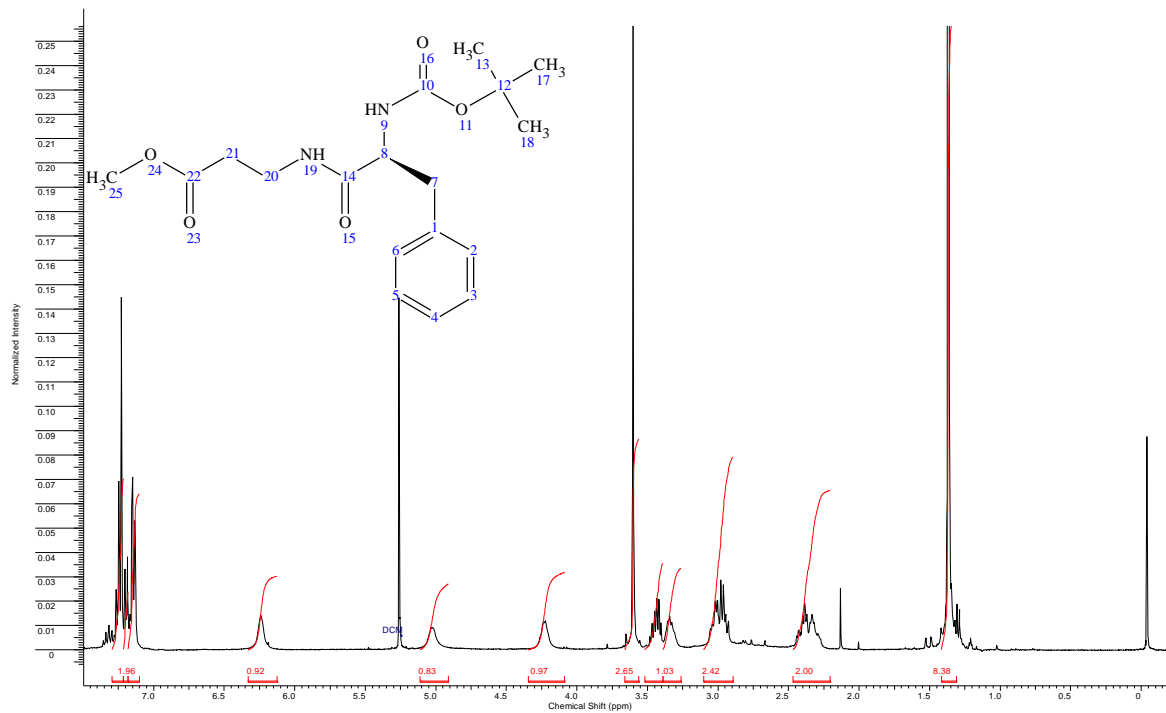
(a)
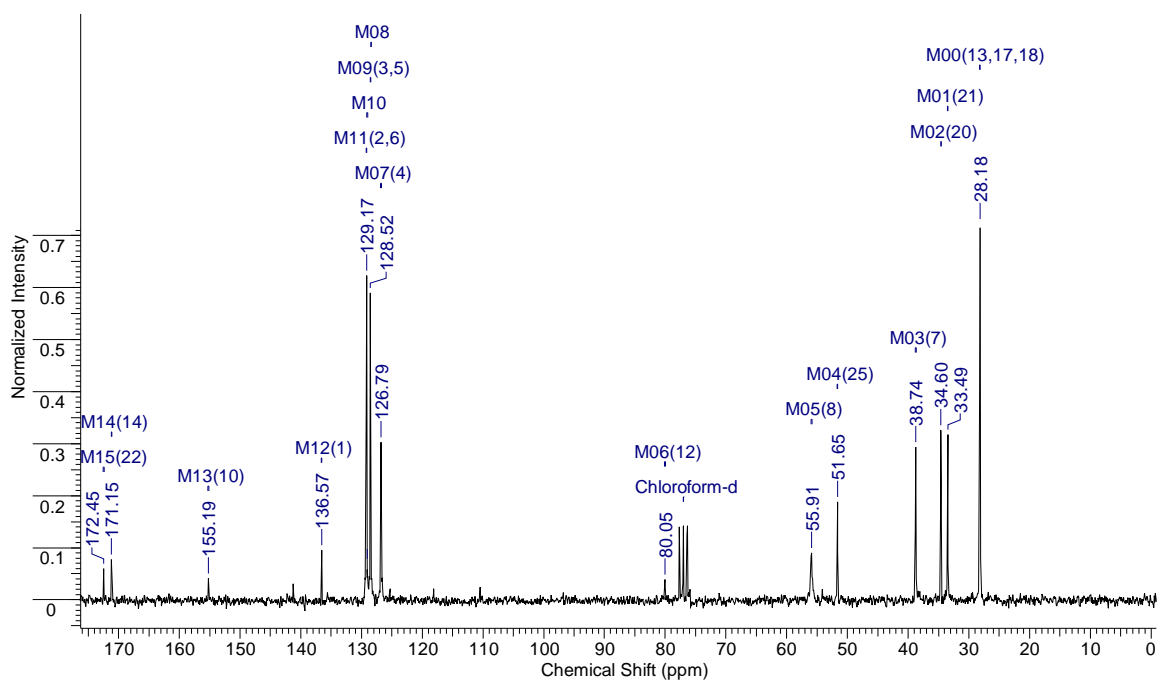
(b)

Figure A.10: - (a) ¹HNMR (b) ¹³CNMR of 2.37b
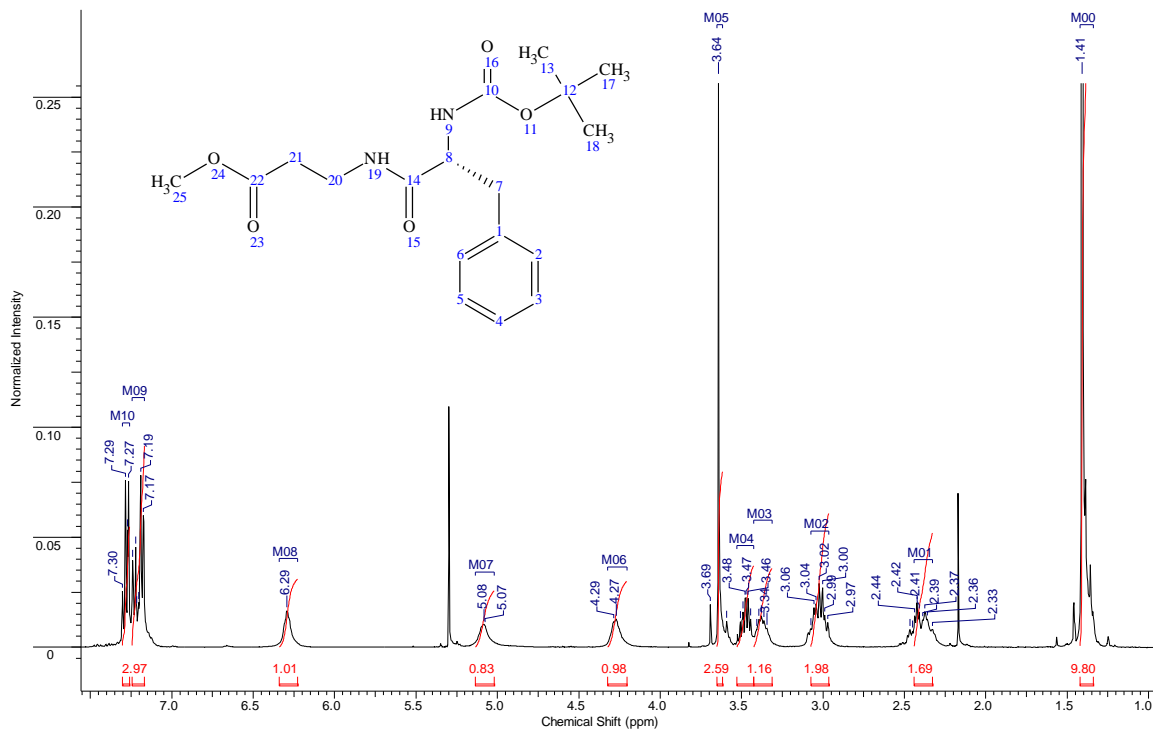
(a)
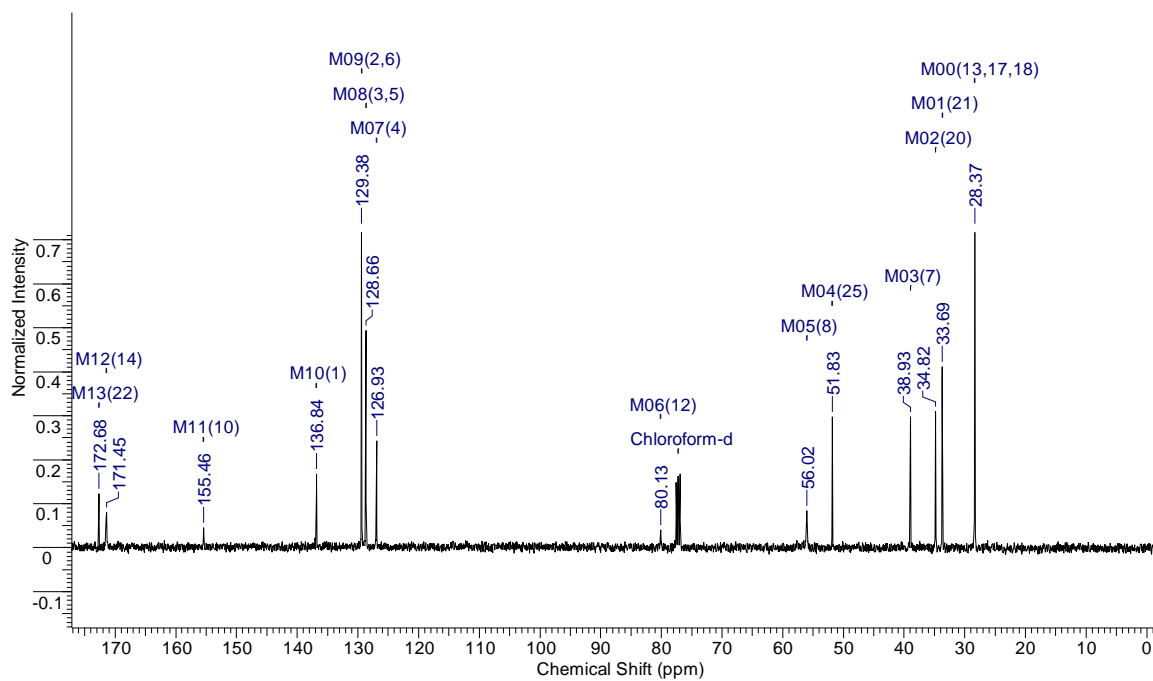
(b)

Figure A.11: - (a) ¹HNMR (b) ¹³CNMR of 2.37c
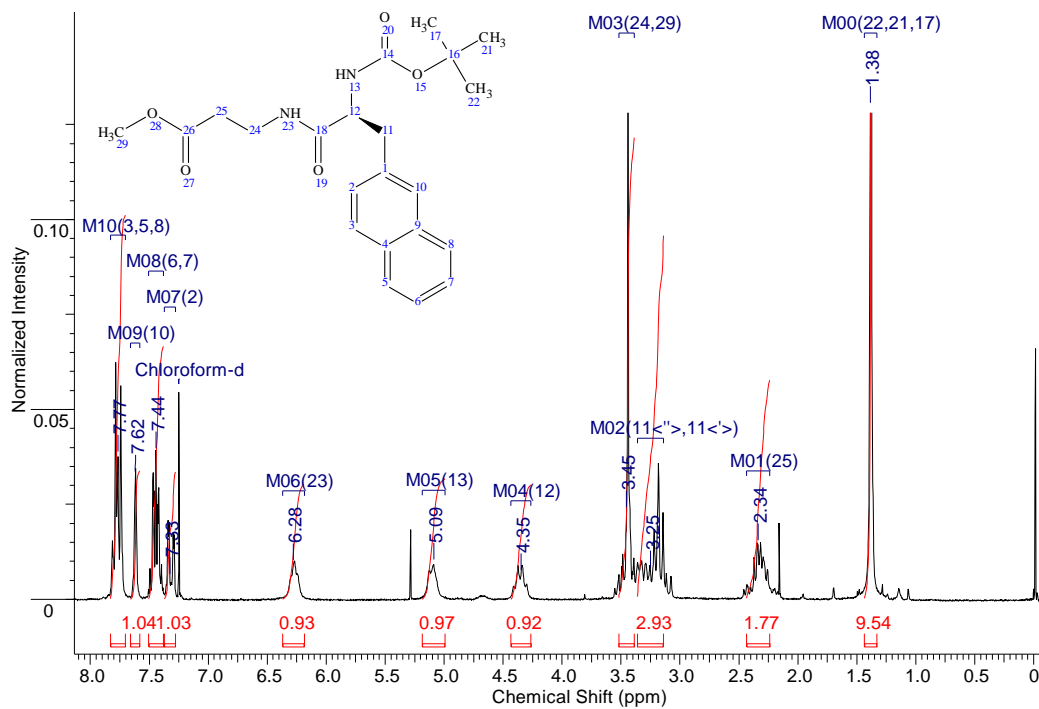
(a)
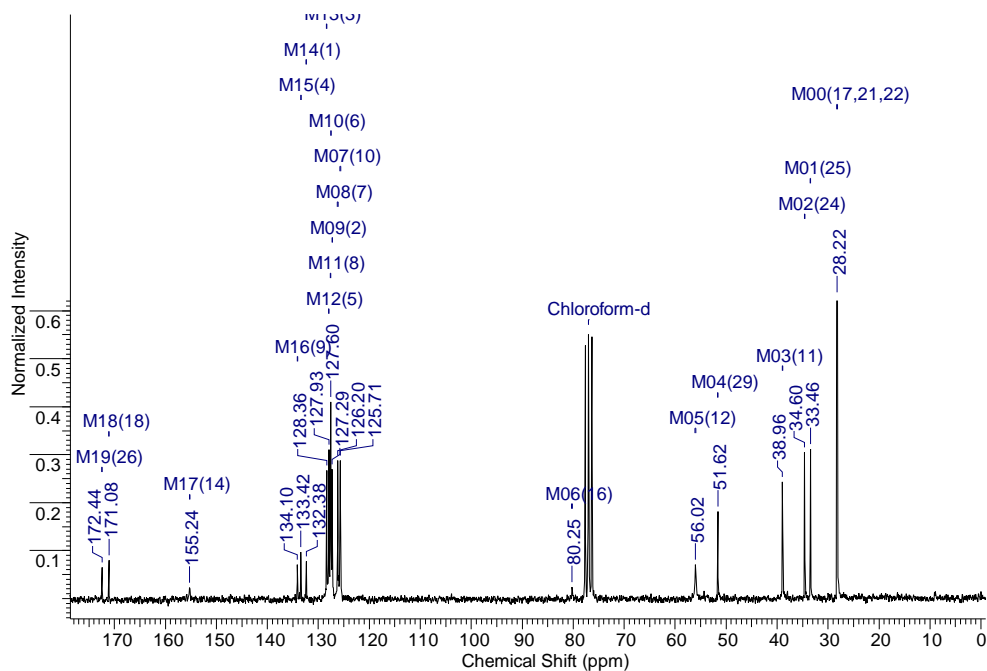
(b)

Figure A.12: - (a) ^{1}HNMR (b) ^{13}CNMR of 2.37d
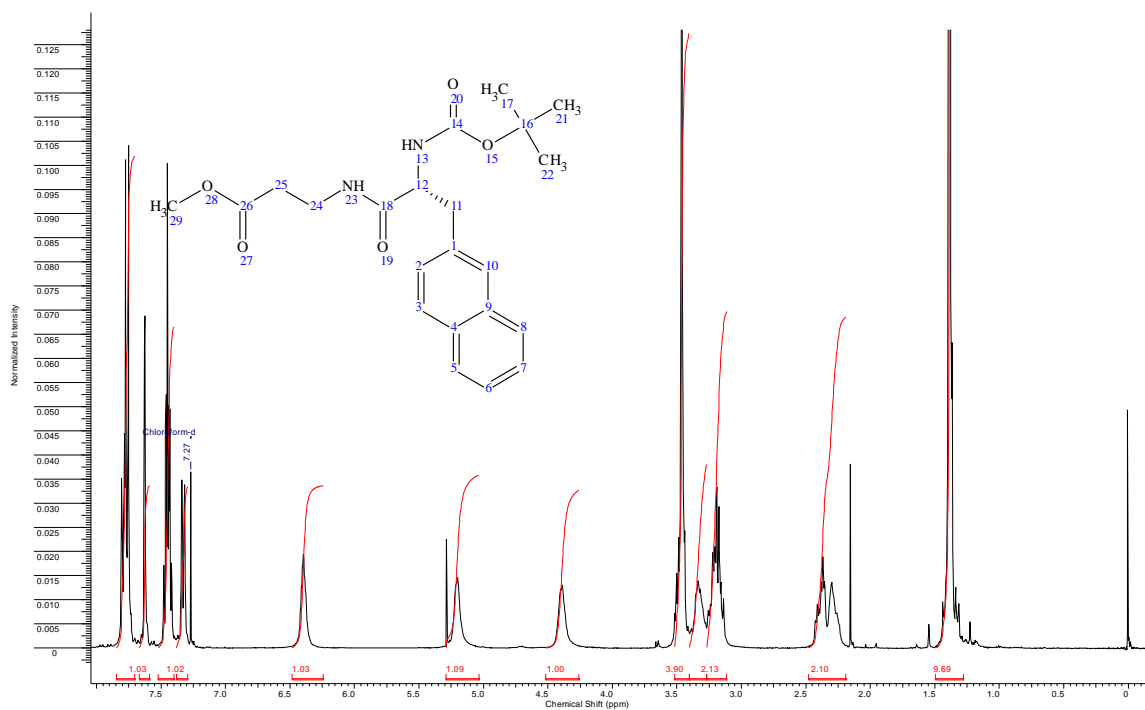
(a)
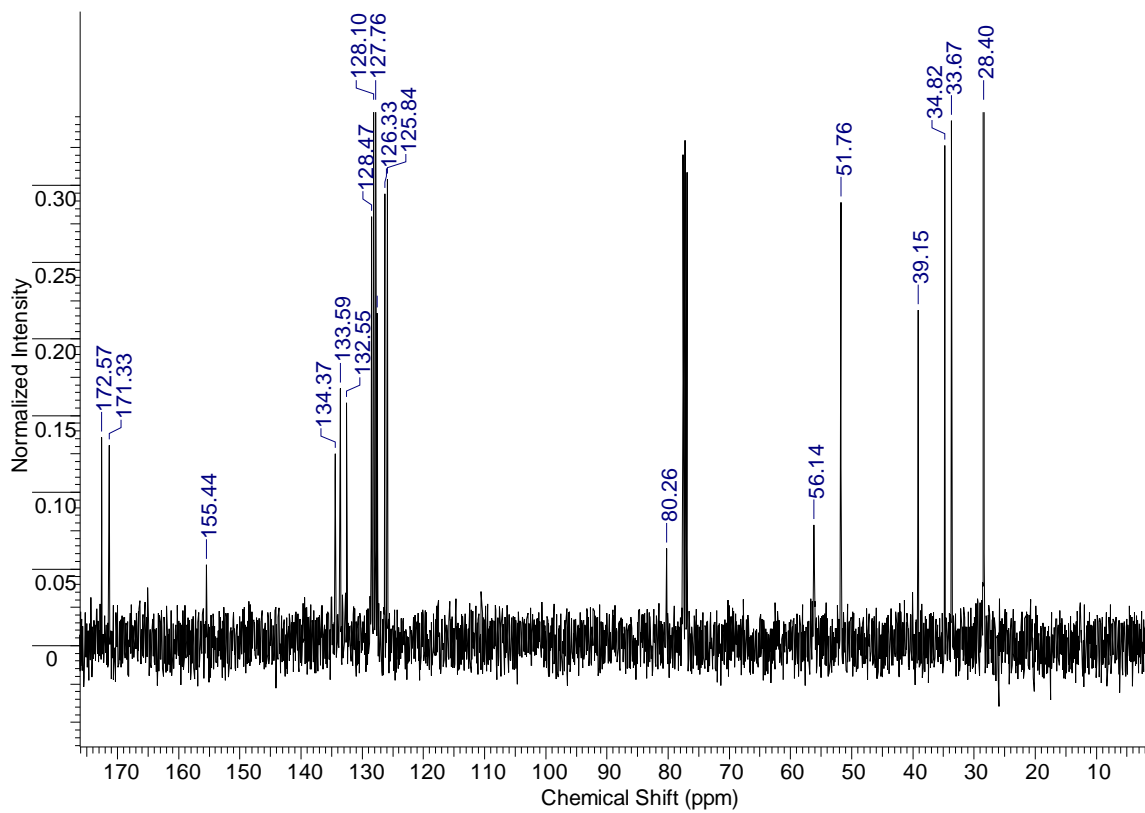
(b)

Figure A.13: - (a) ^{1}HNMR (b) ^{13}CNMR of 2.37e
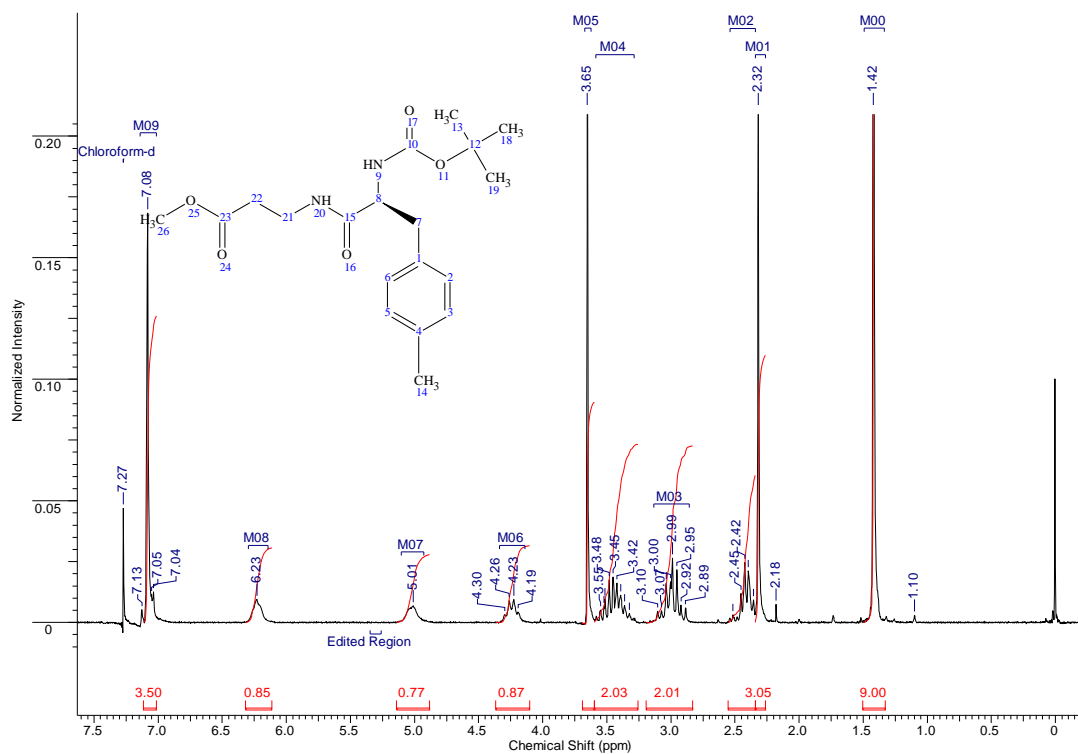
(a)
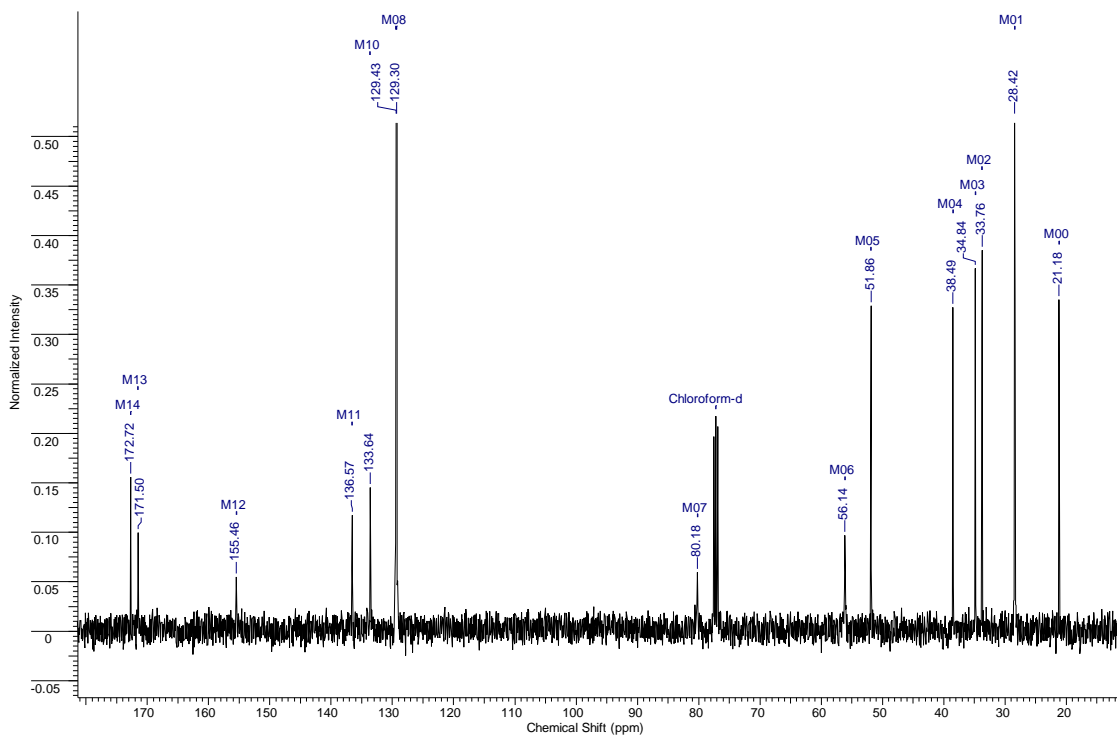
(b)

Figure A.14: - (a) ¹HNMR (b) ¹³CNMR of 2.37f
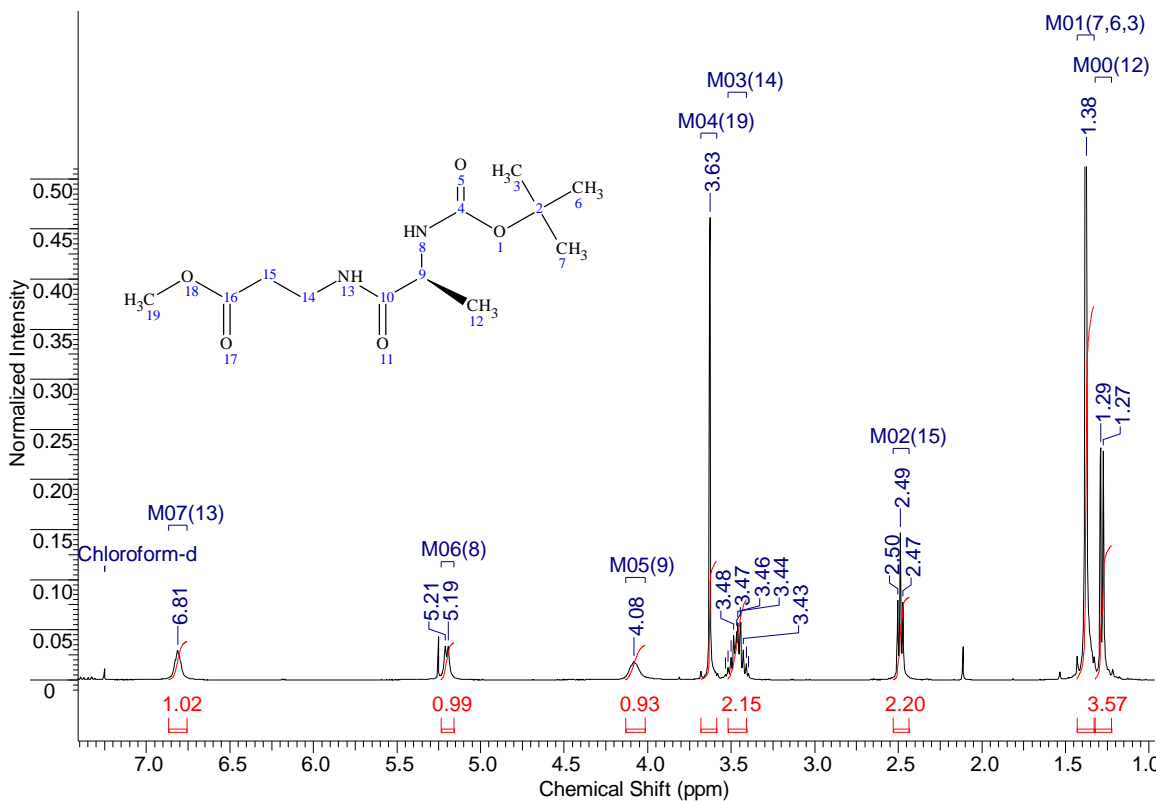
(a)
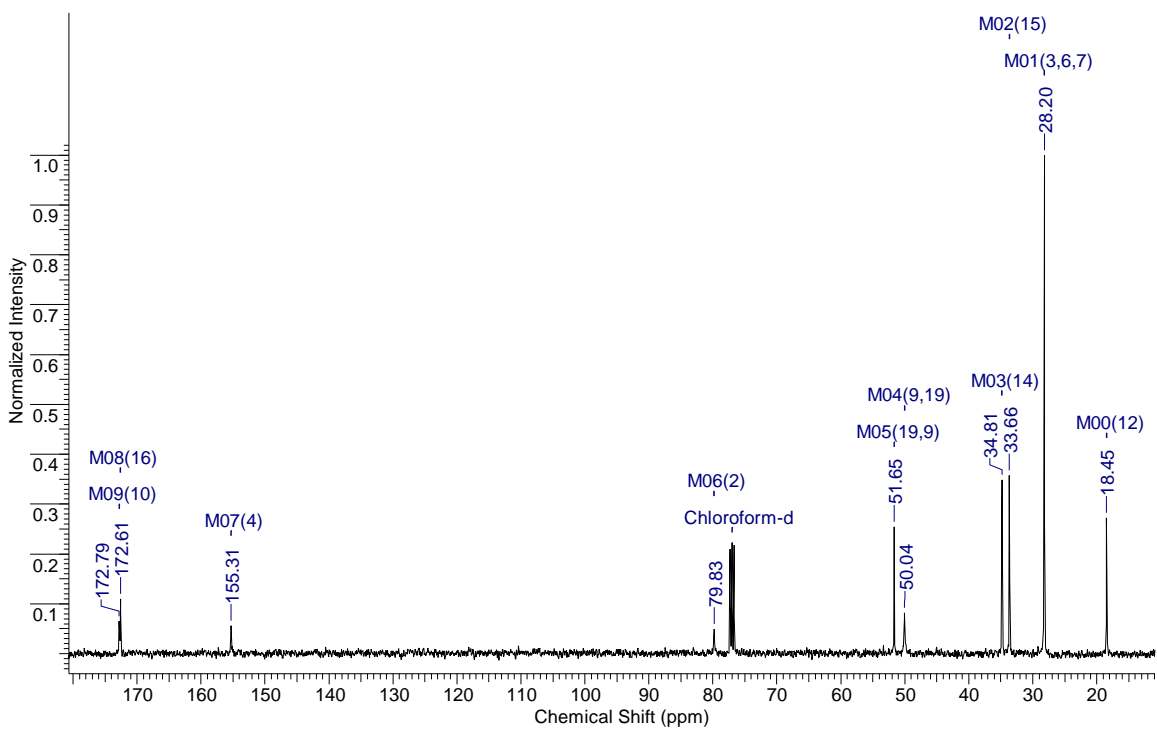
(b)

Figure A.15: - (a) ^{1}HNMR (b) ^{13}CNMR of 2.29a

(a)

(b)

202
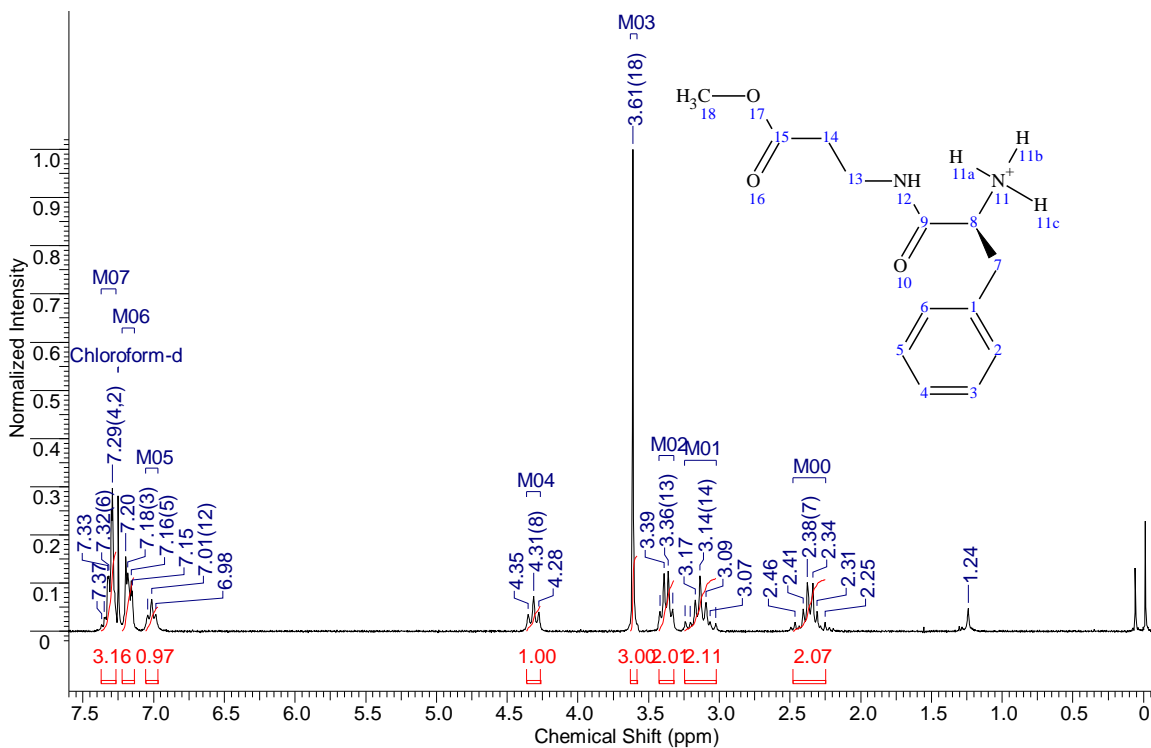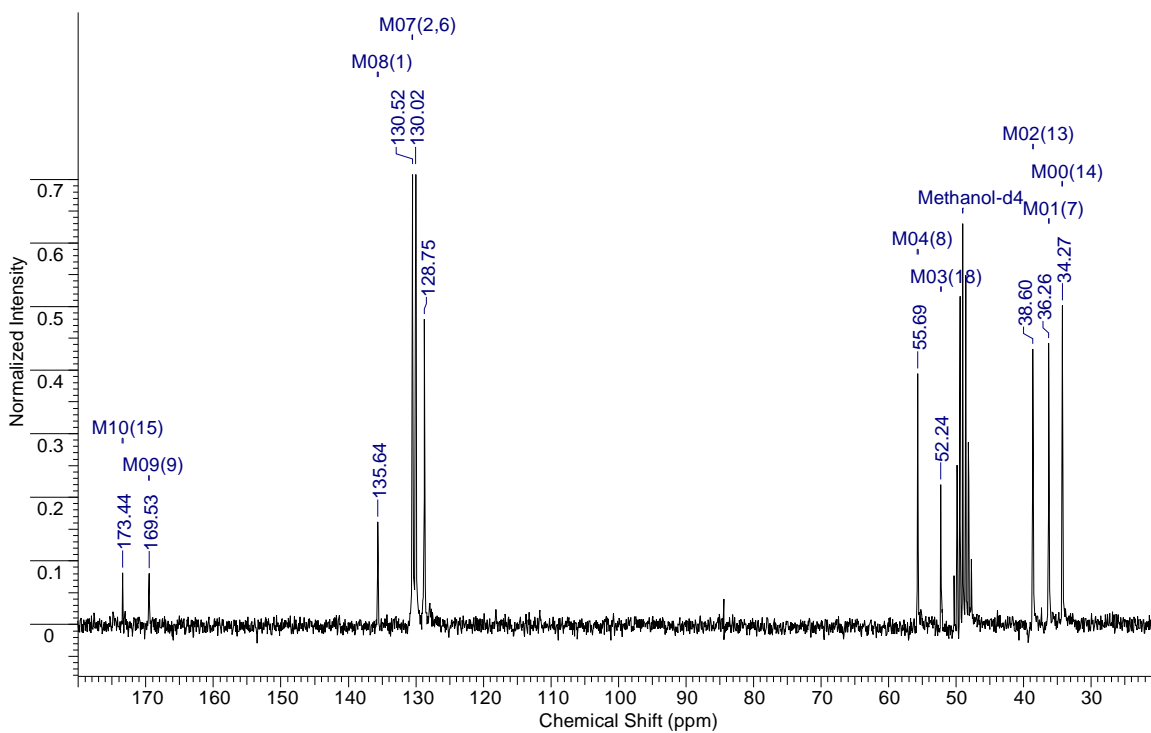
Figure A.16: - (a) ^{1}HNMR (b) ^{13}CNMR of 2.29b
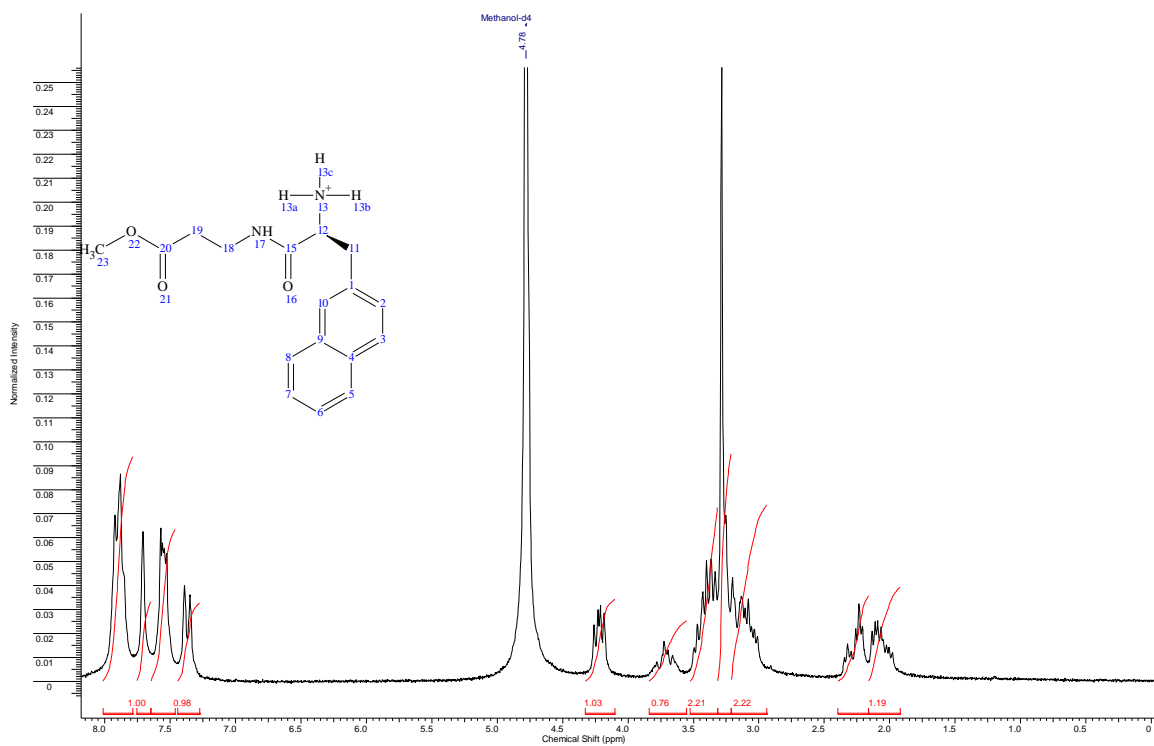
(a)
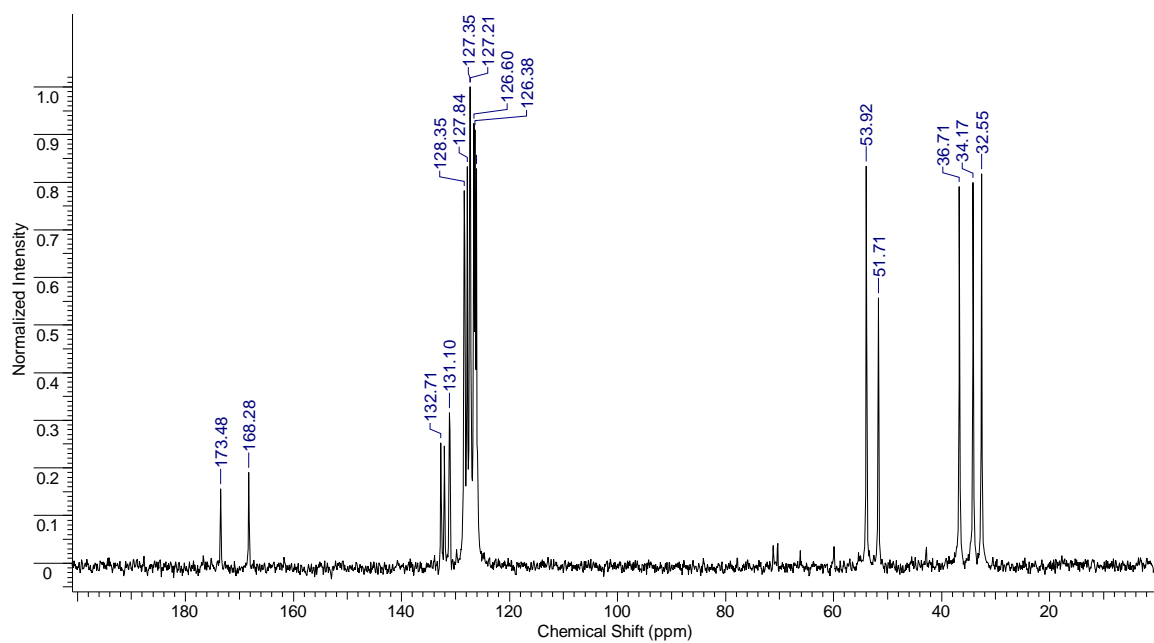
(b)

Figure A.17: - (a) ¹HNMR (b) ¹³CNMR of 2.29c
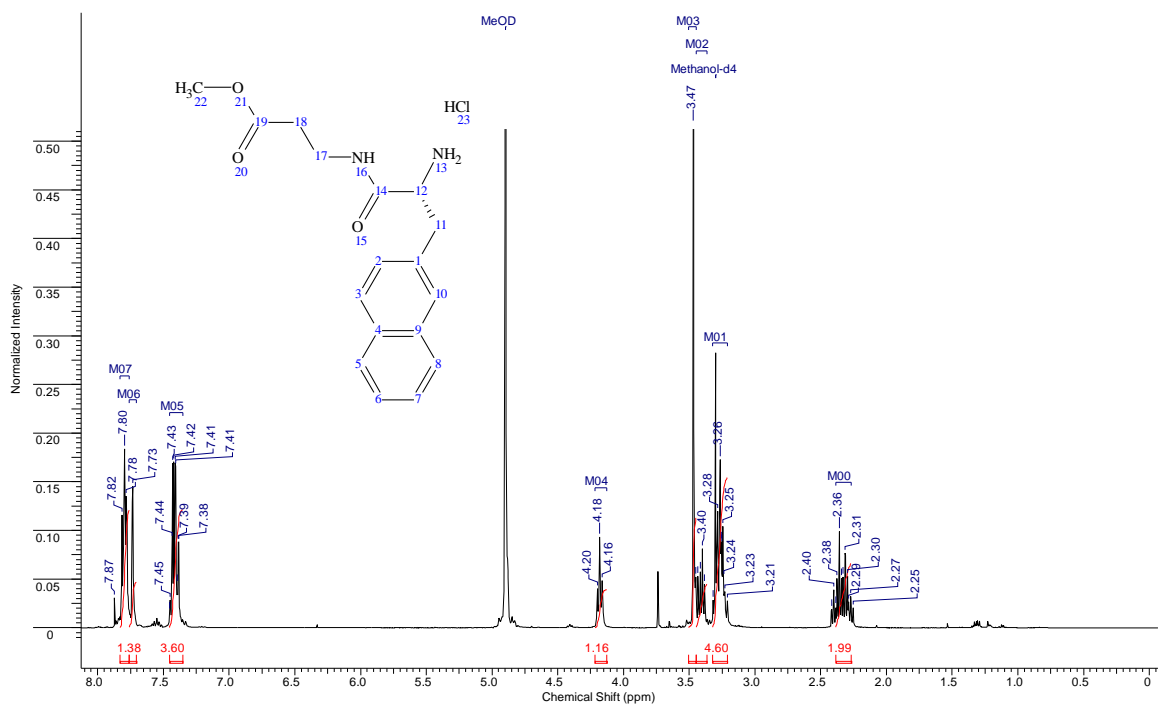

(a)
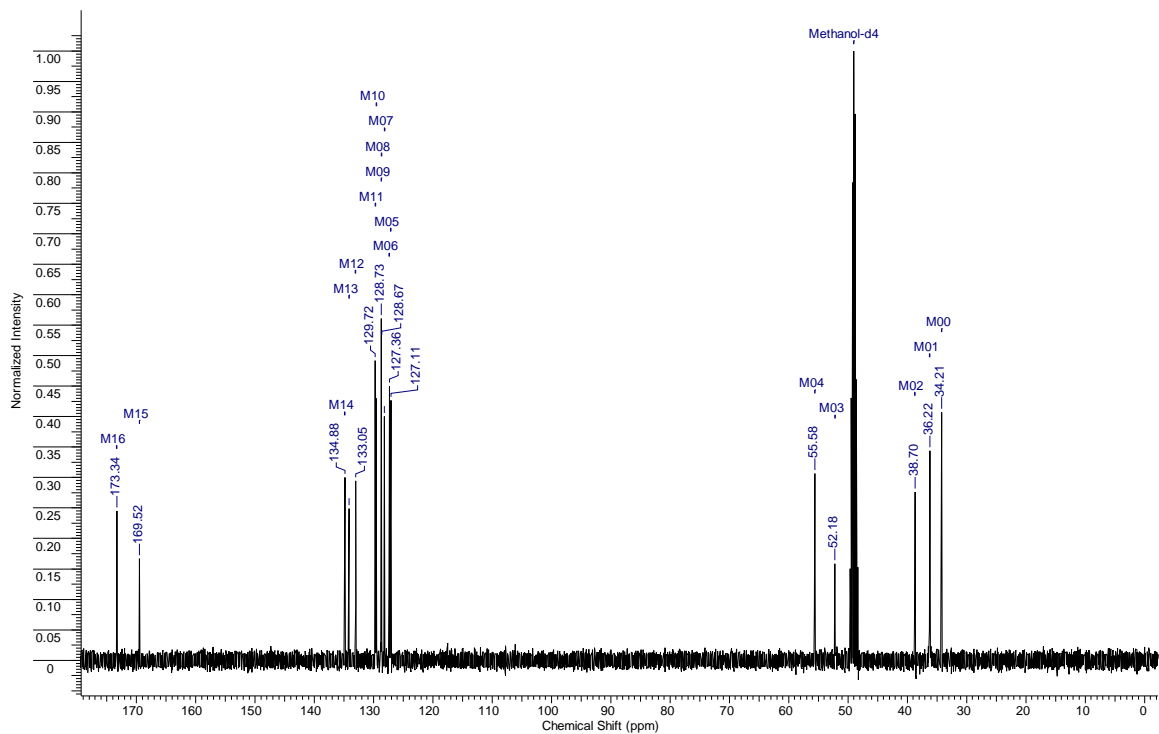
(b)

Figure A.18: - (a) ^{1}HNMR (b) ^{13}CNMR of 2.29d
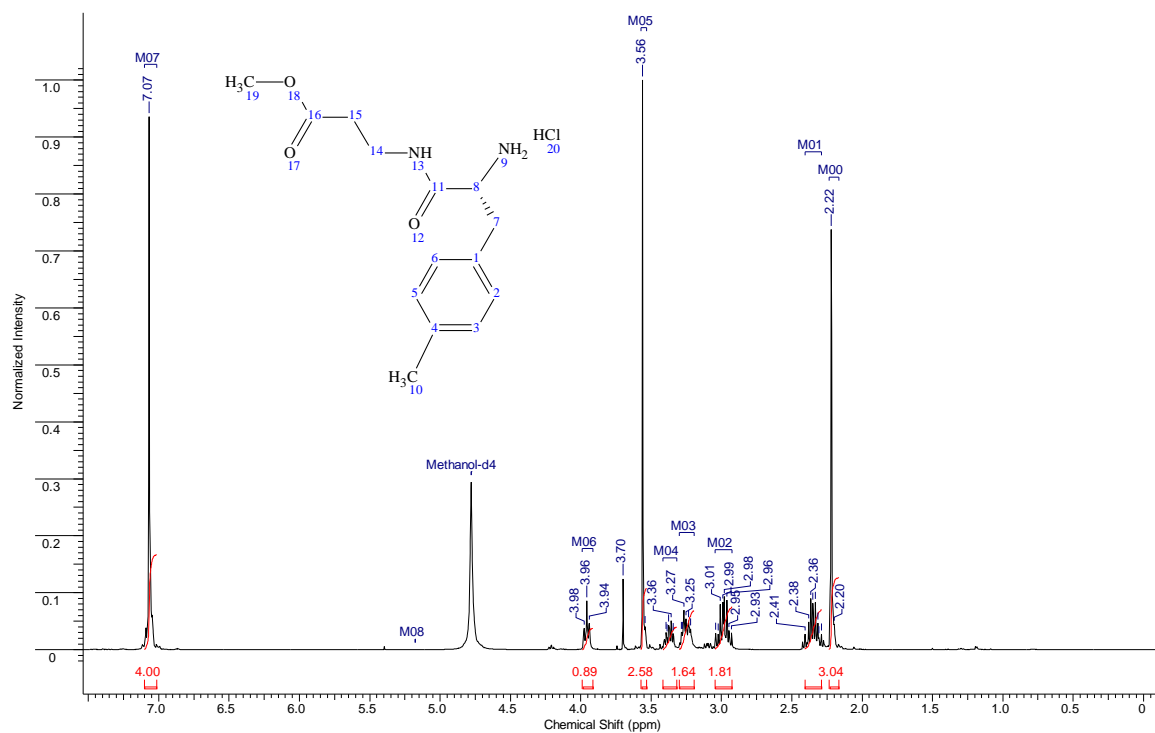
(a)
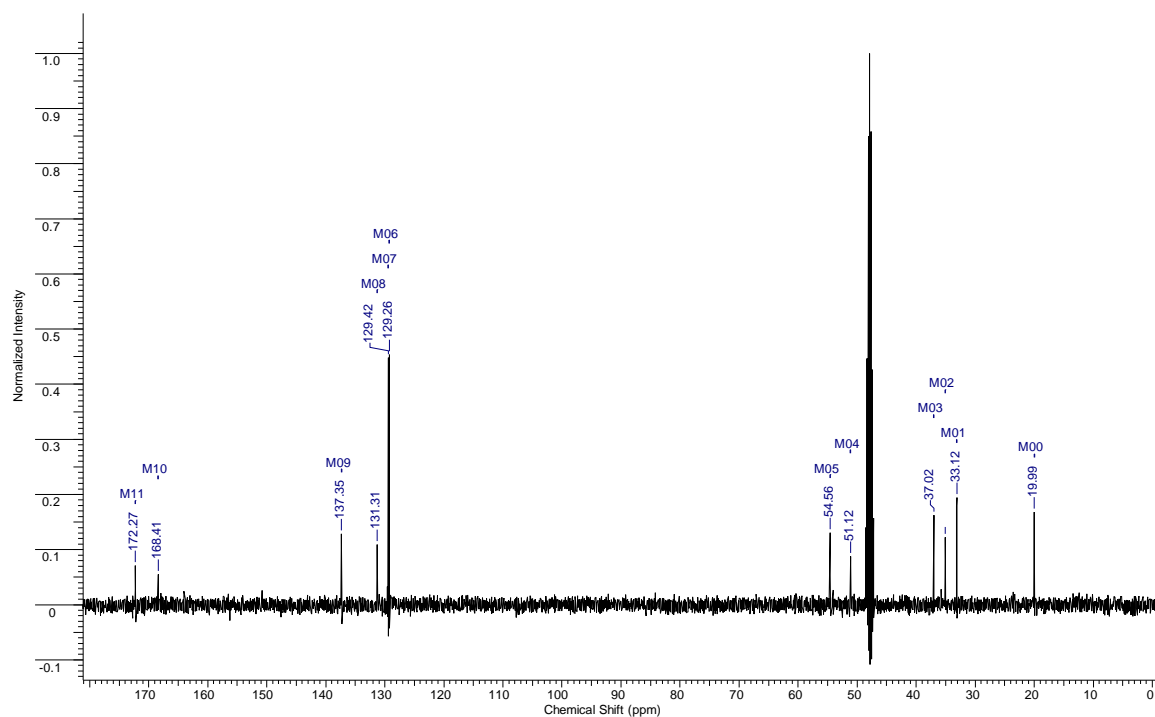
(b)

Figure A.19: - (a) ^{1}HNMR (b) ^{13}CNMR of 2.29e
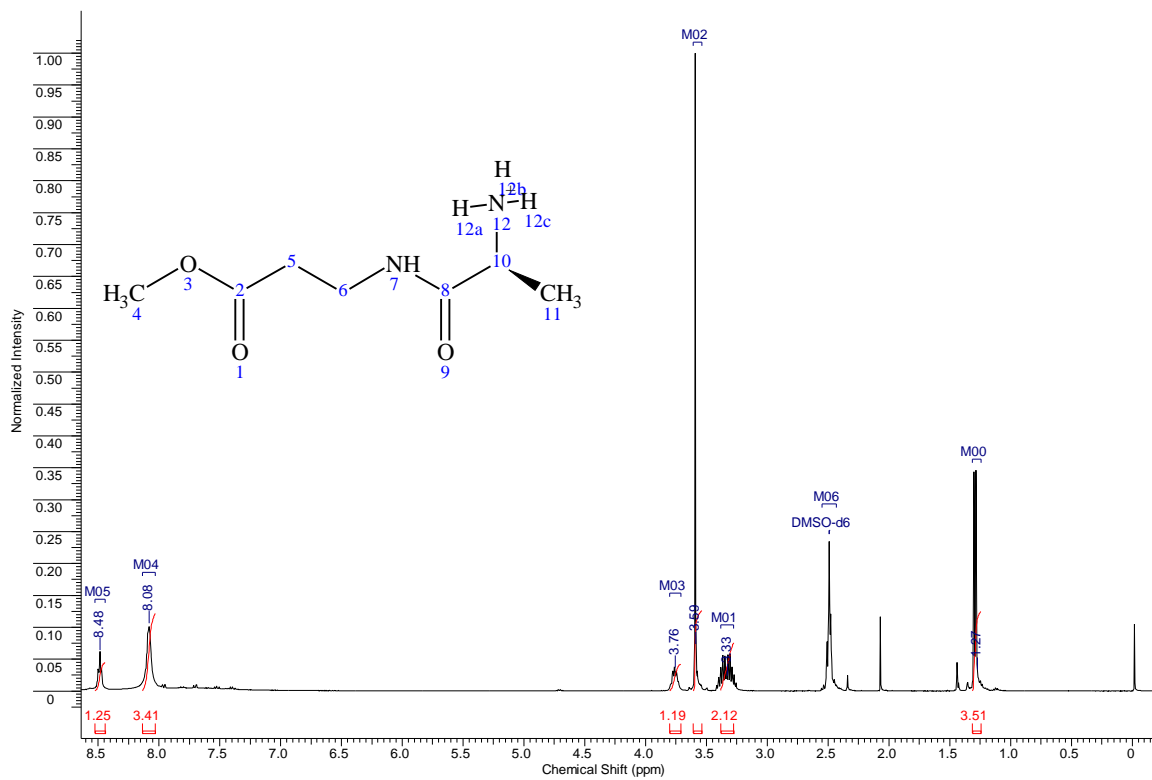
(a)
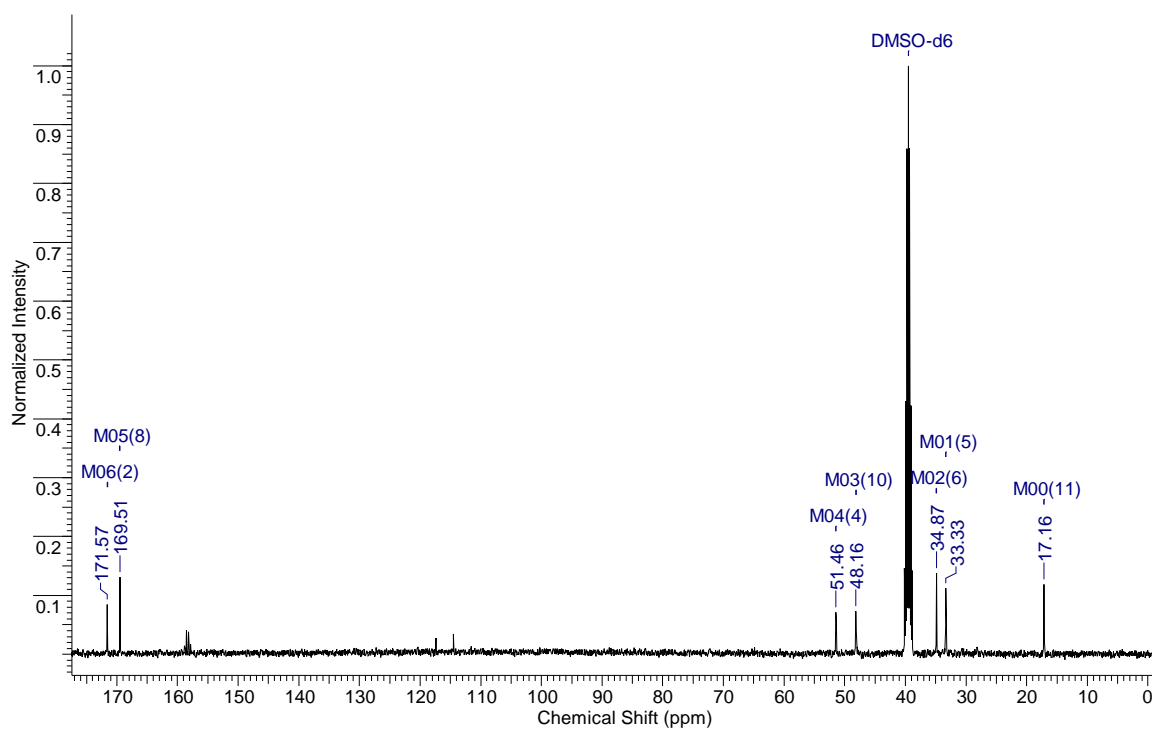
(b)

Figure A.20: - (a) ^{1}HNMR (b) ^{13}CNMR of 2.38a
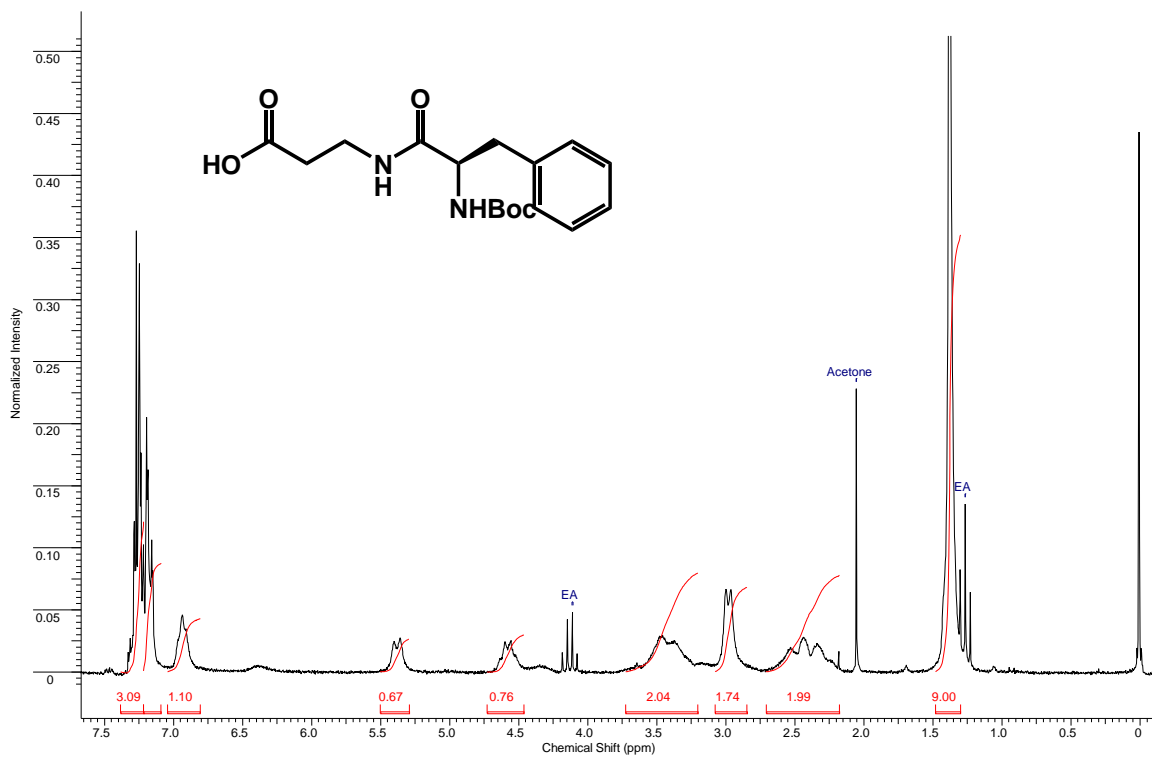
(a)
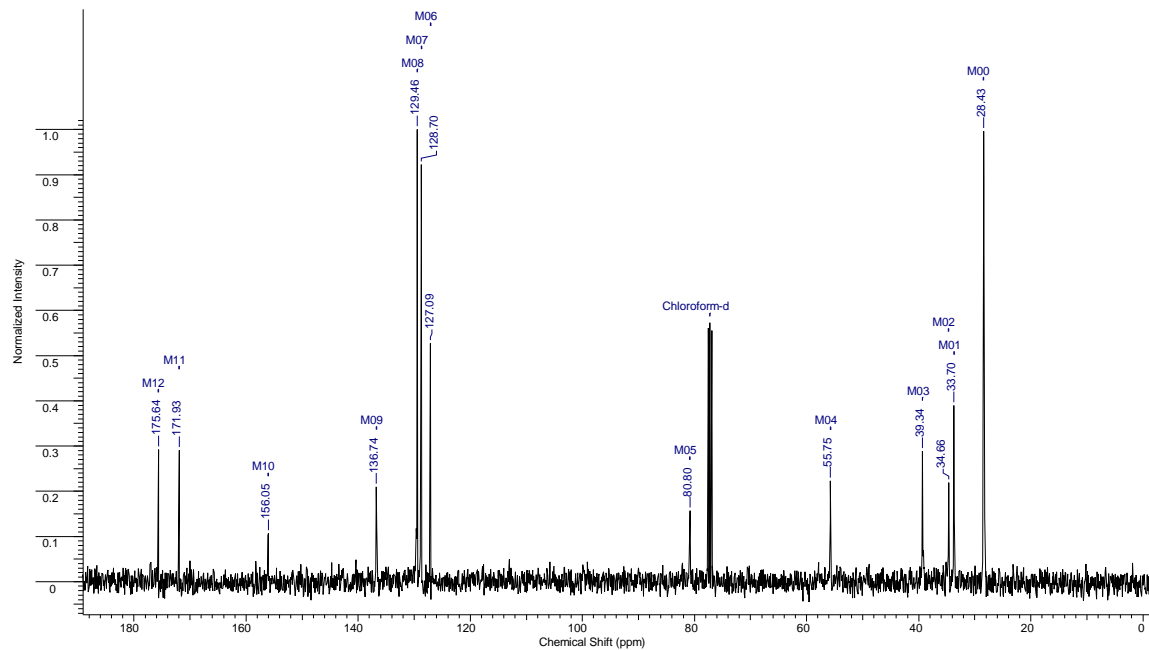
(b)

Figure A.21: - (a) ^{1}HNMR (b) ^{13}CNMR of 2.38b
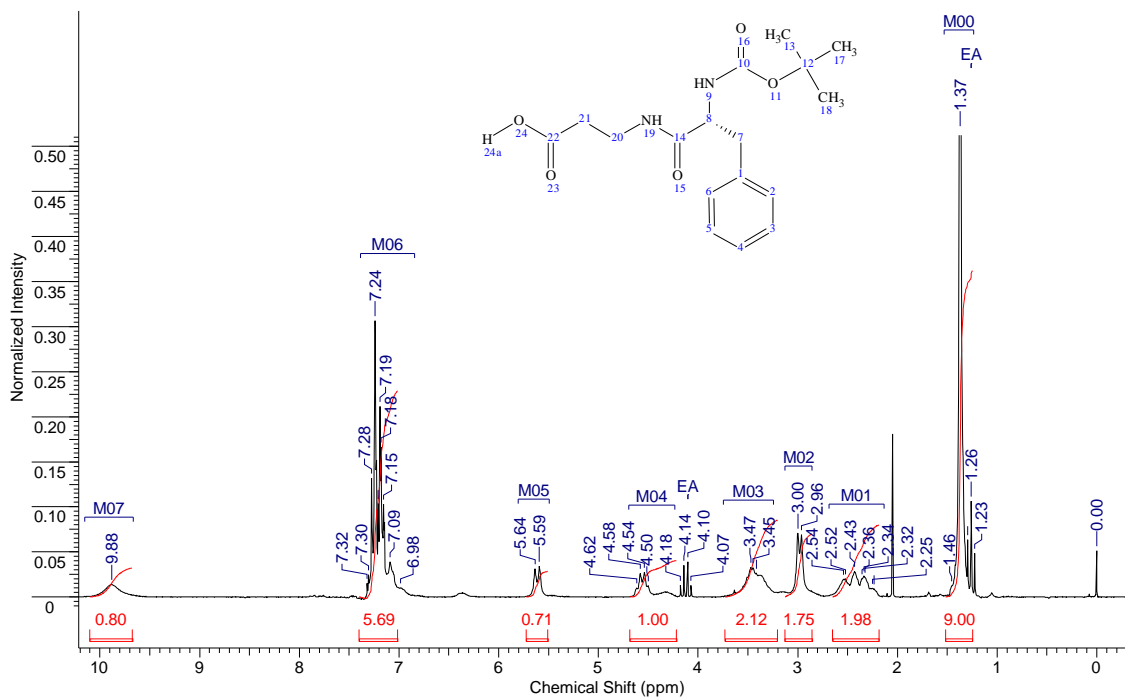
(a)
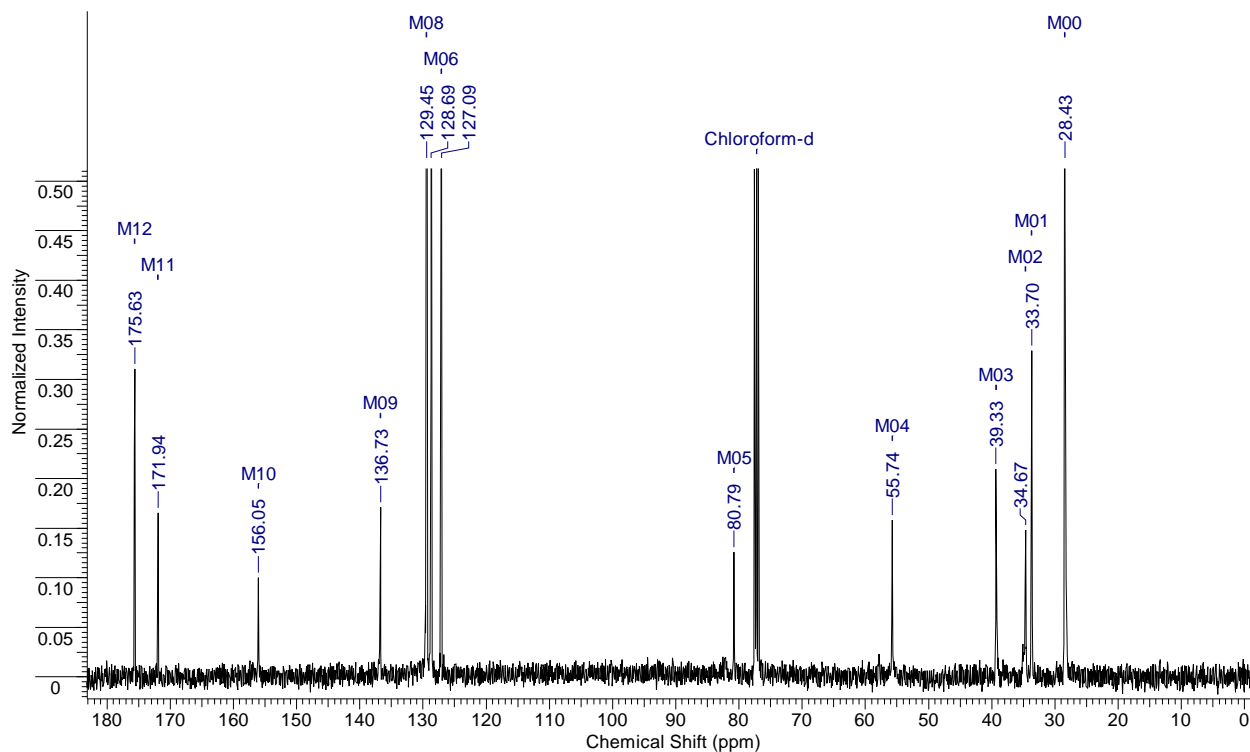
(b)

Figure A.22: - (a) ^{1}HNMR (b) ^{13}CNMR of 2.38c
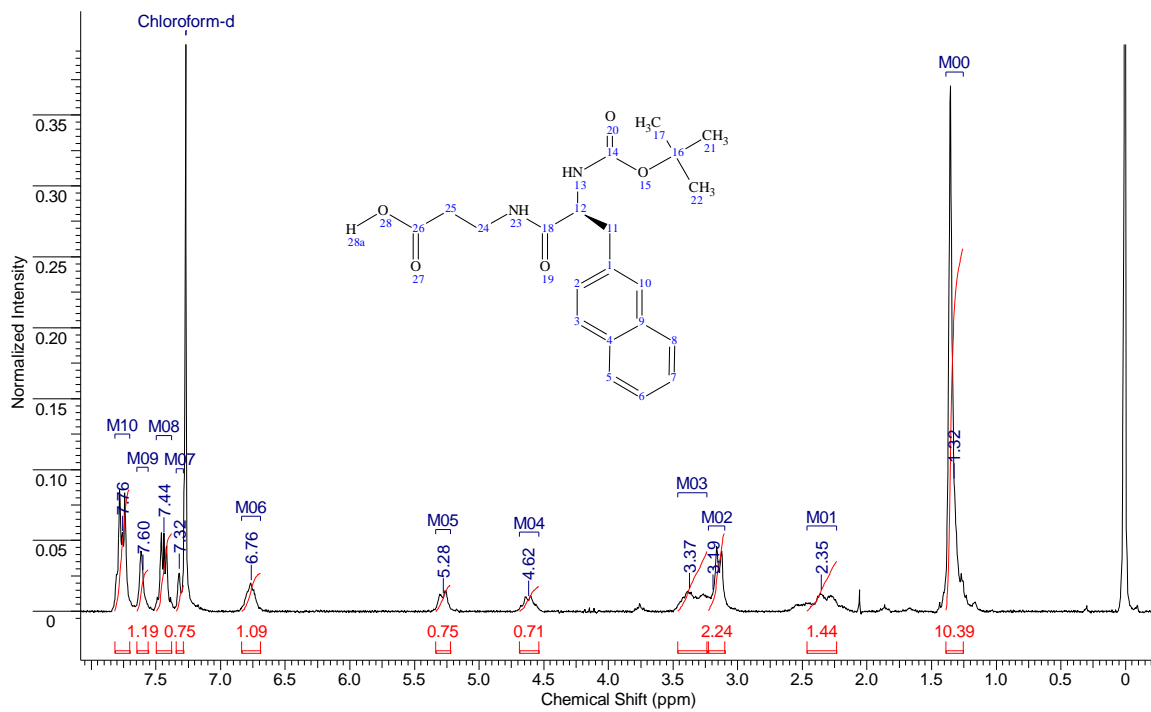
(a)
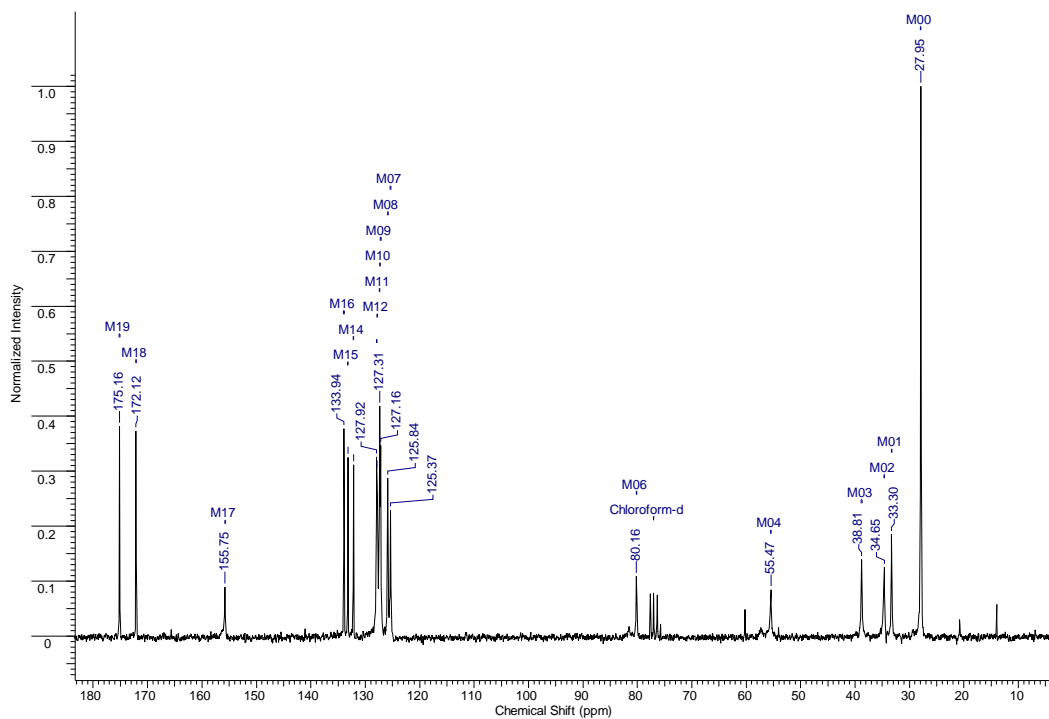
(b)

Figure A.23: - (a) ^{1}HNMR (b) ^{13}CNMR of 2.38d
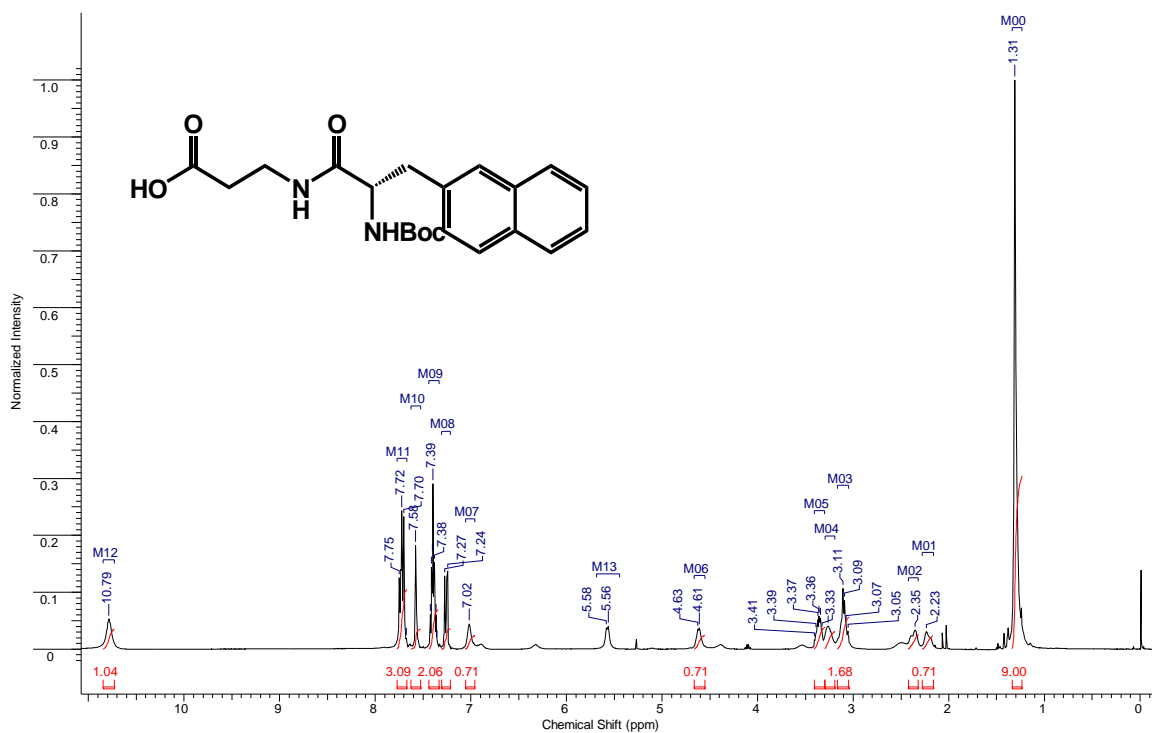
(a)
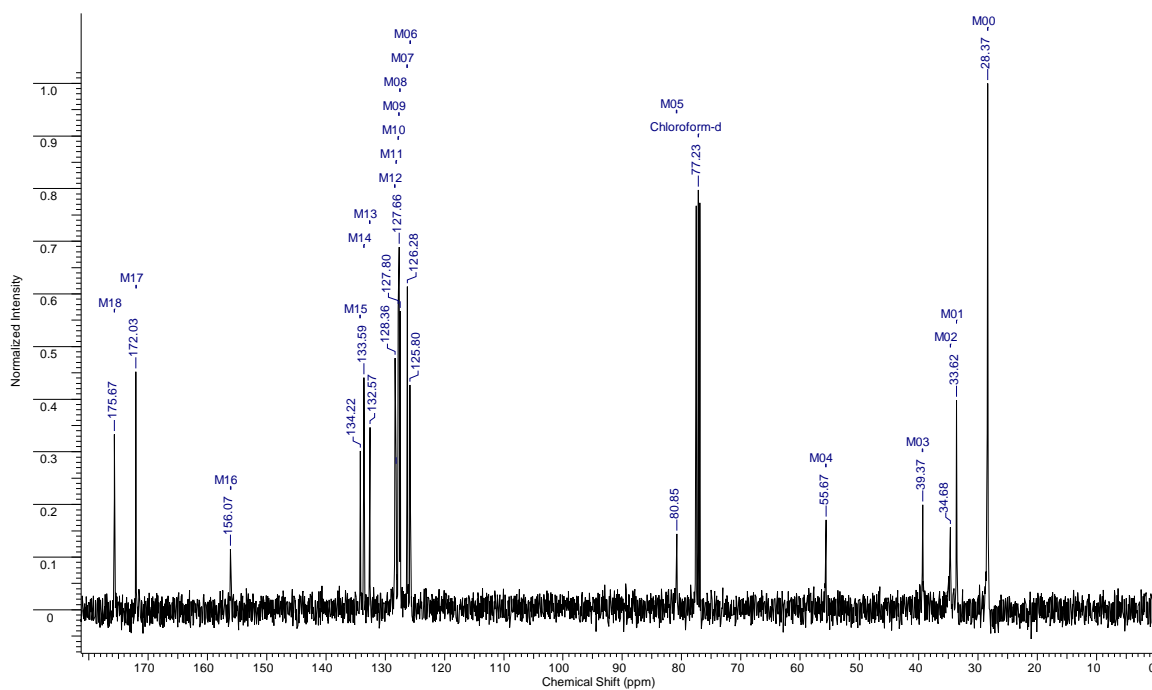
(b)

Figure A.24: - (a) ^{1}HNMR (b) ^{13}CNMR of 2.38e
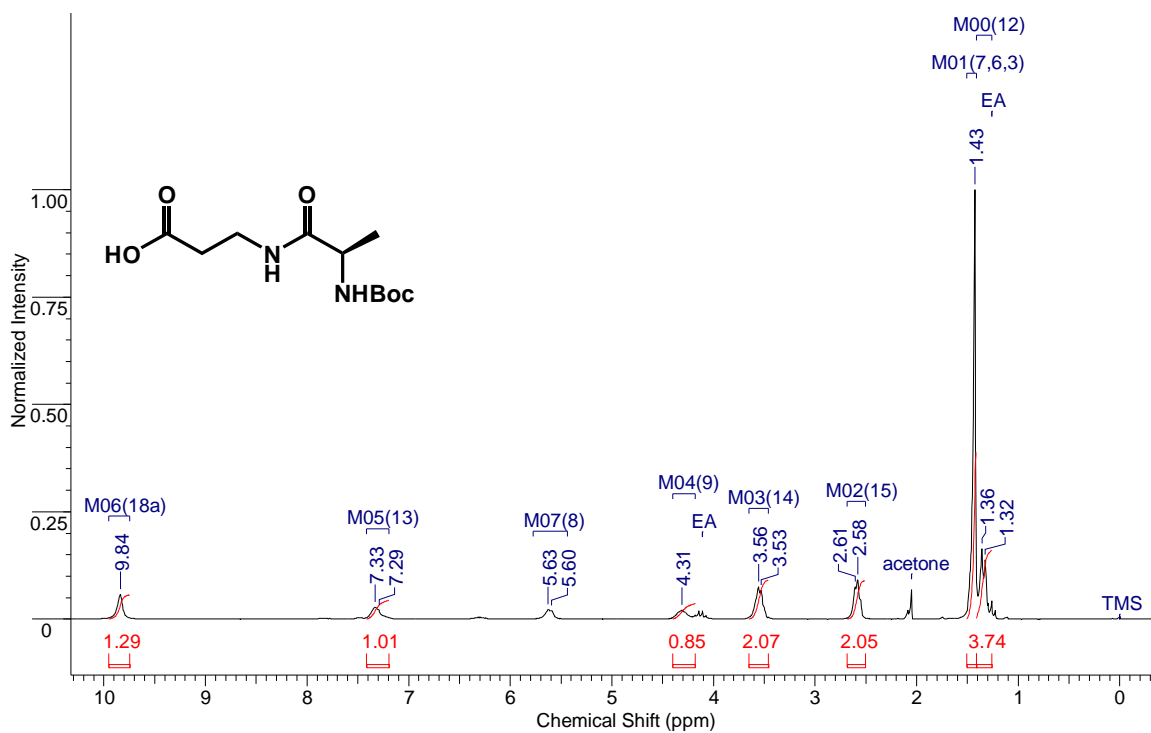
(a)
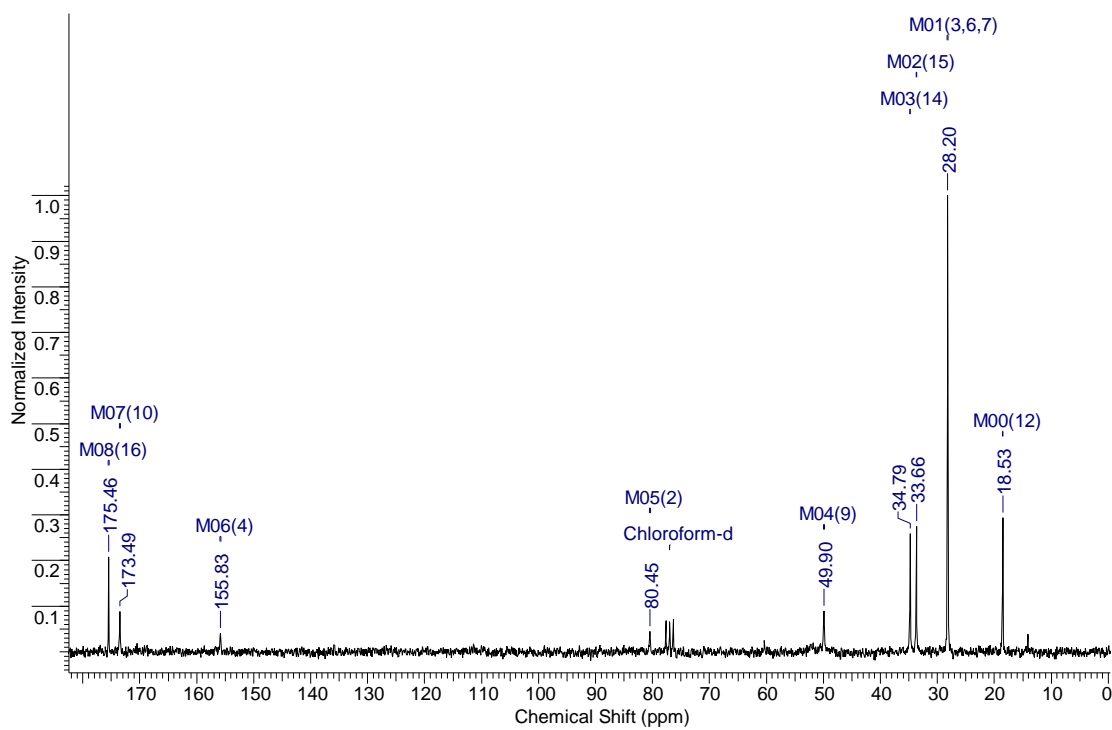
(b)

Figure A.25: - (a) ¹HNMR (b) ¹³CNMR of 2.39a
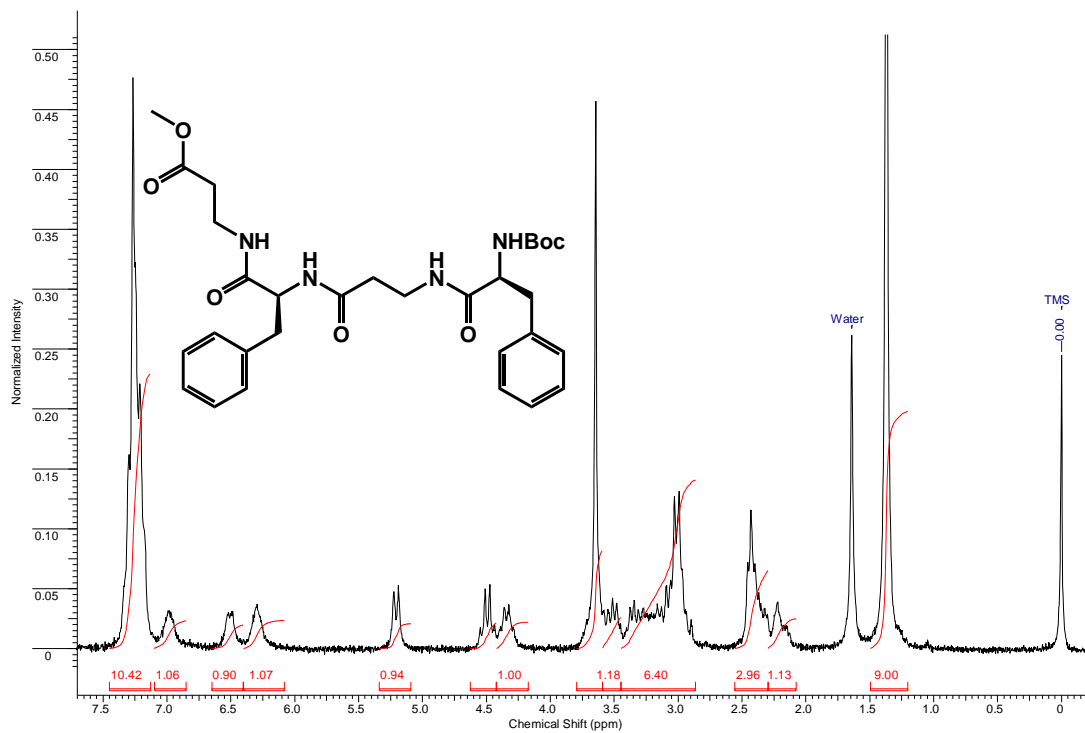
(a)
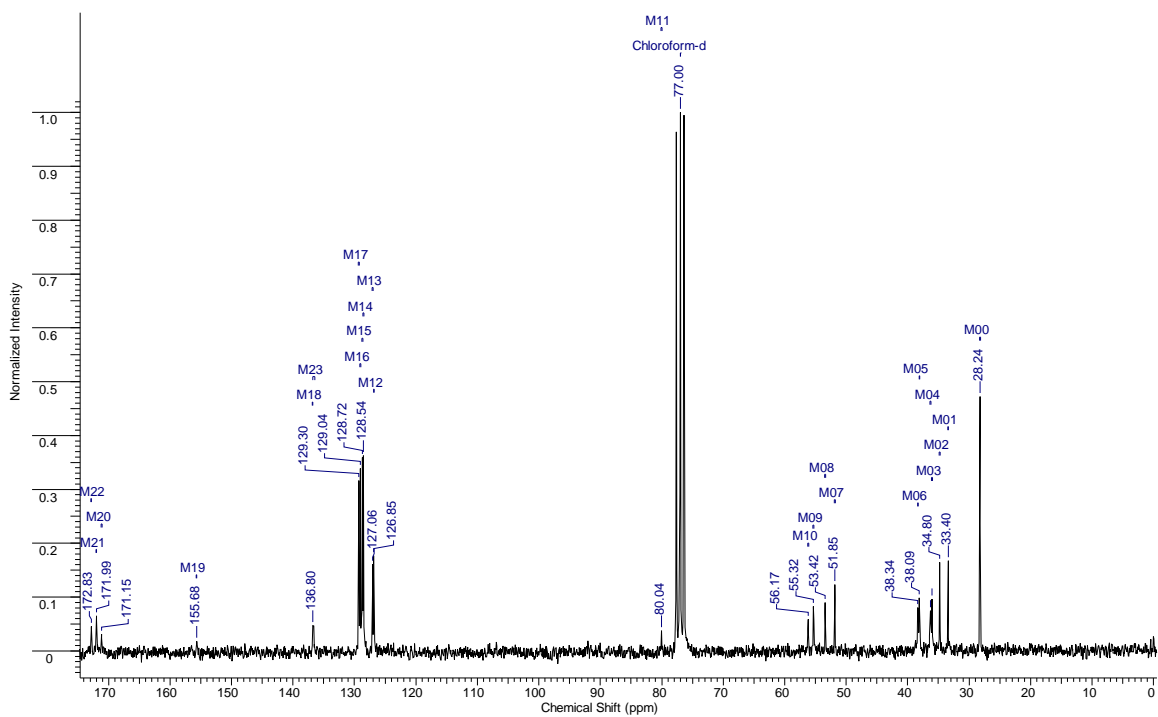
(b)

Figure A.26: - (a) ^{1}HNMR (b) ^{13}CNMR of 2.39b
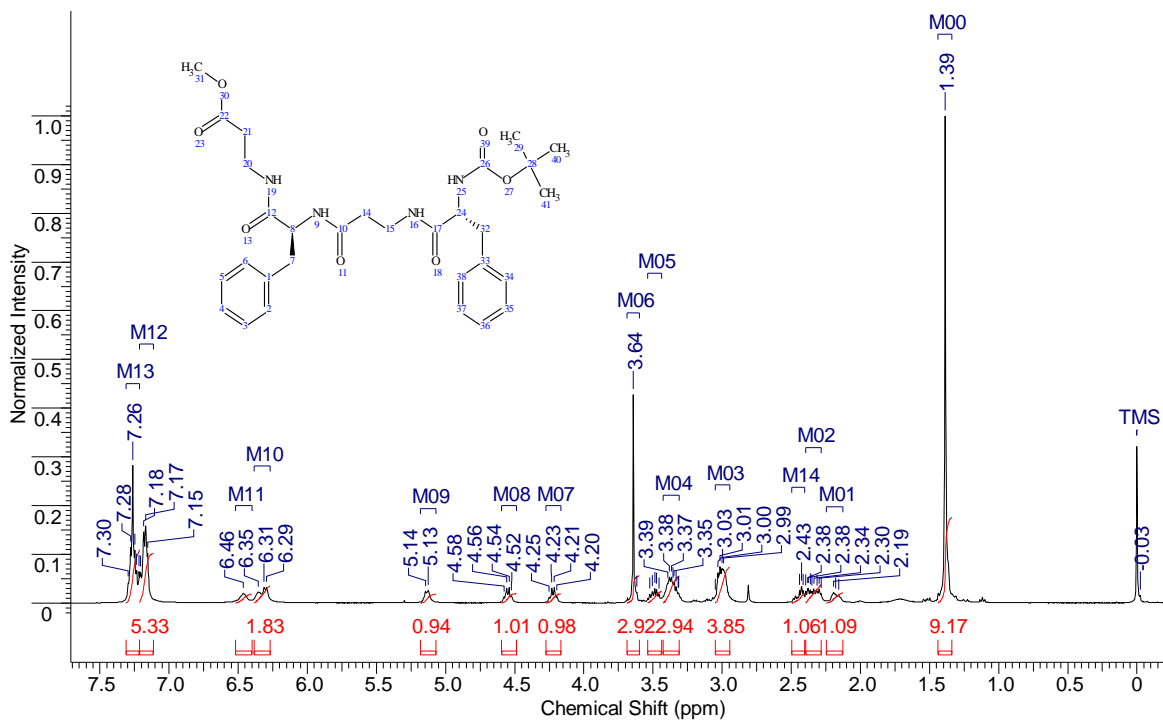
(a)
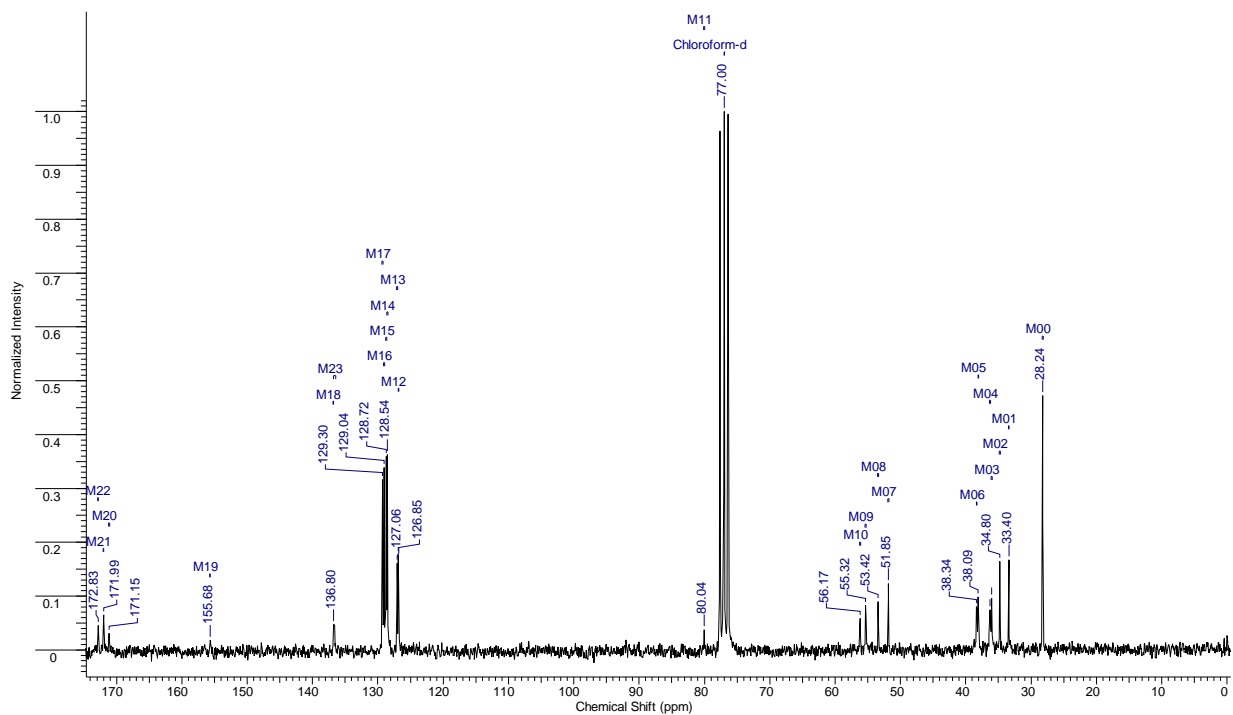
(b)

Figure A.27: - (a) ^{1}HNMR (b) ^{13}CNMR of 2.39c
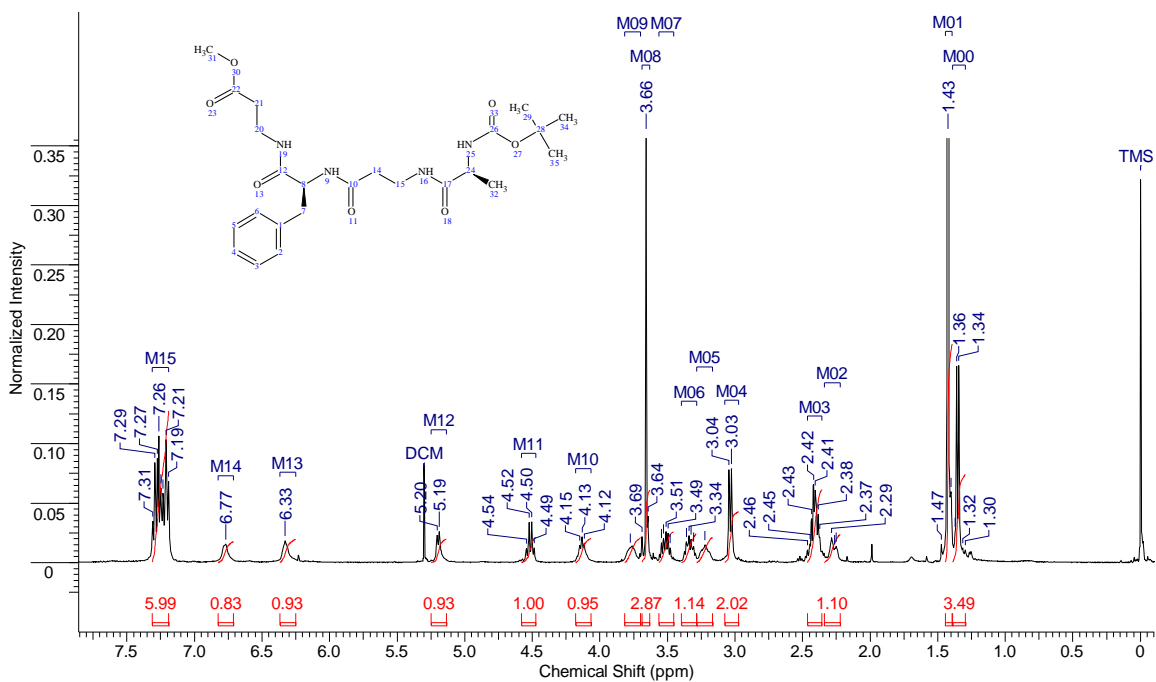
(a)
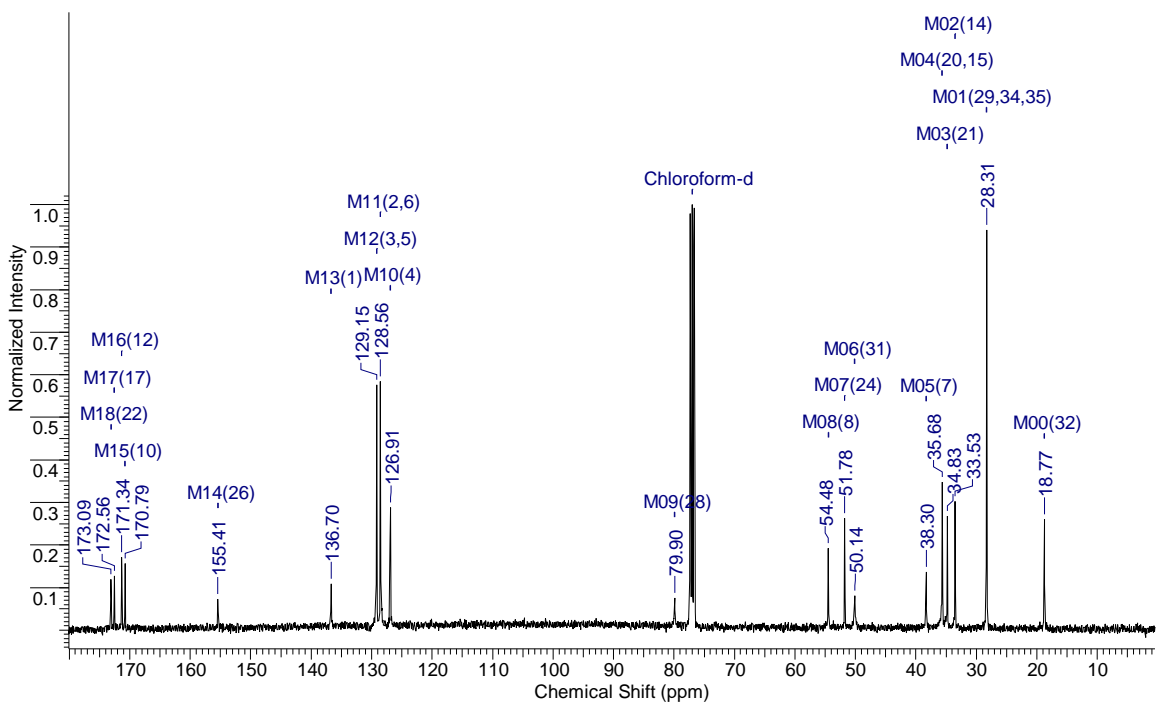
(b)

Figure A.28: - (a) ¹HNMR (b) ¹³CNMR of 2.39d
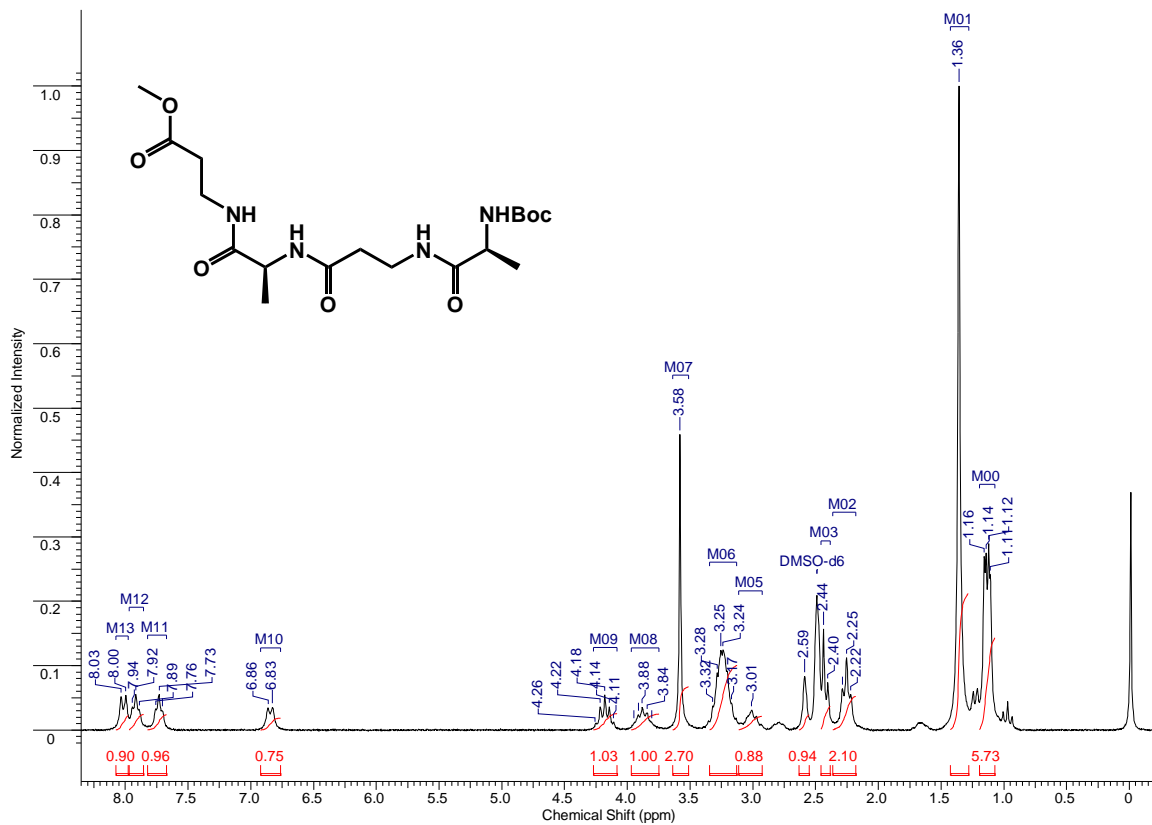
(a)
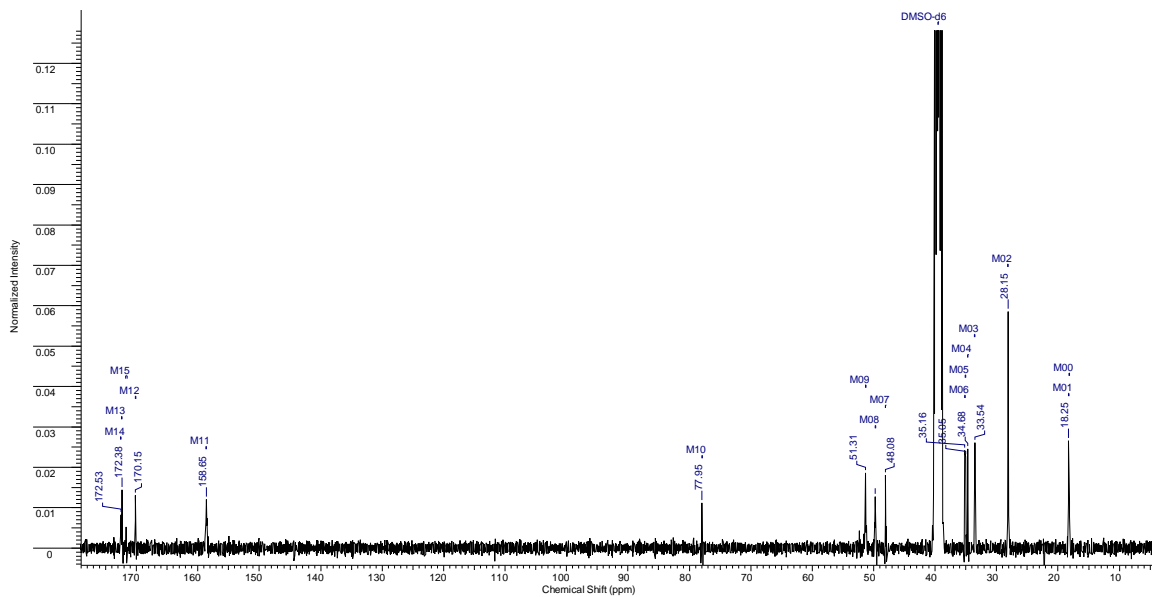
(b)

Figure A.29: - (a) ^{1}HNMR (b) ^{13}CNMR of 2.39e
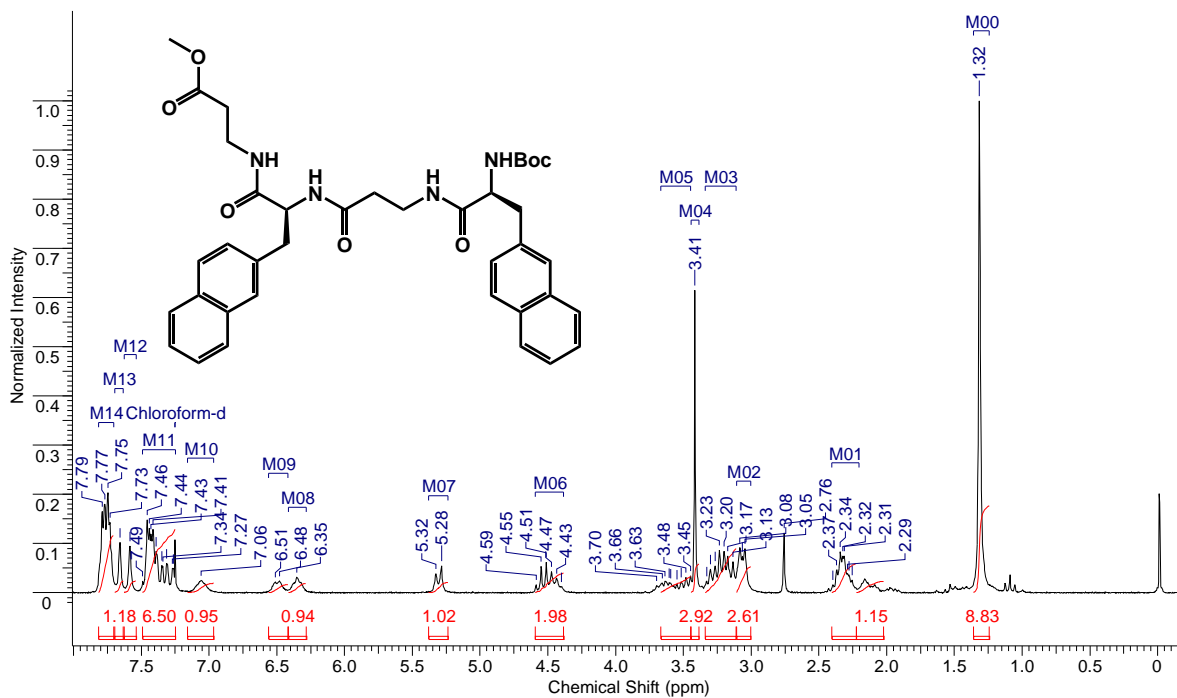
(a)
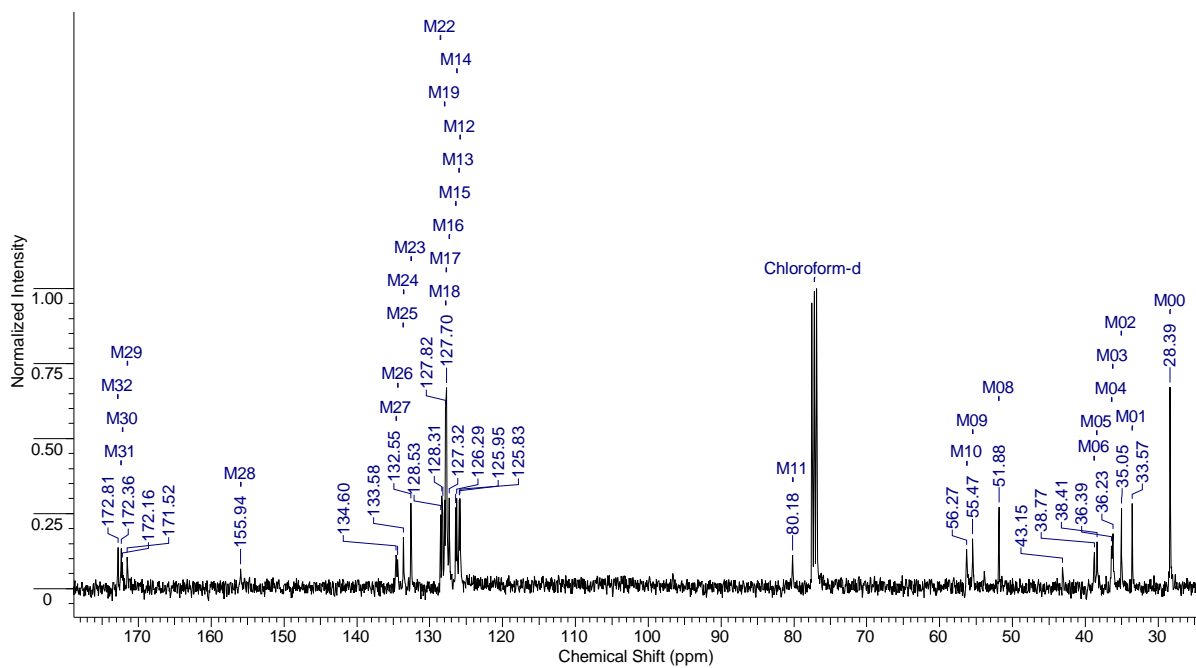
(b)

Figure A.30: - (a) ¹HNMR (b) ¹³CNMR of 2.39f
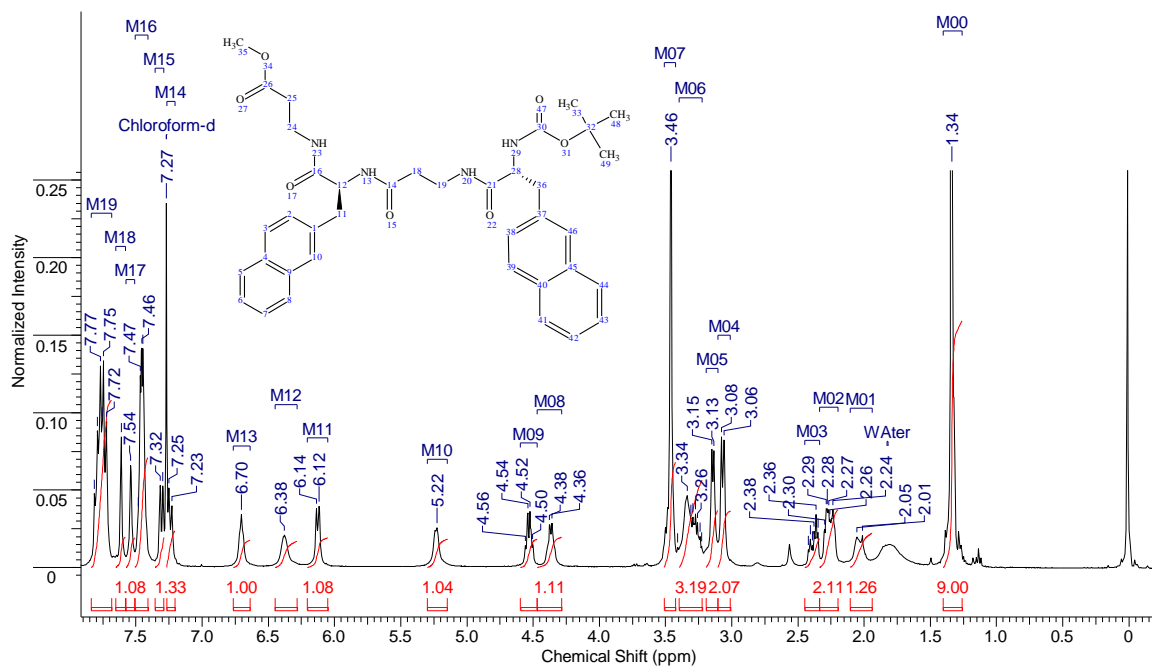
(a)
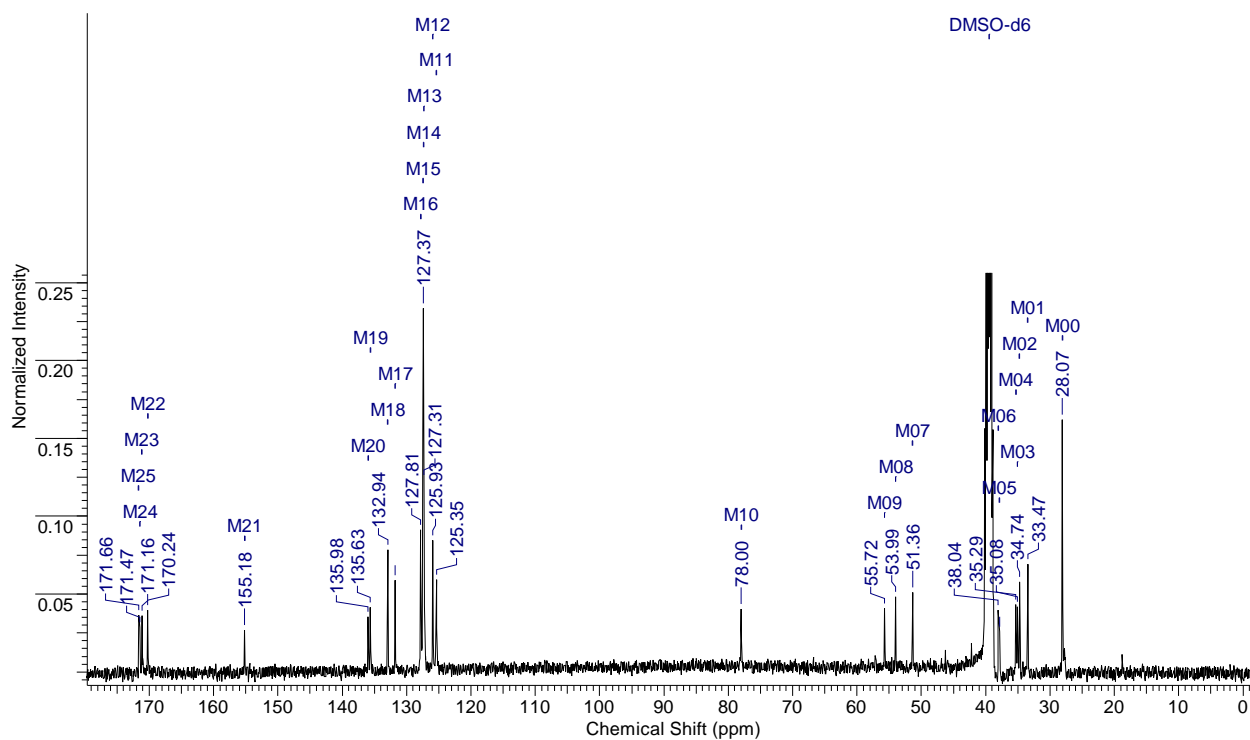
(b)

Figure A.31: - (a) ^{1}HNMR (b) ^{13}CNMR of 2.39g
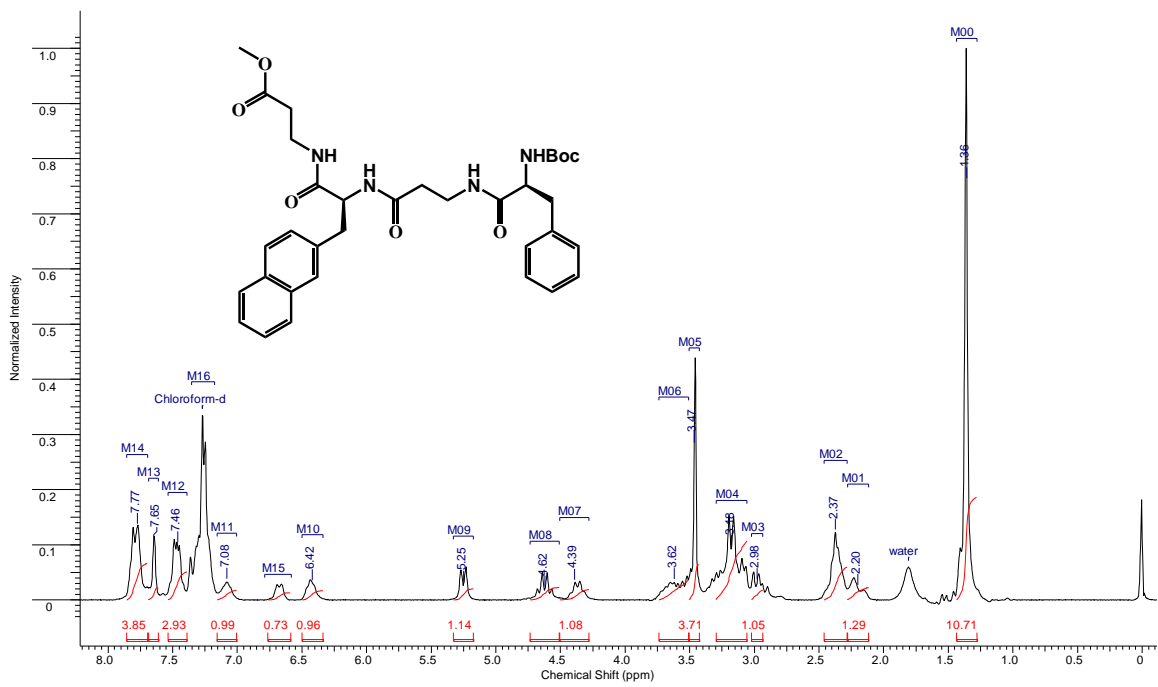
(a)
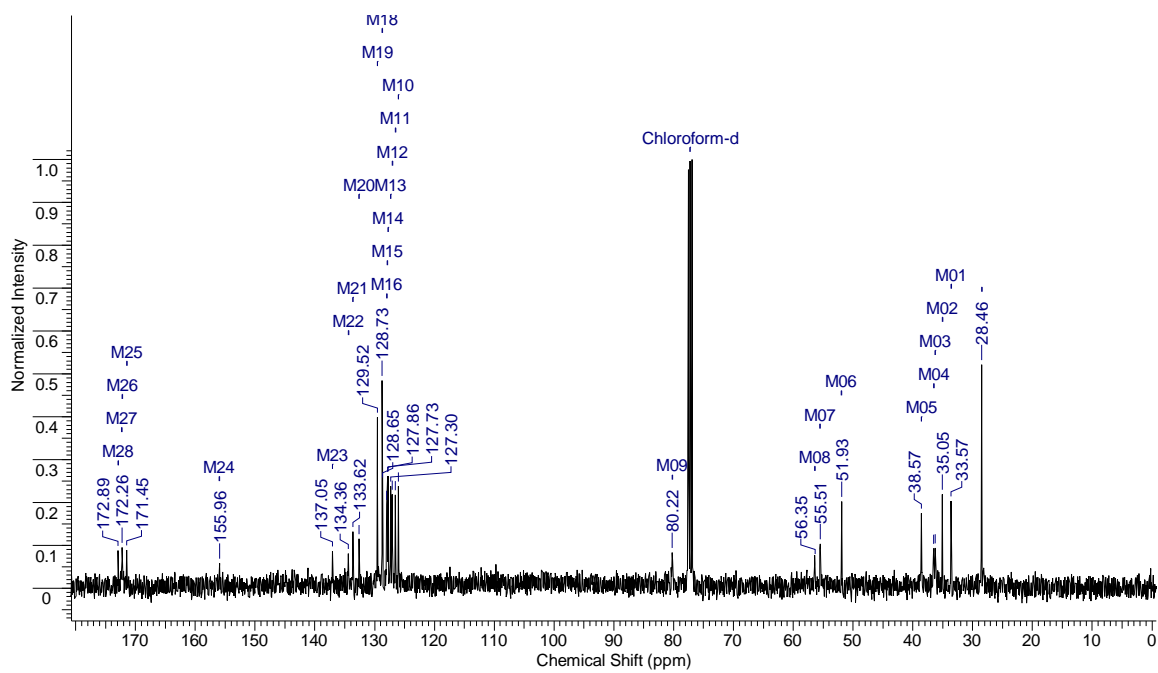
(b)

Figure A.32: - (a) ¹HNMR (b) ¹³CNMR of 2.39h
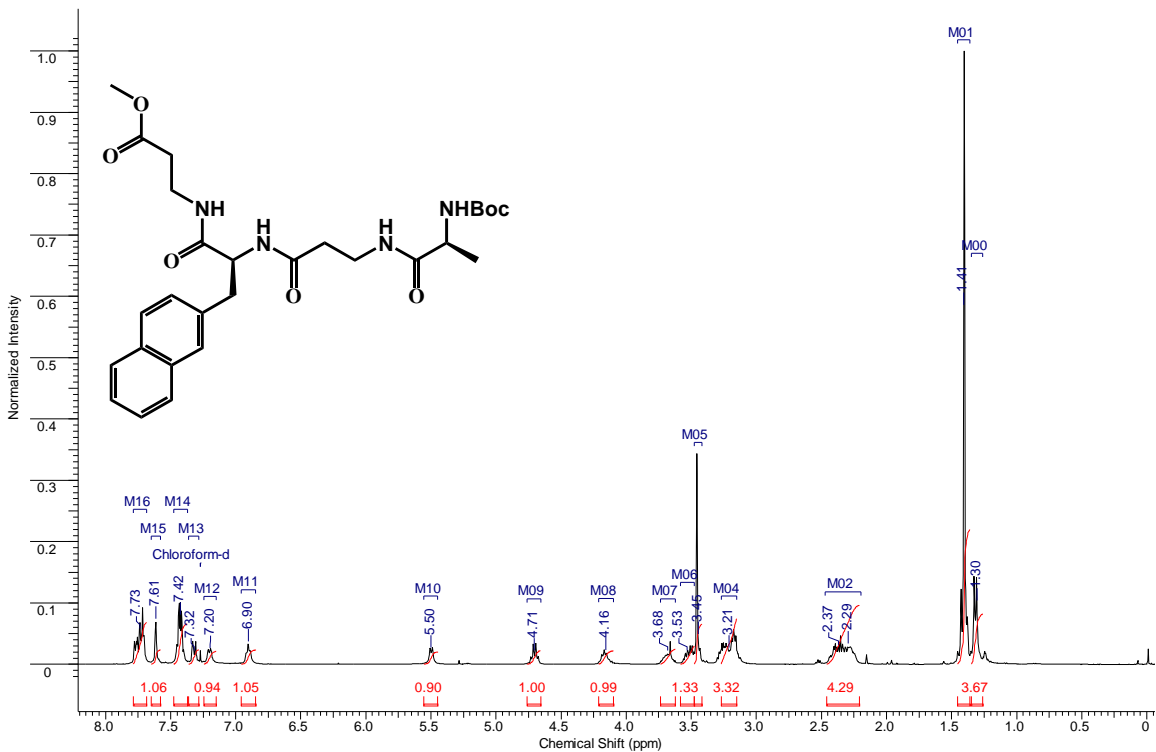
(a)
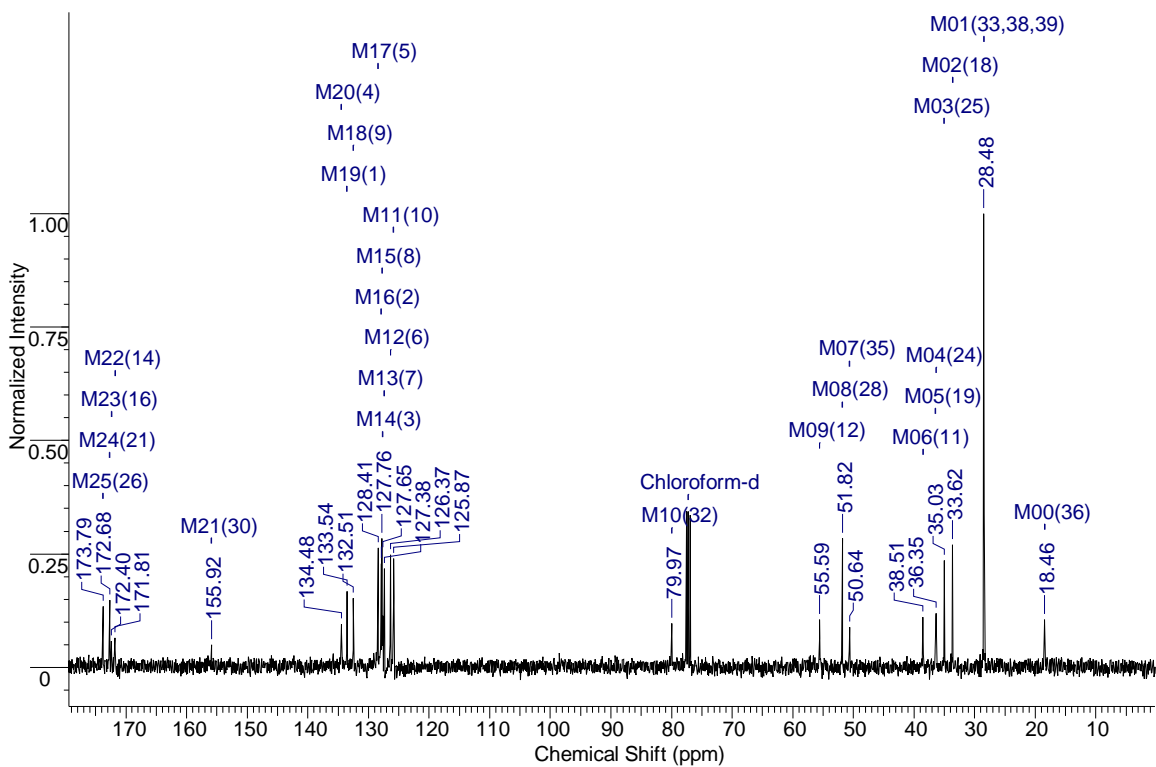
(b)

Figure A.33: - (a) ^{1}HNMR (b) ^{13}CNMR of 2.39i
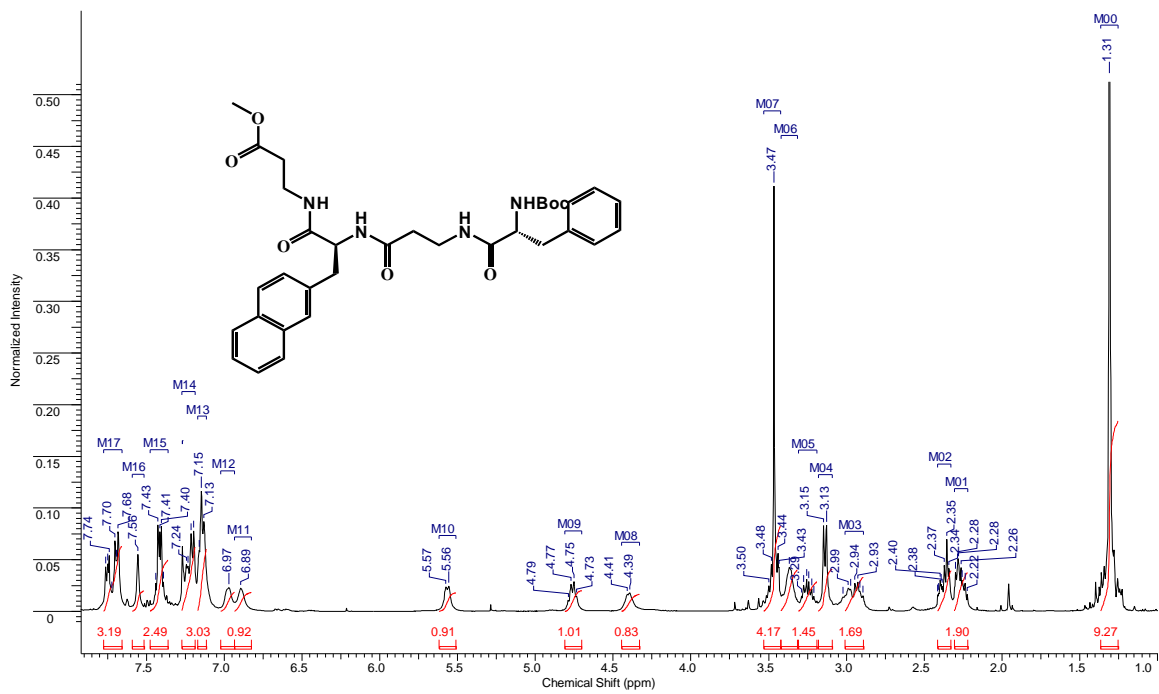
(a)
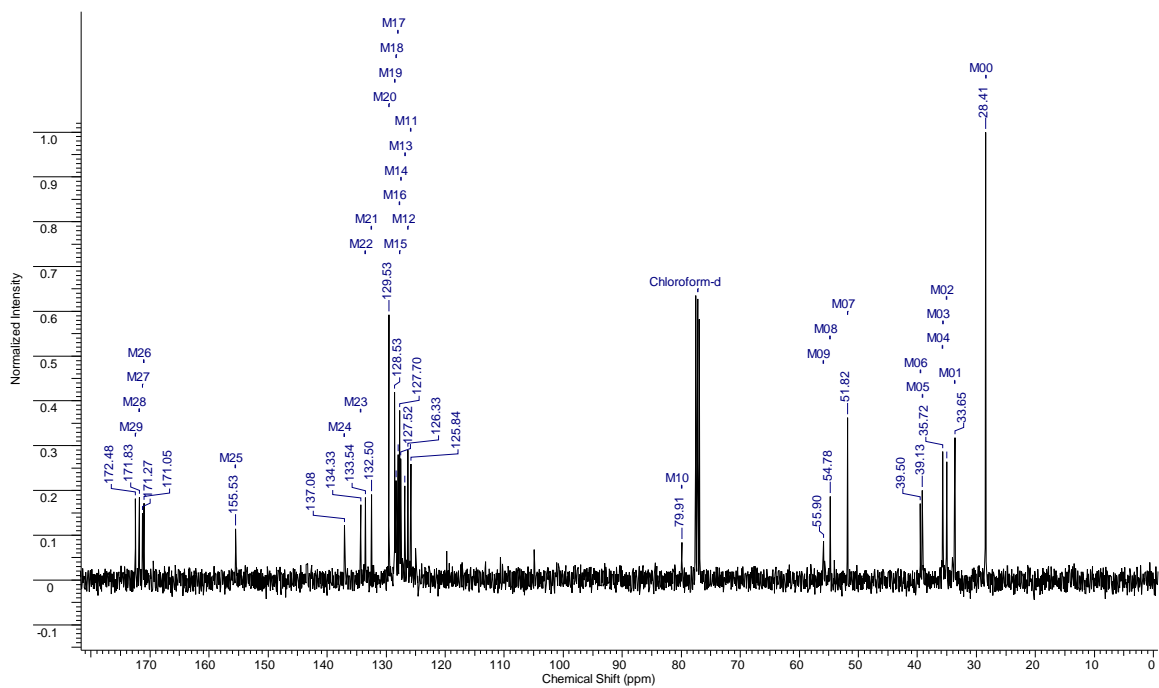
(b)

Figure A.34: - (a) ¹HNMR (b) ¹³CNMR of 2.35a
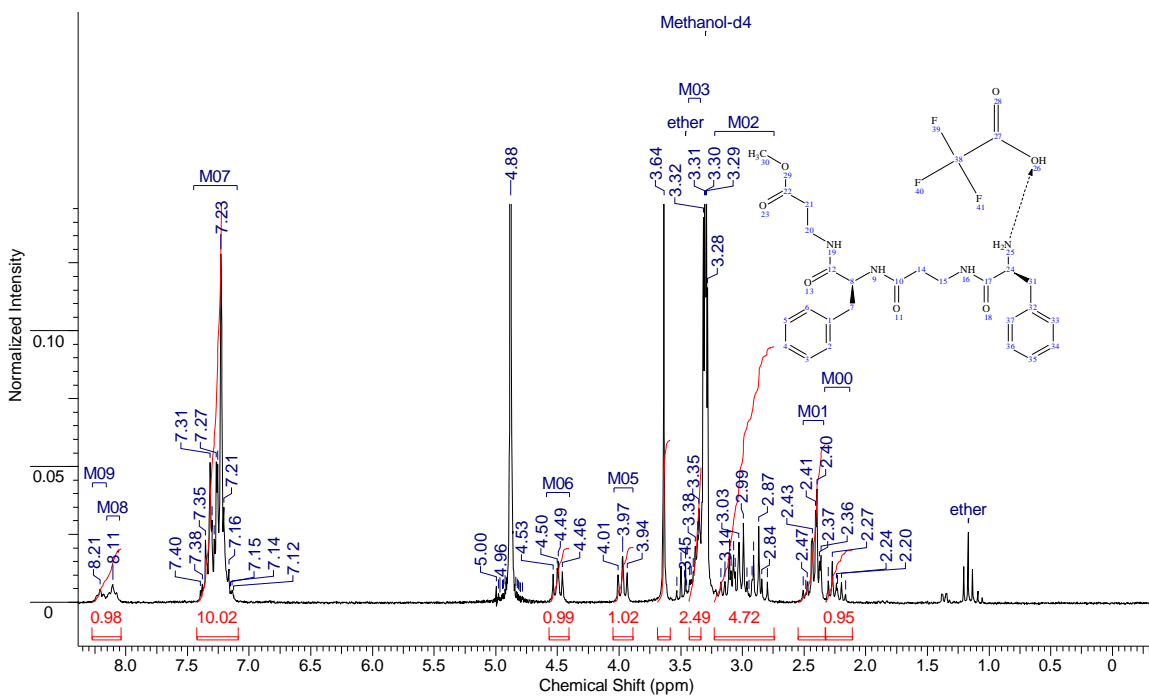
(a)
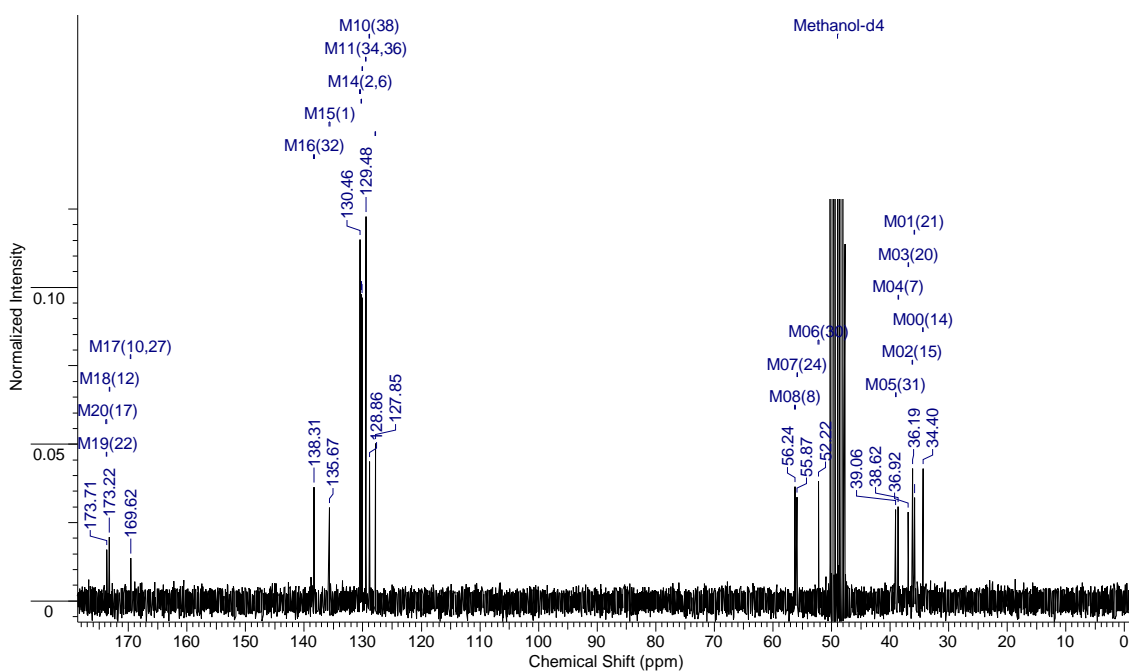
(b)

Figure A.35: - (a) ¹HNMR (b) ¹³CNMR of 2.35b
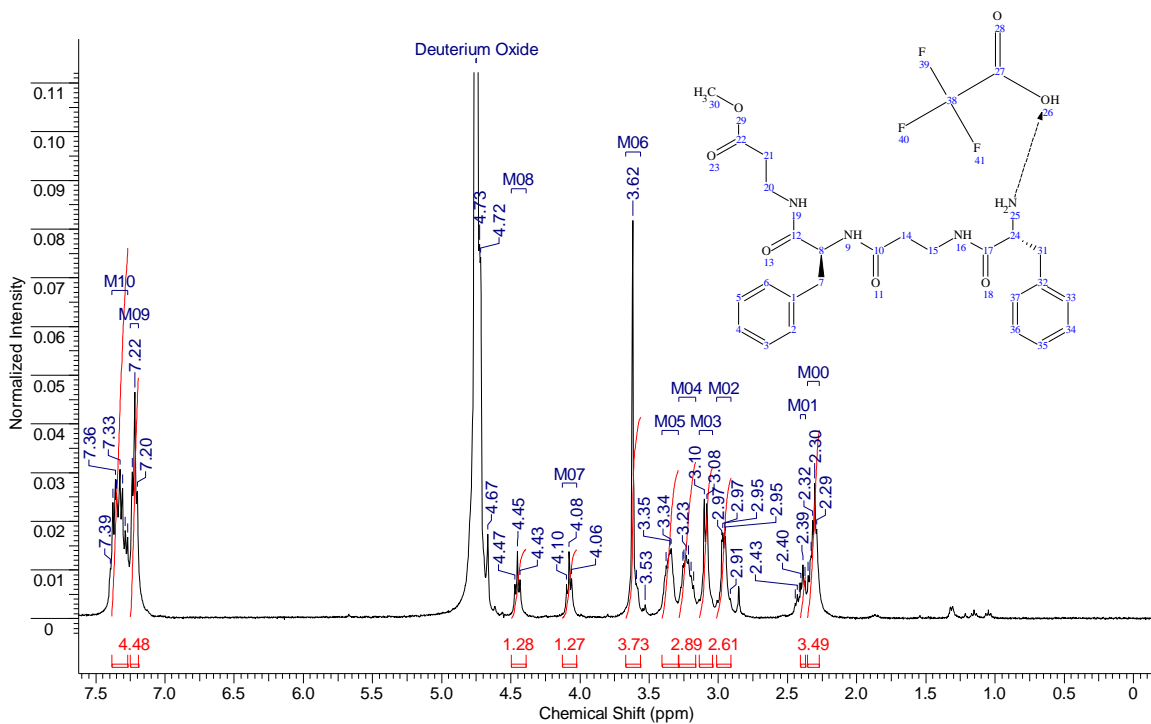
(a)
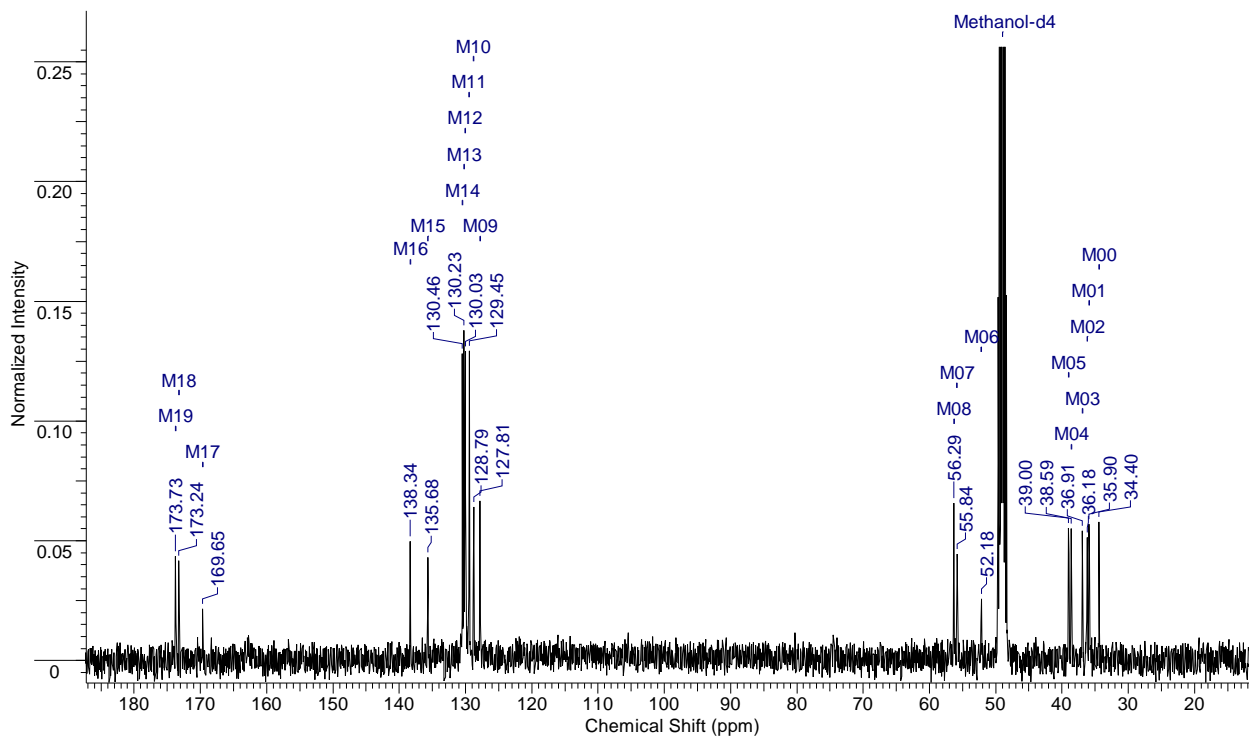
(b)

Figure A.36: - (a) ¹HNMR (b) ¹³CNMR of 2.35c
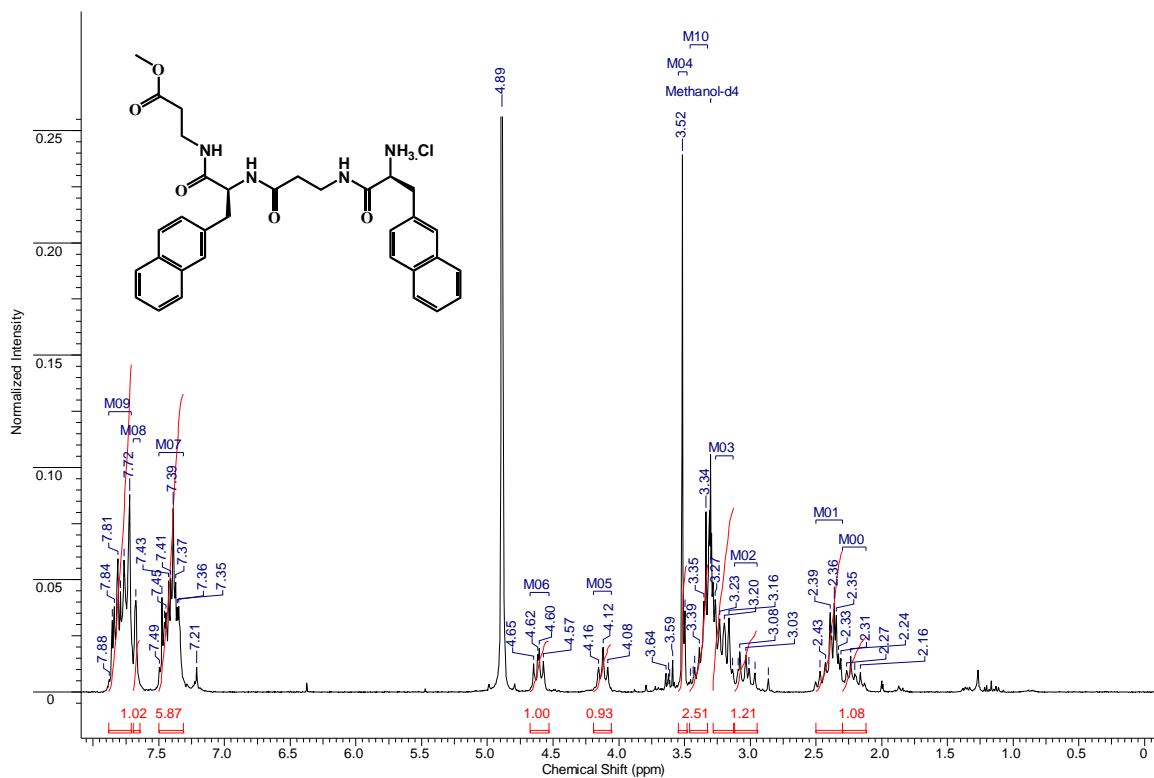
(a)
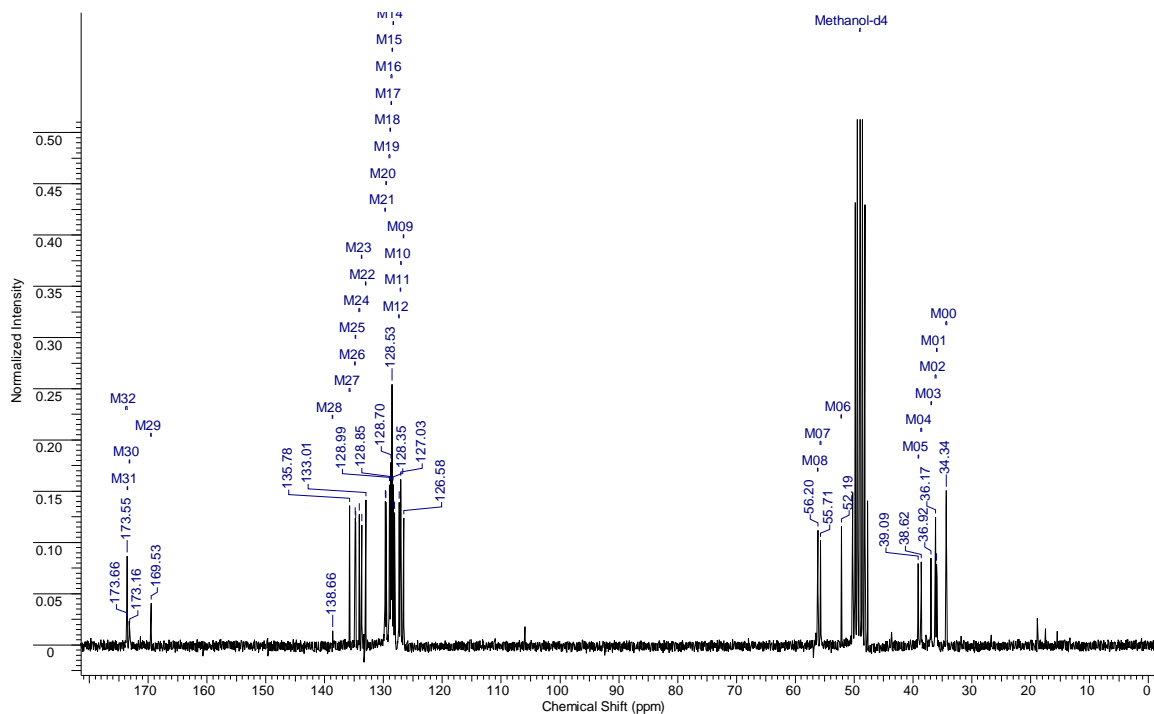
(b)

Figure A.37: - (a) ^{1}HNMR (b) ^{13}CNMR of 2.35d
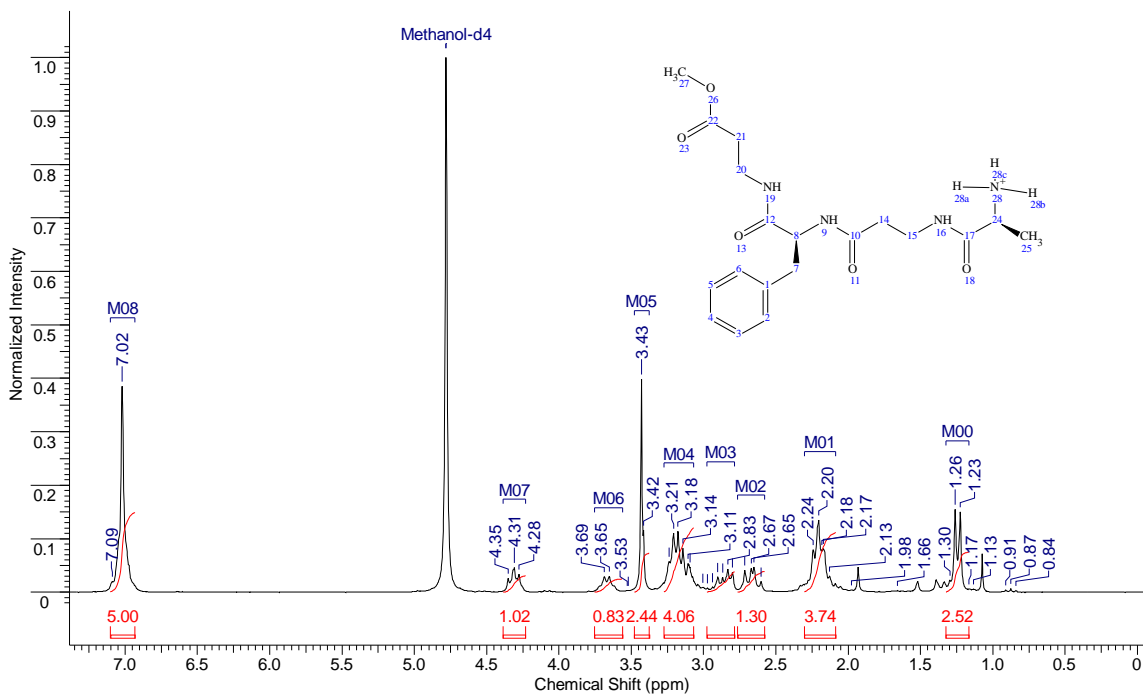
(a)
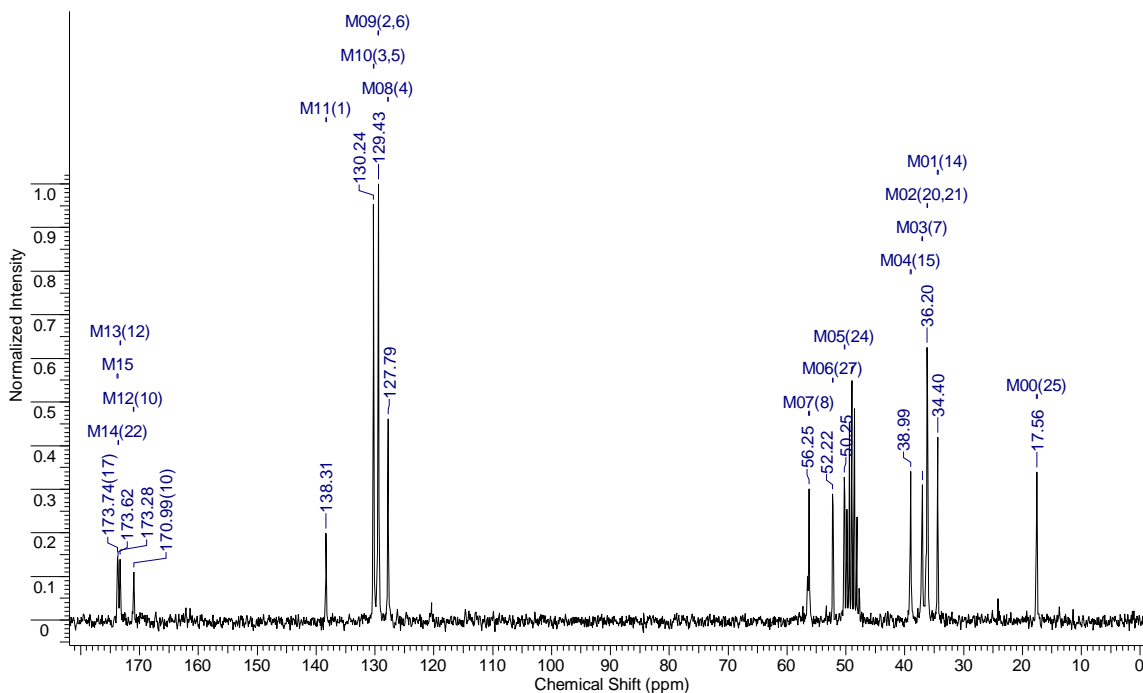
(b)

Figure A.38: - (a) ¹HNMR (b) ¹³CNMR of 2.35e
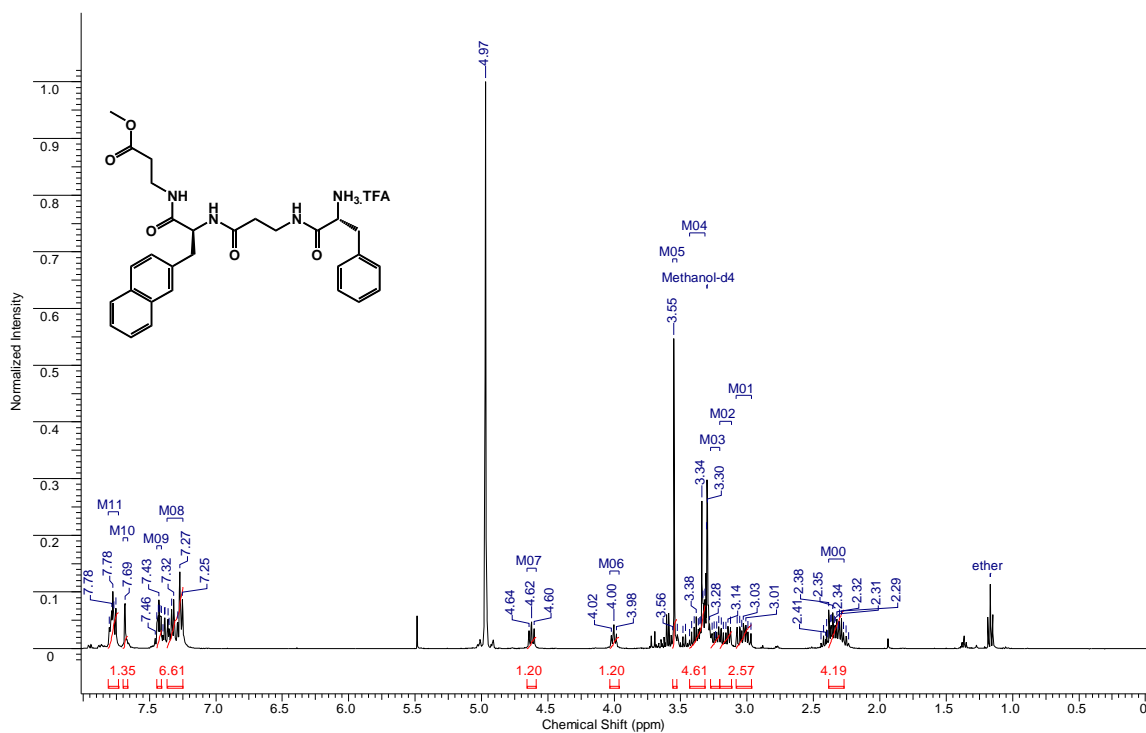
(a)
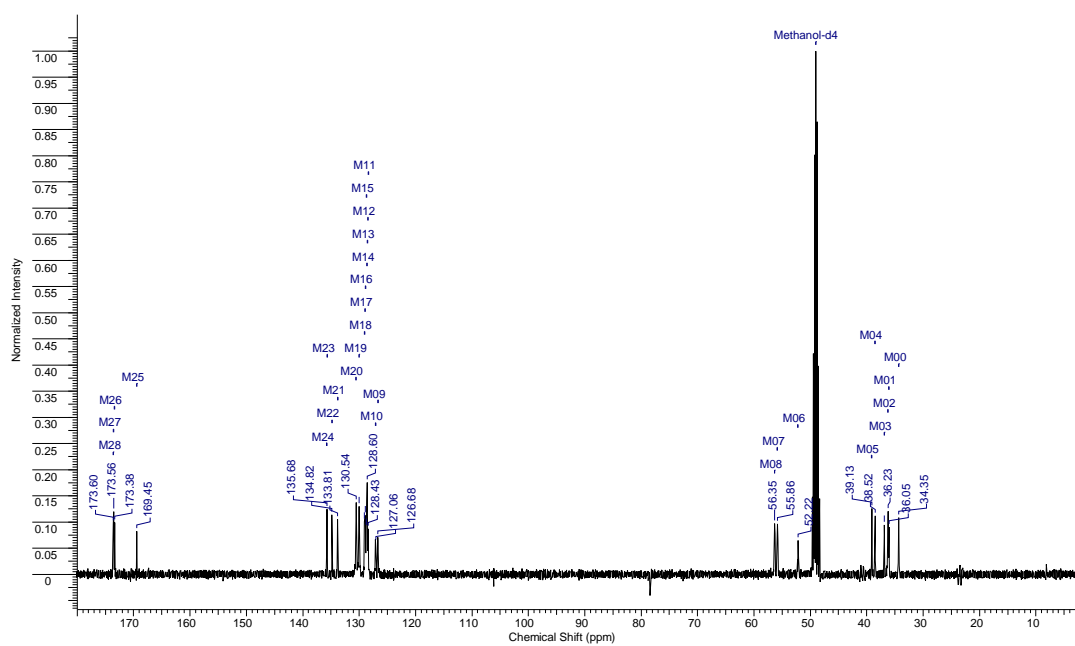
(b)

Figure A.39: - (a) ¹HNMR (b) ¹³CNMR of 2.35f
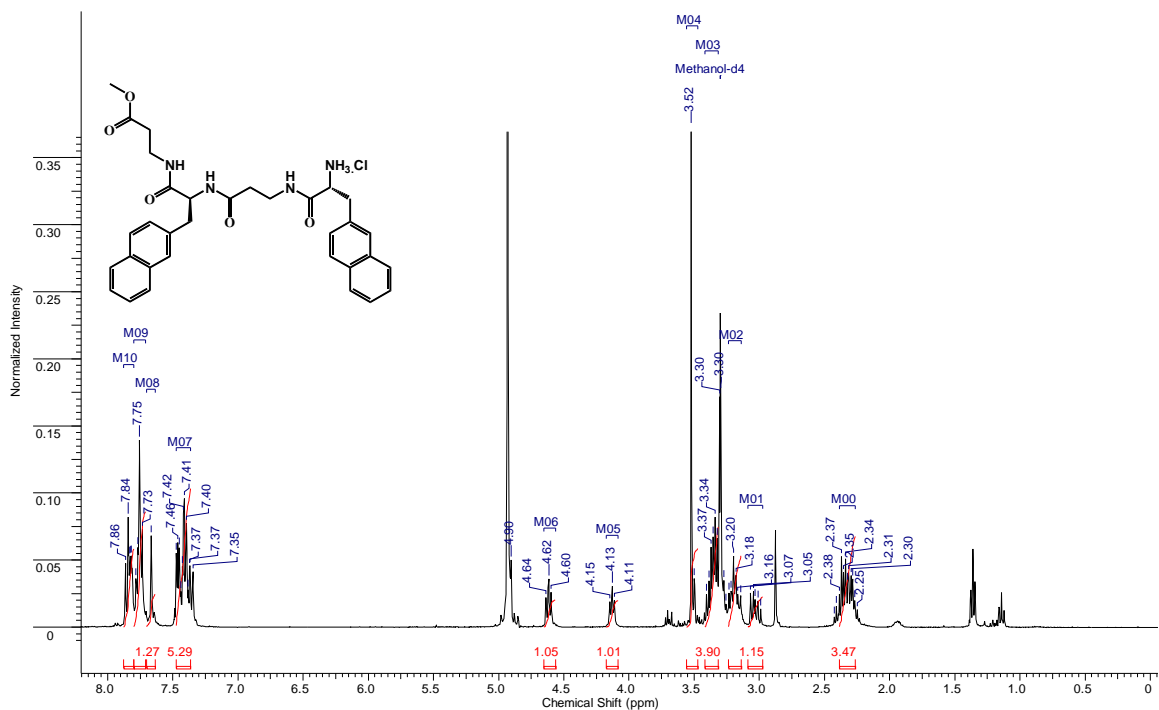
(a)
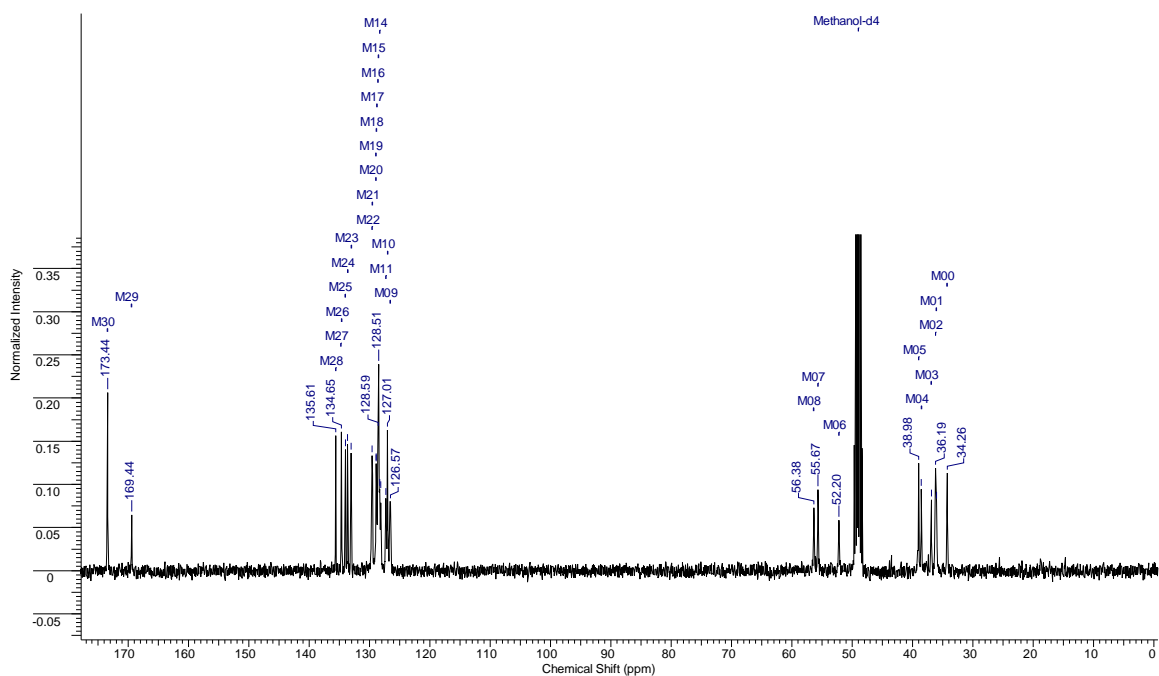
(b)

Figure A.40: - (a) ^{1}HNMR (b) ^{13}CNMR of 3.1a
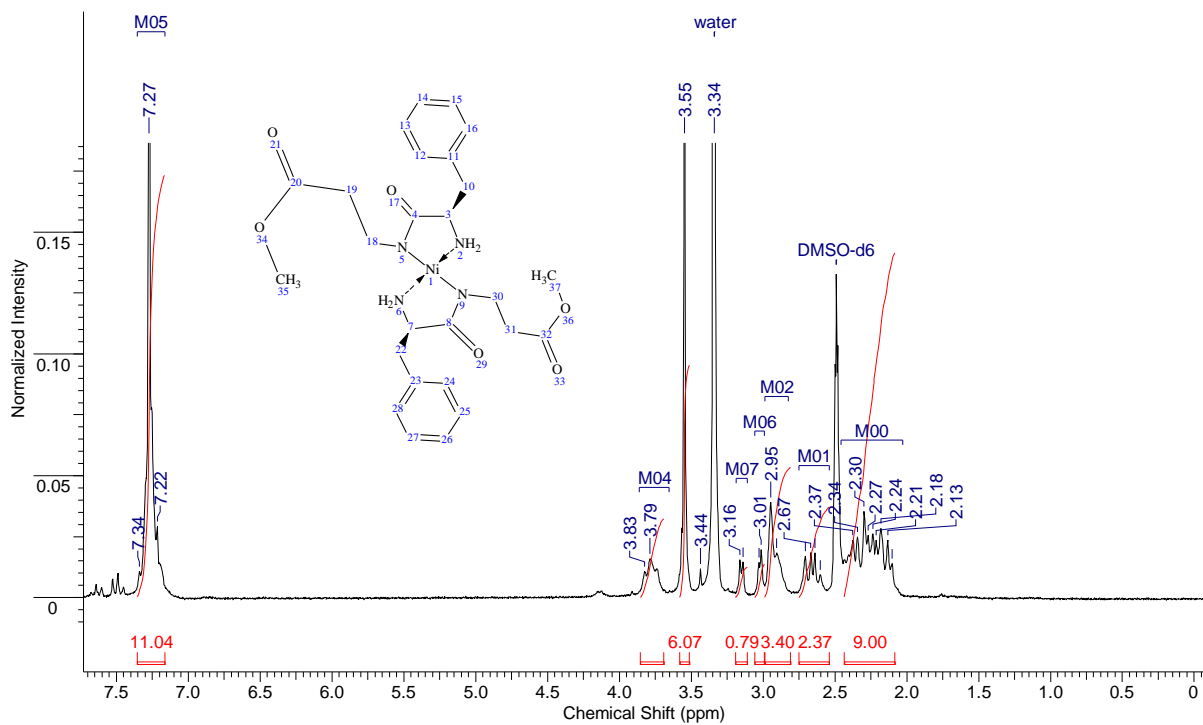
(a)
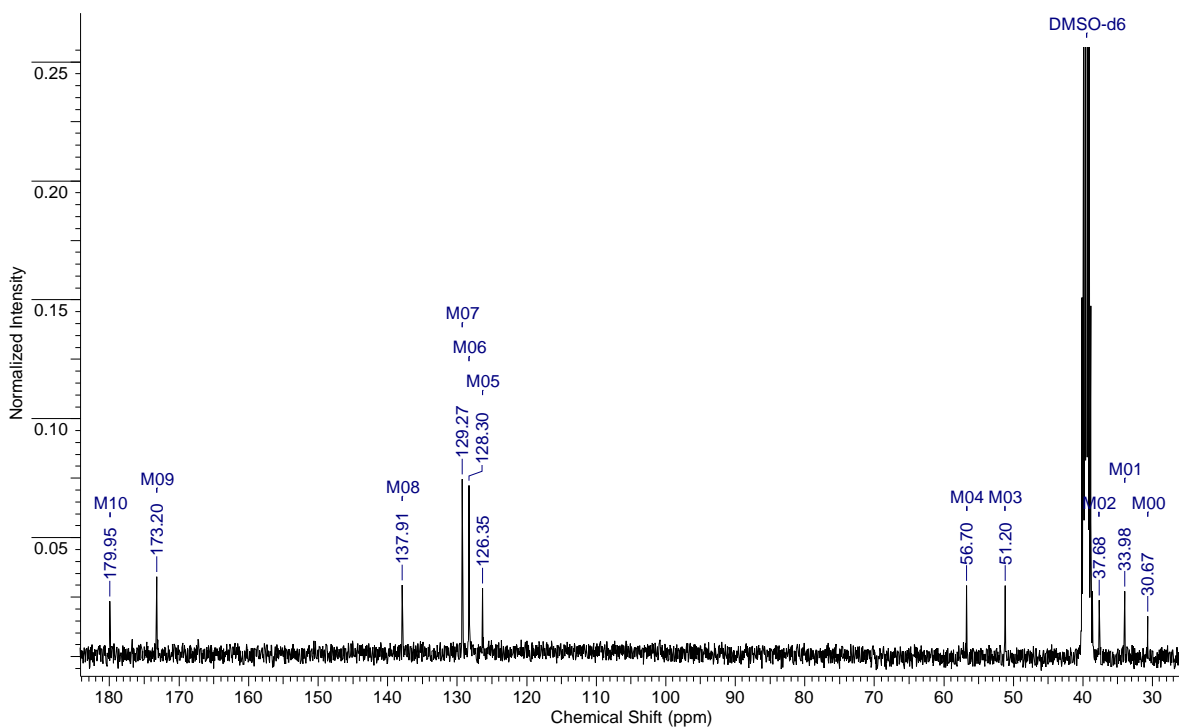
(b)

Figure A.41: - (a) ^{1}HNMR (b) ^{13}C NMR of 3.1b
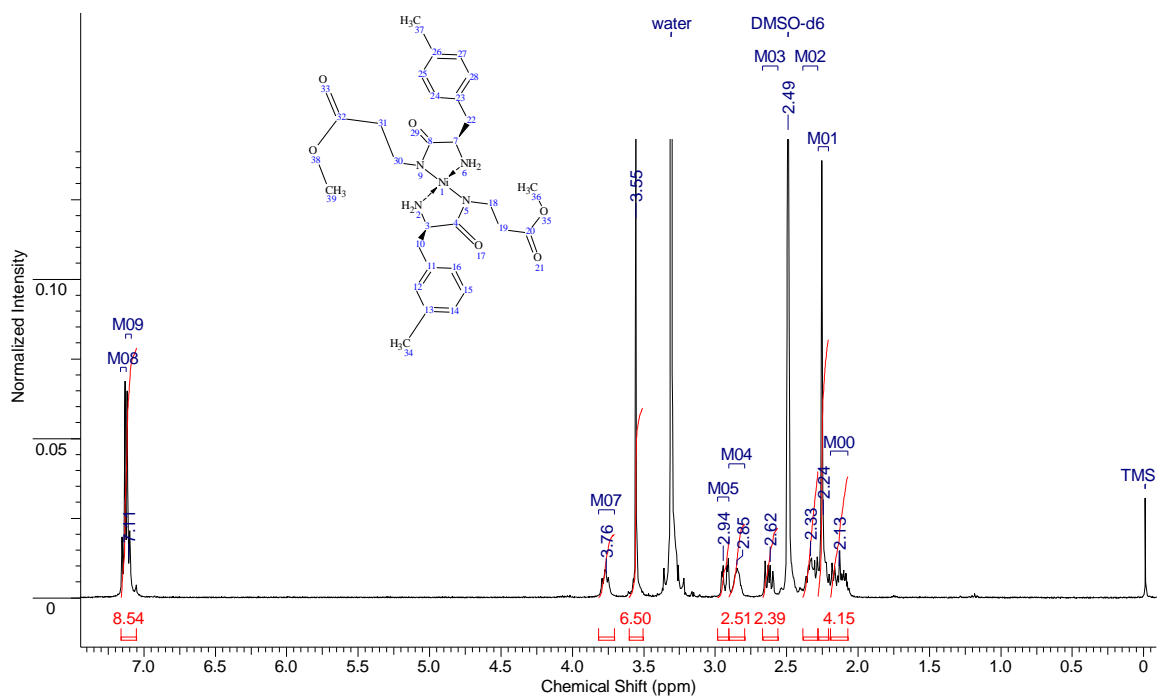
(a)
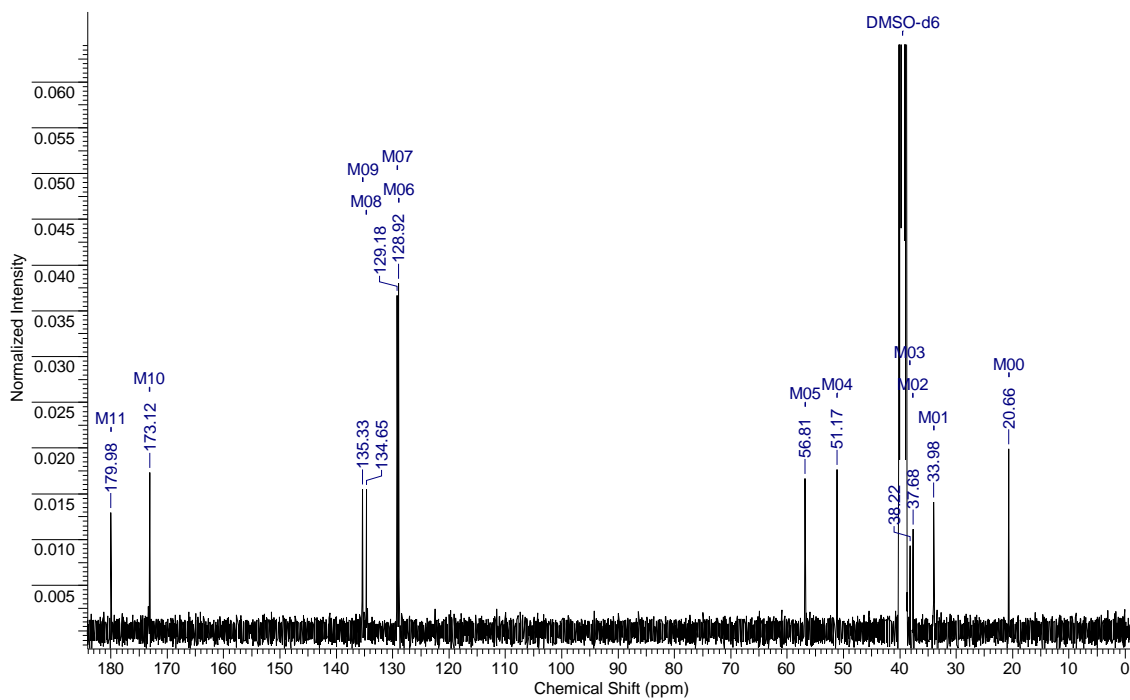
(b)

Figure A.42: - (a) ^{1}HNMR (b) ^{13}CNMR of 3.1c
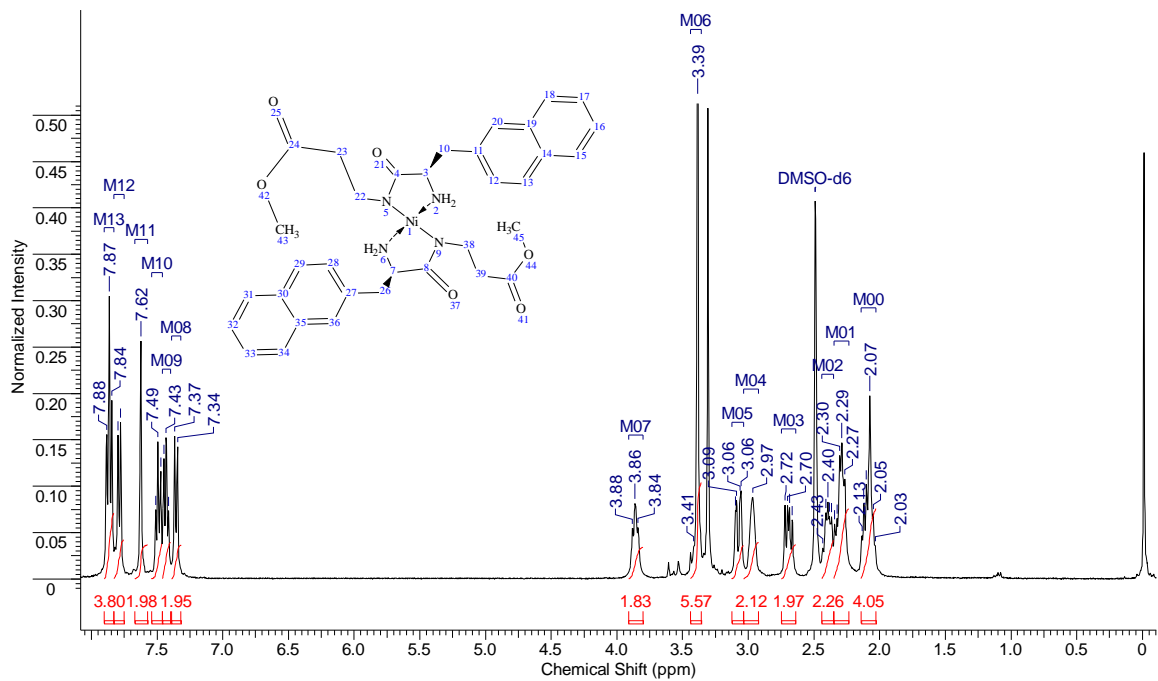

(a)
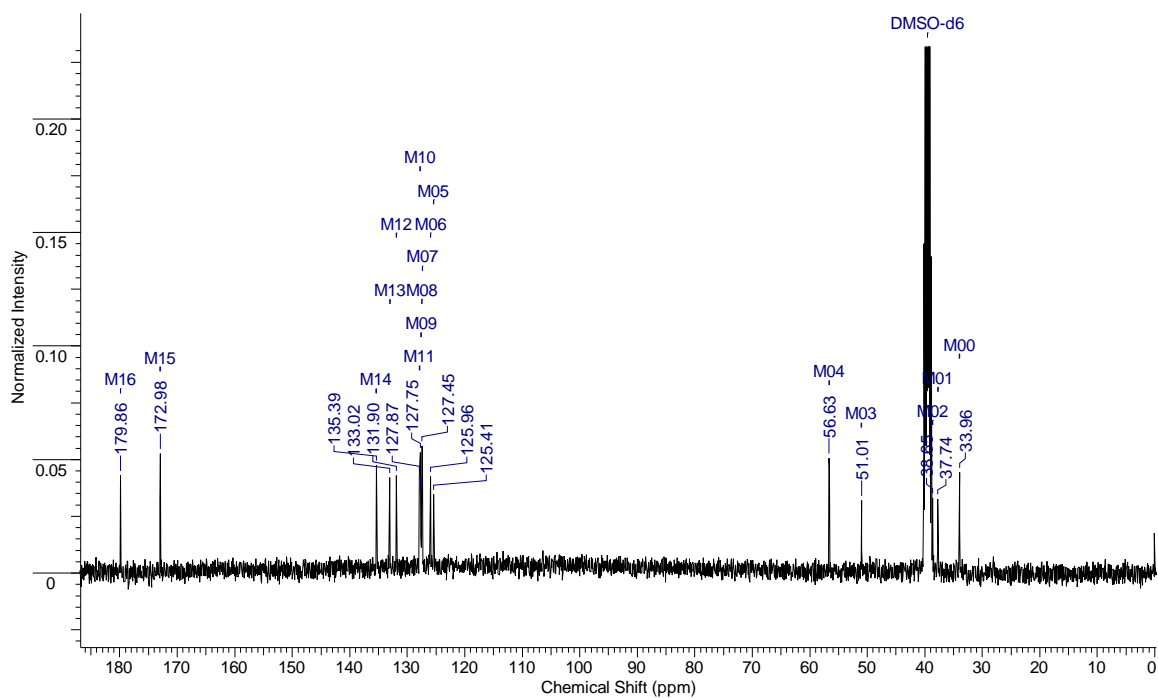
(b)

Figure A.43: - (a) ^{1}HNMR (b) ^{13}CNMR of 3.2a
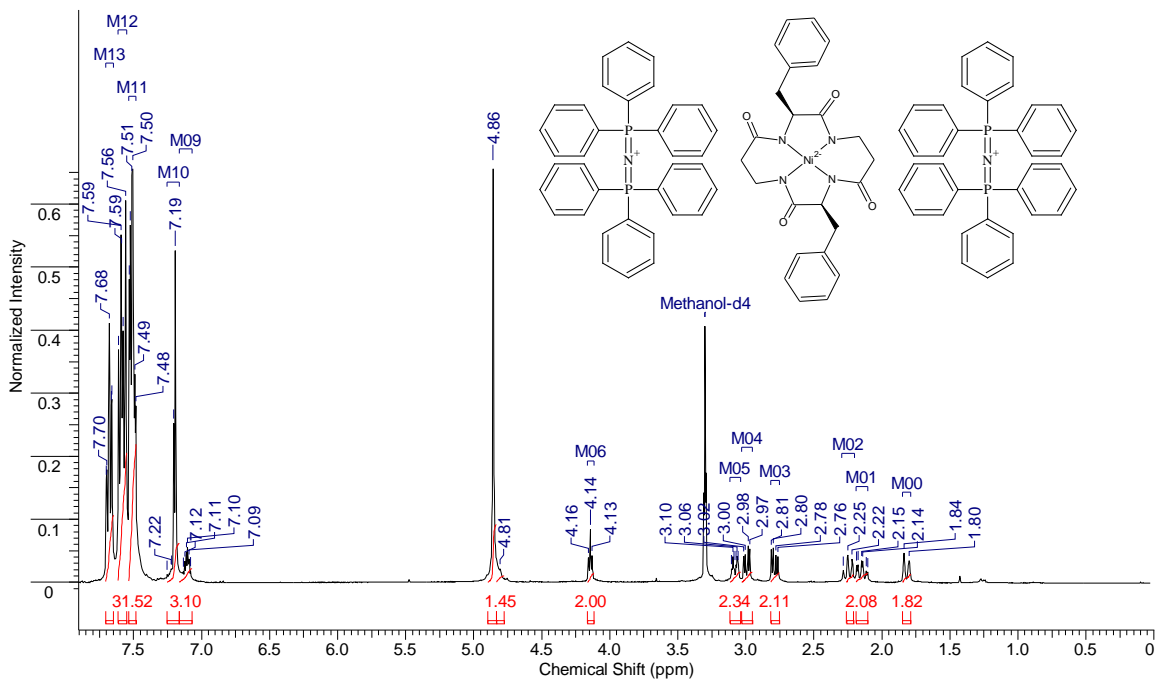
(a)
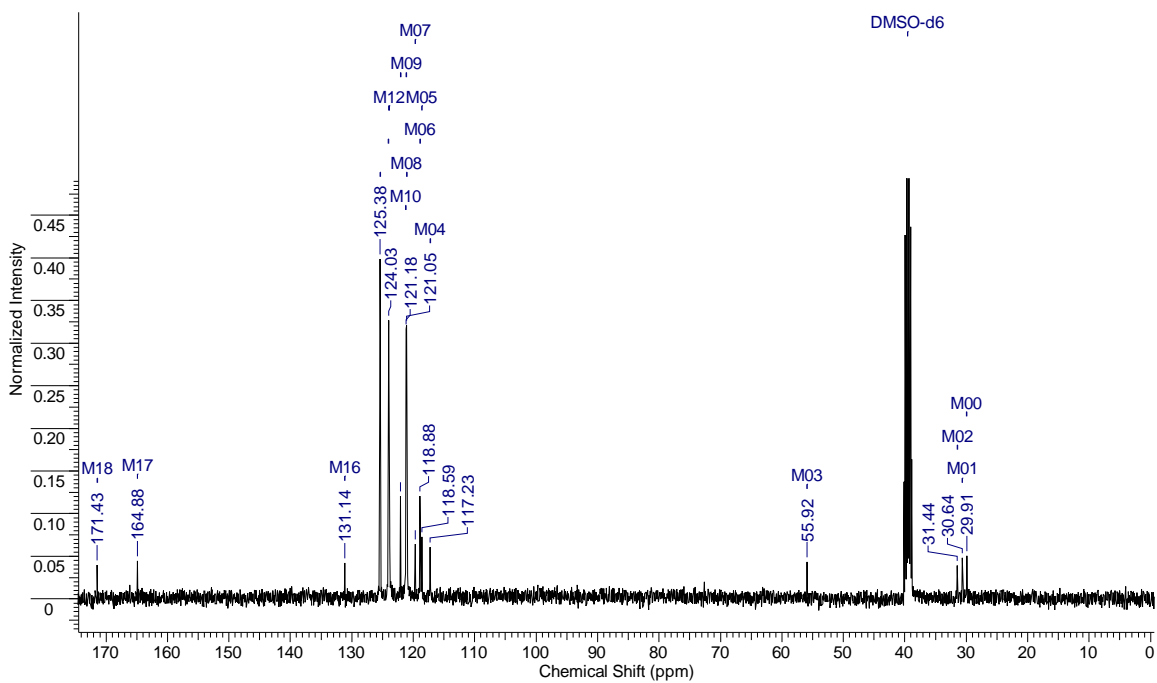
(b)

Figure A.44: - (a) ¹HNMR (b) ¹³CNMR of 3.2b
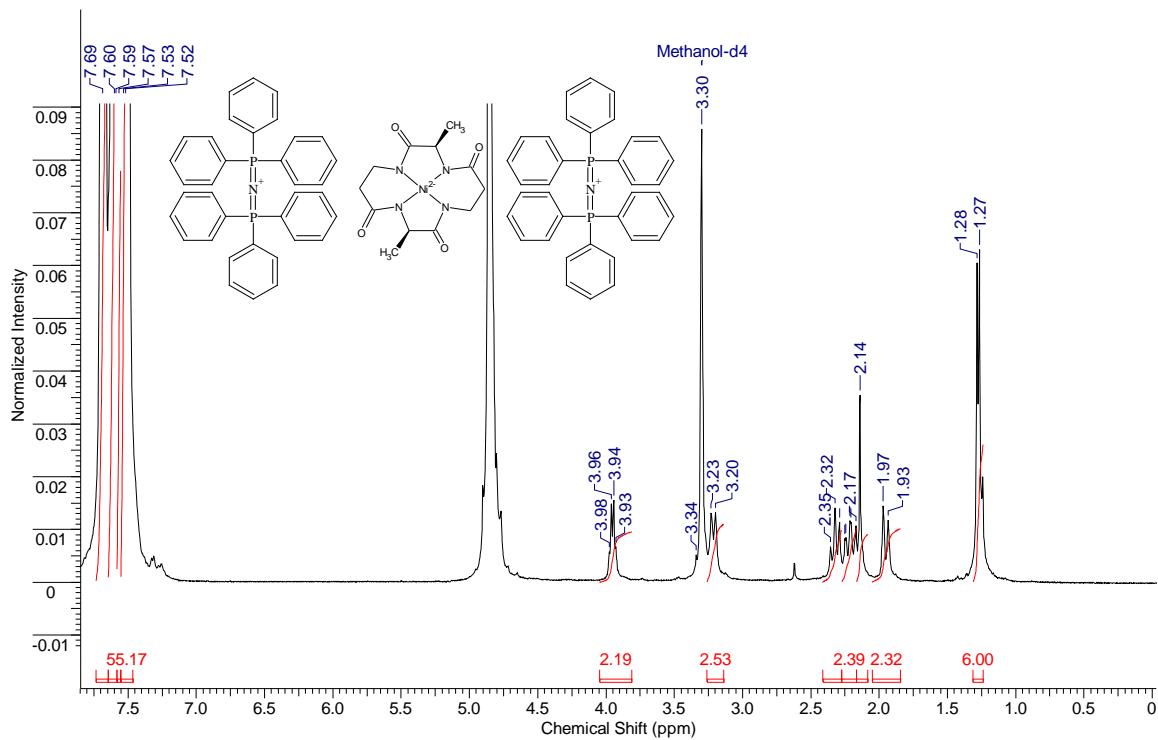
(a)
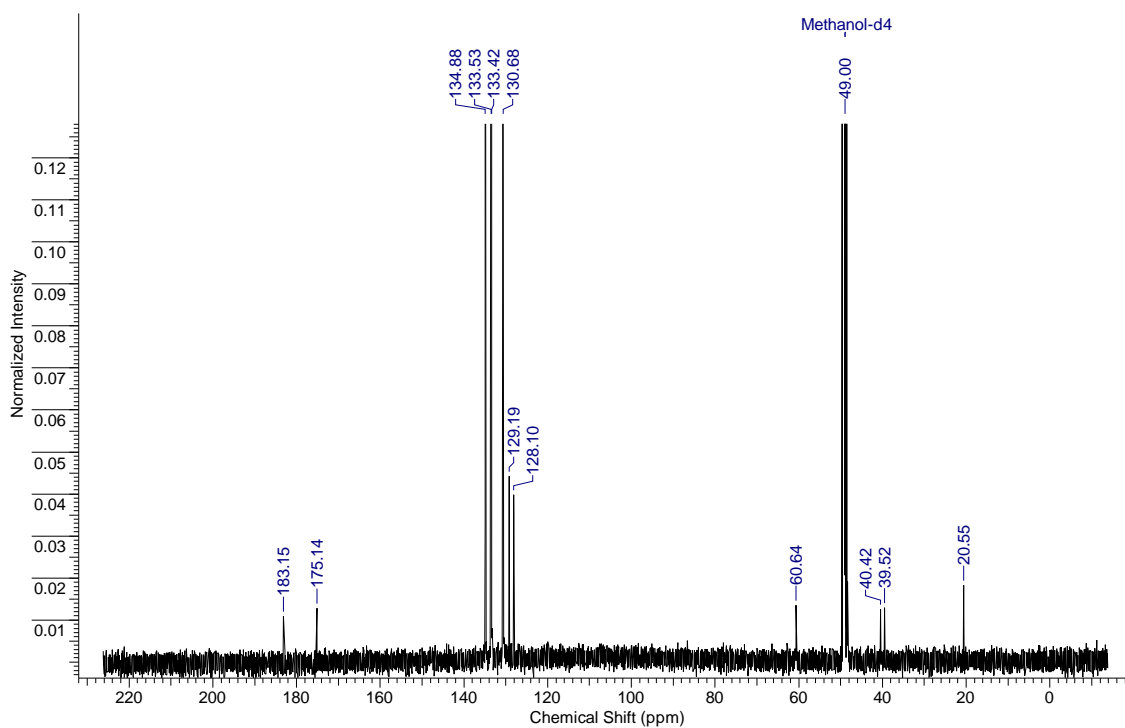
Figure A.45: - (a) ^{1}HNMR (b) ^{13}CNMR of 3.2c

(a)

(b)

Figure A.46: - (a) ^{1}HNMR (b) ^{13}CNMR of 3.2d

(a)
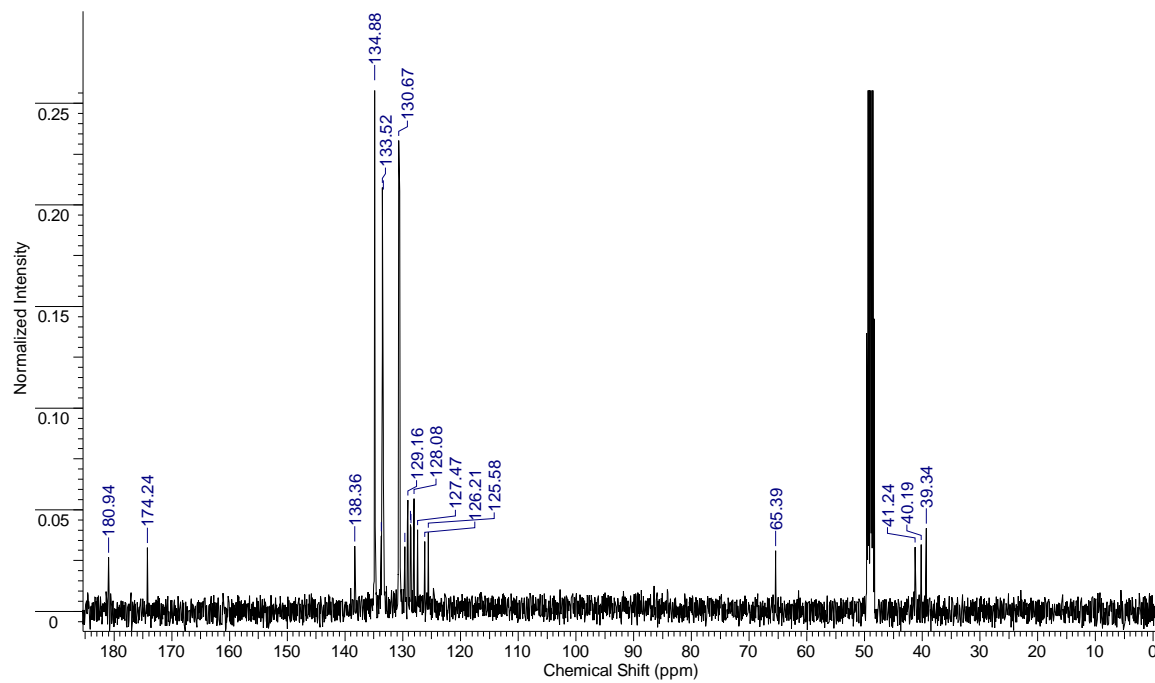
(b)

Figure A.47: - (a) ^{1}HNMR (b) ^{13}CNMR of 3.2e

(a)

(b)

Figure A.48: - (a) ^{1}HNMR (b) ^{13}CNMR of 3.2f
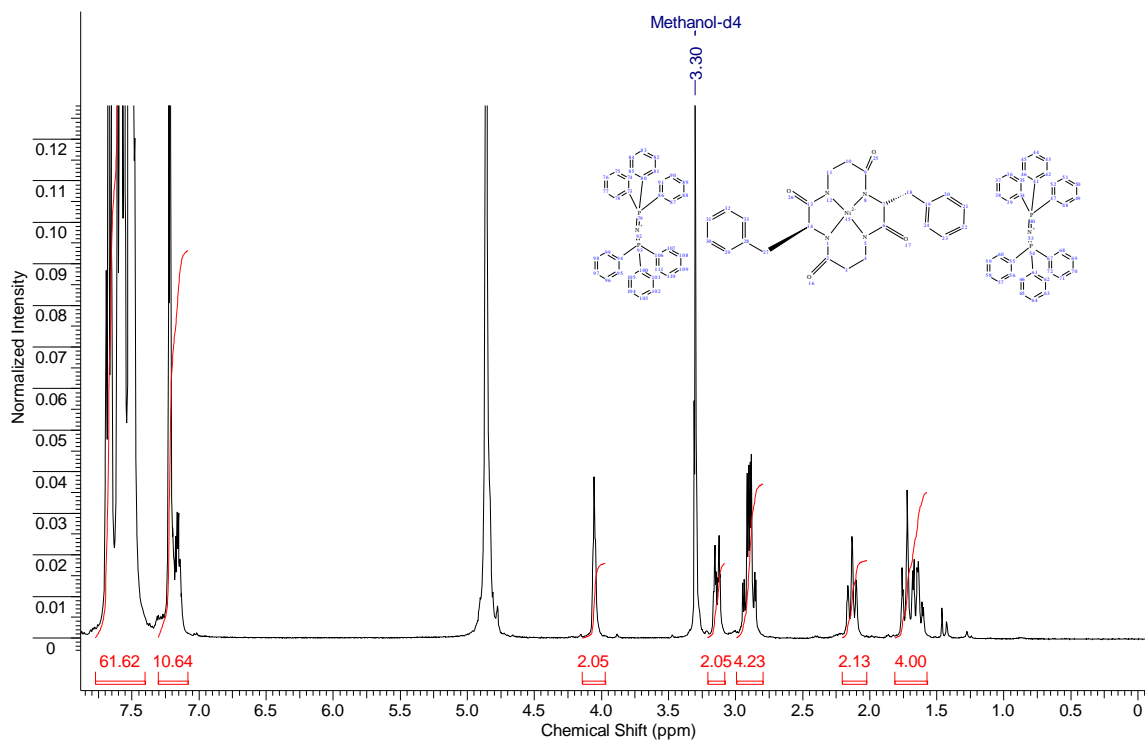
(a)
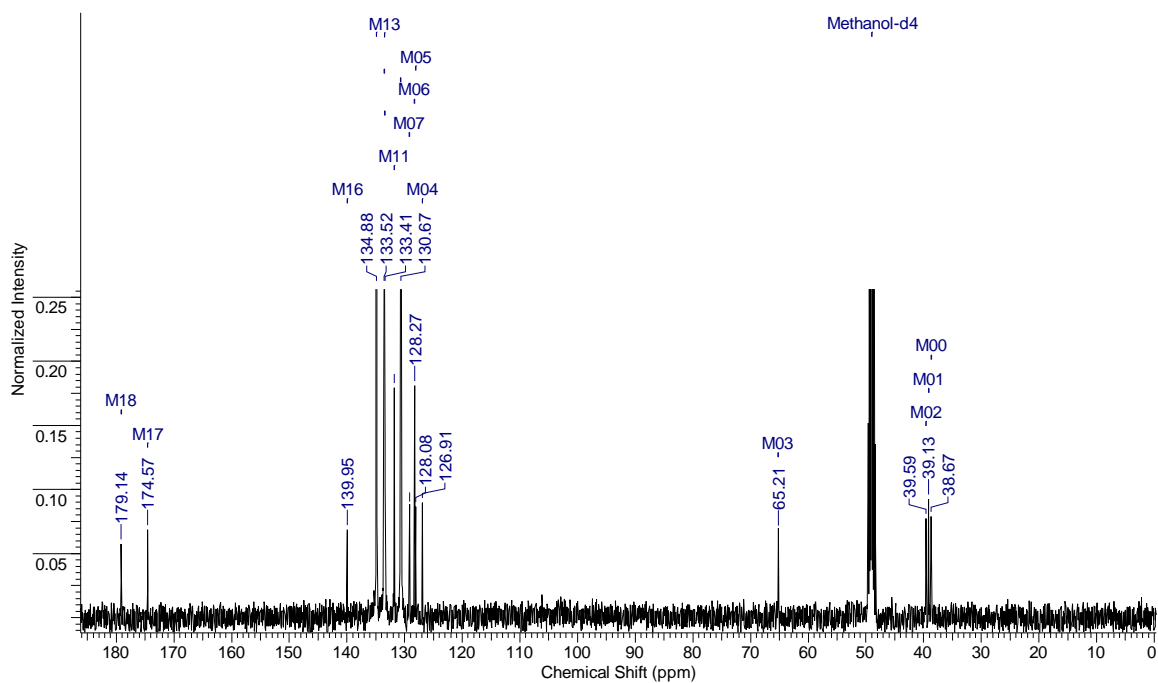
(b)

Figure A.49: - (a) ^{1}HNMR (b) ^{13}CNMR of 4.1a
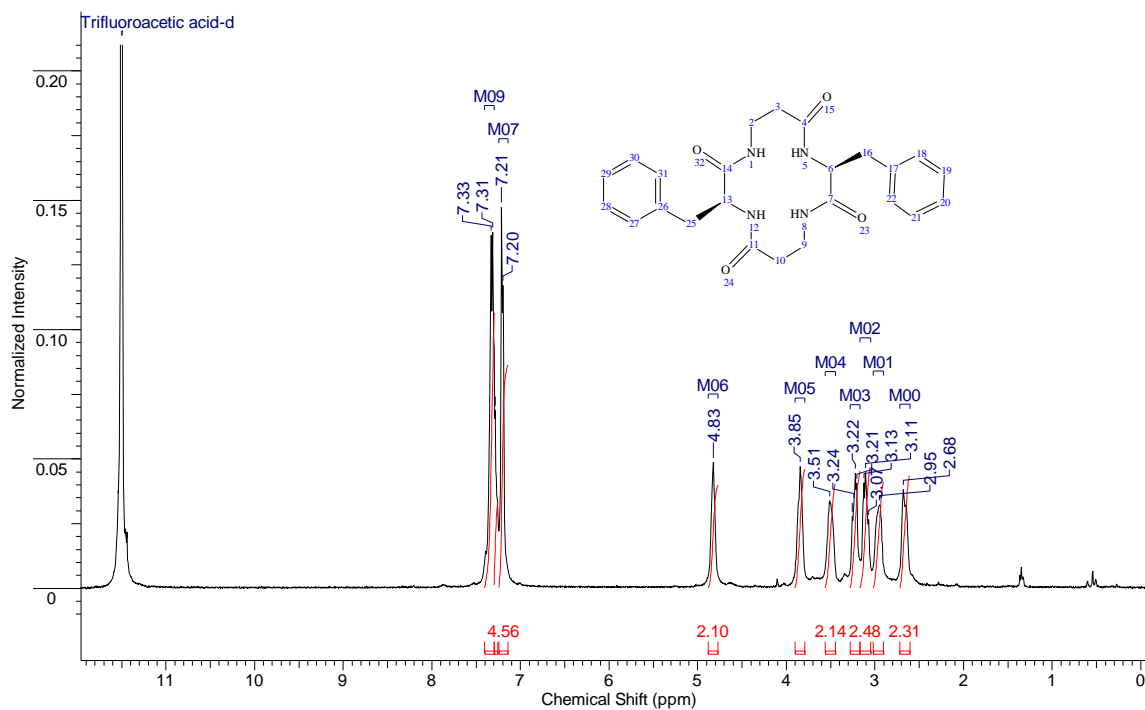
(a)
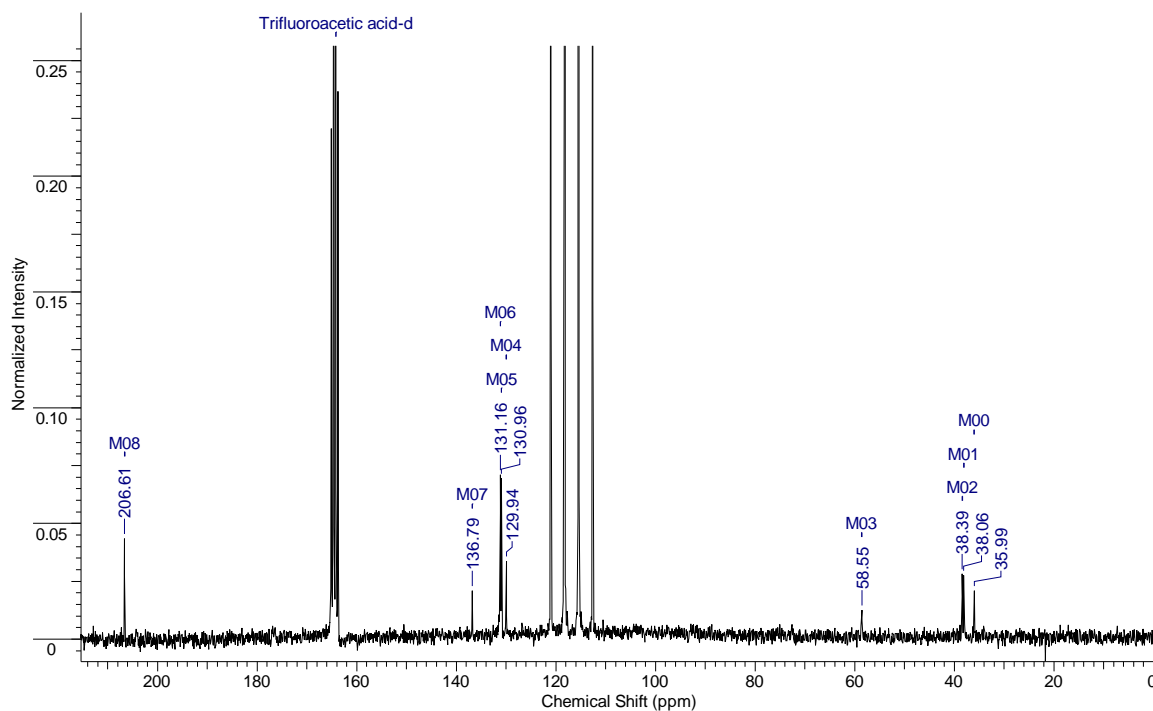
(b)

Figure A.50: - (a) ¹HNMR of 4.1b
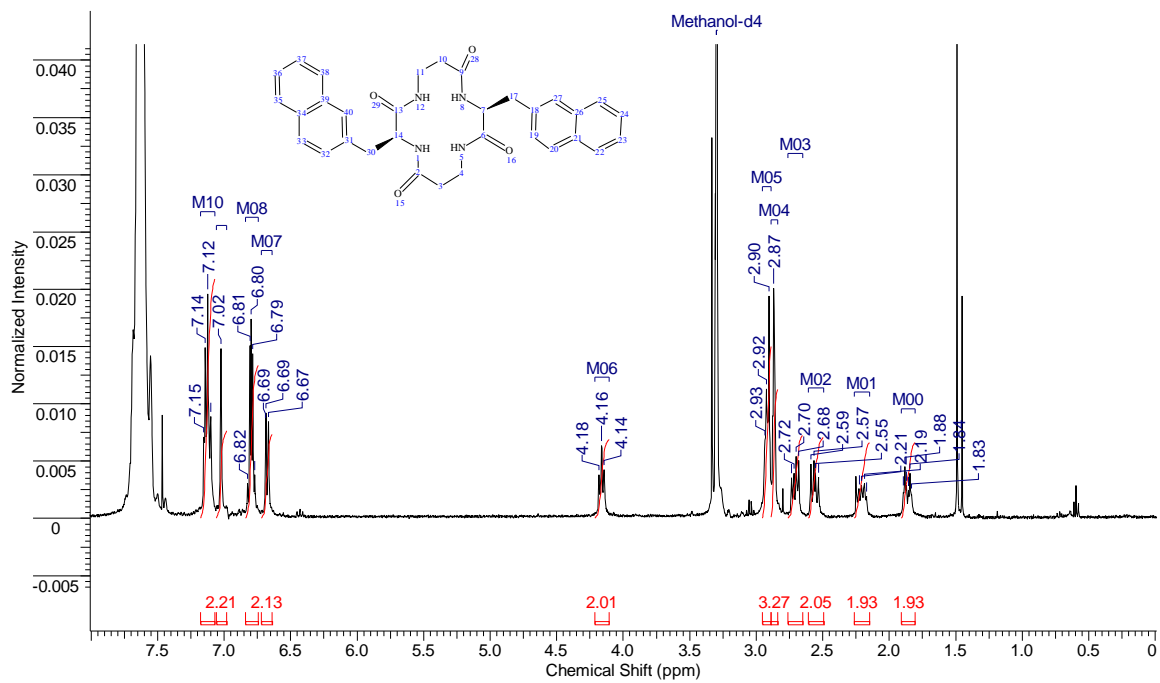
(a)

Figure A.51: - (a) ¹HNMR of 4.1c
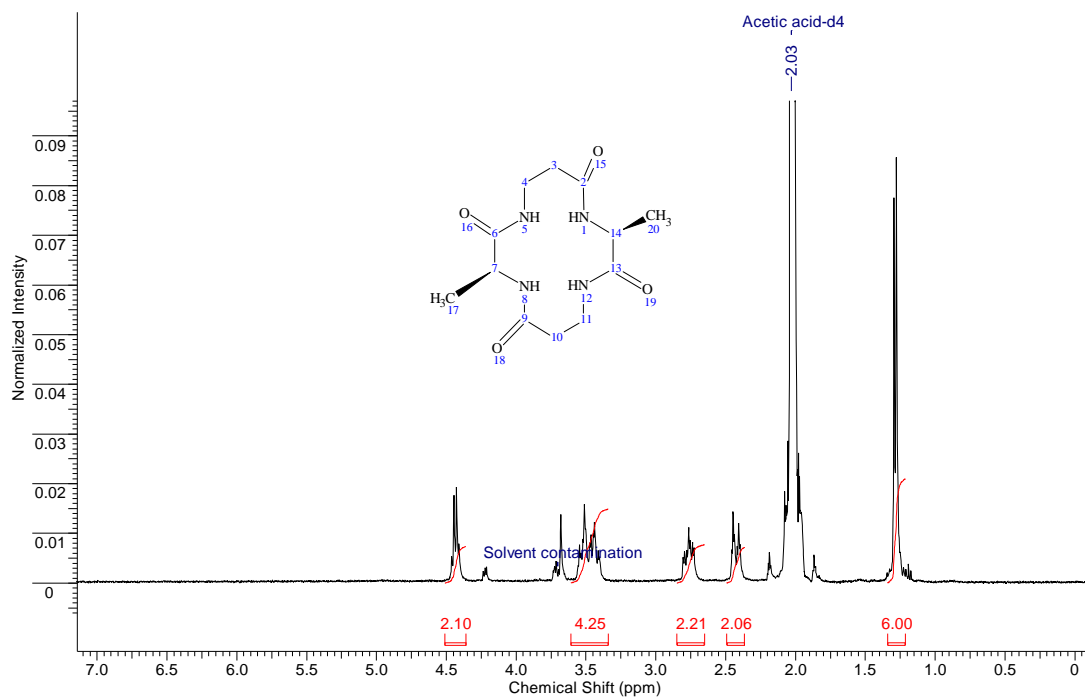
(a)

Figure A.52: - (a) ^{1}HNMR of 4.1d
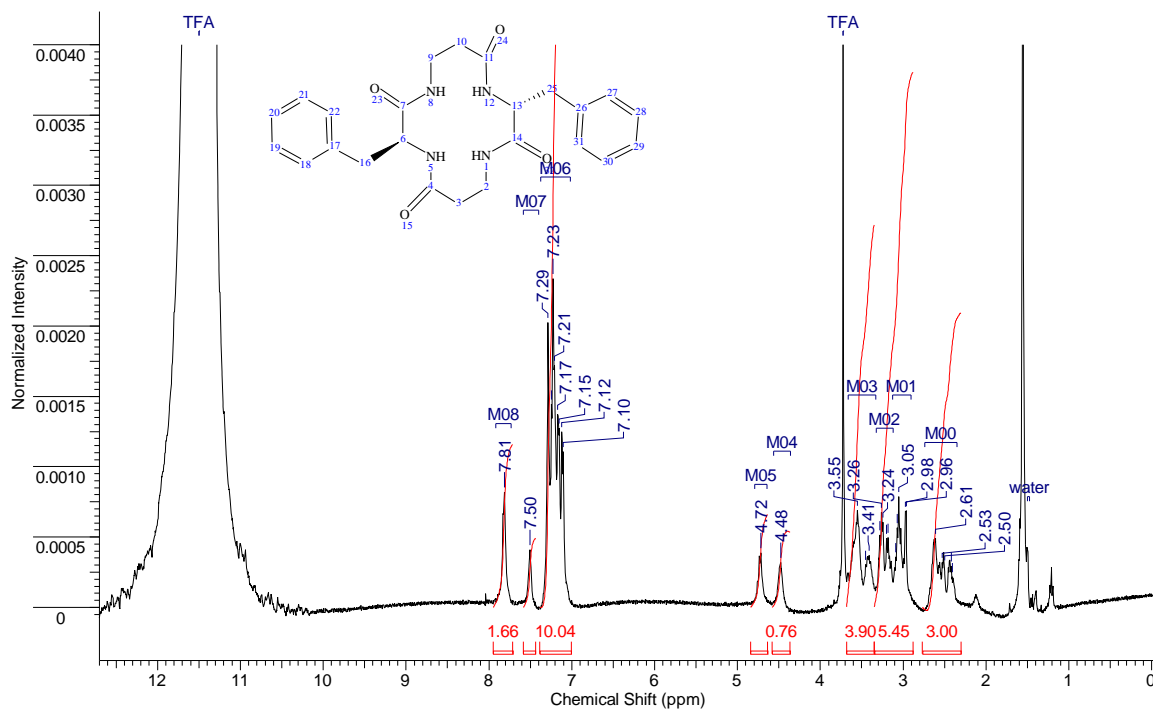
(a)

Figure A.53: - (a) ^{1}HNMR of 4.1e

(a)

238
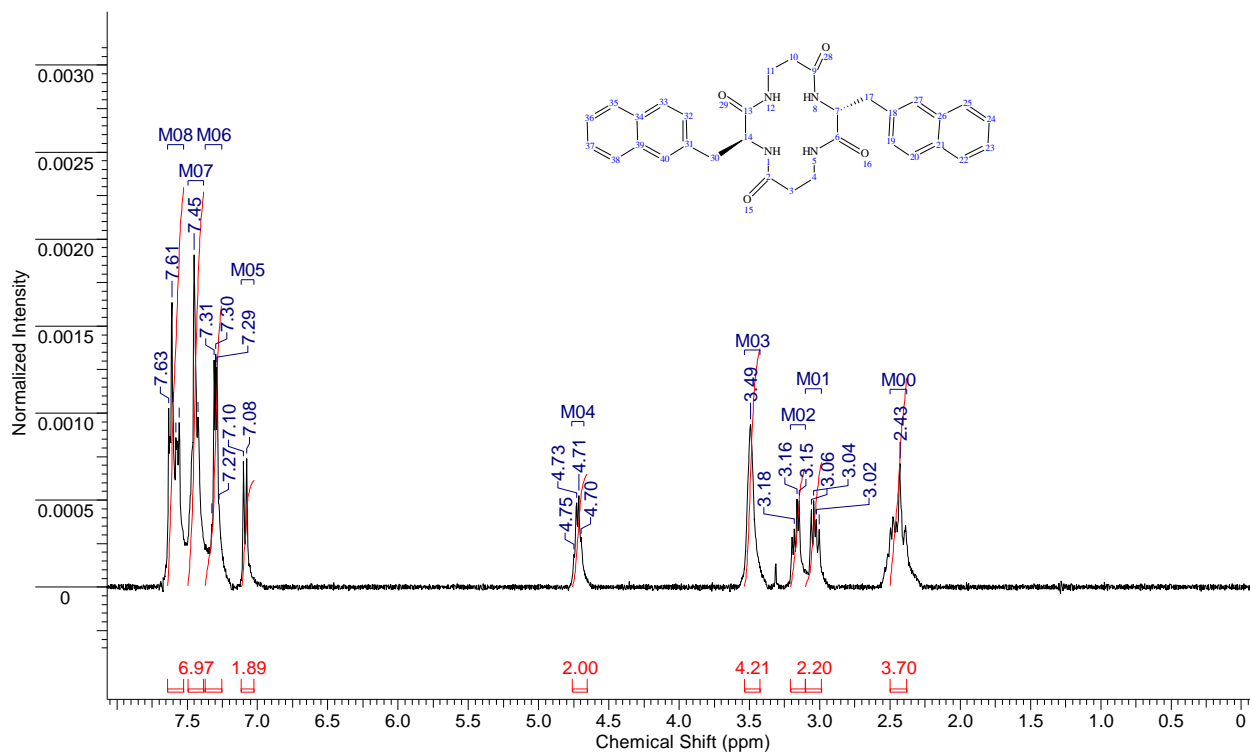
Figure A.54: - (a) ^{1}HNMR of 4.1f
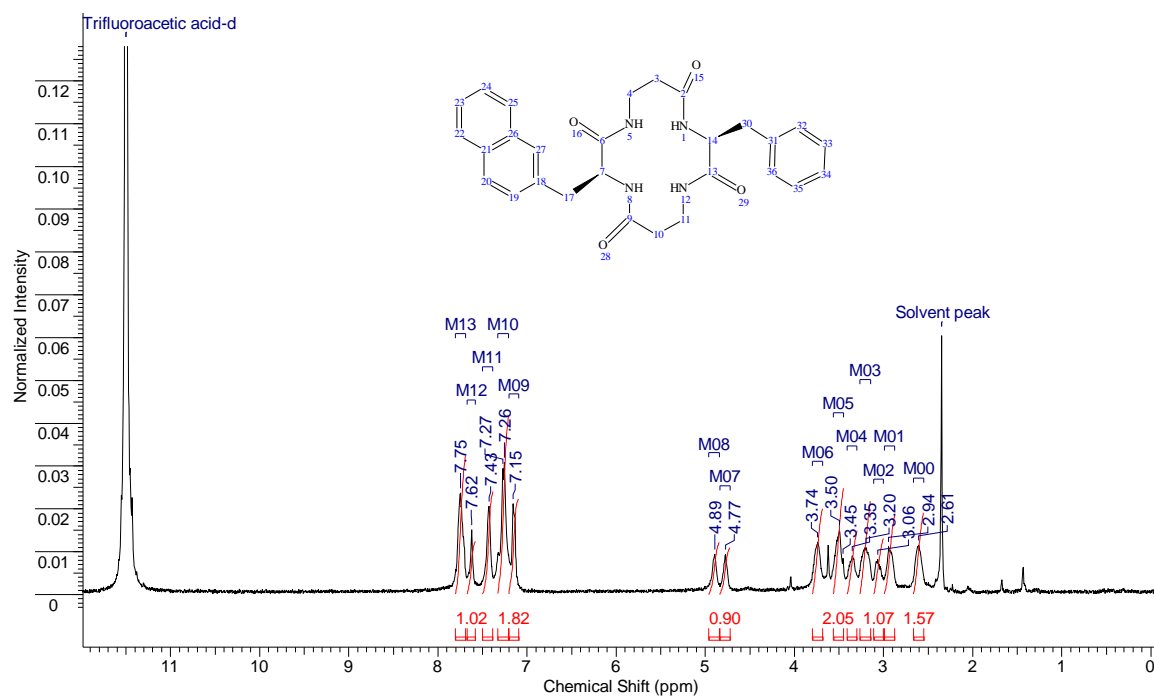
(a)

Figure A.55: - (a) ^{1}HNMR (b) ^{13}CNMR of 4.2a
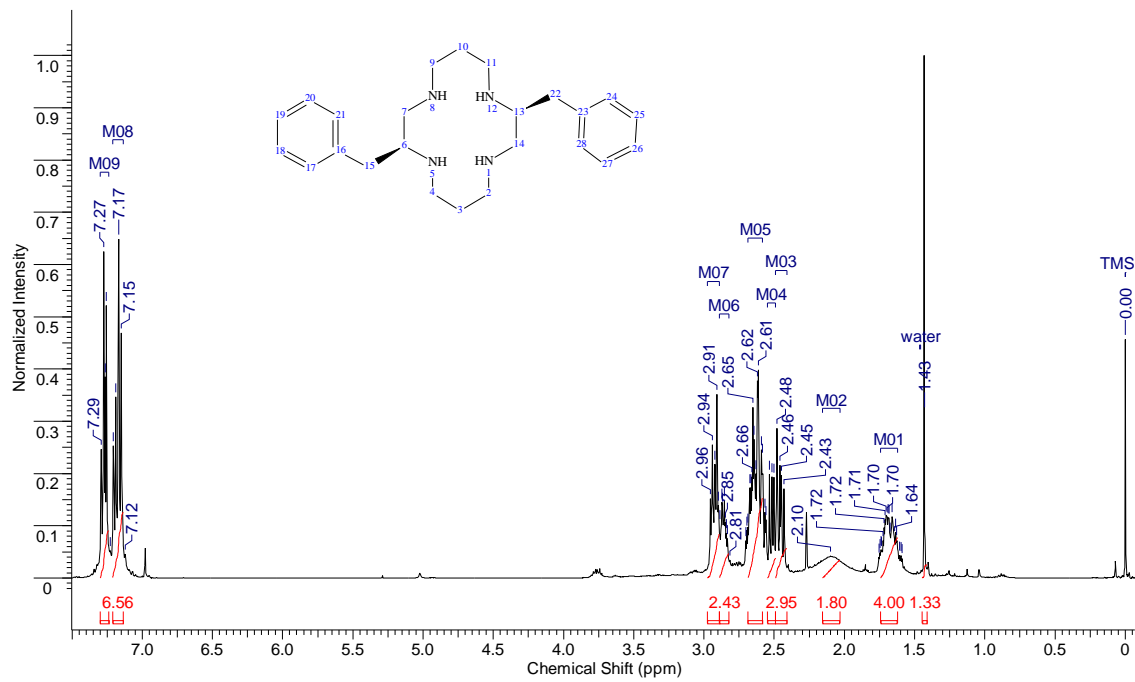
(a)
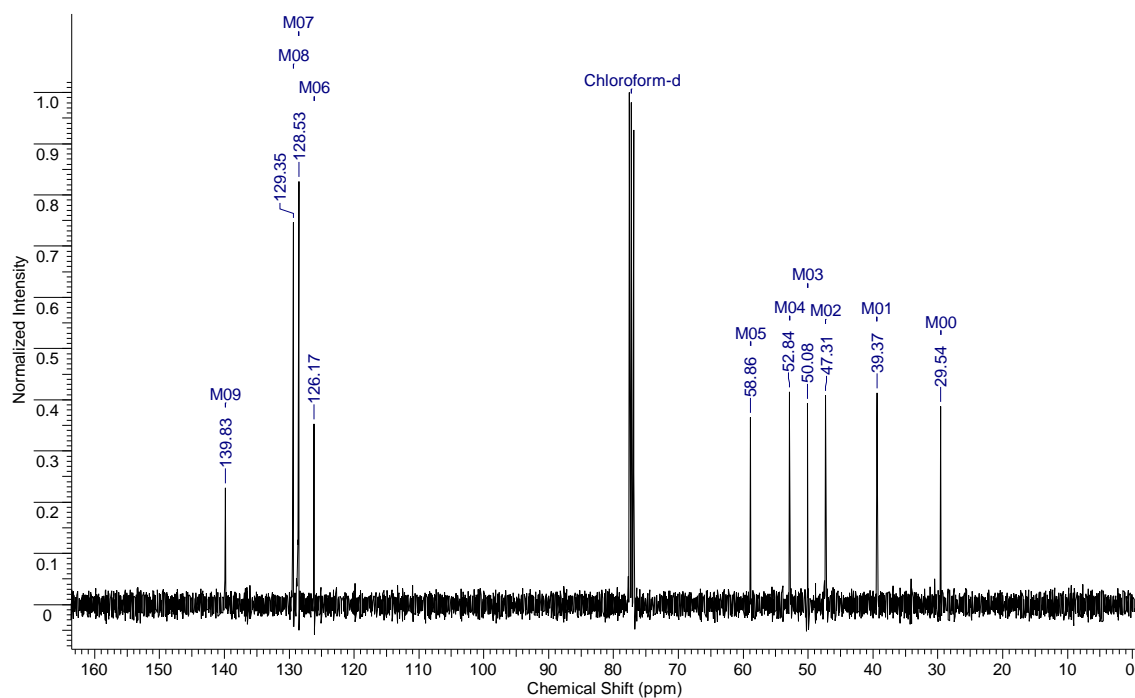
(b)

Figure A.56: - (a) ¹HNMR (b) ¹³CNMR of 4.2b
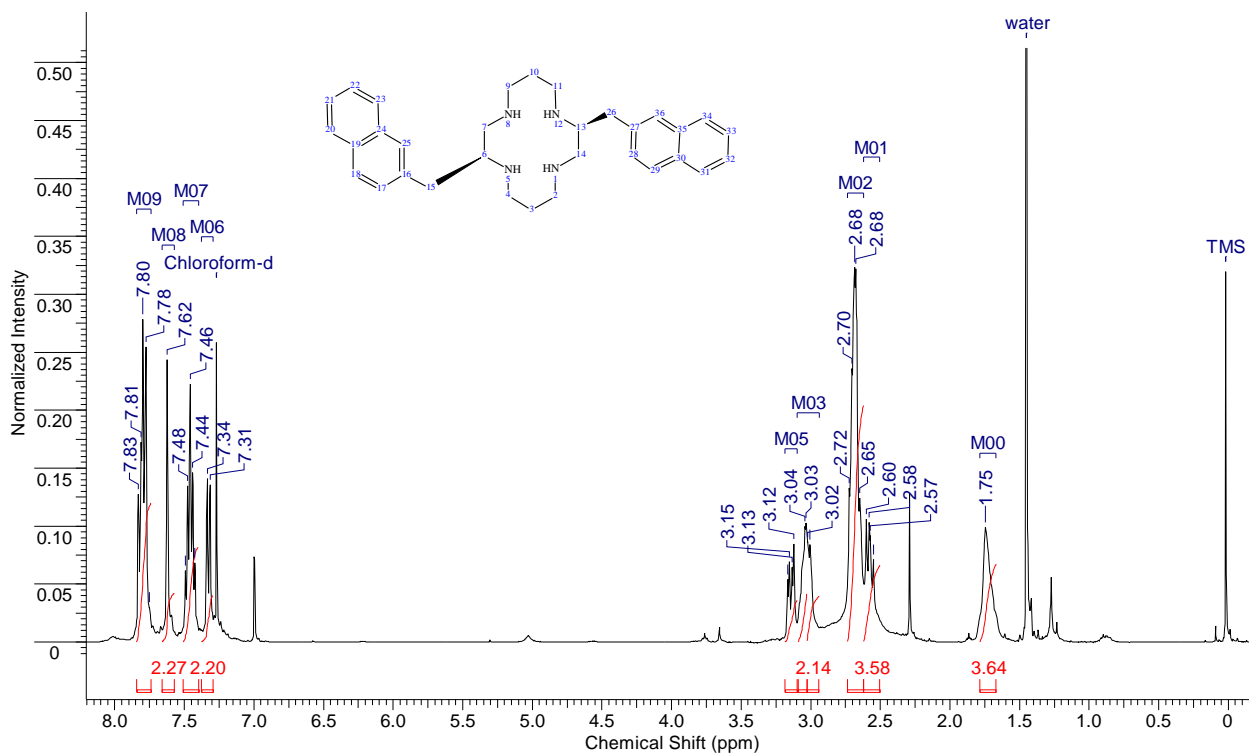
(a)
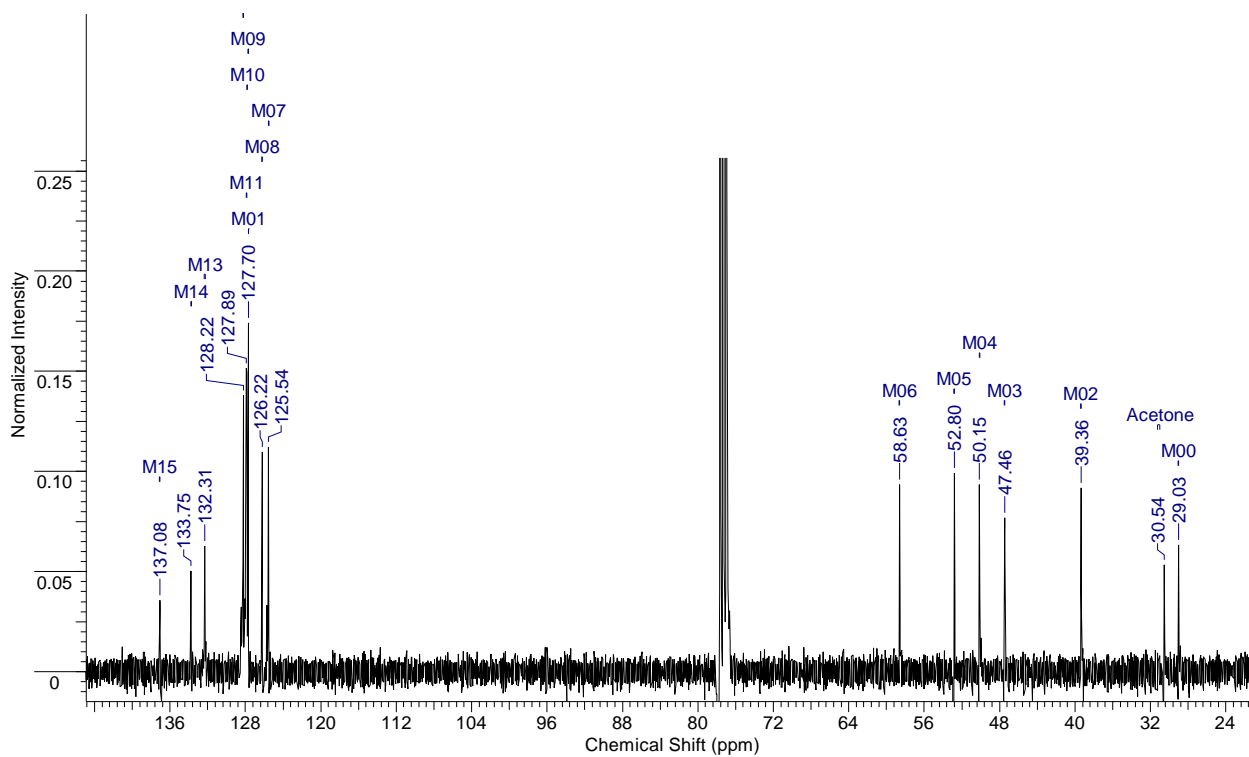
(b)

Figure A.57: - (a) ^{1}HNMR (b) ^{13}CNMR of 4.2c
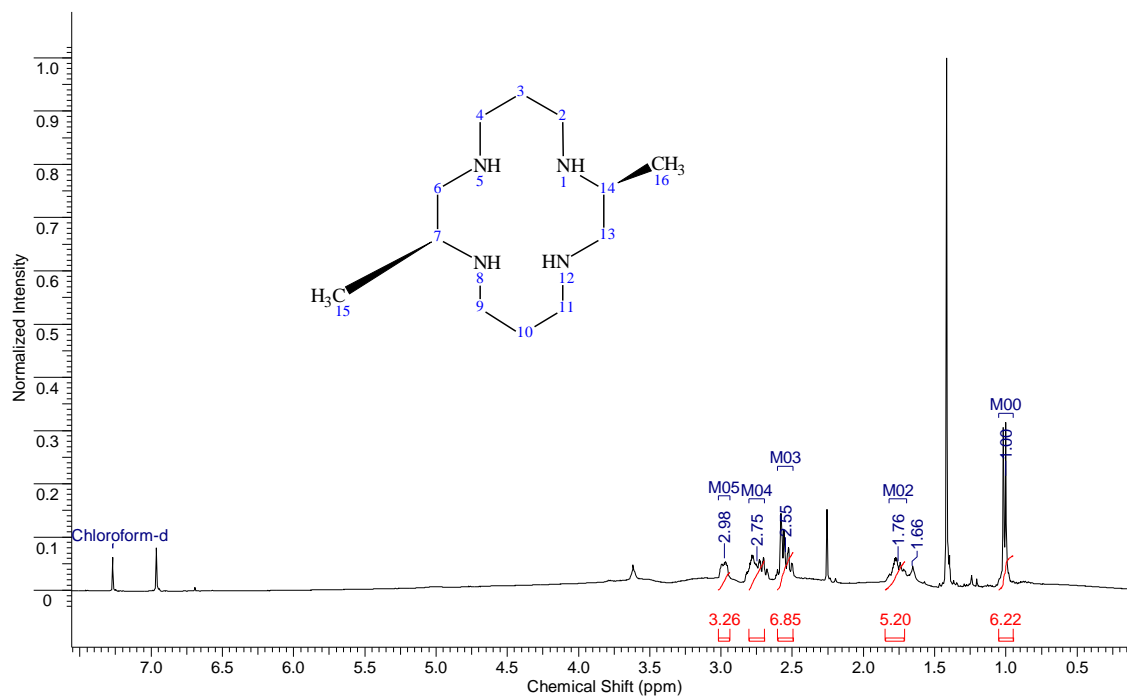
(a)
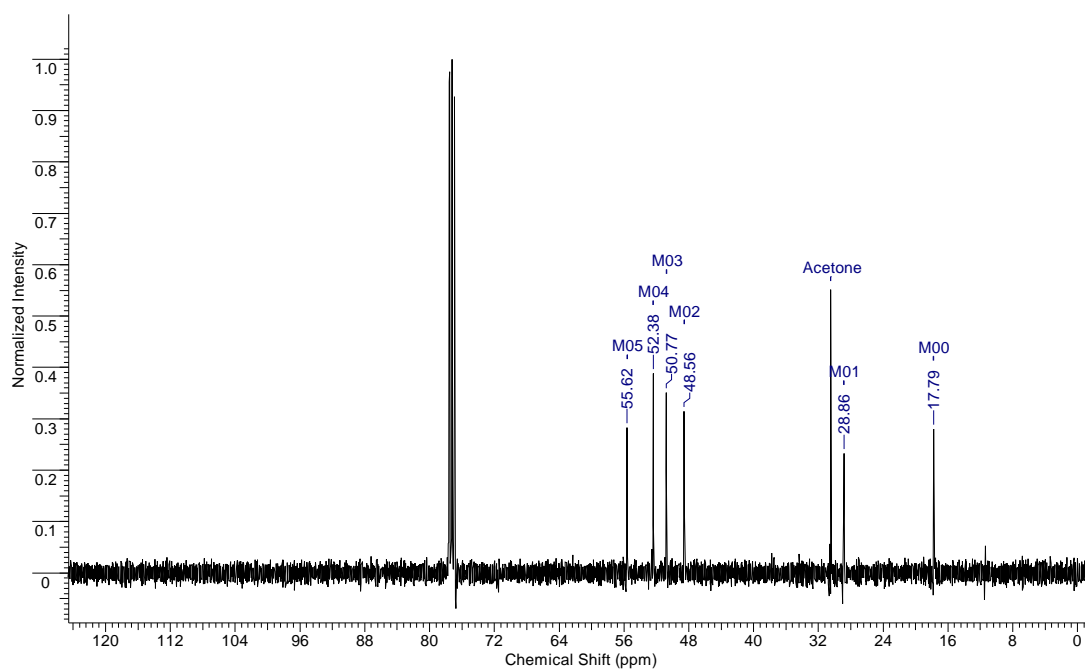
(b)

Appendix B - IR Data

Figure B.1: - IR of 1.6a
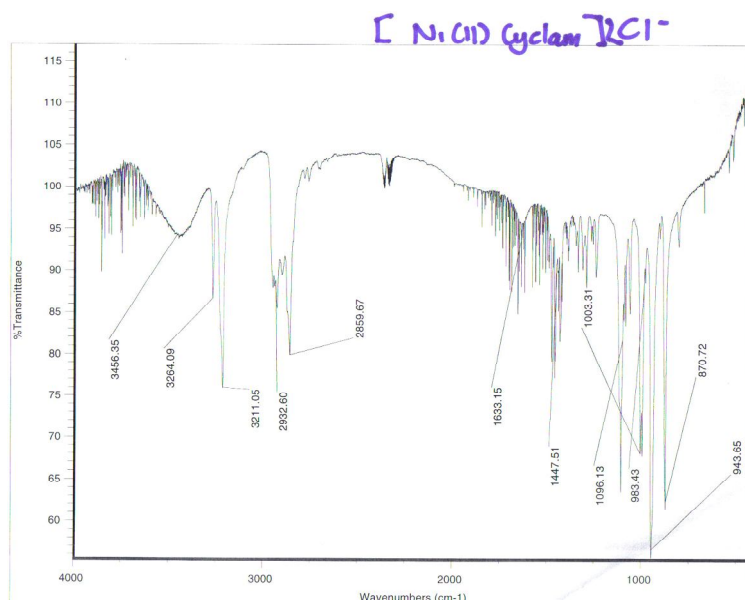
Figure B.2: - IR of 1.6d
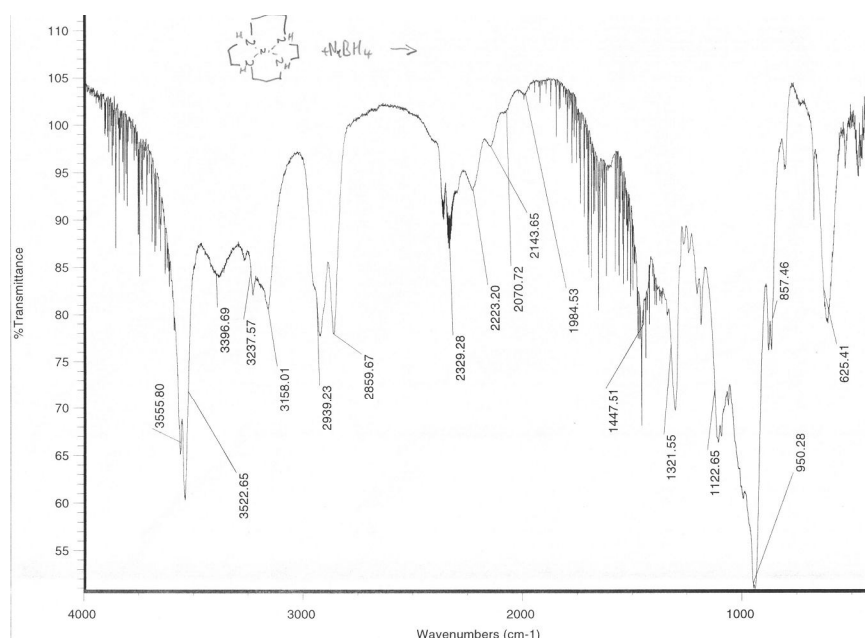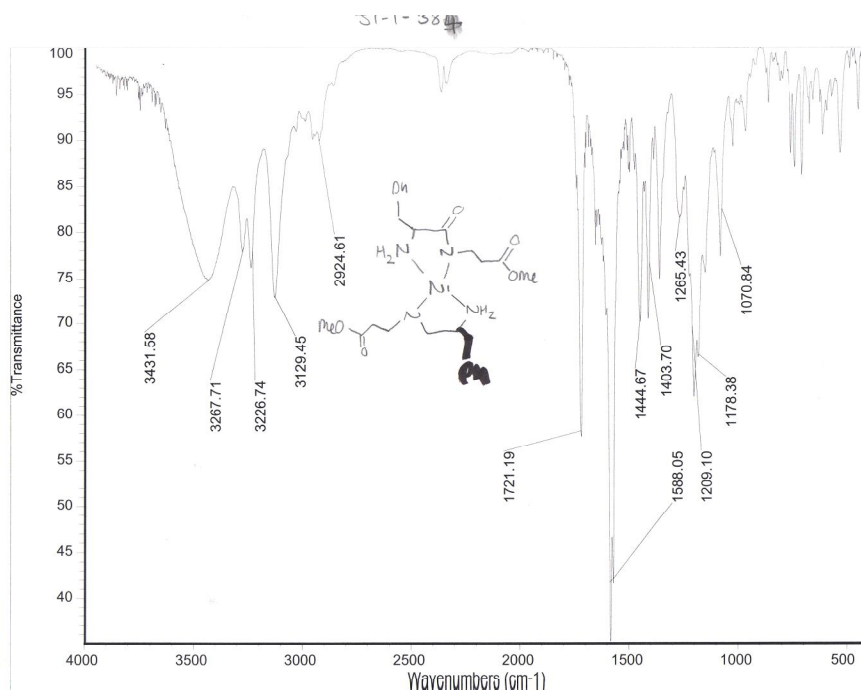
Figure B.3: - IR of 2.37a
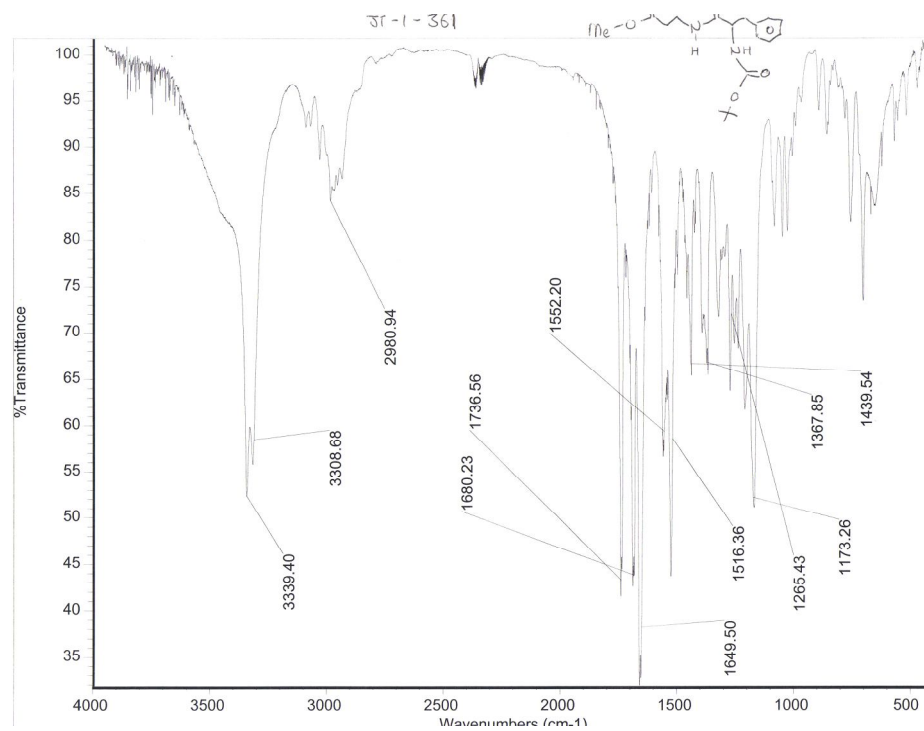
Figure B.4: - IR of 3.1a
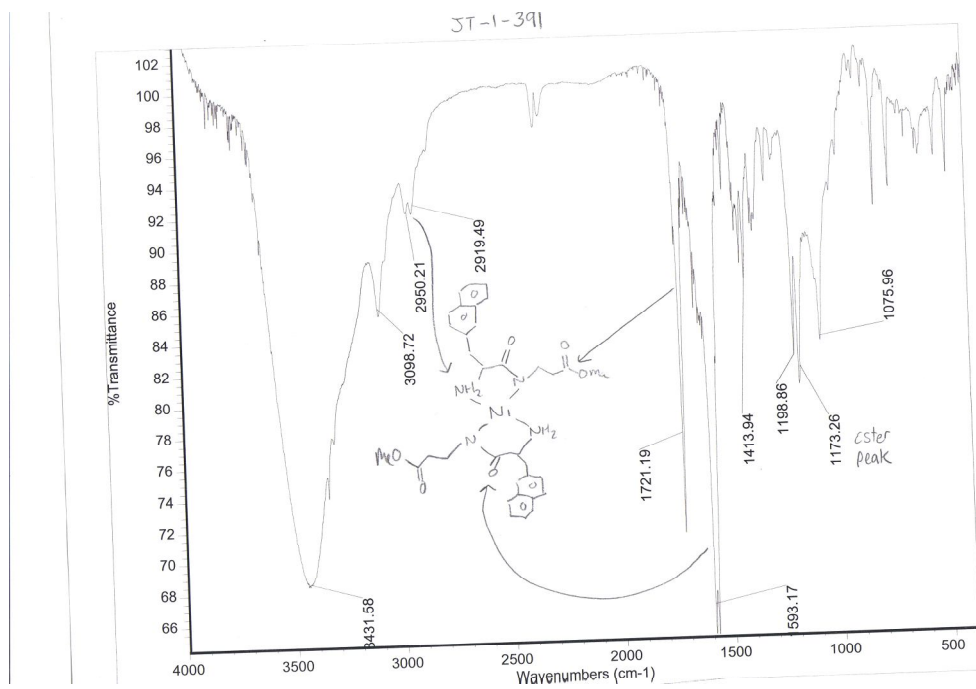
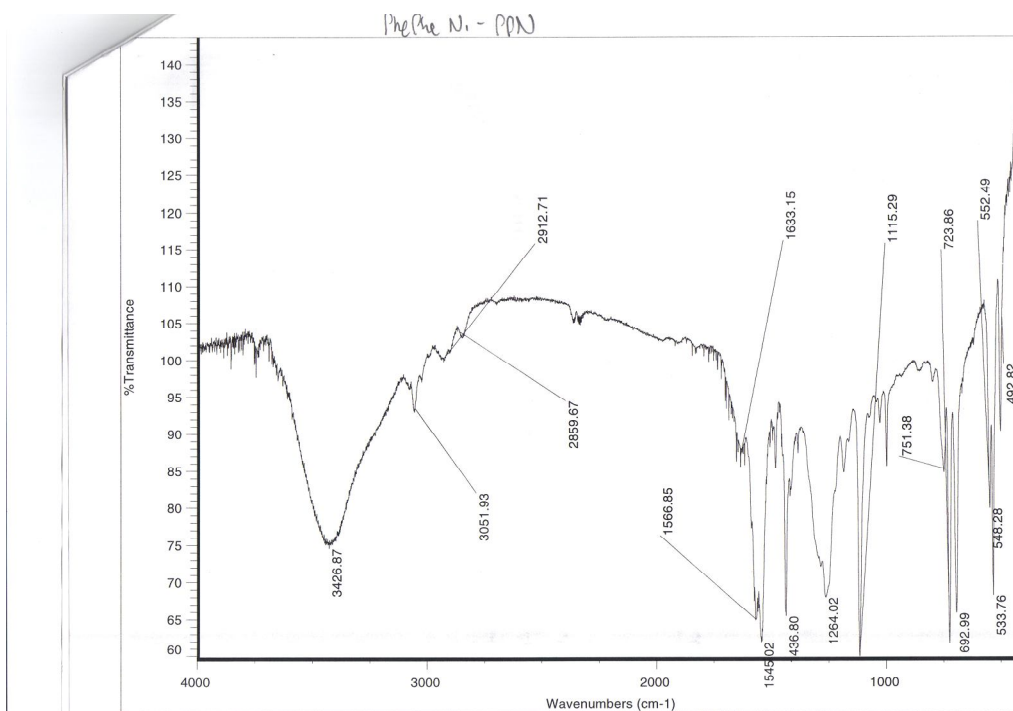**Figure B.5: - IR of 3.1c**

Figure B.6: - IR of 3.2a
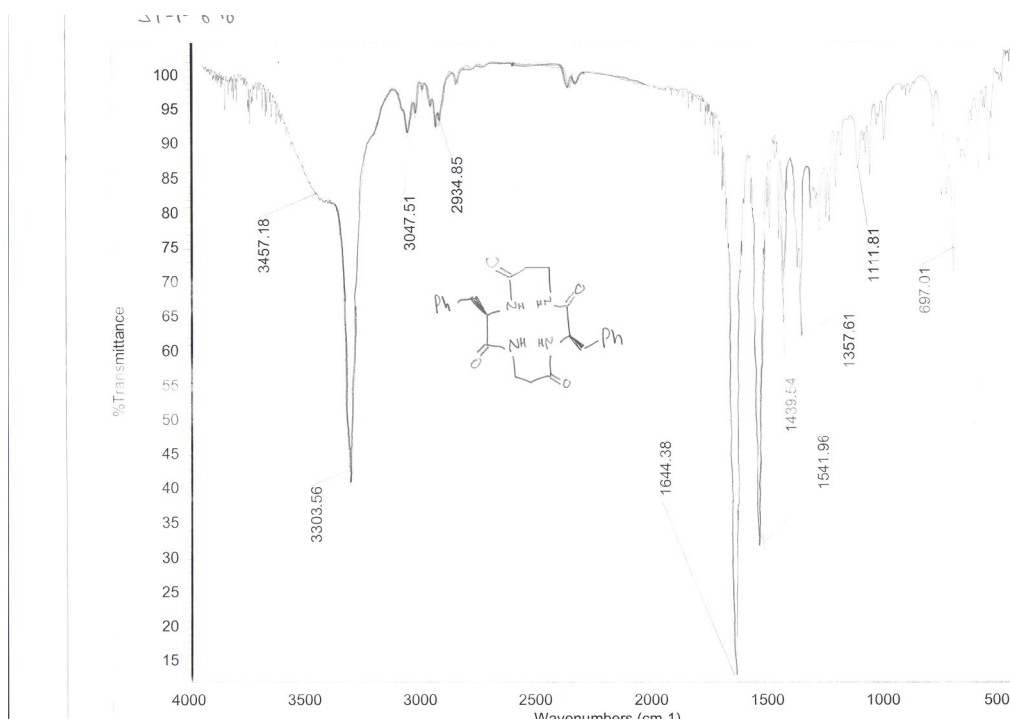
Figure B.7: - IR of 4.1a
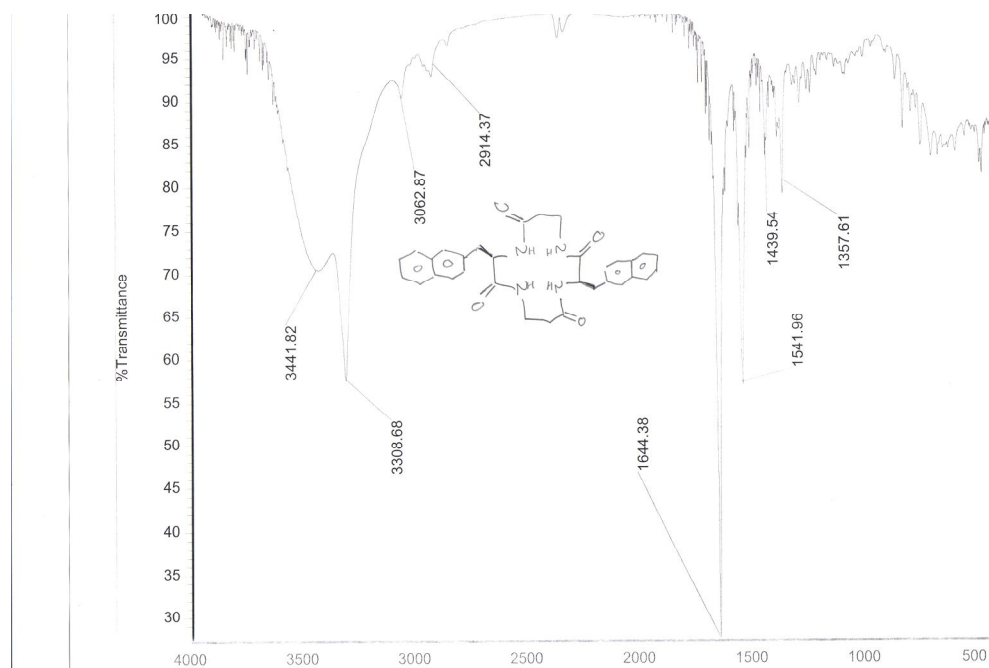

Figure B.8: - IR of 4.1b
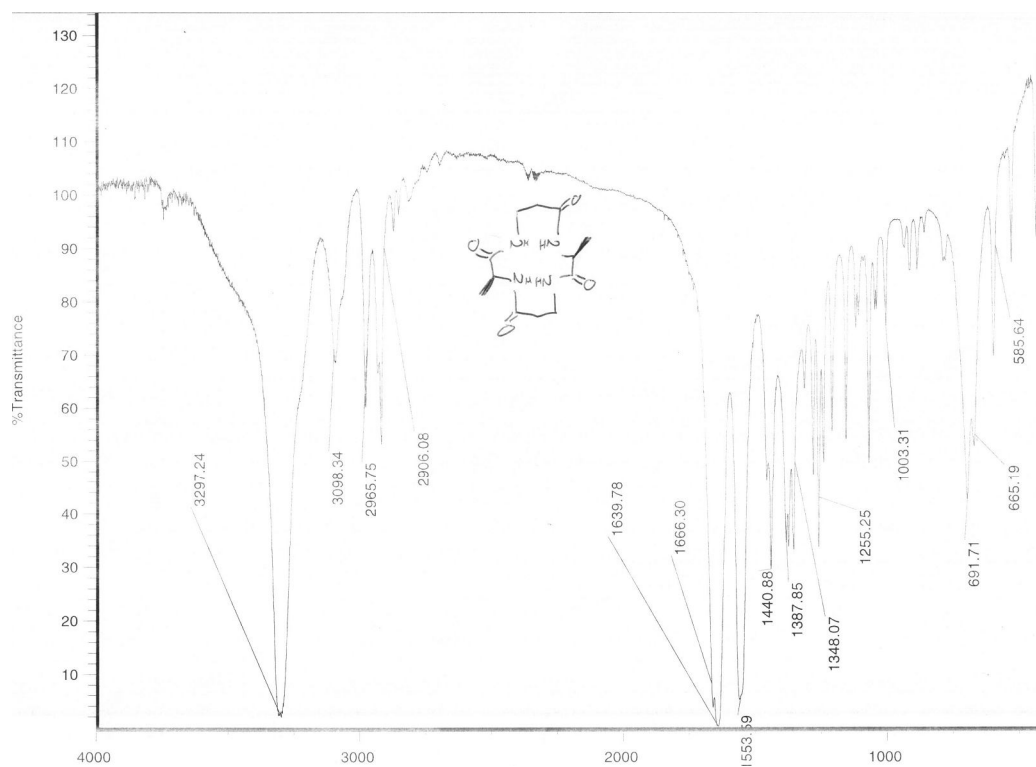
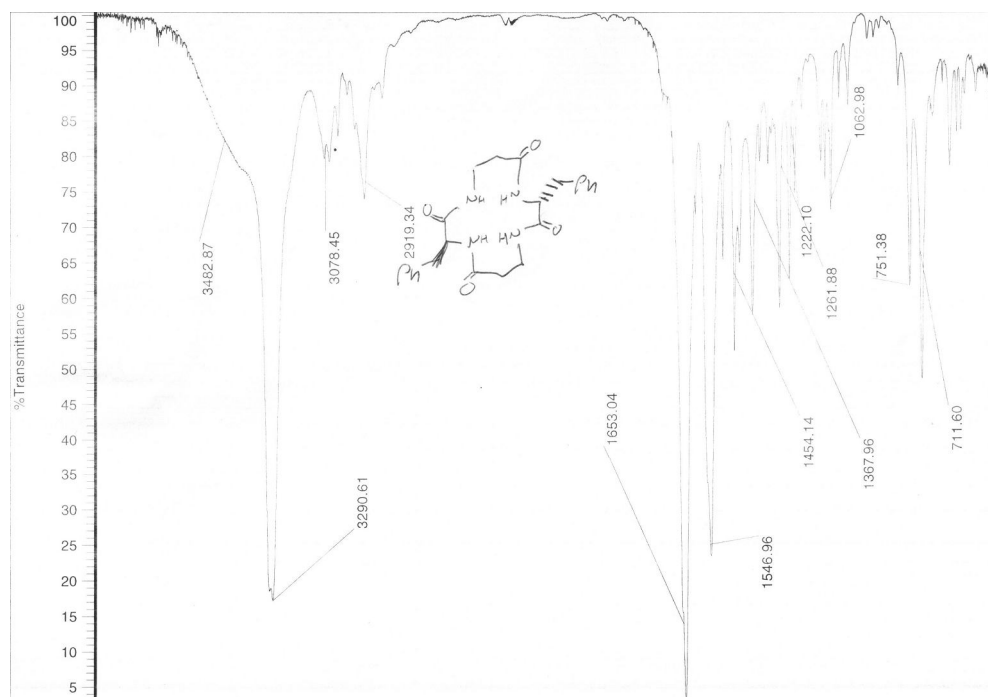**Figure B.9: - IR of 4.1c**

Figure B.10: - IR of 4.1d

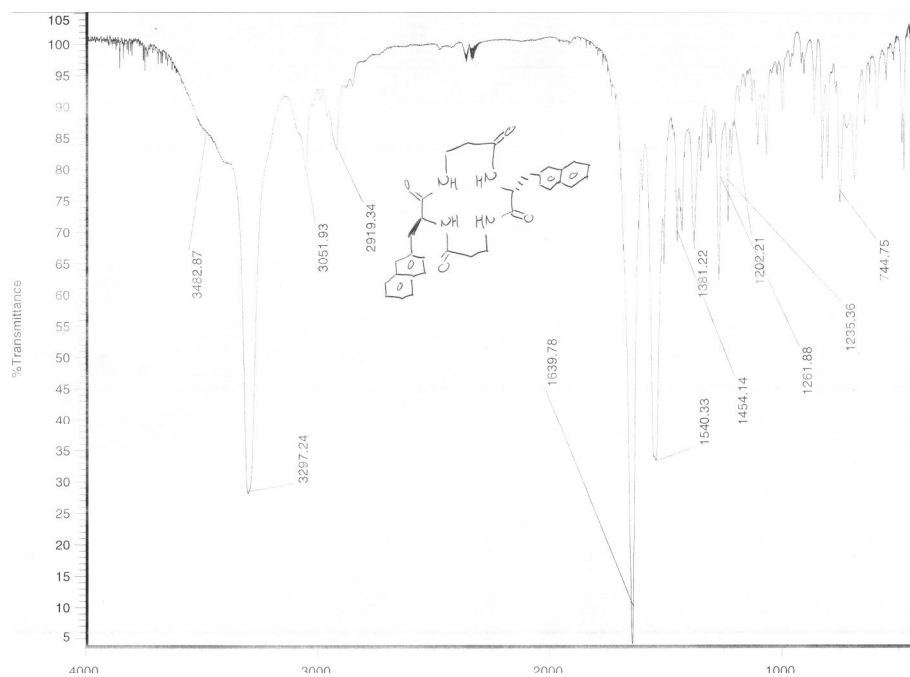**Figure B.11: - IR of 4.1e**

Figure B.12: - IR of 4.1g
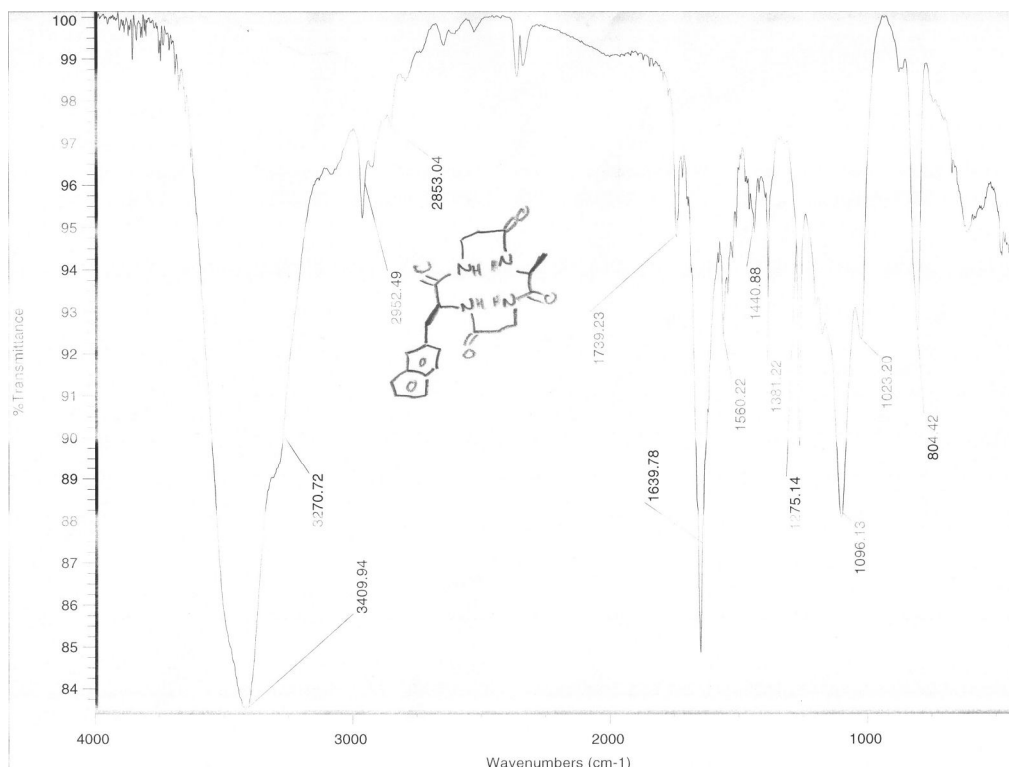
Figure B.13: - IR of 4.1h
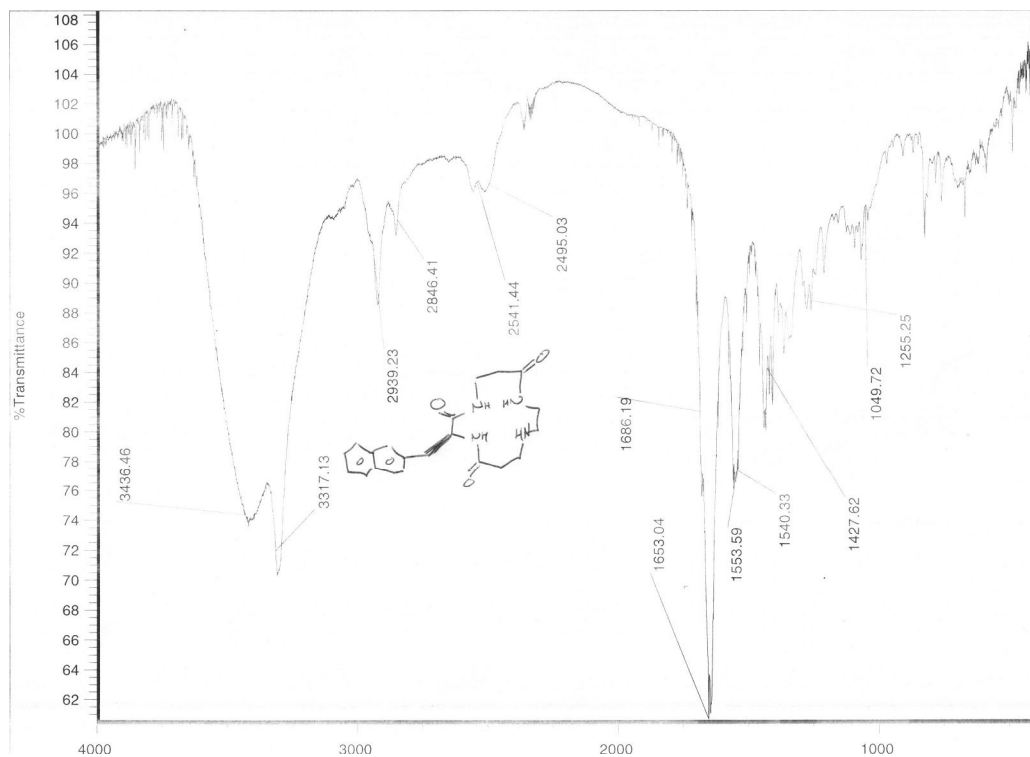
Figure B.14: - IR of 1.3
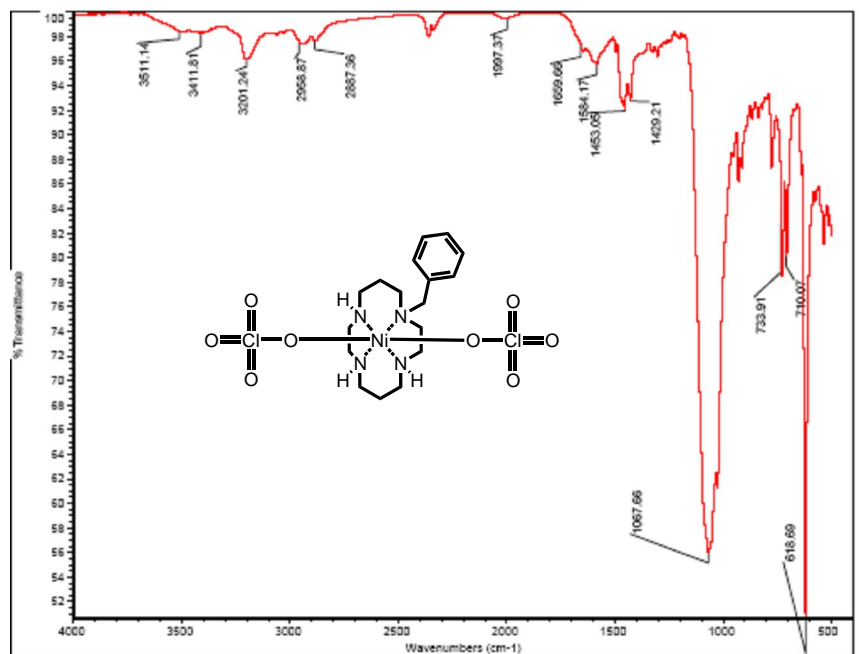
Figure B.15: - IR of 1.5
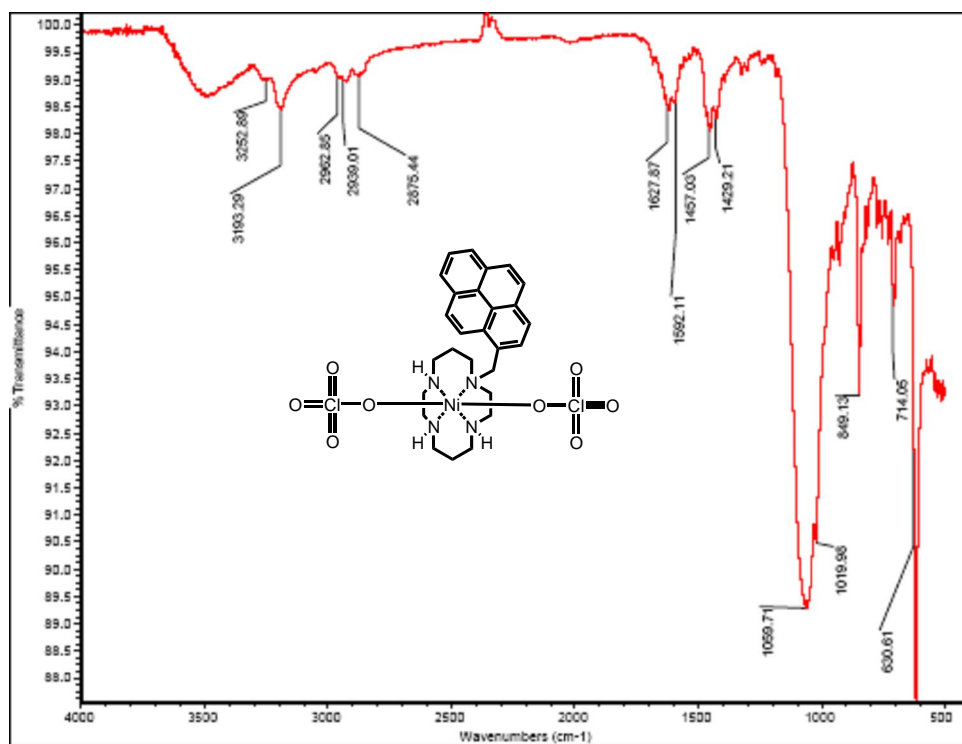
Figure B.16: - IR of 4.4a
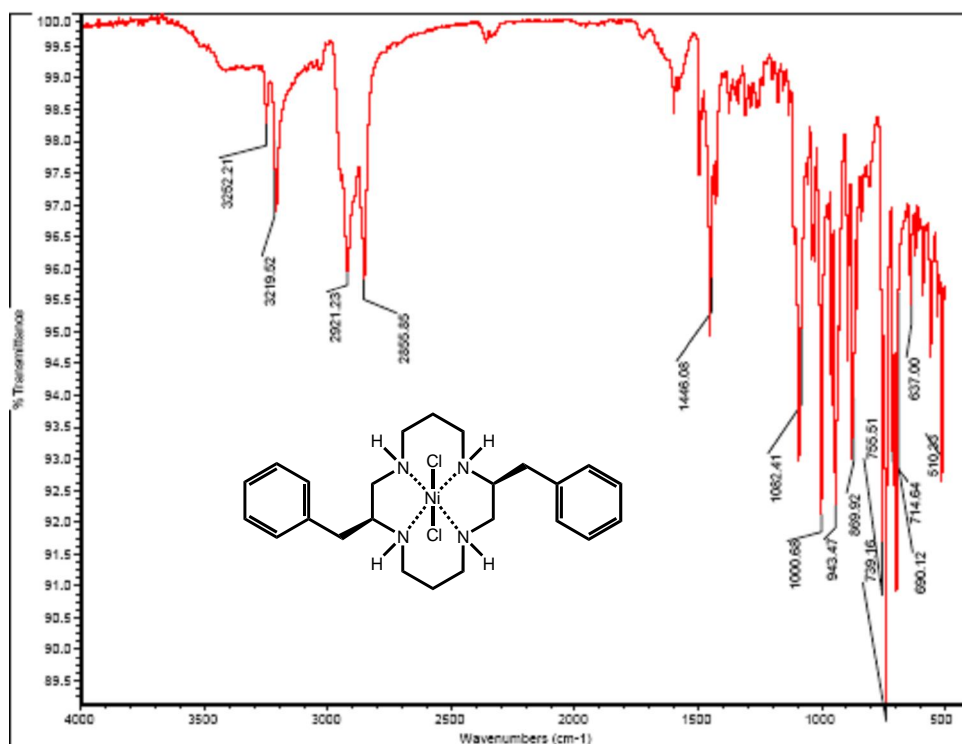
Figure B.17: - IR of 4.4b
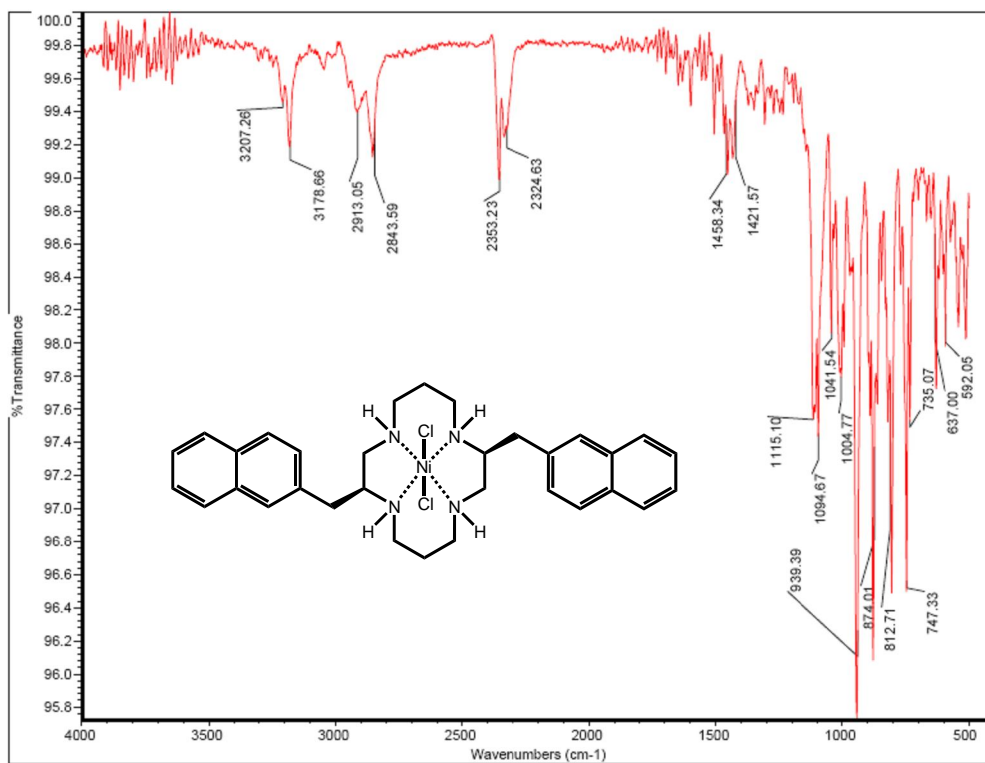
Figure B.18: - IR of 4.3a
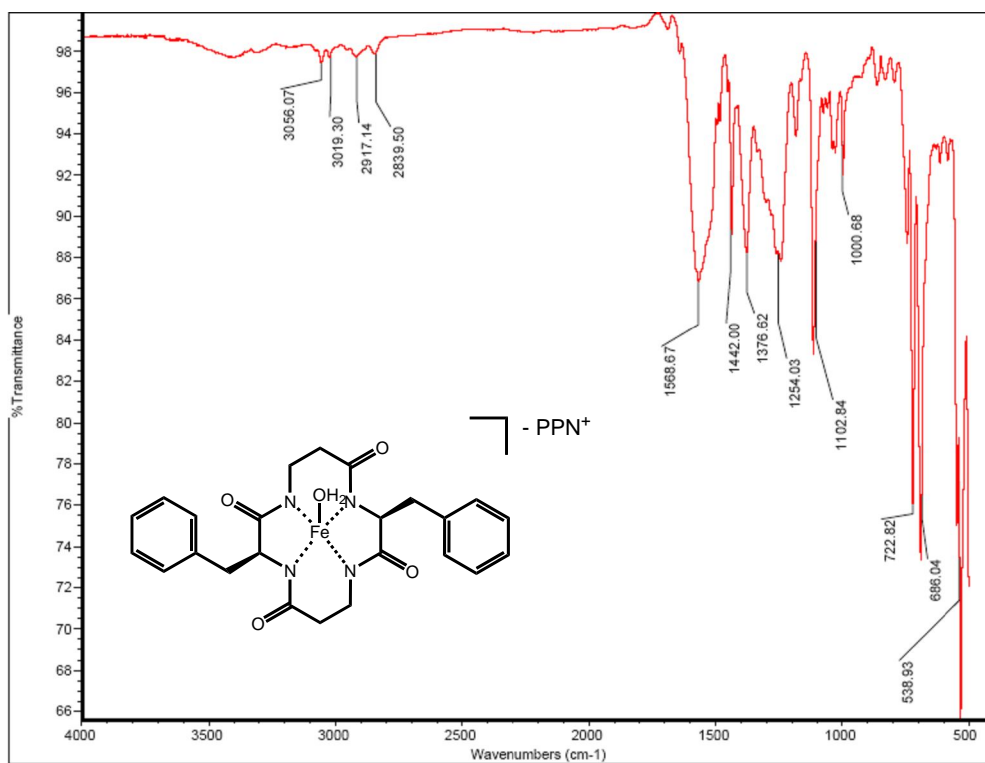
Figure B.19: - IR of 4.3b
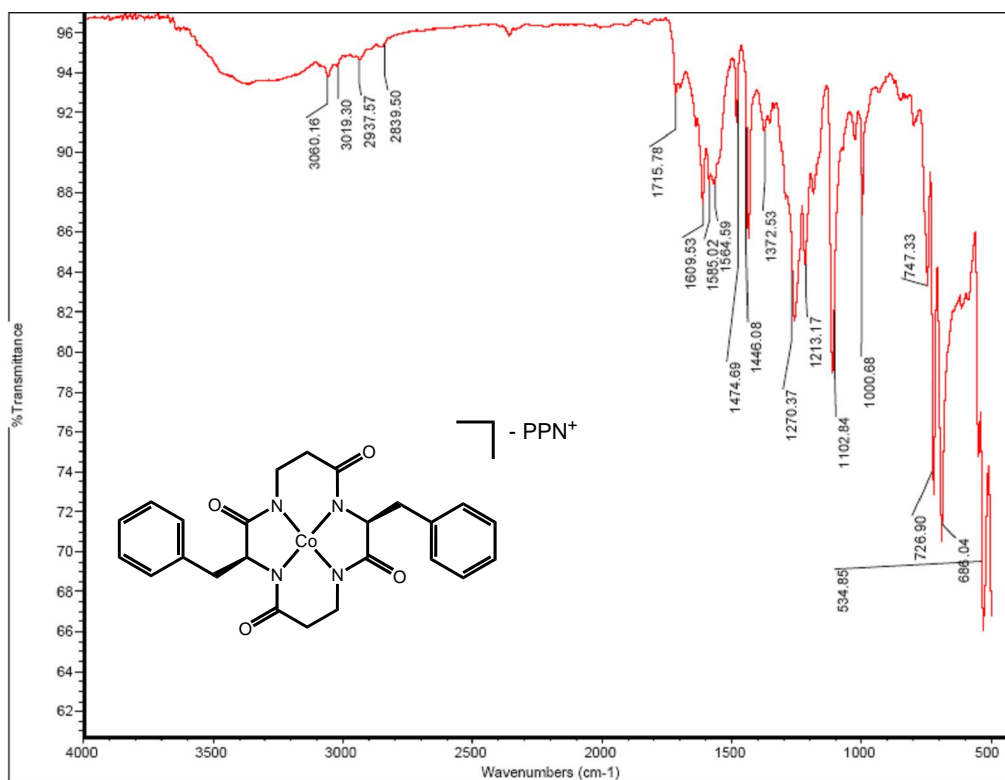
Appendix C - Mass Spectrum Data.

Figure C.1: - Mass spectrum of 1.6a
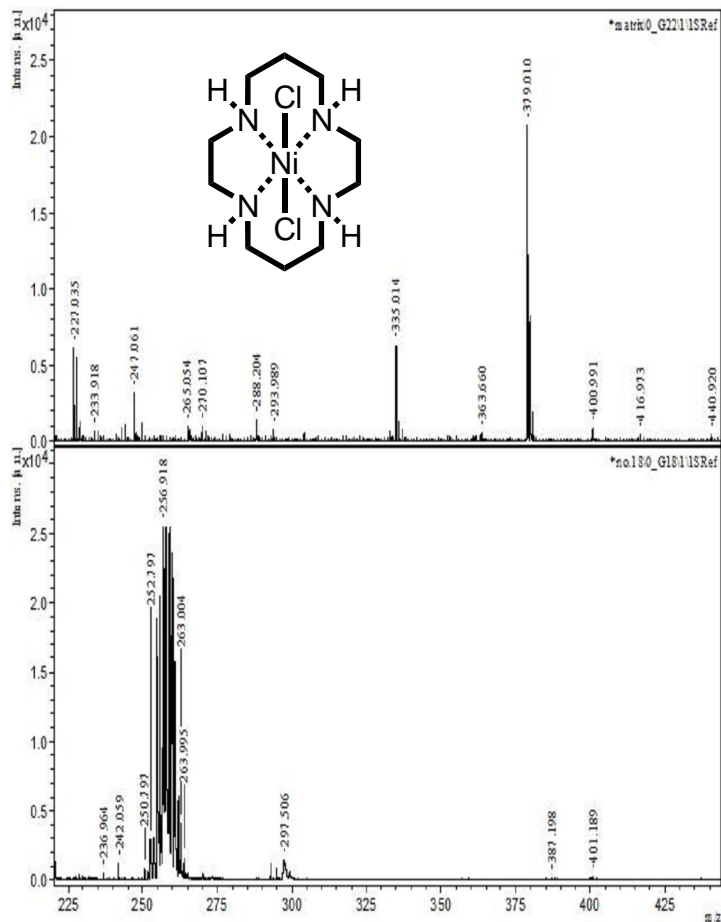
Figure C.2: - Mass spectrum of 1.3
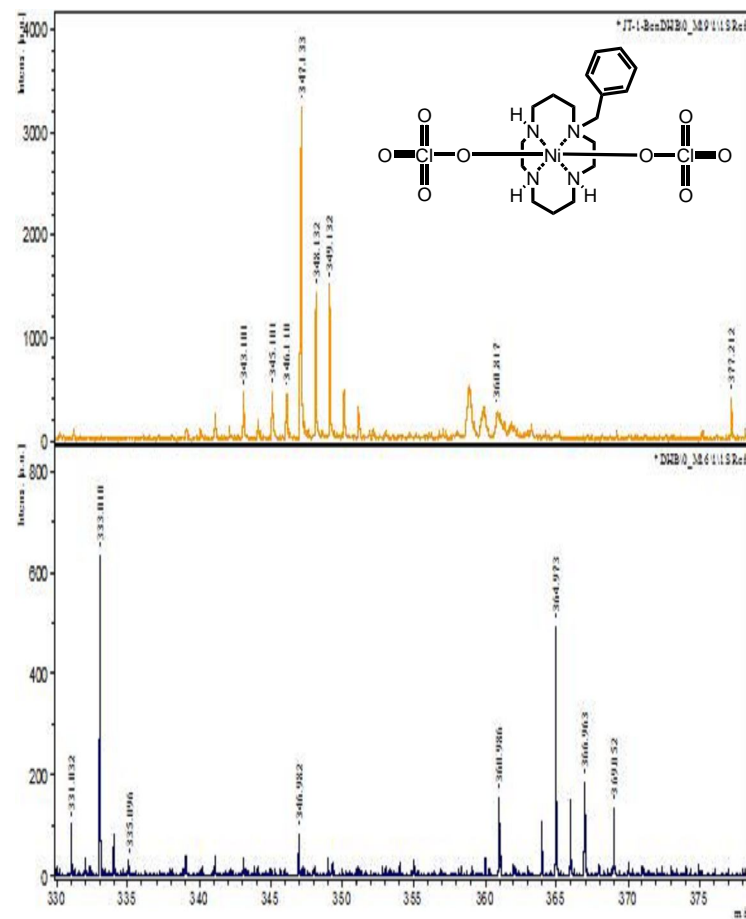
Figure C.3: - Mass spectrum of 1.4
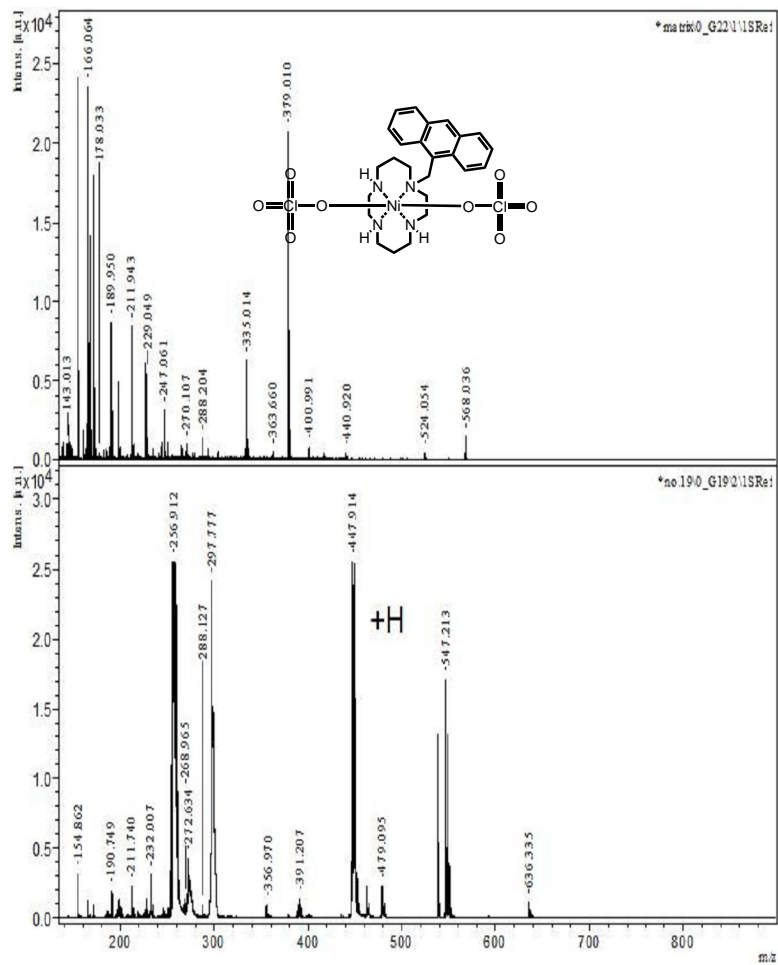
Figure C.4: - Mass spectrum of 1.5
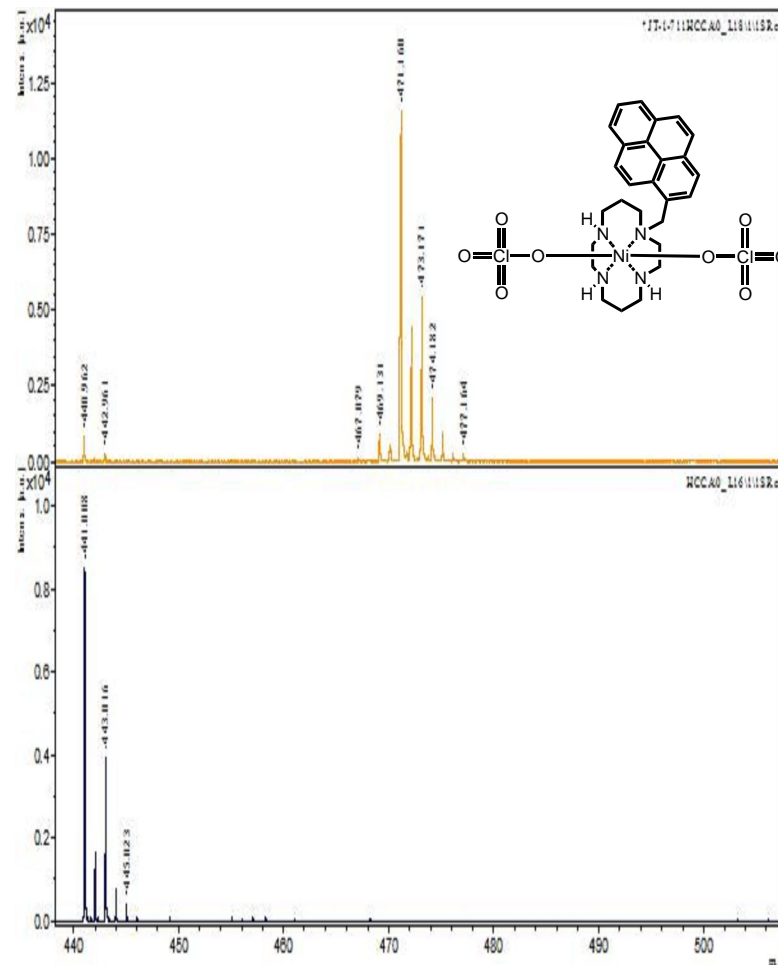
Figure C.5: - Mass spectrum of 2.37a
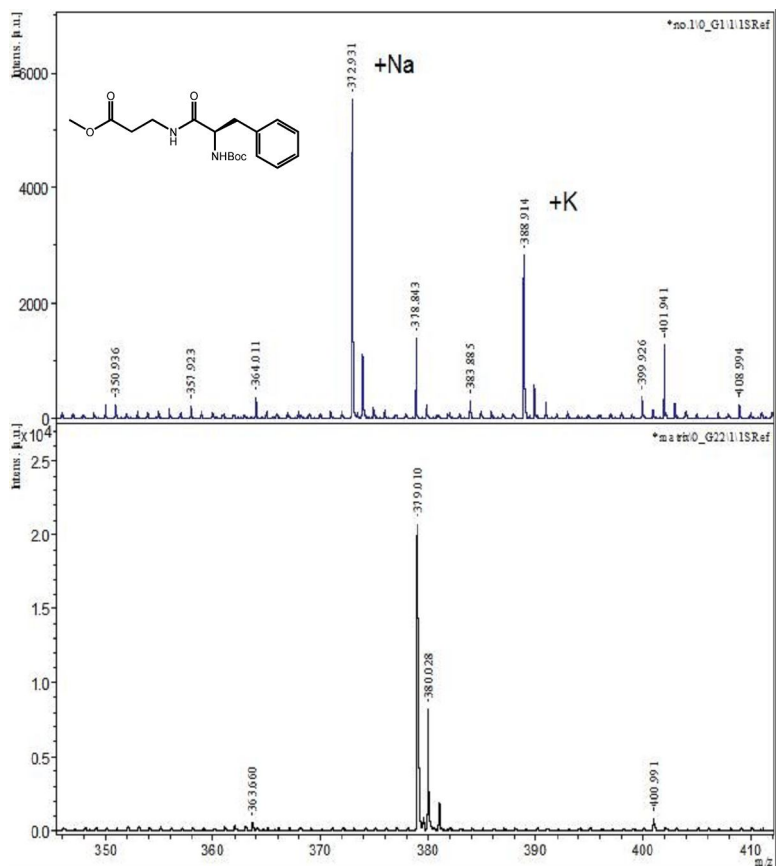
Figure C.6: - Mass spectrum of 2.37b
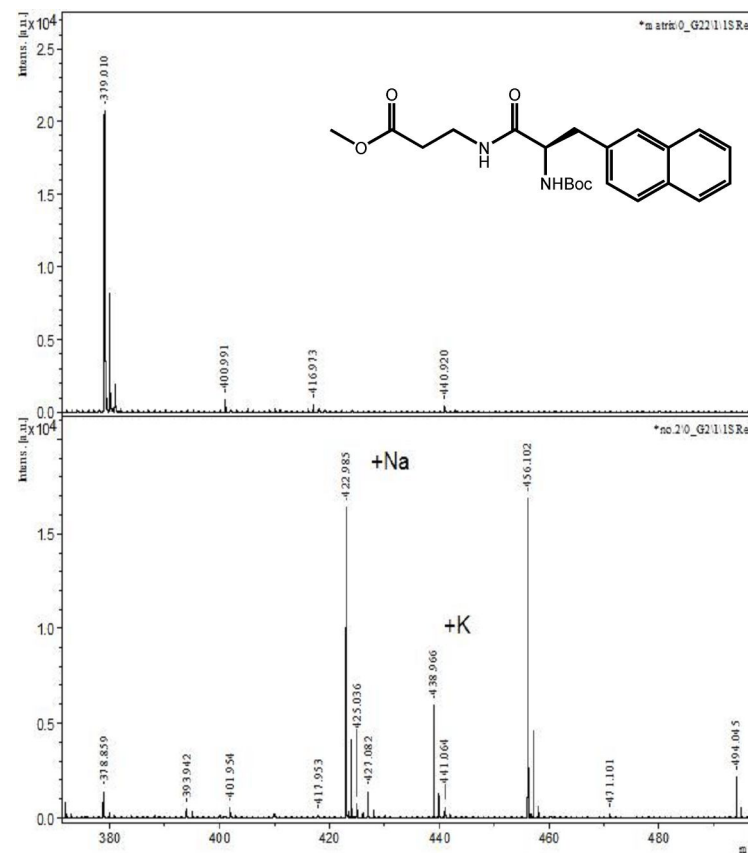
Figure C.7: - Mass spectrum of 2.37e
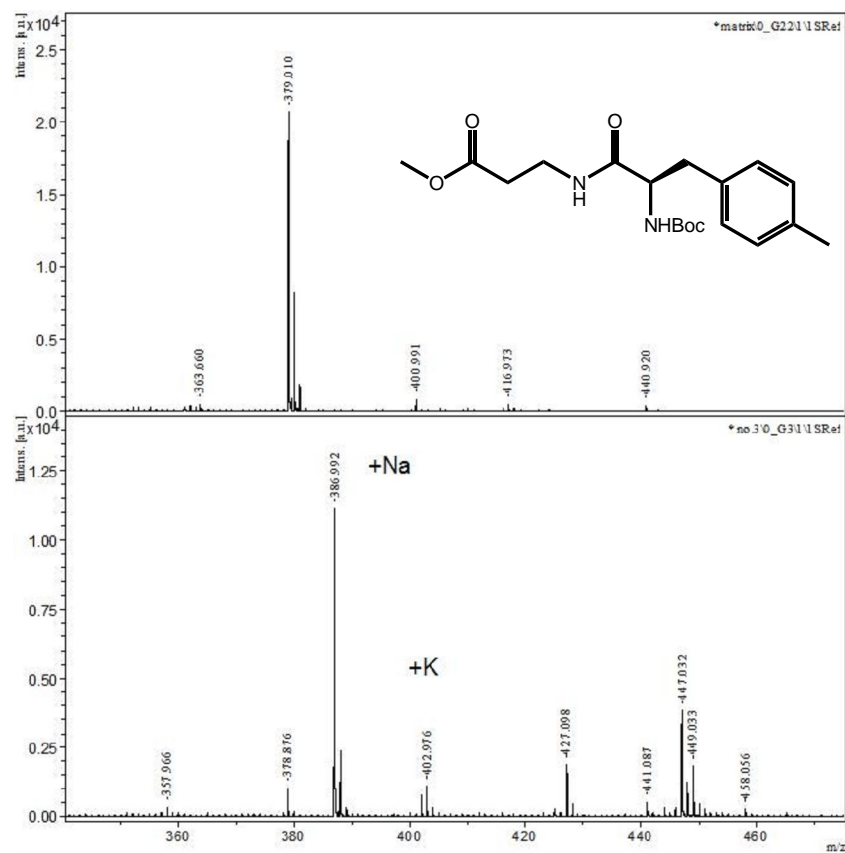
Figure C.8: - Mass spectrum of 2.37f
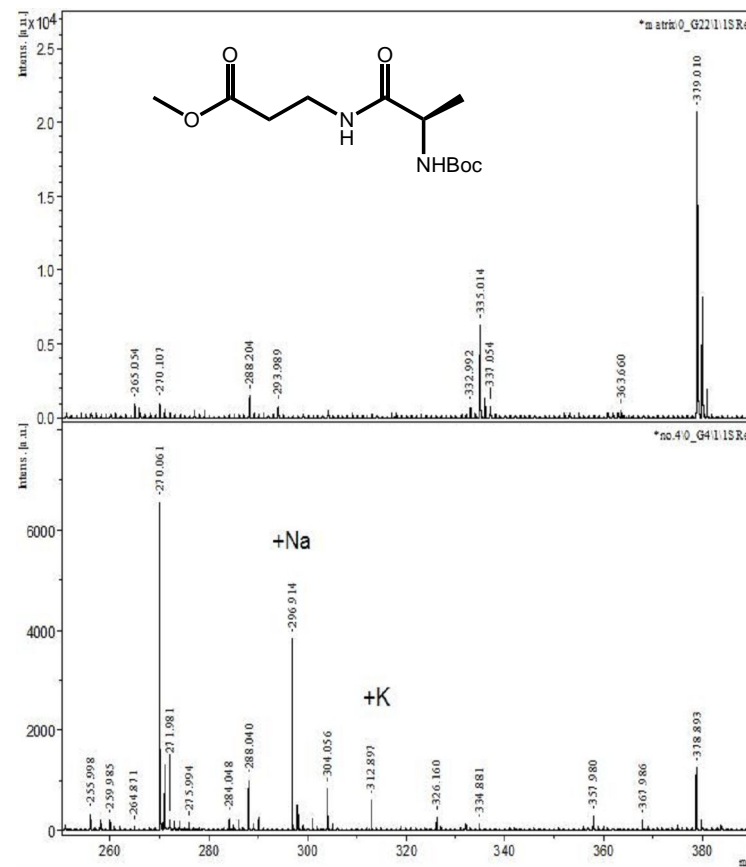
Figure C.9: - Mass spectrum of 2.29a
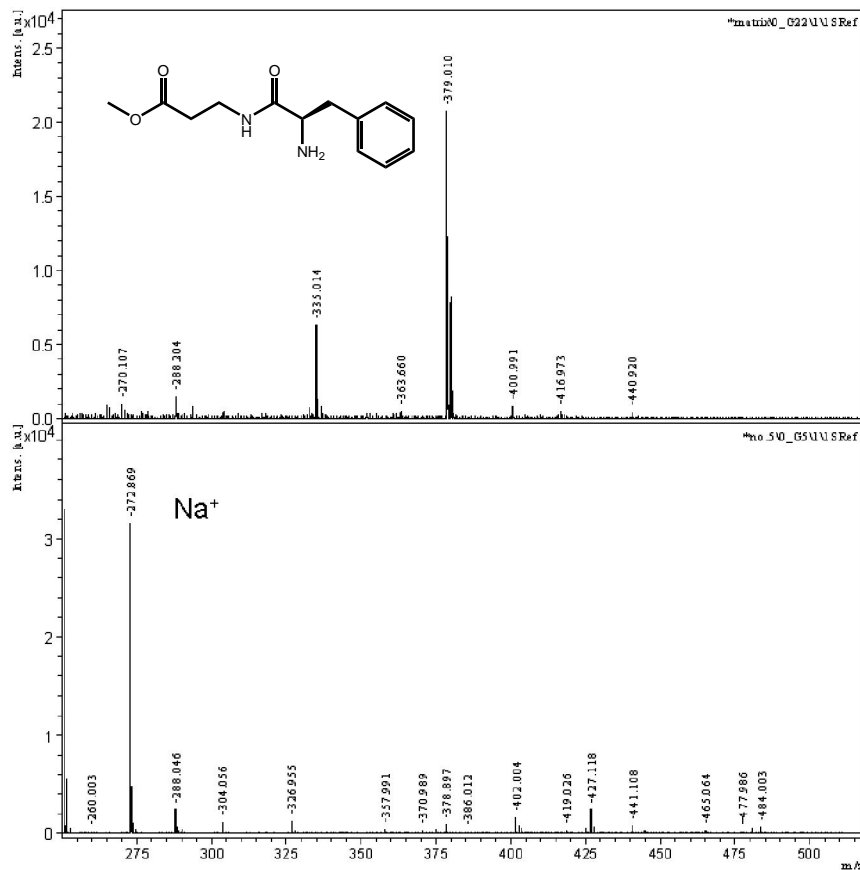
Figure C.10: - Mass spectrum of 2.29b
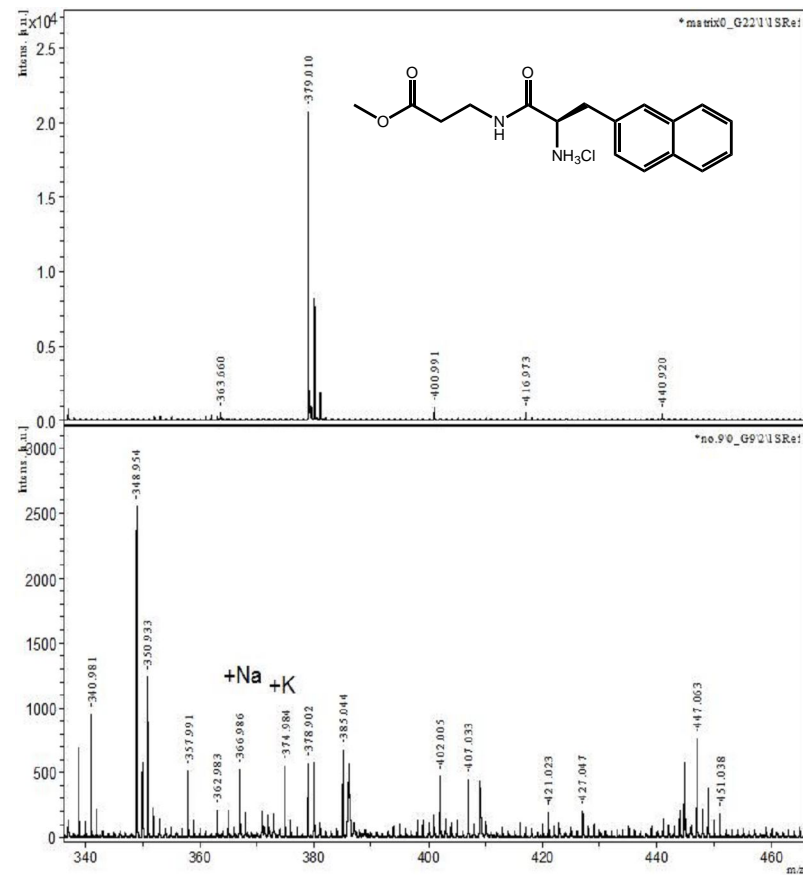
Figure C.11: - Mass spectrum of 2.38a
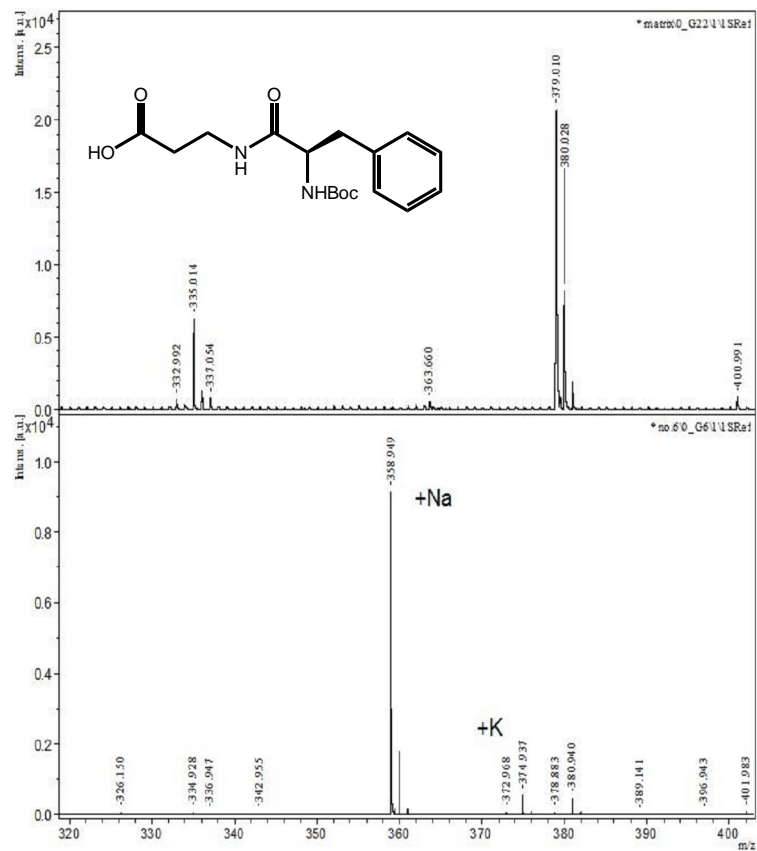
Figure C.12: - Mass spectrum of 2.38b
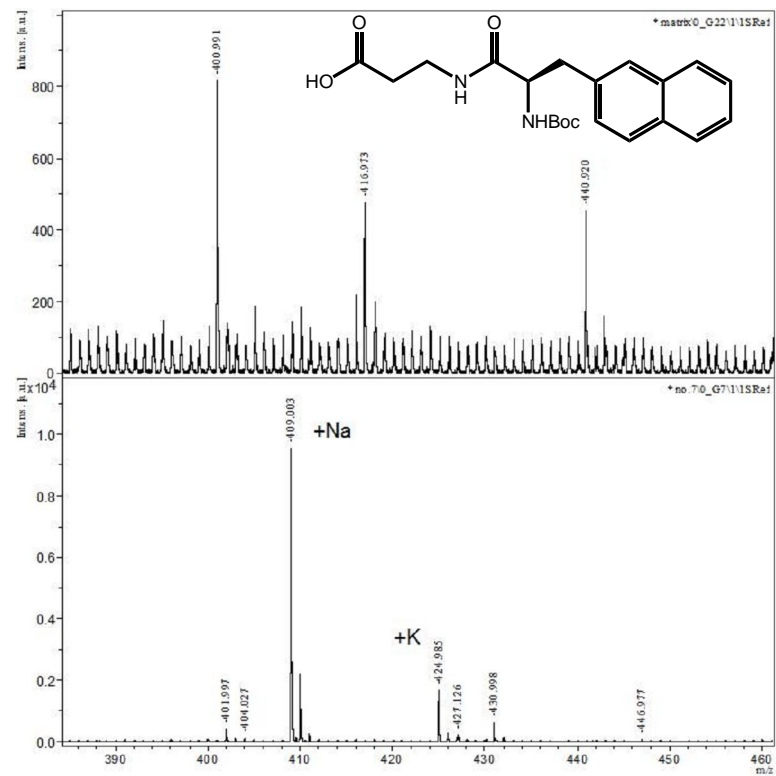
Figure C.13: - Mass spectrum of 2.39a

Figure C.14: - Mass spectrum of 2.39g
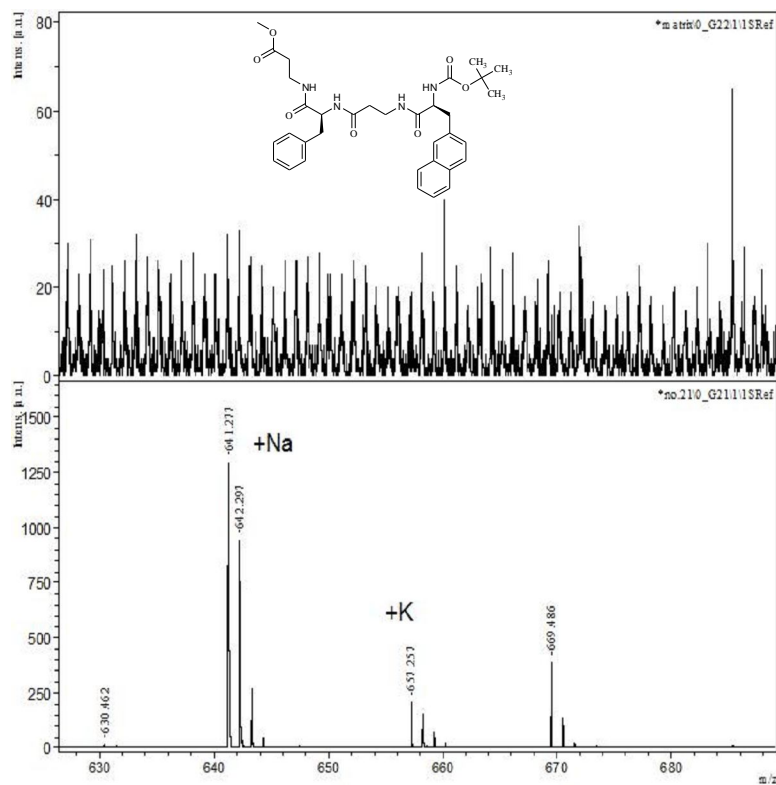
Figure C.15: - Mass spectrum of 2.34a
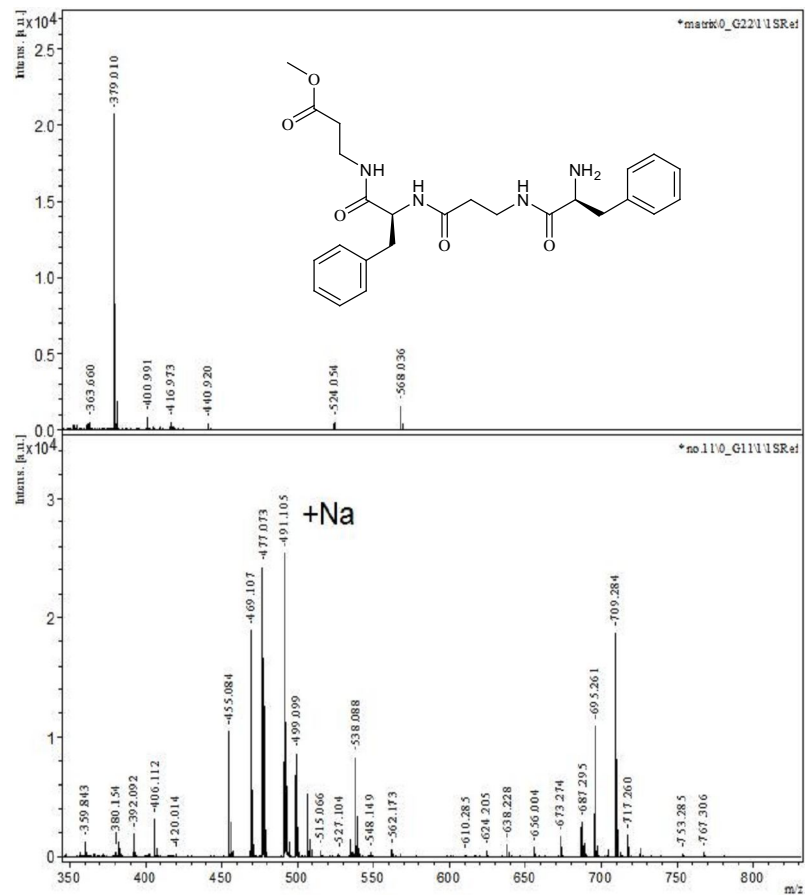
Figure C.16: - Mass spectrum of 2.34c
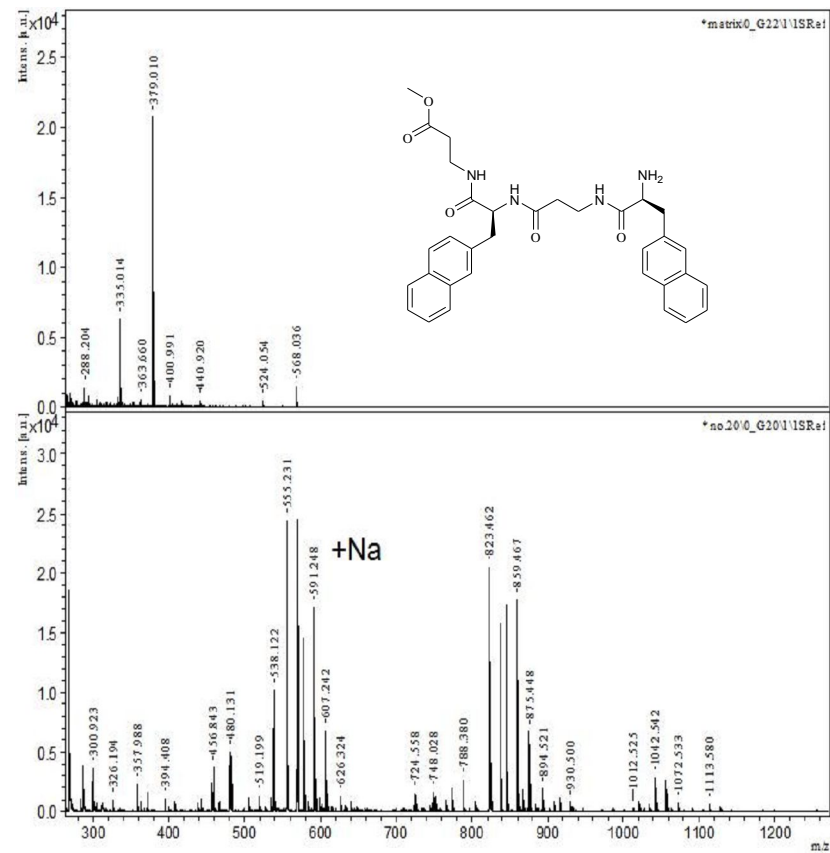
Figure C.17: - Mass spectrum of 2.34d
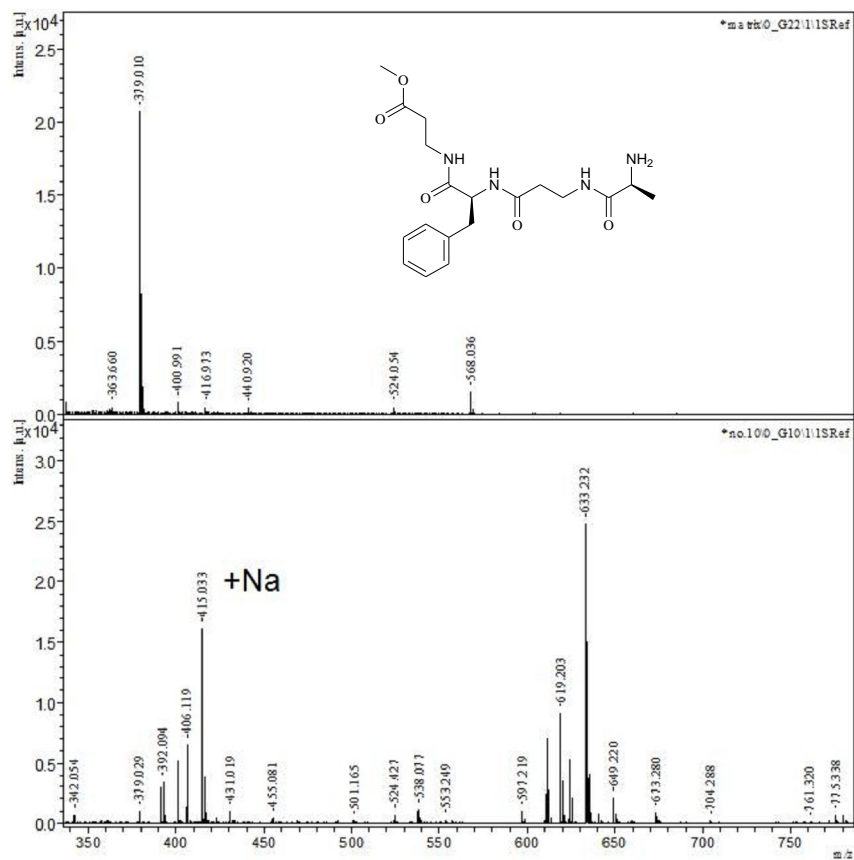
Figure C.18: - Mass spectrum of tripeptide
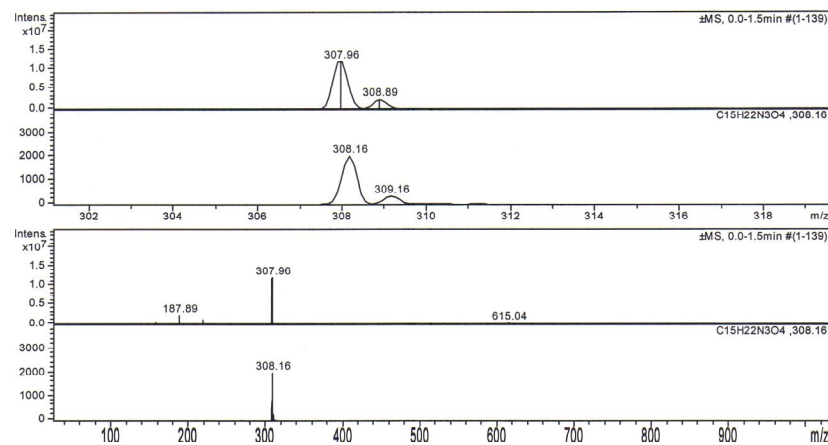
Figure C.19: - Mass spectrum of 2.40a
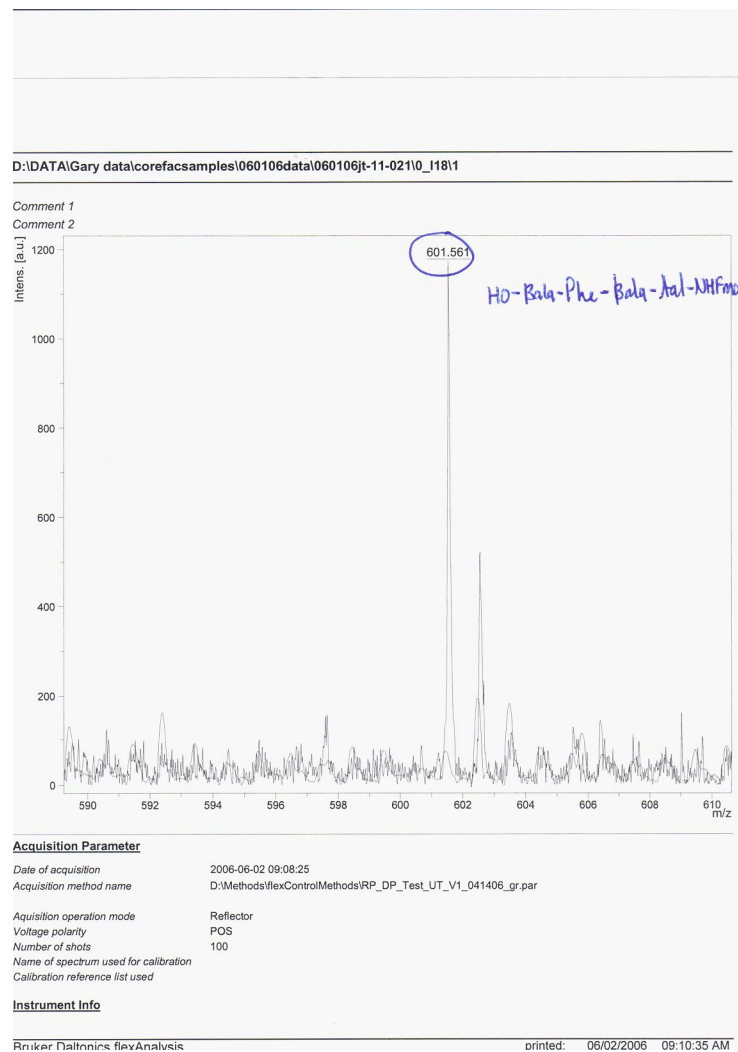
Figure C.20: - Mass spectrum of 2.40b
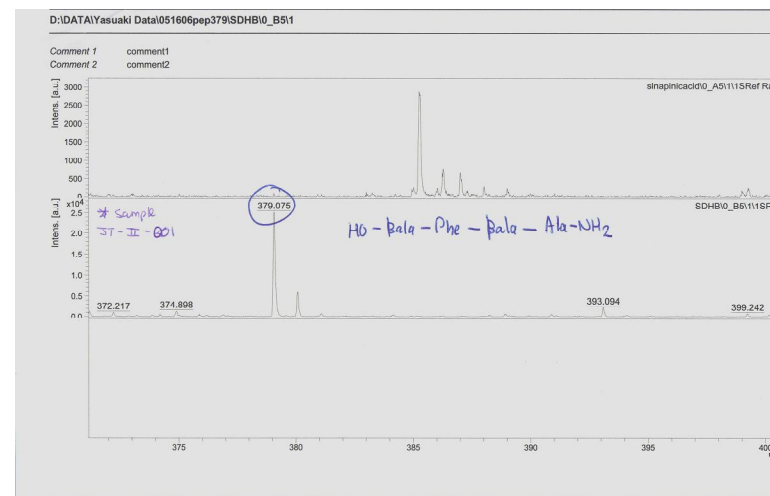
Figure C.21: - Mass spectrum of 2.40c
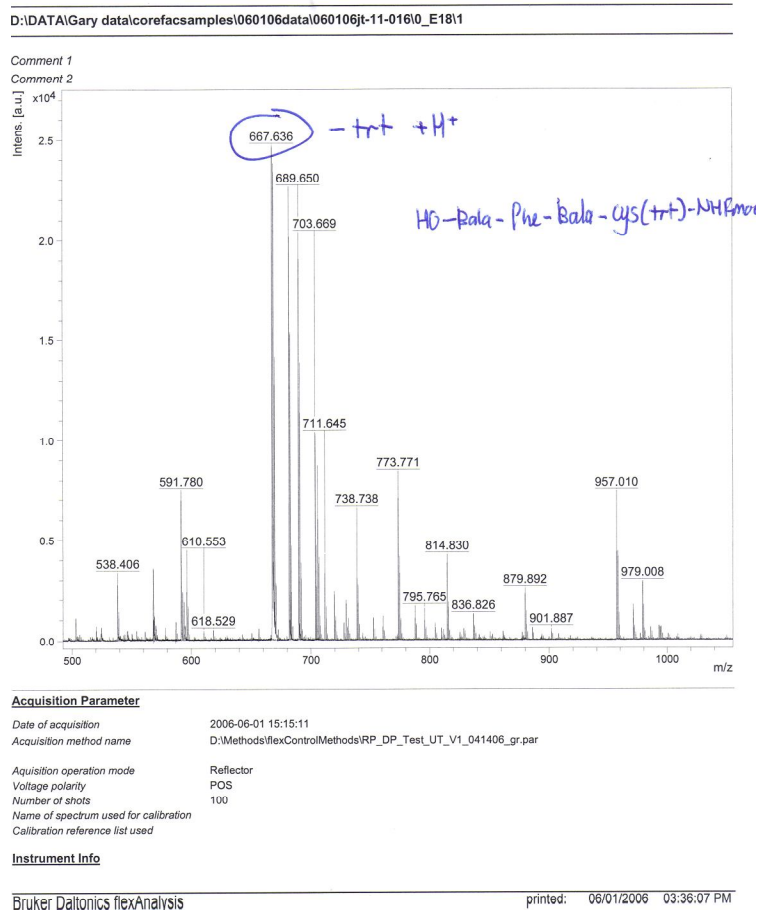
Figure C.22: - Mass spectrum of 2.40d
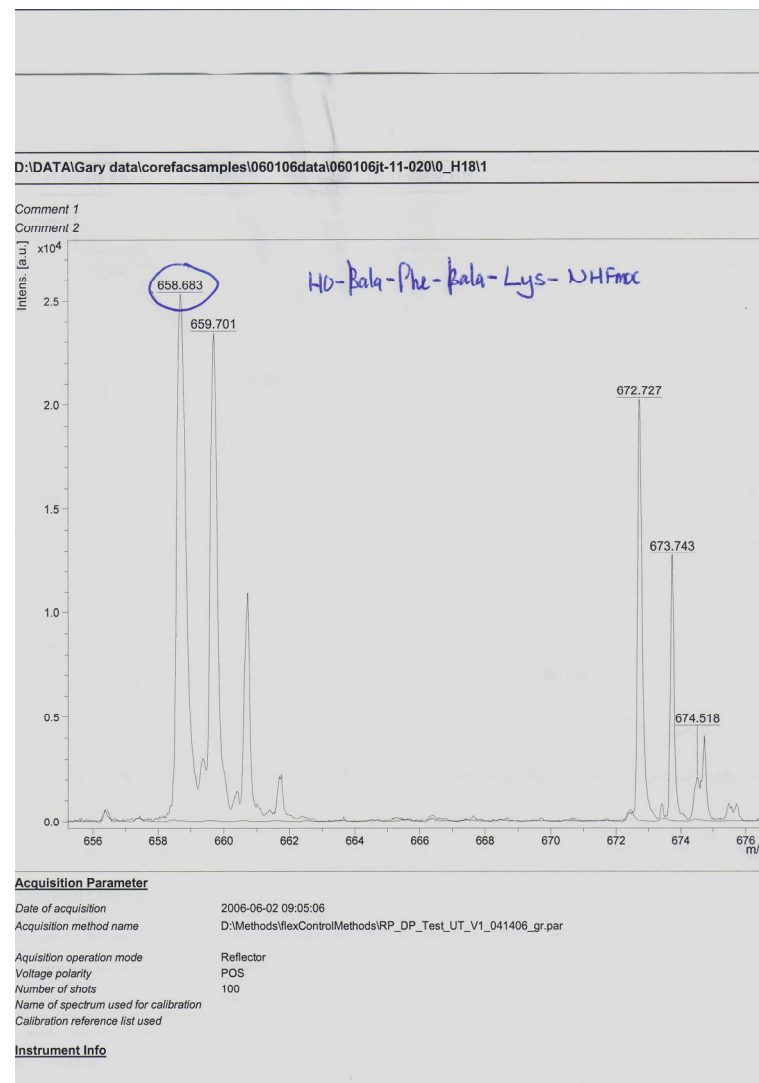
Figure C.23: - Mass spectrum of 2.40e
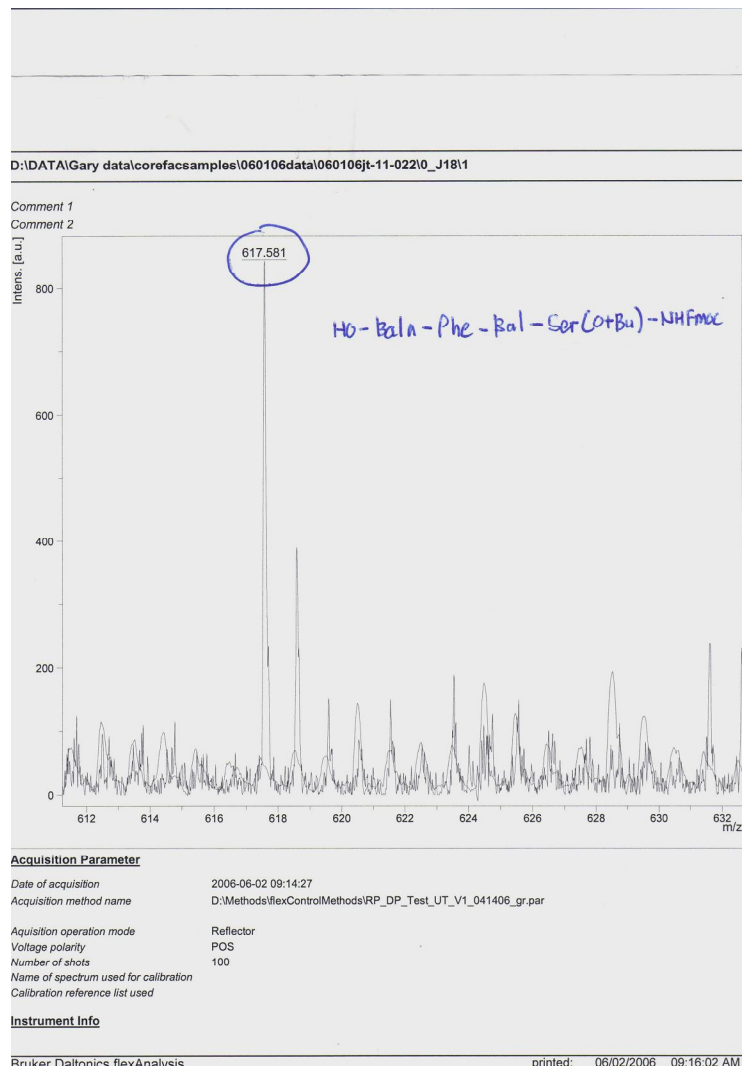
Figure C.24: - Mass spectrum of 2.40f
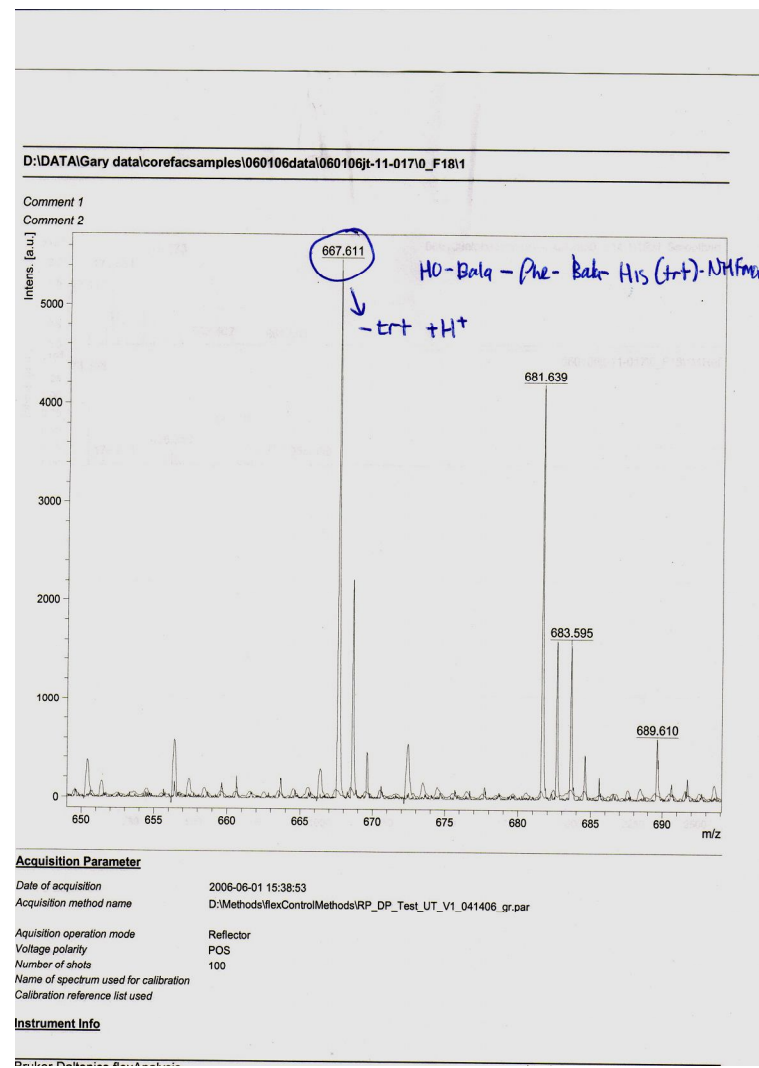
Figure C.25: - Mass spectrum of 2.40g
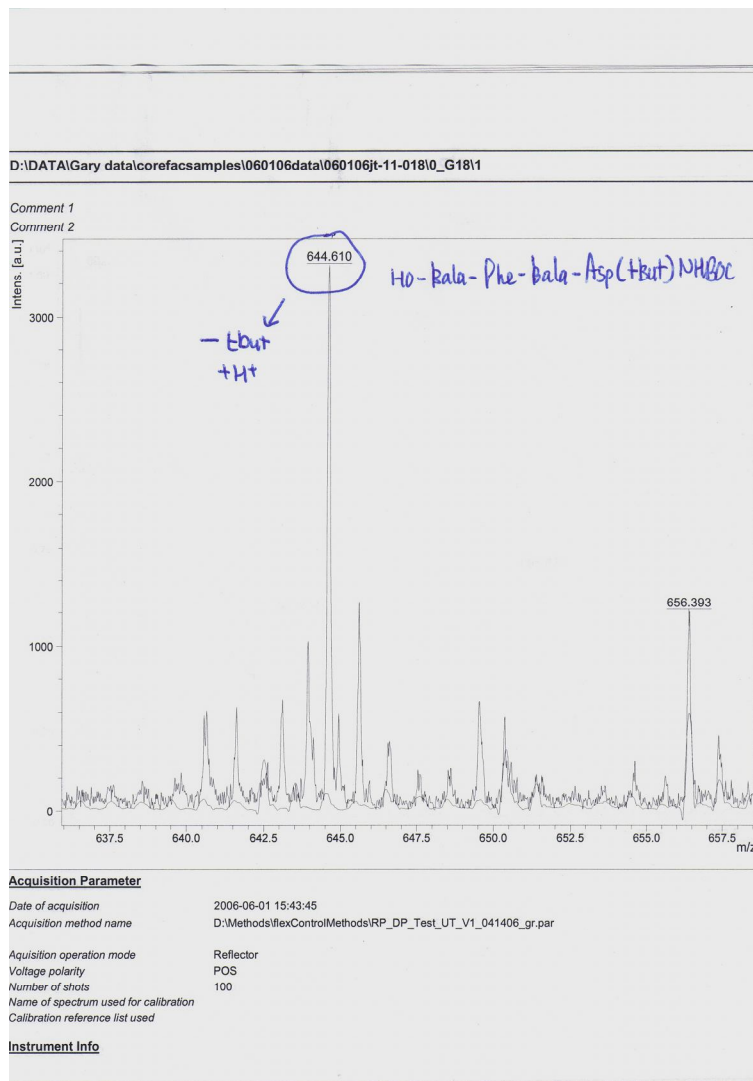
Figure C.26: - Mass spectrum of 2.40h
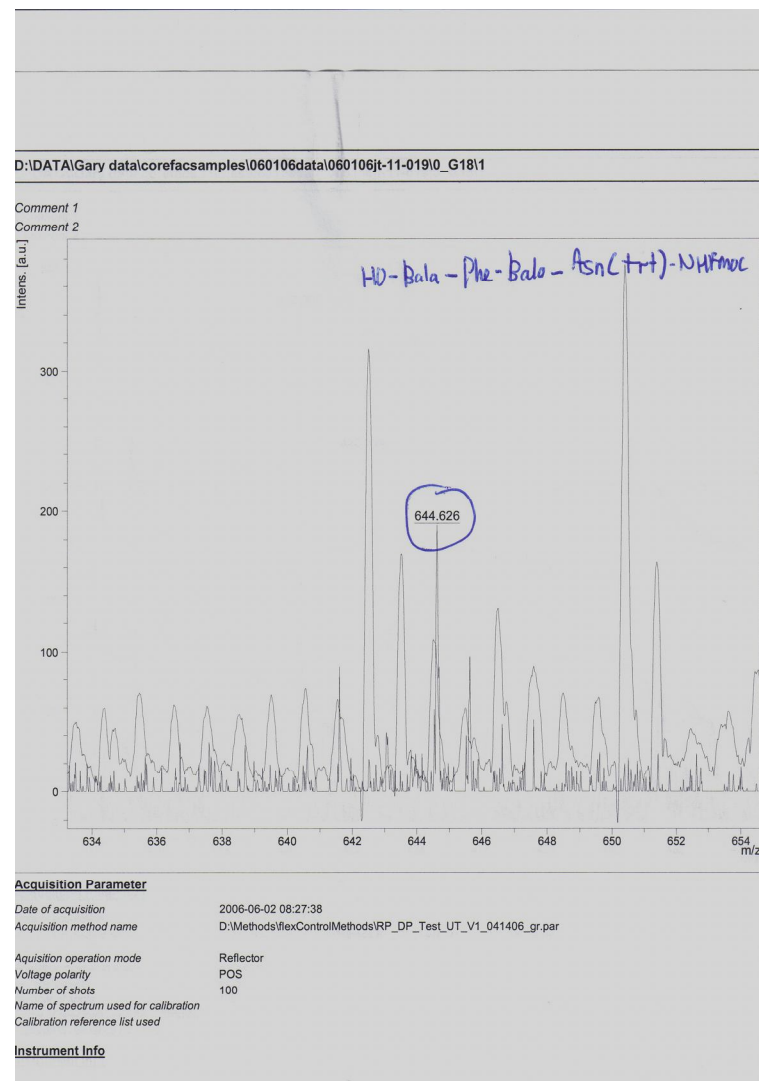
Figure C.27: - Mass spectrum of 2.40i
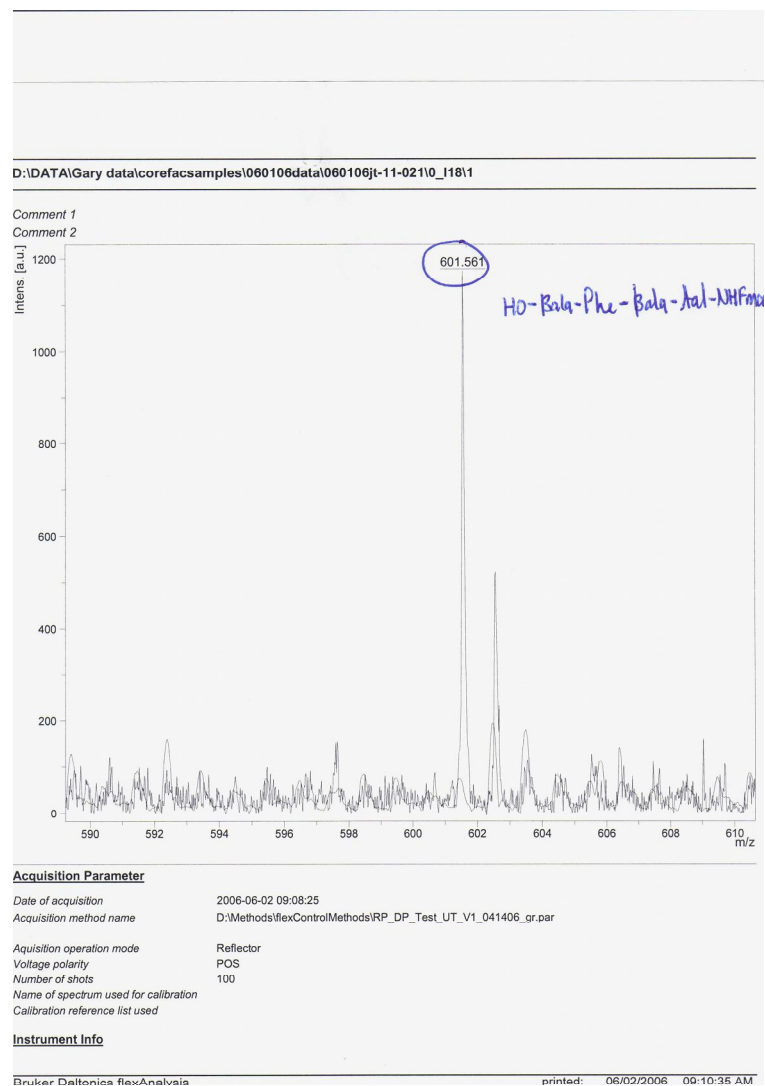
Figure C.28: - Mass spectrum of 3.1b
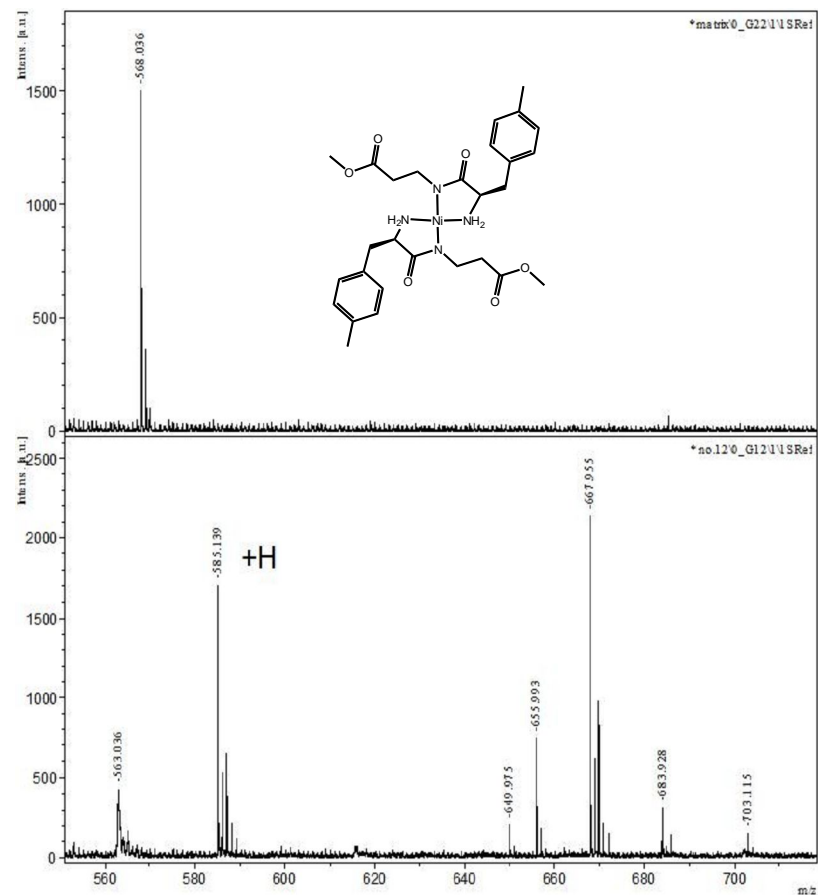
Figure C.29: - Mass spectrum of 3.1c
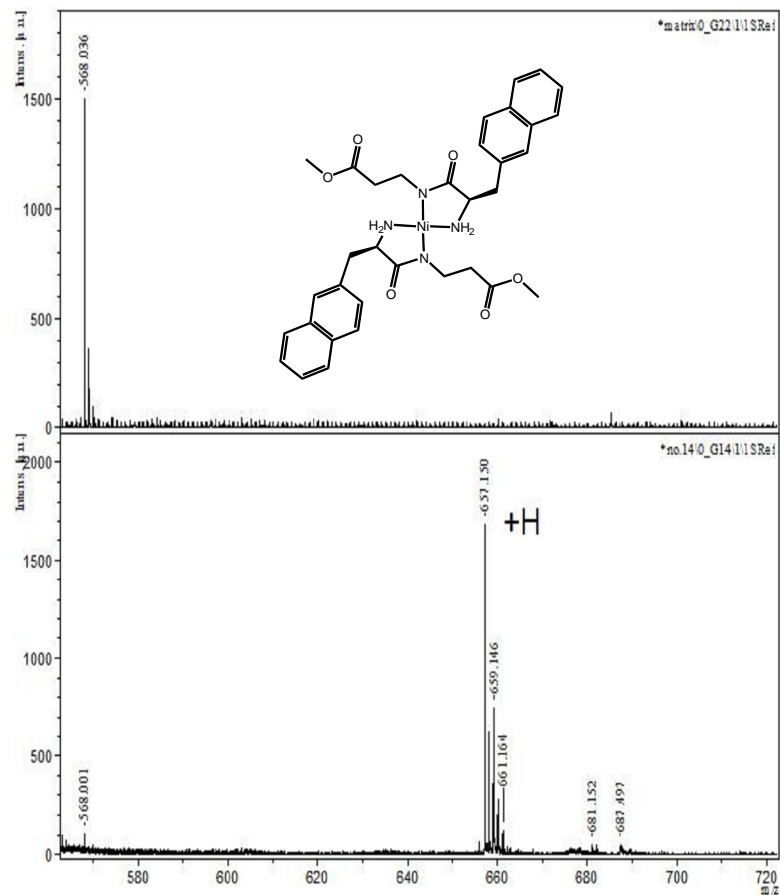
Figure C.30: - Mass spectrum of 3.2a
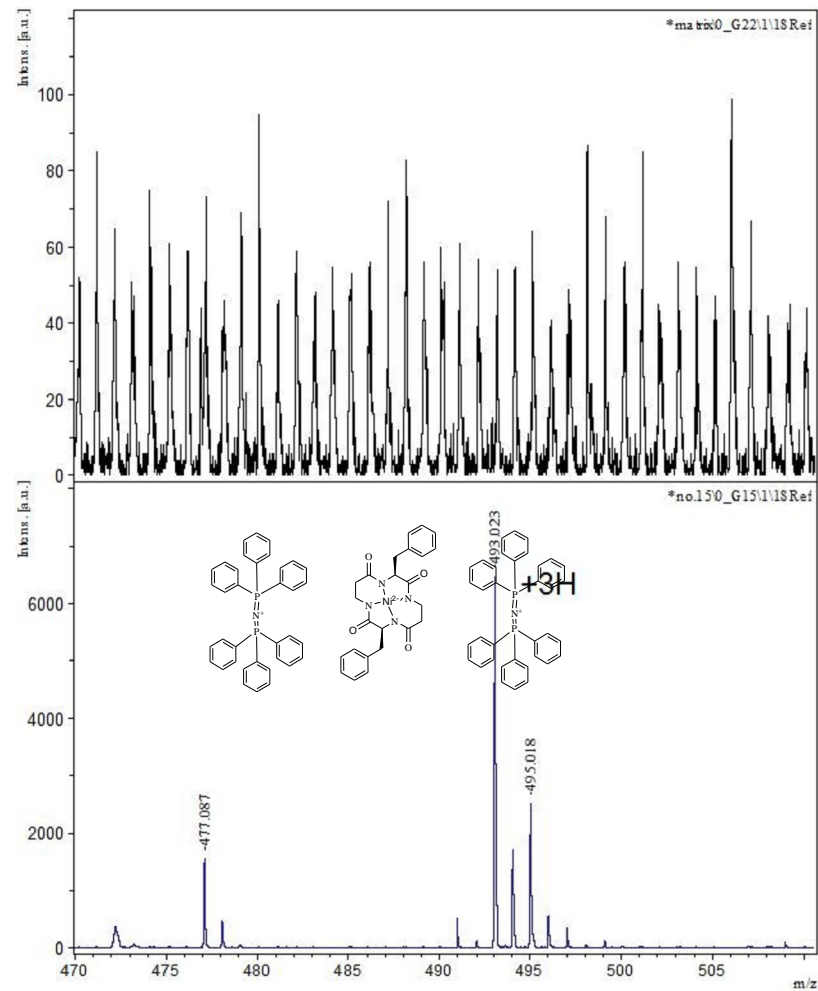
Figure C.31: - Mass spectrum of 3.2c
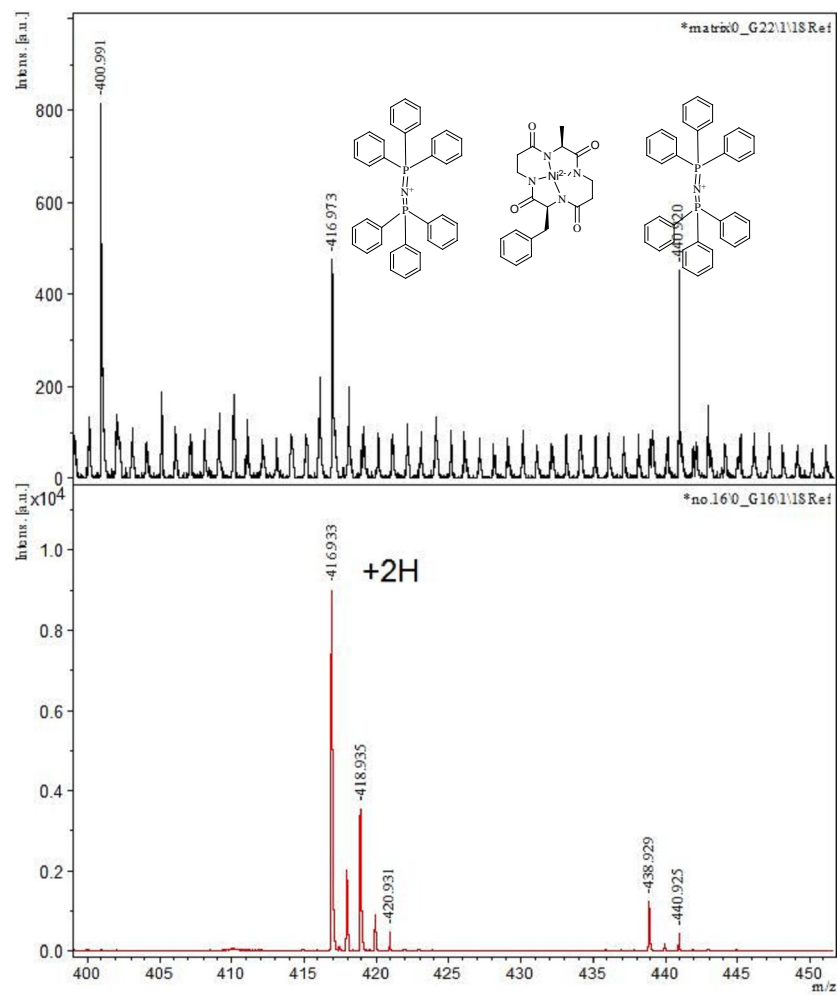
Figure C.32: - Mass spectrum of 3.2b
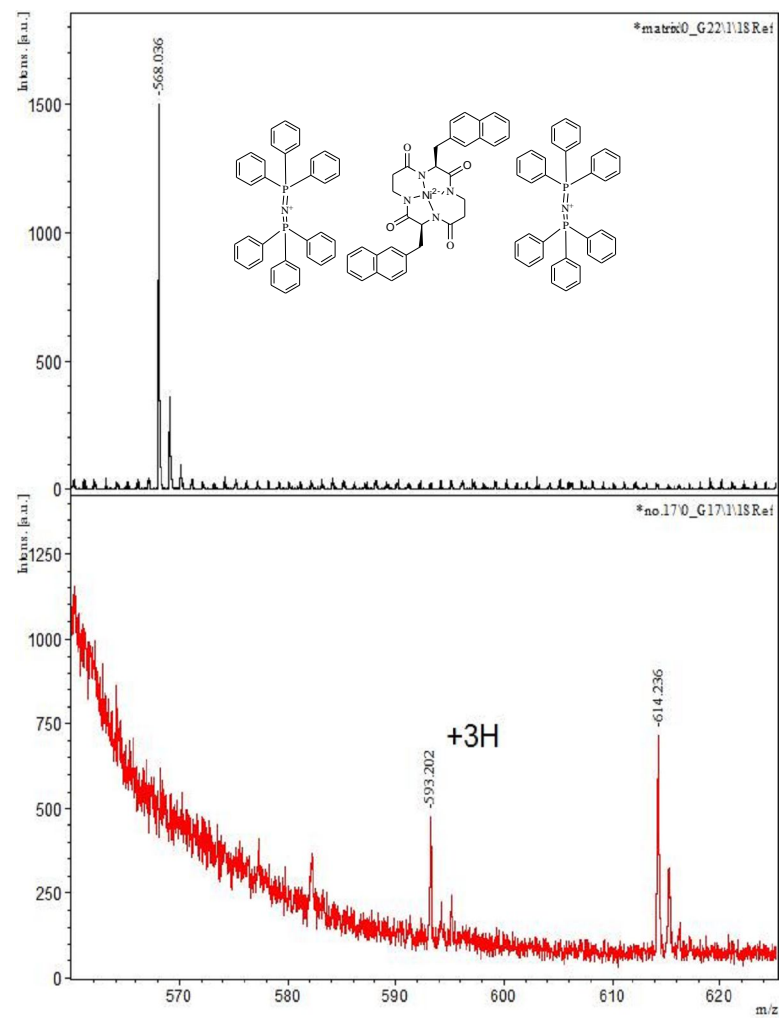
Figure C.33: - Mass spectrum of BocTrpPhe
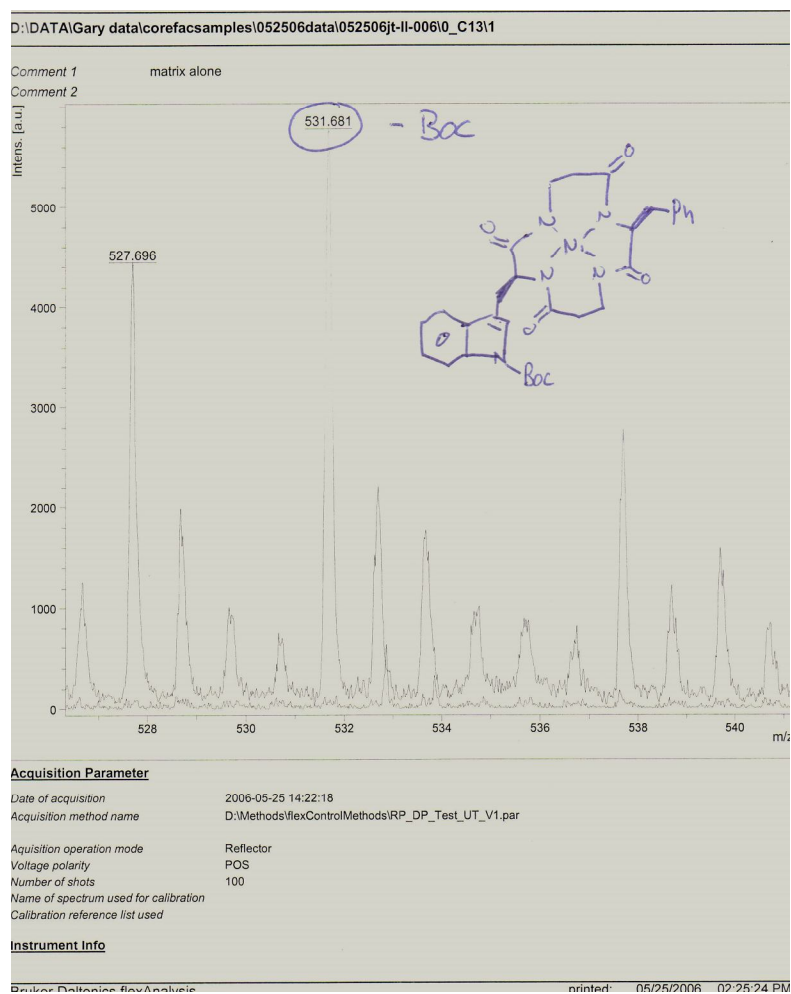
Figure C.34: - Mass spectrum of 3.2g
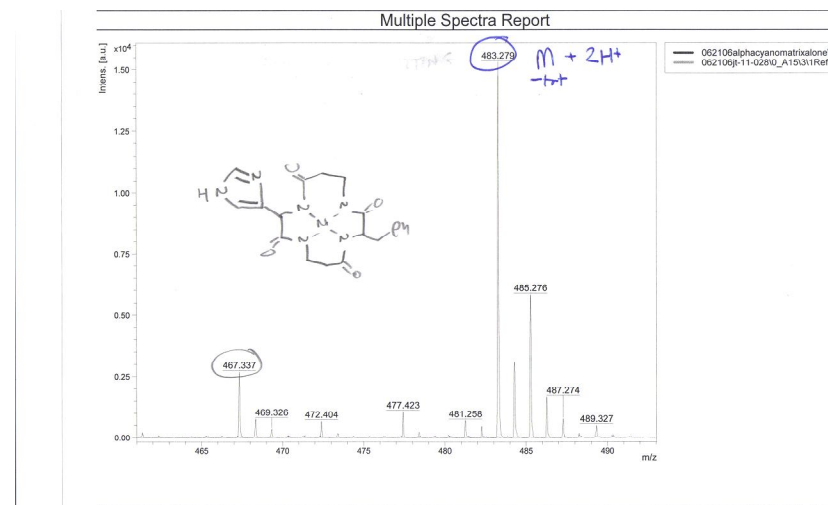
Figure C.35: - Mass spectrum of 3.2h
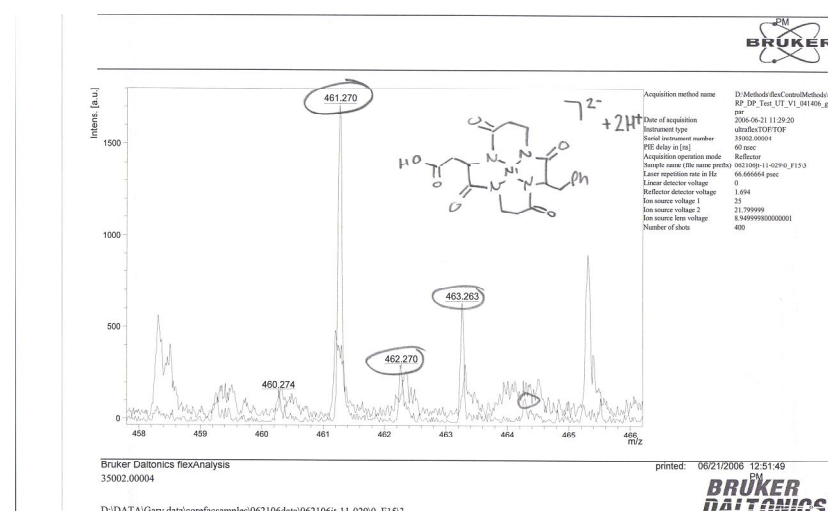
Figure C.36: - Mass spectrum of 3.2i
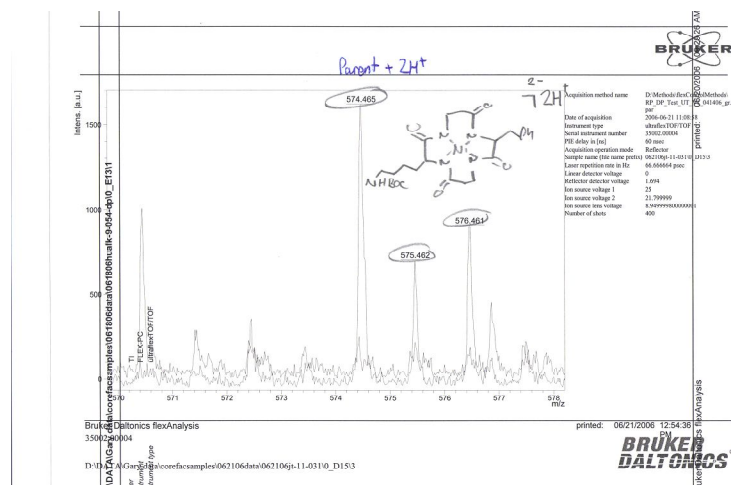
Figure C.38: - Mass spectrum of 3.2a
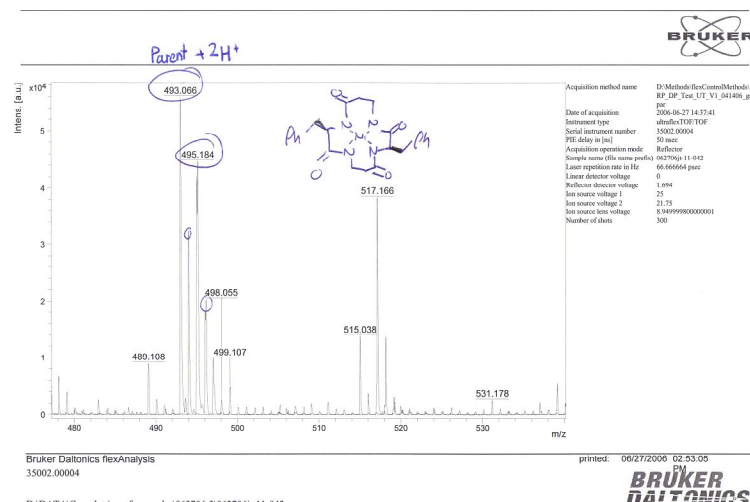
Figure C.37: - Mass spectrum of 3.2j
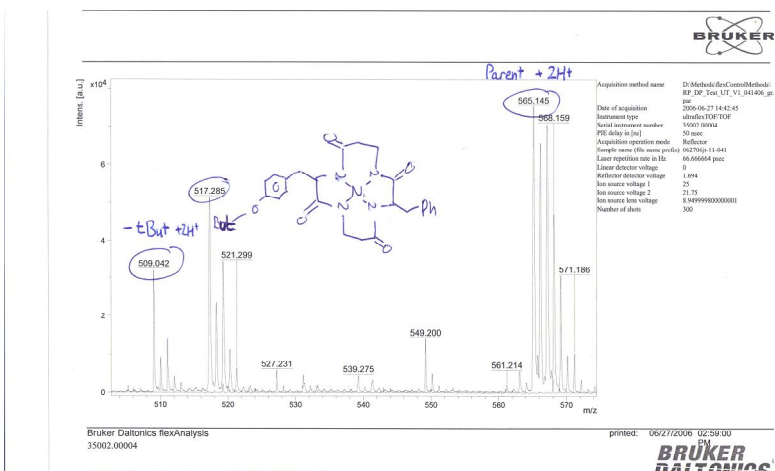
Figure C.39: - Mass spectrum of 3.2k
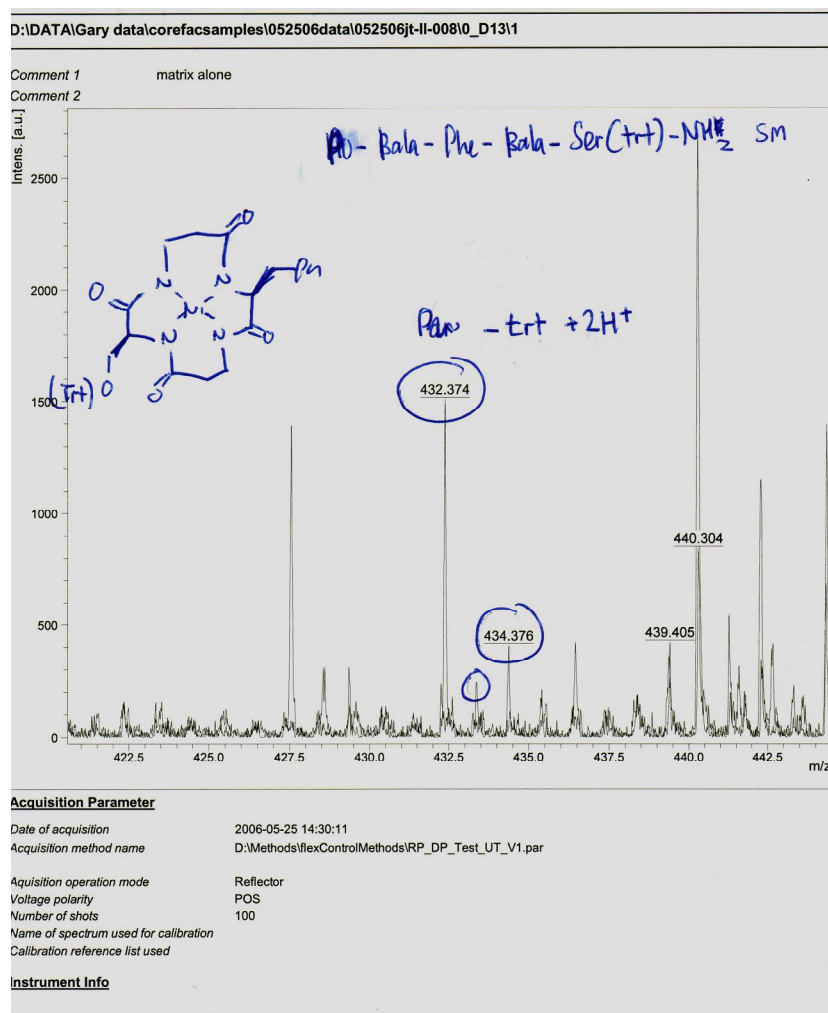
Figure C.40: - Mass spectrum of NapNapNi cyclized from resin 3.2b
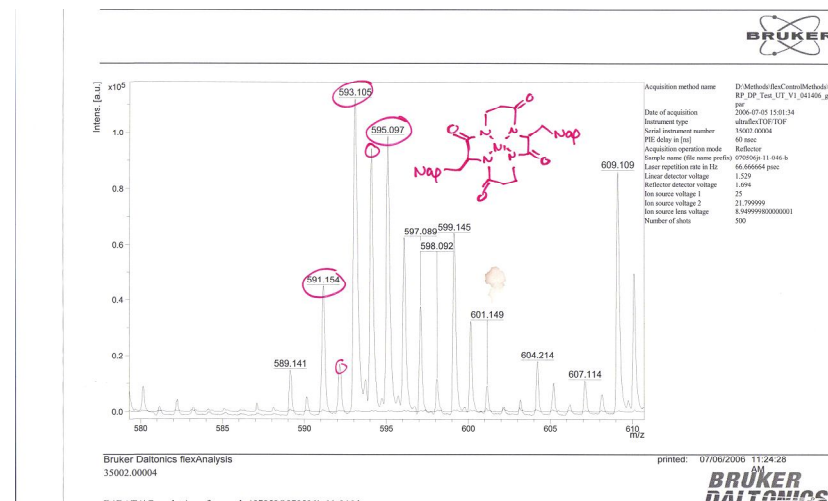
Figure C.41: - Mass spectrum of 4.1a
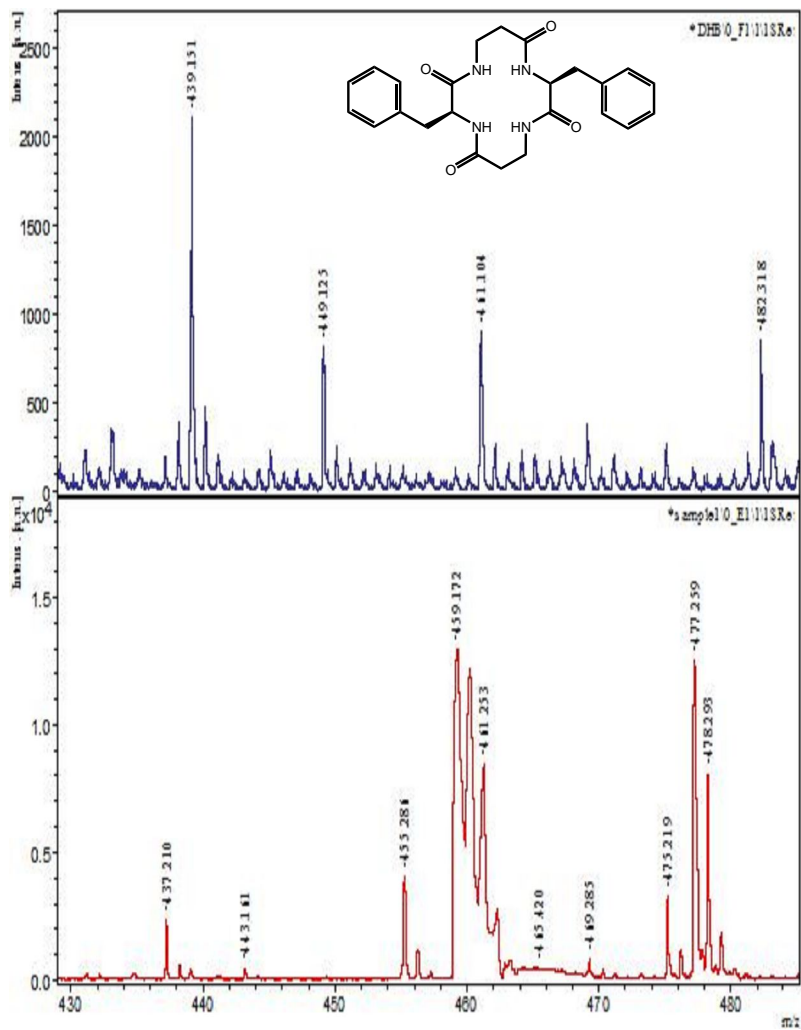
Figure C.42: - Mass spectrum of 4.1c
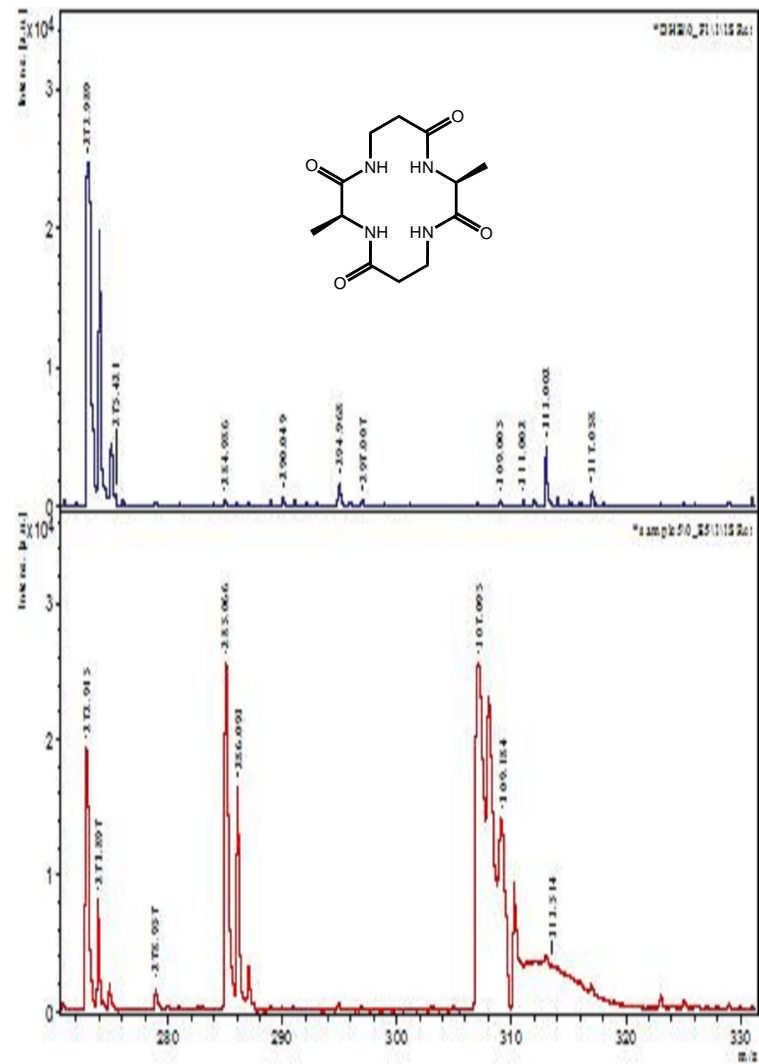
Figure C.43: - Mass spectrum of 4.1c
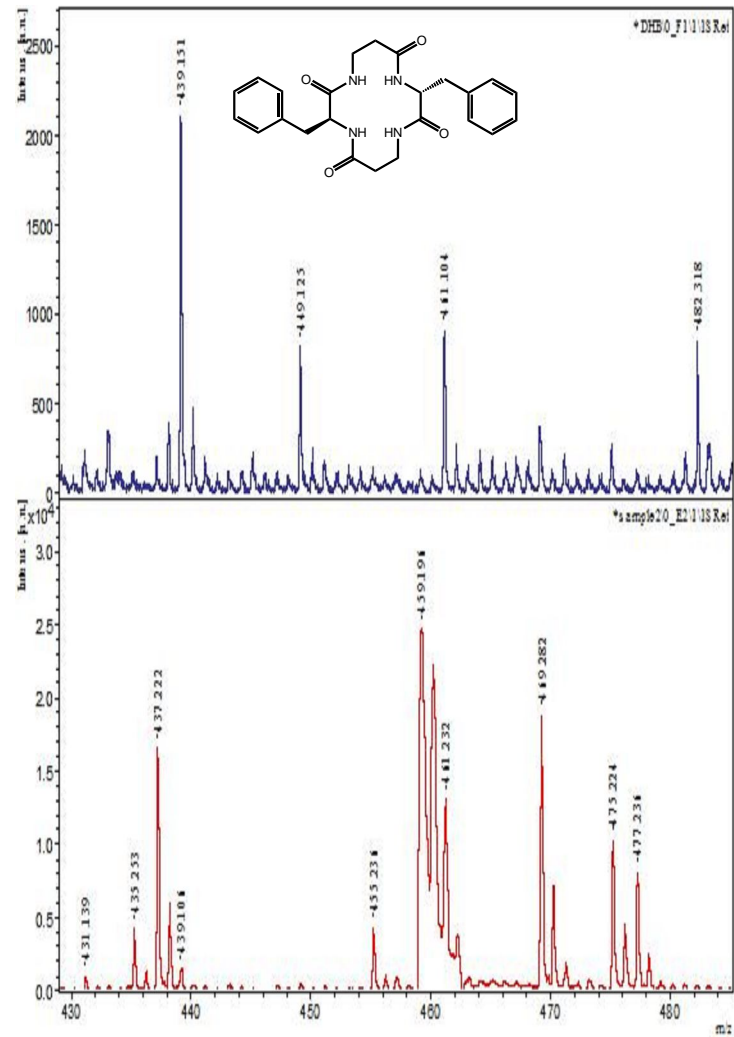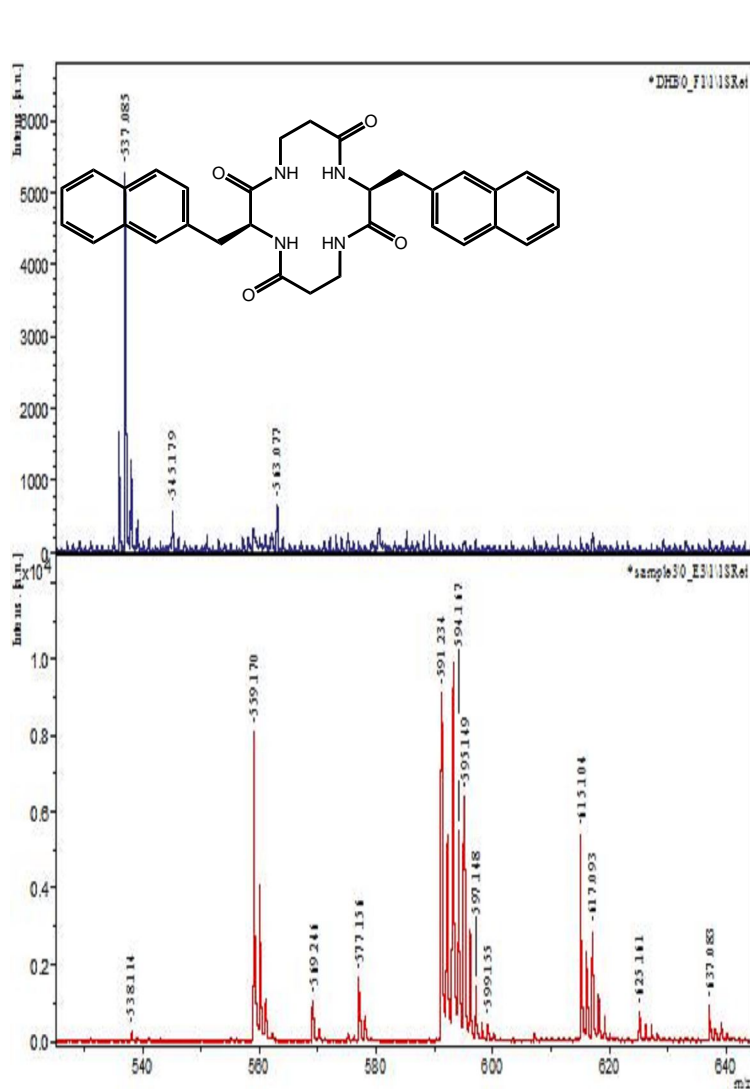
Figure C.44: - Mass spectrum of 4.1d

Figure C.45: - Mass spectrum of 4.1e

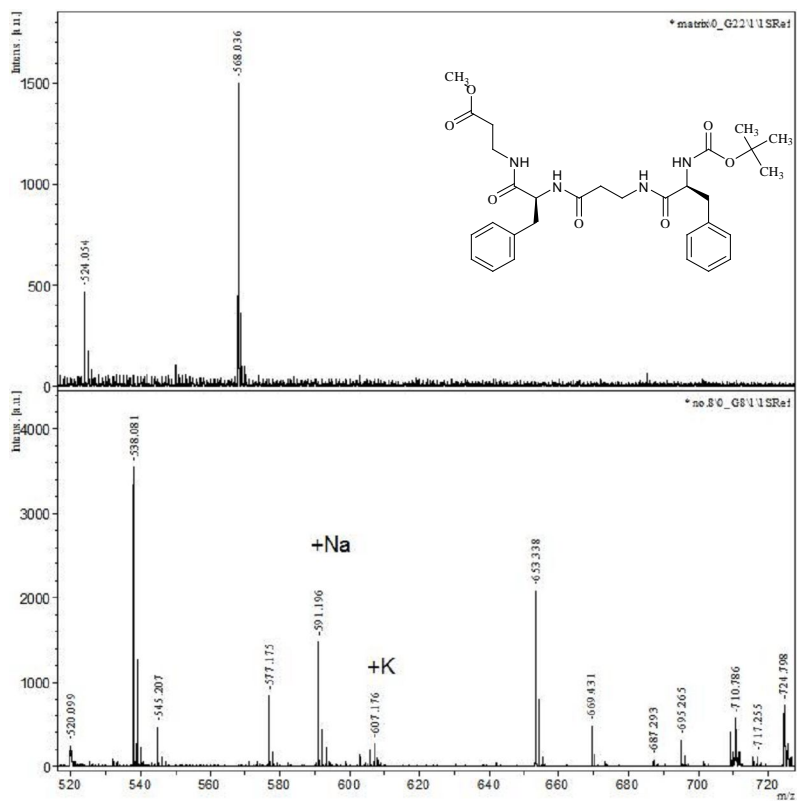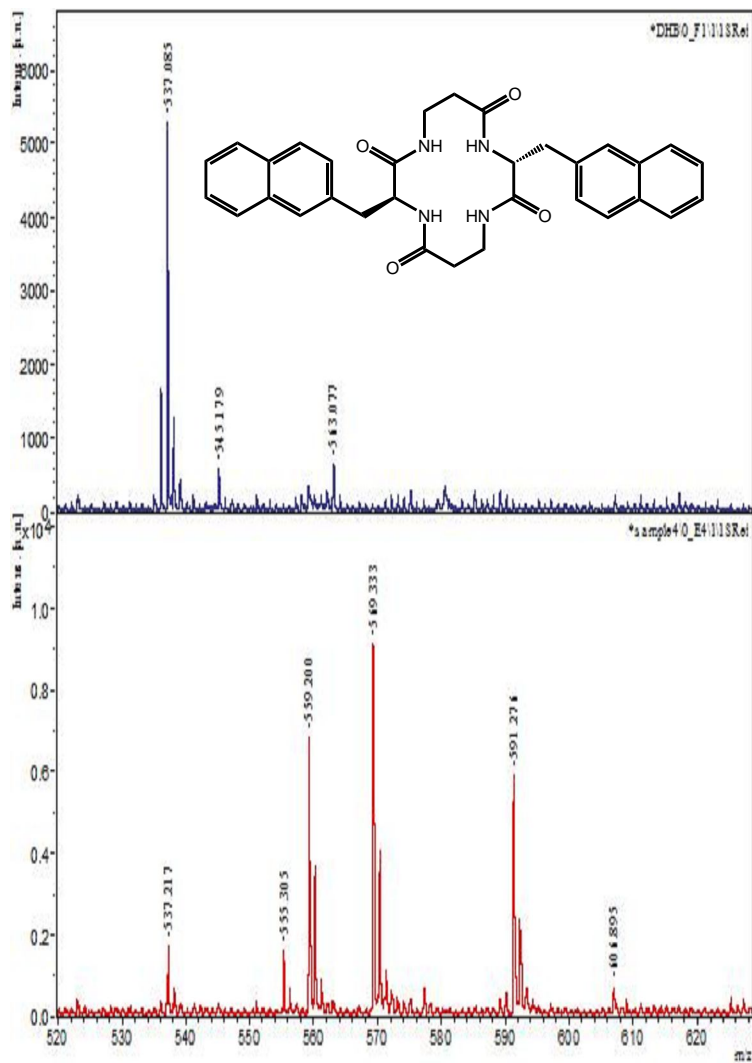**Figure C.46: - Mass spectrum of 4.1h**
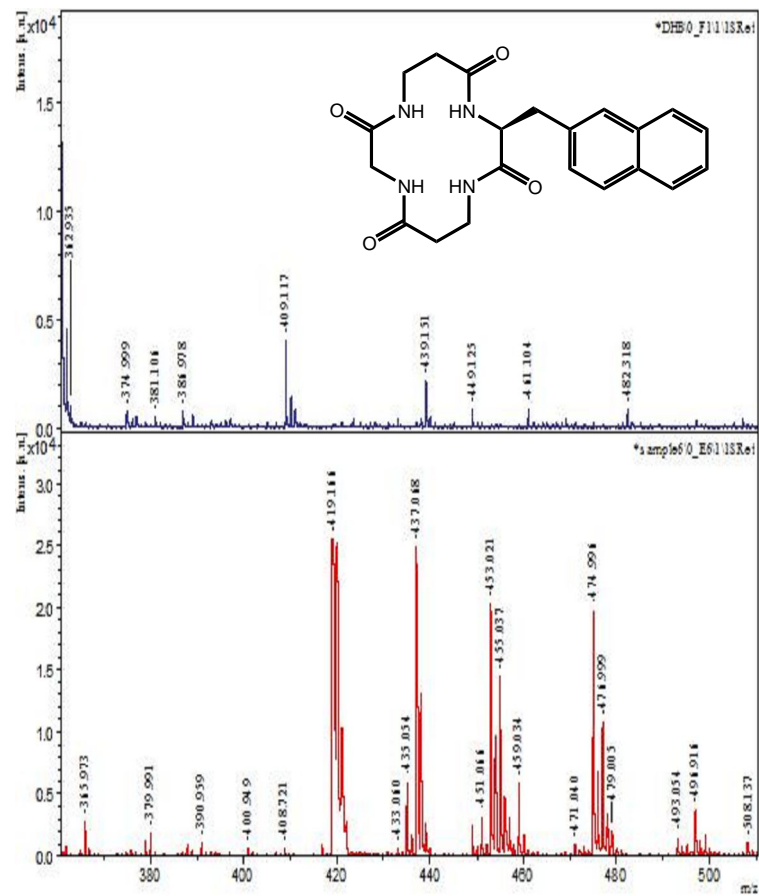
Figure C.47: - Mass spectrum of 4.1g
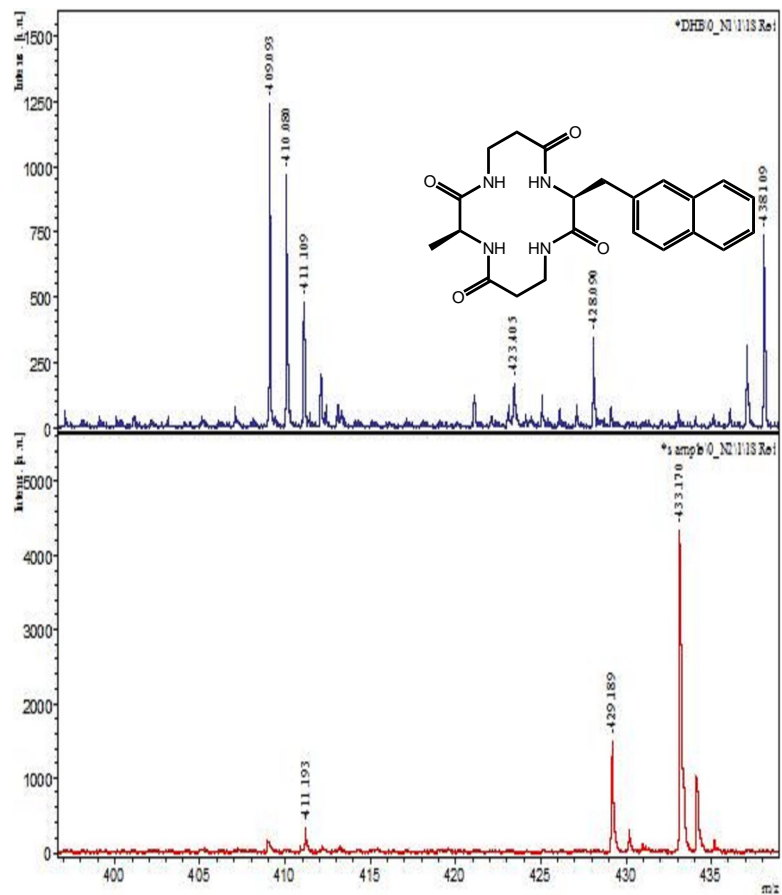
Figure C.48: - Mass spectrum of 4.4a
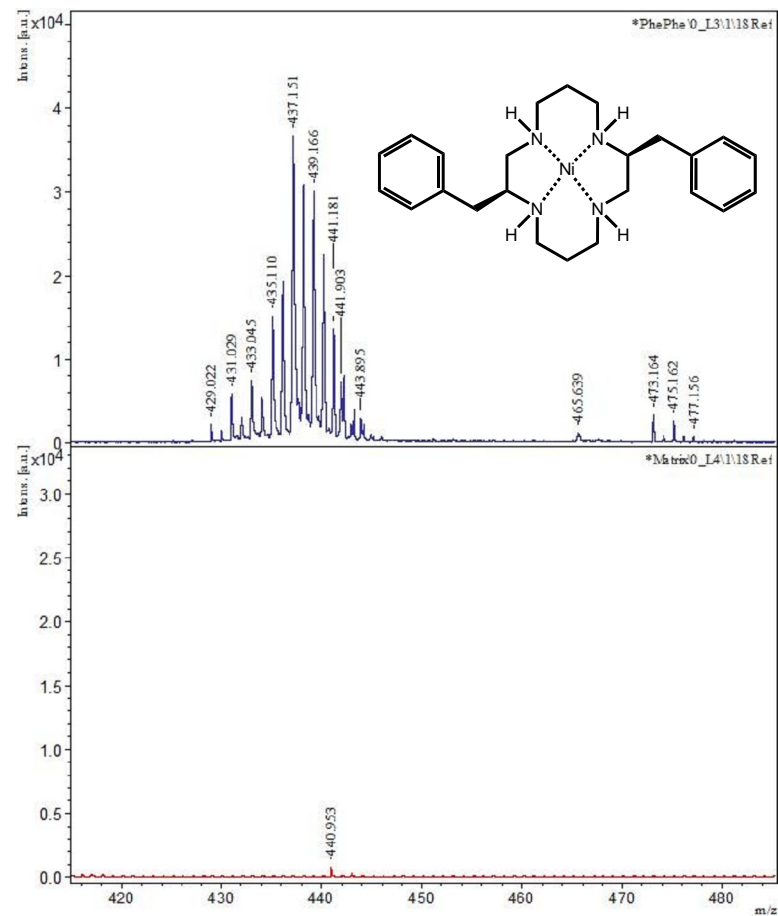
Figure C.49: - Mass spectrum of 4.4b
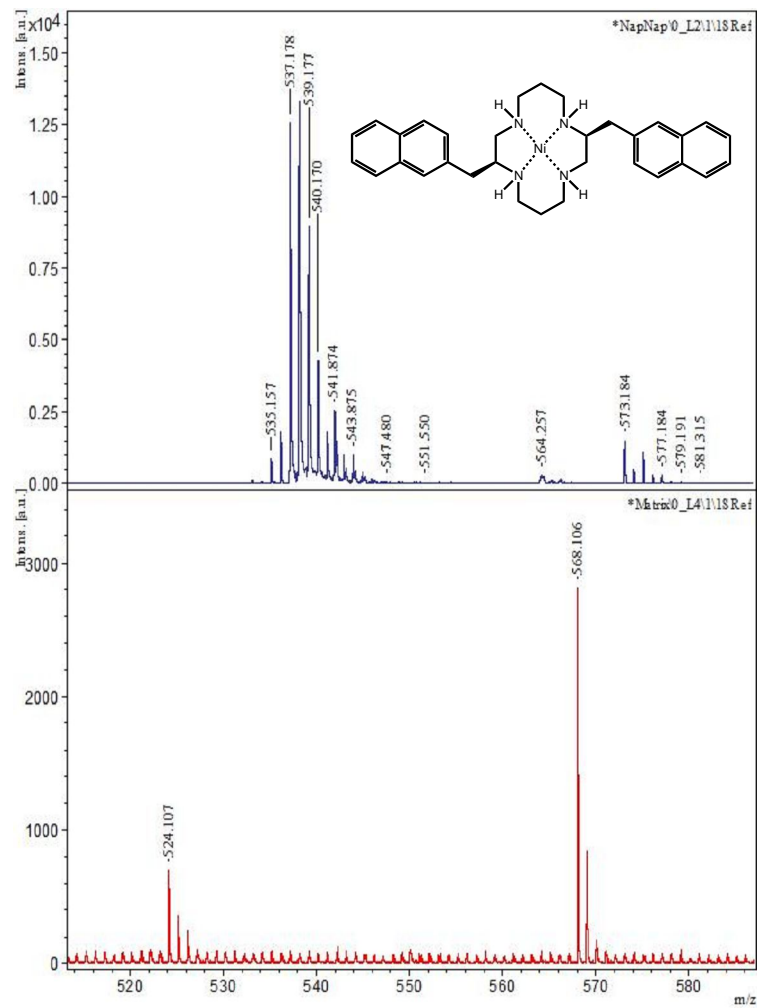
Appendix D - X-ray Crystal Data

Figure D.1: - X-ray data for 1.4

Table 1. Crystal data and structure refinement for jt0708m.

Identification code	jt0708m
Empirical formula	C25 H34 Cl2 N4 Ni O8
Formula weight	648.17
Temperature	120(2) K
Wavelength	0.71073 Å
Crystal system	Monoclinic
Space group	P2(1)/c
Unit cell dimensions	a = 11.4094(17) Å $\alpha= 90°$.
	b = 11.8597(16) Å $\beta= 96.815(5)°$.
	c = 20.544(3) Å $\gamma = 90°$.
Volume	2760.3(7) Å^3
Z	4
Density (calculated)	1.560 g/cm^3
Absorption coefficient	0.953 mm^{-1}
F(000)	1352
Crystal size	0.25 x 0.20 x 0.10 mm^3
Theta range for data collection	1.80 to 31.47°.
Index ranges	-16<=h<=15, -17<=k<=16, -30<=l<=30
Reflections collected	36141
Independent reflections	9092 [R(int) = 0.0426]
Completeness to theta = 31.47°	99.3 %
Absorption correction	None
Max. and min. transmission	0.9108 and 0.7967
Refinement method	Full-matrix least-squares on F^2
Data / restraints / parameters	9092 / 0 / 370
Goodness-of-fit on F^2	1.038
Final R indices [I>2sigma(I)]	R1 = 0.0437, wR2 = 0.1092
R indices (all data)	R1 = 0.0705, wR2 = 0.1228
Largest diff. peak and hole	0.646 and -0.422 e.Å^{-3}

Figure D.2: - X-ray data for 1.6b

Table 1. Crystal data and structure refinement for jt0502m.

Identification code	jt0502m
Empirical formula	C66 H76 B2 N8 Ni
Formula weight	1061.68
Temperature	173(2) K
Wavelength	0.71073 Å
Crystal system	Monoclinic
Space group	P2(1)/c
Unit cell dimensions	a = 16.2945(13) Å $\alpha = 90°$.
	b = 10.2253(7) Å $\beta = 114.774(4)°$.
	c = 19.1985(13) Å $\gamma = 90°$.
Volume	2904.4(4) Å^3
Z	2
Density (calculated)	1.214 g/cm^3
Absorption coefficient	0.382 mm^{-1}
F(000)	1132
Crystal size	0.40 x 0.25 x 0.20 mm^3
Theta range for data collection	2.16 to 27.48°.
Index ranges	-20<=h<=20, -12<=k<=13, -24<=l<=24
Reflections collected	18147
Independent reflections	6015 [R(int) = 0.0941]
Completeness to theta = 27.48°	90.5 %
Absorption correction	None
Refinement method	Full-matrix least-squares on F^2
Data / restraints / parameters	6015 / 0 / 351
Goodness-of-fit on F^2	1.033
Final R indices [I>2sigma(I)]	R1 = 0.0578, wR2 = 0.1487
R indices (all data)	R1 = 0.0826, wR2 = 0.1689
Largest diff. peak and hole	0.322 and -1.117 e.Å^{-3}

Figure D.3: - X-ray data for 1.6d

Table 1. Crystal data and structure refinement for jt0811m.

Identification code	jt0811m
Empirical formula	C10 H32 B2 N4 Ni
Formula weight	288.73
Temperature	120(2) K
Wavelength	0.71073 Å
Crystal system	Monoclinic
Space group	P2(1)/c
Unit cell dimensions	a = 7.1327(5) Å $\quad$ α= 90°.
	b = 12.8026(9) Å $\quad$ β= 109.978(3)°.
	c = 8.6770(5) Å $\quad$ γ = 90°.
Volume	744.68(9) Å^3
Z	2
Density (calculated)	1.288 g/cm^3
Absorption coefficient	1.288 mm^{-1}
F(000)	316
Crystal size	0.20 x 0.15 x 0.15 mm^3
Theta range for data collection	2.96 to 31.51°.
Index ranges	-10<=h<=10, -17<=k<=18, -12<=l<=12
Reflections collected	8351
Independent reflections	2482 [R(int) = 0.0233]
Completeness to theta = 31.51°	100.0 %
Absorption correction	None
Max. and min. transmission	0.8302 and 0.7827
Refinement method	Full-matrix least-squares on F^2
Data / restraints / parameters	2482 / 0 / 97
Goodness-of-fit on F^2	1.046
Final R indices [I>2sigma(I)]	R1 = 0.0248, wR2 = 0.0638
R indices (all data)	R1 = 0.0301, wR2 = 0.0669
Largest diff. peak and hole	0.447 and -0.440 e.Å^{-3}

Figure D.4: - X-ray data for 2.37a

Table 1. Crystal data and structure refinement for jt0809m.

Identification code	jt0809m
Empirical formula	C36 H54 N4 O11
Formula weight	718.83
Temperature	120(2) K
Wavelength	0.71073 Å
Crystal system	Orthorhombic
Space group	P2(1)2(1)2(1)
Unit cell dimensions	a = 12.5832(9) Å $\alpha = 90°$.
	b = 17.6865(12) Å $\beta = 90°$.
	c = 18.0311(12) Å $\gamma = 90°$.
Volume	4012.9(5) Å^3
Z	4
Density (calculated)	1.190 g/cm^3
Absorption coefficient	0.088 mm^{-1}
F(000)	1544
Crystal size	0.25 x 0.20 x 0.15 mm^3
Theta range for data collection	2.57 to 32.57°.
Index ranges	-18<=h<=16, -26<=k<=17, -27<=l<=25
Reflections collected	28685
Independent reflections	7696 [R(int) = 0.0372]
Completeness to theta = 25.00°	99.8 %
Absorption correction	None
Max. and min. transmission	0.9869 and 0.9783
Refinement method	Full-matrix least-squares on F^2
Data / restraints / parameters	7696 / 0 / 486
Goodness-of-fit on F^2	1.029
Final R indices [I>2sigma(I)]	R1 = 0.0449, wR2 = 0.0898
R indices (all data)	R1 = 0.0772, wR2 = 0.1013
Absolute structure parameter	-1.3(7)
Largest diff. peak and hole	0.205 and -0.234 e.Å^{-3}

Figure D.5: - X-ray data for 3.1a

Table 1. Crystal data and structure refinement for jt0701m.

Identification code	jt0701m
Empirical formula	C26 H34 N4 Ni O6
Formula weight	557.28
Temperature	133(2) K
Wavelength	0.71073 Å
Crystal system	Orthorhombic
Space group	P2(1)2(1)2(1)

Unit cell dimensions

$a = 10.8295(7)$ Å $\quad \alpha = 90°.$

$b = 10.8356(7)$ Å $\quad \beta = 90°.$

$c = 45.297(3)$ Å $\quad \gamma = 90°.$

Volume	5315.4(6) Å^3
Z	8
Density (calculated)	1.393 g/cm^3
Absorption coefficient	0.777 mm^{-1}
F(000)	2352
Crystal size	0.25 x 0.25 x 0.06 mm^3
Theta range for data collection	1.80 to 29.57°.
Index ranges	-15<=h<=14, -15<=k<=15, -62<=l<=62
Reflections collected	284919
Independent reflections	8256 [R(int) = 0.0949]
Completeness to theta = 29.57°	100.0 %
Absorption correction	Semi-empirical from equivalents
Max. and min. transmission	0.9549 and 0.8294
Refinement method	Full-matrix least-squares on F^2
Data / restraints / parameters	8256 / 377 / 746
Goodness-of-fit on F^2	1.039
Final R indices [I>2sigma(I)]	R1 = 0.0475, wR2 = 0.1056
R indices (all data)	R1 = 0.0595, wR2 = 0.1115
Absolute structure parameter	0.43(2)
Largest diff. peak and hole	1.137 and -0.805 e.Å^{-3}

Figure D.6: - X-ray data for 3.1b

Identification code	JT-1-547
Empirical formula	$C_{28}H_{38}N_4O_6Ni$
Formula weight	585.33
Temperature	150 K
Wavelength	0.71073 Á
Crystal system	Monoclinic
Space group	$P2_1$
Unit cell dimensions	a = 10.1769(8) Å
	b = 9.1013(8) Å
	c = 15.1983(12) Å
	$\alpha = 90°$
	$\beta = 92.735(4)$ °
	$\gamma = 90°$
Volume	1406.1(2) Å^3
Z	2
Calculated density	1.382 g/cm^3
Absorption coefficient	0.738mm^{-1}
F(000)	620
Crystal size	0.22 x 0.20 x 0.06 mm
Crystal habit	Plate
Crystal color	Orange
θ range for data collection	3.43 to 26.00^o
Limiting indices	$-12 \leq h \leq 12$
	$-11 \leq k \leq 11$
	$-18 \leq l \leq 18$
Reflections collected / unique	27340/5518 [R(int) = 0.0680]
Completeness to $\theta = 26.00$	99.6 %
Refinement method	Full-matrix least-squares on F^2
Data / restraints / parameters	5518 / 1 / 356
Refinement threshold	I>2σ(I)
Data > threshold	4240
Goodness-of-fit on F^2	1.012
Final R indices [I>2σ(I)]	R1 = 0.0402, wR2 = 0.0742
R indices (all data)	R1 = 0.0660, wR2 = 0.0830
Largest diff. peak and hole	0.364 and -0.409 e.A^{-3}

Figure D.7: - X-ray data for 3.3a

Table 1. Crystal data and structure refinement for jt0707m.

Identification code	jt0707m
Empirical formula	C193.50 H172.50 N12 Ni2 O31.50 P8
Formula weight	3535.11
Temperature	120(2) K
Wavelength	0.71073 Å
Crystal system	Triclinic
Space group	P-1
Unit cell dimensions	a = 17.3668(11) Å α= 64.893(3)°.
	b = 22.7993(15) Å β= 83.504(3)°.
	c = 25.3453(17) Å γ = 84.426(3)°.
Volume	9015.5(10) Å^3
Z	2
Density (calculated)	1.302 g/cm^3
Absorption coefficient	0.355 mm^{-1}
F(000)	3691
Crystal size	0.30 x 0.25 x 0.15 mm^3
Theta range for data collection	0.99 to 30.06°.
Index ranges	-24<=h<=24, -32<=k<=32, -33<=l<=35
Reflections collected	239493
Independent reflections	89022 [R(int) = 0.0763]
Completeness to theta = 30.06°	96.5 %
Absorption correction	None
Max. and min. transmission	0.9486 and 0.9009
Refinement method	Full-matrix least-squares on F^2
Data / restraints / parameters	89022 / 3 / 3757
Goodness-of-fit on F^2	0.972
Final R indices [I>2sigma(I)]	R1 = 0.0573, wR2 = 0.1363
R indices (all data)	R1 = 0.1048, wR2 = 0.1639
Absolute structure parameter	-0.010(6)
Largest diff. peak and hole	1.361 and -0.744 e.Å^{-3}

Figure D.8: - X-ray data for 3.2f

Table 1. Crystal data and structure refinement for jt0801m.

Identification code	jt0801m
Empirical formula	C60 H58 N5 Ni O6 P2
Formula weight	1065.76
Temperature	100(2) K
Wavelength	0.71073 Å
Crystal system	Triclinic
Space group	P1

Unit cell dimensions

$a = 10.4869(9)$ Å $\alpha = 115.667(4)°$.

$b = 16.9295(14)$ Å $\beta = 104.894(4)°$.

$c = 17.1207(14)$ Å $\gamma = 95.491(5)°$.

Volume	2571.7(4) Å^3
Z	2
Density (calculated)	1.376 g/cm^3
Absorption coefficient	0.498 mm^{-1}
F(000)	1118
Crystal size	0.25 x 0.15 x 0.08 mm^3
Theta range for data collection	2.42 to 32.58°.
Index ranges	-15<=h<=15, -25<=k<=25, -25<=l<=25
Reflections collected	102256
Independent reflections	18624 [R(int) = 0.0429]
Completeness to theta = 32.58°	99.5 %
Absorption correction	None
Max. and min. transmission	0.9612 and 0.8855
Refinement method	Full-matrix least-squares on F^2
Data / restraints / parameters	18624 / 108 / 739
Goodness-of-fit on F^2	1.104
Final R indices [I>2sigma(I)]	R1 = 0.0527, wR2 = 0.1319
R indices (all data)	R1 = 0.0749, wR2 = 0.1438
Largest diff. peak and hole	1.962 and -0.593 e.Å^{-3}

Figure D.9: - X-ray data for 3.2e

Table 1. Crystal data and structure refinement for jt0806m.

Identification code	jt0806m
Empirical formula	C68 H58 N5 Ni O4 P2
Formula weight	1129.84
Temperature	120(2) K
Wavelength	0.71073 Å
Crystal system	Monoclinic
Space group	P2(1)/c
Unit cell dimensions	a = 14.9124(5) Å $\quad\alpha= 90°$.
	b = 28.3252(9) Å $\quad\beta= 101.860(2)°$.
	c = 26.0270(9) Å $\quad\gamma = 90°$.
Volume	10759.0(6) Å^3
Z	8
Density (calculated)	1.395 g/cm^3
Absorption coefficient	0.479 mm^{-1}
F(000)	4728
Crystal size	0.30 x 0.20 x 0.15 mm^3
Theta range for data collection	1.08 to 31.00°.
Index ranges	-21<=h<=21, -40<=k<=40, -30<=l<=37
Reflections collected	144435
Independent reflections	32178 [R(int) = 0.0375]
Completeness to theta = 31.00°	93.8 %
Absorption correction	None
Max. and min. transmission	0.9317 and 0.8697
Refinement method	Full-matrix least-squares on F^2
Data / restraints / parameters	32178 / 25 / 1274
Goodness-of-fit on F^2	2.079
Final R indices [I>2sigma(I)]	R1 = 0.0928, wR2 = 0.2895
R indices (all data)	R1 = 0.1220, wR2 = 0.3029
Largest diff. peak and hole	1.754 and -1.062 e.Å^{-3}

Figure D.10: - X-ray data for 4.3a

Table 1. Crystal data and structure refinement for jt0901m.

Identification code	jt0901m
Empirical formula	C60 H62 Fe N5 O9.50 P2
Formula weight	1122.94
Temperature	120(2) K
Wavelength	0.71073 Å
Crystal system	Orthorhombic
Space group	P2(1)2(1)2(1)
Unit cell dimensions	a = 10.6733(9) Å $\alpha = 90°$.
	b = 13.4712(11) Å $\beta = 90°$.
	c = 38.259(3) Å $\gamma = 90°$.
Volume	5501.0(8) Å^3
Z	4
Density (calculated)	1.356 g/cm^3
Absorption coefficient	0.396 mm^{-1}
F(000)	2356
Crystal size	0.28 x 0.10 x 0.06 mm^3
Theta range for data collection	2.13 to 30.65°.
Index ranges	-15<=h<=8, -19<=k<=16, -54<=l<=42
Reflections collected	93207
Independent reflections	16670 [R(int) = 0.1950]
Completeness to theta = 30.65°	99.2 %
Absorption correction	None
Max. and min. transmission	0.9766 and 0.8972
Refinement method	Full-matrix least-squares on F^2
Data / restraints / parameters	16670 / 12 / 719
Goodness-of-fit on F^2	1.071
Final R indices [I>2sigma(I)]	R1 = 0.0917, wR2 = 0.1919
R indices (all data)	R1 = 0.2069, wR2 = 0.2399
Absolute structure parameter	0.02(3)
Largest diff. peak and hole	0.928 and -1.052 e.Å^{-3}

Figure D.11: - X-ray data for 4.3b

Table 1. Crystal data and structure refinement for jt0902m.

Identification code	jt0902m
Empirical formula	C60 H54 Co N5 O4 P2
Formula weight	1029.95
Temperature	120(2) K
Wavelength	0.71073 Å
Crystal system	Monoclinic
Space group	P2
Unit cell dimensions	a = 15.6796(11) Å $\quad\quad$ α= 90°.
	b = 8.9697(7) Å $\quad\quad$ β= 94.201(4)°.
	c = 17.8778(13) Å $\quad\quad$ γ = 90°.
Volume	2507.6(3) Å^3
Z	2
Density (calculated)	1.364 g/cm^3
Absorption coefficient	0.461 mm^{-1}
F(000)	1076
Crystal size	0.20 x 0.16 x 0.14 mm^3
Theta range for data collection	1.30 to 31.00°.
Index ranges	-22<=h<=22, -12<=k<=12, -25<=l<=25
Reflections collected	39874
Independent reflections	14883 [R(int) = 0.0860]
Completeness to theta = 25.00°	99.9 %
Absorption correction	None
Max. and min. transmission	0.9383 and 0.9134
Refinement method	Full-matrix least-squares on F^2
Data / restraints / parameters	14883 / 313 / 651
Goodness-of-fit on F^2	1.024
Final R indices [I>2sigma(I)]	R1 = 0.0812, wR2 = 0.1559
R indices (all data)	R1 = 0.1664, wR2 = 0.1825
Absolute structure parameter	0.11(3)
Largest diff. peak and hole	0.960 and -0.977 e.Å^{-3}

Figure D.12: - X-ray data for 4.4a

Table 1. Crystal data and structure refinement for jt0803m.

Identification code	jt0803m
Empirical formula	C26 H44 Cl2 N4 Ni O2
Formula weight	574.26
Temperature	120(2) K
Wavelength	0.71073 Å
Crystal system	Triclinic
Space group	P1
Unit cell dimensions	a = 6.8356(4) Å $\qquad$ α= 86.977(2)°.
	b = 8.0965(4) Å $\qquad$ β= 81.399(2)°.
	c = 12.9985(7) Å $\qquad$ γ = 82.068(2)°.
Volume	704.12(7) Å^3
Z	1
Density (calculated)	1.354 g/cm^3
Absorption coefficient	0.908 mm^{-1}
F(000)	306
Crystal size	0.25 x 0.15 x 0.10 mm^3
Theta range for data collection	2.54 to 33.11°.
Index ranges	-10<=h<=10, -12<=k<=12, -19<=l<=19
Reflections collected	15175
Independent reflections	9039 [R(int) = 0.0180]
Completeness to theta = 33.11°	97.9 %
Absorption correction	None
Max. and min. transmission	0.9146 and 0.8048
Refinement method	Full-matrix least-squares on F^2
Data / restraints / parameters	9039 / 3 / 336
Goodness-of-fit on F^2	0.981
Final R indices [I>2sigma(I)]	R1 = 0.0251, wR2 = 0.0558
R indices (all data)	R1 = 0.0281, wR2 = 0.0568
Absolute structure parameter	0.021(6)
Largest diff. peak and hole	0.585 and -0.226 e.Å^{-3}

Figure D.13: - X-ray data for 4.4b.

Table 1. Crystal data and structure refinement for jt0710m.

Identification code	jt0710m
Empirical formula	C34 H44 Cl2 N4 Ni O2
Formula weight	670.34
Temperature	120(2) K
Wavelength	0.71073 Å
Crystal system	Triclinic
Space group	P1
Unit cell dimensions	a = 6.872(4) Å α= 89.33(4)°.
	b = 8.172(6) Å β= 86.34(4)°.
	c = 15.032(8) Å γ = 84.67(4)°.
Volume	838.8(9) Å^3
Z	1
Density (calculated)	1.327 g/cm^3
Absorption coefficient	0.774 mm^{-1}
F(000)	354
Crystal size	0.25 x 0.20 x 0.15 mm^3
Theta range for data collection	2.72 to 29.94°.
Index ranges	-9<=h<=9, -11<=k<=11, -21<=l<=20
Reflections collected	24197
Independent reflections	24197 [R(int) = 0.0000]
Completeness to theta = 29.94°	98.7 %
Absorption correction	None
Max. and min. transmission	0.8928 and 0.8301
Refinement method	Full-matrix least-squares on F^2
Data / restraints / parameters	24197 / 3 / 318
Goodness-of-fit on F^2	1.047
Final R indices [I>2sigma(I)]	R1 = 0.1038, wR2 = 0.2644
R indices (all data)	R1 = 0.2403, wR2 = 0.3355
Absolute structure parameter	0.08(3)

Largest diff. peak and hole1.020 and -1.294 e.Å^{-3}

Figure D.14: - X-ray data for 4.4c.

Table 1. Crystal data and structure refinement for jt0812m.

Identification code	jt0812m
Empirical formula	C65 H84 Cl4 N8 Ni2 O
Formula weight	1252.62
Temperature	120(2) K
Wavelength	0.71073 Å
Crystal system	Monoclinic
Space group	C2/c
Unit cell dimensions	a = 25.861(3) Å $\alpha= 90°$.
	b = 6.6117(6) Å $\beta= 101.243(7)°$.
	c = 36.006(4) Å $\gamma = 90°$.
Volume	6038.3(11) Å^3
Z	4
Density (calculated)	1.378 g/cm^3
Absorption coefficient	0.851 mm^{-1}
F(000)	2648
Crystal size	0.18 x 0.12 x 0.06 mm^3
Theta range for data collection	3.06 to 30.51°.
Index ranges	-35<=h<=33, -9<=k<=9, -51<=l<=51
Reflections collected	30422
Independent reflections	8626 [R(int) = 0.1708]
Completeness to theta = 27.50°	95.1 %
Absorption correction	None
Max. and min. transmission	0.9507 and 0.8619
Refinement method	Full-matrix least-squares on F^2
Data / restraints / parameters	8626 / 0 / 382
Goodness-of-fit on F^2	0.940
Final R indices [I>2sigma(I)]	R1 = 0.0736, wR2 = 0.1286
R indices (all data)	R1 = 0.2224, wR2 = 0.1746
Largest diff. peak and hole	0.558 and -0.432 e.Å^{-3}

Figure D.15: - X-ray data for 4.4d

Table 1. Crystal data and structure refinement for jt0808m.

Identification code	jt0808m
Empirical formula	C12 H28 Cl2 N4 Ni O8
Formula weight	485.99
Temperature	120(2) K
Wavelength	0.71073 Å
Crystal system	Orthorhombic
Space group	P2(1)2(1)2(1)

Unit cell dimensions

$a = 8.3101(4)$ Å $\alpha = 90°$.
$b = 13.4696(6)$ Å $\beta = 90°$.
$c = 17.3408(8)$ Å $\gamma = 90°$.

Volume	1941.02(16) Å^3
Z	4
Density (calculated)	1.663 g/cm^3
Absorption coefficient	1.323 mm^{-1}
F(000)	1016
Crystal size	0.25 x 0.20 x 0.15 mm^3
Theta range for data collection	2.35 to 31.49°.
Index ranges	-12<=h<=12, -19<=k<=19, -25<=l<=25
Reflections collected	27290
Independent reflections	6371 [R(int) = 0.0631]
Completeness to theta = 31.49°	99.6 %
Absorption correction	None
Max. and min. transmission	0.8262 and 0.7333
Refinement method	Full-matrix least-squares on F^2
Data / restraints / parameters	6371 / 40 / 275
Goodness-of-fit on F^2	1.065
Final R indices [I>2sigma(I)]	R1 = 0.0626, wR2 = 0.1685
R indices (all data)	R1 = 0.0765, wR2 = 0.1781
Absolute structure parameter	0.01(2)

Largest diff. peak and hole 2.870 and -0.980 e.Å^{-3}